Copy 2

[redacted]

NASA MEMO 5-30-59L

NASA MEMO 5-30-59L

CLASSIFICATION CHANGE

To Unclassified

By authority of NASA Memo dtd 5-2-73 3/5/69 H. Maines

Changed by M. R. Ruda Date 6-11-73

NASA

MEMORANDUM

AN INVESTIGATION OF A 0.05-SCALE MODEL OF THE XSM-64A NAVAHO MISSILE AND BOOSTER

PART I - FORCE STUDY AT MACH NUMBERS FROM 1.77 TO 3.51

By James D. Church and Nancy L. Taylor

Langley Research Center
Langley Field, Va.

NASA FILE COPY

REVIEW COPY

CLASSIFIED DOCUMENT - TITLE CONFIDENTIAL

This material contains information affecting the National Defense of the United States within the meaning of the espionage laws, Title 18, U.S.C., Secs. 793 and 794, the transmission or revelation of which in any manner to an unauthorized person is prohibited by law.

NATIONAL AERONAUTICS AND SPACE ADMINISTRATION

WASHINGTON

[redacted]

[redacted]

NATIONAL AERONAUTICS AND SPACE ADMINISTRATION

MEMORANDUM 5-30-59L

AN INVESTIGATION OF A 0.05-SCALE MODEL OF THE XSM-64A NAVAHO MISSILE AND BOOSTER

PART I - FORCE STUDY AT MACH NUMBERS FROM 1.77 TO 3.51*

By James D. Church and Nancy L. Taylor

ABSTRACT

An investigation has been conducted in the Langley Unitary Plan wind tunnel of the aerodynamic loads and the static longitudinal and lateral stability of a missile-booster combination and its various components. The Reynolds number range of the test was 2.4×10^6 to 2.9×10^6. Included are some effects of various controls and separately measured loads on wing, tip aileron, rudder, booster, booster separating surface, booster fin, and booster yaw and pitch thrust chambers.

INDEX HEADINGS

Air Inlets, Side	1.4.1.4
Missiles - Components in Combination	1.7.2.1
Missiles, Specific Types	1.7.2.2
Stability, Static	1.8.1.1
Control	1.8.2
Loads, Aerodynamic	4.1.1

*Title, Confidential.

[redacted]

NATIONAL AERONAUTICS AND SPACE ADMINISTRATION

MEMORANDUM 5-30-59L

AN INVESTIGATION OF A 0.05-SCALE MODEL OF THE XSM-64A NAVAHO MISSILE AND BOOSTER

PART I - FORCE STUDY AT MACH NUMBERS FROM 1.77 TO 3.51*

By James D. Church and Nancy L. Taylor

SUMMARY

An investigation has been conducted in the Langley Unitary Plan wind tunnel to determine the aerodynamic loads and the static longitudinal and lateral stability of a 0.05-scale model of the XSM-64A Navaho missile and booster and its various components. Tests were conducted through a Mach number range of 1.77 to 3.51 with a corresponding Reynolds number range of 2.4×10^6 to 2.9×10^6. Results are presented for an angle-of-attack range of -8° to 4° for the missile-booster combination and -10° to 10° for the missile-alone configuration. Tests for both configurations were conducted through an angle-of-sideslip range of -8° to 8°. Also presented are some effects on the model characteristics of the deflection of various components including canard, tip aileron, vertical stabilizer, speed brakes, and booster pitch and yaw thrust chambers. The various components on which loads were measured include the wing, tip aileron, rudder, booster, booster separating surface, booster fin, and booster yaw and pitch thrust chambers. These data are presented without analysis.

INTRODUCTION

An investigation was conducted on a 0.05-scale model of the XSM-64A Navaho missile and missile-booster combination in the Langley Unitary Plan wind tunnel. This configuration represents a surface-to-surface missile intended for long-range supersonic operation within the atmosphere.

*Title, Confidential.

The system is initially boosted to a Mach number M of approximately 3.5 by a liquid-rocket package suspended beneath the missile. After the missile separates from the booster, a cruise flight at M = 3.2 is provided by the missile's ram-jet engines. Upon reaching the target area, the missile dives (with speed brakes extended) at approximately M = 1.8.

The purpose of the present investigation was to determine the total forces acting on the missile and the portion of these loads carried by the booster and the various model lifting and control surfaces. Data for the missile-booster combination were obtained at Mach numbers of 2.29, 2.75, 3.22, and 3.51 for angles of attack from -8° to 4°. Missile-alone measurements were made at Mach numbers of 1.77, 2.75, and 3.22 for angles of attack from -10° to 10°. The angle-of-sideslip range for both of these configurations was -8° to 8°.

The results presented consist of the separate forces and moments measured on models of the missile, booster, and various component parts of both the missile and booster. Included are some effects of deflection of the missile canard, aileron, rudder, and the booster thrust chambers. In addition, several model modifications were examined. These results are presented without analysis.

The force results presented herein are augmented by a report on pressure-distribution measurements already obtained for the same model configurations. (See ref. 1.) Included in this reference are pressures measured on one of the booster thrust chambers with and without the jet simulator.

SYMBOLS

In general, all data are referred to the body axes illustrated in figure 1(a). However, the three pitch components of the missile balance (presented about the body axes for lateral tests) are referred to the wind axes (fig. 1(b)) for the pitch tests. A statement of the location of the various moment reference points is contained in the section entitled "Presentation of Results." Table I lists the areas and lengths upon which the coefficients are based and figure 2 gives additional pertinent information and indicates the location of the various reference centers.

A base area of thrust chambers, sq ft

b span of surface, in.

C_N model total normal-force coefficient, F_N/qS_W

[redacted]

$(C_A)_B$ base axial-force coefficient

$(C_A)_C$ cavity axial-force coefficient

C_A model total axial-force coefficient, F_A/qS_W

C_m model total pitching-moment coefficient, $M_Y/qS_W\bar{c}_W$

C_l model total rolling-moment coefficient, M_X/qS_Wb_W

C_n model total yawing-moment coefficient, M_Z/qS_Wb_W

C_Y model total side-force coefficient, F_Y/qS_W

C_L model total lift coefficient (wind axis), F_L/qS_W

$(C_D)_i$ missile internal (two ducts) drag coefficient (wind axis)

C_D model total drag coefficient (wind axis), F_D/qS_W

$C_{m,w}$ model total pitching-moment coefficient (wind axis), $M_{Yw}/qS_W\bar{c}_W$

$C_{N,W}$ missile-wing normal-force coefficient, $\dfrac{(F_N)_W}{q\left(\frac{S_W}{2}\right)_{exp}}$

$C_{m,W}$ missile-wing pitching-moment coefficient, $\dfrac{(M_Y)_W}{q\left(\frac{S_W}{2}\right)_{exp}(\bar{c}_W)_{exp}}$

$C_{b,W}$ missile-wing bending-moment coefficient, $\dfrac{(M_X)_W}{q\left(\frac{S_W}{2}\right)_{exp}\left(\frac{b_W}{2}\right)_{exp}}$

$C_{h,A}$ missile-aileron hinge-moment coefficient, $\dfrac{(M_Y)_A}{qS_A\bar{c}_A}$

$C_{N,R}$ missile-vertical-stabilizer normal-force coefficient, $\frac{(F_Y)_R}{qS_R}$

$C_{h,R}$ missile-vertical-stabilizer hinge-moment (yaw) coefficient, $\frac{(M_Z)_R}{qS_R\bar{c}_R}$

$C_{b,R}$ missile-vertical-stabilizer bending-moment coefficient, $\frac{(M_X)_R}{qS_R b_R}$

$(C_{N,B})_M$ booster normal-force coefficient at missile pitch center, $\frac{(F_N)_B}{qS_W}$

$(C_{A,B})_M$ booster axial-force coefficient at missile pitch center, $\frac{(F_A)_B}{qS_W}$

$(C_{m,B})_M$ booster pitching-moment coefficient about missile pitch center, $\frac{(M_Y)_B}{qS_W\bar{c}_W}$

$C_{N,S}$ booster-separation-surface normal-force coefficient, $\frac{(F_N)_S}{qS_S}$

$C_{b,S}$ booster-separating-surface bending-moment coefficient, $\frac{(M_X)_S}{qS_S b_S}$

$C_{N,F}$ booster-fin normal-force coefficient, $\frac{(F_N)_F}{qS_F}$

$C_{m,F}$ booster-fin pitching-moment coefficient, $\frac{(M_Y)_F}{qS_F\bar{c}_F}$

$C_{b,F}$ booster-fin bending-moment coefficient, $\frac{(M_X)_F}{qS_F b_F}$

$C_{N,PT}$ booster-pitch-thrust-chamber normal-force coefficient, $\frac{(F_N)_{PT}}{qA}$

$C_{h,PT}$ booster-pitch-thrust-chamber hinge-moment coefficient, $\frac{(M_Y)_{PT}}{qAD}$

$C_{n,PT}$ booster-pitch-thrust-chamber yawing-moment coefficient, $\frac{(M_Z)_{PT}}{qAD}$

$C_{Y,PT}$ booster-pitch-thrust-chamber side-force coefficient, $\frac{(F_Y)_{PT}}{qA}$

$C_{N,YT}$ booster-yaw-thrust-chamber normal-force coefficient, $\frac{(F_N)_{YT}}{qA}$

$C_{m,YT}$ booster-yaw-thrust-chamber pitching-moment coefficient, $\frac{(M_Y)_{YT}}{qAD}$

$C_{h,YT}$ booster-yaw-thrust-chamber hinge-moment coefficient, $\frac{(M_Z)_{YT}}{qAD}$

$C_{Y,YT}$ booster-yaw-thrust-chamber side-force coefficient, $\frac{(F_Y)_{YT}}{qA}$

$\bar{c}$ mean aerodynamic chord of surface, in.

D base diameter of thrust chambers, in.

F_N force normal to chord plane of surface or axis of component, lb

F_A force along missile X-axis (fuselage reference line), lb

F_Y force perpendicular to normal plane of surface or axis of component, lb

F_L force along Z_W-axis, lb

F_D	force alone X_w-axis, lb
M	free-stream Mach number
M_Y	moment about Y-axis passing through model, surface, or component pitch center, in-lb
M_X	moment about X-axis of model or root chord of surface, in-lb
M_Z	moment about Z-axis passing through model, surface, or component pitch center, in-lb
M_{Yw}	moment about Y_w-axis, in-lb
m/m_c	mass-flow ratio based on free-stream conditions and inlet capture area
q	free-stream dynamic pressure, lb/sq ft
R	Reynolds number based on $\bar{c}_w$
S	surface area, sq ft
α	angle of attack referred to missile-fuselage reference line (parallel to wing chord plane), deg
β	angle of sideslip referred to missile center line, deg
δ_a	angle of aileron relative to missile wing chord plane, deg
δ_e	angle of canard surface relative to missile-fuselage reference line, deg
δ_r	angle of vertical stabilizer relative to missile center line, deg
δ_{SB}	angle of speed brakes relative to missile-fuselage reference line, deg
δ_{PT}	angle of booster pitch thrust chambers relative to axis shown in figure 2(h), deg
δ_{YT}	angle of booster yaw thrust chamber relative to axis shown in figure 2(h), deg

Subscripts:

W	missile wing (total surface)
exp	indicates exposed portion of a surface
A	missile aileron
R	missile vertical stabilizer
B	complete booster
S	booster separating surface
F	booster fin
PT	booster pitch thrust chamber
YT	booster yaw thrust chamber

MODEL AND APPARATUS

The tests were conducted in both the low and high Mach number test sections of the Langley Unitary Plan wind tunnel. This tunnel is of the variable-pressure, return-flow type with test sections measuring 4 feet square and approximately 7 feet long. Mach number may be varied continuously from approximately 1.5 to 2.9 and 2.3 to 4.7 in the low and high Mach number test sections, respectively, by means of asymmetric, sliding-block nozzles.

Details of the model are shown in figure 2 and the geometric characteristics are given in table I. Photographs of the model are presented in figure 3.

The missile configuration (see fig. 2(a)) was comprised of a canard surface mounted on an ogival nose section, a pair of side-mounted nacelles faired to the body and containing the model inlet and duct systems, a midwing affixed to the sides of the nacelles 0.10 inch below the body center line, and a single all-movable vertical stabilizer mounted on top of the rear of the fuselage.

The fuselage was circular in cross section from the Von Kármán nose ogive rearward to the inlets. From the -10° canted inlets aft, the cross section was a blend of the circular body and the side-mounted nacelles as shown in the upper half of figure 2(b). Control surface and wing

airfoils were 3.5 to 4 percent thick and modified biconvex in section. All surfaces were swept 0° at the 50-percent-chord line and were set at zero dihedral angle except the canard which was at an angle of 15°. Canard, vertical stabilizer, and wing plan forms were trapezoidal. The wing panels had triangular-shaped tip ailerons affixed to their outboard ends.

The booster configuration consisted of a conical nose faired to a cylindrical afterbody with two conical segments, separating surfaces located about midway along the afterbody, and rear-located stabilizing fins as illustrated in figures 2(a) and 2(b).

The booster fuselage was circular in cross section along its entire length. Mounted externally along the cylindrical afterbody were several simulated structural longerons. The phase of the tests involving nozzle measurements employed three nozzles affixed to the rear portion of the booster as shown in figure 2(h). Also illustrated in this figure are several modifications to these nozzles, referred to as bug-eye and shroud fairings. The jet simulator shown in this figure was not a part of the basic model but was incorporated in an attempt to determine the effects of flow through the nozzle. (See ref. 1.)

The booster was suspended beneath the missile by a balance that measured booster forces and moments. Located well forward between the missile and booster was an A-frame. (See fig. 3(a).) This A-frame was so mounted that there was no interference involved in the booster balance measurements.

A six-component balance was mounted in the missile to obtain total forces and moments. The forces and moments on the other components were measured by means of individual strain-gage instrumentation as listed in the following table:

Component	Forces and moments measured
Missile wing	Normal force, pitching moment, and bending moment
Aileron	Hinge moment
Vertical stabilizer.	Normal force, yawing moment, and bending moment
Booster	Normal force, axial force, and pitching moment
Separating surface	Normal force and bending moment
Fin	Normal force, bending moment, and pitching moment
Pitch and yaw thrust chambers	Normal force, pitching moment, yawing moment, and side force

[redacted]

The main balance of the missile was attached to the central tunnel support system by means of various stings as illustrated in figure 2(i). A rotary coupling and the central tunnel support system were employed to obtain varying angles of attack simultaneously with varying angles of sideslip.

TESTS

Tests were made of the missile-booster combination and the missile-alone configurations through an angle-of-attack range from about -8° to 4° and -10° to 10°, respectively, at approximately 0° angle of sideslip. At angles of attack of approximately 0° and $\pm5^\circ$, tests were conducted on both configurations for an angle-of-sideslip range from about -8° to 8°. All basic model tests were made with a canard deflection of 0°.

Tests which were made to determine the effect of deflection of the missile canard surface on the various component loads (and the canard-control effectiveness) utilized deflections δ_e of $\pm5^\circ$, and in some cases $\pm10^\circ$. Effects of the missile wing-tip aileron were determined by tests conducted at aileron deflections δ_a of $\pm10^\circ$, 20°, and, for the missile-booster combination, 30°. Missile rudder settings δ_r of 5°, 10°, and 15° were employed to determine the effects of this surface. Determination of the effects of missile speed-brake deflection (δ_{SB}) was accomplished by tests made at deflections of 10°, 30°, and 50°. The effects of booster-thrust-chamber deflection were obtained at settings of -10° and 5° for the pitch nozzle (δ_{PT}) and 8° for the yaw nozzle (δ_{YT}).

Average test conditions of Mach number, stagnation and dynamic pressures, and Reynolds number are as follows:

M	Stagnation pressure, lb/sq in. abs	Dynamic pressure, lb/sq ft	Reynolds number
1.77	9.5	548	2.74×10^6
2.29	11.1	476	2.39
2.75	17.1	518	2.90
3.22	20.4	419	2.69
3.51	25.9	416	2.92

Stagnation temperature was maintained at 150° F for all Mach numbers except 1.77 for which it was 125° F. The Reynolds number is based on the mean aerodynamic chord of the wing.

The use of sting mounting arrangements other than the basic arrangement (sting A) (see fig. 2(i)) was necessary because the tests to determine the effects of missile rudder deflection (stings C and D) utilized a remotely controlled motor which entirely filled the missile cavity normally occupied by the basic sting and also because the portion of the investigation incorporating the booster thrust chamber required the use of sting B to avoid shock interference with the chambers, which would have resulted with the use of the basic sting. Table II is presented to facilitate the identification of which tests were conducted with the various sting arrangements.

Tests were made to determine the effects of various added components such as an A-frame, located between the missile and booster, and the following booster nozzle modifications: bug-eye fairings, shrouds, and a jet simulator.

CORRECTIONS AND ACCURACY

No corrections have been applied to the data to account for stream angularity or buoyancy, inasmuch as the calibration of the test sections had not been completed at the time of the tests. However, final calibration results show that, although no measurable buoyancy exists, a correction should have been applied to the angle in the vertical plane of the test section. The corrections for Mach numbers of 1.77, 2.29, 2.75, 3.22, and 3.51 have been found to be 0.45°, 0.35°, 0.25°, 0.10°, and 0.10°, respectively. Inasmuch as the model wings were alined with the tunnel vertical plane at zero angles of sideslip, only those angles (α and β) presented at $\beta \neq 0$ are in error.

The maximum deviation of local Mach number in the portion of the tunnel occupied by the model was ±0.015 for all but the two highest Mach numbers, where the deviation was ±0.035. The angles of attack and sideslip have been corrected for deflections of the balance and sting under loads. The total axial force, before resolution into drag coefficient, was corrected for base and cavity pressures on both the missile and the booster. The booster axial force has been corrected for the base and cavity pressures of the booster only. In addition, the total pitching moment (with the booster mounted) has been adjusted to represent free-stream static pressure acting on the booster base and cavity. A typical variation of the axial-force coefficient due to the base and cavity pressure for both the missile-booster and the missile-alone configurations are contained in the results.

The estimated probable accuracy of the measured quantities, based on individual strain-gage calibrations and experience with repeatability of the data, is as follows:

Total loads:
- C_N, C_L . . . . . ±0.012
- C_A, C_D . . . . . ±0.0010
- C_m, $C_{m,w}$ . . . . . ±0.002
- C_l . . . . . ±0.0005
- C_n . . . . . ±0.0007
- C_Y . . . . . ±0.005

Missile wing:
- $C_{N,W}$ . . . . . ±0.021
- $C_{m,W}$ . . . . . ±0.0022
- $C_{b,W}$ . . . . . ±0.003

Aileron:
- $C_{h,A}$ . . . . . ±0.0025

Missile rudder:
- $C_{N,R}$ . . . . . ±0.032
- $C_{h,R}$ . . . . . ±0.0025
- $C_{b,R}$ . . . . . ±0.010

Booster:
- $(C_{N,B})_M$ . . . . . ±0.001
- $(C_{A,B})_M$ . . . . . ±0.0008
- $(C_{m,B})_M$ . . . . . ±0.001

Booster separating surface:
- $C_{N,S}$ . . . . . ±0.013
- $C_{b,S}$ . . . . . ±0.007

Booster fin:
- $C_{N,F}$ . . . . . ±0.015
- $C_{m,F}$ . . . . . ±0.0024
- $C_{b,F}$ . . . . . ±0.005

Booster pitch thrust chamber:
- $C_{N,PT}$ . . . . . ±0.015
- $C_{h,PT}$ . . . . . ±0.022
- $C_{Y,PT}$ . . . . . ±0.012
- $C_{n,PT}$ . . . . . ±0.016

Booster yaw thrust chamber:
- $C_{N,YT}$ . . . . . ±0.013
- $C_{m,YT}$ . . . . . ±0.019
- $C_{Y,YT}$ . . . . . ±0.011
- $C_{h,YT}$ . . . . . ±0.017

Angles:
- α, deg . . . . . ±0.2
- β, deg . . . . . ±0.2
- δ_a, deg . . . . . ±0.1
- δ_e, deg . . . . . ±0.1
- δ_r, deg . . . . . ±0.1

PRESENTATION OF RESULTS

The data obtained on the six-component missile balance are presented about the body axis except for the pitch tests where the wind axis is employed. Moment coefficients from this balance were taken about a point on the fuselage reference line at 6 percent chord of the missile wing mean aerodynamic chord (0.1 inch above the chord plane and at missile longitudinal station 33.00).

All other model component results are presented about axes fixed to the model. Moment coefficients for the lifting surfaces were taken about the root chord points illustrated in figure 2 (designated as reference center). Positive bending moments are defined as the results of positive normal forces. Loads obtained by the balance supporting the booster

beneath the missile were measured with respect to the booster axes and pitch center (booster station 40.22). These forces and moments were then transferred to the missile pitch center for the presentation.

To facilitate location of the data for any particular configuration, an abbreviated outline of figure content follows (see also table II):

	Figure
Typical schlieren photographs	4
Typical base and cavity axial-force and internal drag coefficients	5
Missile-Booster Combination	
Total loads:	
Pitch characteristics (wind axis) -	
Effect of A-frame	6
Effect of canard deflection	7
Effect of booster nozzle	8
Effect of bug-eye fairing	9
Effect of nozzle shrouds	10
Effect of jet simulator	11
Effect of missile aileron actuator housing	12
Lateral characteristics -	
Effect of A-frame	13
Effect of rudder deflection	14
Effect of booster nozzle	15
Effect of aileron deflection	16
Wing loads:	
Pitch characteristics -	
Effect of A-frame	17
Effect of canard deflection	18
Effect of aileron deflection	19
Lateral characteristic -	
Effect of A-frame	20
Aileron hinge moment:	
Effect of aileron deflection	21
Rudder loads:	
Lateral characteristics -	
Effect of canard deflection	22
Effect of rudder deflection	23

Figure

Booster loads:
Pitch characteristics -
Effect of A-frame 24
Effect of canard deflection 25
Effect of booster nozzle 26
Effect of bug-eye fairing 27
Effect of nozzle shrouds 28
Effect of jet simulator 29
Effect of aileron deflection 30

Booster-separating-surface loads:
Pitch characteristics -
Effect of A-frame 31
Effect of canard deflection 32
Effect of aileron deflection 33
Lateral characteristics -
Effect of A-frame 34

Booster-fin loads:
Pitch characteristics -
Effect of canard deflection 35
Effect of aileron deflection 36
Lateral characteristics 37

Booster-thrust-chamber loads:
Pitch characteristics -
Effect of nozzle deflection 38
Effect of bug-eye fairing 39
Effect of nozzle shrouds 40
Lateral characteristics -
Effect of nozzle deflection 41

Missile alone

Total loads:
Pitch characteristics (wind axis) -
Effect of canard surface 42
Effect of canard deflection 43
Effect of speed-brake deflection 44
Lateral characteristics -
Effect of canard and rudder surfaces 45
Effect of canard deflection 46
Effect of rudder deflection 47
Effect of aileron deflection 48

Figure

Wing loads:
Pitch characteristics -
Effect of canard surface 49
Effect of canard deflection 50
Effect of aileron deflection 51
Lateral characteristics -
Effect of canard and rudder surfaces 52
Effect of canard deflection 53

Aileron hinge moment:
Effect of aileron deflection 54

Rudder loads:
Lateral characteristics -
Effect of canard deflection 55
Effect of rudder deflection 56

Langley Research Center,
National Aeronautics and Space Administration,
Langley Field, Va., March 3, 1959.

REFERENCE

1. Church, James D., and Taylor, Nancy L.: An Investigation of a 0.05-Scale Model of the XSM-64A Navaho Missile and Booster. Part II - Pressure Study at Mach Numbers From 2.29 to 3.22. NASA MEMO 5-31-59L, 1959.

TABLE I

PHYSICAL PROPERTIES OF THE 0.05-SCALE MODEL OF THE XSM-64A

[Areas and lengths of all surfaces except the missile wing are based on the exposed portions of the surfaces. Since the model total force and moment coefficients are based on total wing area, the exposed area is listed for reference purposes only for the case of the wing. The aileron area and span are listed for a single tip aileron.]

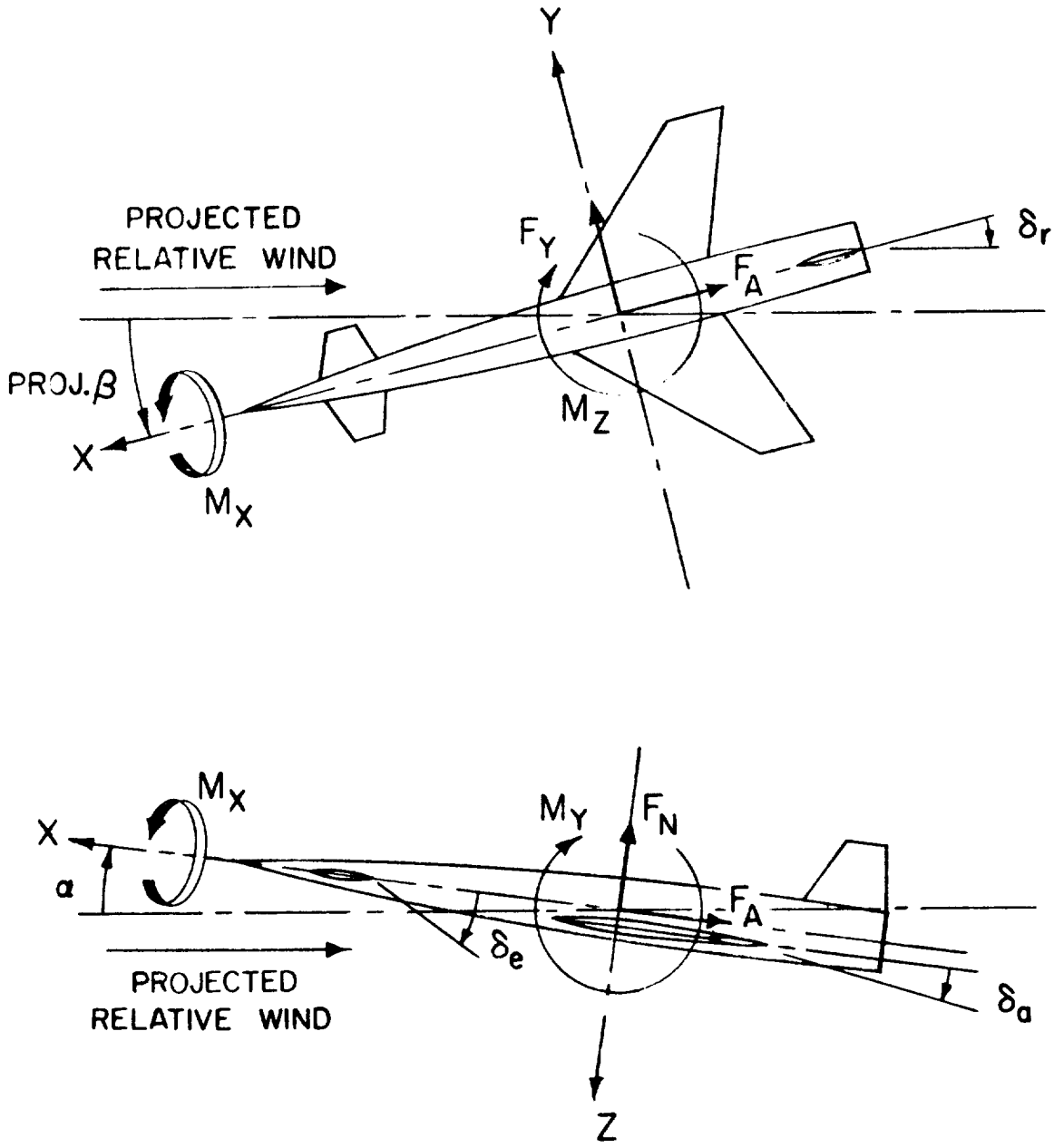
	Missile					Booster	
	Wing		Aileron	Canard surface	Vertical stabilizer	Fin	Separating surface
	Total	Exposed					
Area, sq ft	1.903	1.056	0.0394	0.130	0.100	0.354	0.0600
Span, ft	2.138	1.562	0.195	0.504	0.396	1.000	0.267
Mean aerodynamic chord, ft	1.137	0.589	0.269	0.285	0.263	0.374	0.237
Aspect ratio	2.40	2.31	0.965	1.95	1.56	2.82	1.185
Sweep of 50%-chord line	0		0	0	0	0	0
Taper ratio	0		0	0.285	0.500	0.416	0.422
Airfoil section perpendicular to 50%-chord line	4%-thick modified biconvex		4%-thick modified biconvex	3.5%-thick modified biconvex	3.5%-thick modified biconvex	5%-thick modified hexagonal	5%-thick modified hexagonal
Dihedral angle, deg	0		0	15		-35	0
Incidence angle, deg	0		Variable	Variable	Variable	-3	-10

	Fuselage			
	Fineness ratio	Cone angle, deg	Base area, sq ft	Cavity area, sq ft
Missile	7.60	22	0.0575	0.0284
Booster	10.87	28	0.0812	0.0376

TABLE II

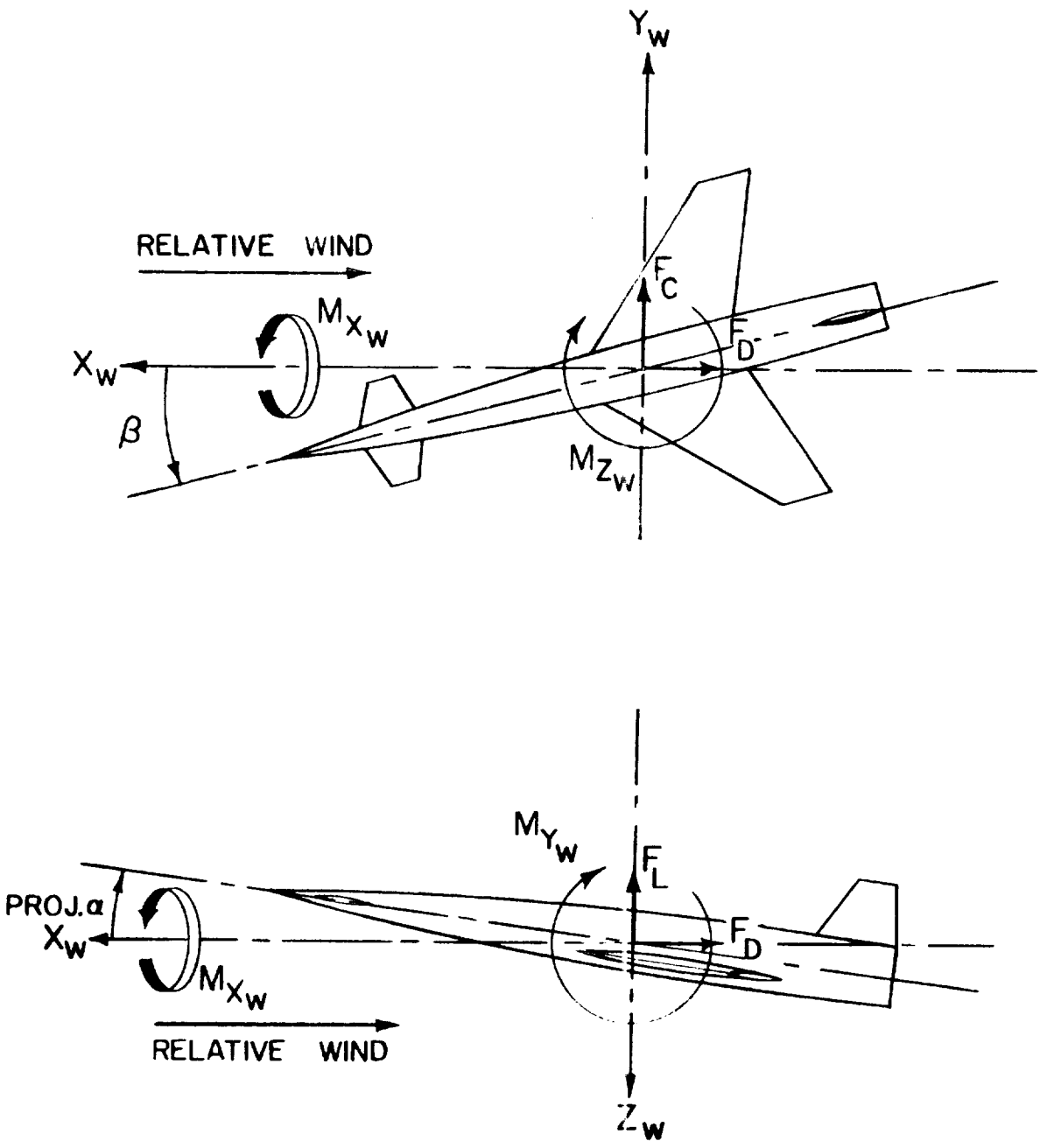
INDEX TO STING ARRANGEMENTS

Sting	M	Figure
Missile-booster configuration		
A	2.29, 2.75, 3.51	5-7, 13, 14, 17, 18, 20, 24, 25, 31, 32, 34, 35, 37
	3.22	Same as above; also 16(a), 19(a), 21(a), 30(a), 33, 36
B	2.75, 3.22	8-12, 15, 16(b,c), 19(b,c), 21(b,c), 26-29, 30(b,c), 38-41
C	2.75, 3.22	22, 23
Missile-alone configuration		
A	1.77	5, 42-54
	2.75, 3.22	5, 43, 44, 46-48, 50, 51, 53, 54
D	1.77, 2.75, 3.22	55, 56



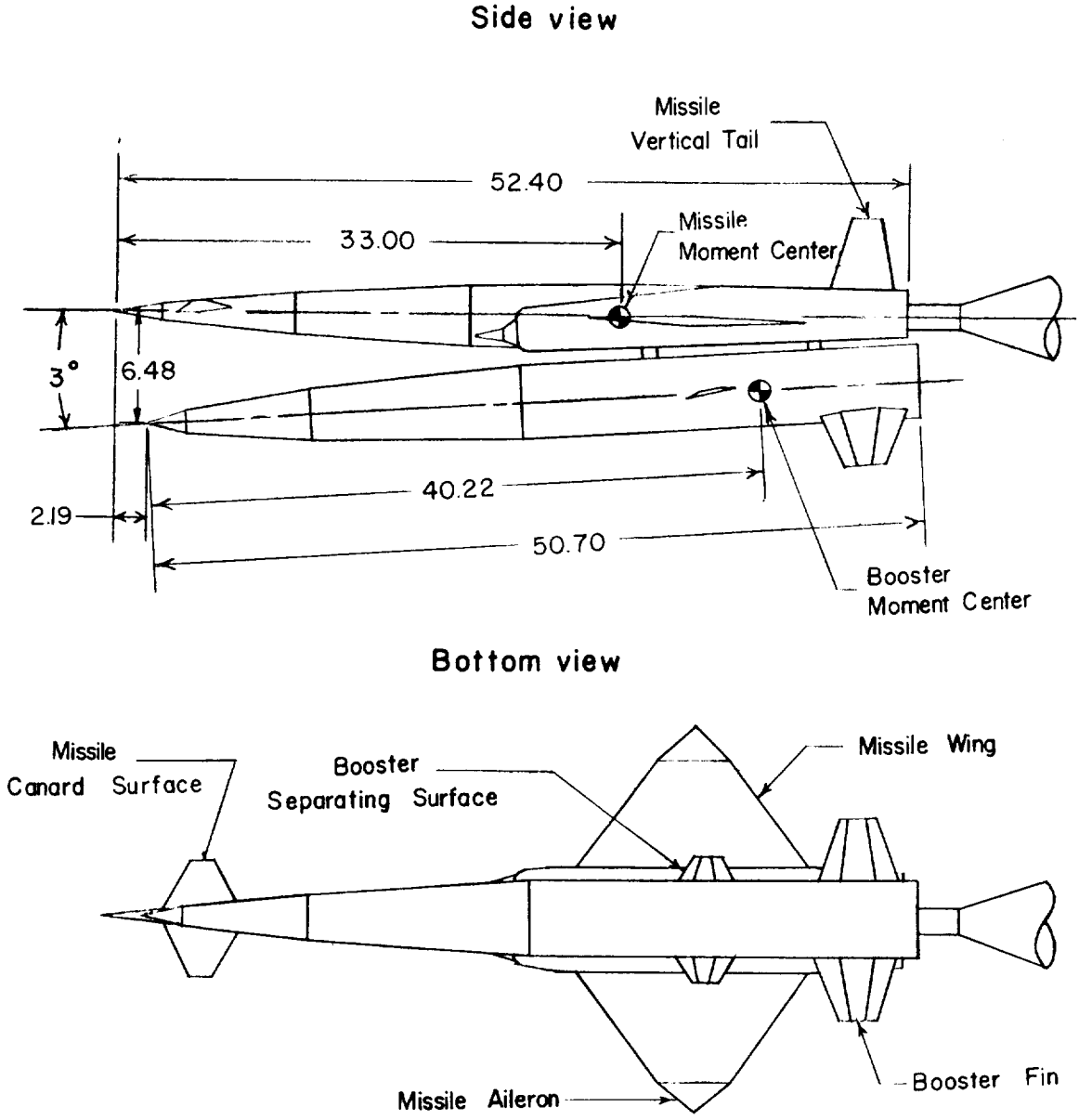
(a) Body axis.

Figure 1.- System of axes. Arrows indicate directions of positive forces, moments, and angles.



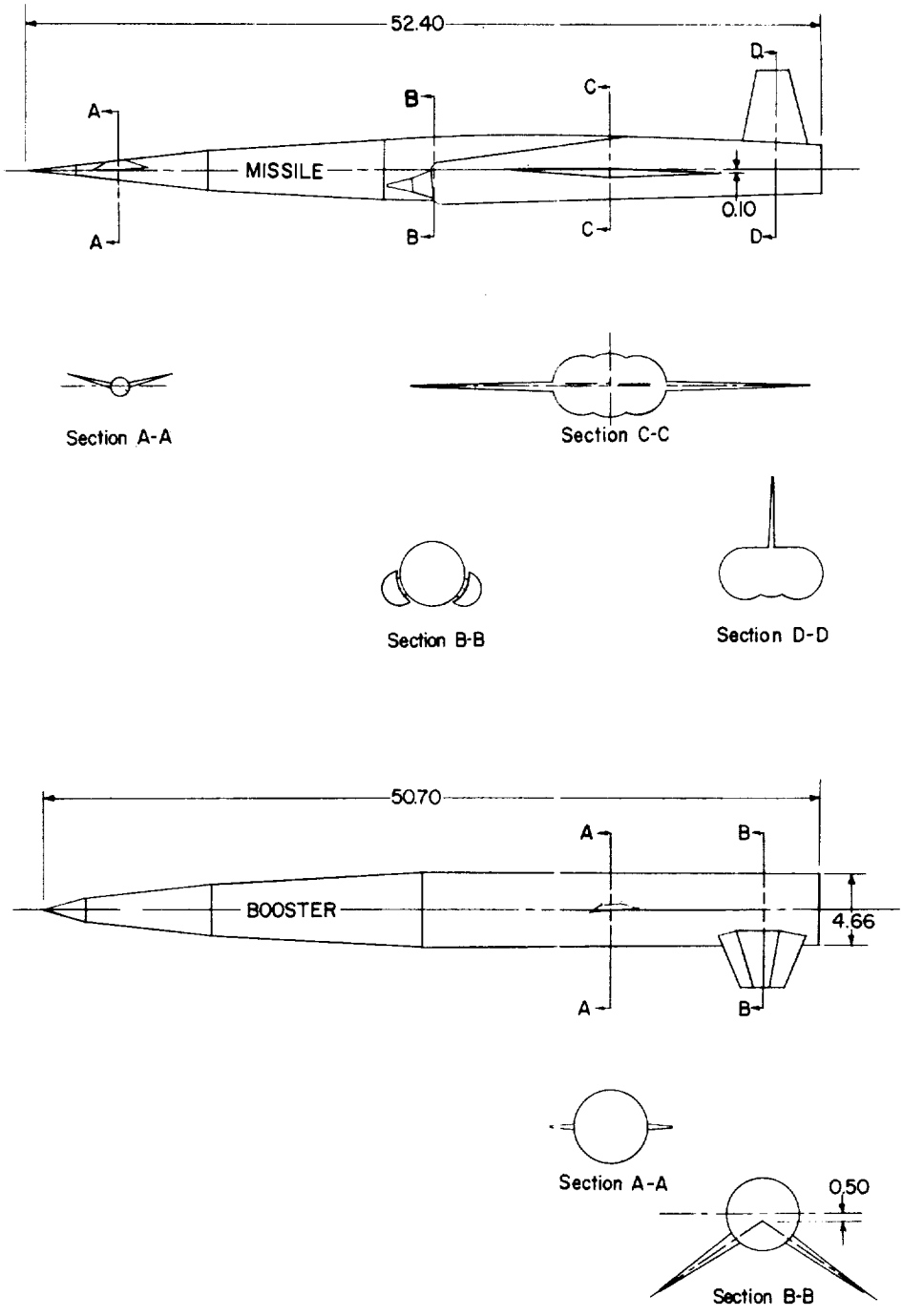
(b) Wind axis.

Figure 1.- Concluded.



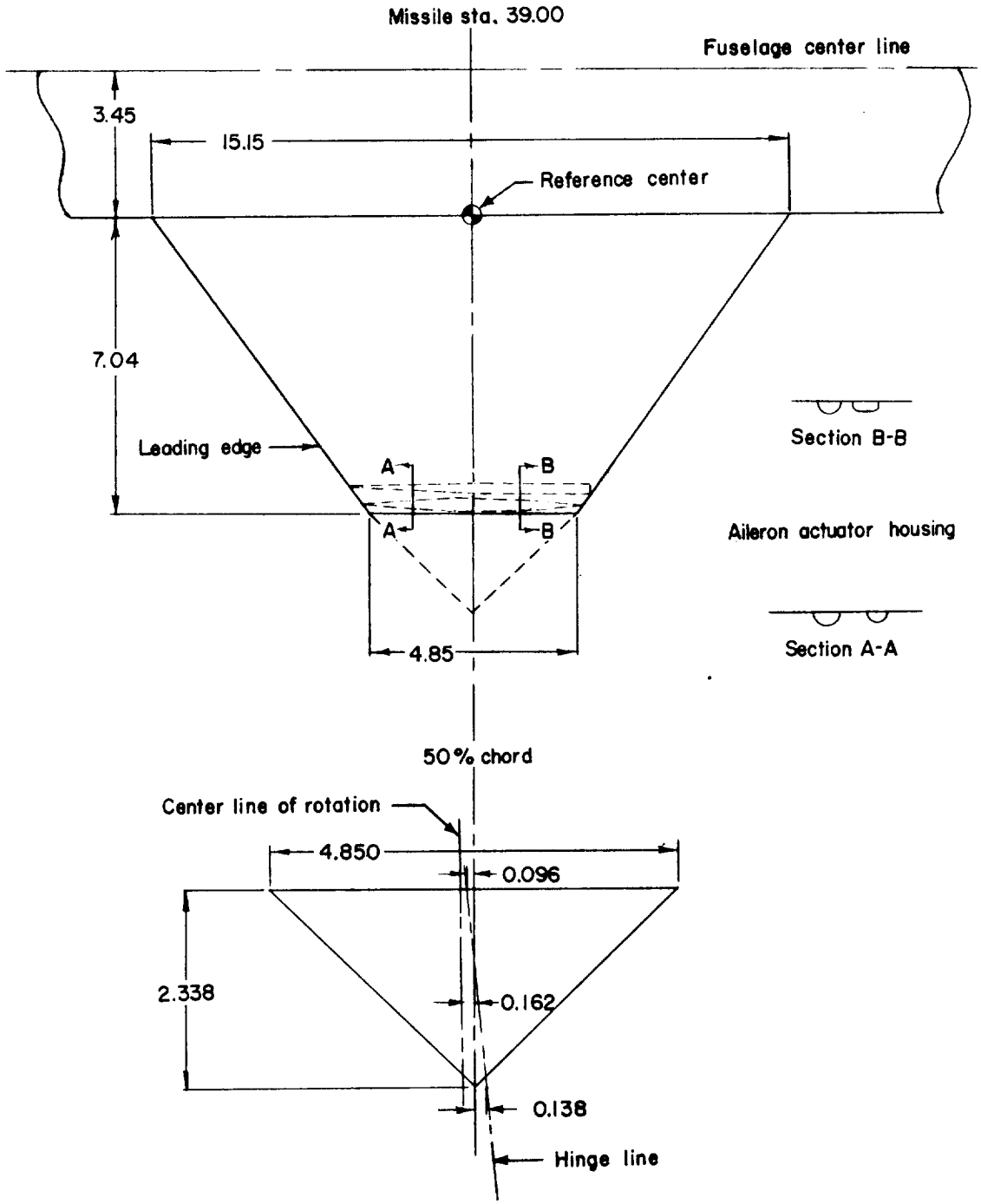
(a) General views.

Figure 2.- Sketches of 0.05-scale model of SXM-64A Navaho missile. All dimensions in inches.



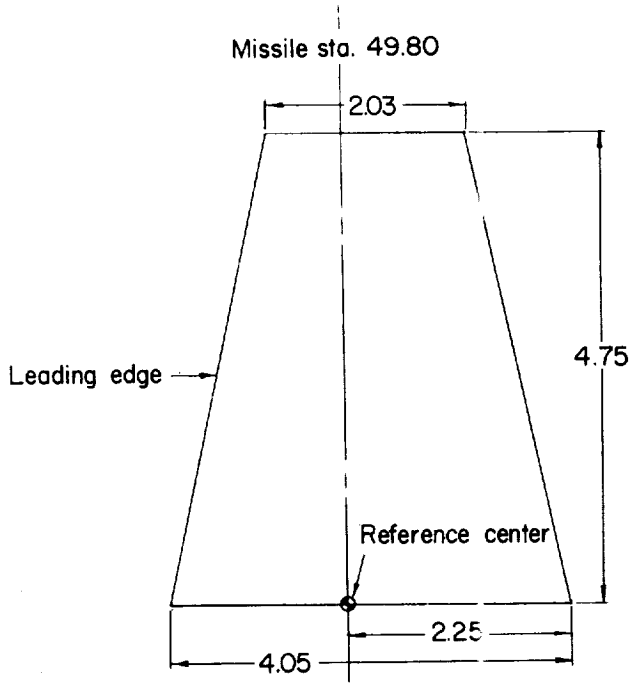
(b) Body details.

Figure 2.- Continued.

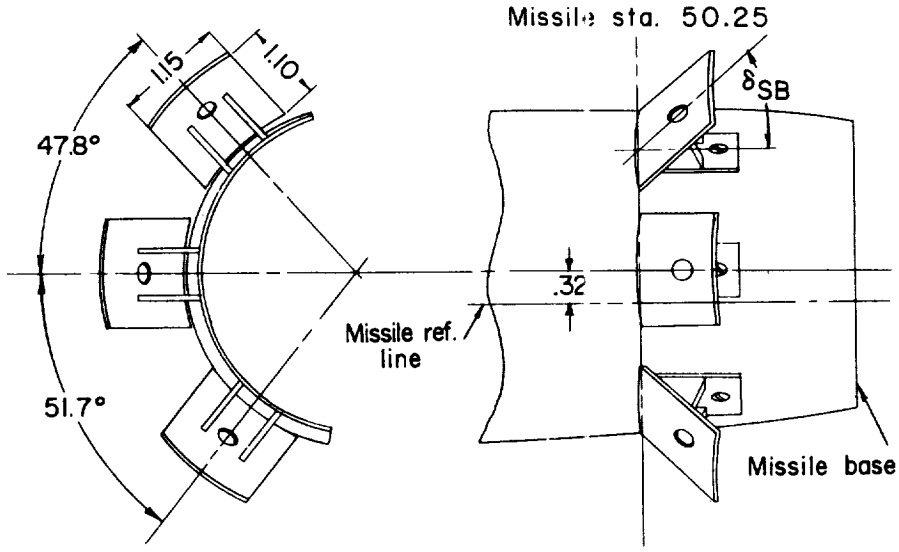


(c) Missile wing and aileron.

Figure 2.- Continued.

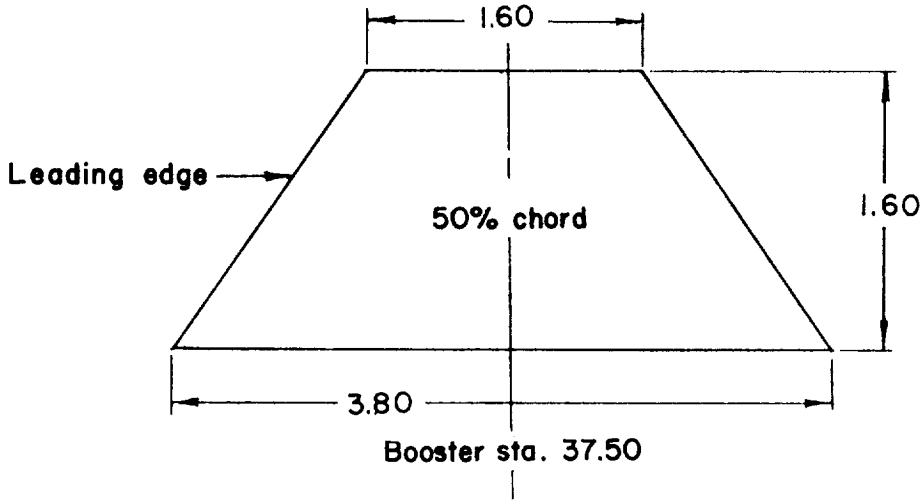


(d) Missile rudder.

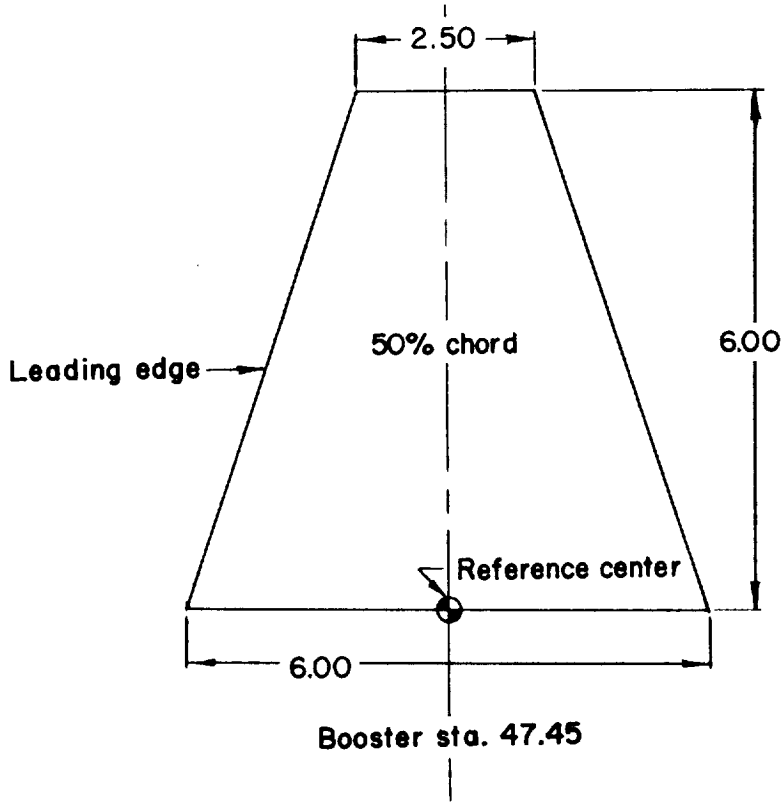


(e) Speed brakes.

Figure 2.- Continued.

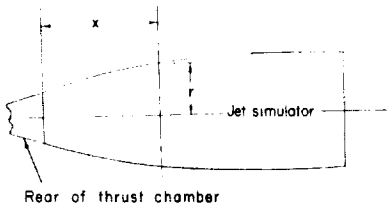


(f) Booster separating surface.

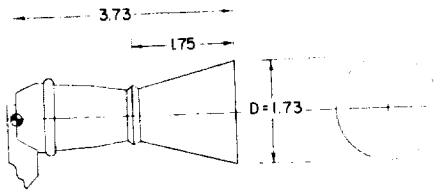


(g) Booster fin.

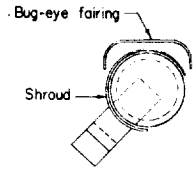
Figure 2.- Continued.



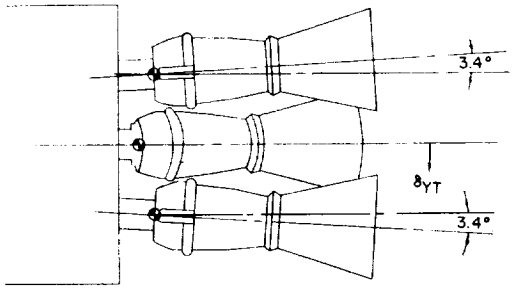
x	r	x	r
0	0.965	5.046	1.860
0.721	1.095	5.766	1.900
1.441	1.298	6.488	1.931
2.163	1.460	7.208	1.954
2.883	1.600	7.929	1.960
3.604	1.708	8.650	1.960
4.325	1.794	9.371	1.954
		10.091	1.946



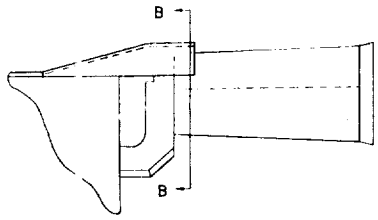
Thrust chamber



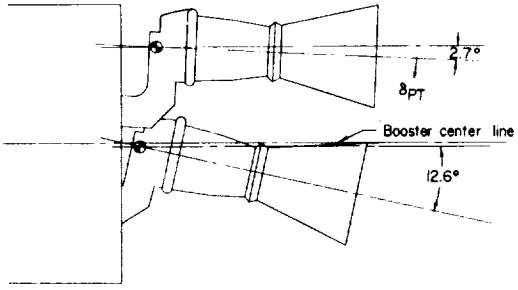
Section B-B



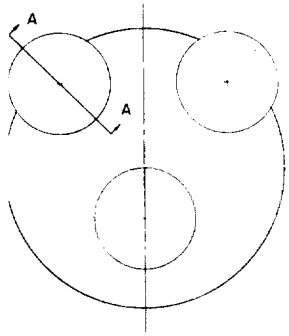
Top view



Chamber modifications
Viewed at section A-A



Side view

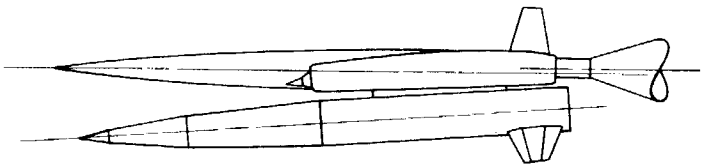


End view

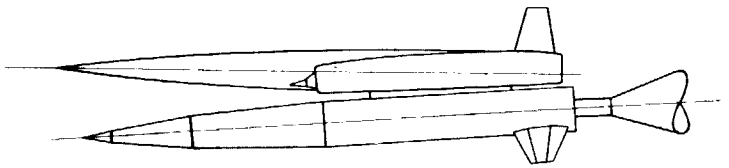
(h) Booster thrust chambers.

Figure 2.- Continued.

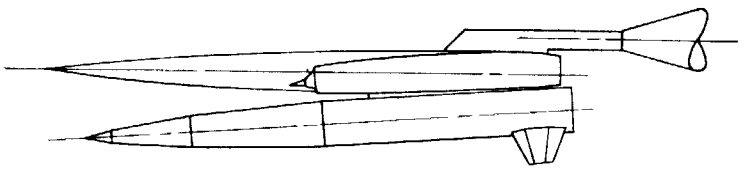
L-340



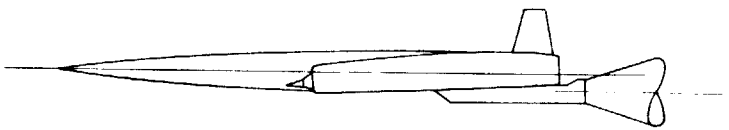
Sting A; missile-booster combination and missile alone.



Sting C; missile-booster combination only.



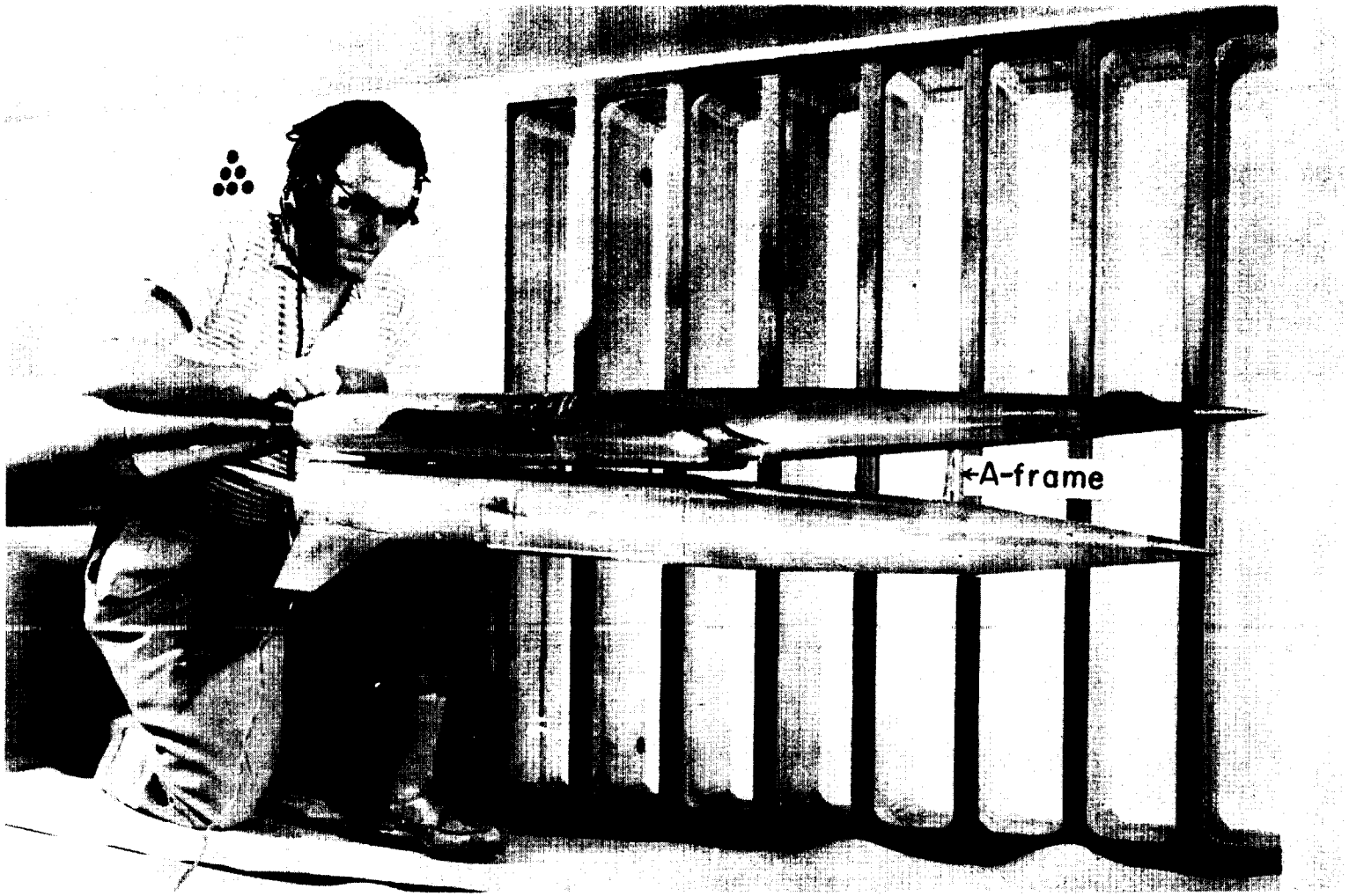
Sting B; missile-booster combination and missile alone.



Sting D; missile alone only.

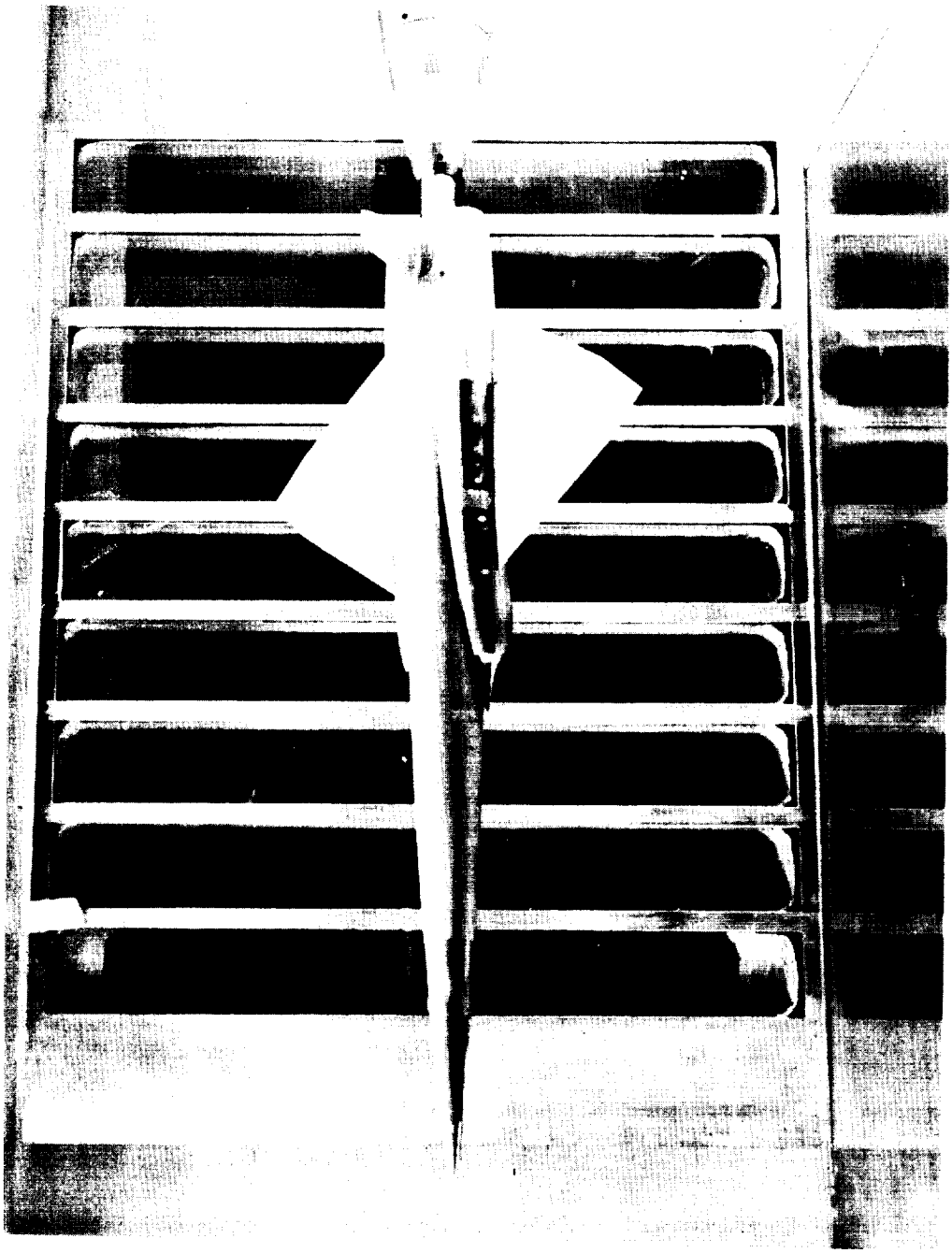
(i) Sting mounting arrangements.

Figure 2.- Concluded.



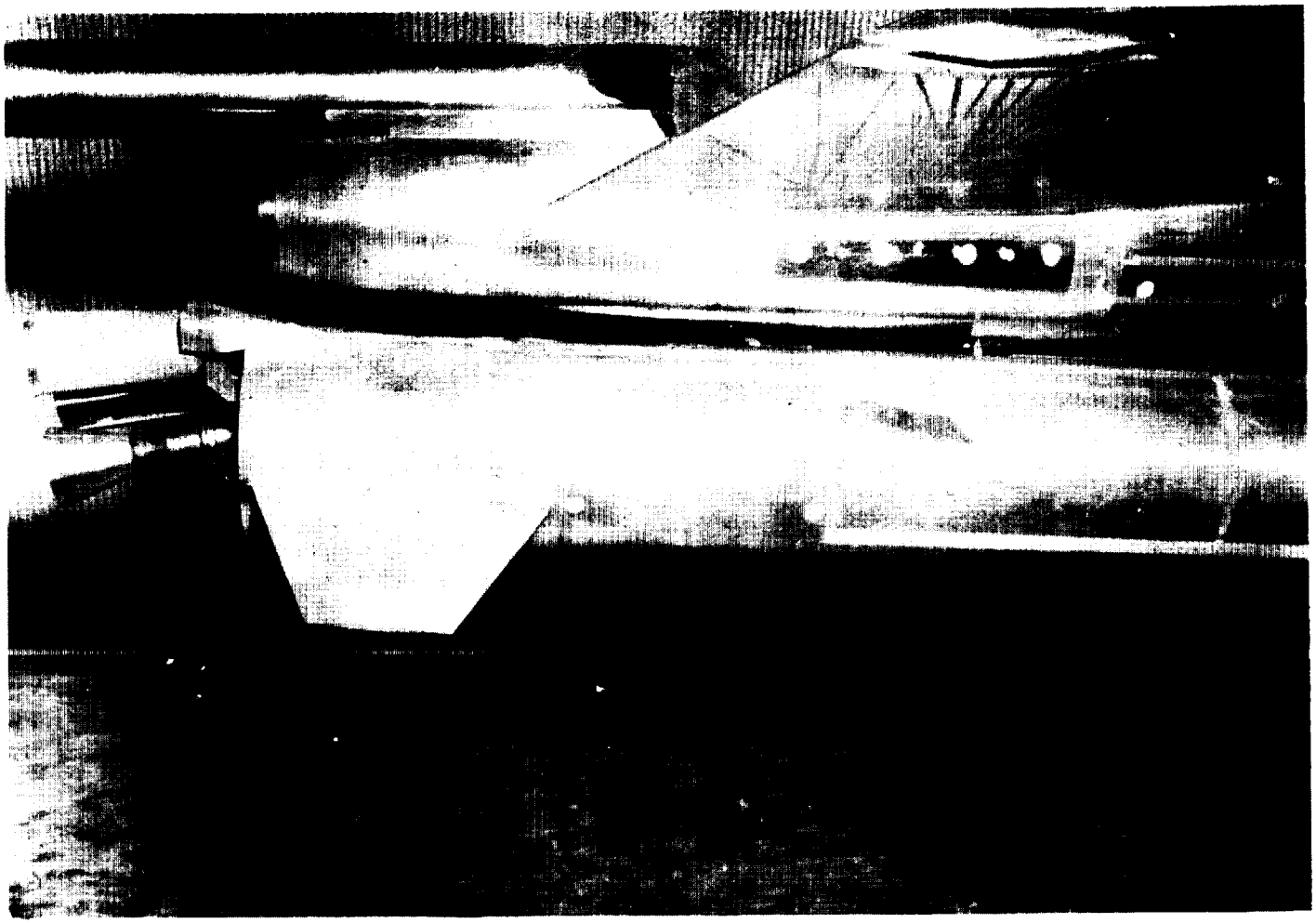
(a) Missile-booster combination; sting A. L-95496.1

Figure 3.- Photographs of model.



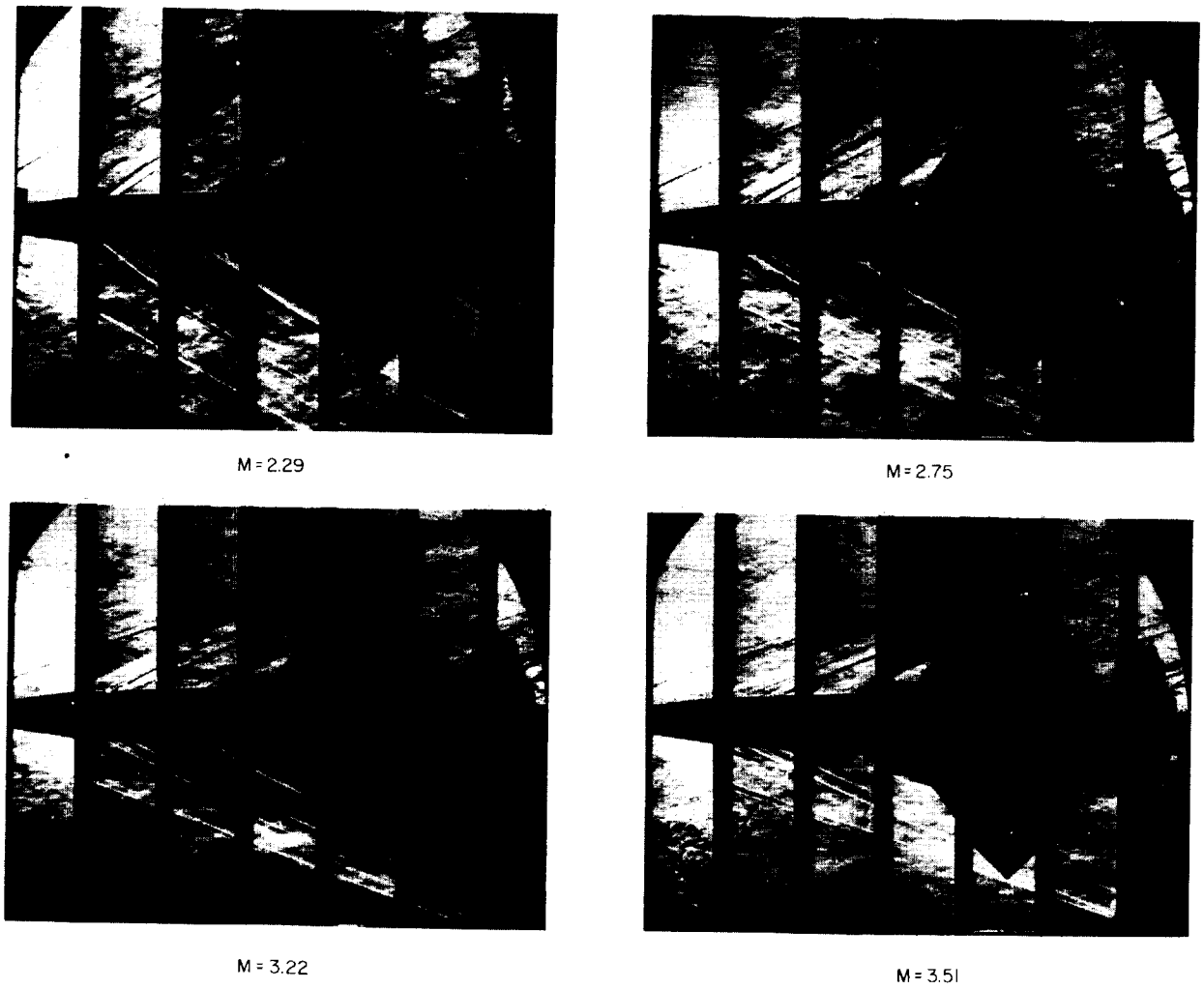
(b) Missile alone; sting A. L-92672

Figure 3.- Continued.



(c) Booster thrust chambers; sting B. L-95595

Figure 3.- Concluded.



(a) Missile-booster combination; $\alpha = 0^{\circ}$; sting A. L-59-1866

Figure 4.- Typical schlieren photographs.



M = 1.77



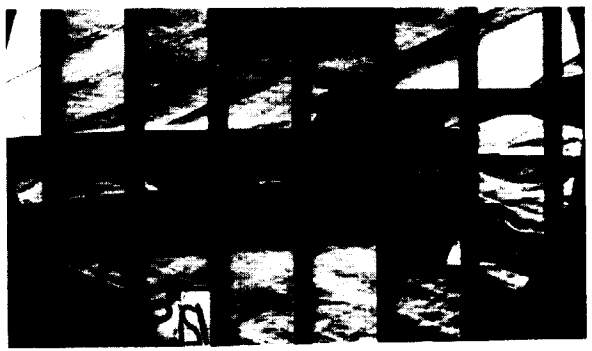
M = 2.75



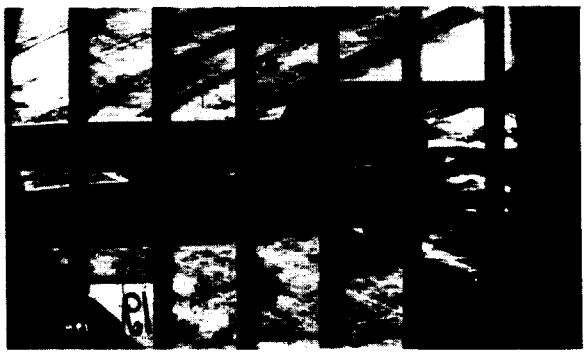
M = 3.22

(b) Missile alone; $\alpha = 0^{\circ}$; sting A. L-59-1867

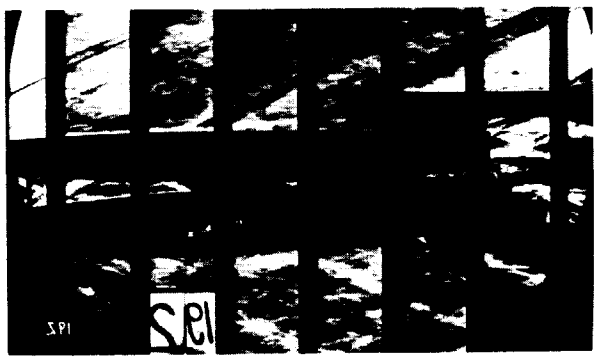
Figure 4.- Continued.



Thrust chambers off



Thrust chambers on

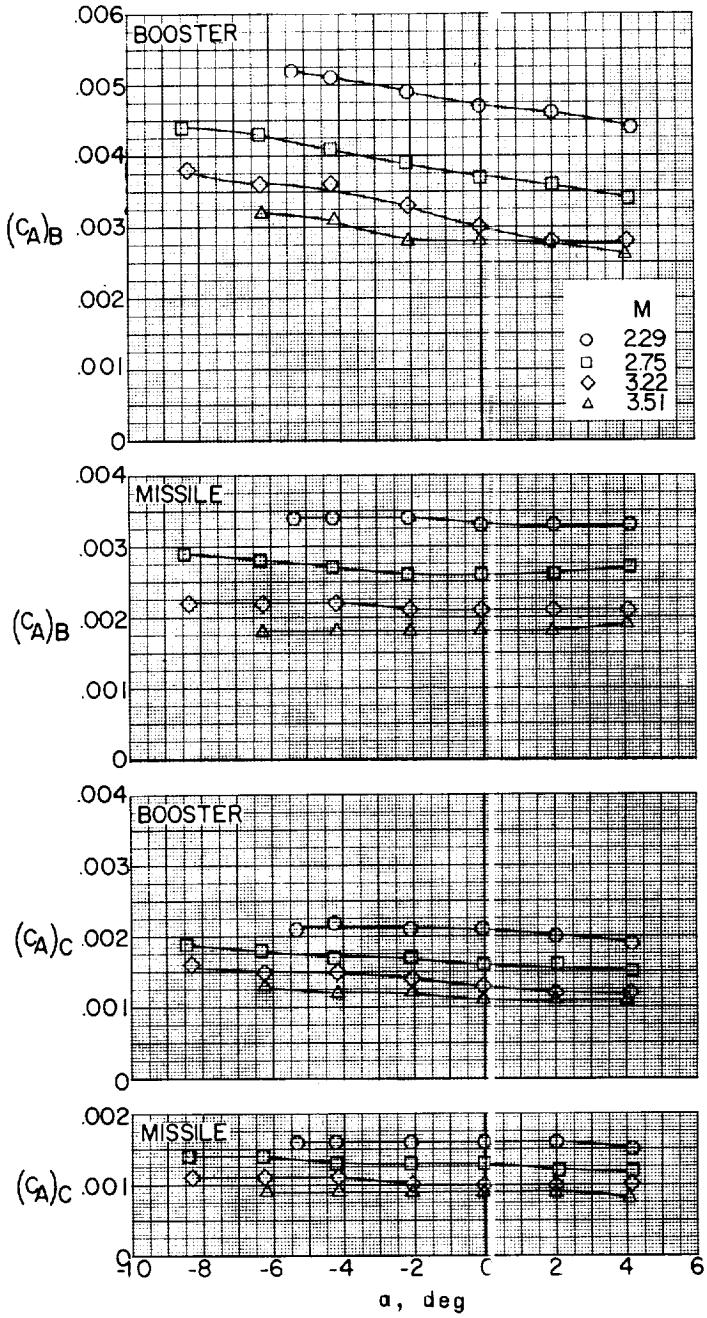


Thrust chambers with jet simulator

L-59-1868

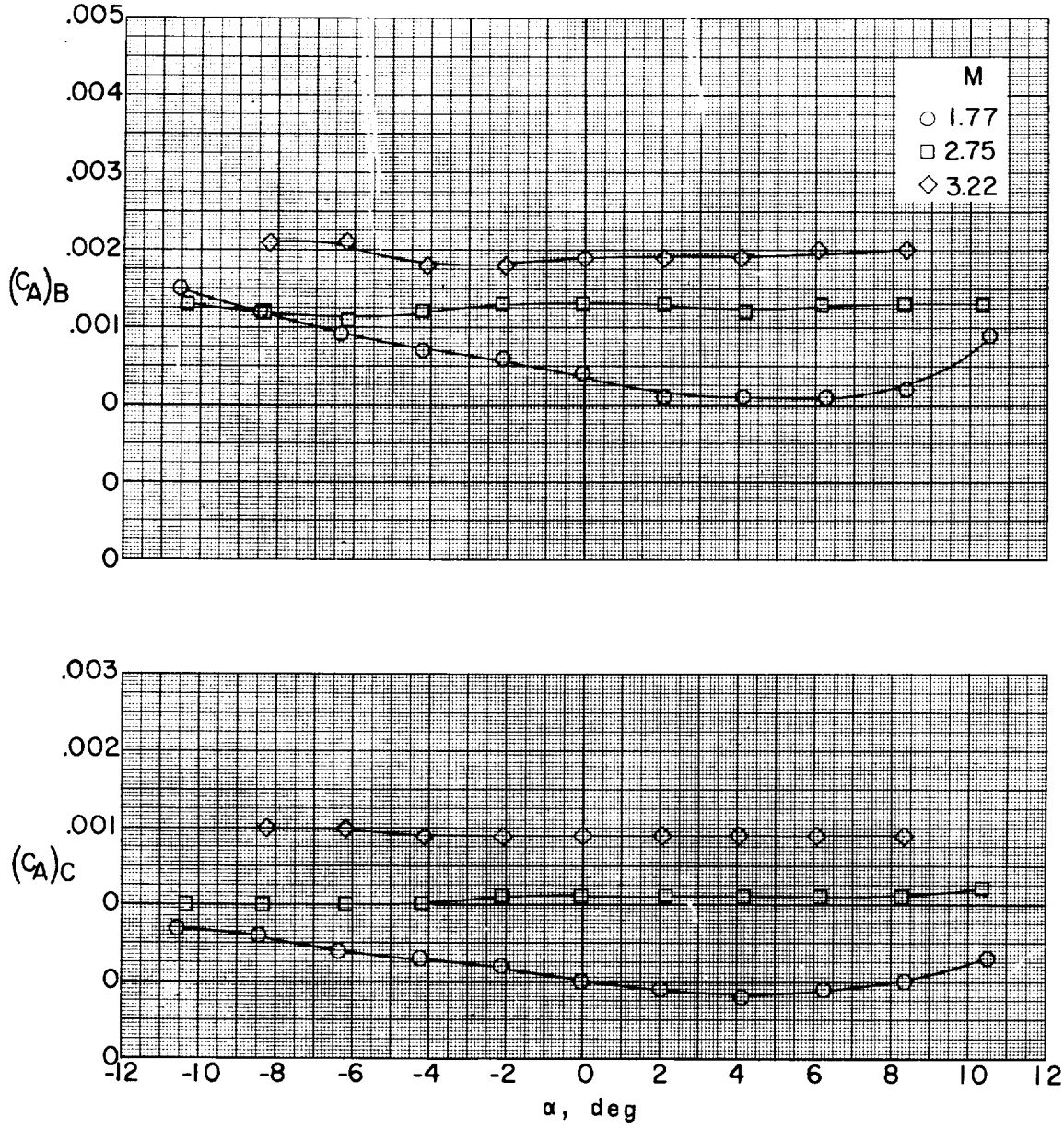
(c) Missile-booster combination; M = 2.75; $\alpha = 0^{\circ}$; sting B.

Figure 4.- Concluded.



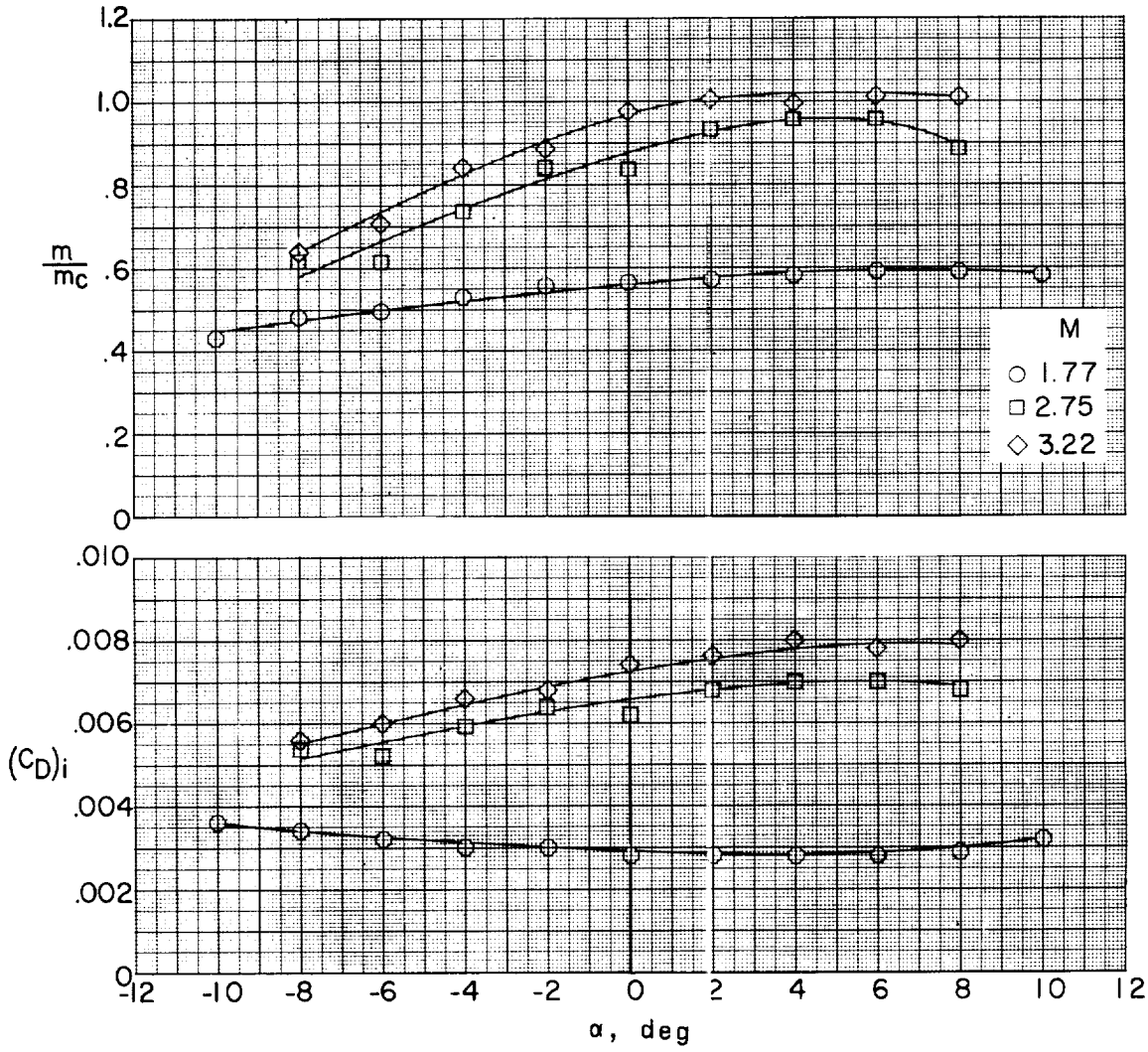
(a) Missile-booster combination.

Figure 5.- Typical variations of axial-force coefficient due to base and cavity pressures and internal drag coefficient with angle of attack.



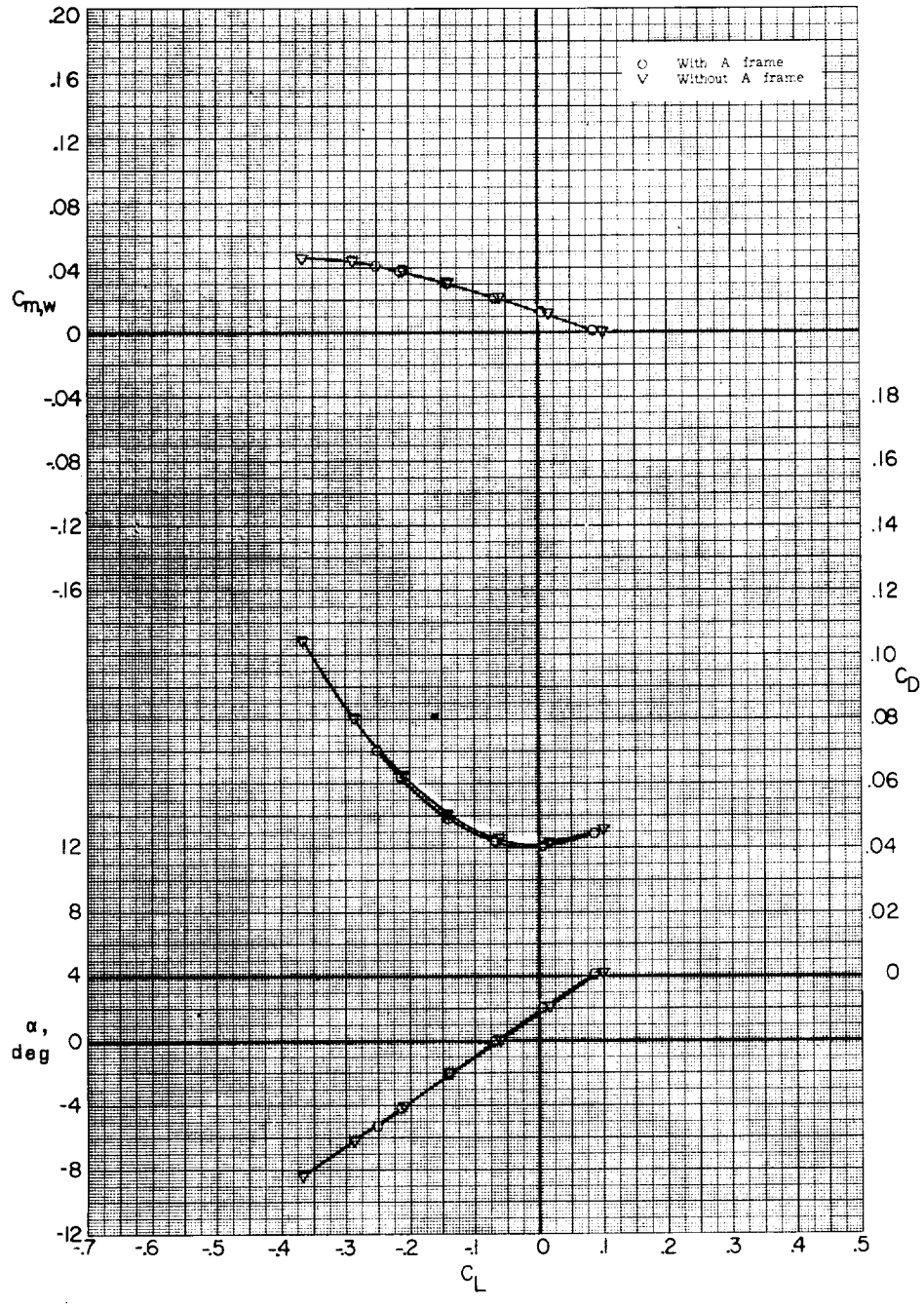
(b) Missile alone.

Figure 5.- Continued.



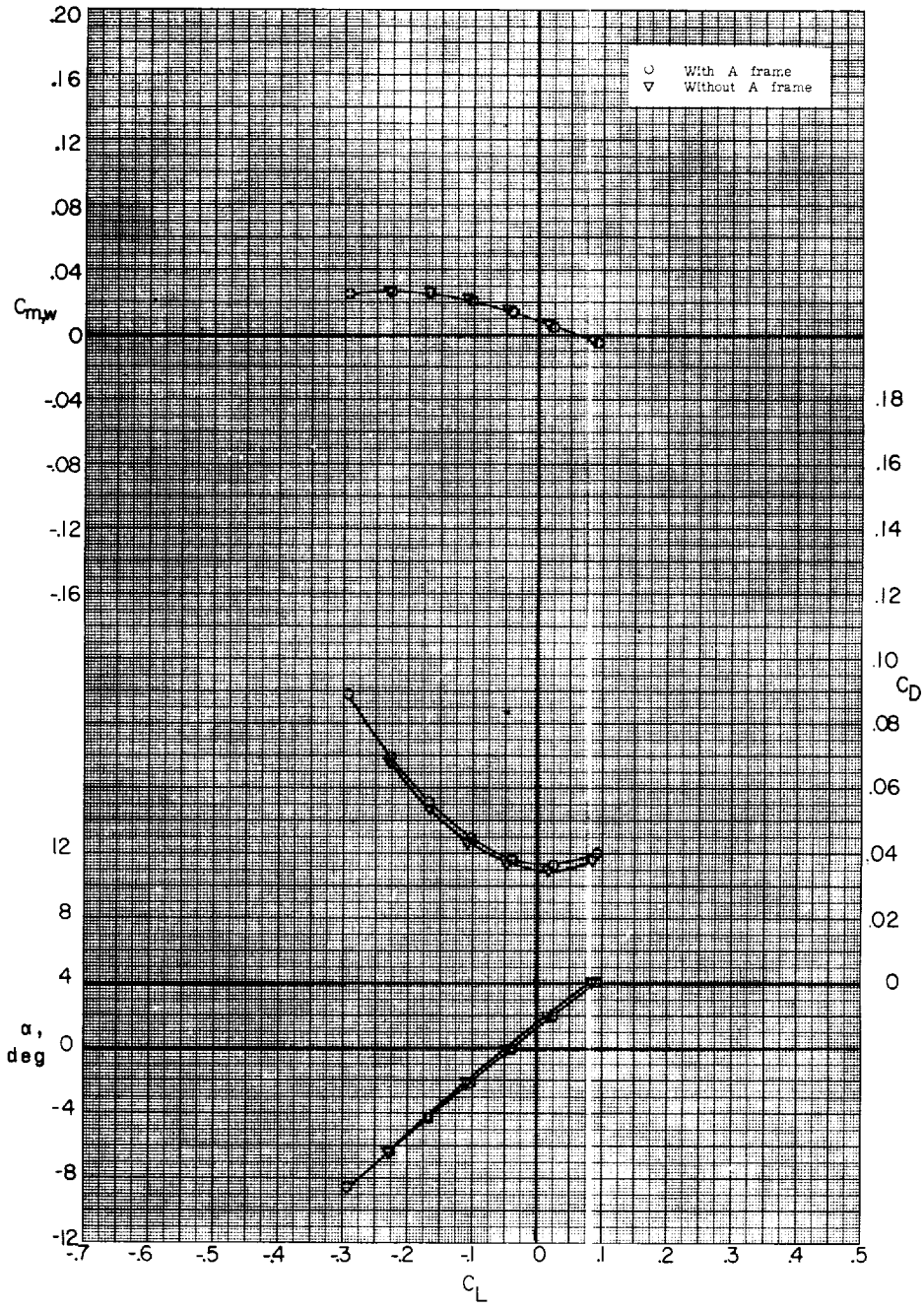
(c) Internal drag coefficient (two ducts) and mass-flow ratio.

Figure 5.- Concluded.



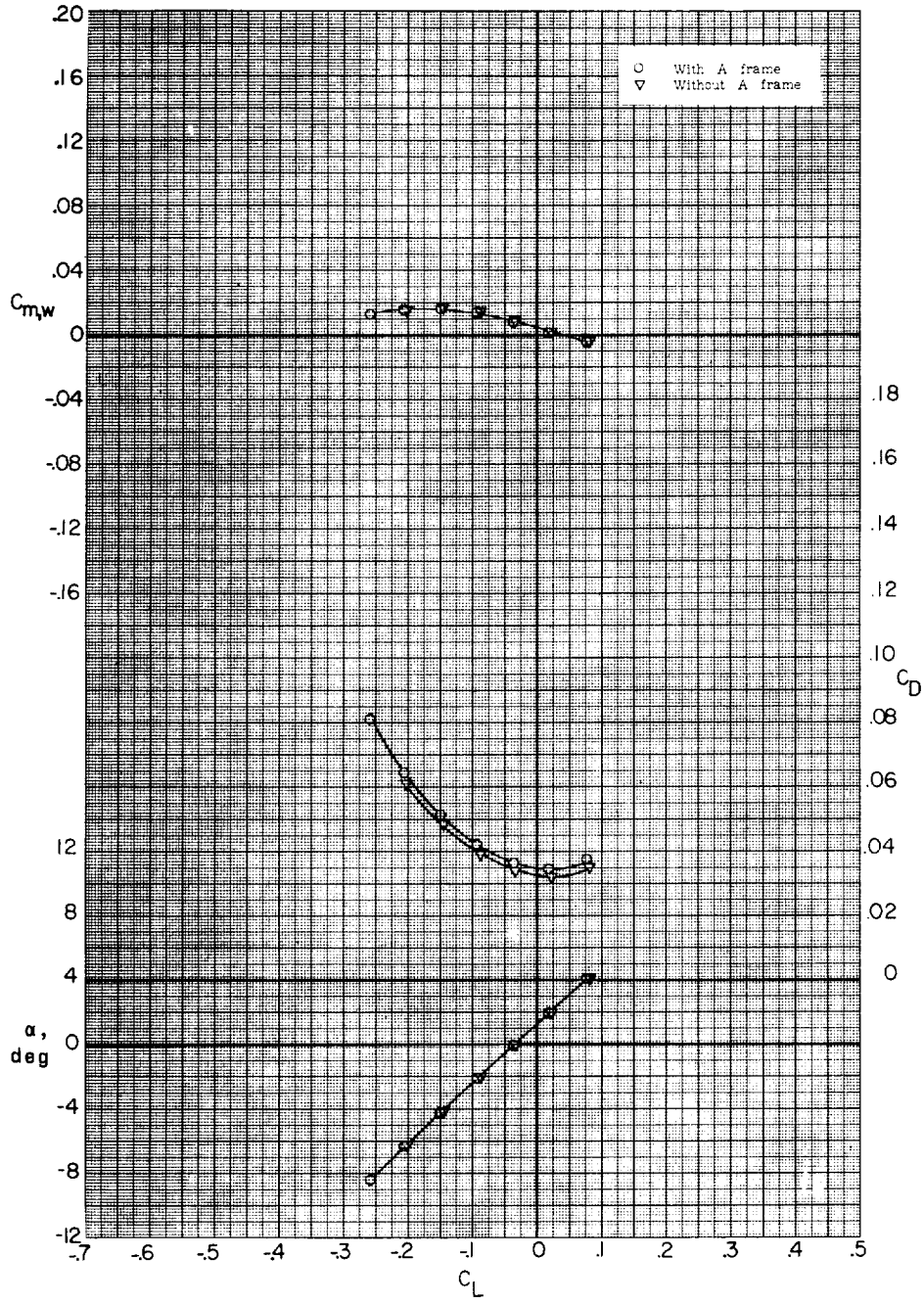
(a) M = 2.29.

Figure 6.- Effect of A-frame on pitch characteristics of missile-booster combination. $\delta_e = 0^\circ$; $\beta = 0.3^\circ$; sting A.



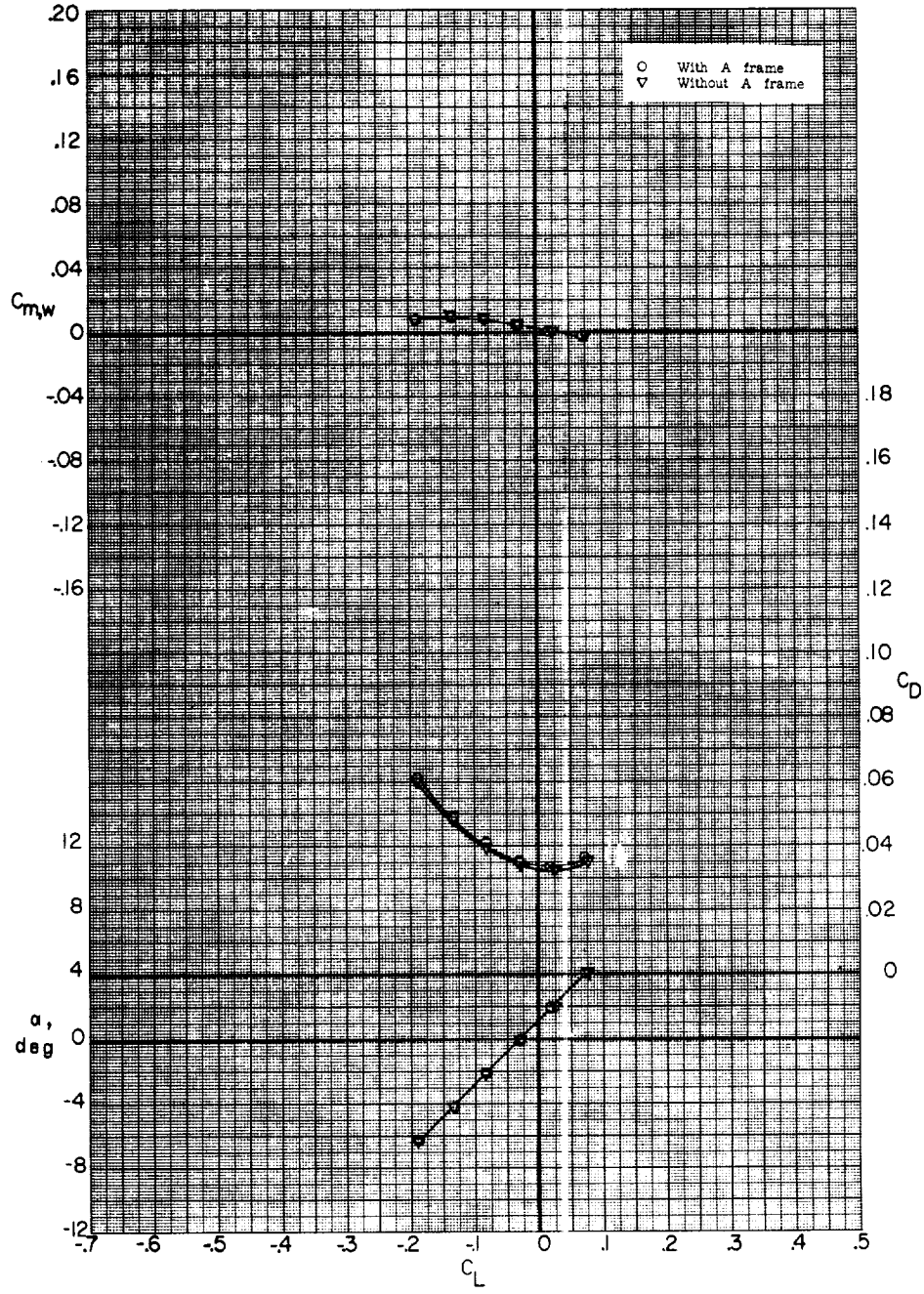
(b) M = 2.75.

Figure 6.- Continued.



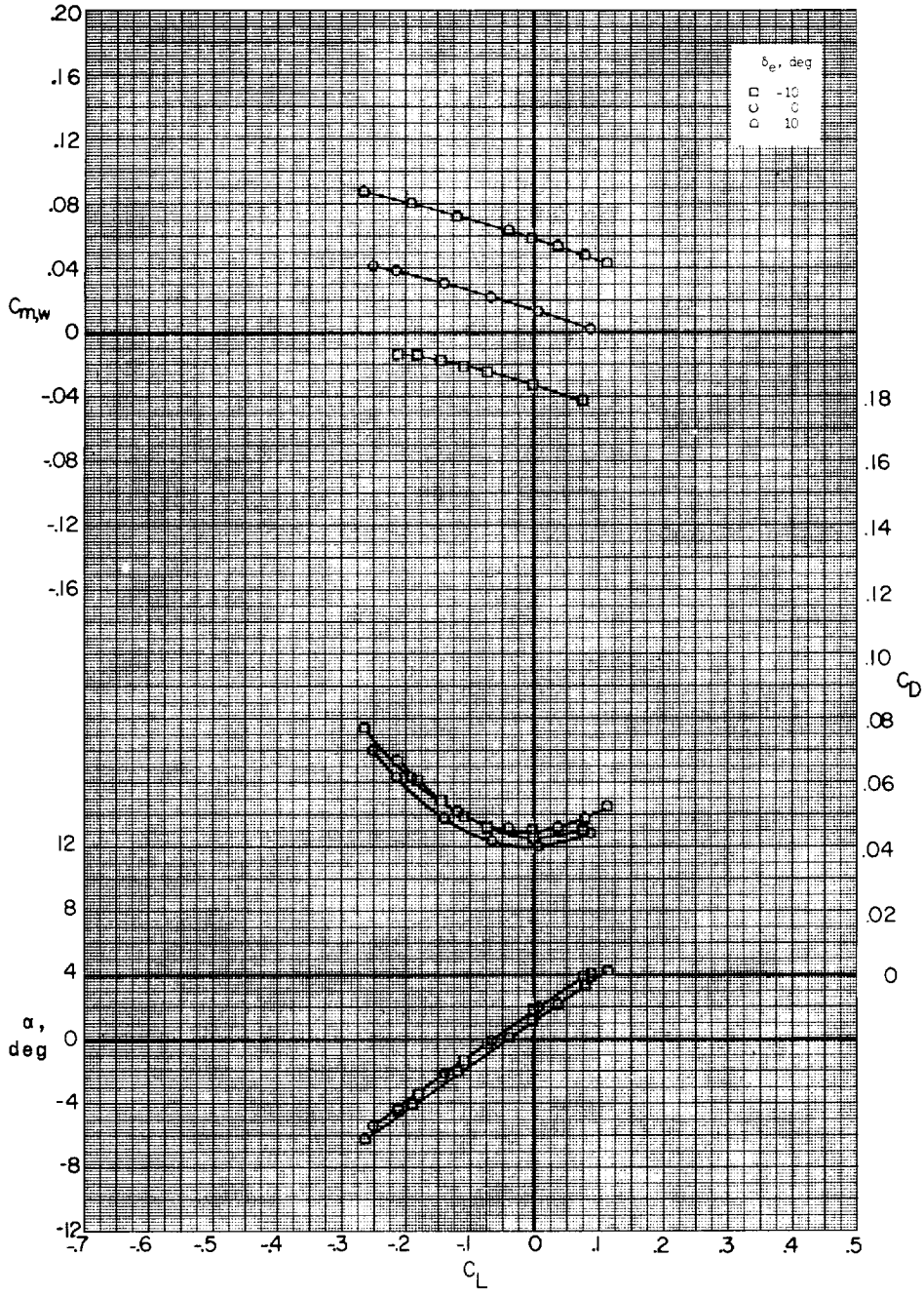
(c) M = 3.22.

Figure 6.- Continued.



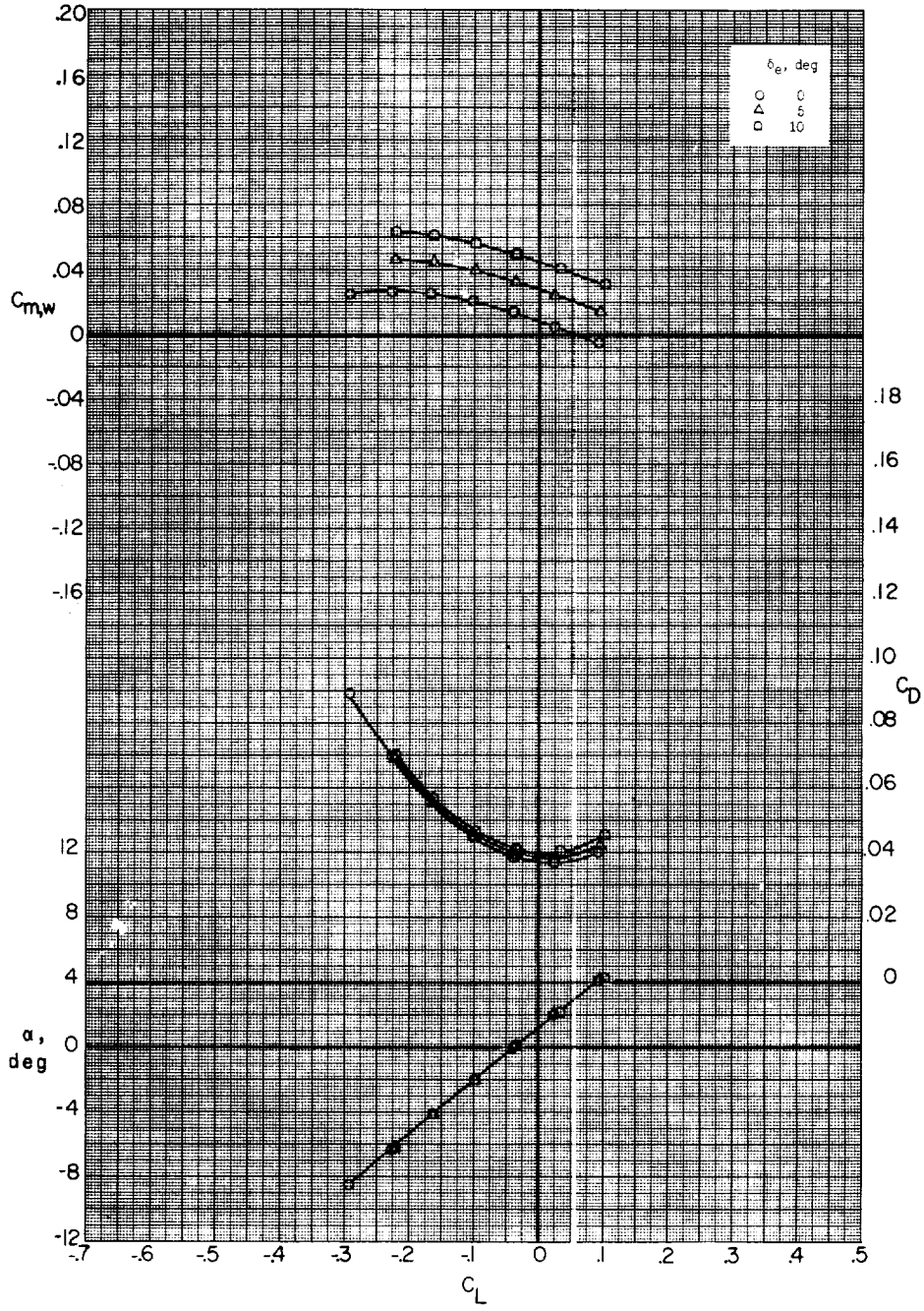
(d) M = 3.51.

Figure 6.- Concluded.



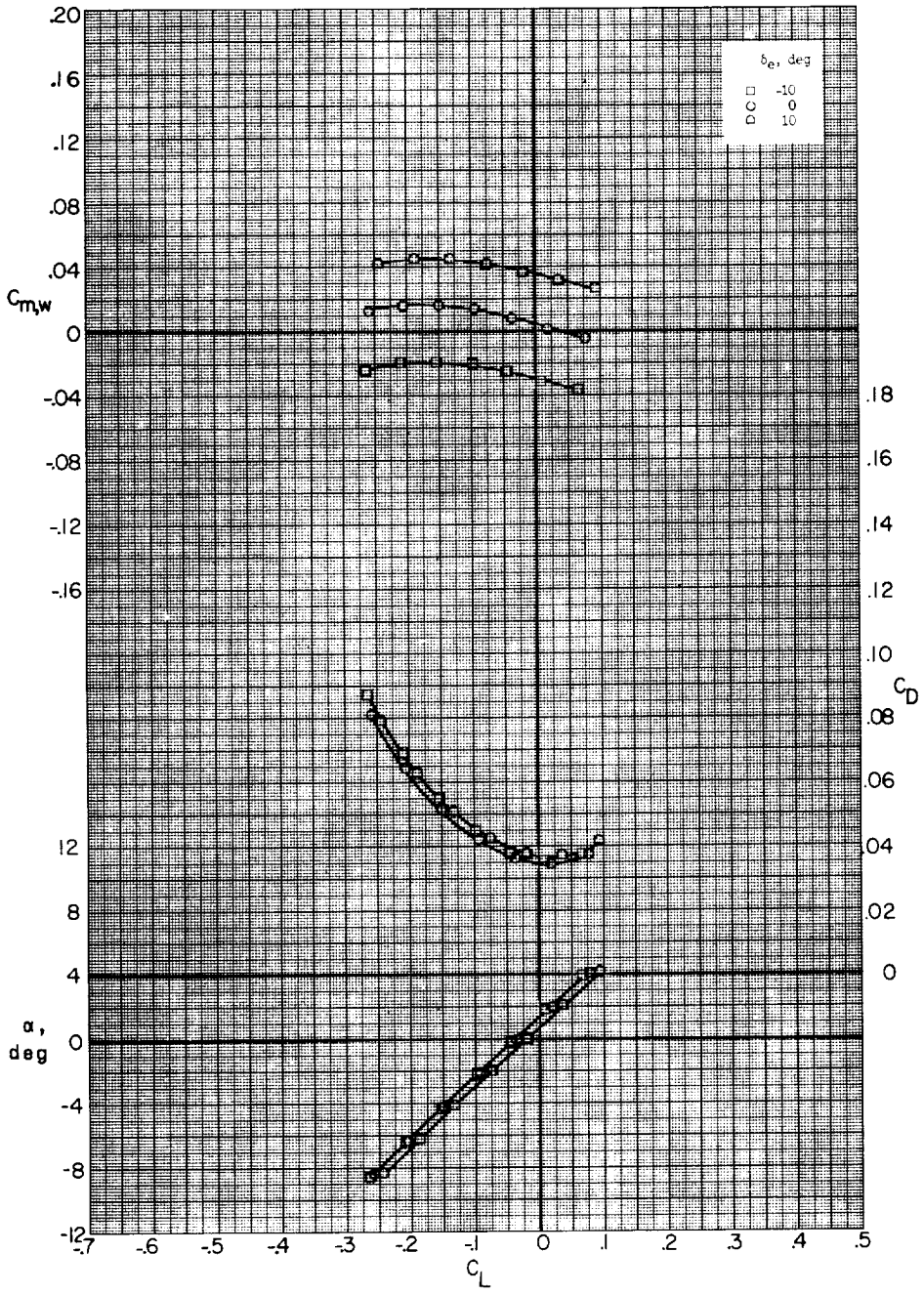
(a) M = 2.29.

Figure 7.- Effect of canard deflection on pitch characteristics of missile-booster combination with A-frame mounted. $\beta = 0.3^{o}$; sting A.



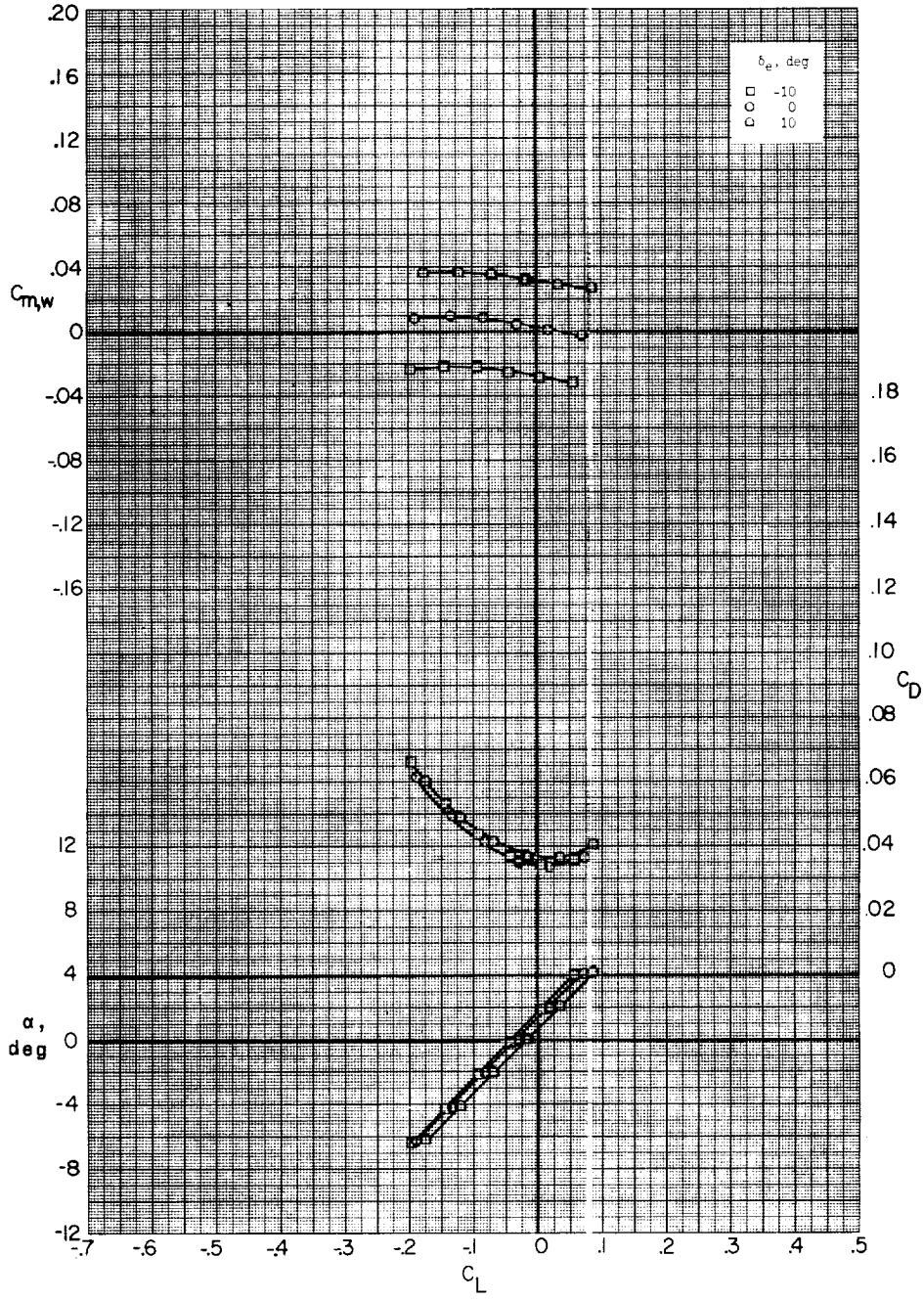
(b) M = 2.75.

Figure 7.- Continued.



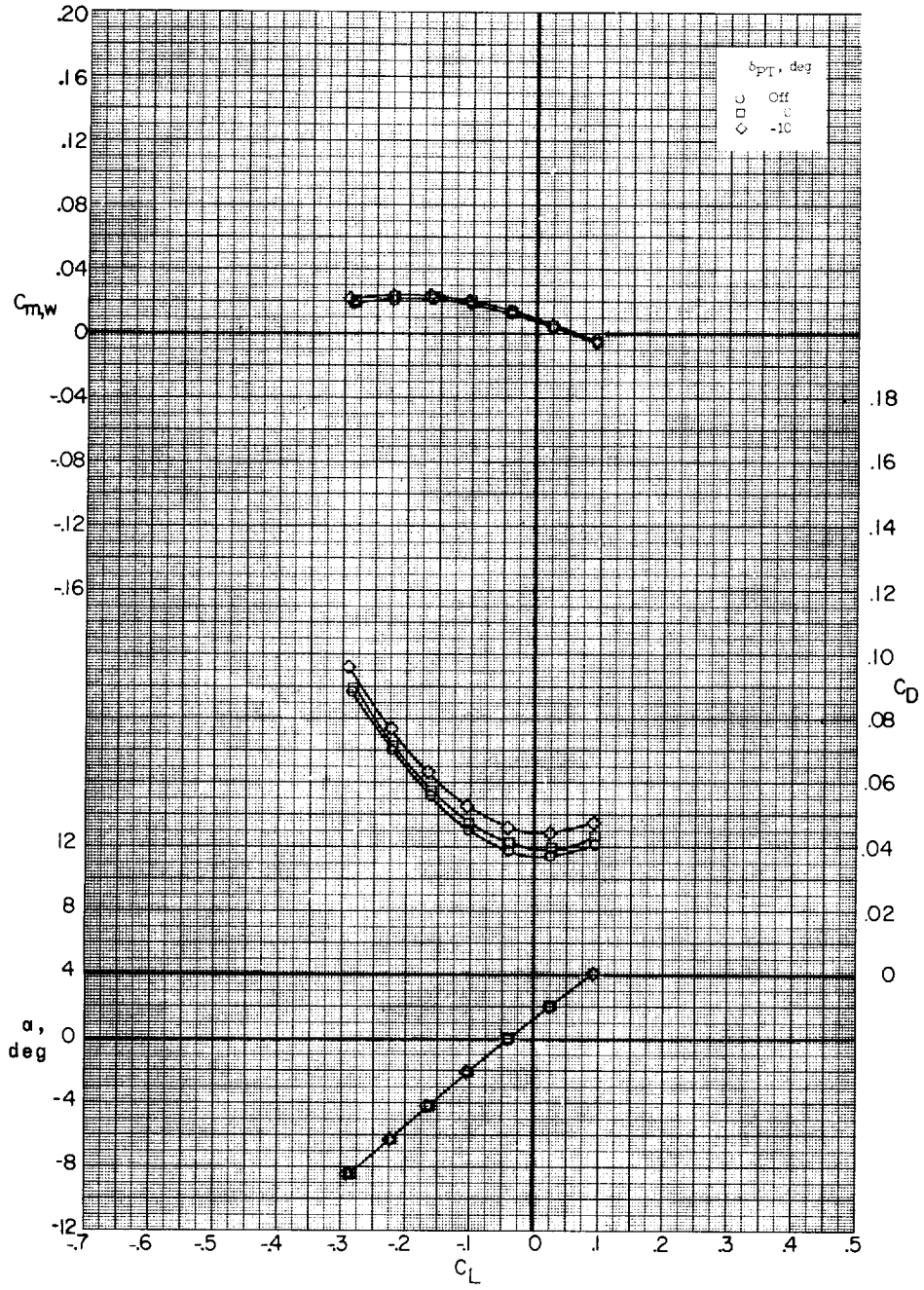
(c) M = 3.22.

Figure 7.- Continued.



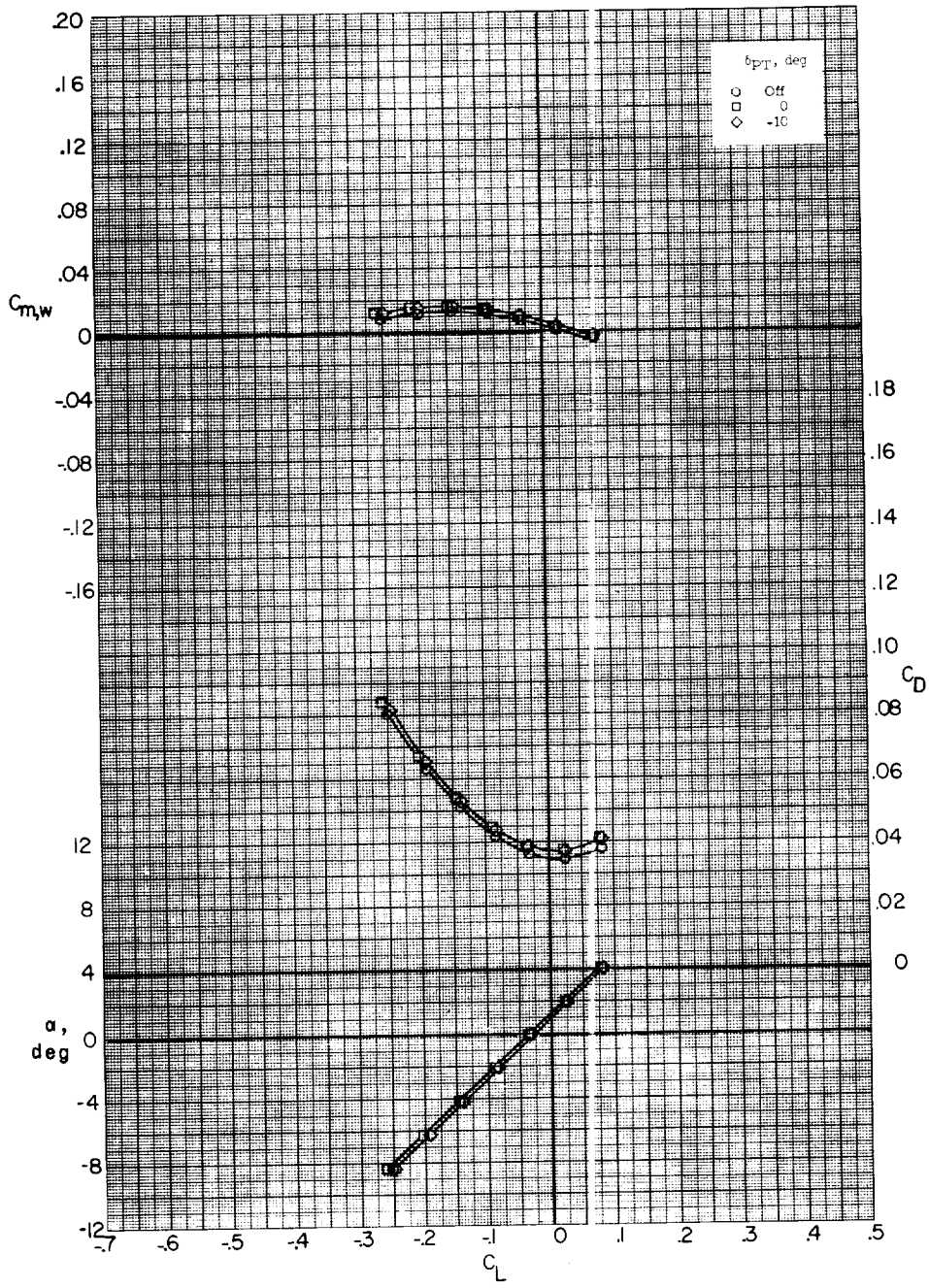
(d) M = 3.51.

Figure 7.- Concluded.



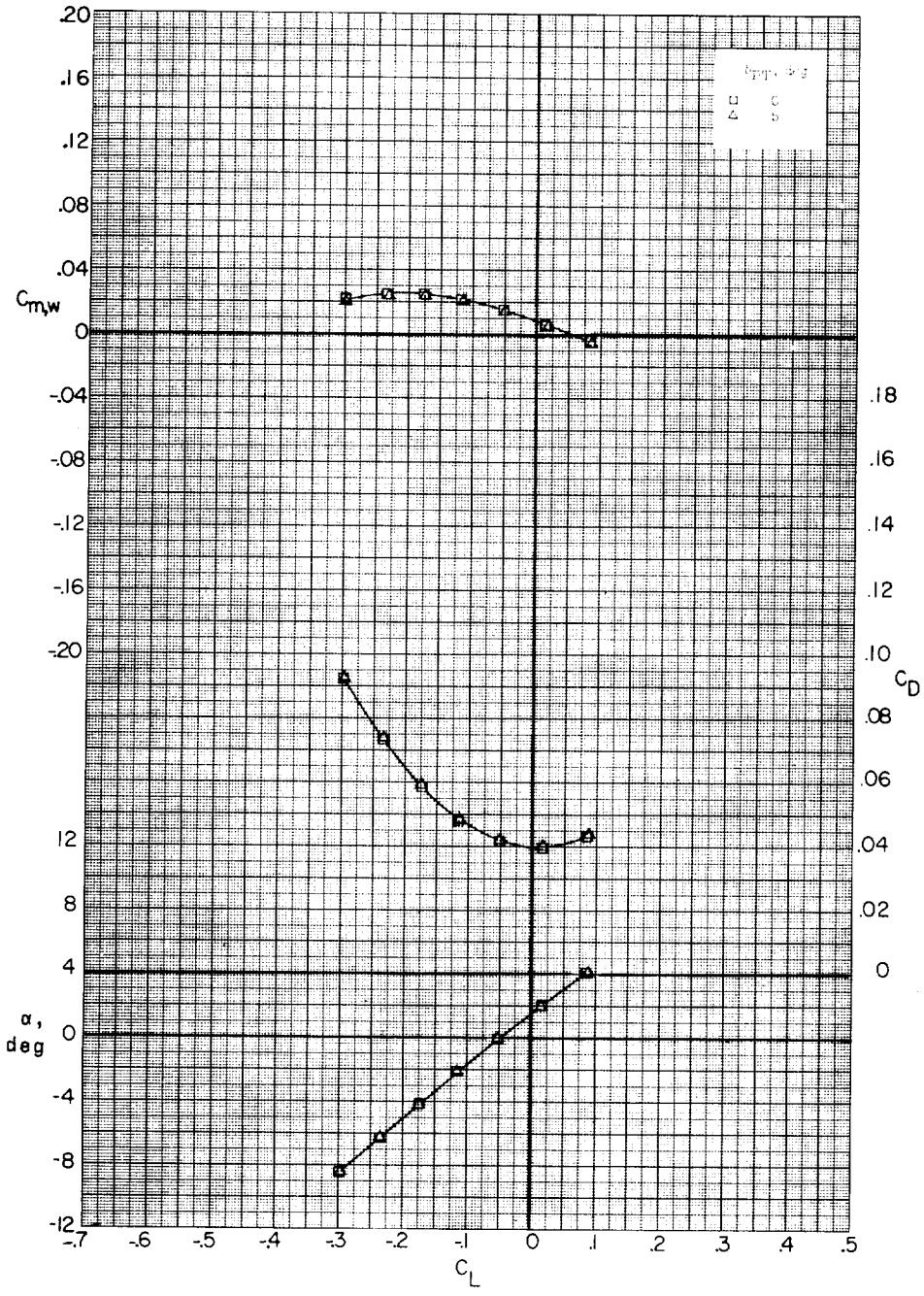
(a) M = 2.75; with bug-eye fairing.

Figure 8.- Effect of booster nozzle on pitch characteristics of missile-booster combination with A-frame mounted. $\delta_{YT} = 0^{\circ}$; $\beta = 0.2^{\circ}$; sting B.



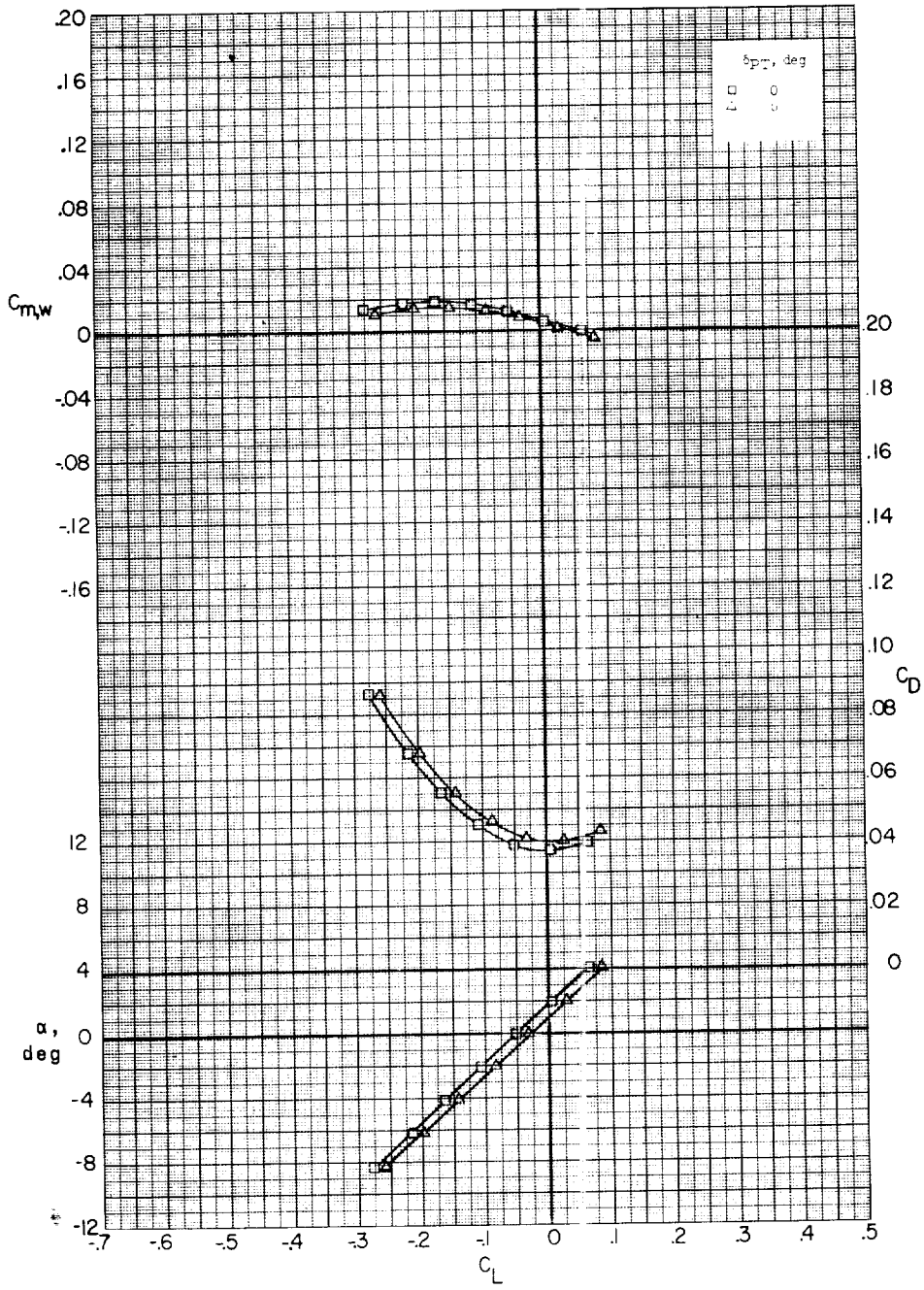
(b) M = 3.22; with bug-eye fairing.

Figure 8.- Continued.



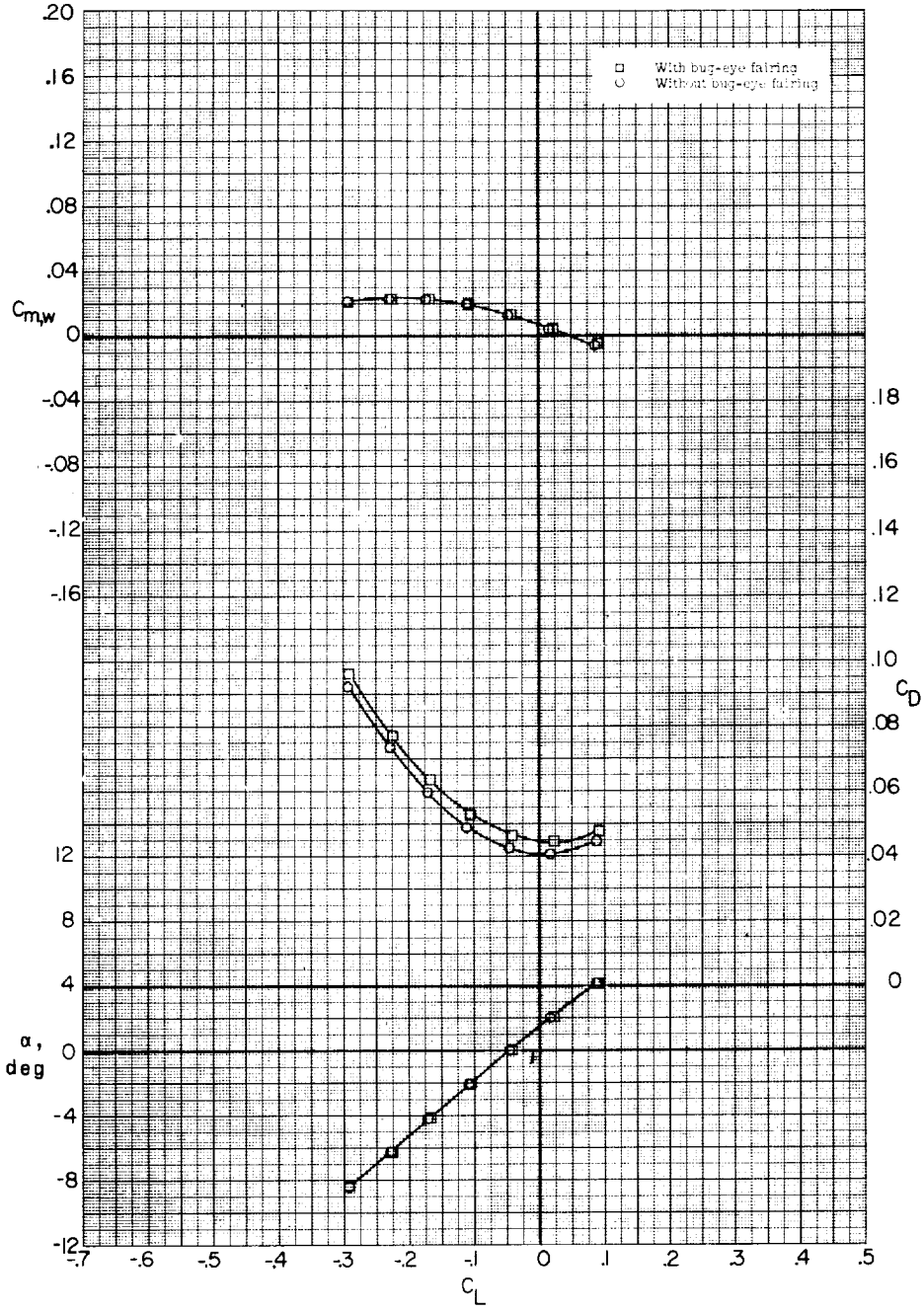
(c) M = 2.75; with bug-eye and nozzle-shroud fairings.

Figure 8.- Continued.



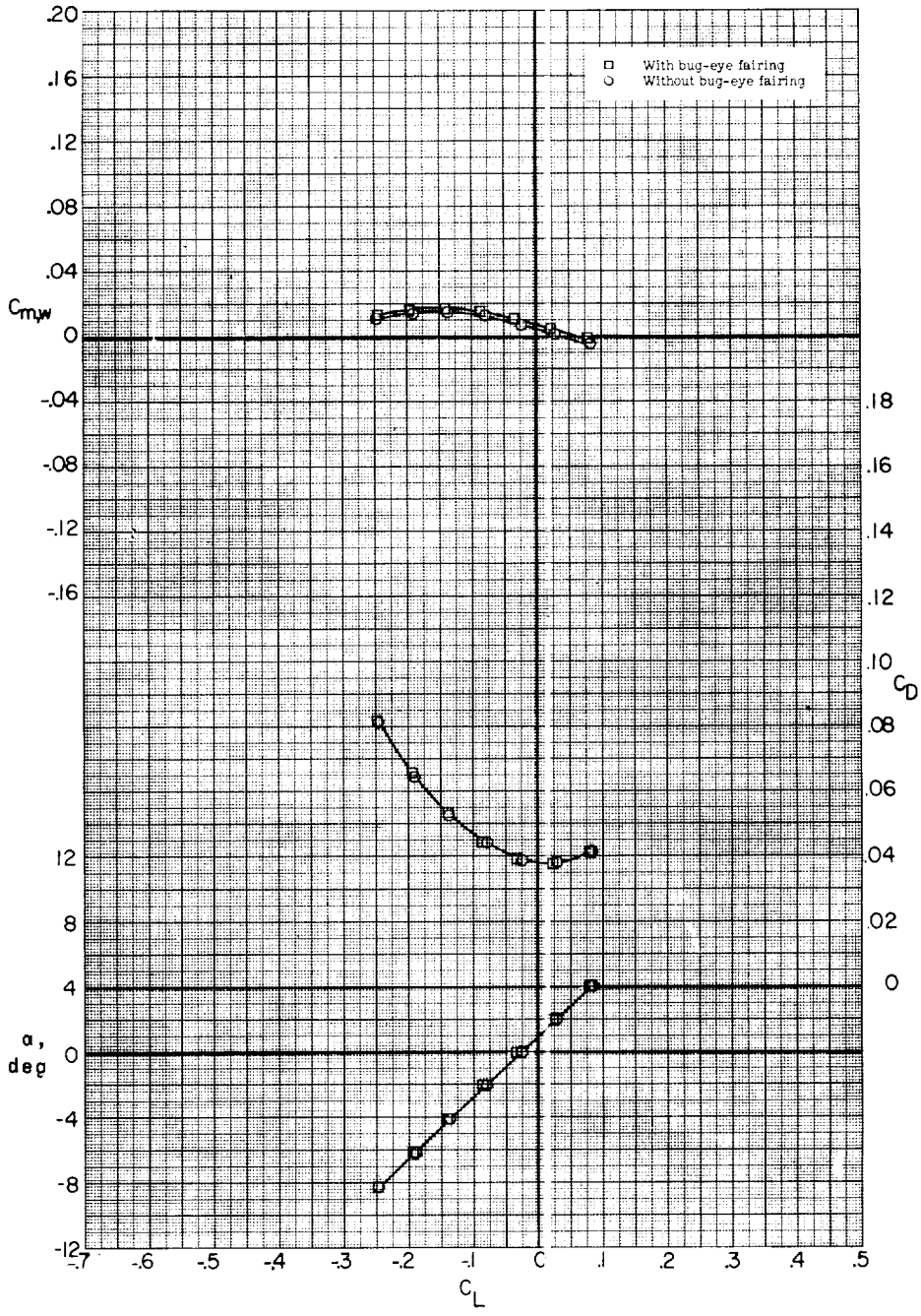
(d) M = 3.22; with bug-eye and nozzle-shroud fairings.

Figure 8.- Concluded.



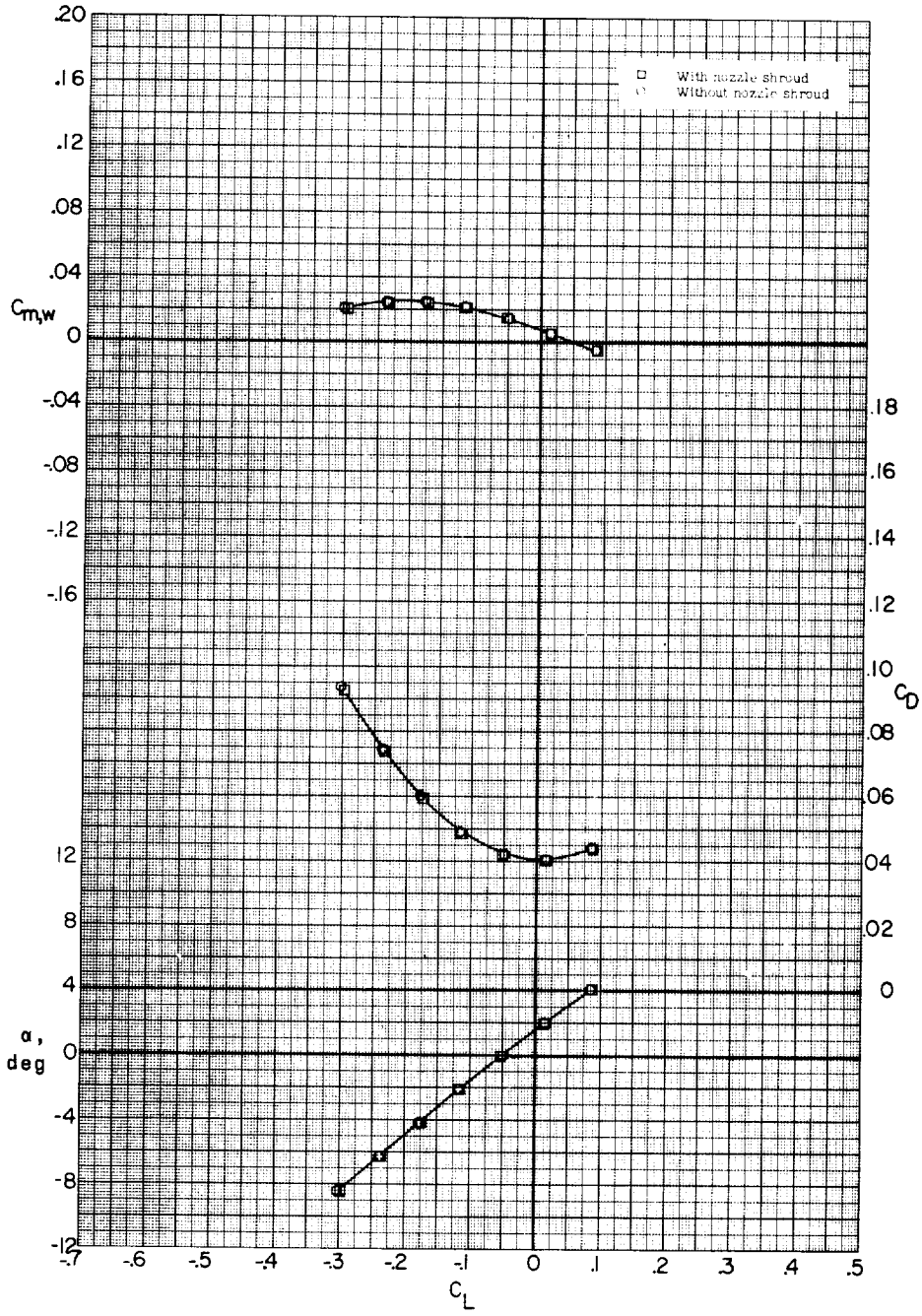
(a) M = 2.75.

Figure 9.- Effect of bug-eye fairing on pitch characteristics of missile-booster combination with A-frame mounted. $\delta_{PT} = -10^\circ$; $\delta_{YT} = 0^\circ$; $\beta = 0.2^\circ$; sting B.



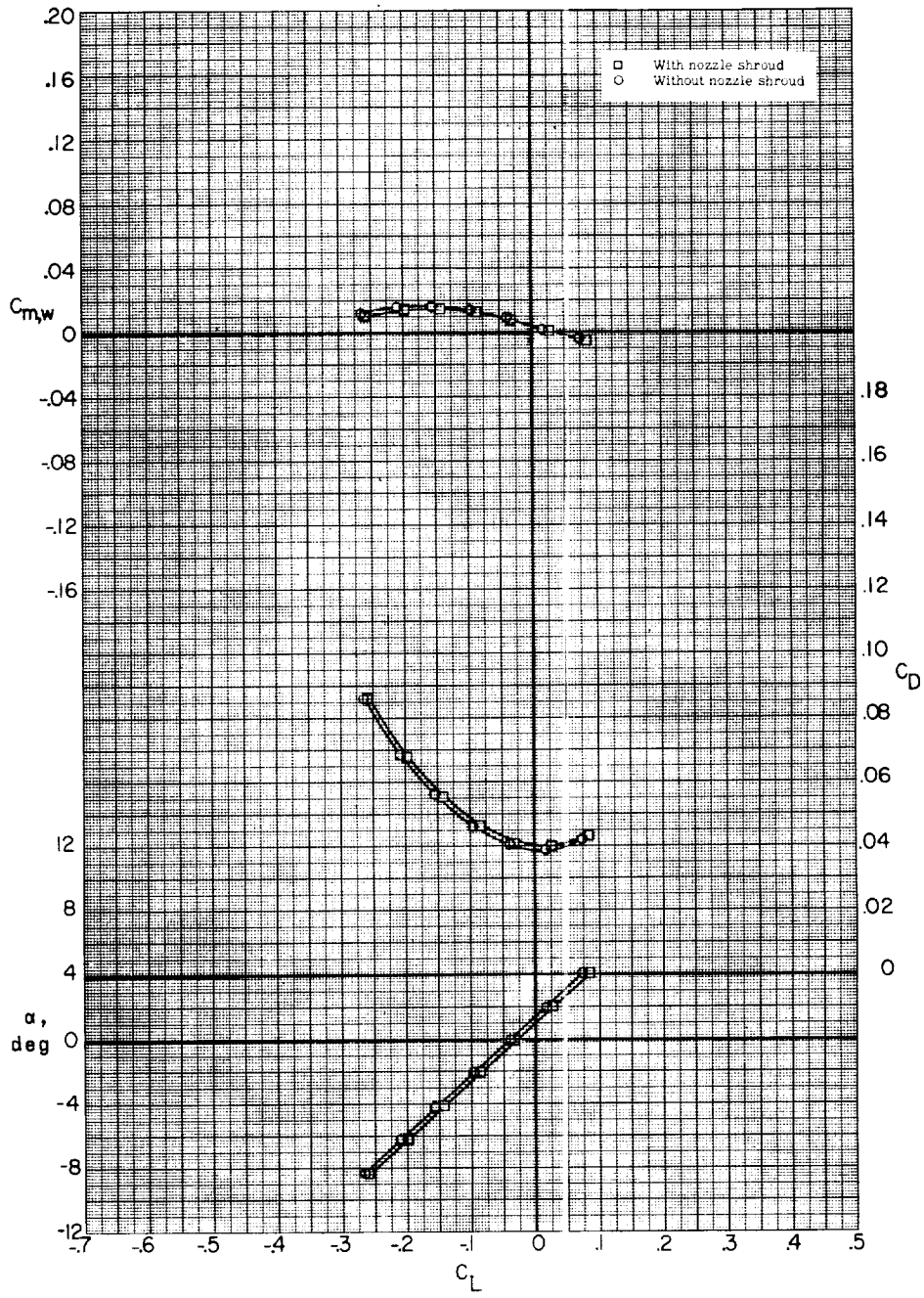
(b) M = 3.22.

Figure 9.- Concluded.



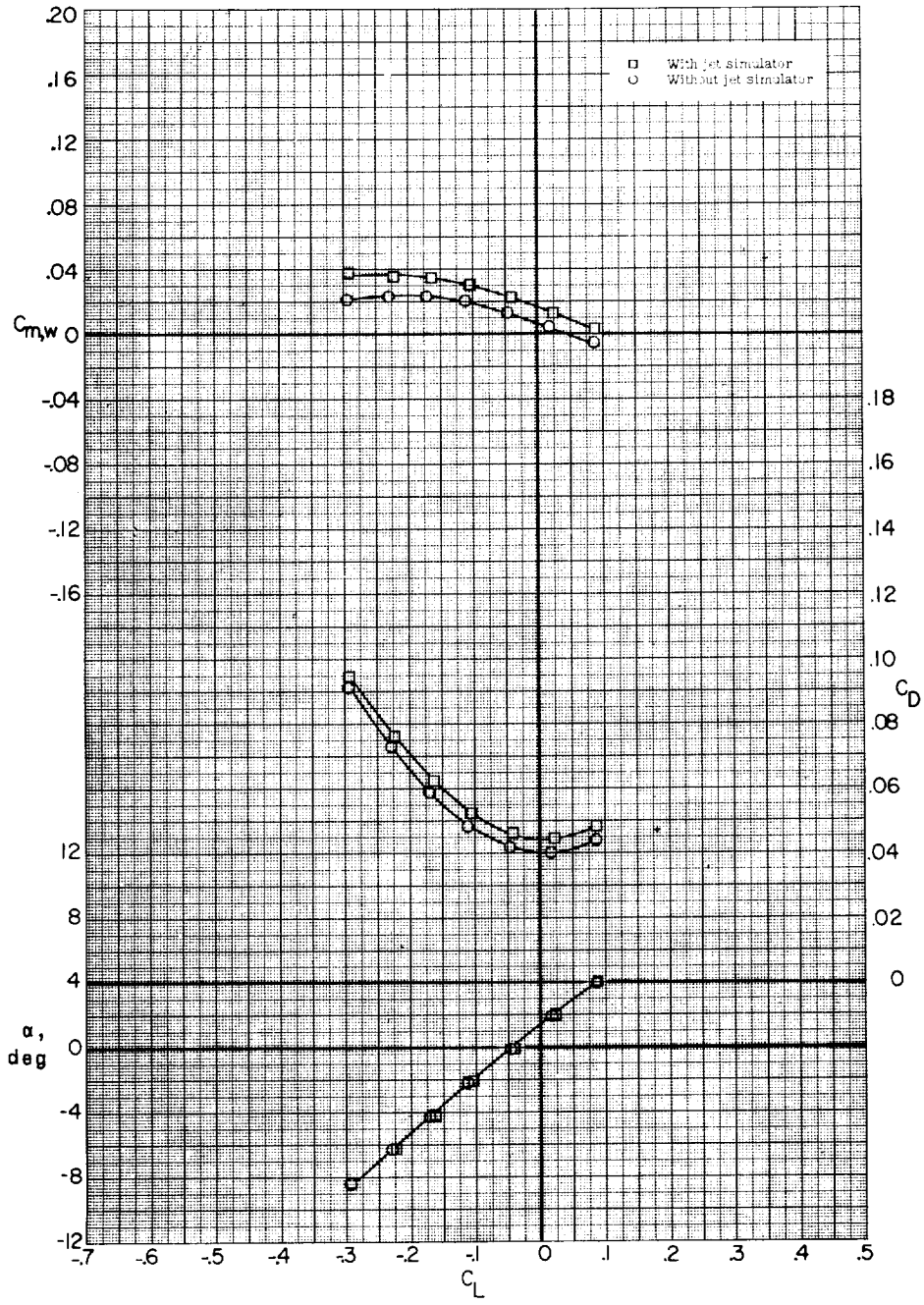
(a) M = 2.75.

Figure 10.- Effect of nozzle shrouds on pitch characteristics of missile-booster combination with bug-eye fairing and A-frame mounted. $\delta_{PT} = 5^{\circ}$; $\delta_{YT} = 0^{\circ}$; $\beta = 0.2^{\circ}$; sting B.



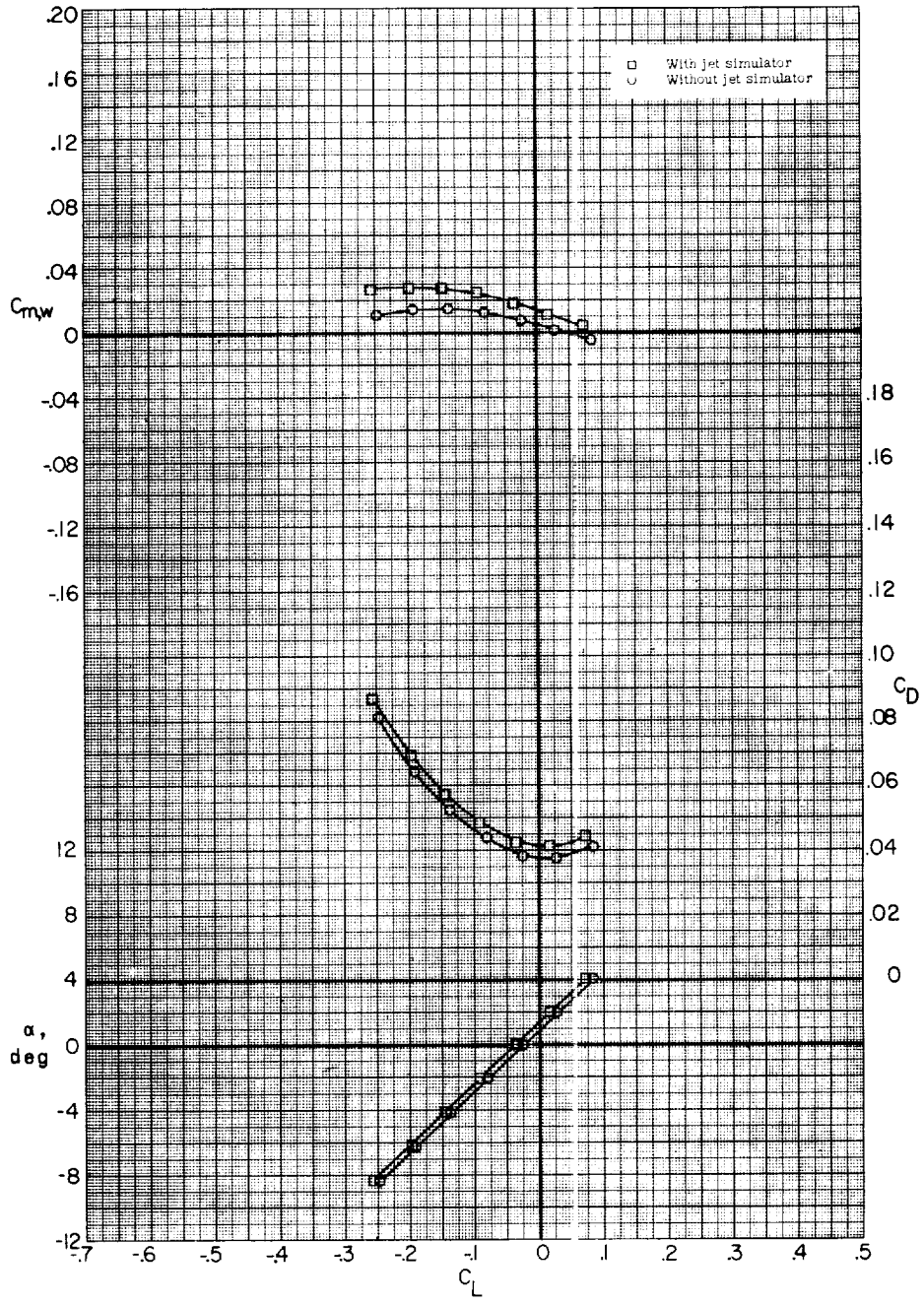
(b) M = 3.22.

Figure 10.- Concluded.



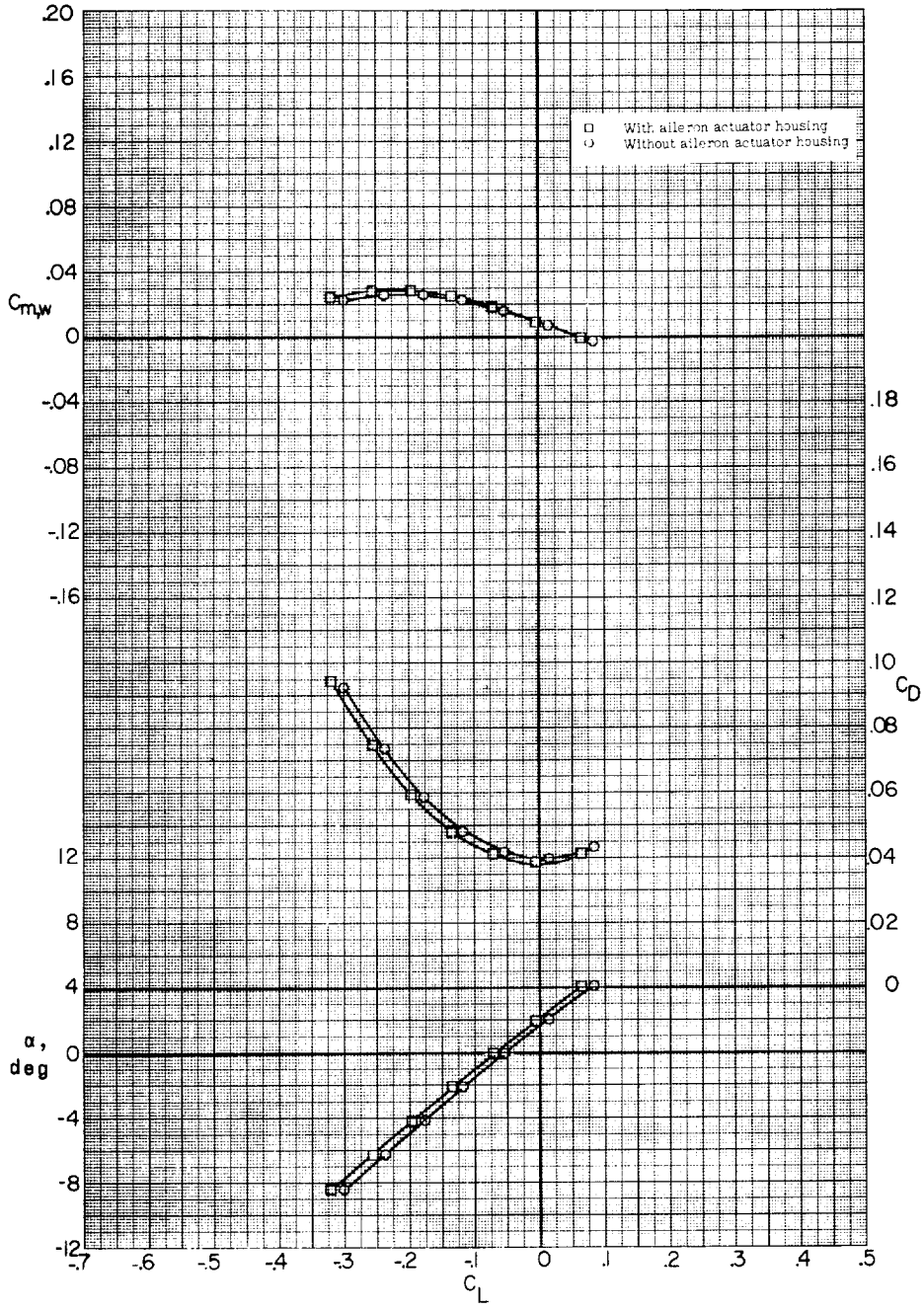
(a) M = 2.75.

Figure 11.- Effects of jet simulator mounted at rear of rocket nozzle on pitch characteristics of missile-booster combination with A-frame mounted. $\delta_{PT} = -10^{\circ}$; $\delta_{YT} = 0^{\circ}$; $\beta = 0.2^{\circ}$; sting B.



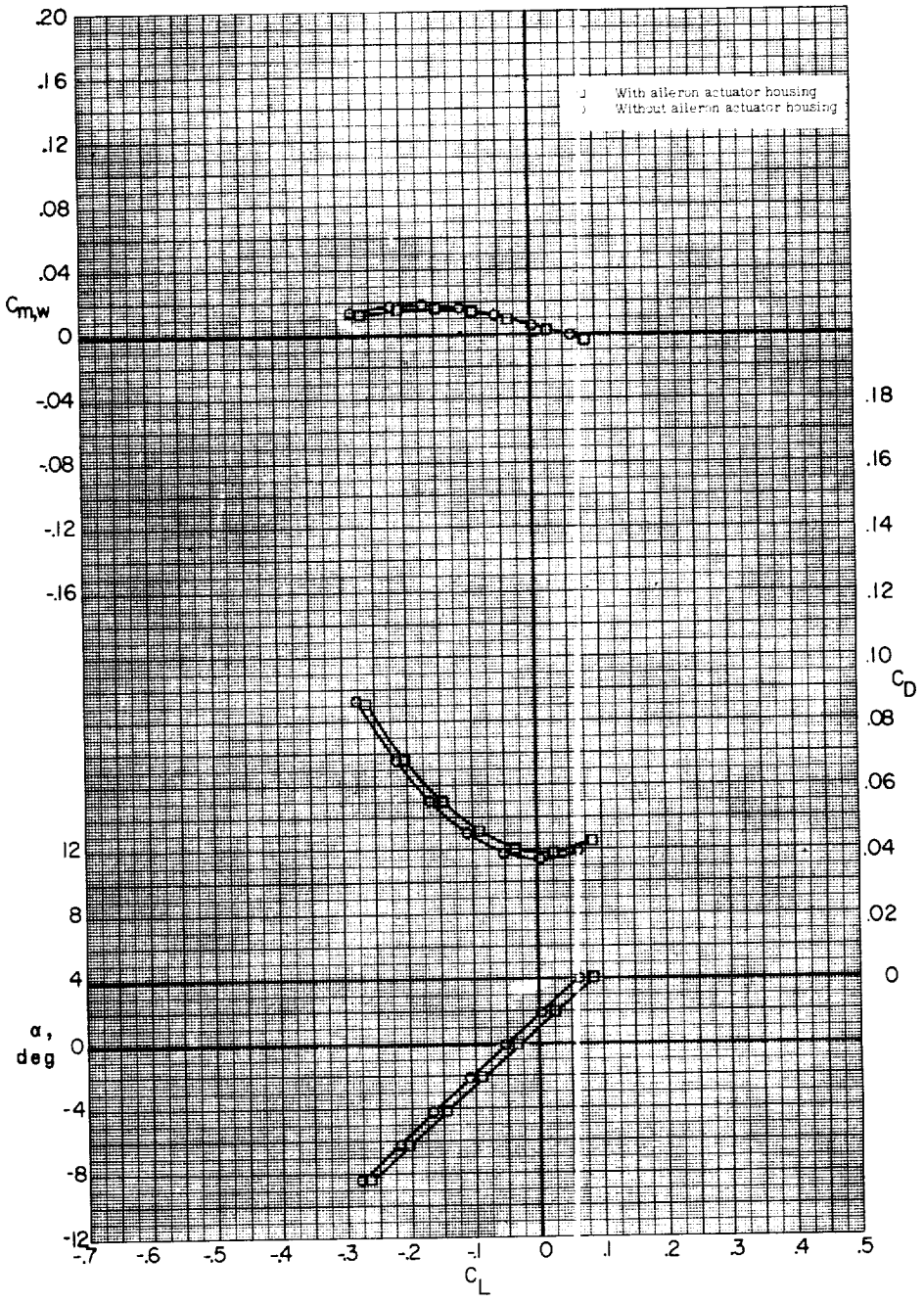
(b) M = 3.22.

Figure 11.- Concluded.



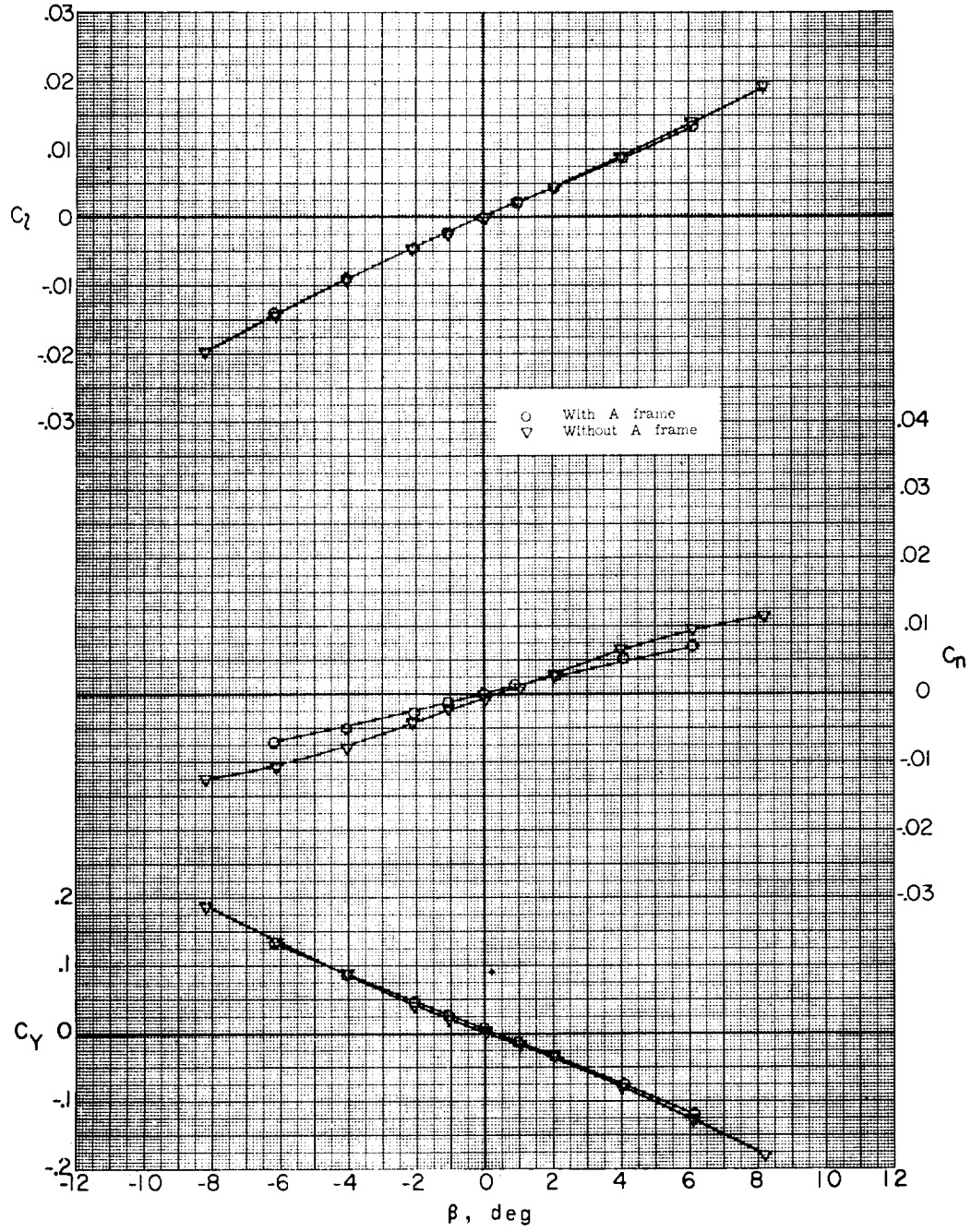
(a) M = 2.75.

Figure 12.- Effect of missile aileron actuator housing on pitch characteristics of missile-booster combination with A-frame mounted. $\delta_a = 0^o$; $\beta = 0.2^o$; sting B.



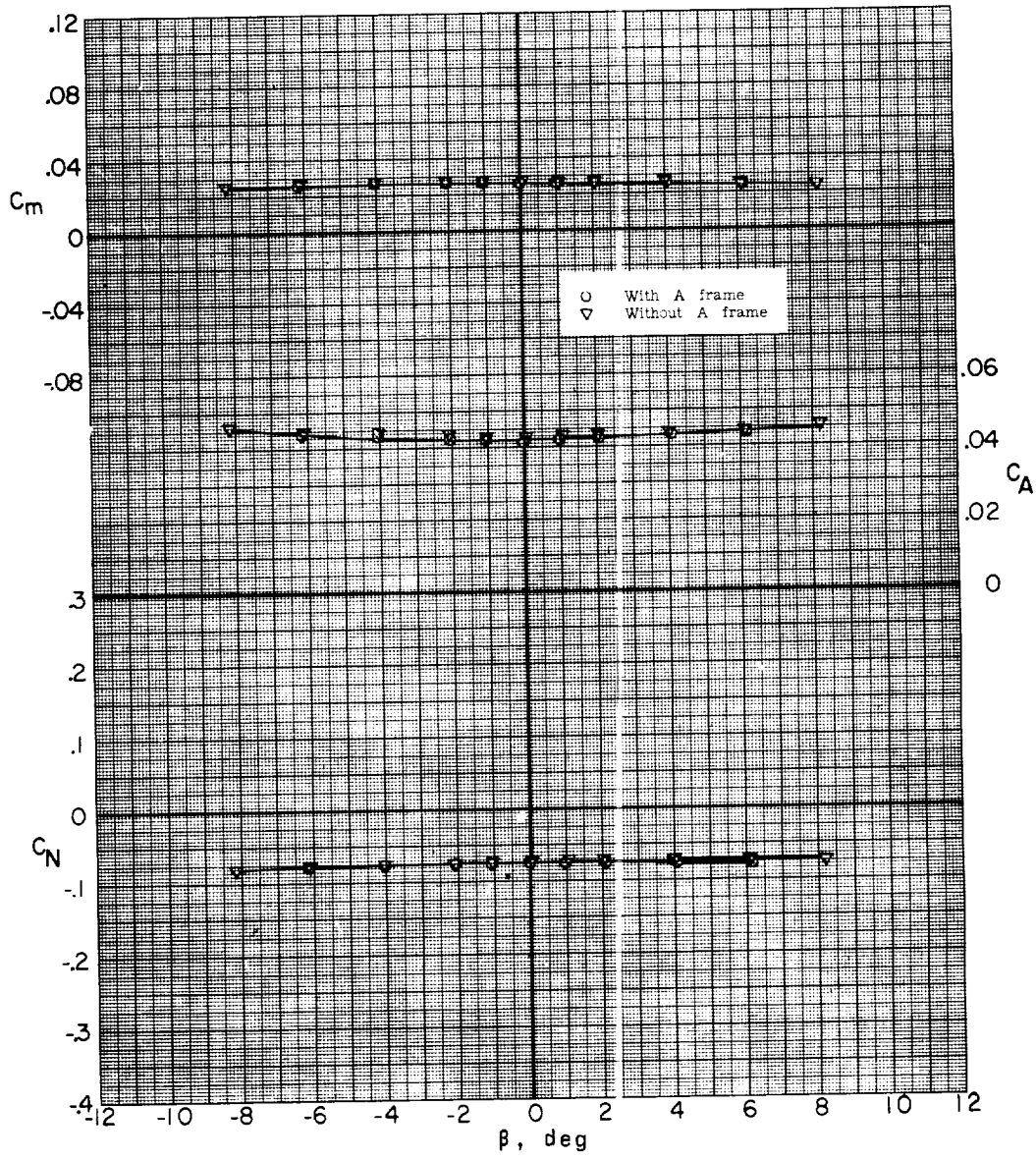
(b) M = 3.22.

Figure 12.- Concluded.



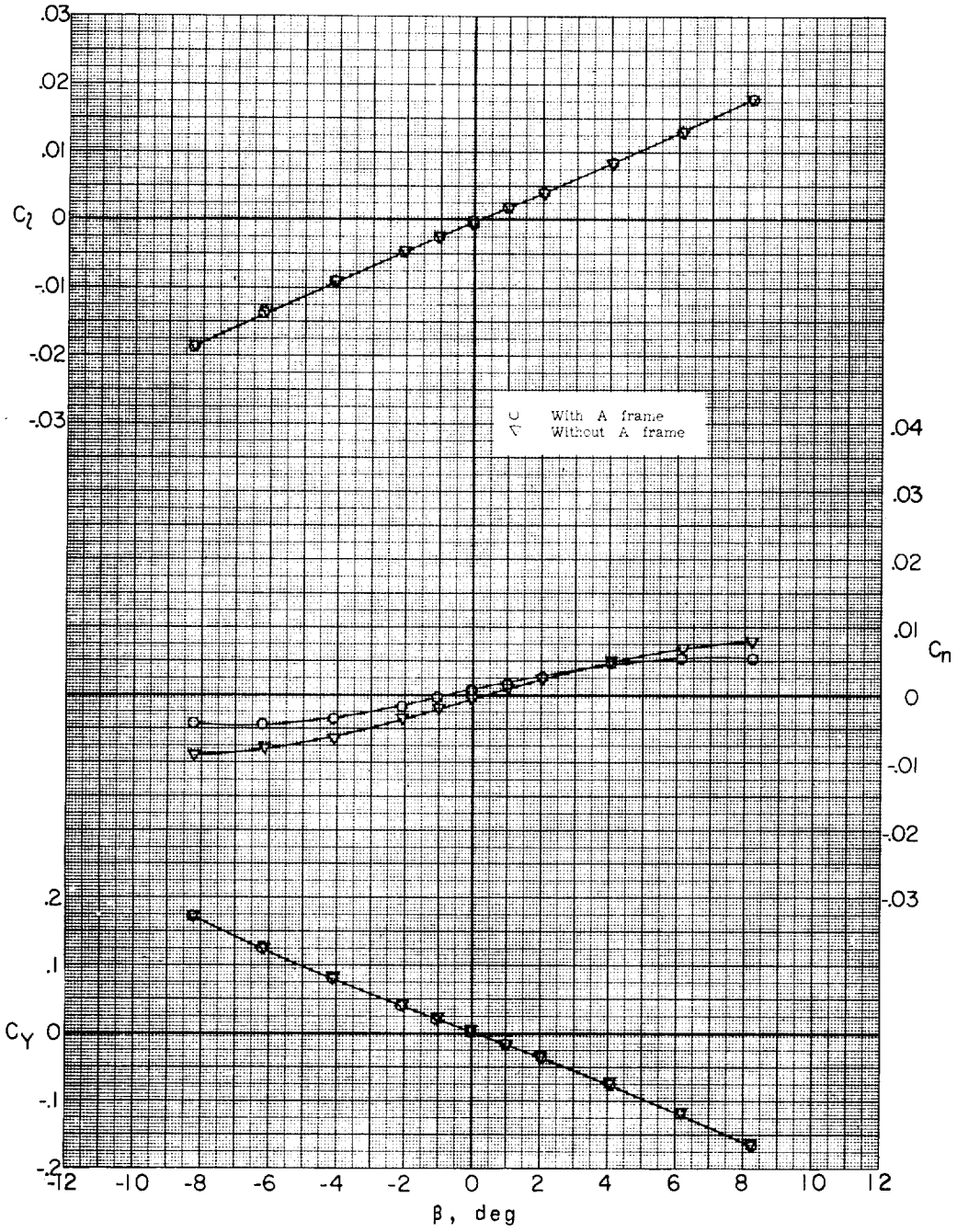
(a) M = 2.29.

Figure 13.- Effect of A-frame on lateral characteristics of missile-booster combination. $\delta_e = 0^\circ$; $\alpha = -0.3^\circ$; sting A.



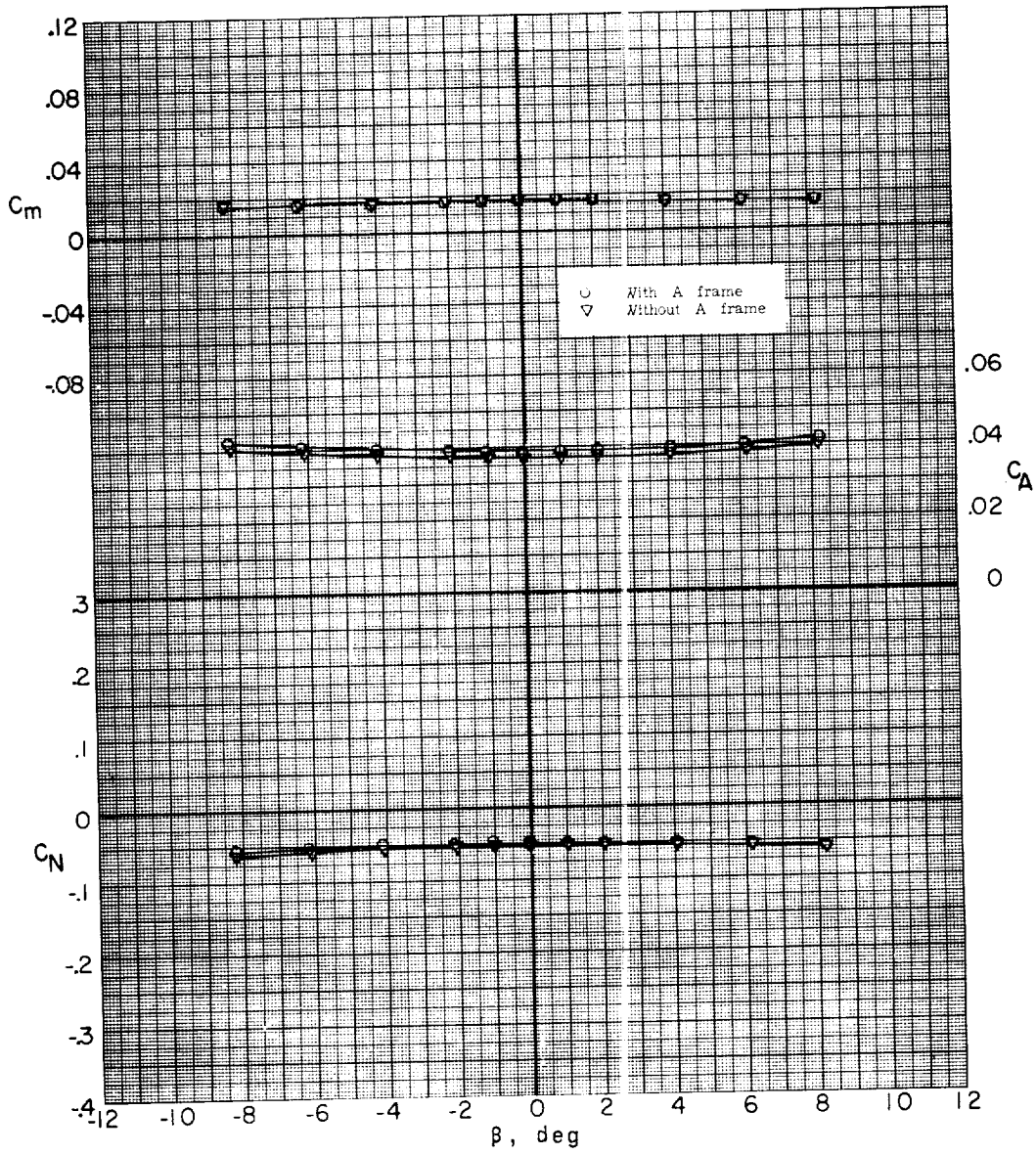
(a) Concluded.

Figure 13.- Continued.



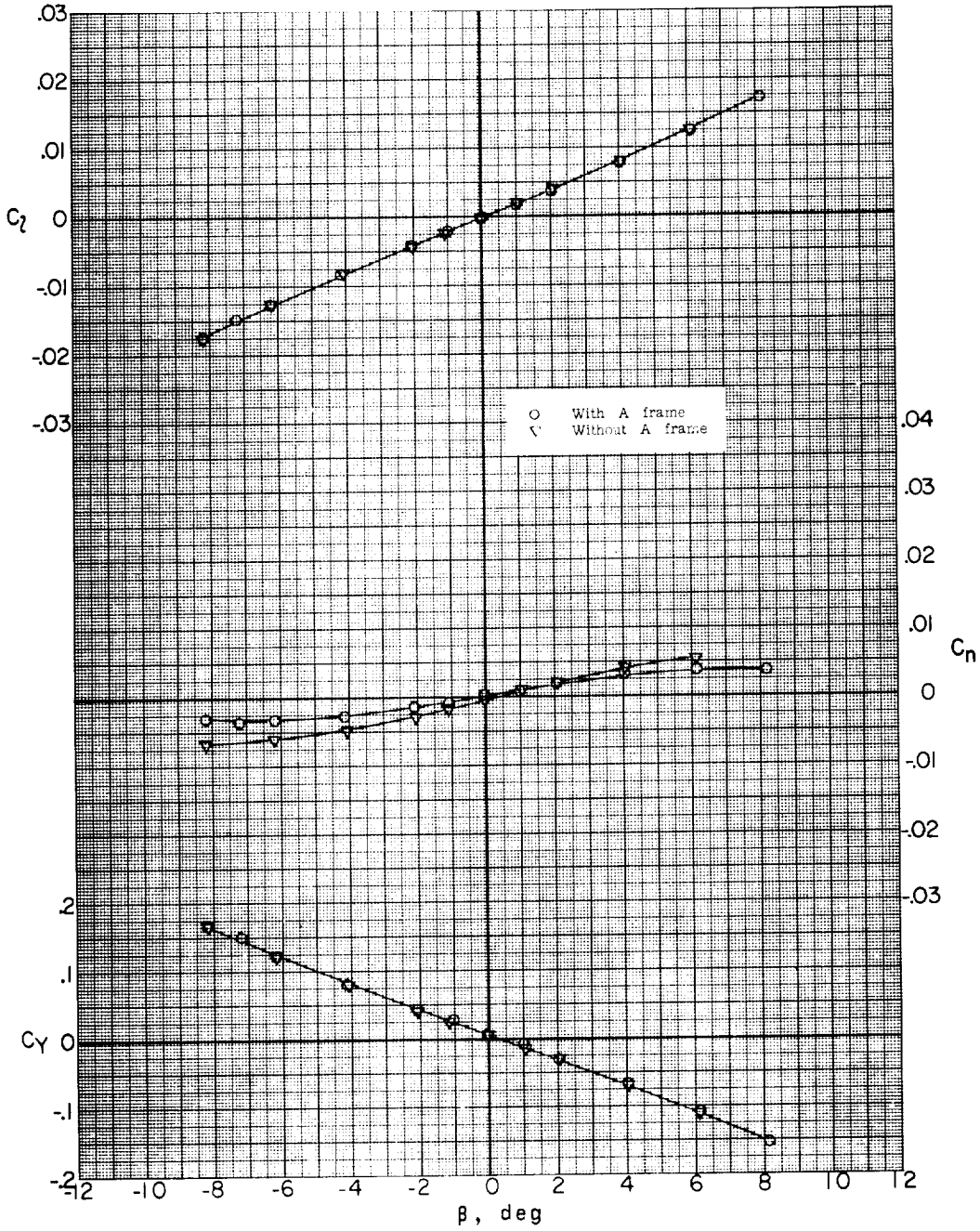
(b) M = 2.75.

Figure 13.- Continued.



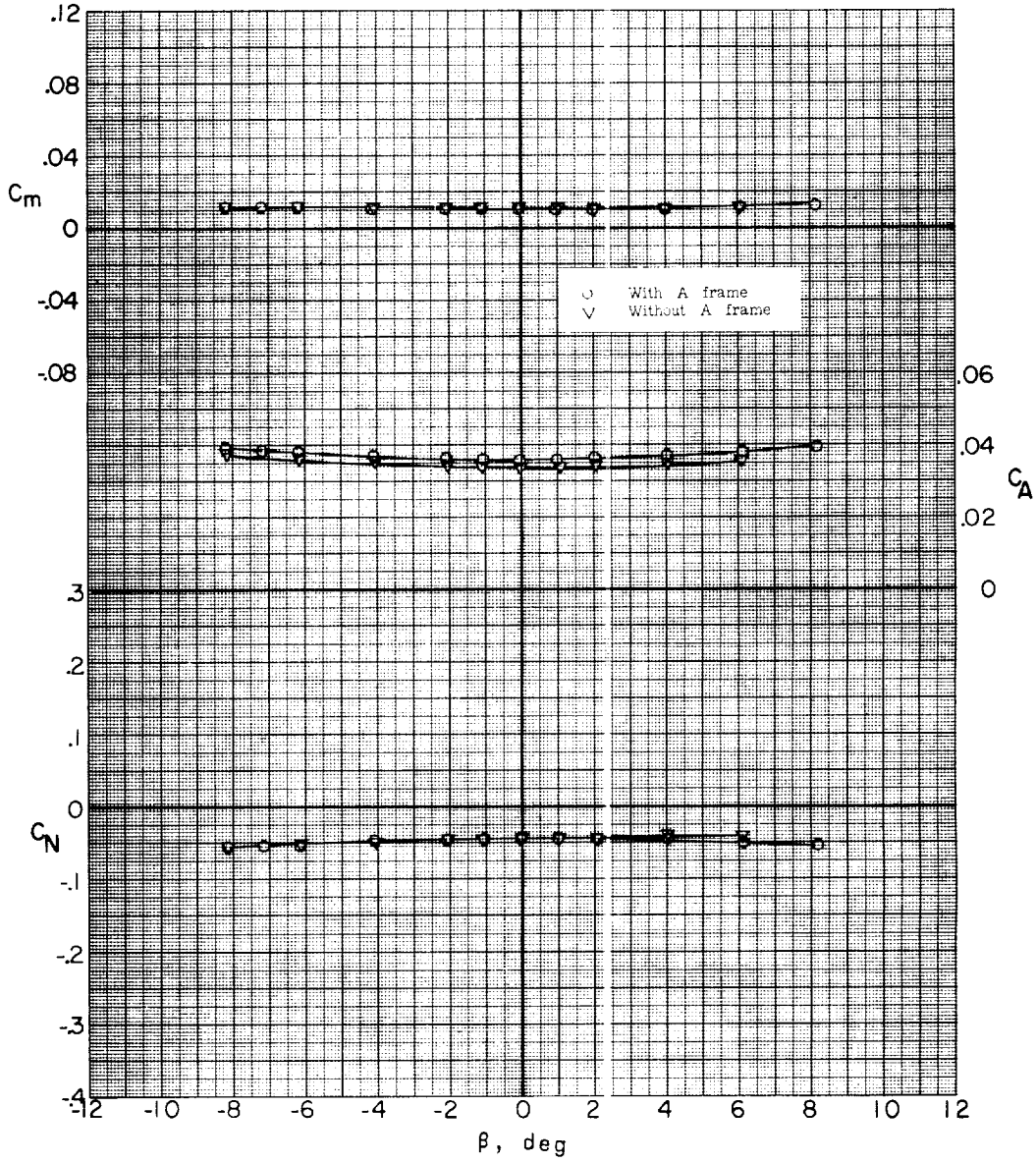
(b) Concluded.

Figure 13.- Continued.



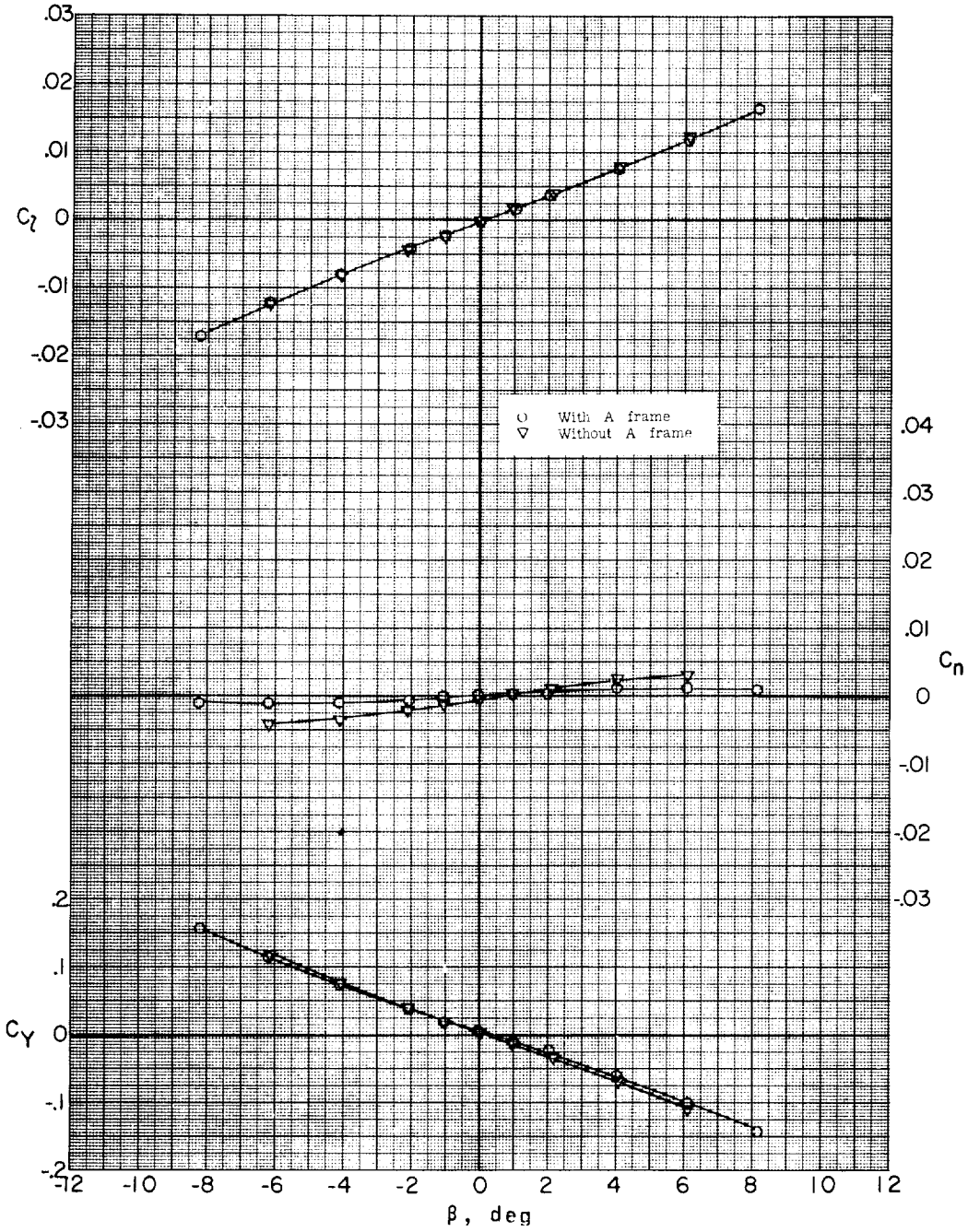
(c) M = 3.22.

Figure 13.- Continued.



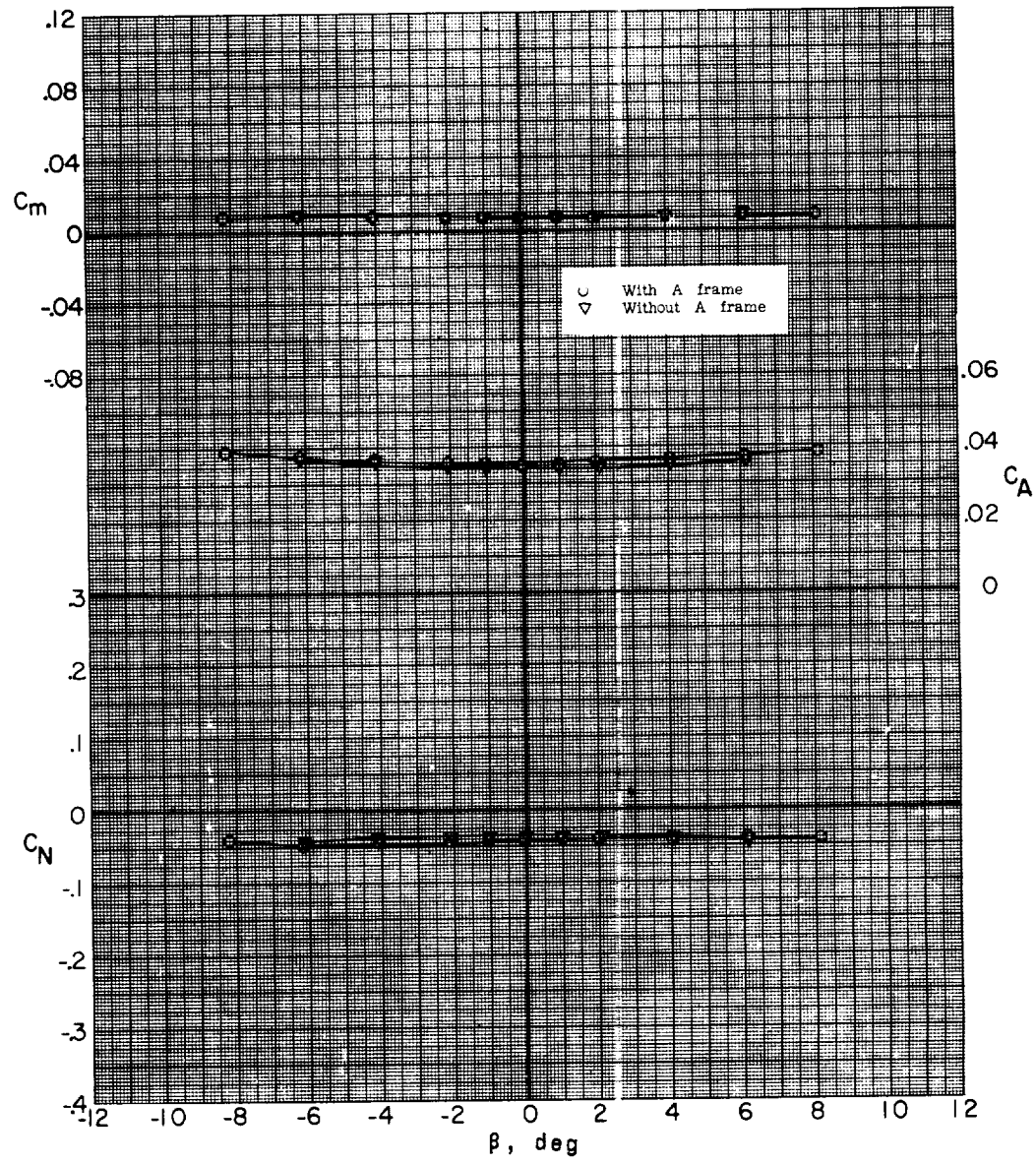
(c) Concluded.

Figure 13.- Continued.



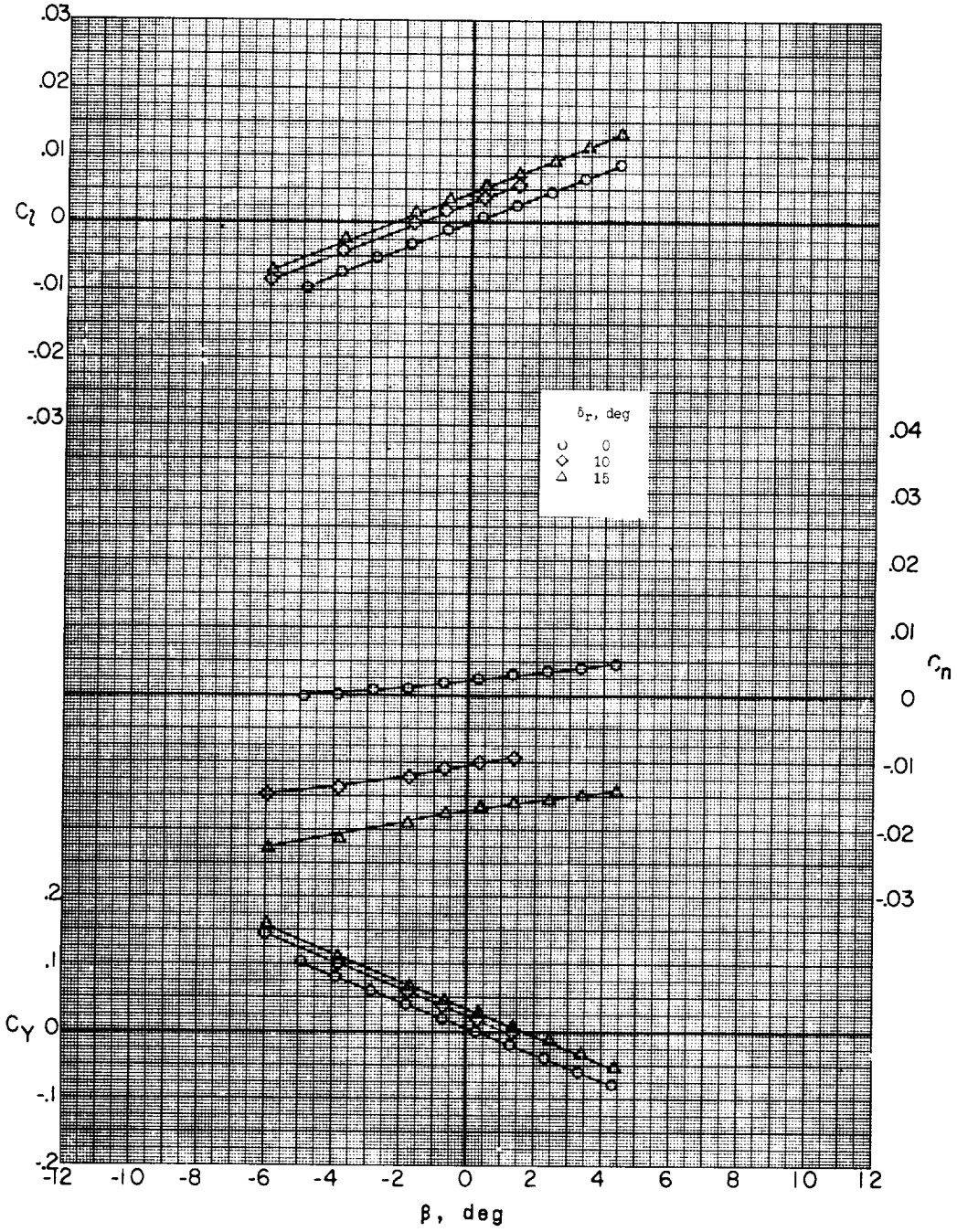
(d) M = 3.51.

Figure 13.- Continued.



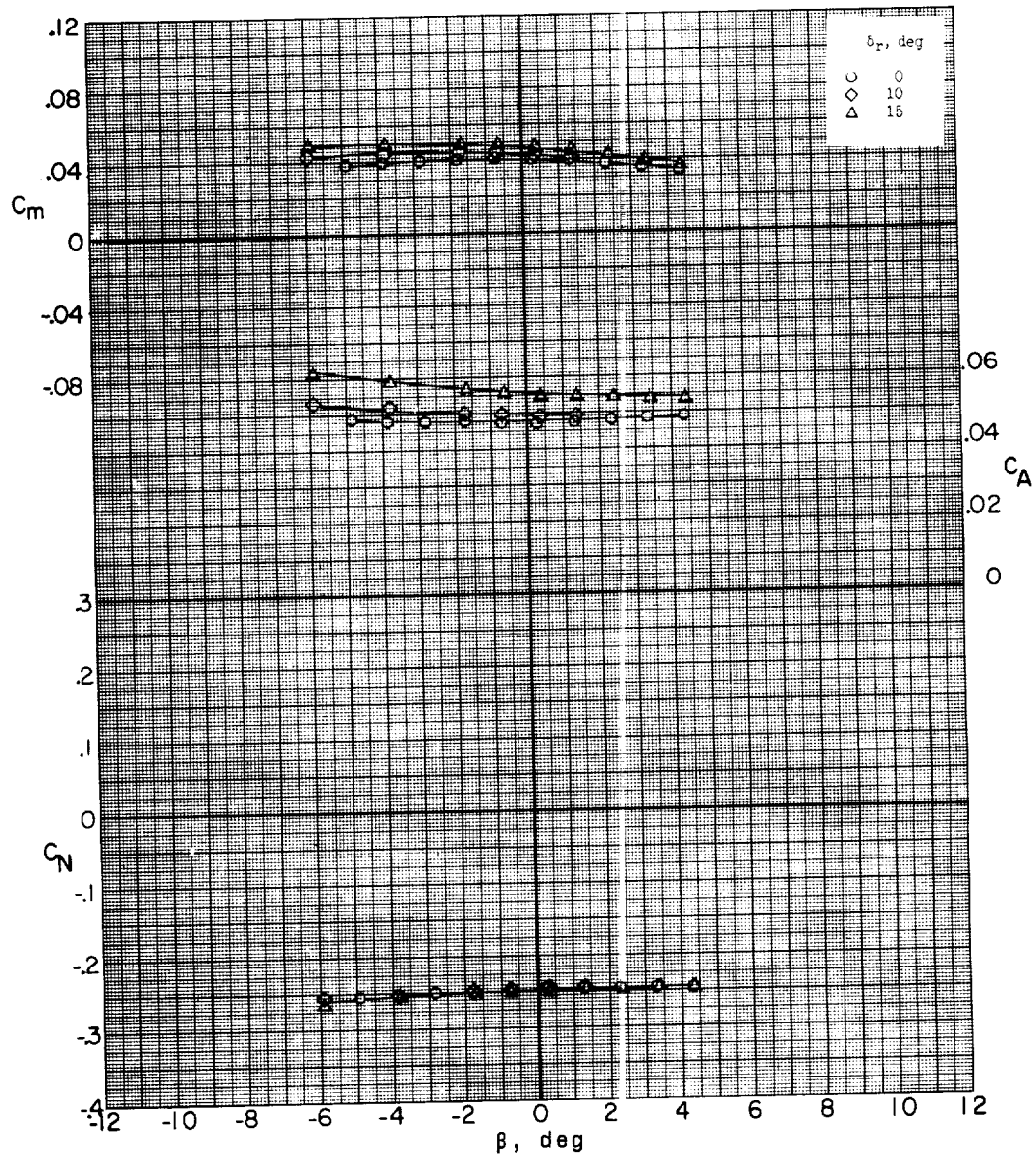
(d) Concluded.

Figure 13.- Concluded.



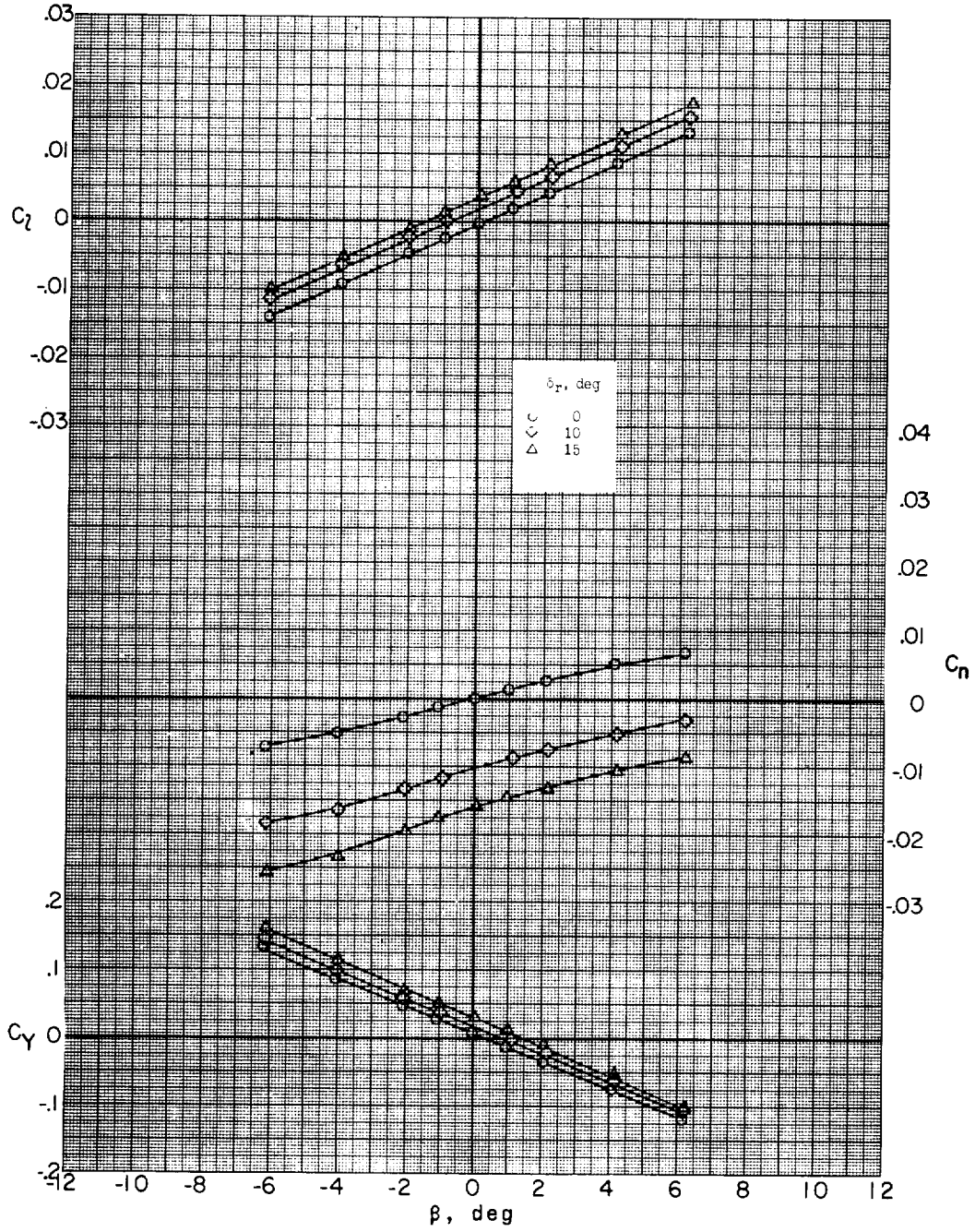
(a) M = 2.29; $\alpha = -5.3^{\circ}$.

Figure 14.- Effect of rudder deflection on lateral characteristics of missile-booster combination with A-frame mounted. $\delta_e = 0^{\circ}$; sting A.



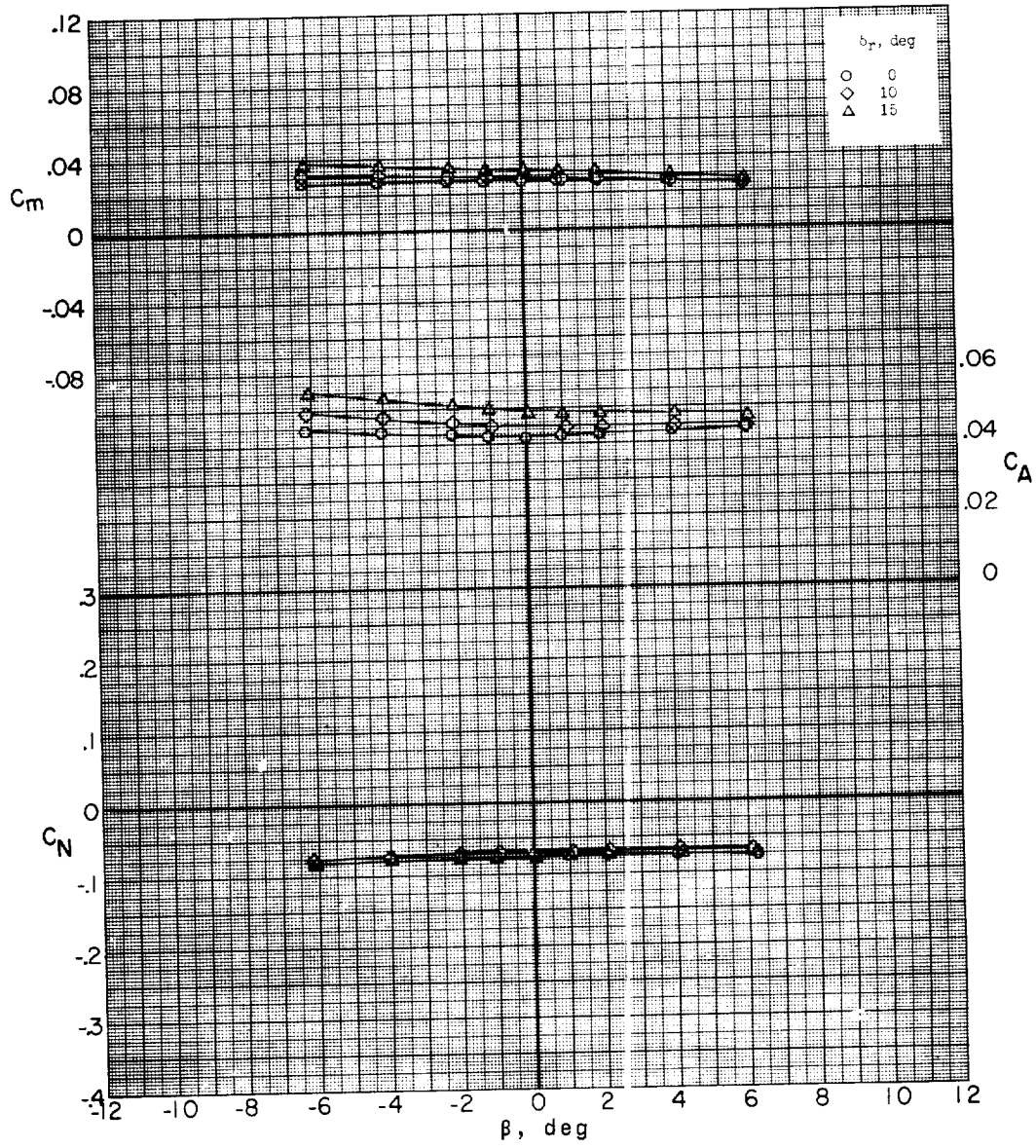
(a) Concluded.

Figure 14.- Continued.



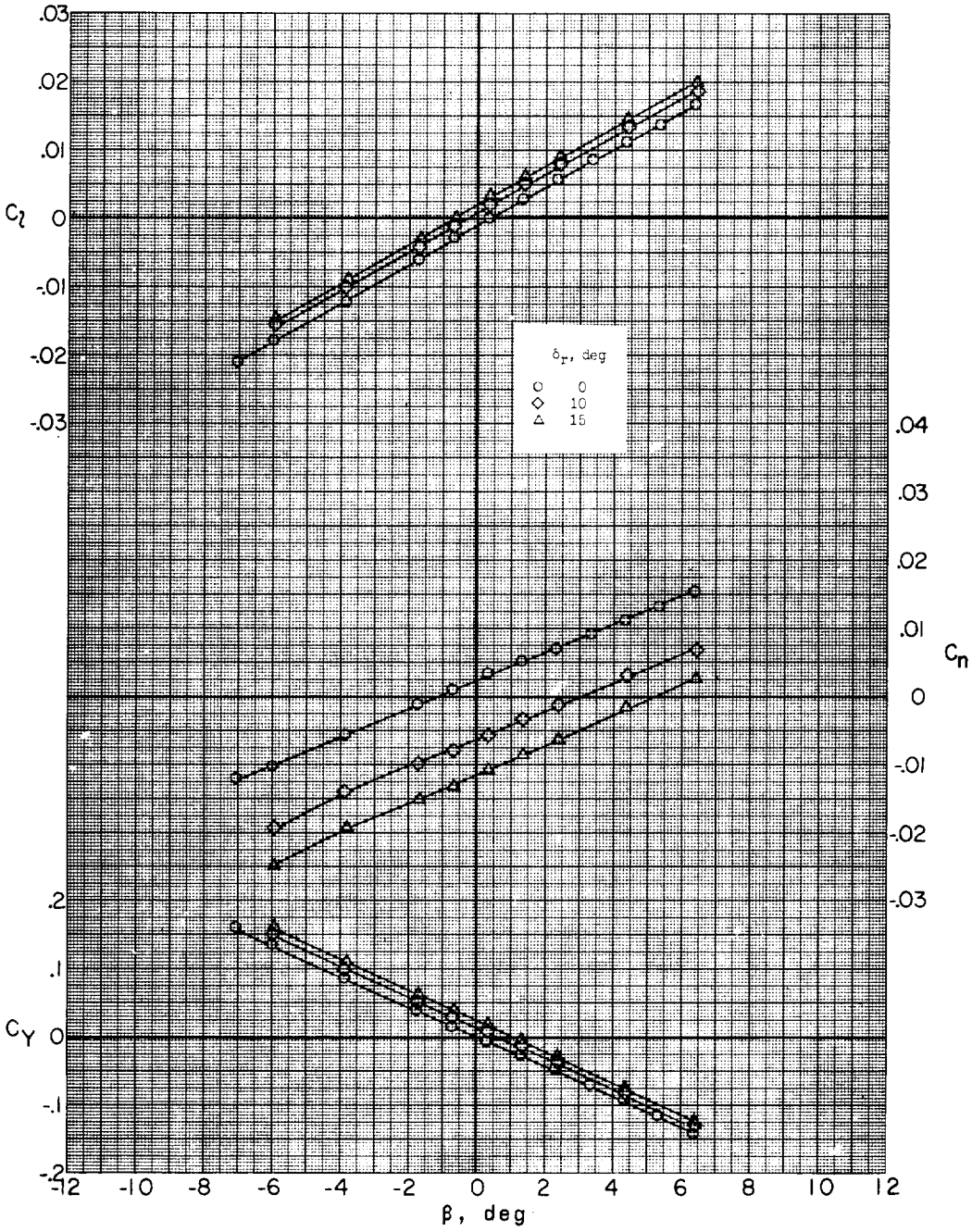
(b) M = 2.29; $\alpha = -0.3^{\circ}$.

Figure 14.- Continued.



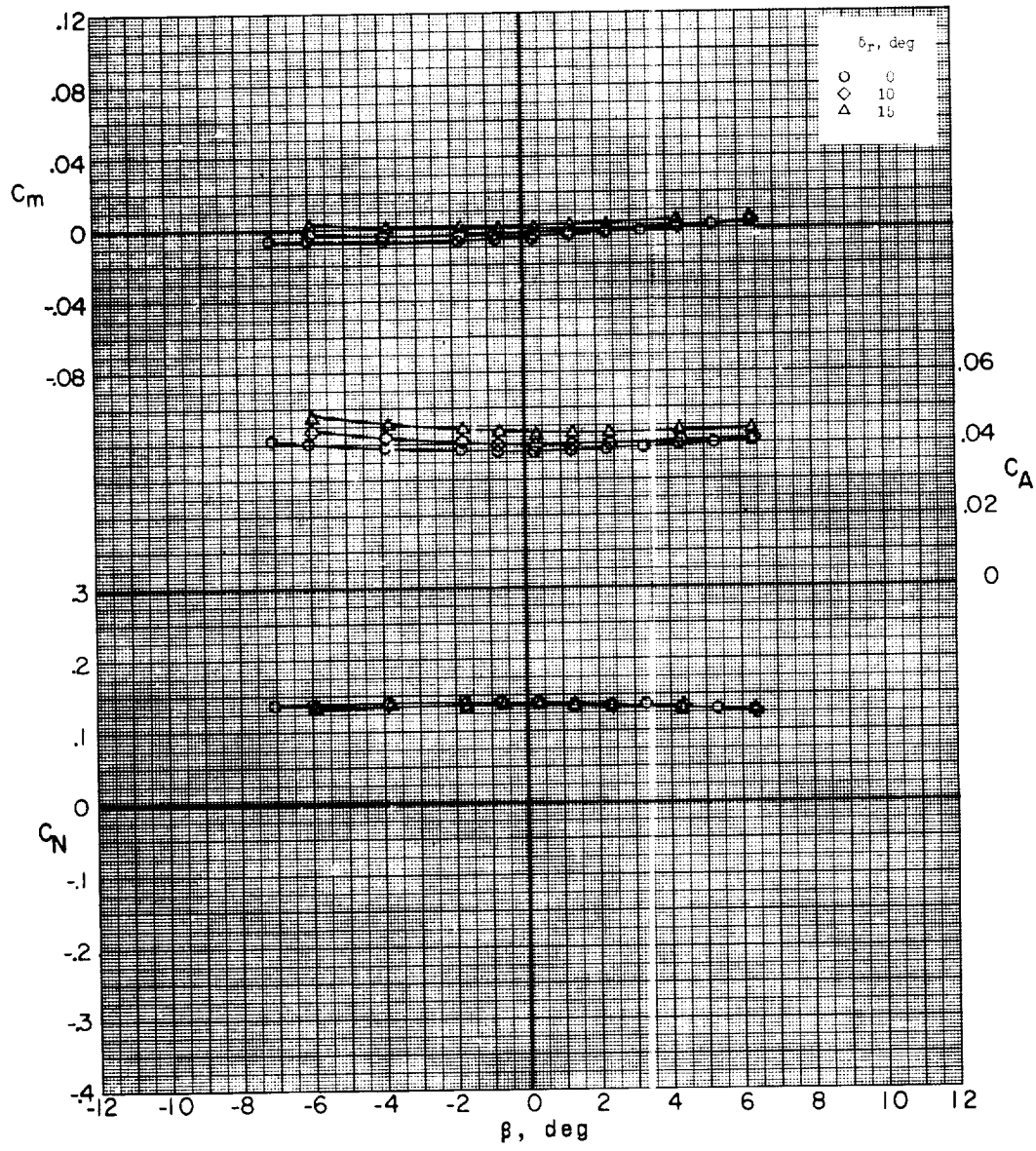
(b) Concluded.

Figure 14.- Continued.



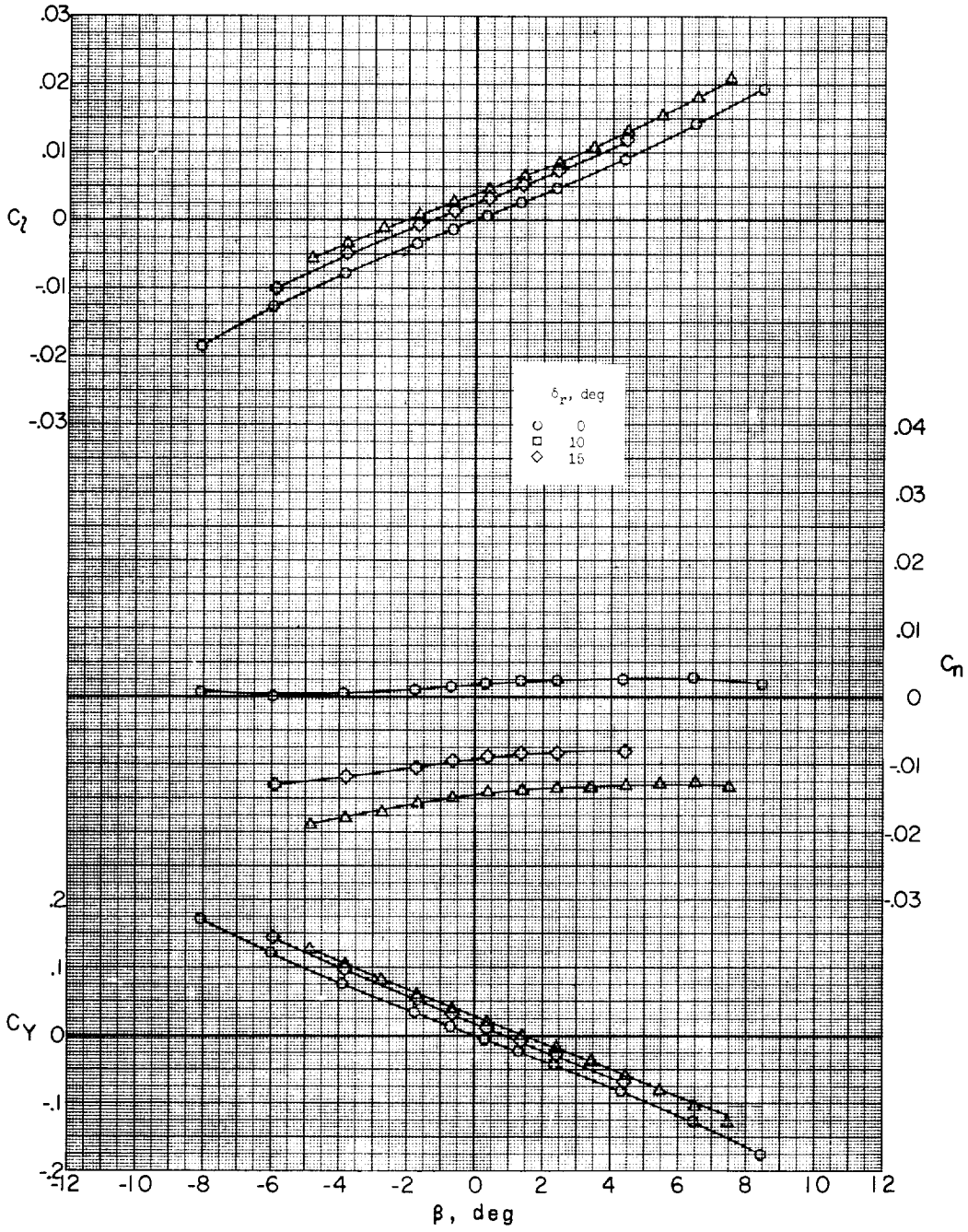
(c) M = 2.29; $\alpha = 5.2^{\circ}$.

Figure 14.- Continued.



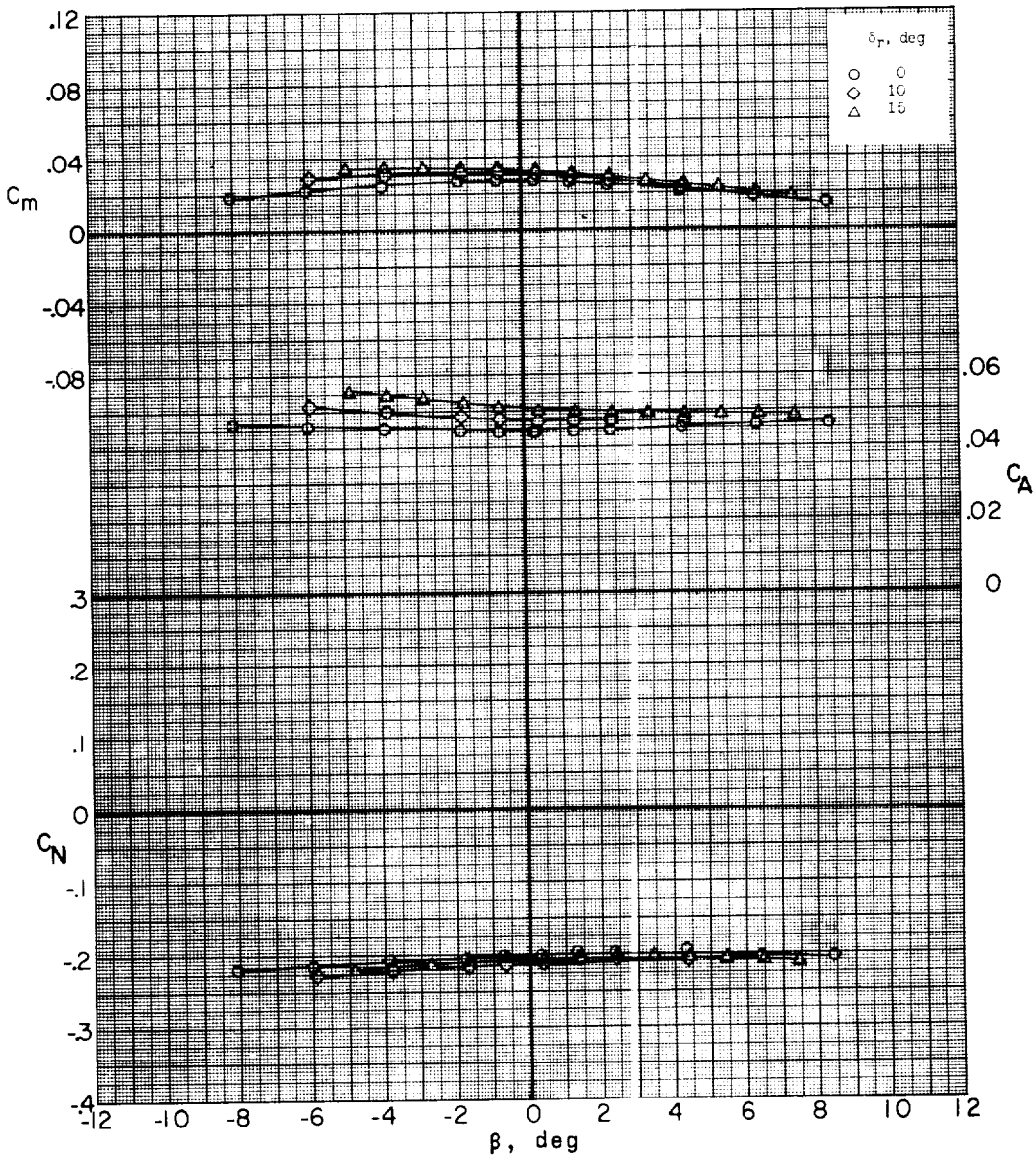
(c) Concluded.

Figure 14.- Continued.



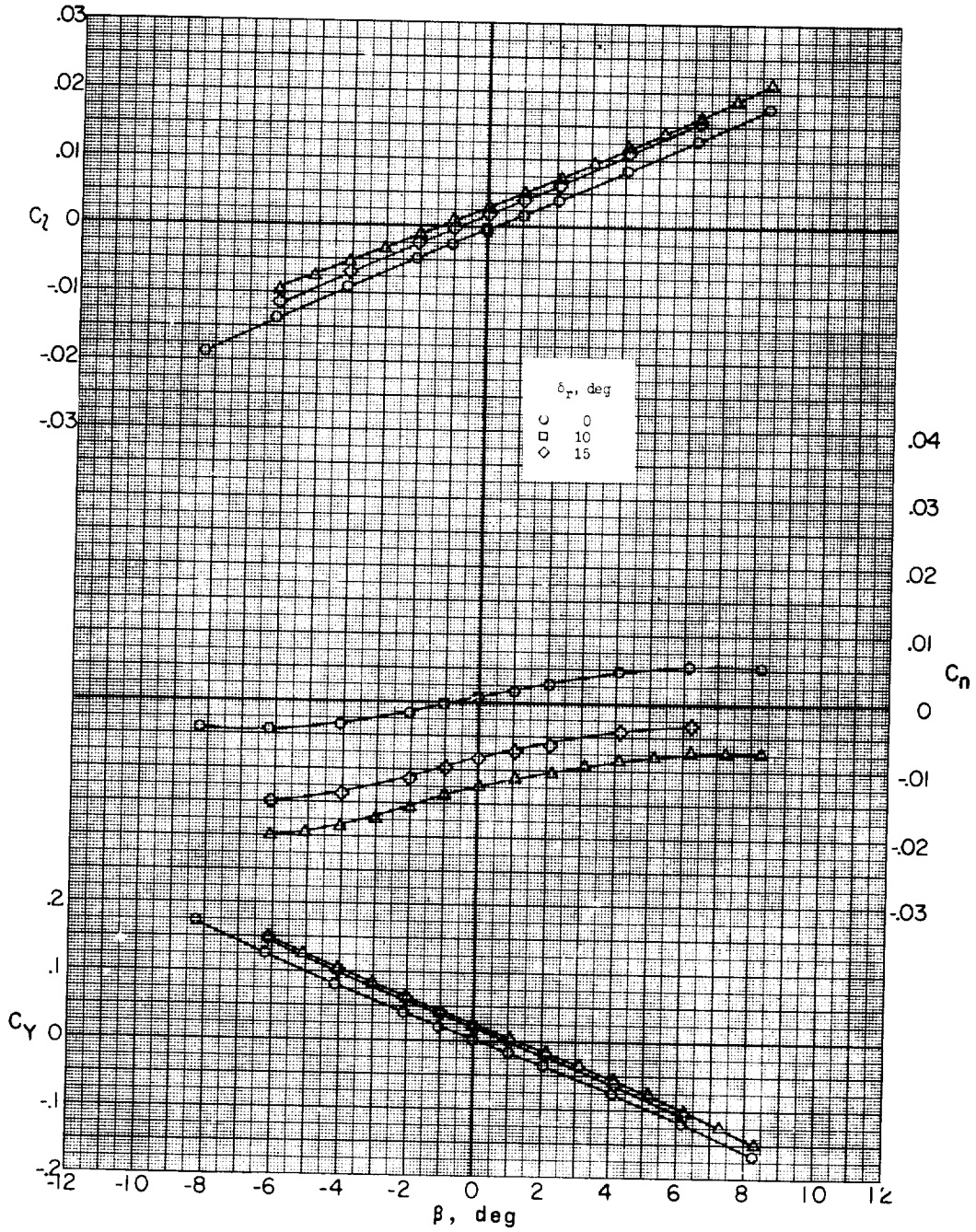
(d) M = 2.75; $\alpha = -5.2^{\circ}$.

Figure 14.- Continued.



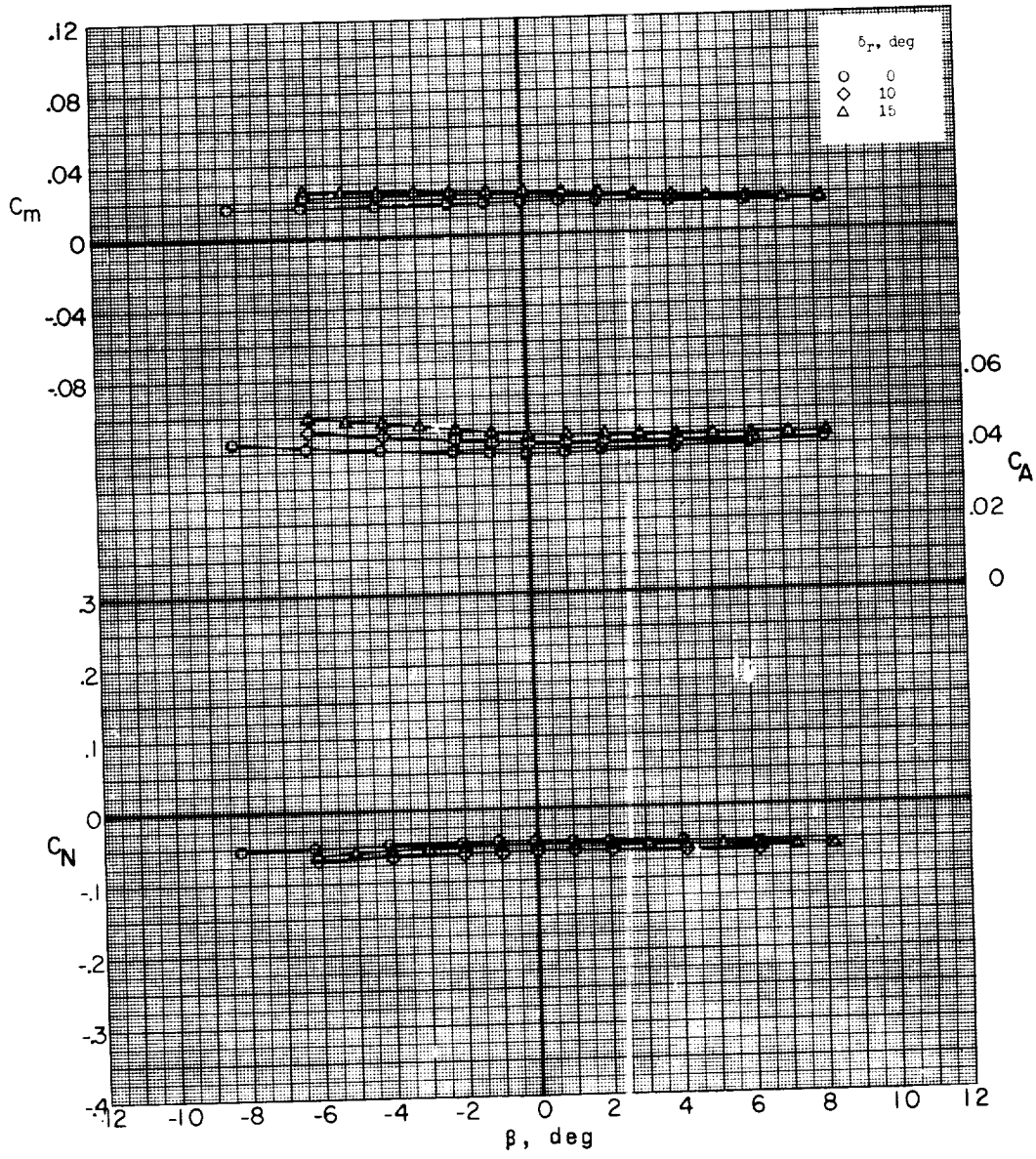
(d) Concluded

Figure 14.- Continued.



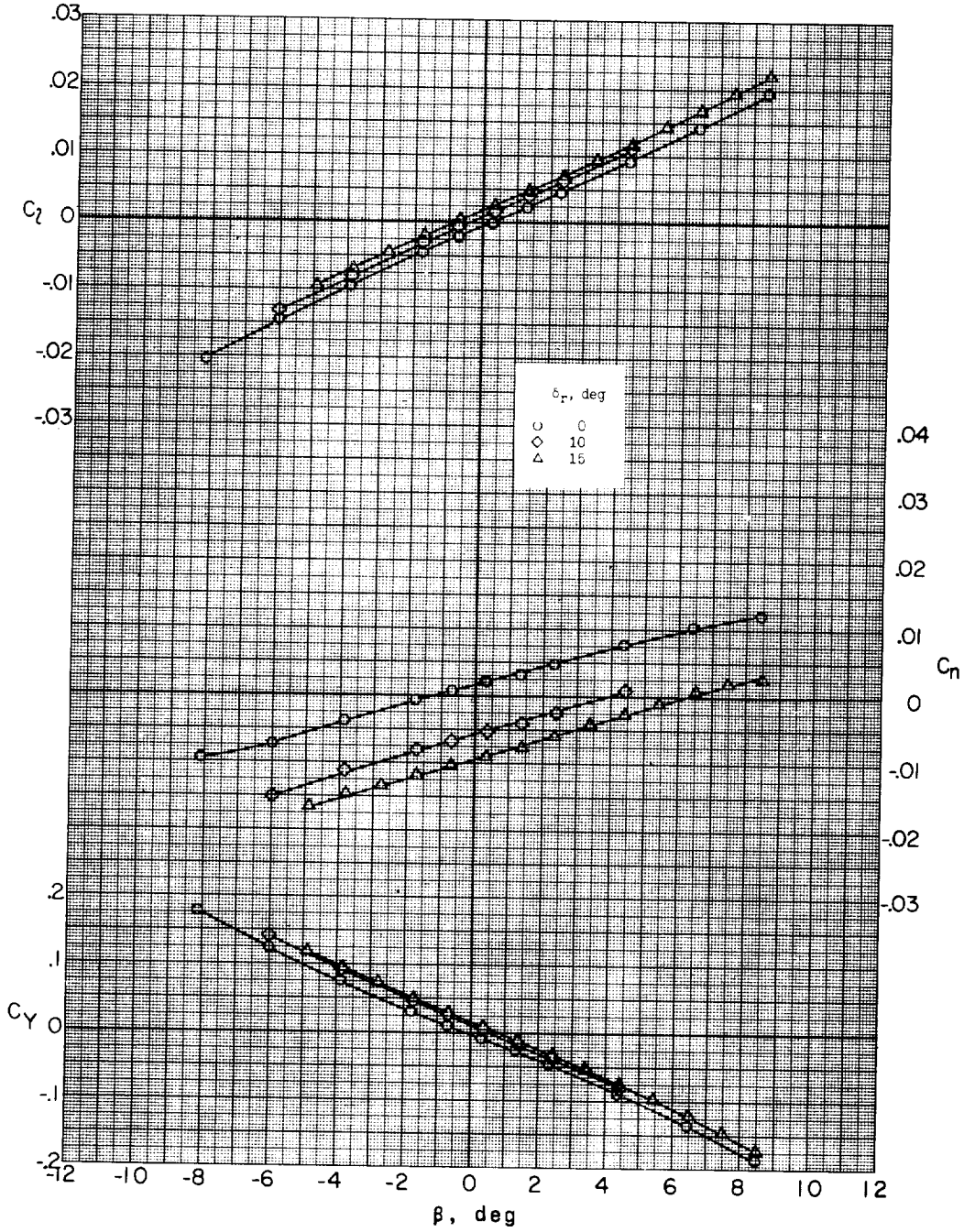
(e) M = 2.75; $\alpha = -0.3^\circ$.

Figure 14.- Continued.



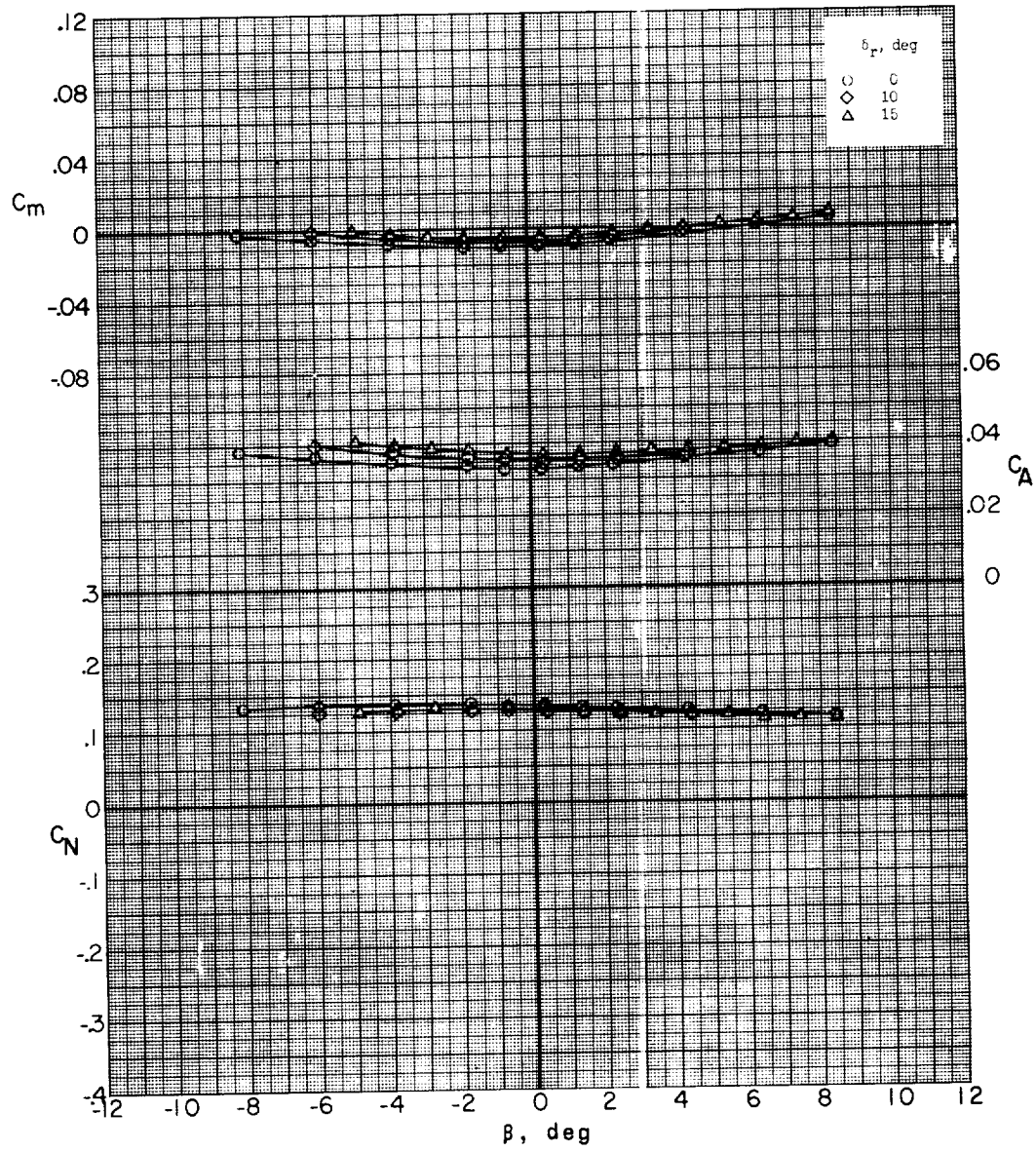
(e) Concluded.

Figure 14.- Continued.



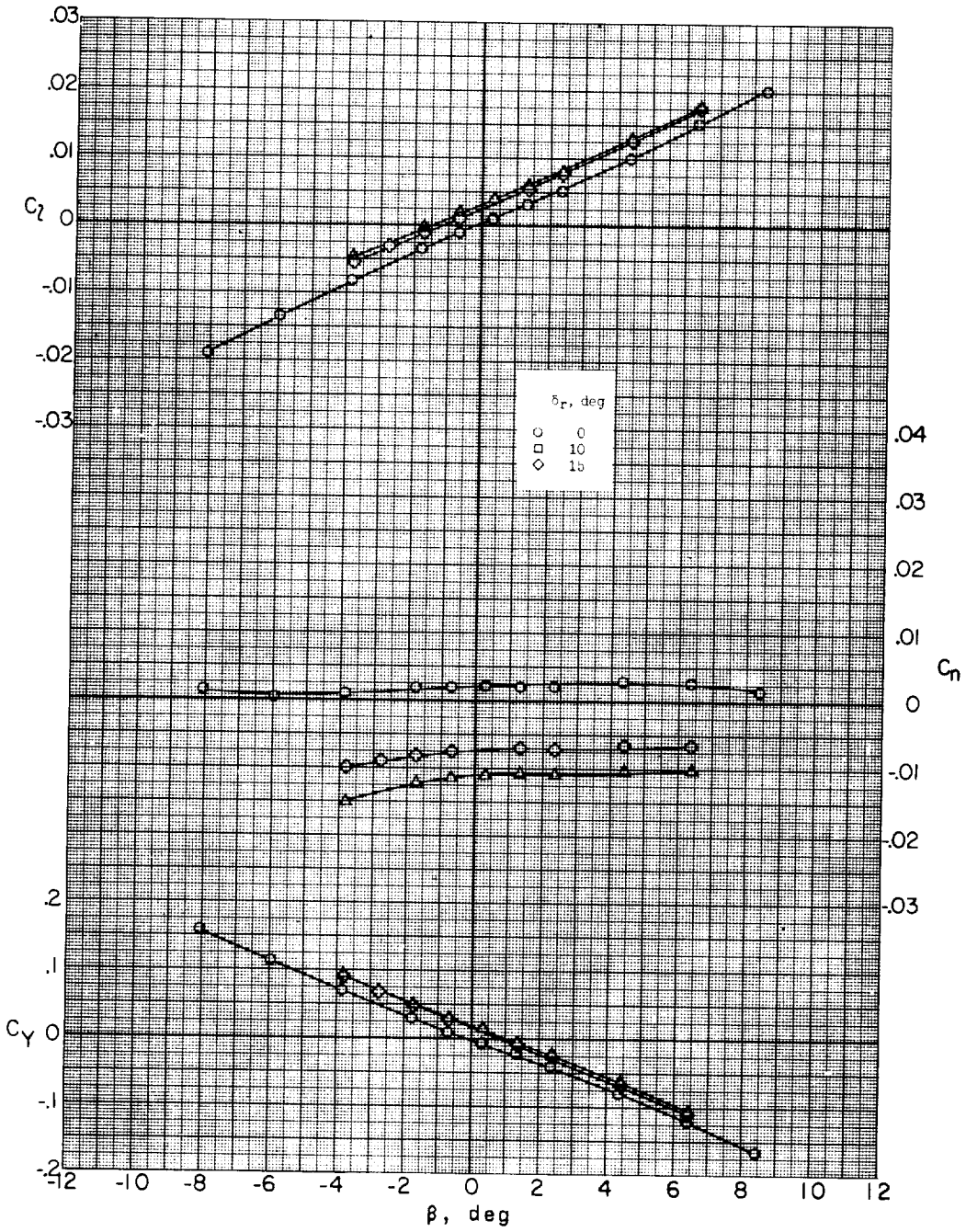
(f) M = 2.75; $\alpha = 5.2^{\circ}$.

Figure 14.- Continued.



(f) Concluded.

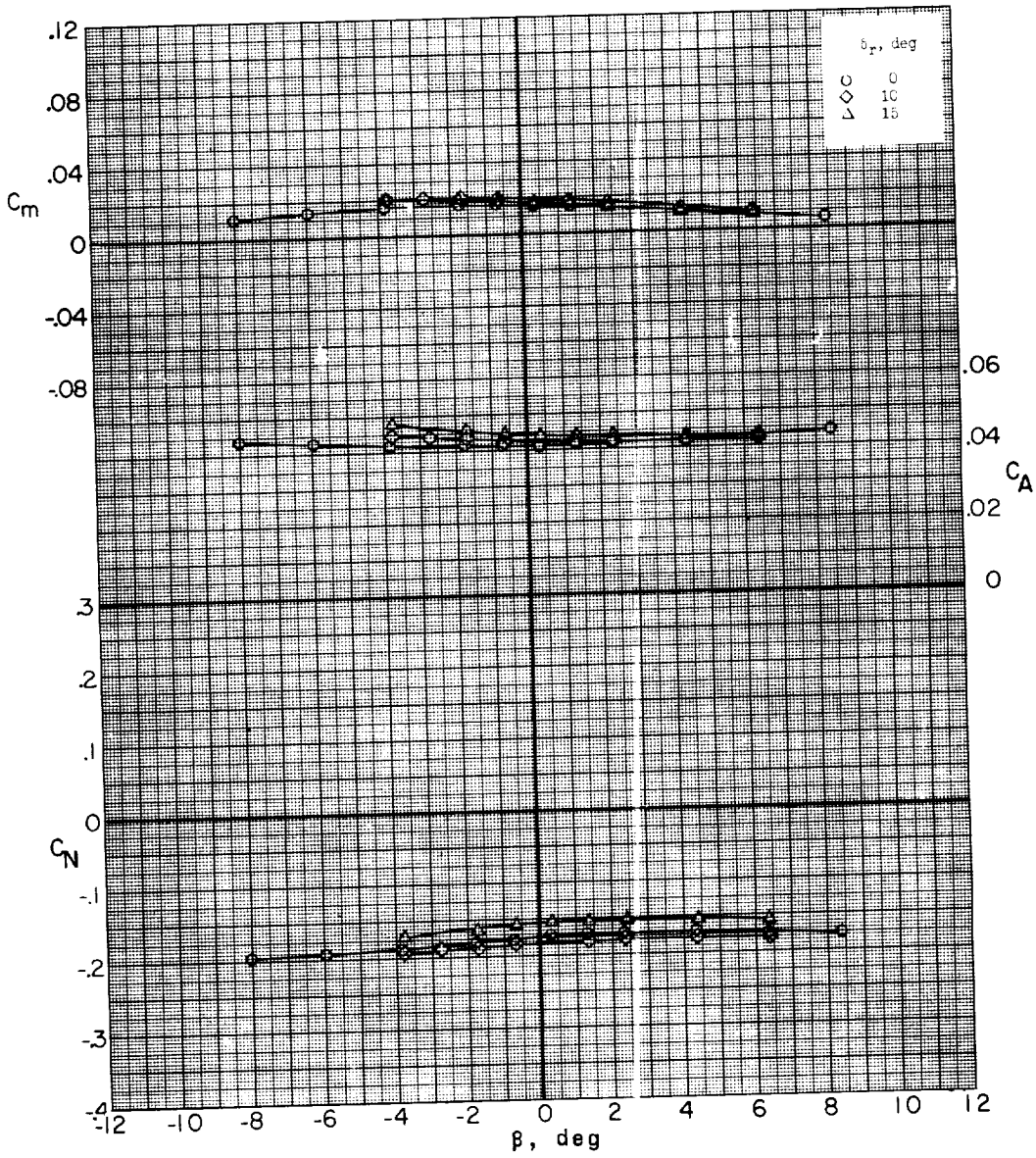
Figure 14.- Continued.



(g) M = 3.22; α = -5.2°.

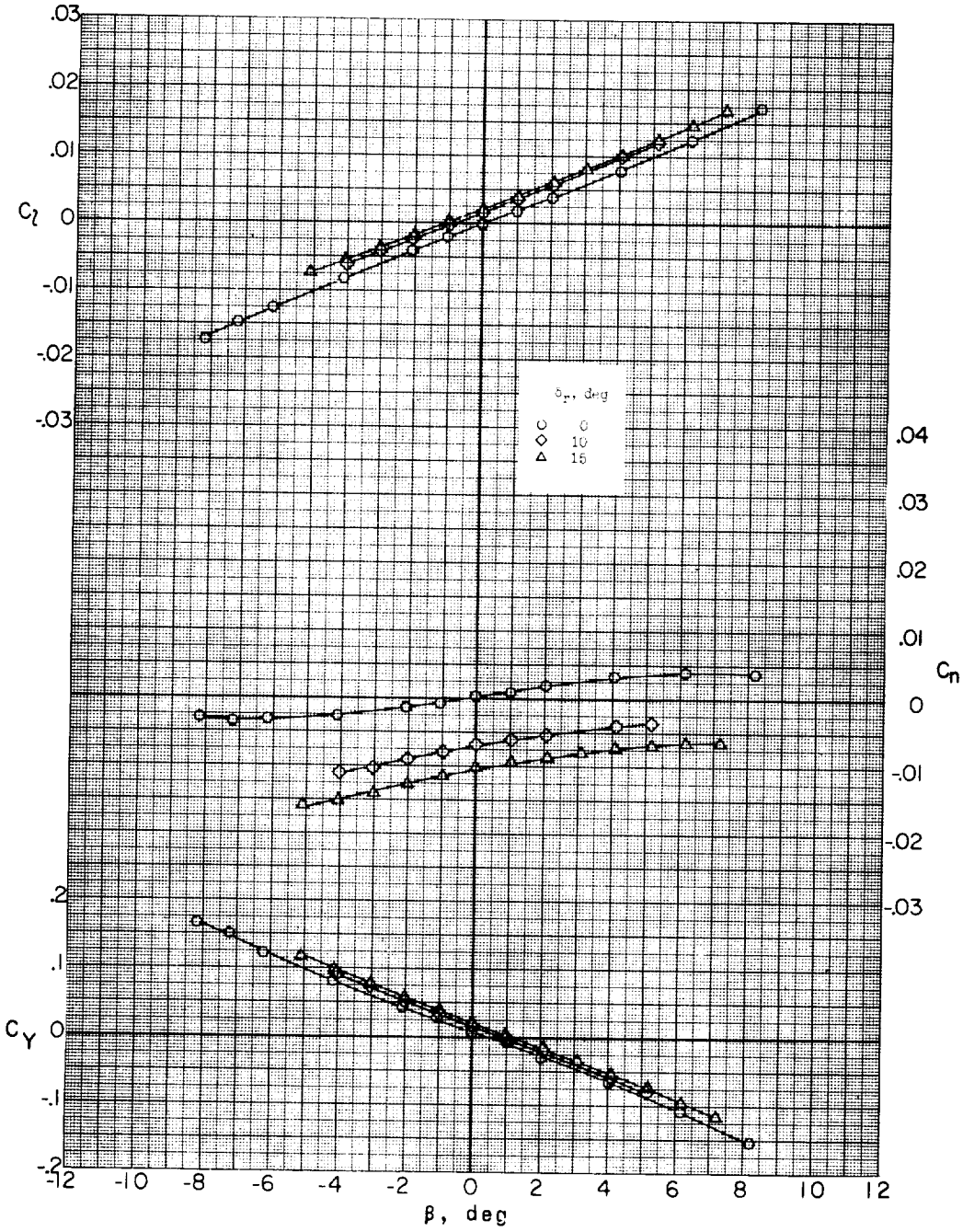
Figure 14.- Continued.

CONFIDENTIAL



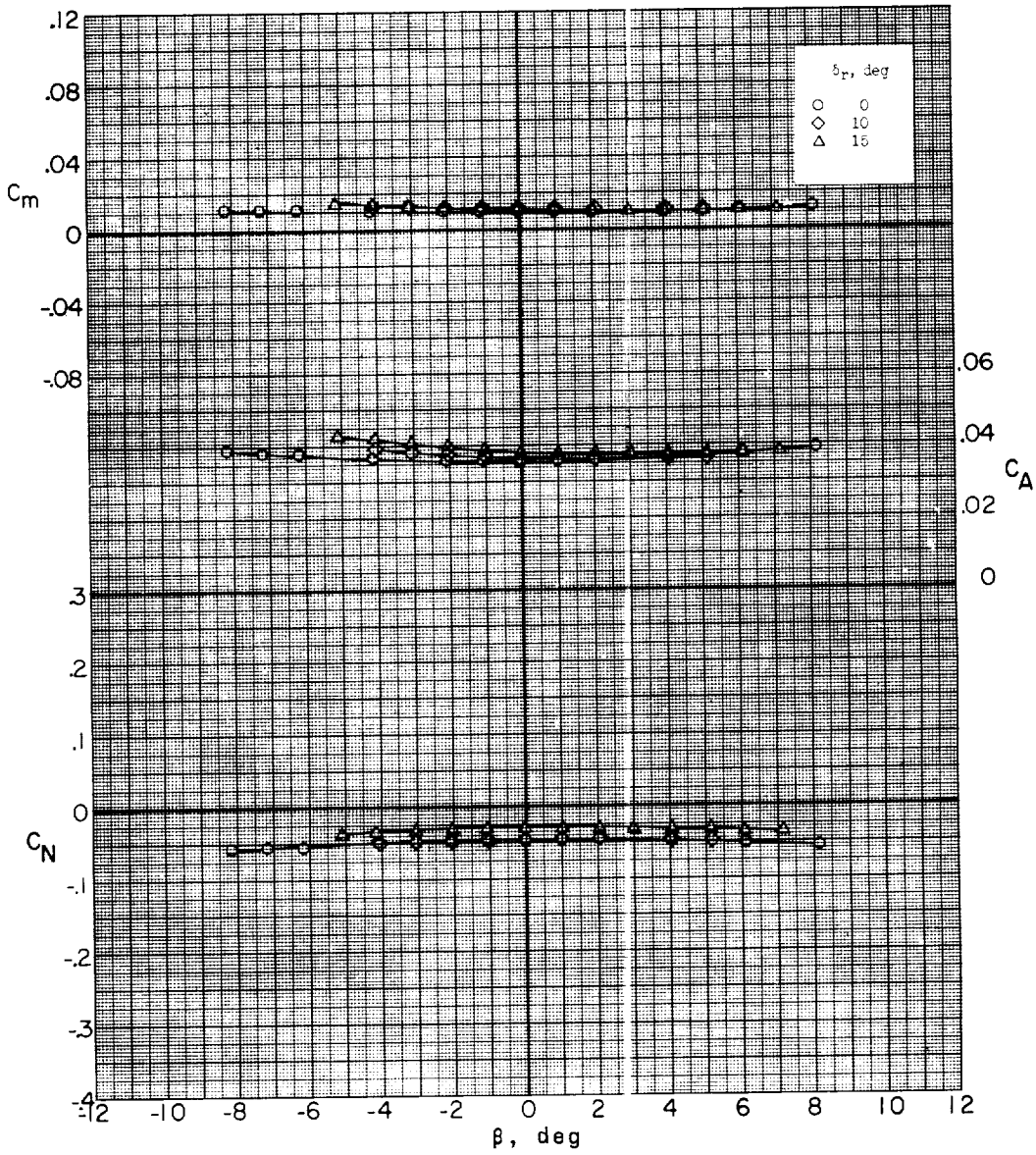
(g) Concluded.

Figure 14.- Continued.



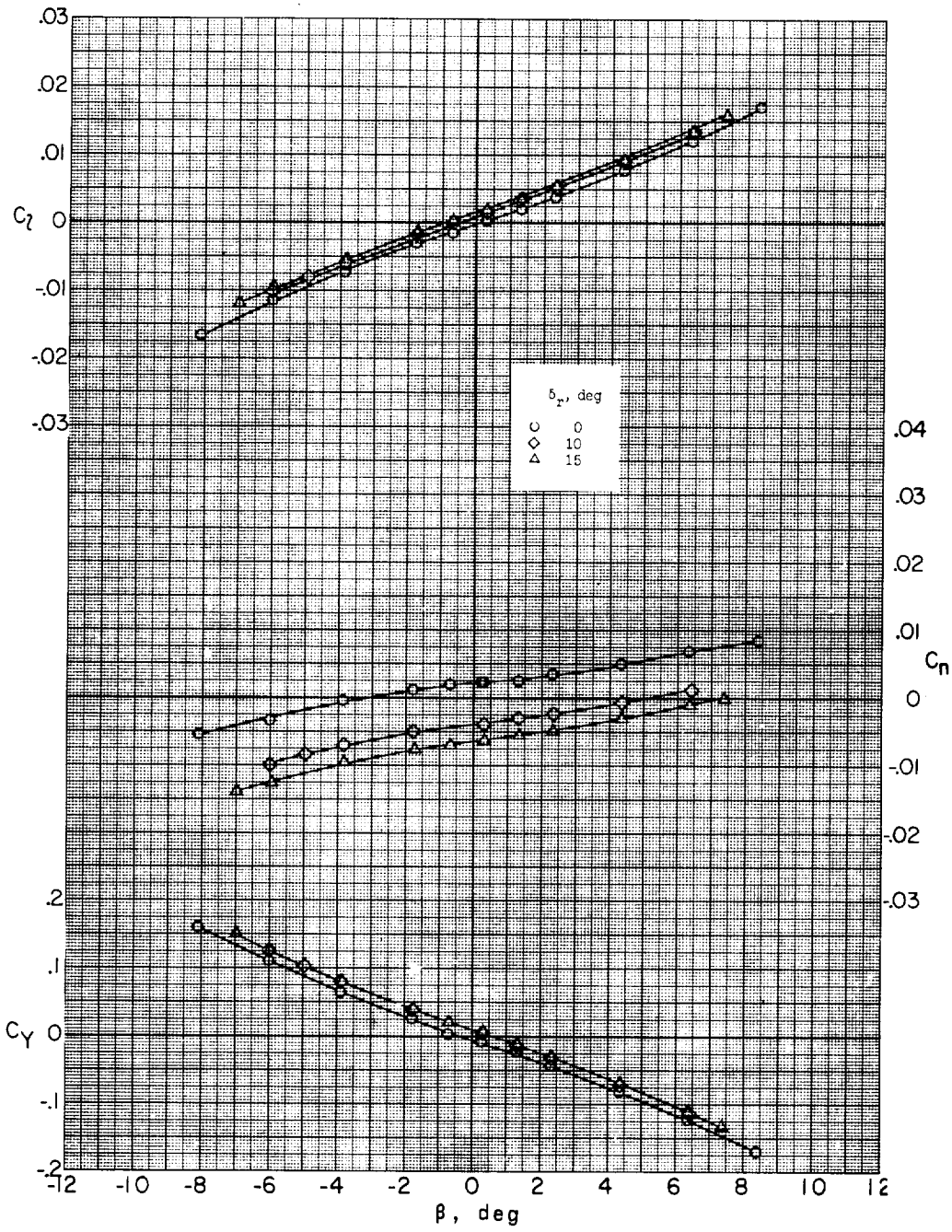
(h) $M = 3.22$; $\alpha = -0.3^{\circ}$.

Figure 14.- Continued.



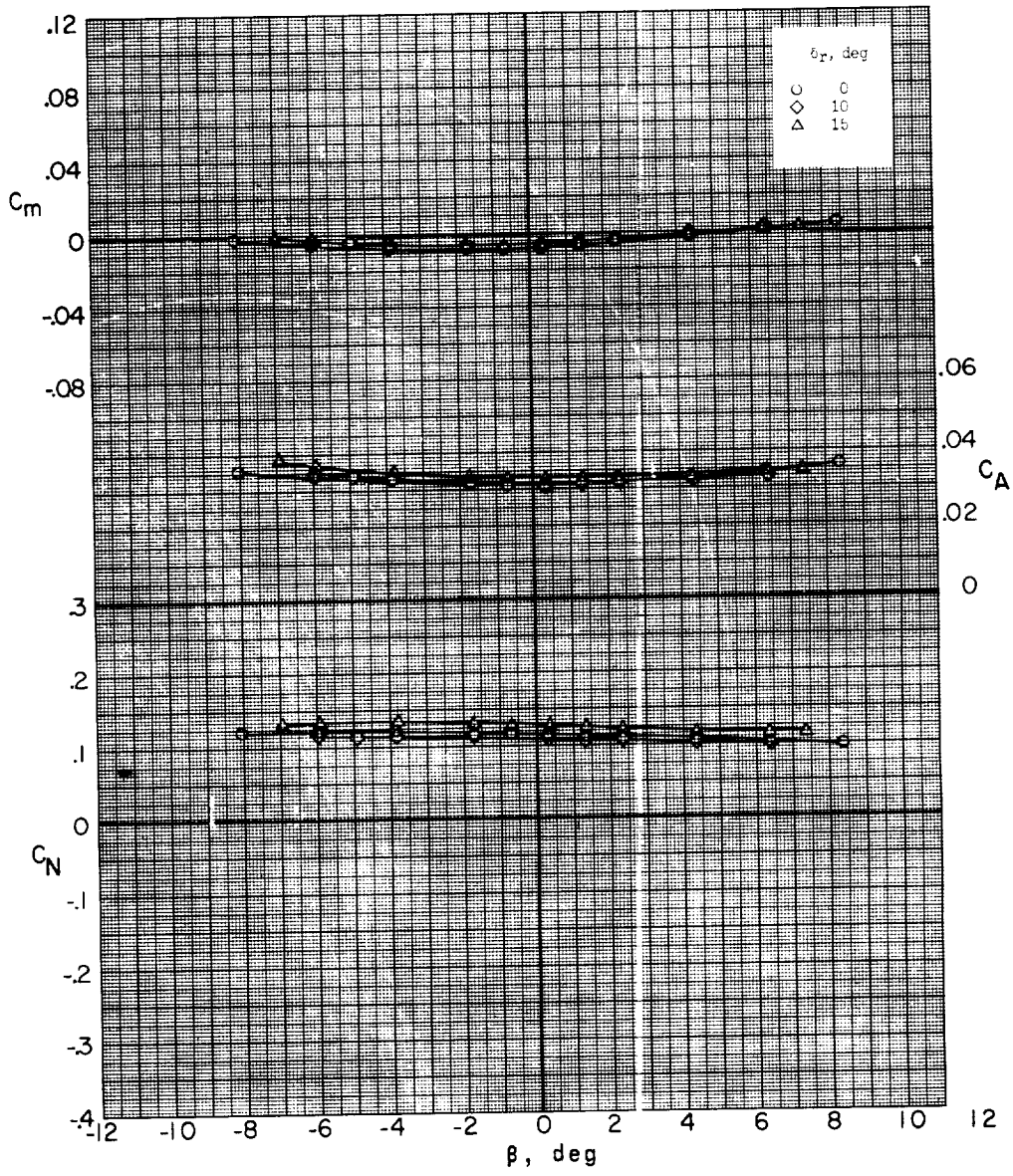
(h) Concluded.

Figure 14.- Continued.



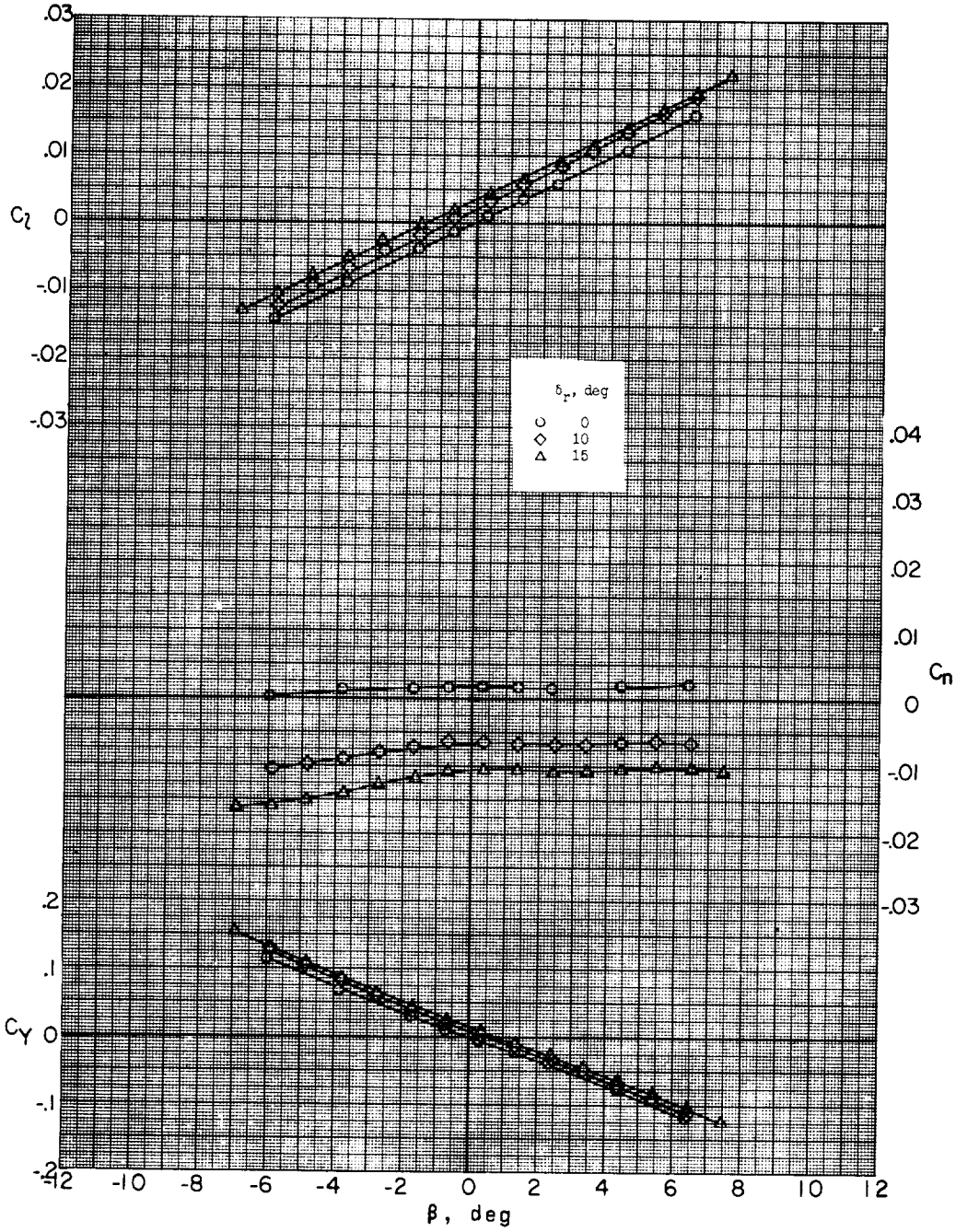
(i) M = 3.22; $\alpha = 5.1^{\circ}$.

Figure 14.- Continued.



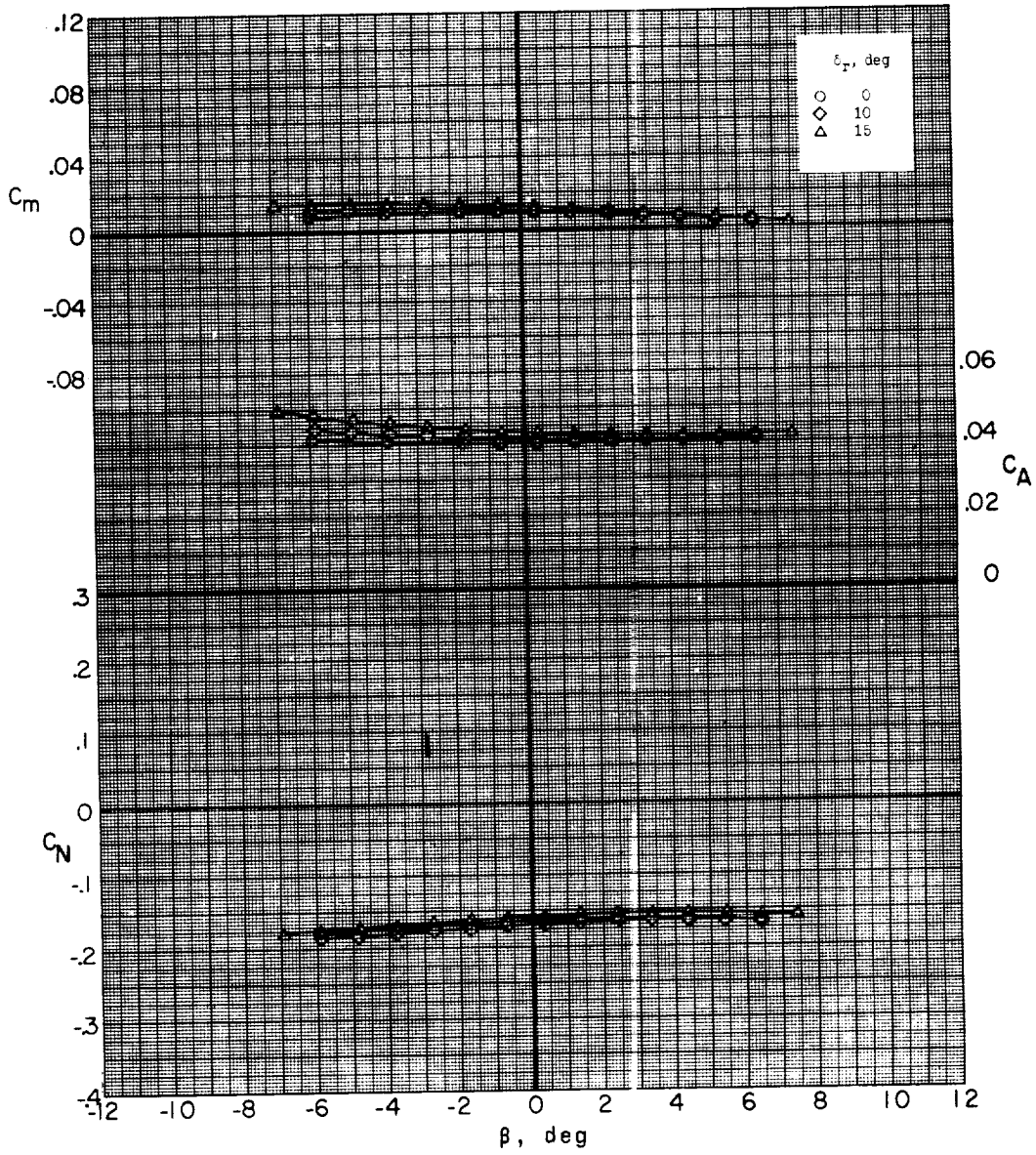
(i) Concluded.

Figure 14.- Continued.



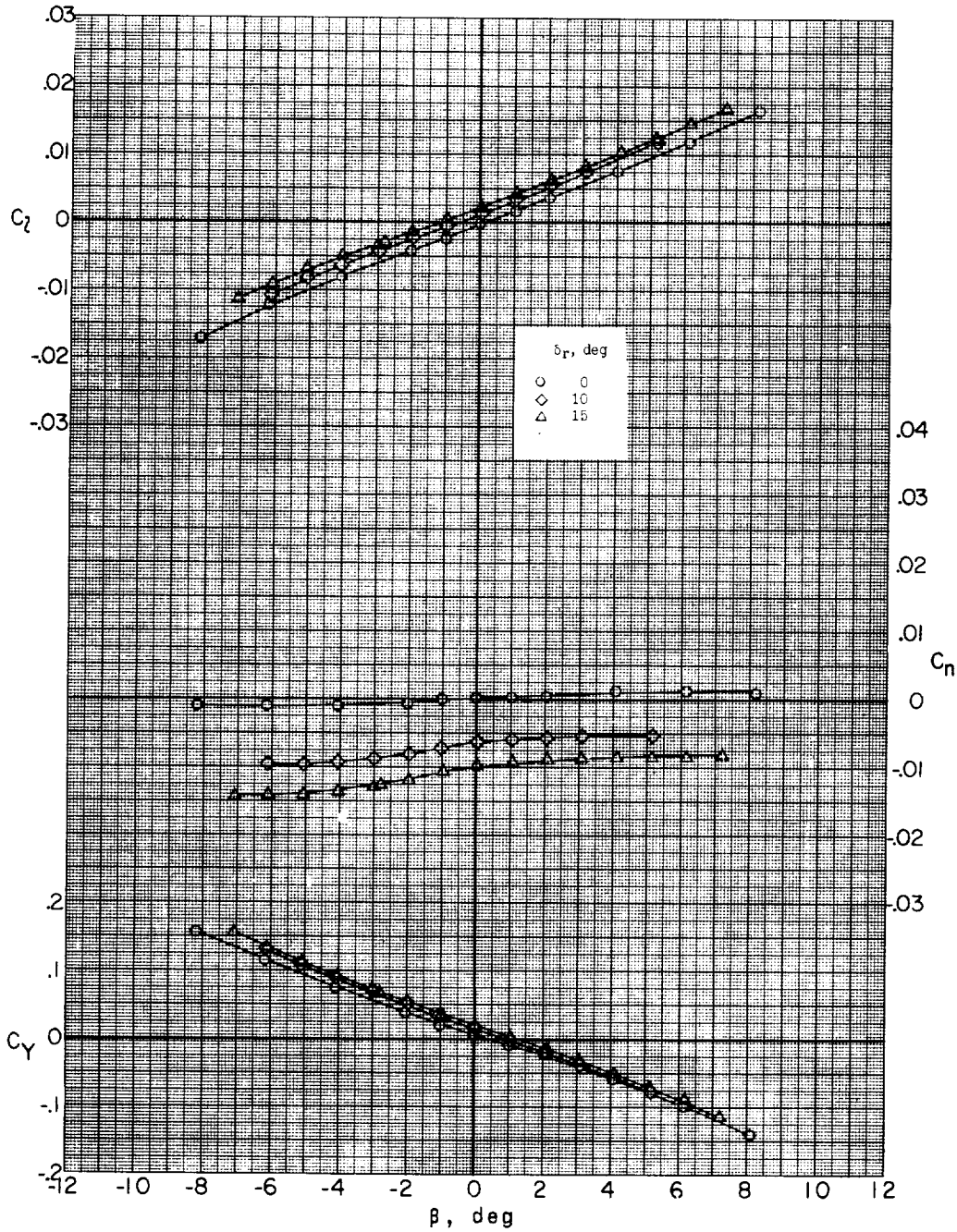
(j) M = 3.51; α = -5.2°.

Figure 14.- Continued.



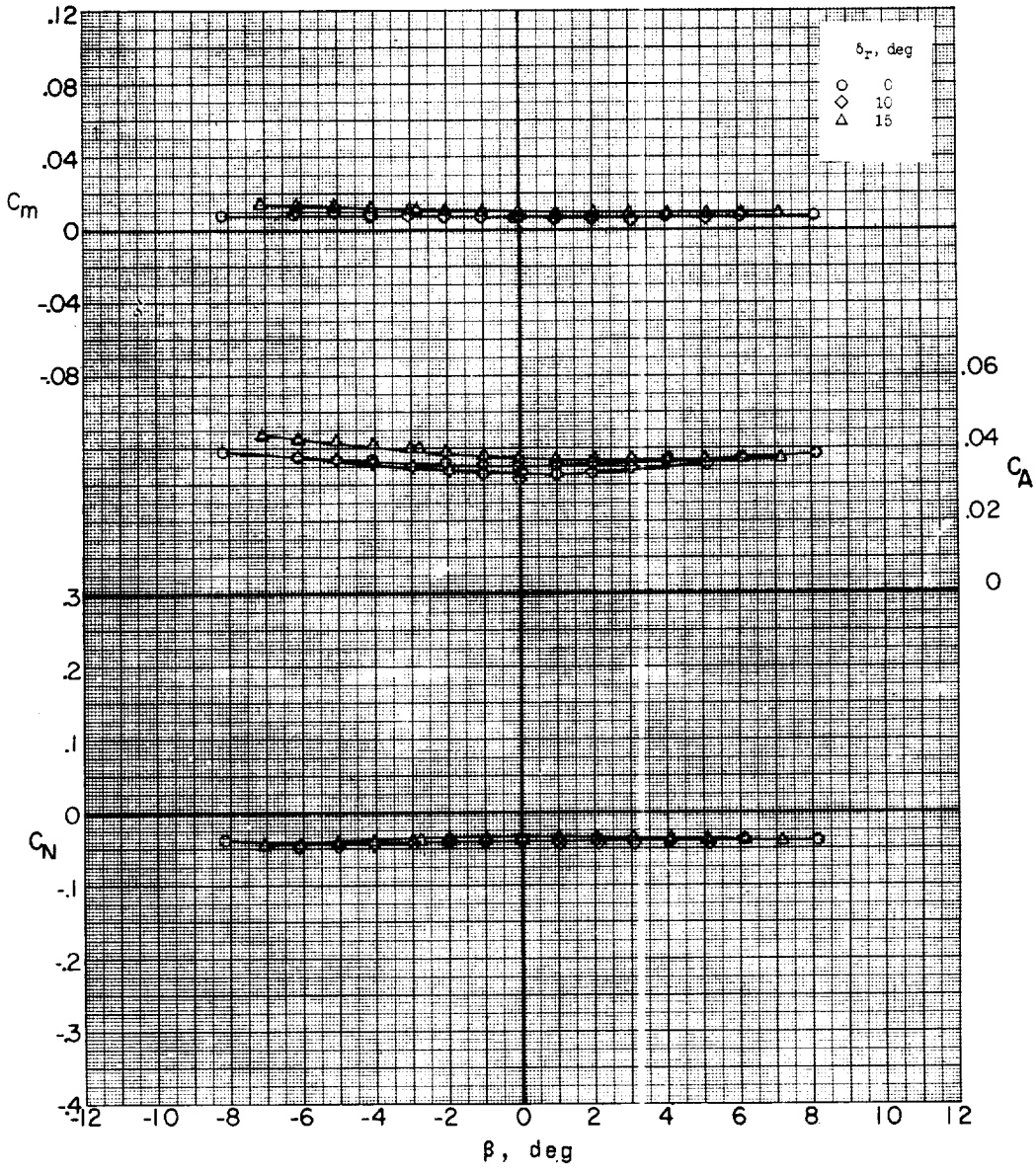
(j) Concluded.

Figure 14.- Continued.



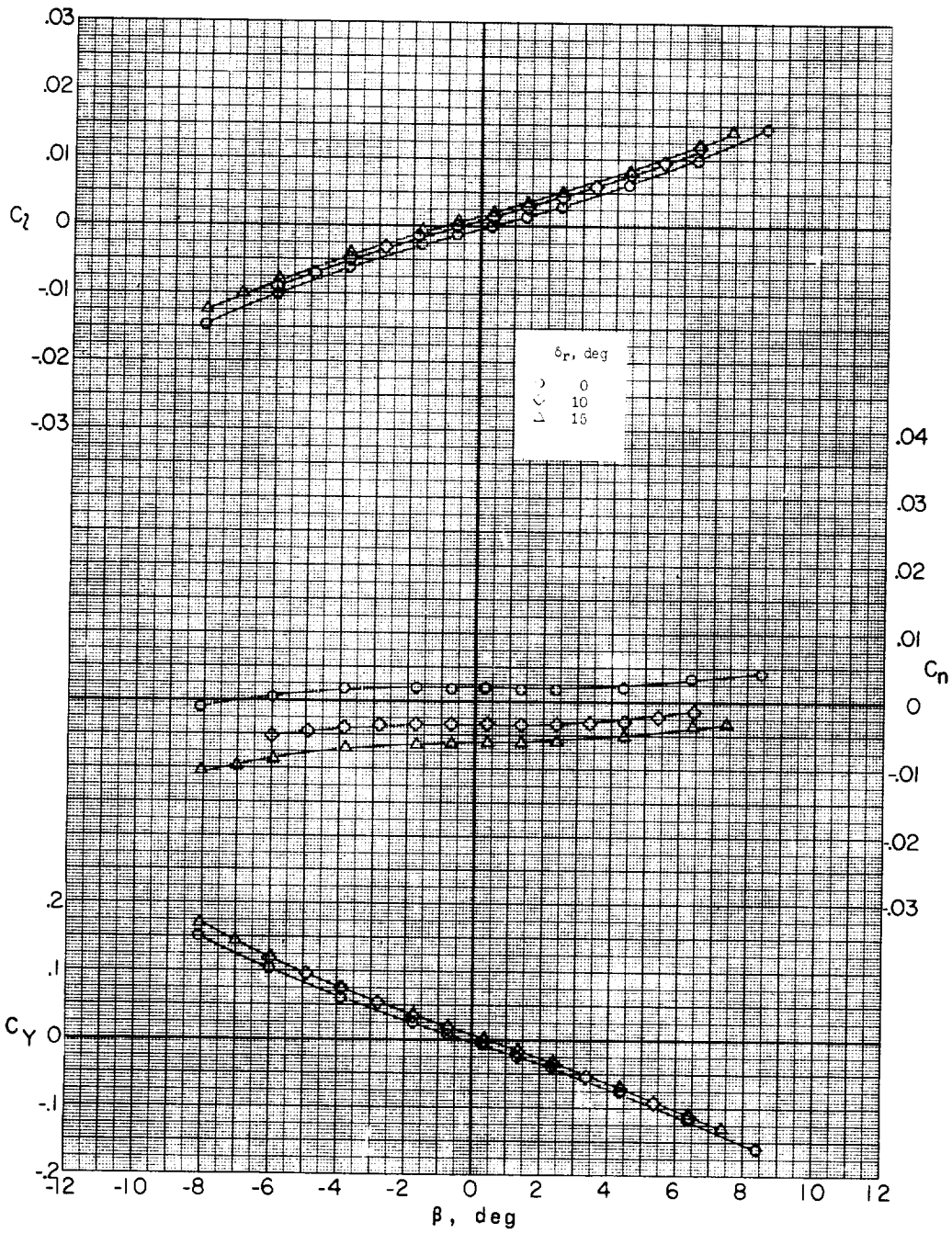
(k) M = 3.51; $\alpha = -0.3^\circ$.

Figure 14.- Continued.



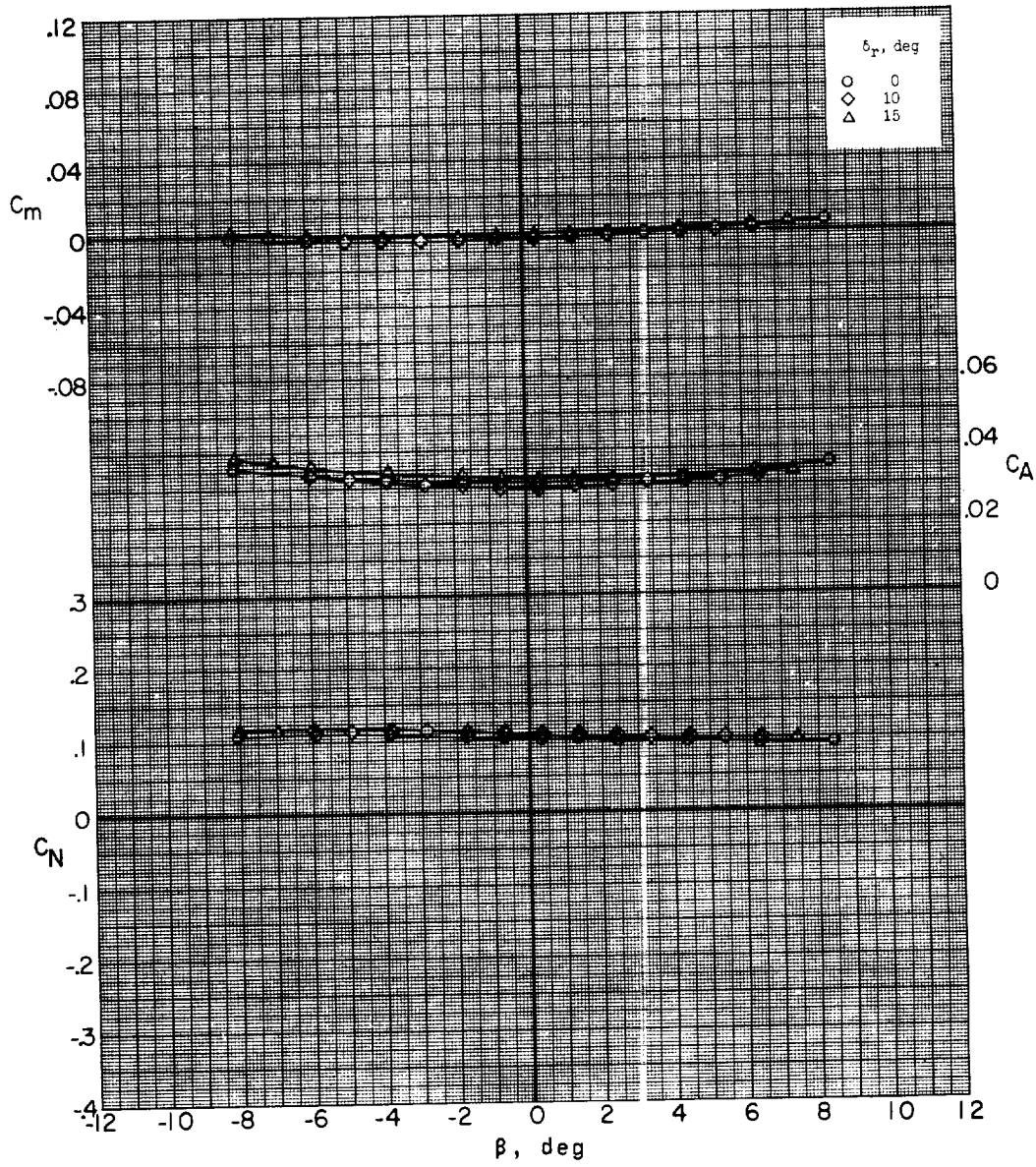
(k) Concluded.

Figure 14.- Continued.



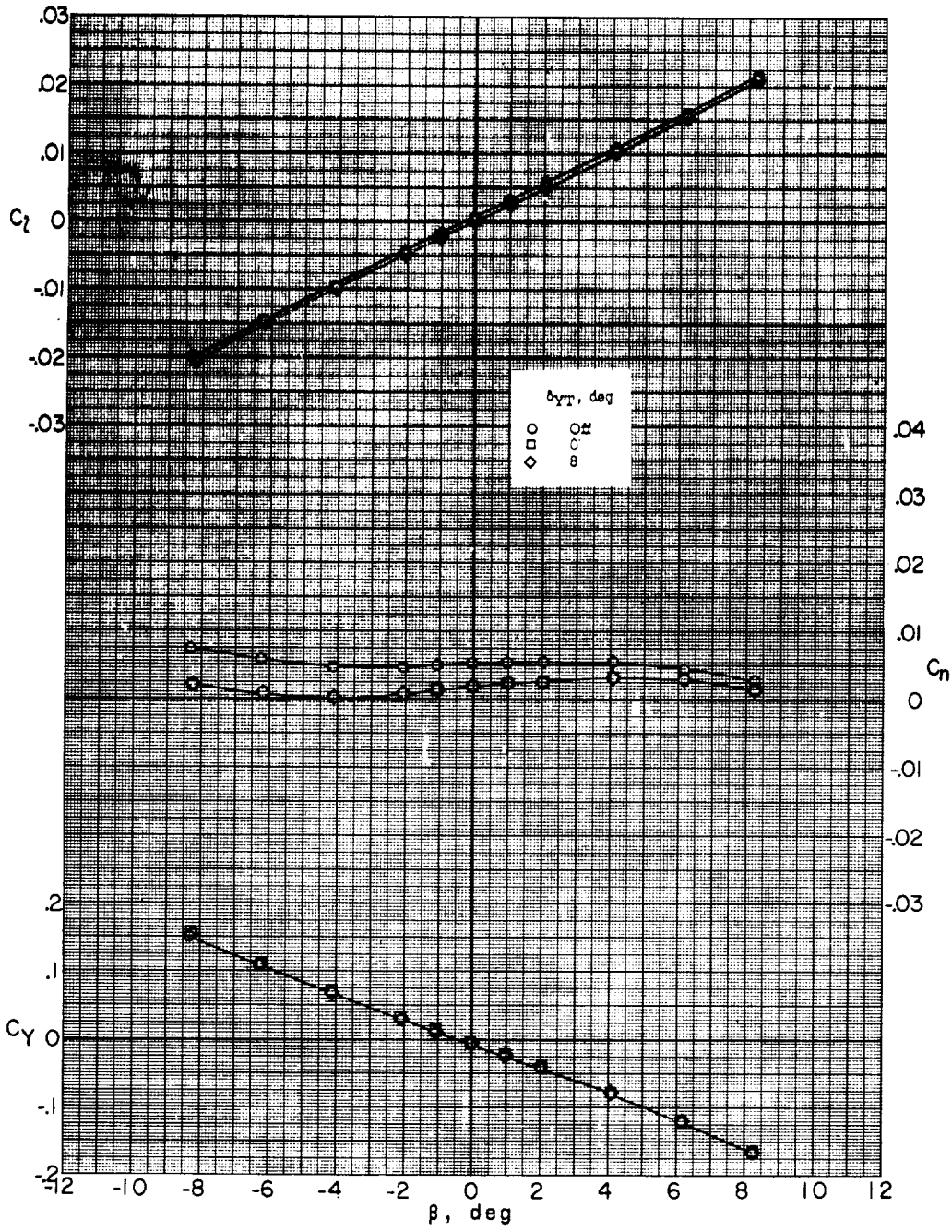
(l) M = 3.51; $\alpha = 5.1^{\circ}$.

Figure 14.- Continued.



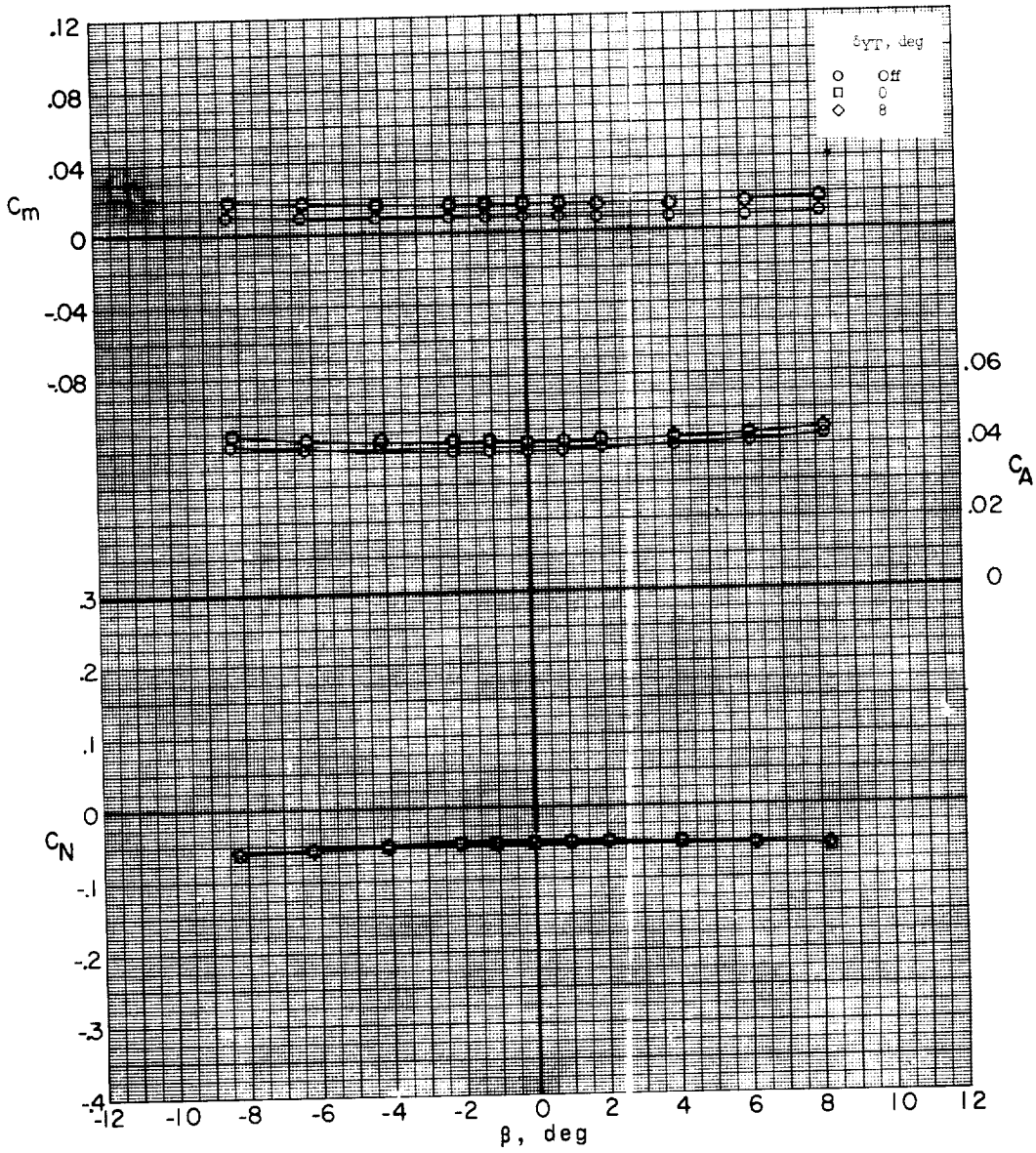
(l) Concluded.

Figure 14.- Concluded.



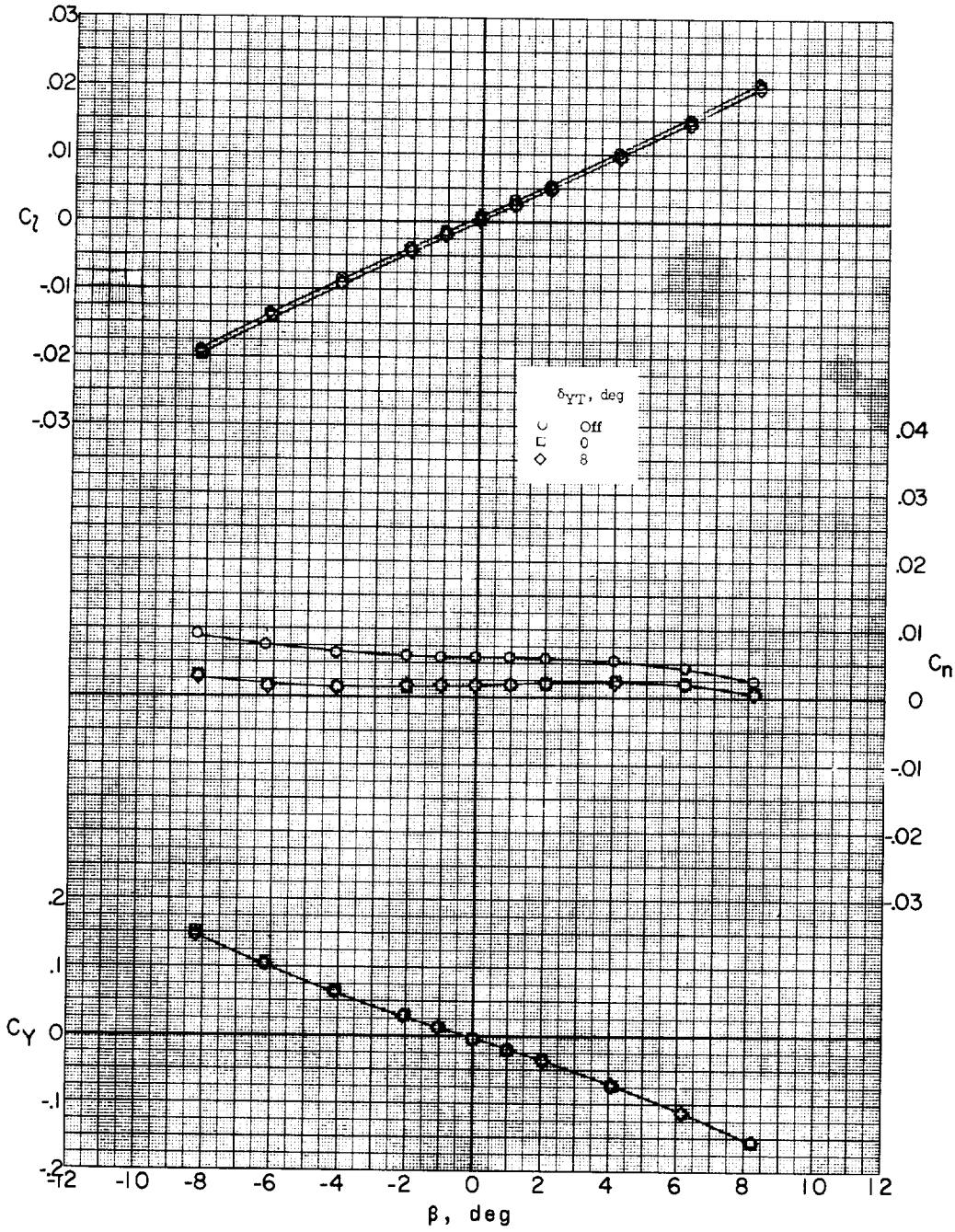
(a) M = 2.75.

Figure 15.- Effect of booster nozzle on lateral characteristics of missile-booster combination with bug-eye fairing and A-frame mounted. $\delta_{PT} = 0^\circ$; $\alpha = -0.3^\circ$; sting B.



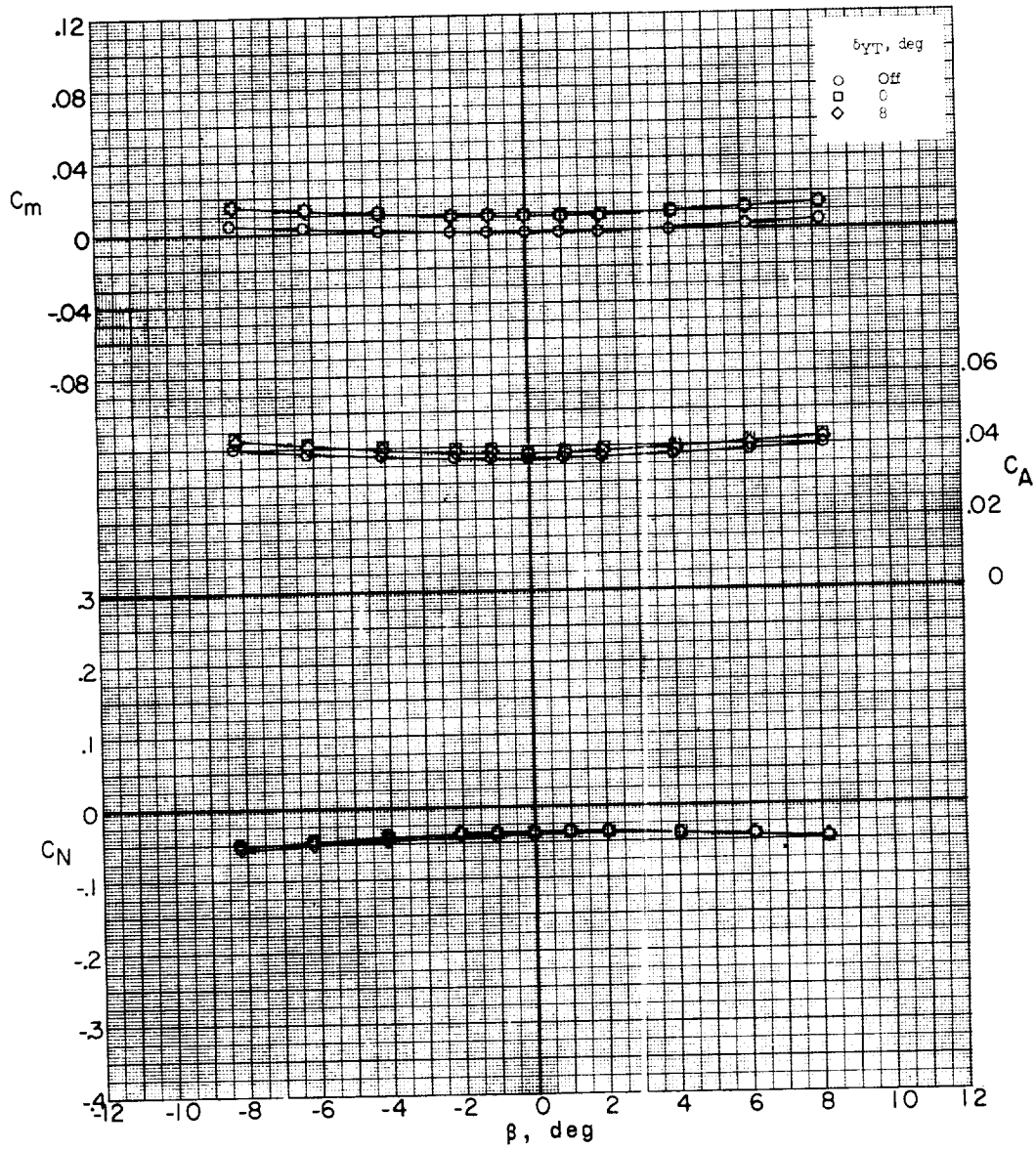
(a) Concluded.

Figure 15.- Continued.



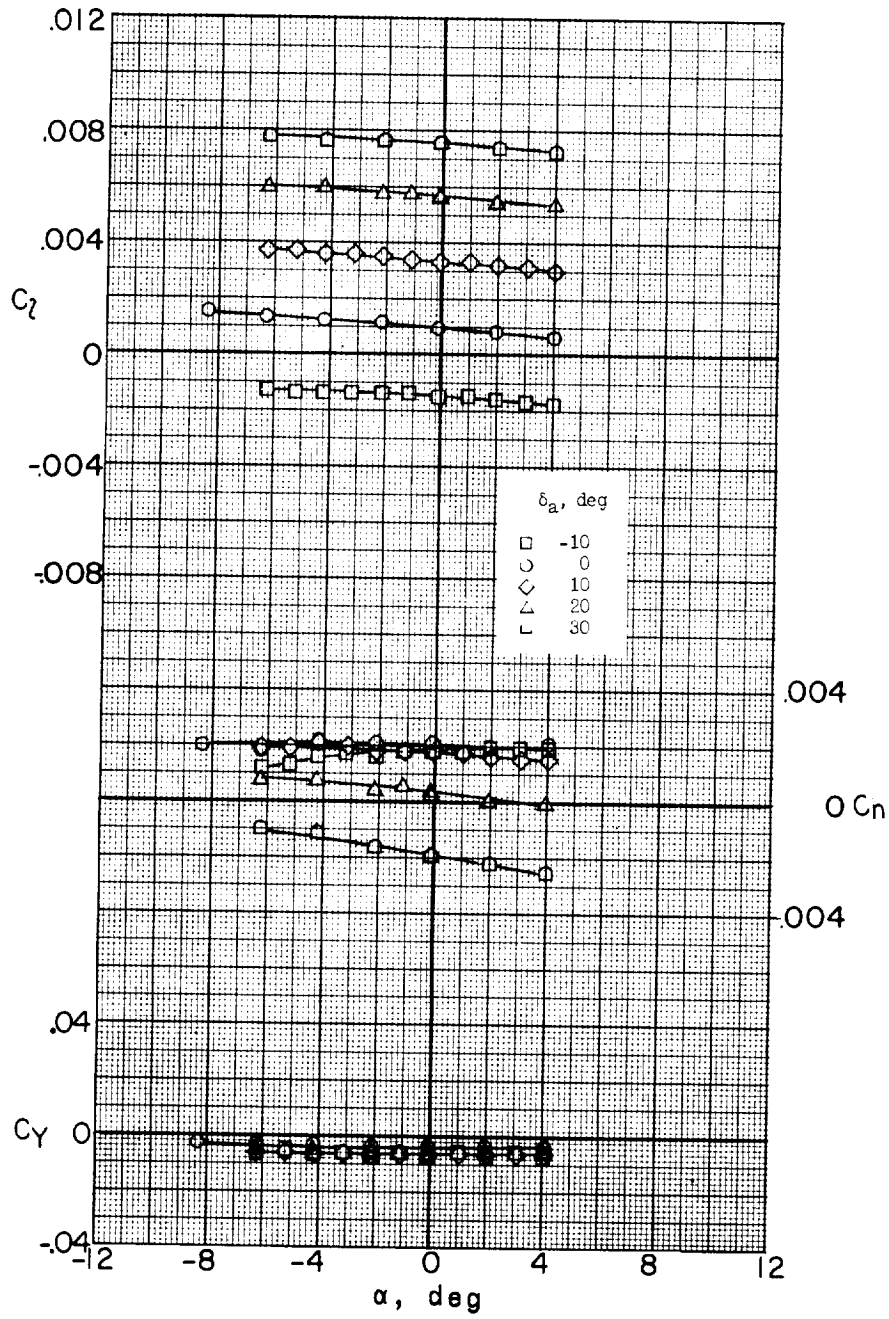
(b) M = 3.22.

Figure 15.- Continued.



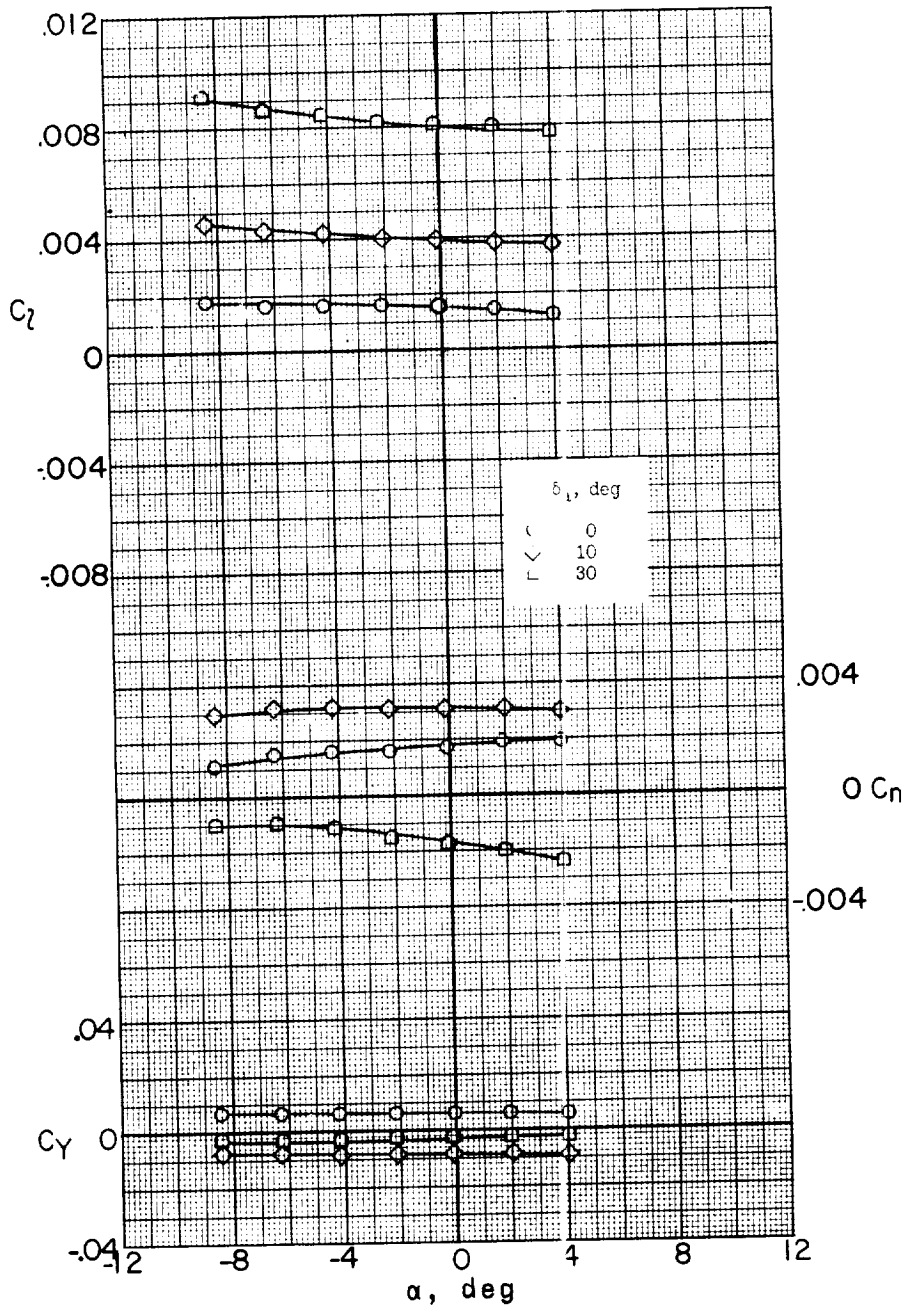
(b) Concluded.

Figure 15.- Concluded.



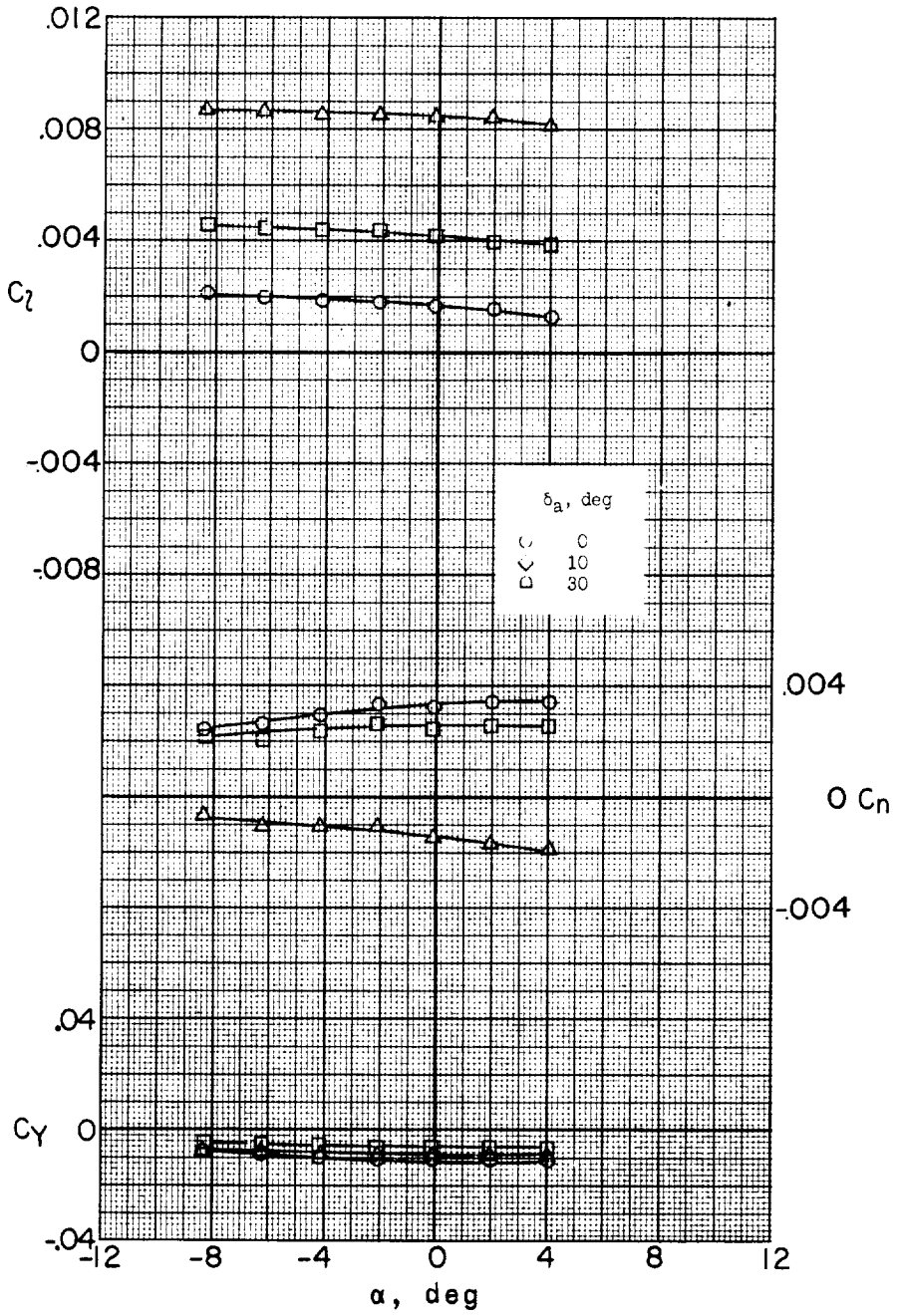
(a) M = 3.22; sting A.

Figure 16.- Effect of aileron deflection on lateral characteristics of missile-booster combination with A-frame mounted. $\delta_e = 0^\circ$; $\beta = 0.2^\circ$.



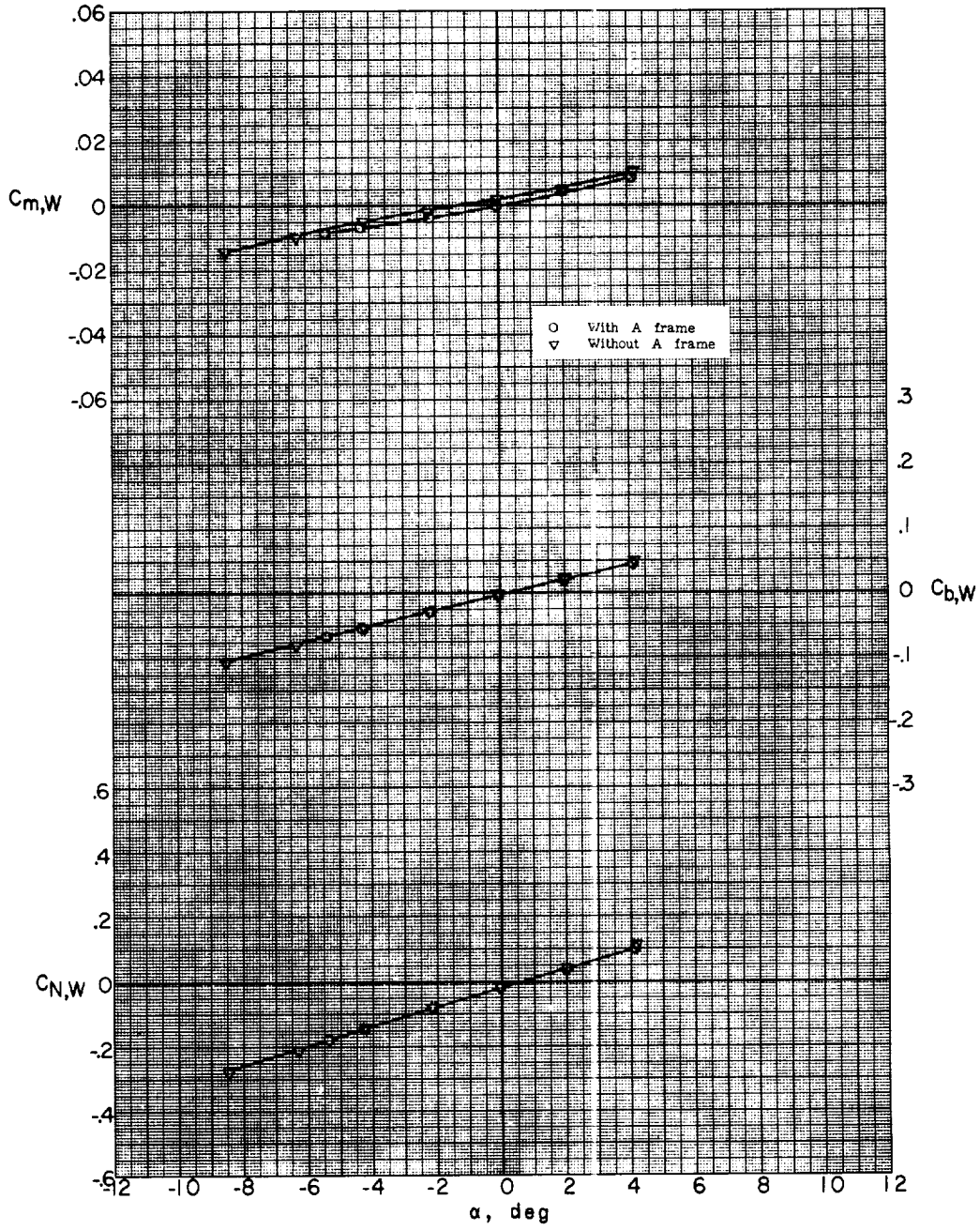
(b) M = 2.75; with missile aileron actuator housing; sting B.

Figure 16.- Continued.



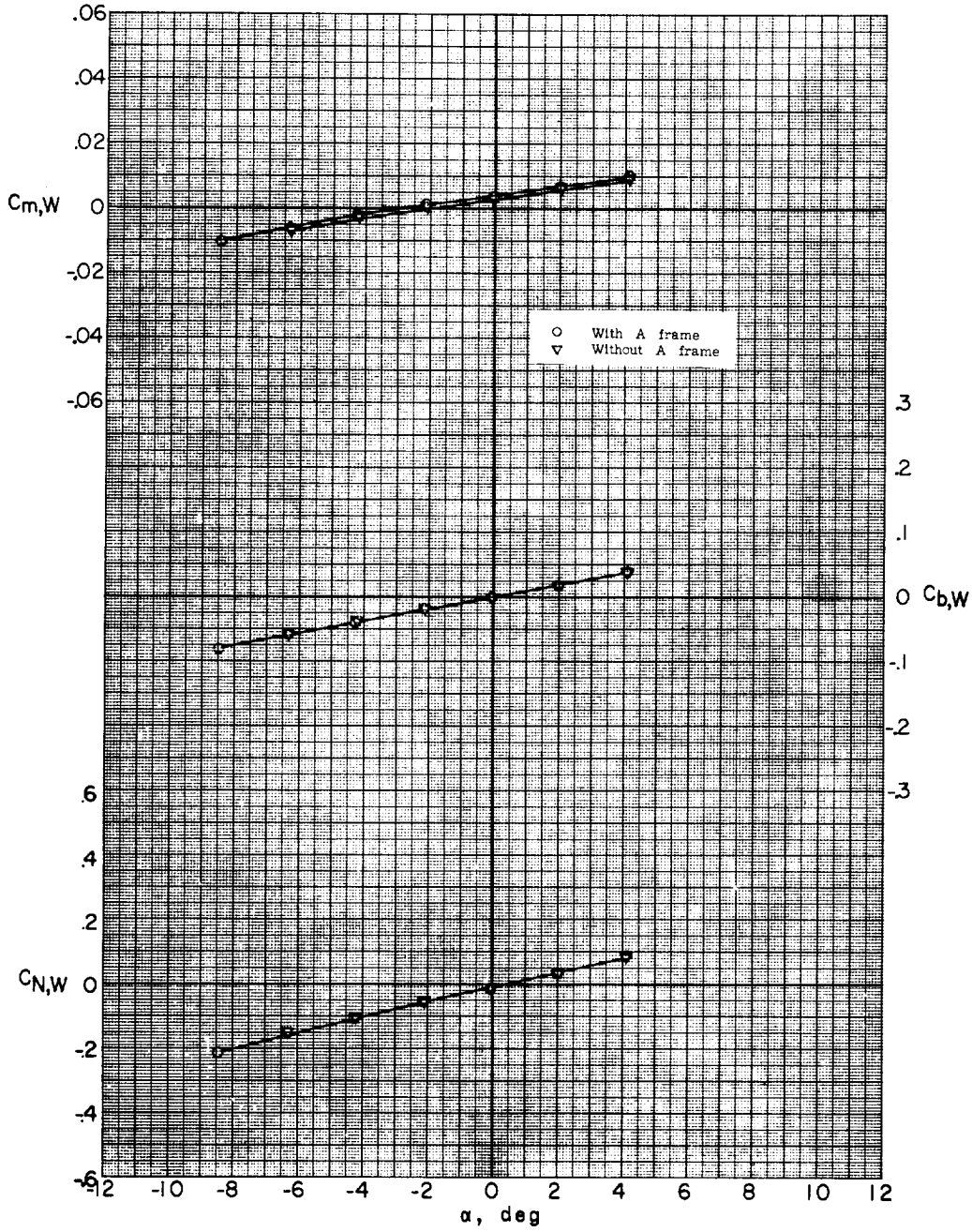
(c) M = 3.22; with missile aileron actuator housing; sting B.

Figure 16.- Concluded.



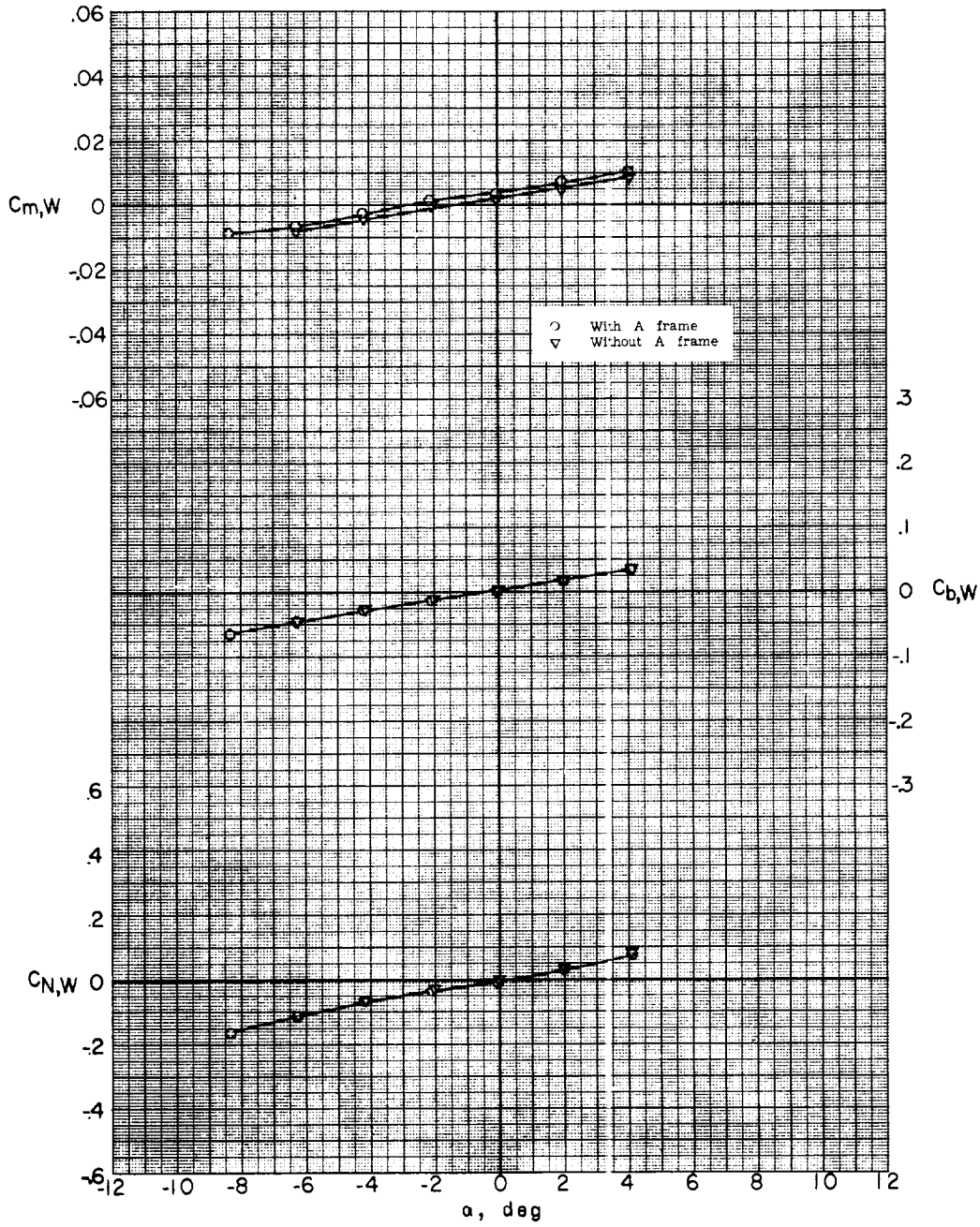
(a) M = 2.29.

Figure 17.- Effect of A-frame on pitch characteristics of missile wing. Missile-booster combination; $\delta_e = 0^\circ$; $\beta = 0.3^\circ$; sting A.



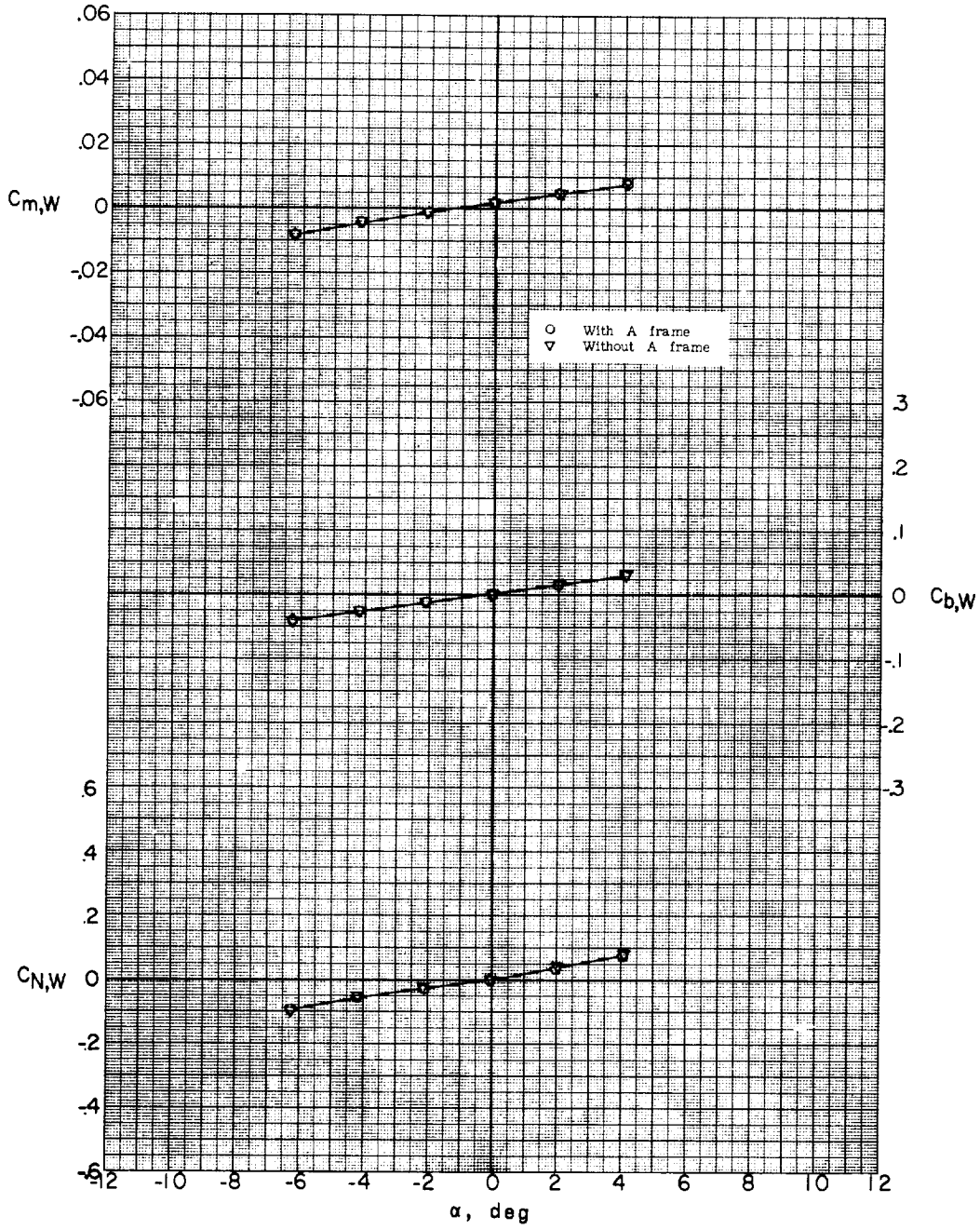
(b) M = 2.75.

Figure 17.- Continued.



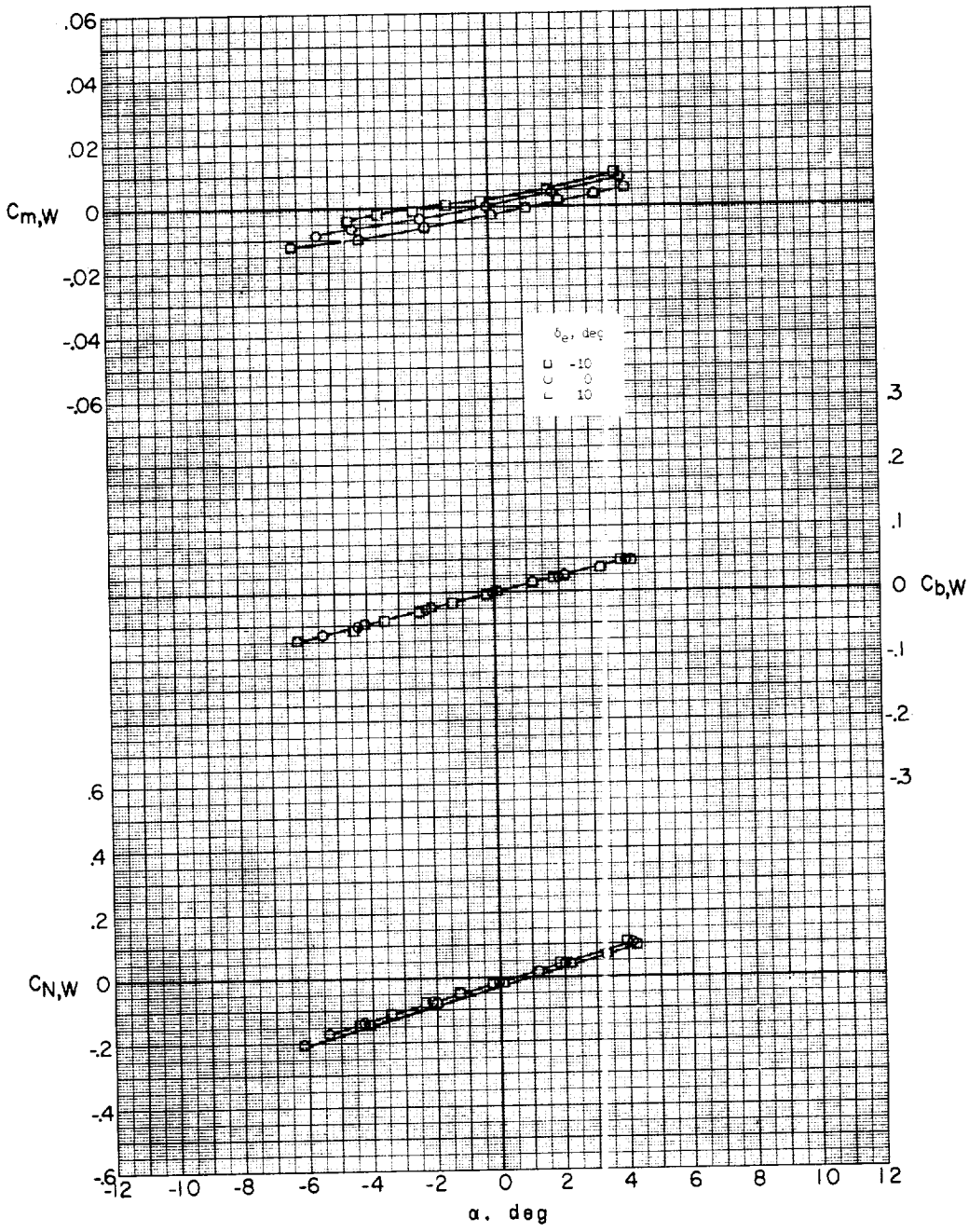
(c) M = 3.22.

Figure 17.- Continued.



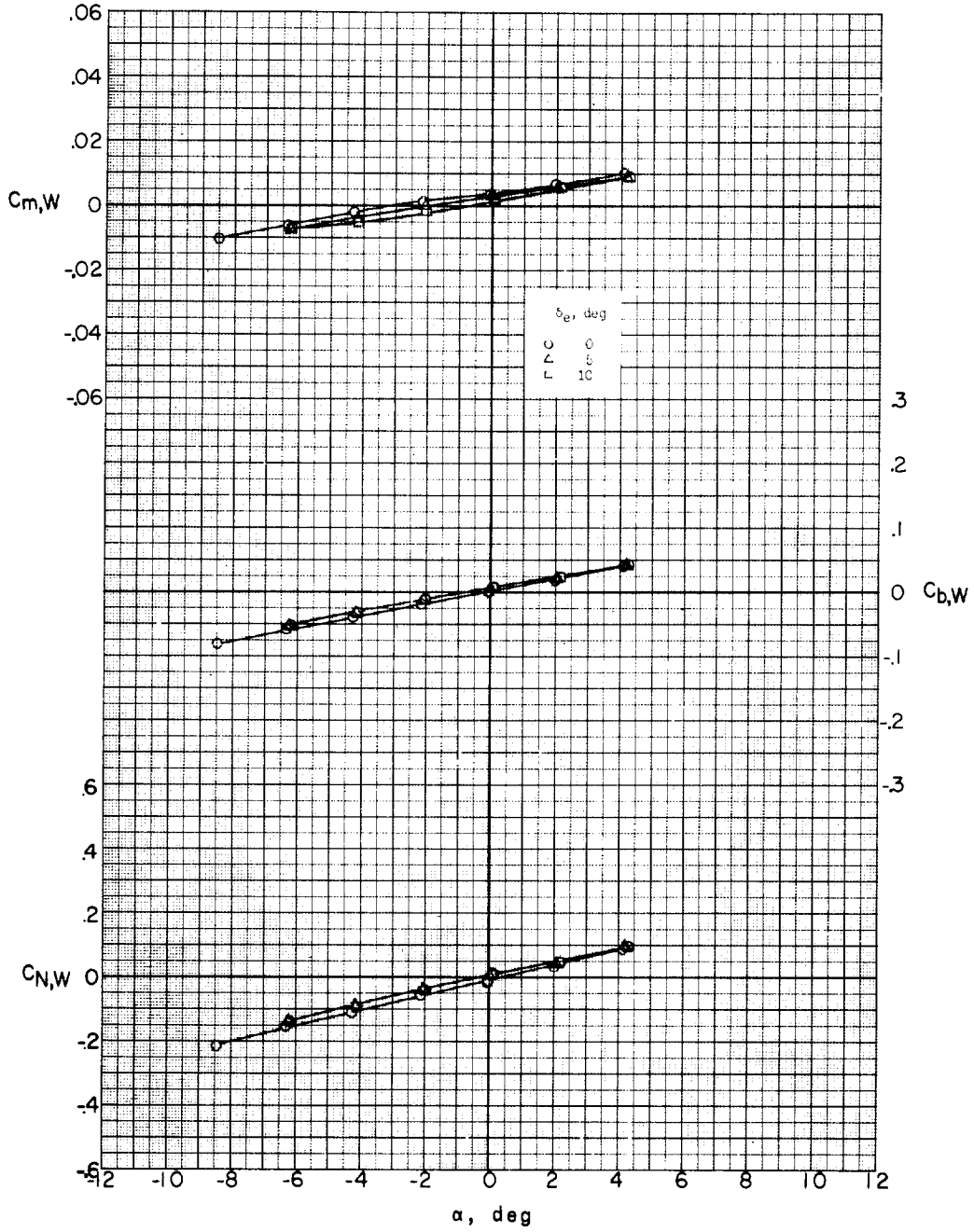
(d) M = 3.51.

Figure 17.- Concluded.



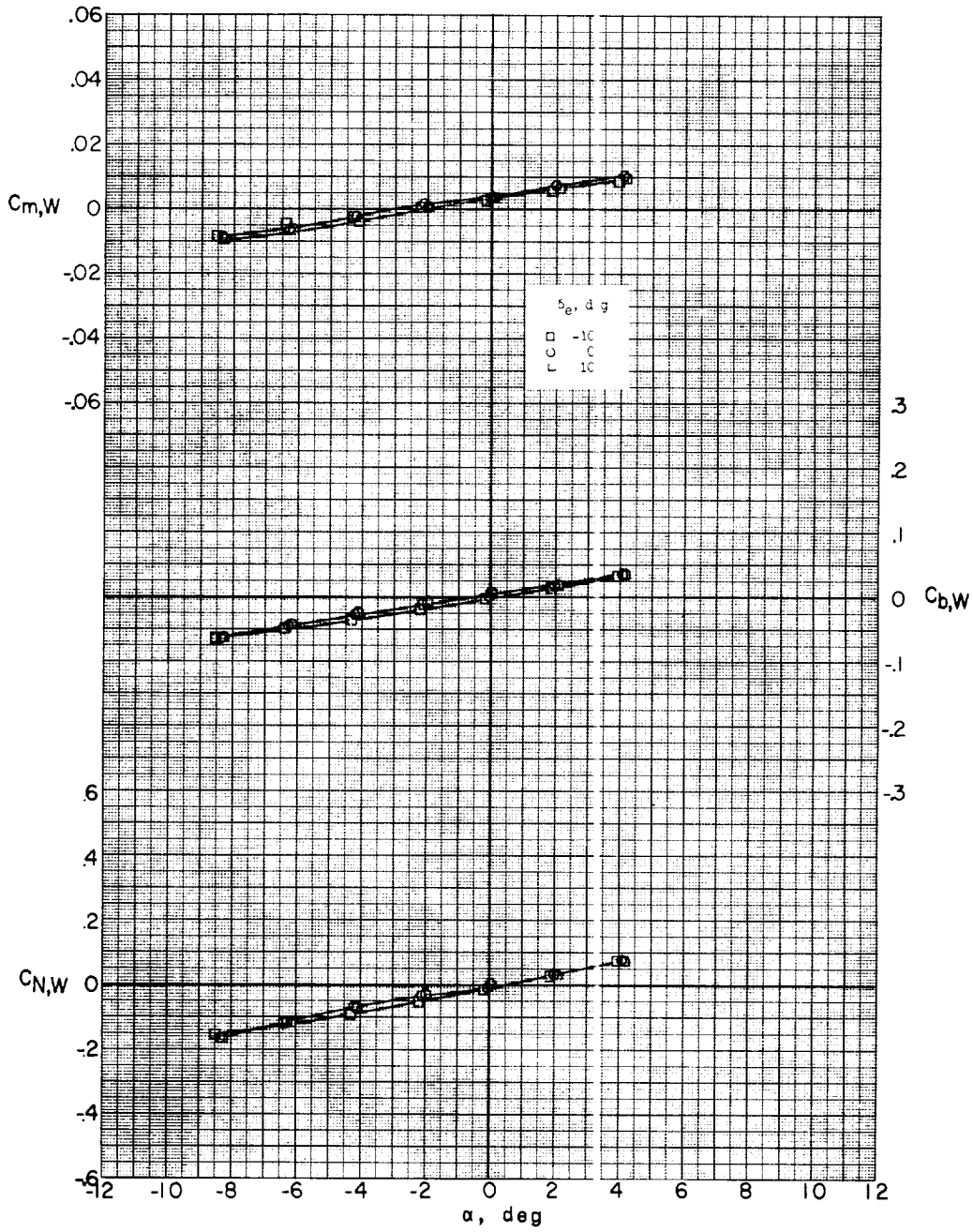
(a) M = 2.29

Figure 18.- Effect of canard deflection on pitch characteristics of missile wing. Missile-booster combination with A-frame mounted; $\beta = 0.3^{\circ}$; sting A.



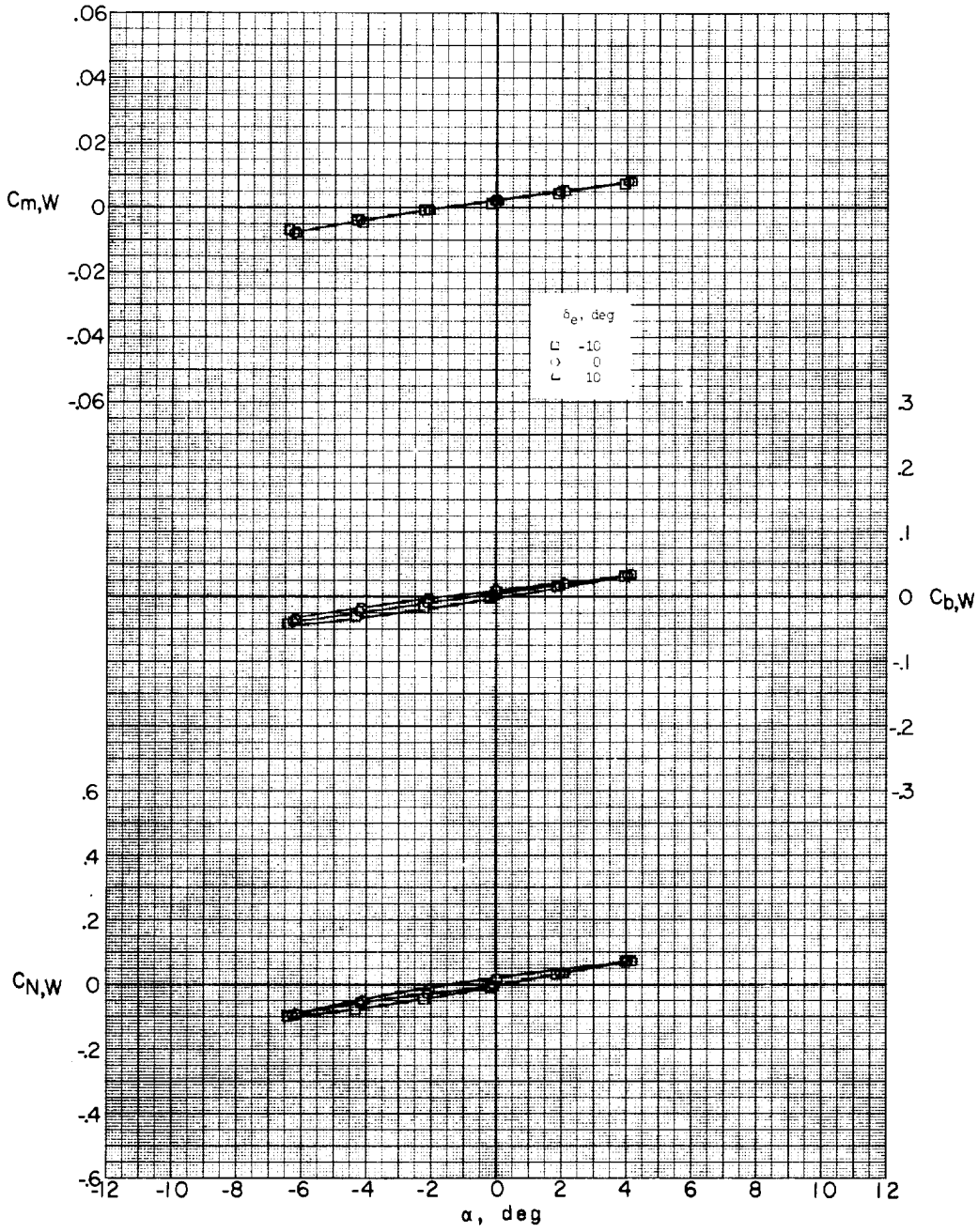
(b) M = 2.75.

Figure 18.- Continued.



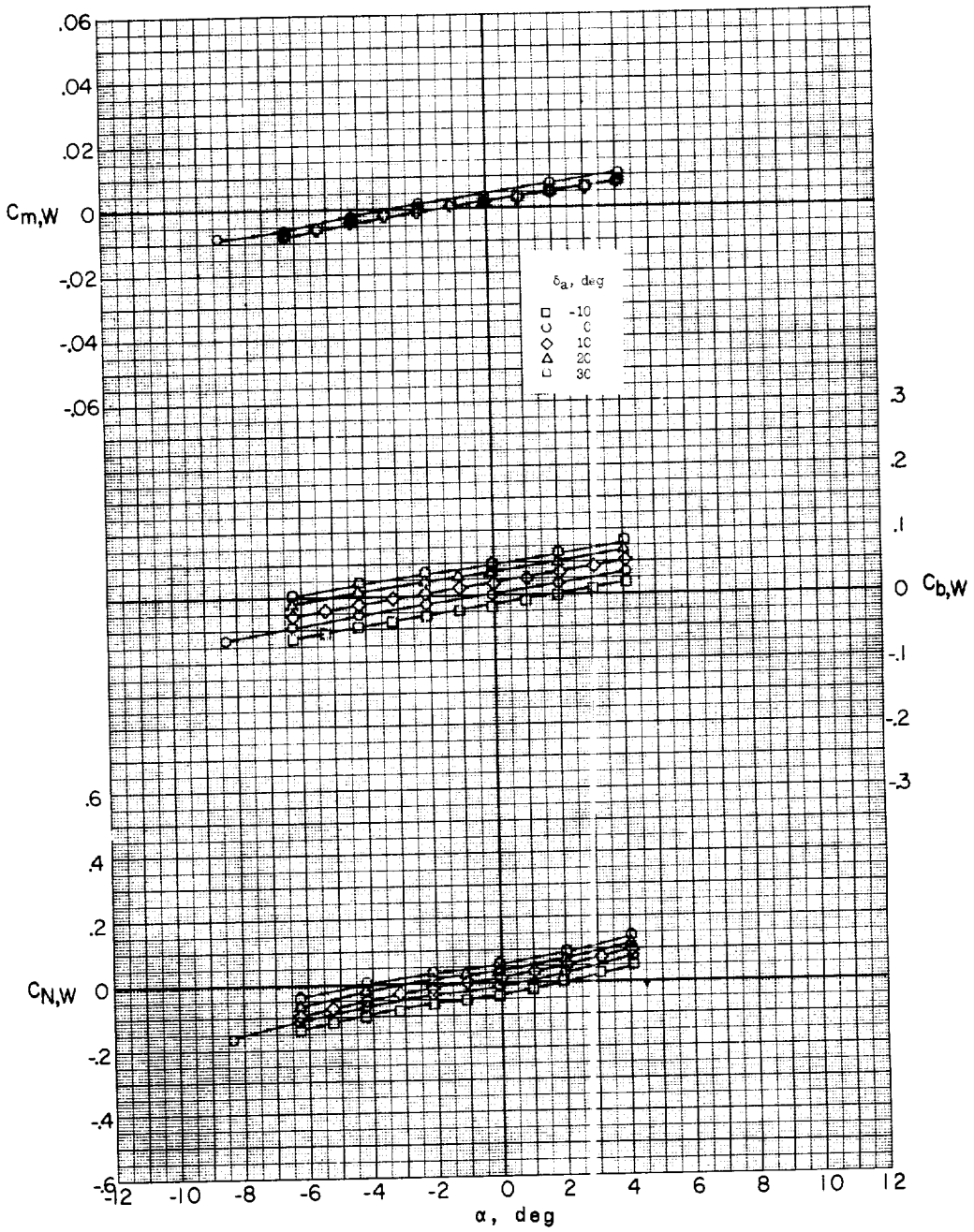
(c) M = 3.22.

Figure 18.- Continued.



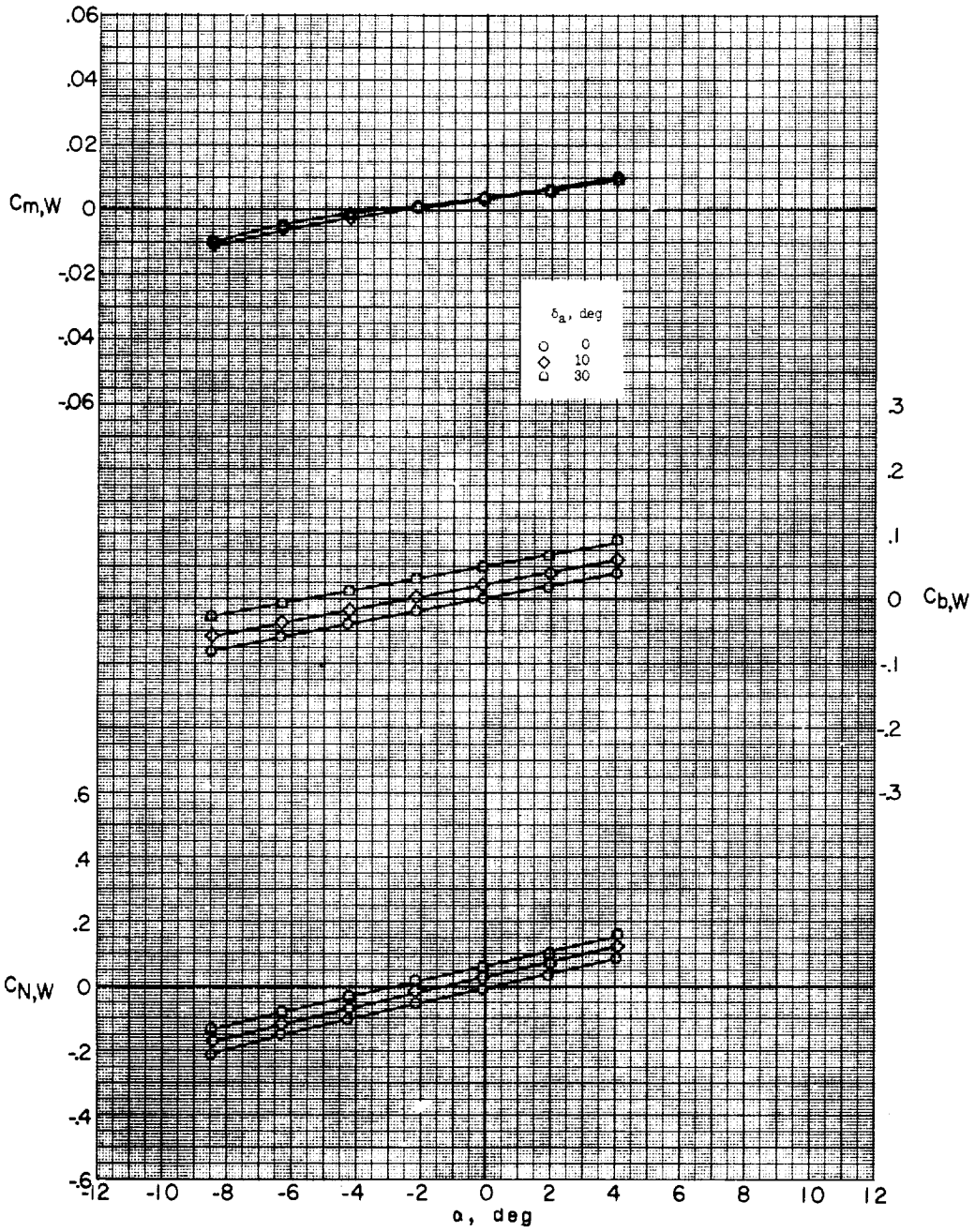
(d) M = 3.51.

Figure 18.- Concluded.



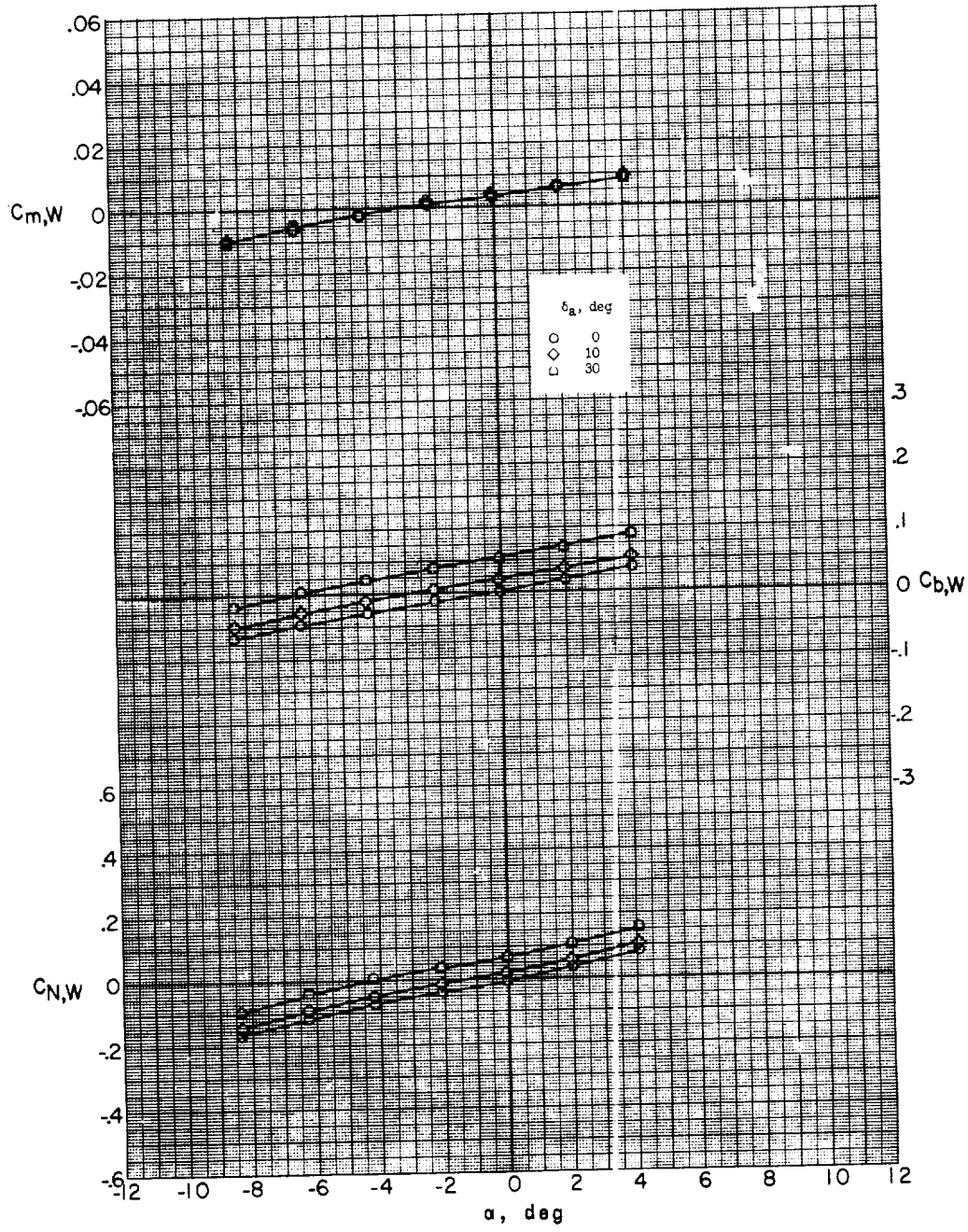
(a) M = 3.22; sting A.

Figure 19.- Effect of aileron deflection on pitch characteristics of missile wing. Missile-booster combination with A-frame mounted; $\delta_e = 0^o$; $\beta = 0.2^o$.



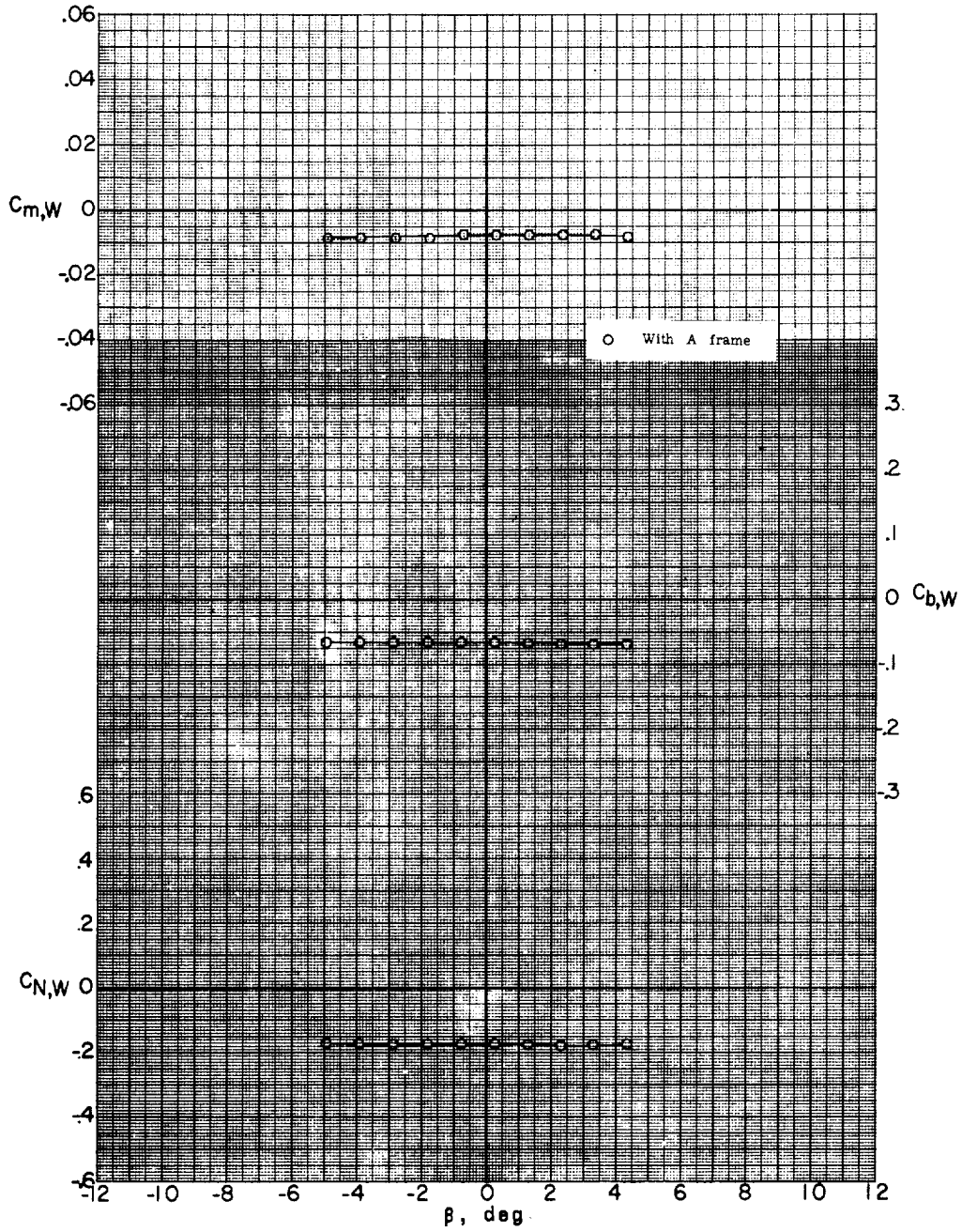
(b) M = 2.75; with missile aileron actuator housing; sting B.

Figure 19.- Continued.



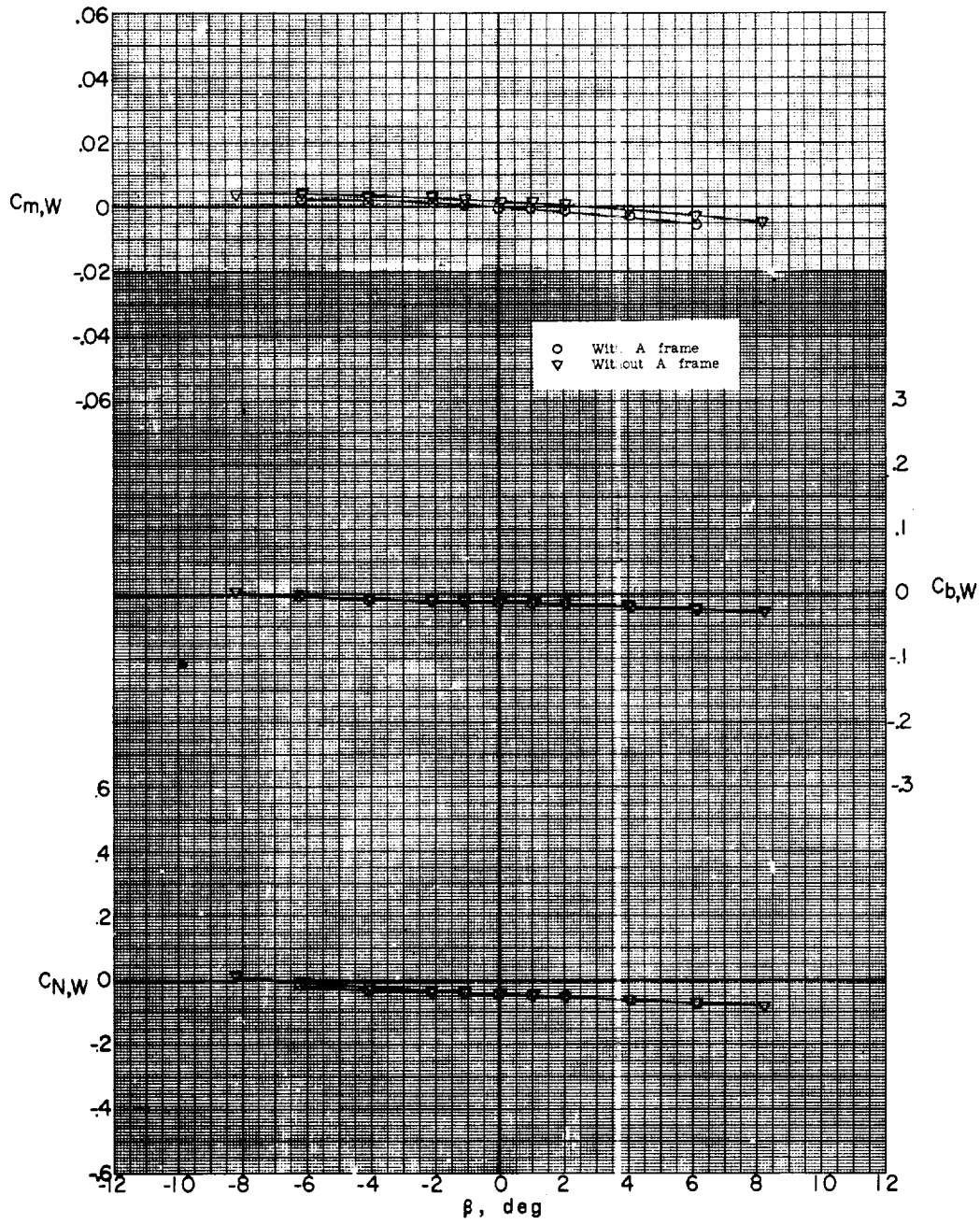
(c) M = 3.22; with missile aileron actuator housing; sting B.

Figure 19.- Concluded.



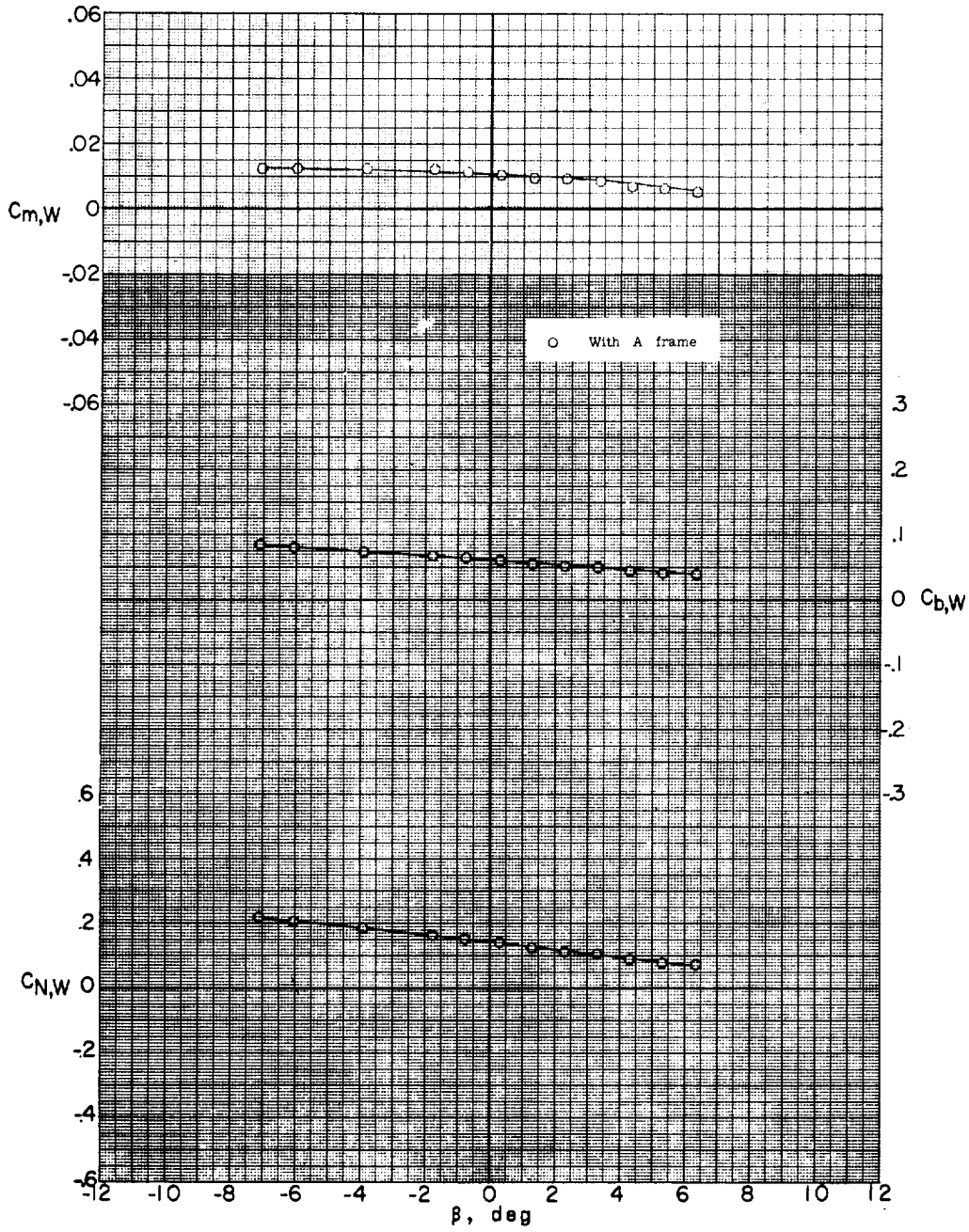
(a) M = 2.29; $\alpha = -5.3^{\circ}$.

Figure 20.- Effect of A-frame on lateral characteristics of missile wing. Missile-booster combination; $\delta_e = 0^{\circ}$; sting A.



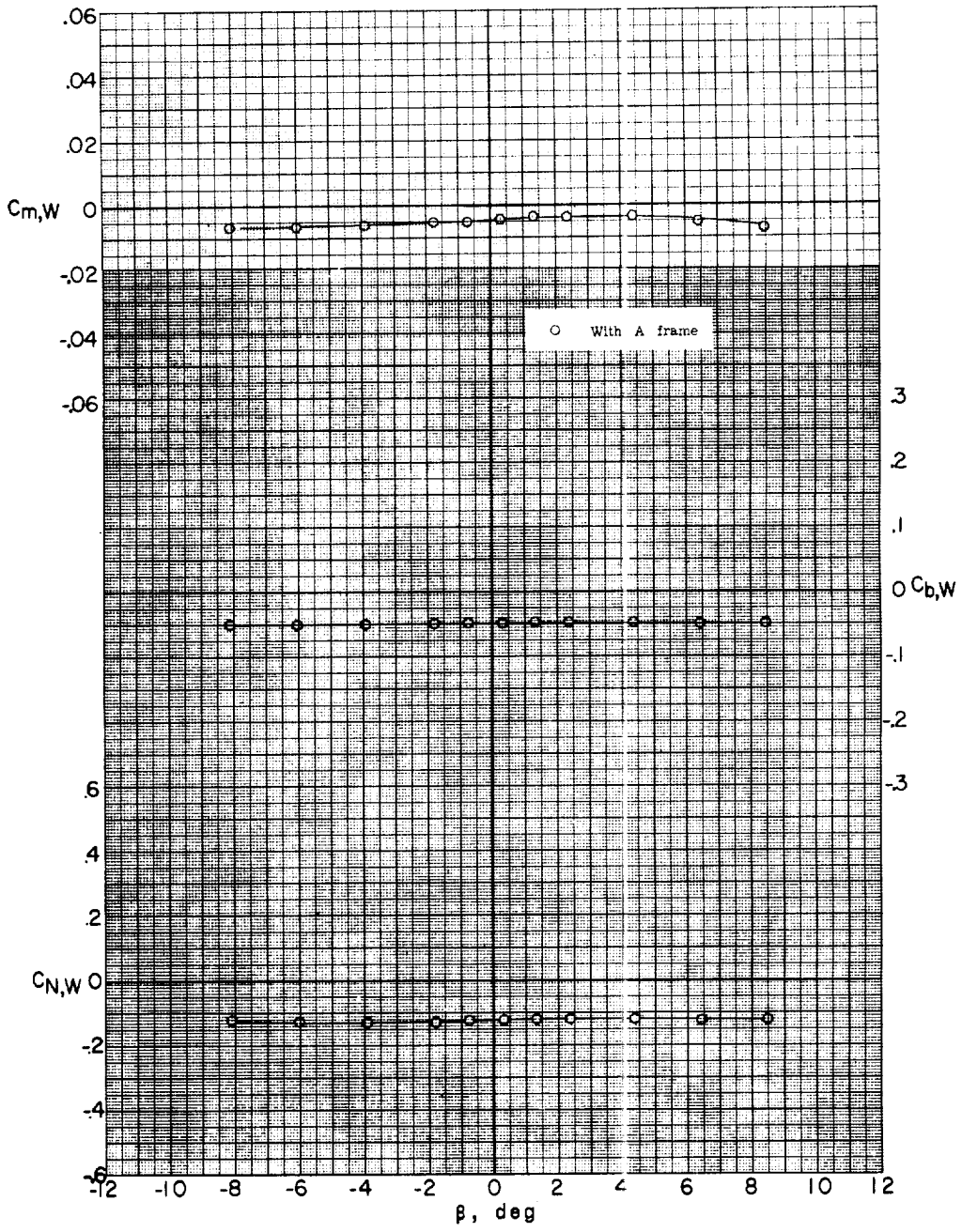
(b) M = 2.29; α = -0.3°.

Figure 20.- Continued.



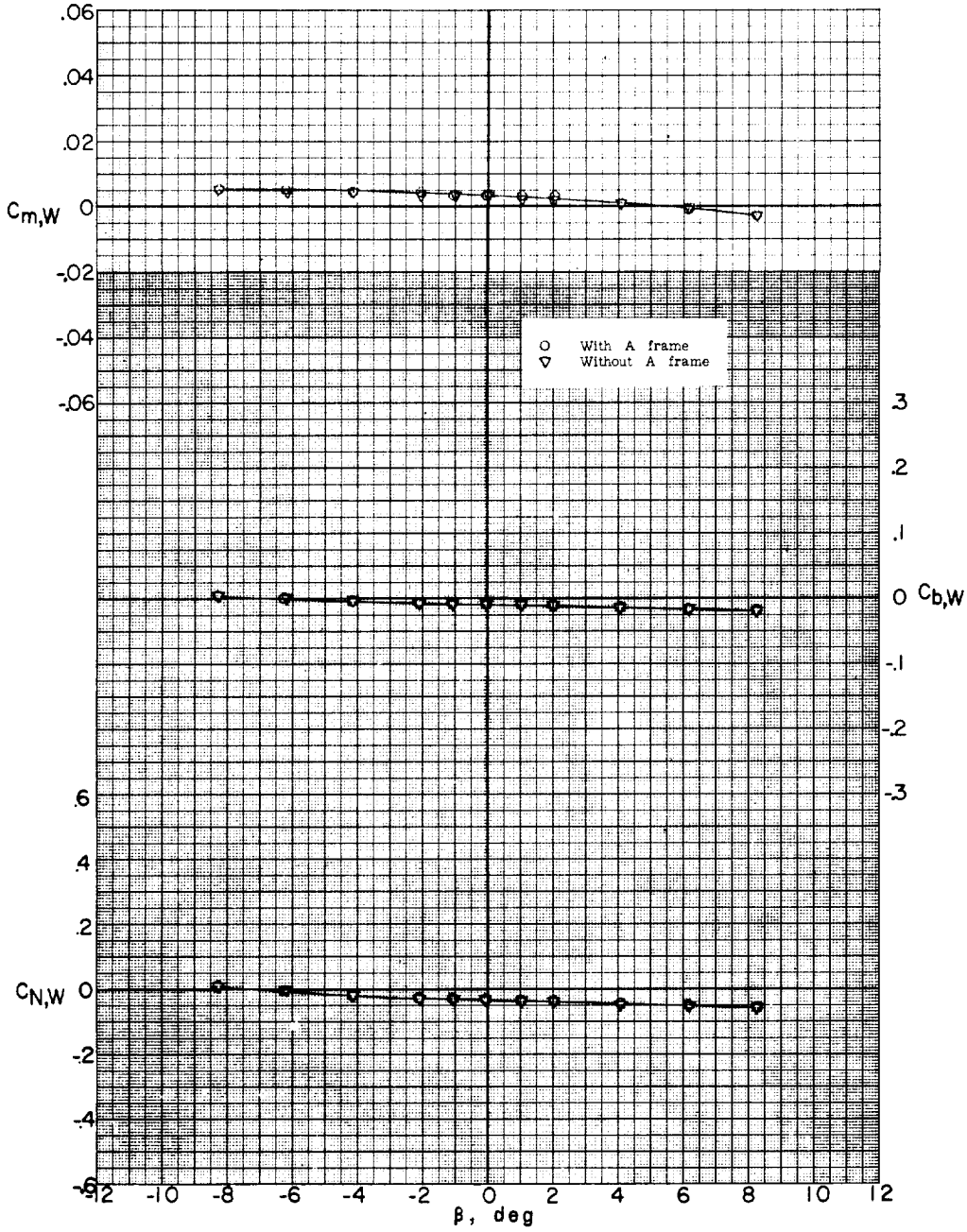
(c) M = 2.29; $\alpha = 5.1^{\circ}$.

Figure 20.- Continued.



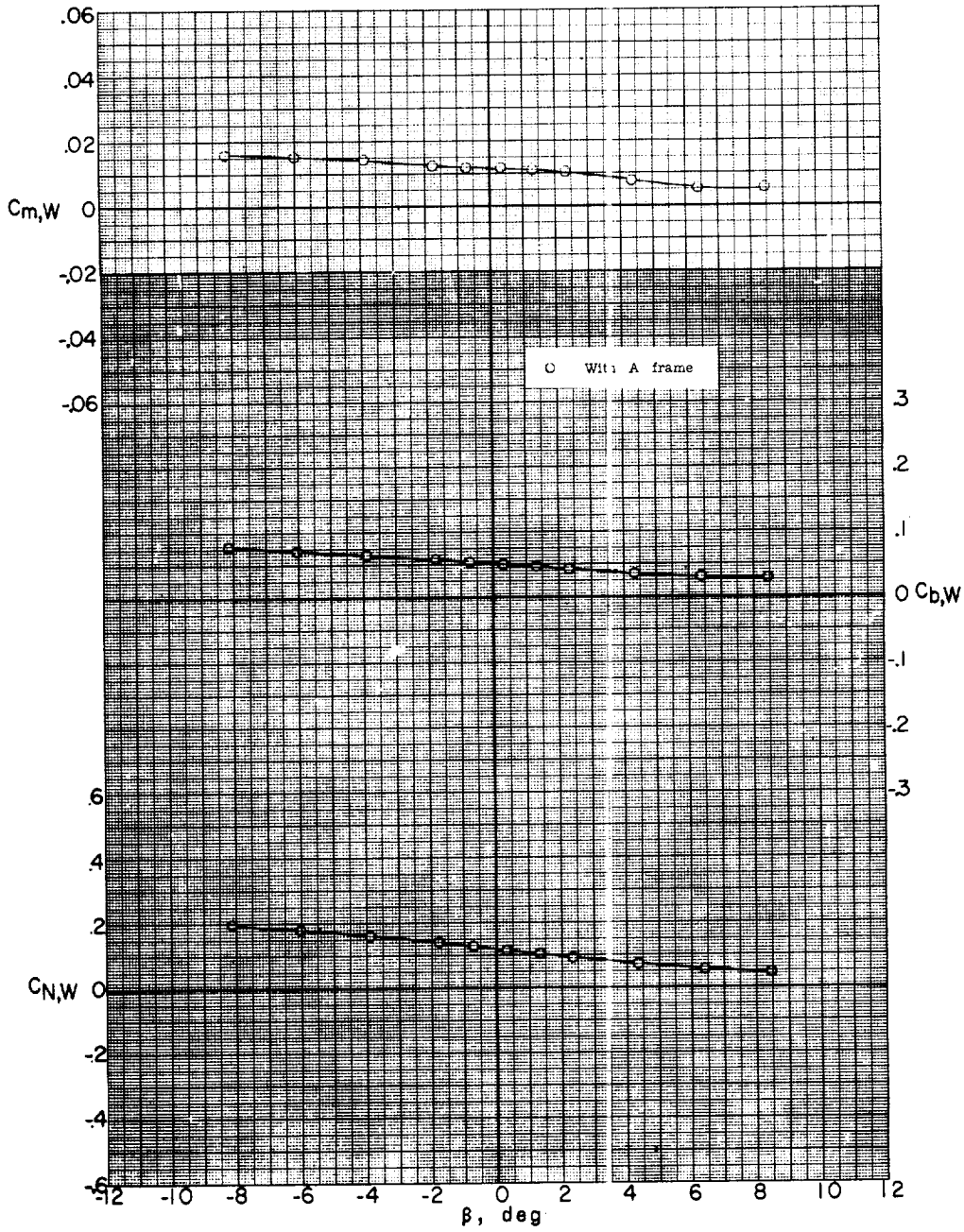
(d) M = 2.75; $\alpha = -5.3^{\circ}$.

Figure 20.- Continued.



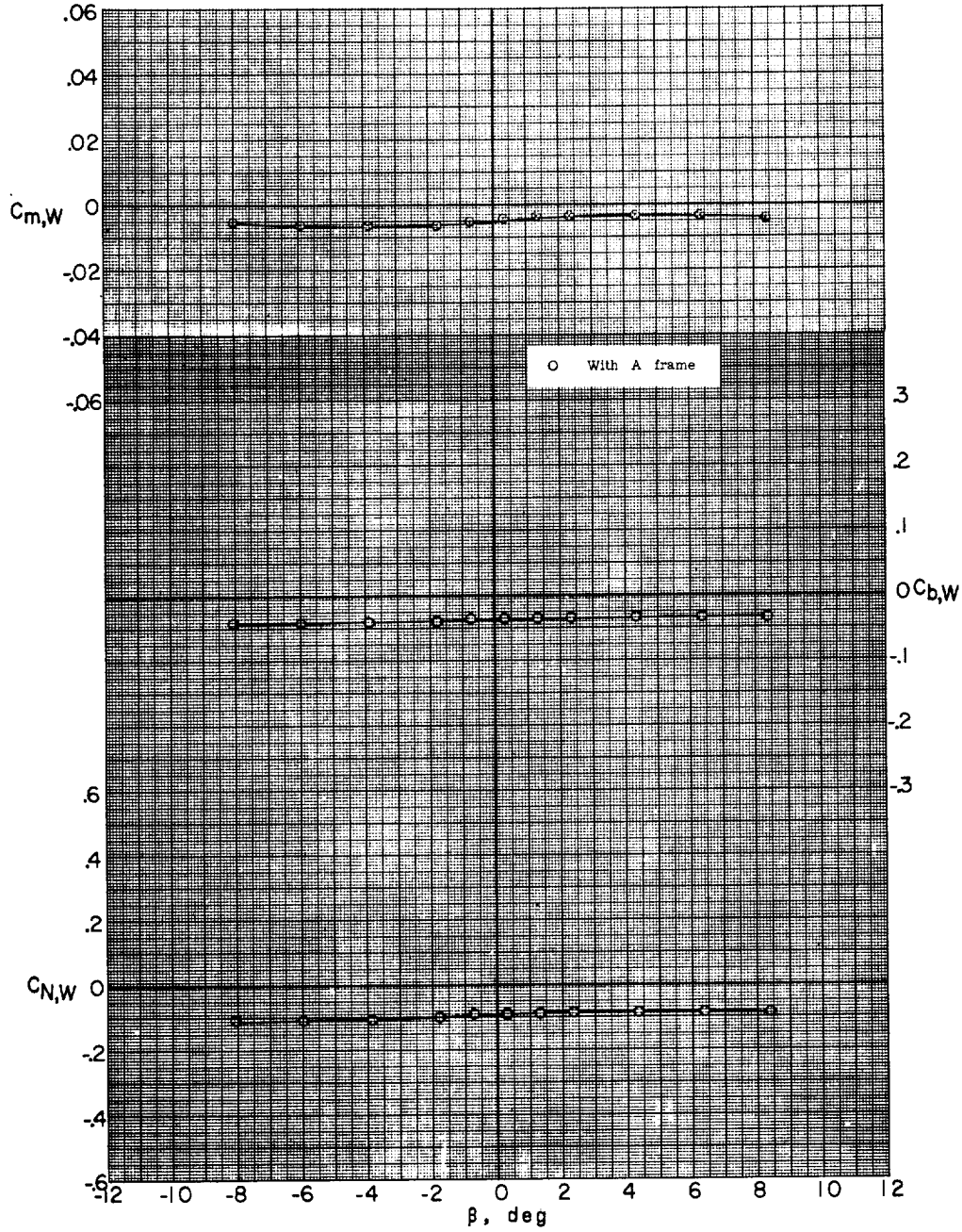
(e) M = 2.75; $\alpha = -0.3^{\circ}$.

Figure 20.- Continued.



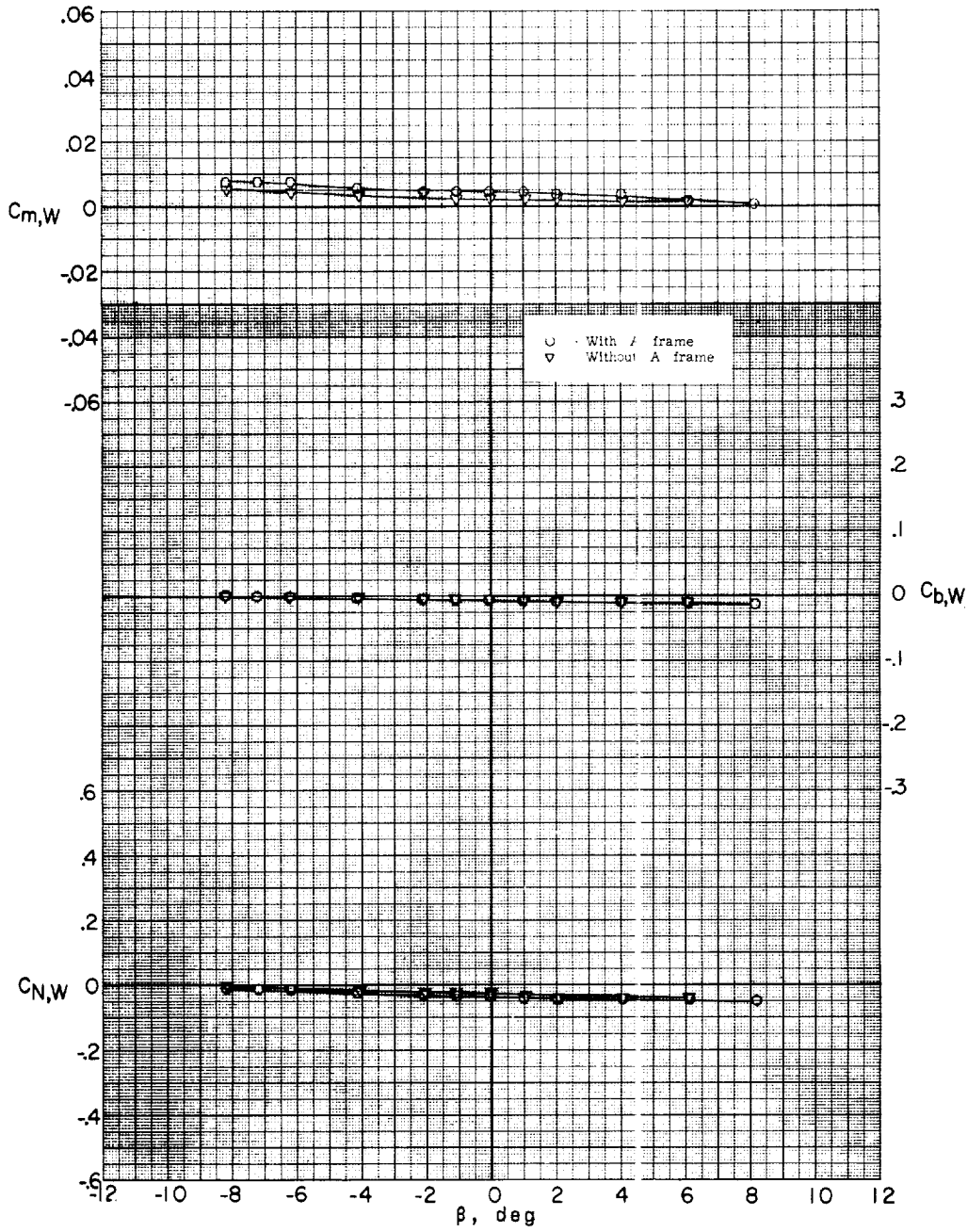
(f) M = 2.75; $\alpha = 5.2^{\circ}$.

Figure 20.- Continued.



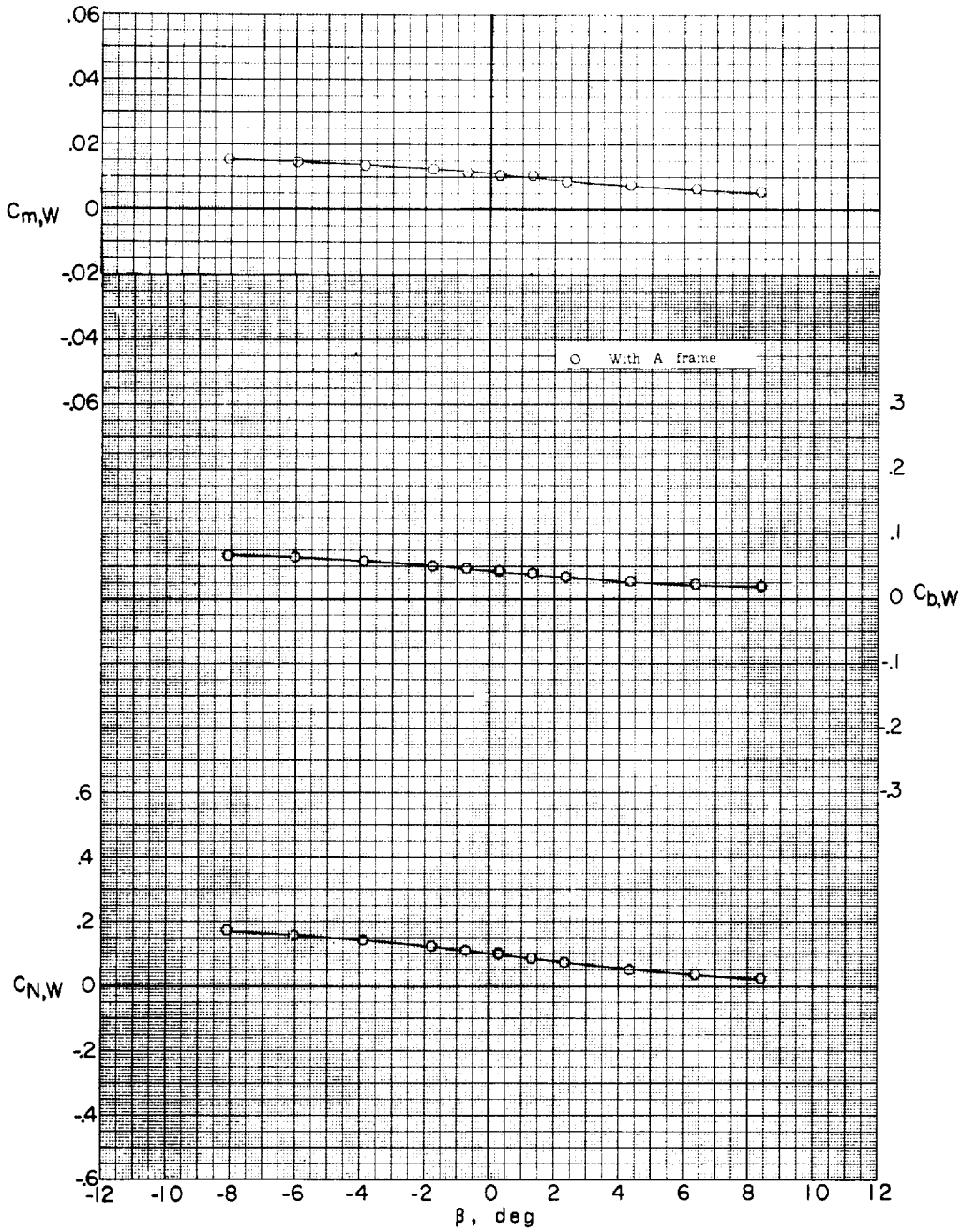
(g) M = 3.22; α = -5.2°.

Figure 20.- Continued.



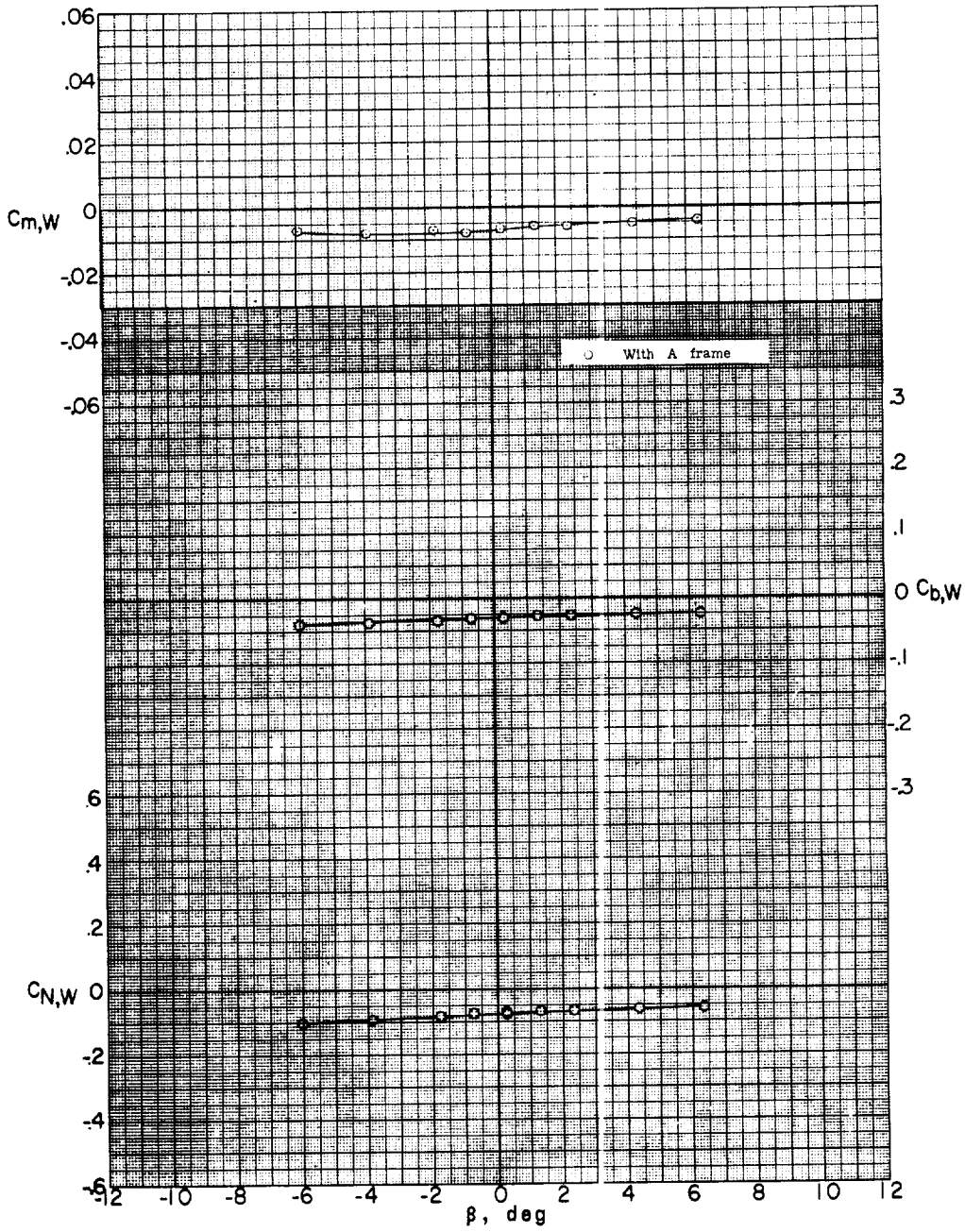
(h) $M = 3.22$; $\alpha = -0.3^{\circ}$.

Figure 20.- Continued.



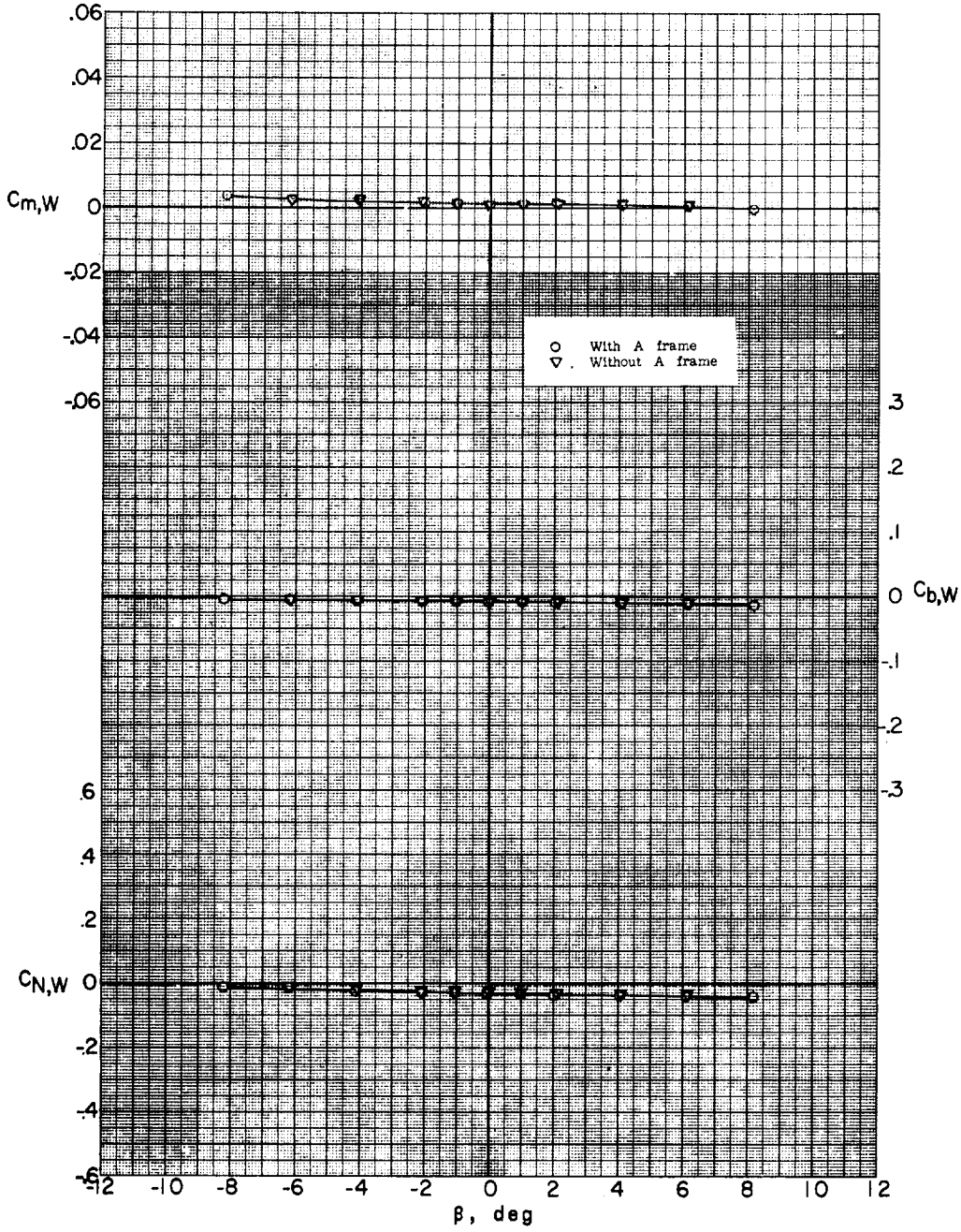
(i) M = 3.22; $\alpha = 5.1^{\circ}$.

Figure 20.- Continued.



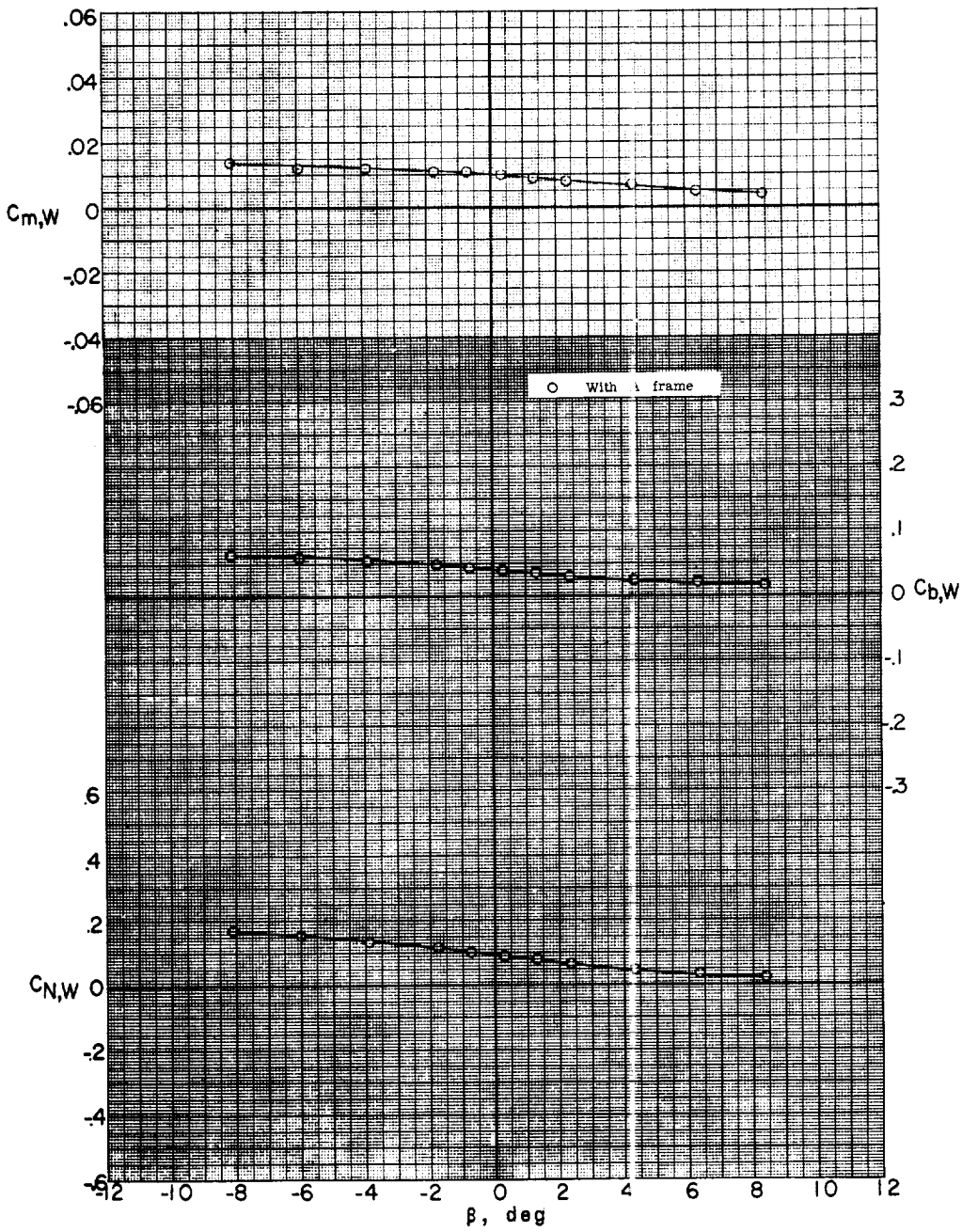
(j) M = 3.51; $\alpha = -5.2^{\circ}$.

Figure 20.- Continued.



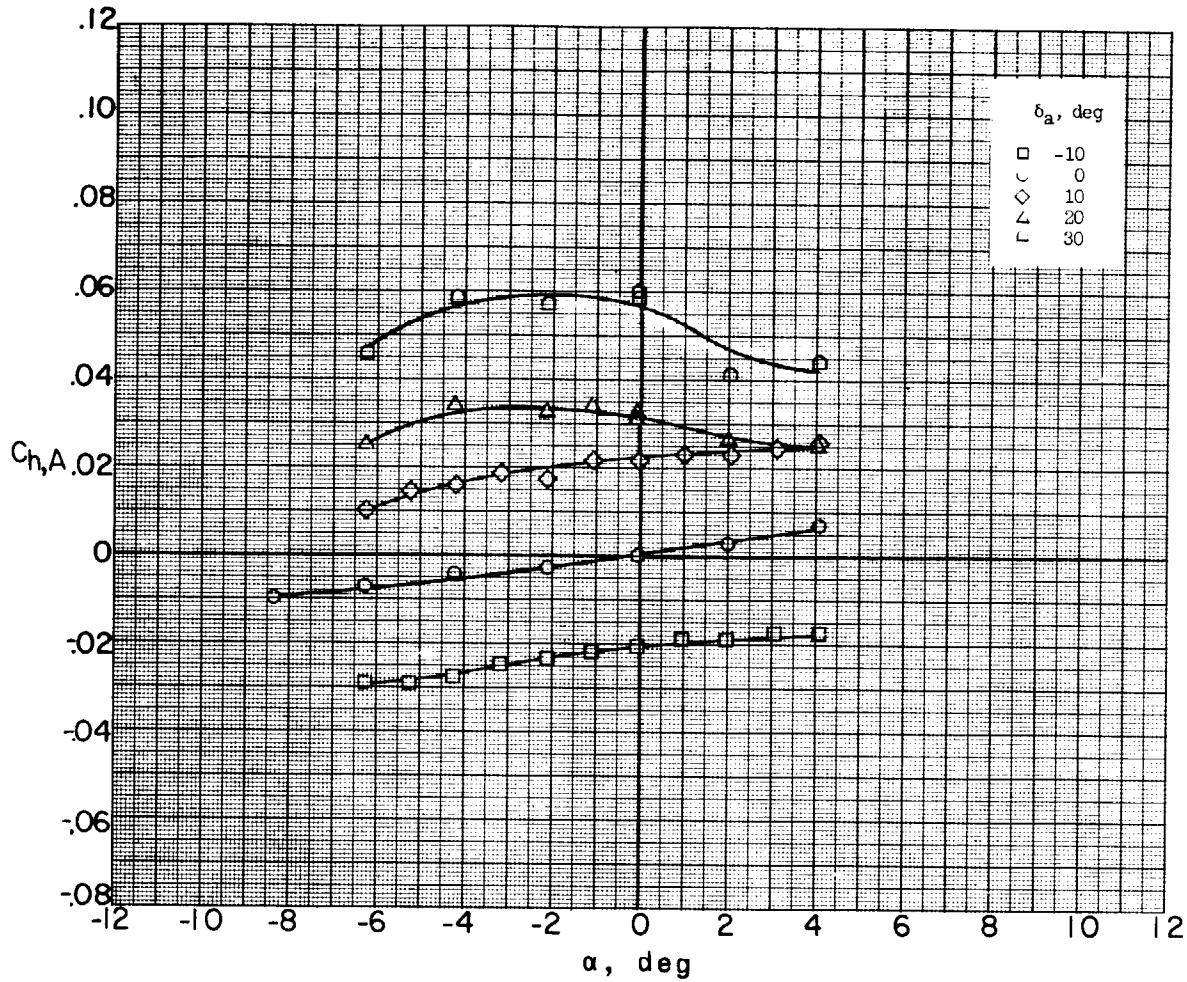
(k) $M = 3.51$; $\alpha = -0.3^{\circ}$.

Figure 20.- Continued.



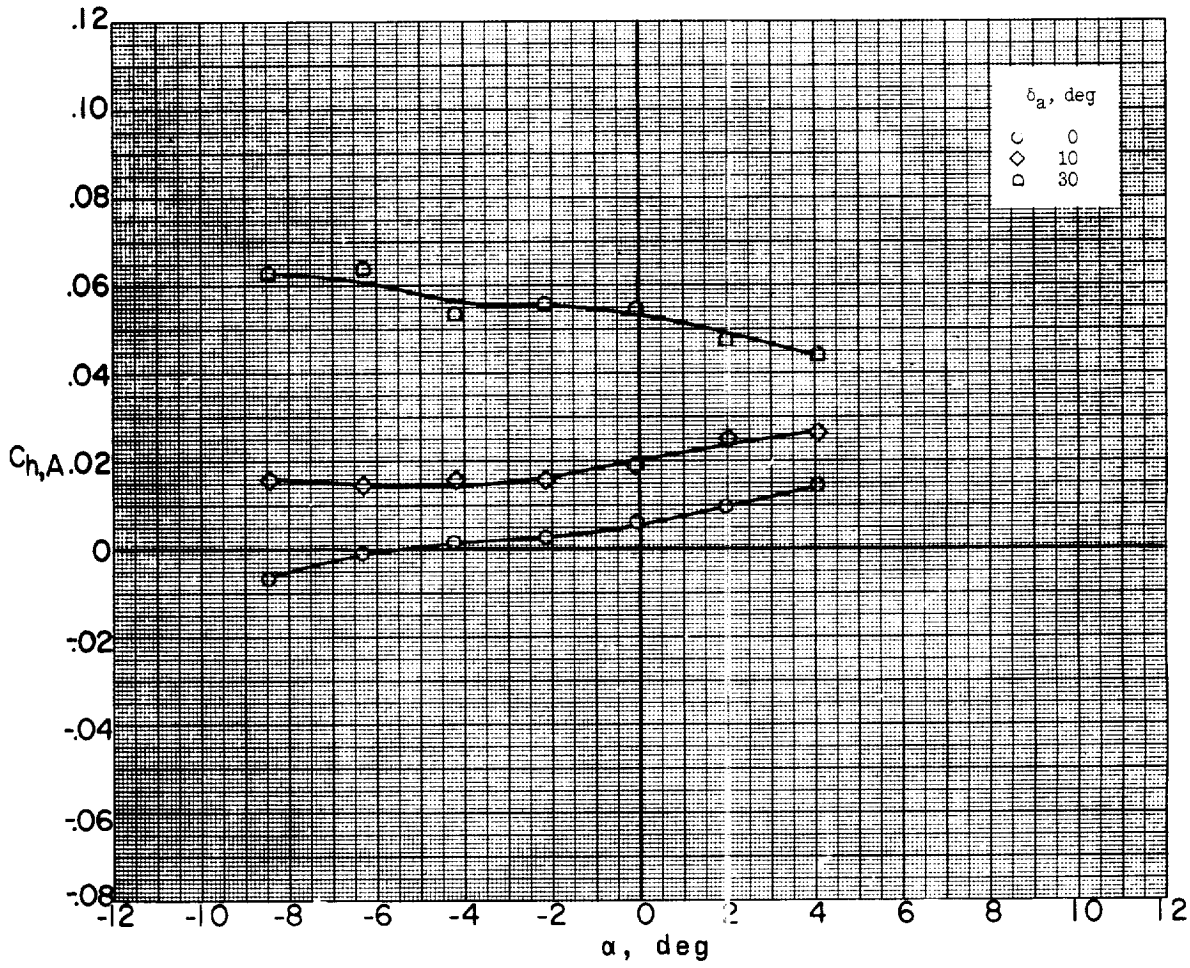
(l) M = 3.51; α = 5.1°.

Figure 20.- Concluded.



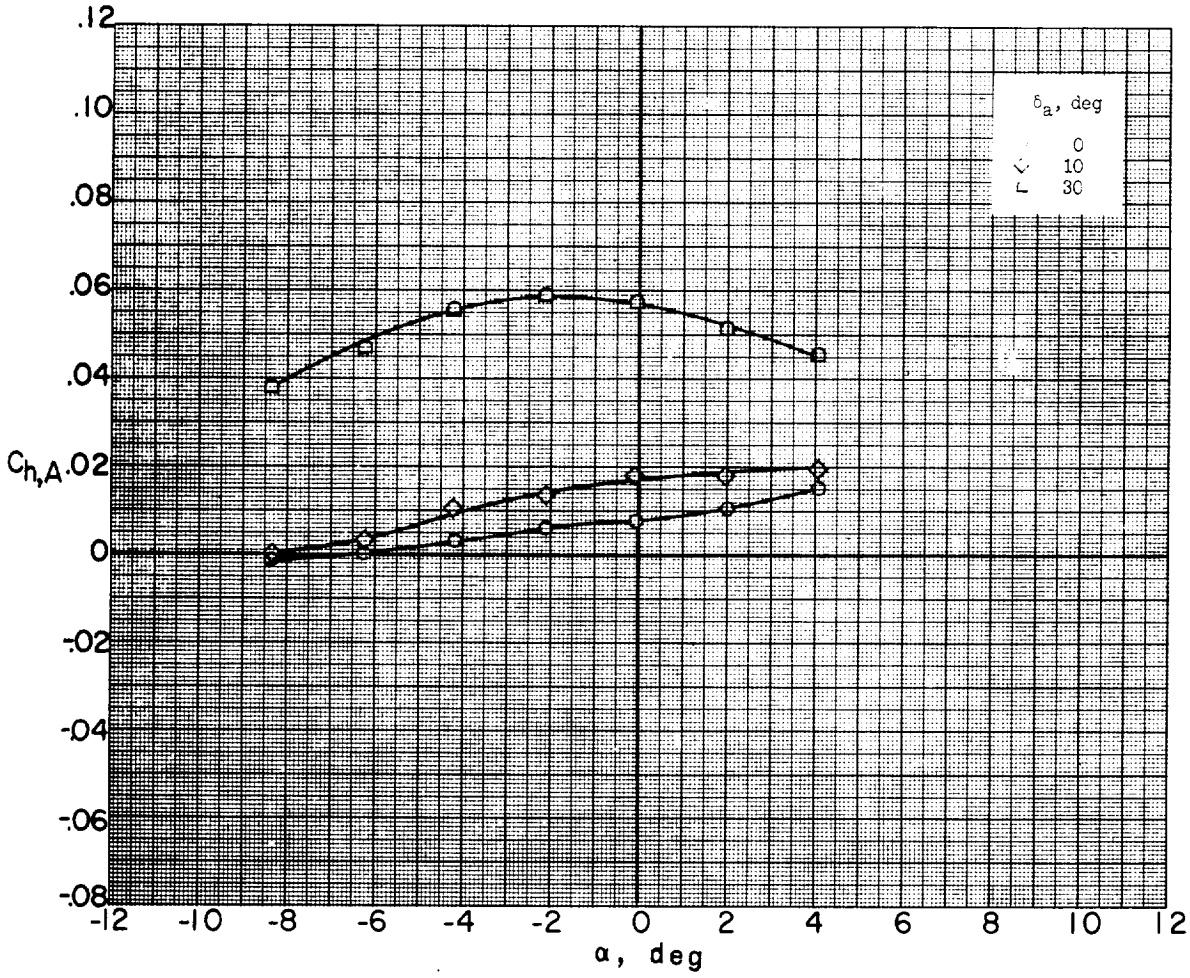
(a) M = 3.22; sting A.

Figure 21.- Effect of aileron deflection on aileron hinge-moment characteristics. Missile-booster combination with A-frame mounted; $\delta_e = 0^o$; $\beta = 0.2^o$.



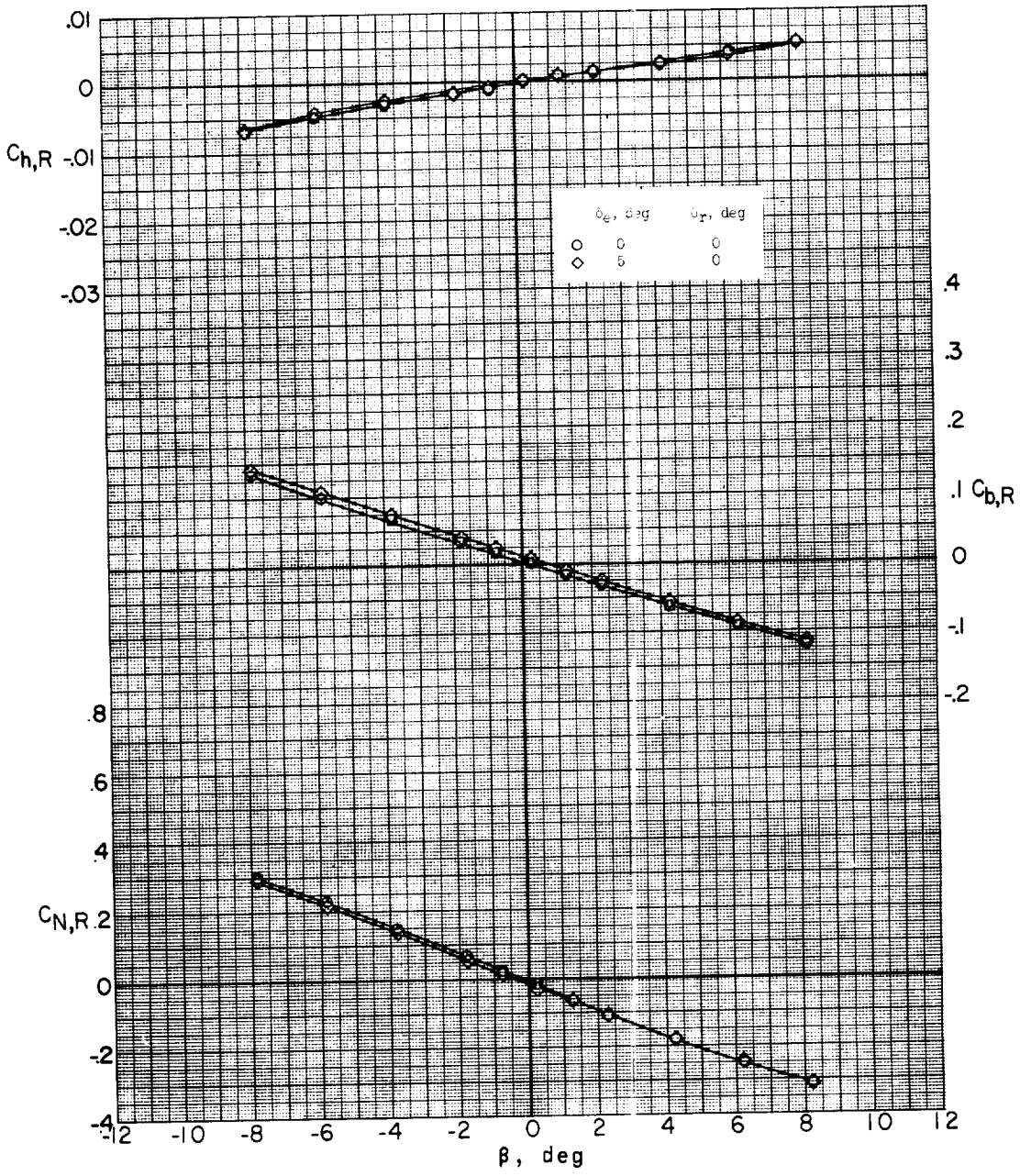
(b) M = 2.75; with missile aileron actuator housing; sting B.

Figure 21.- Continued.



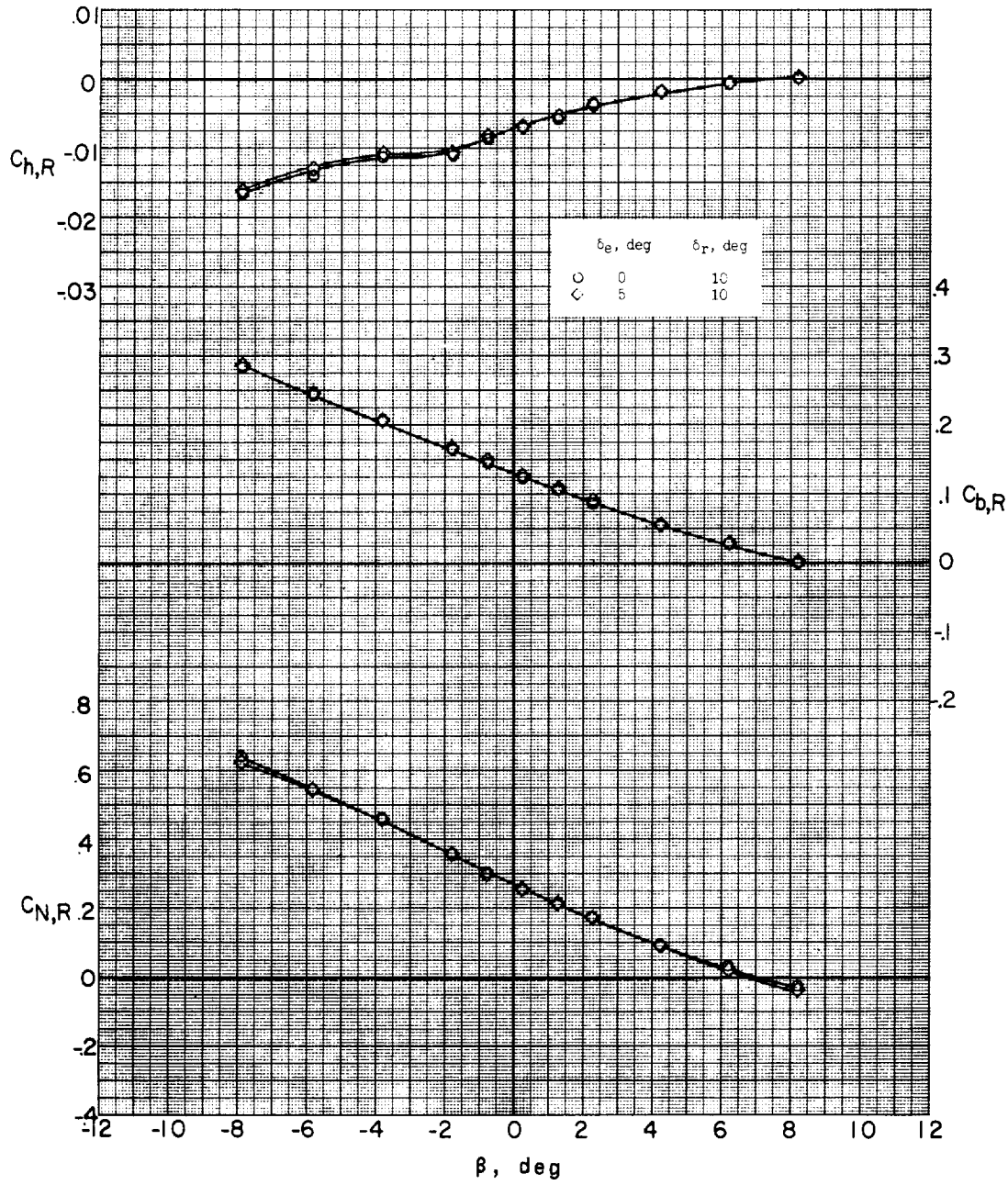
(c) M = 3.22; with missile aileron actuator housing; sting B.

Figure 21.- Concluded.



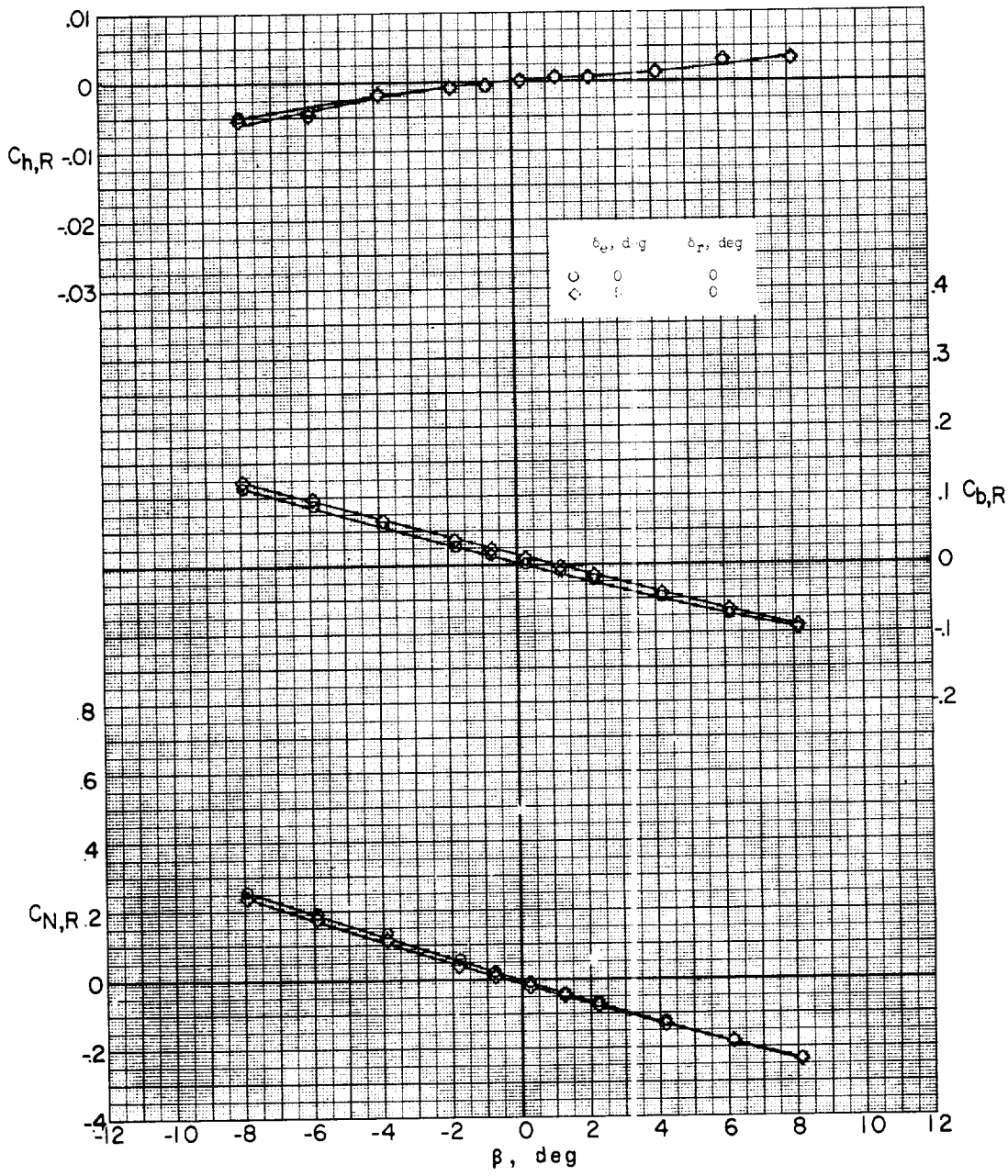
(a) M = 2.75; $\alpha = -5.0^{\circ}$.

Figure 22.- Effect of canard deflection on lateral characteristics of missile rudder at two rudder deflections. Missile-booster combination with A-frame mounted; sting C.



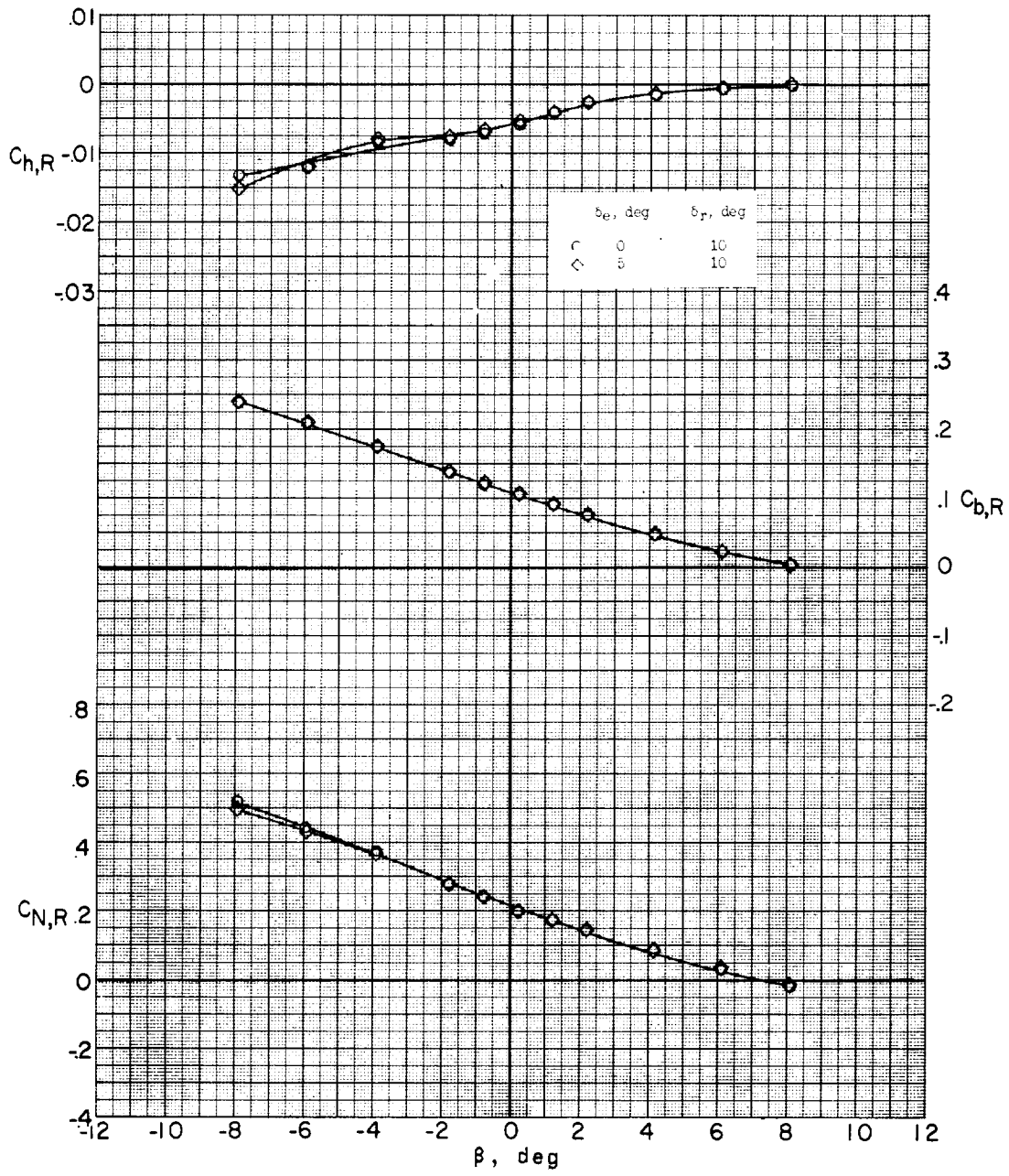
(a) Concluded.

Figure 22.- Continued.



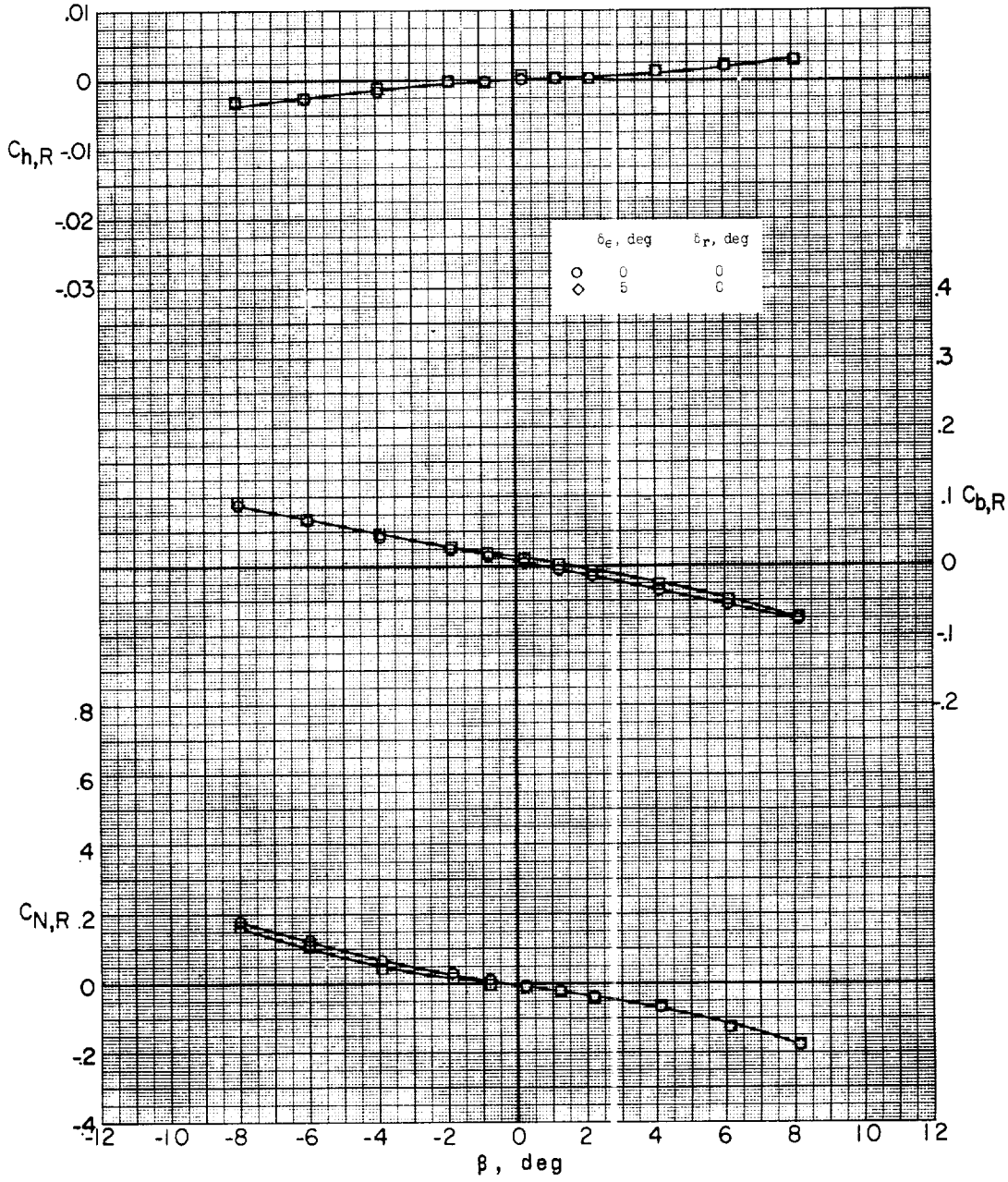
(b) M = 2.75; $\alpha = 0^{\circ}$.

Figure 22.- Continued.



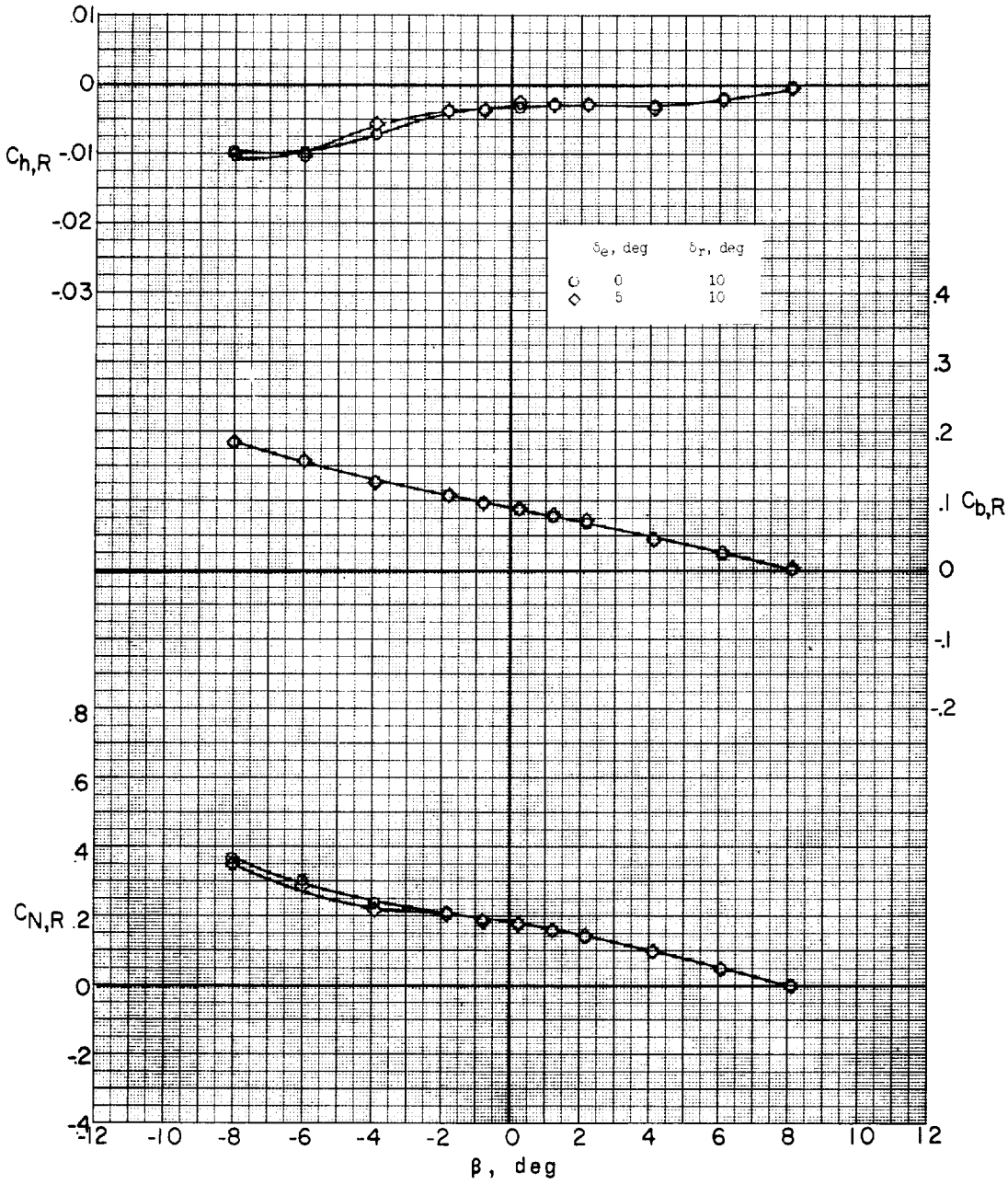
(b) Concluded.

Figure 22.- Continued.



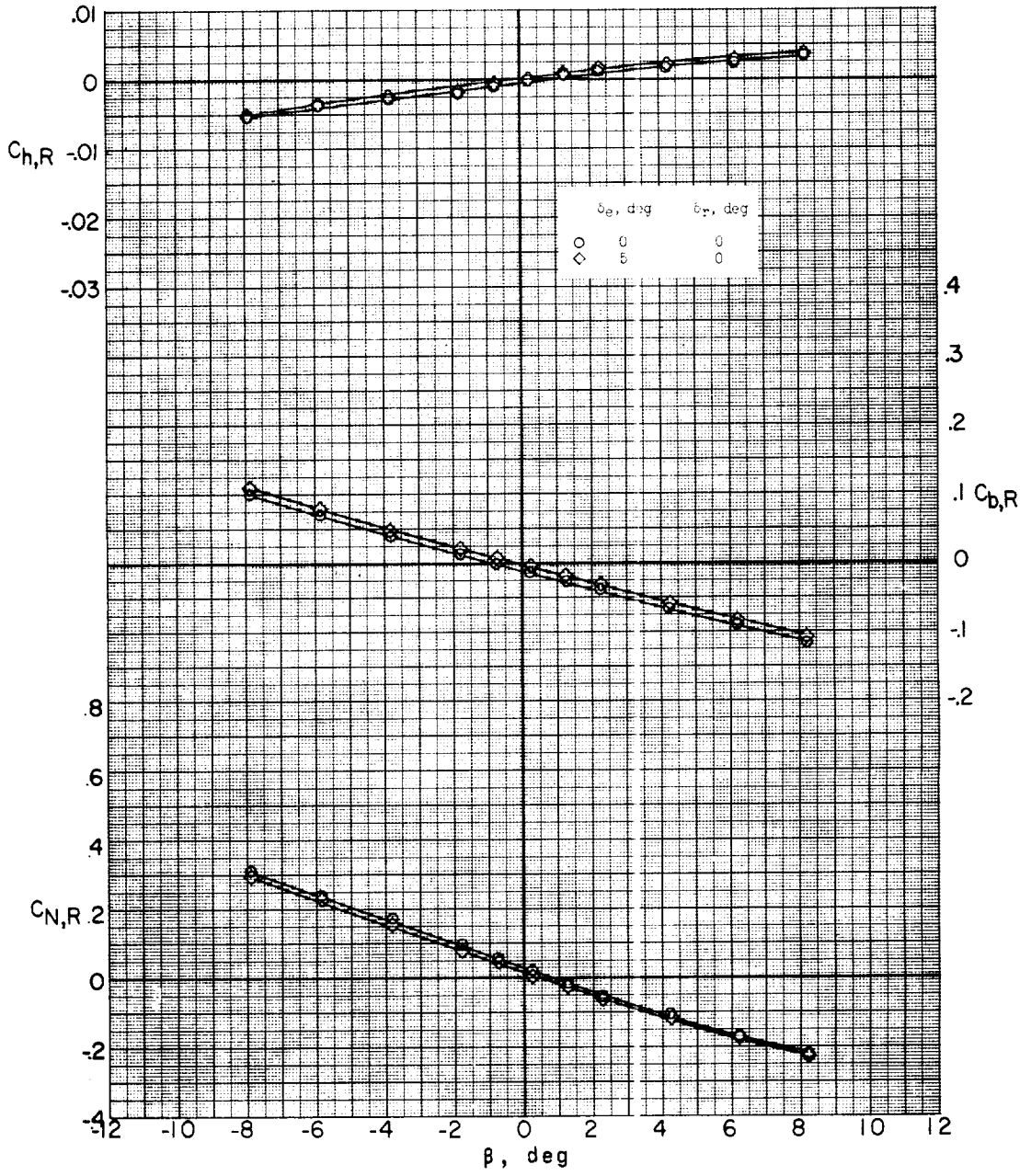
(c) M = 2.75; $\alpha = 5.0^{\circ}$.

Figure 22.- Continued.



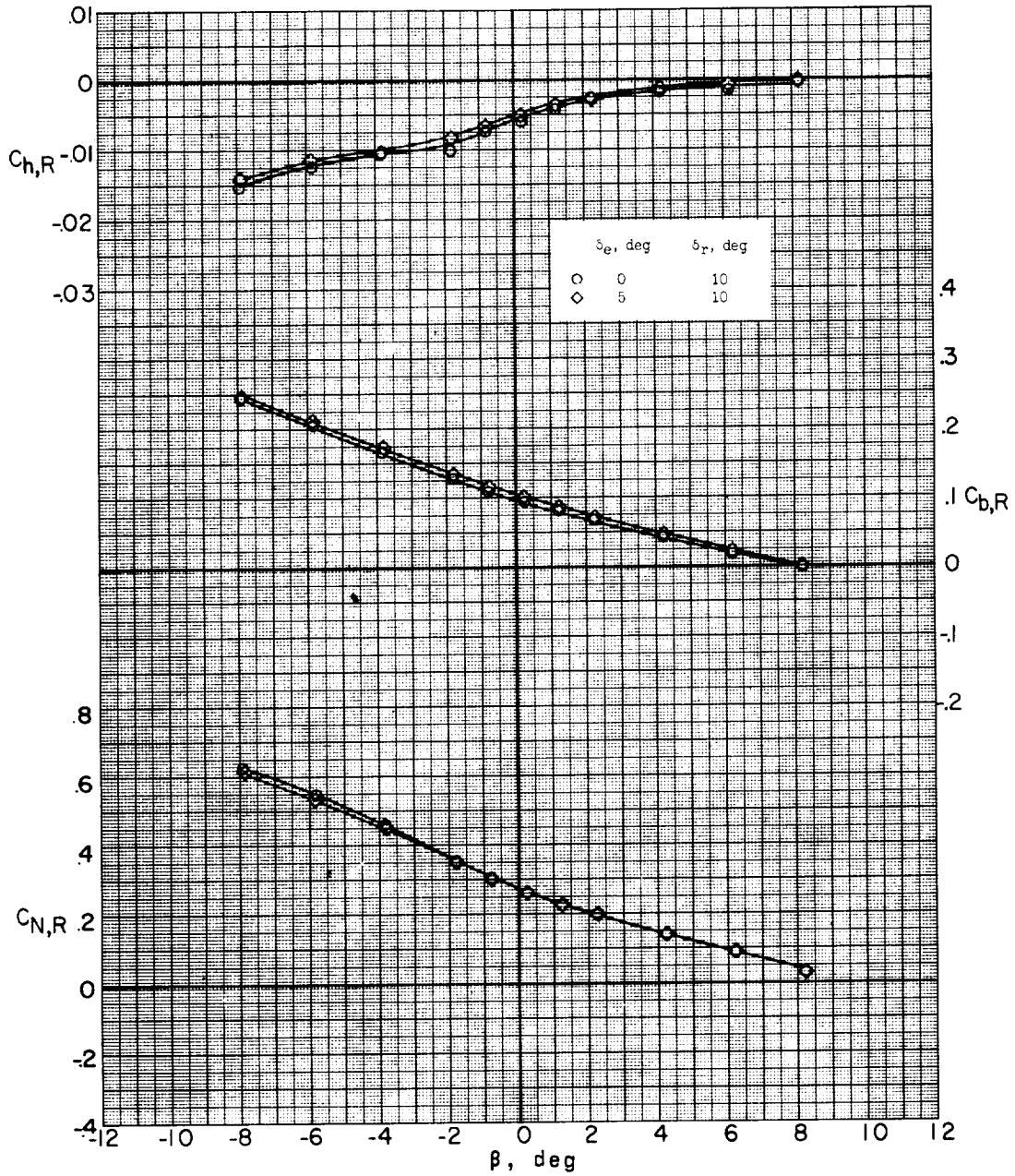
(c) Concluded.

Figure 22.- Continued.



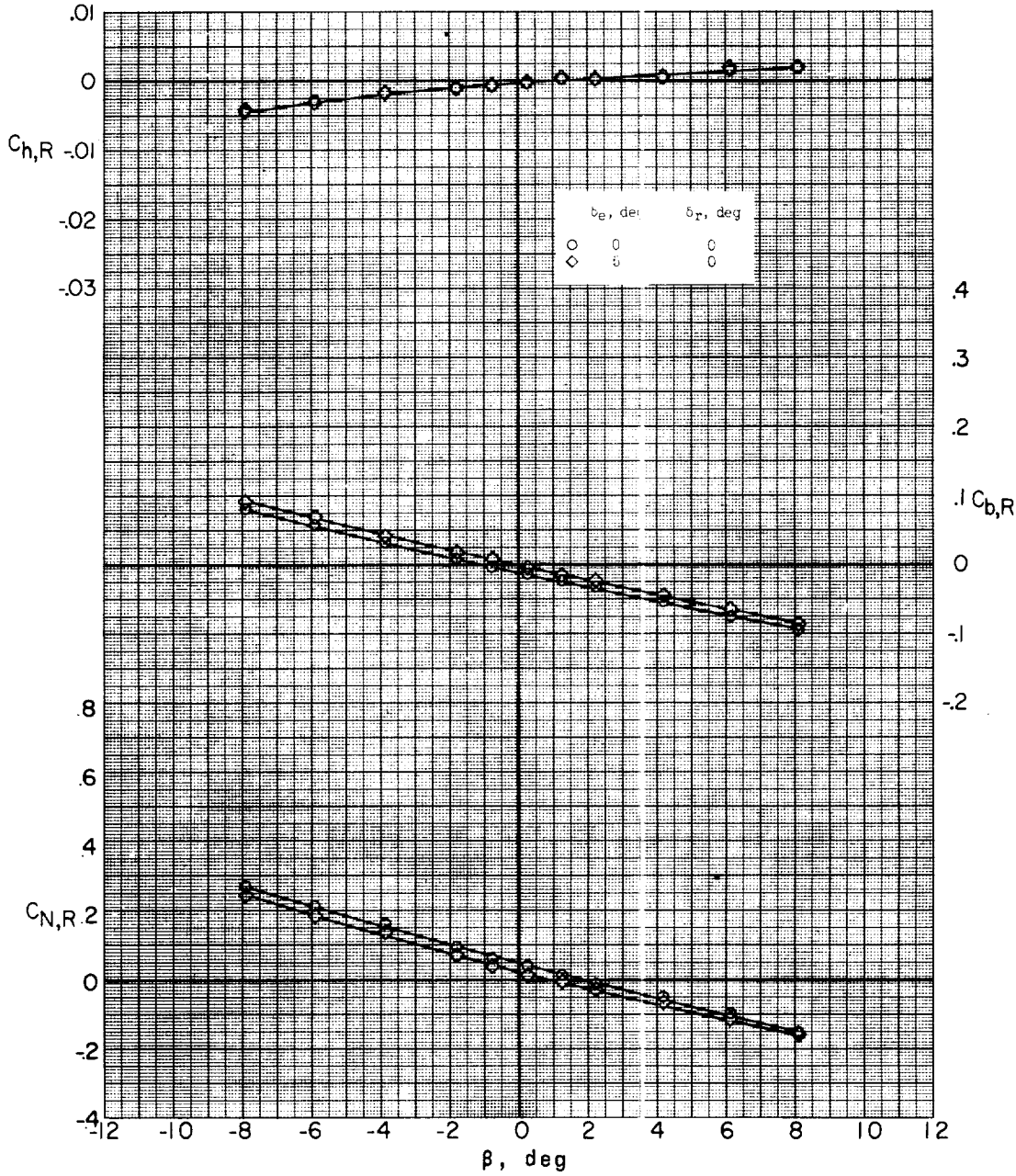
(d) M = 3.22; $\alpha = -5.0^{\circ}$.

Figure 22.- Continued.



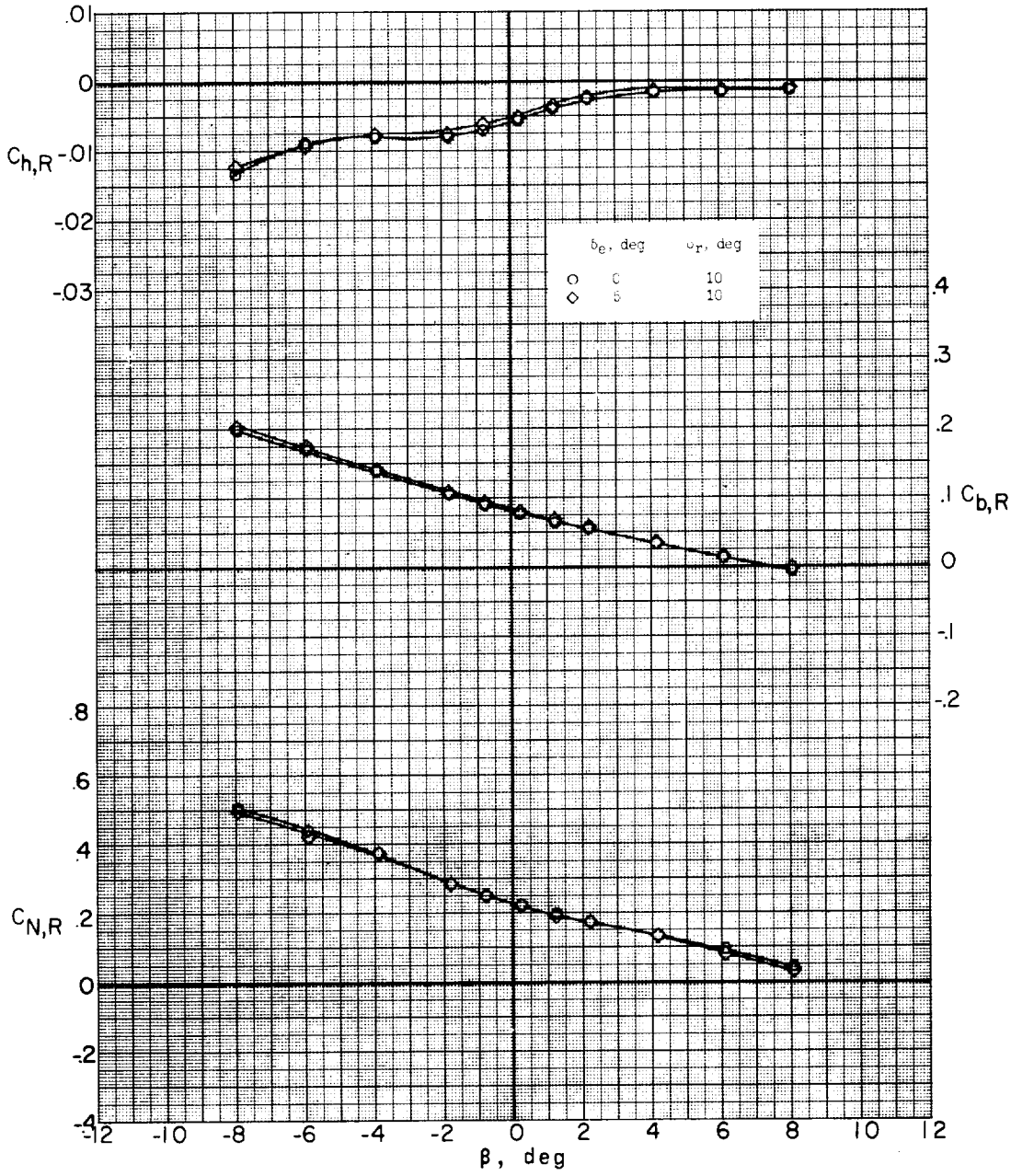
(d) Concluded.

Figure 22.- Continued.



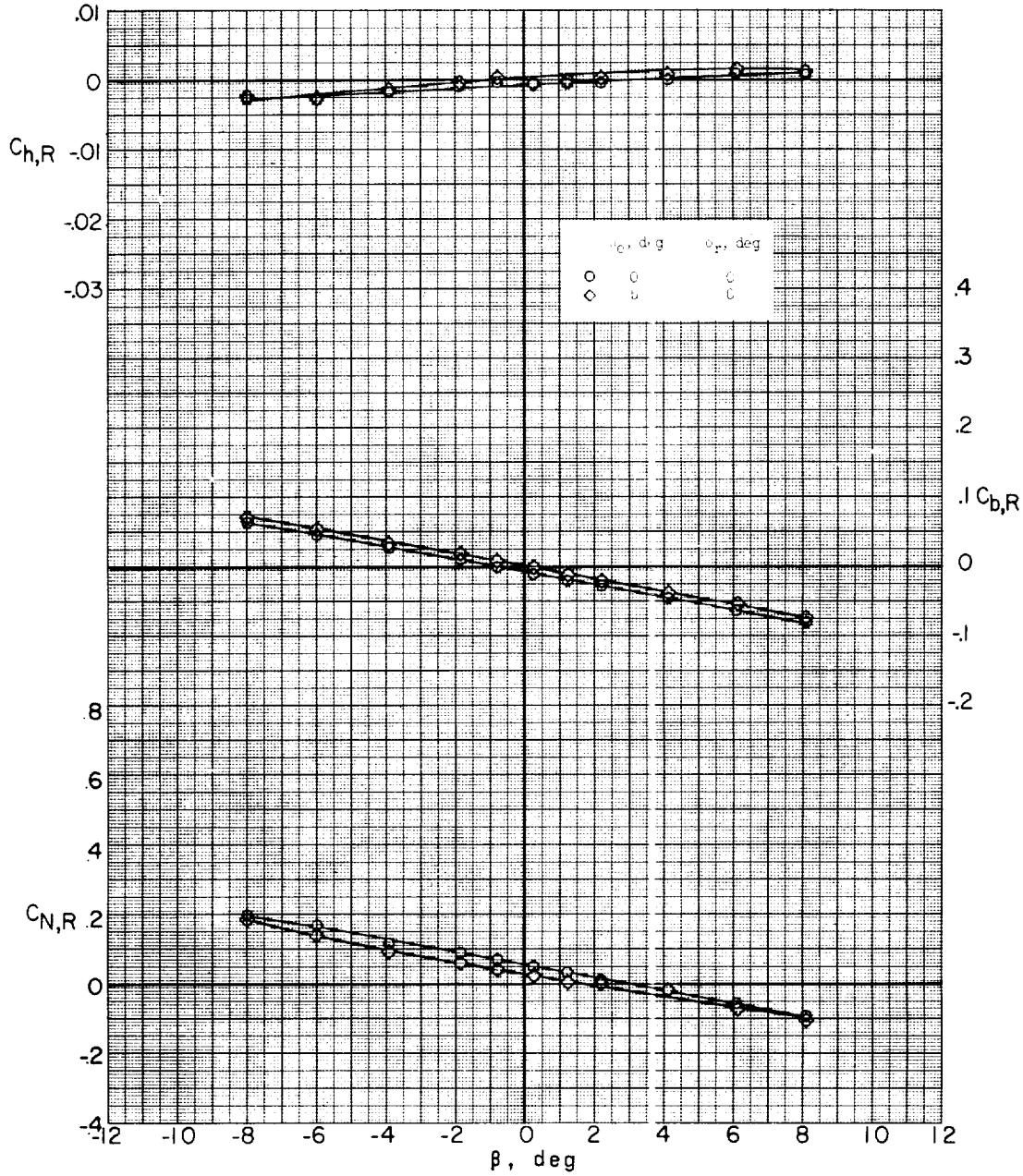
(e) M = 3.22; $\alpha = 0^{\circ}$.

Figure 22.- Continued.



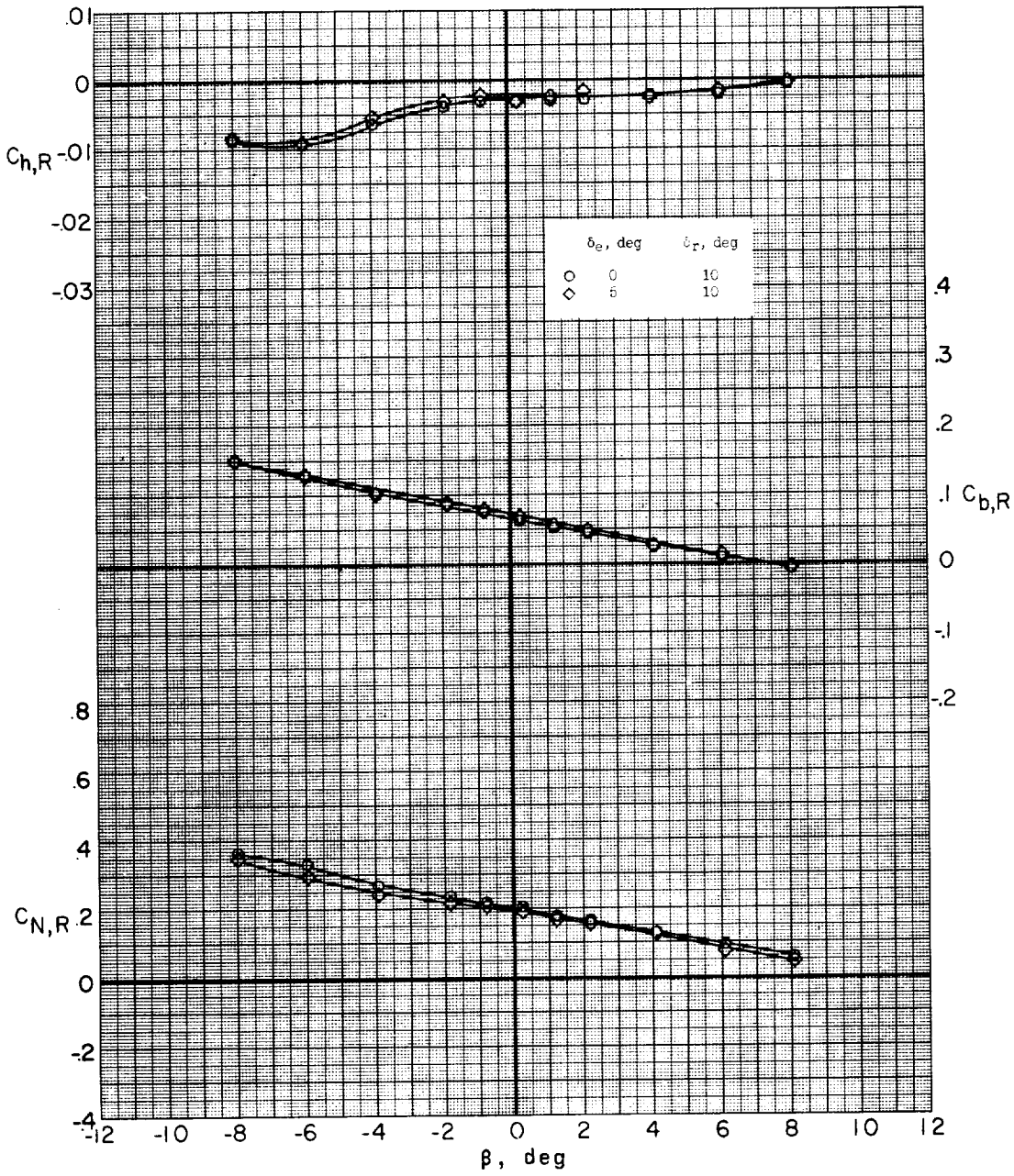
(e) Concluded.

Figure 22.- Continued.



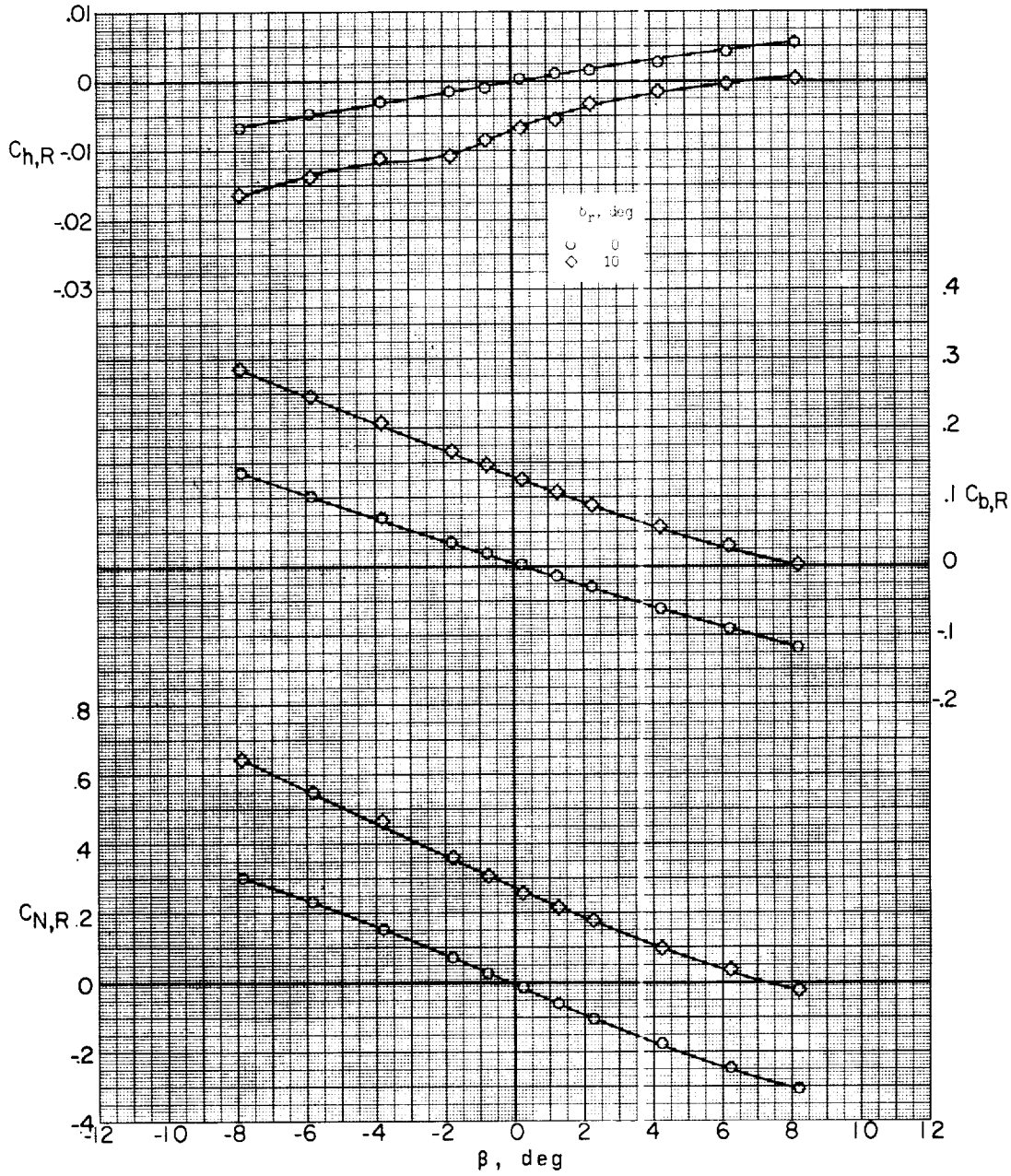
(f) M = 3.22; $\alpha = 5.0^{\circ}$.

Figure 22.- Continued.



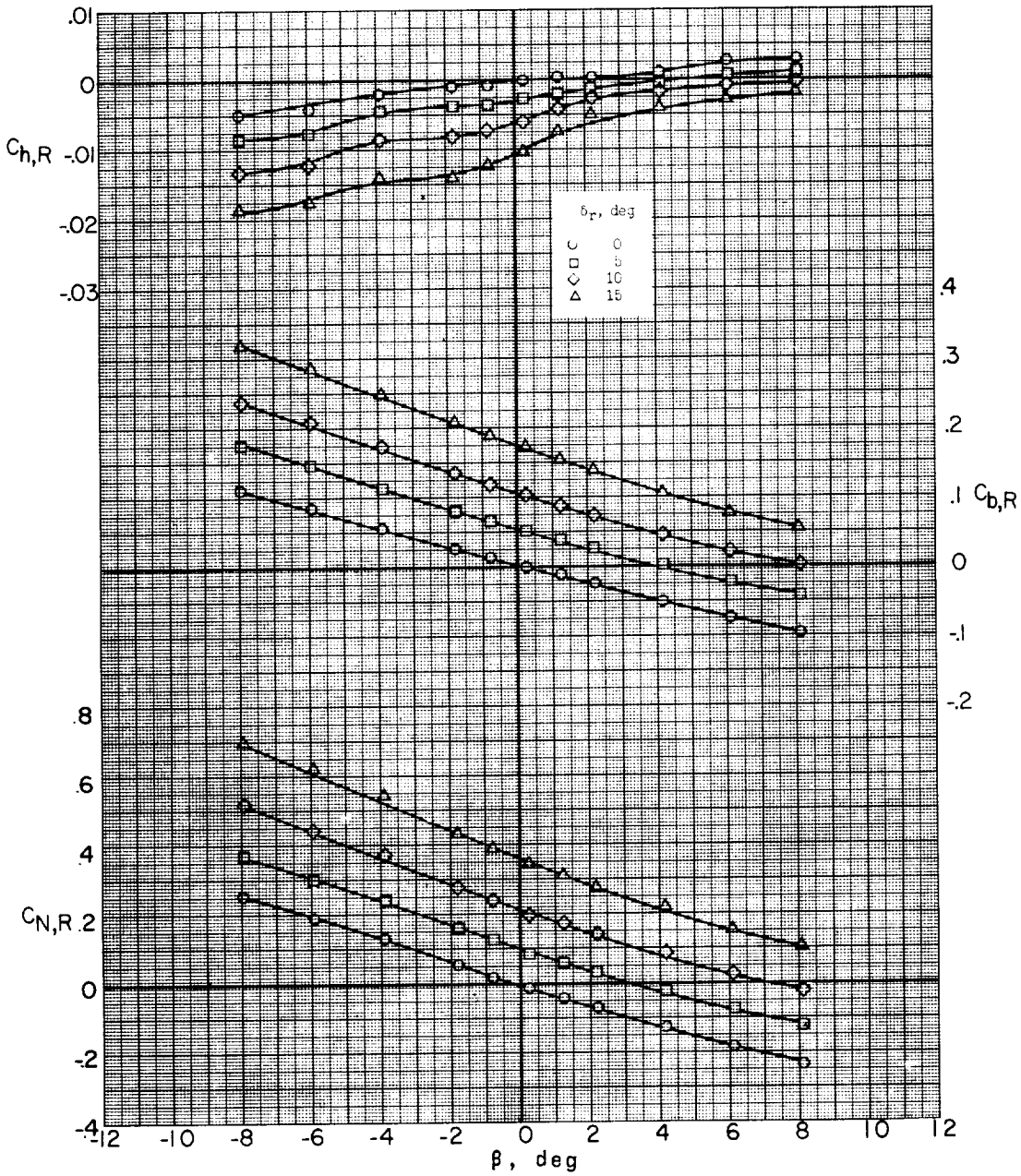
(f) Concluded.

Figure 22.- Concluded.



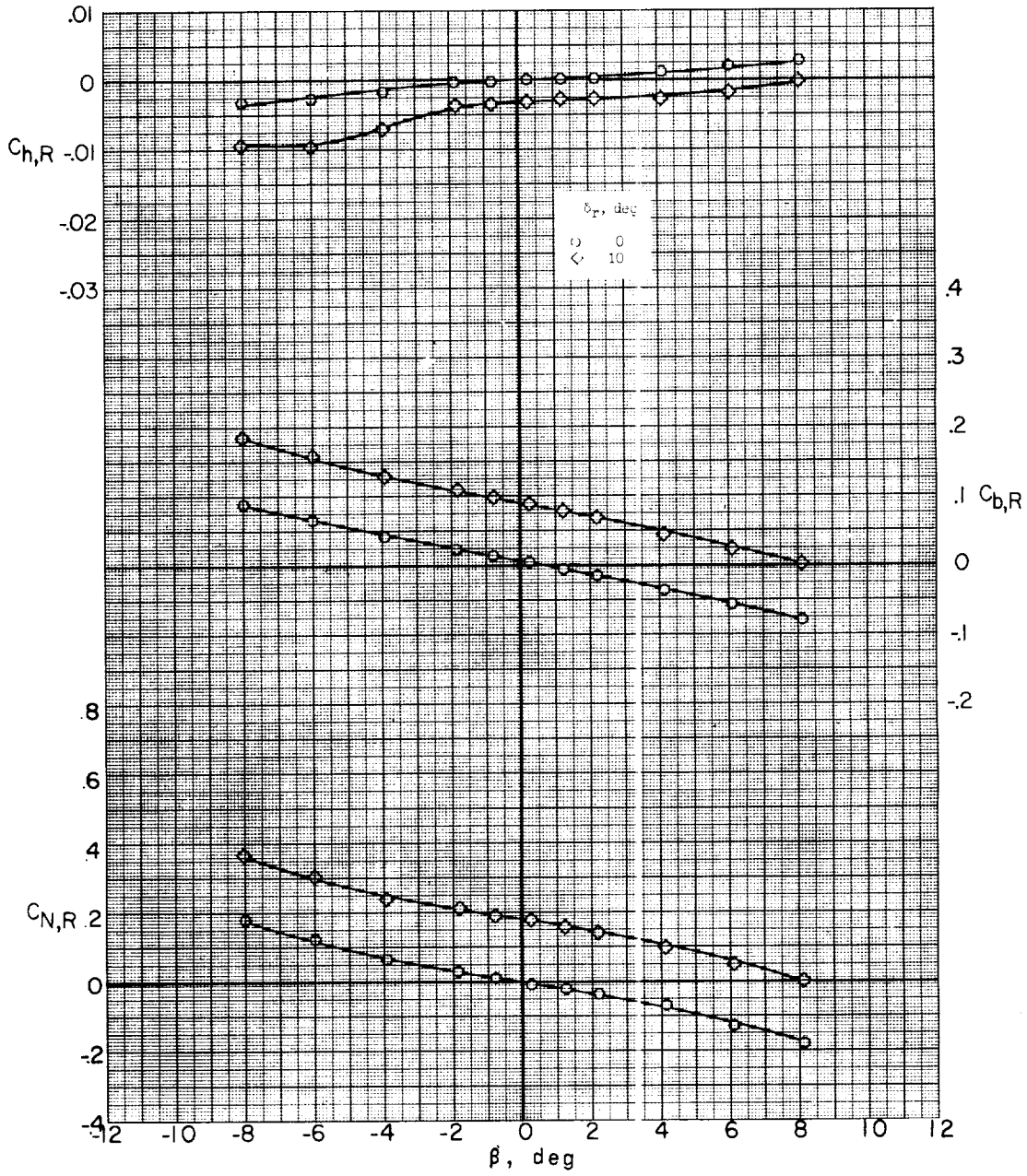
(a) M = 2.75; α = -5.0°.

Figure 23.- Effect of rudder deflection on lateral characteristics of missile rudder. Missile-booster combination with A-frame mounted; δ_e = 0°; sting C.



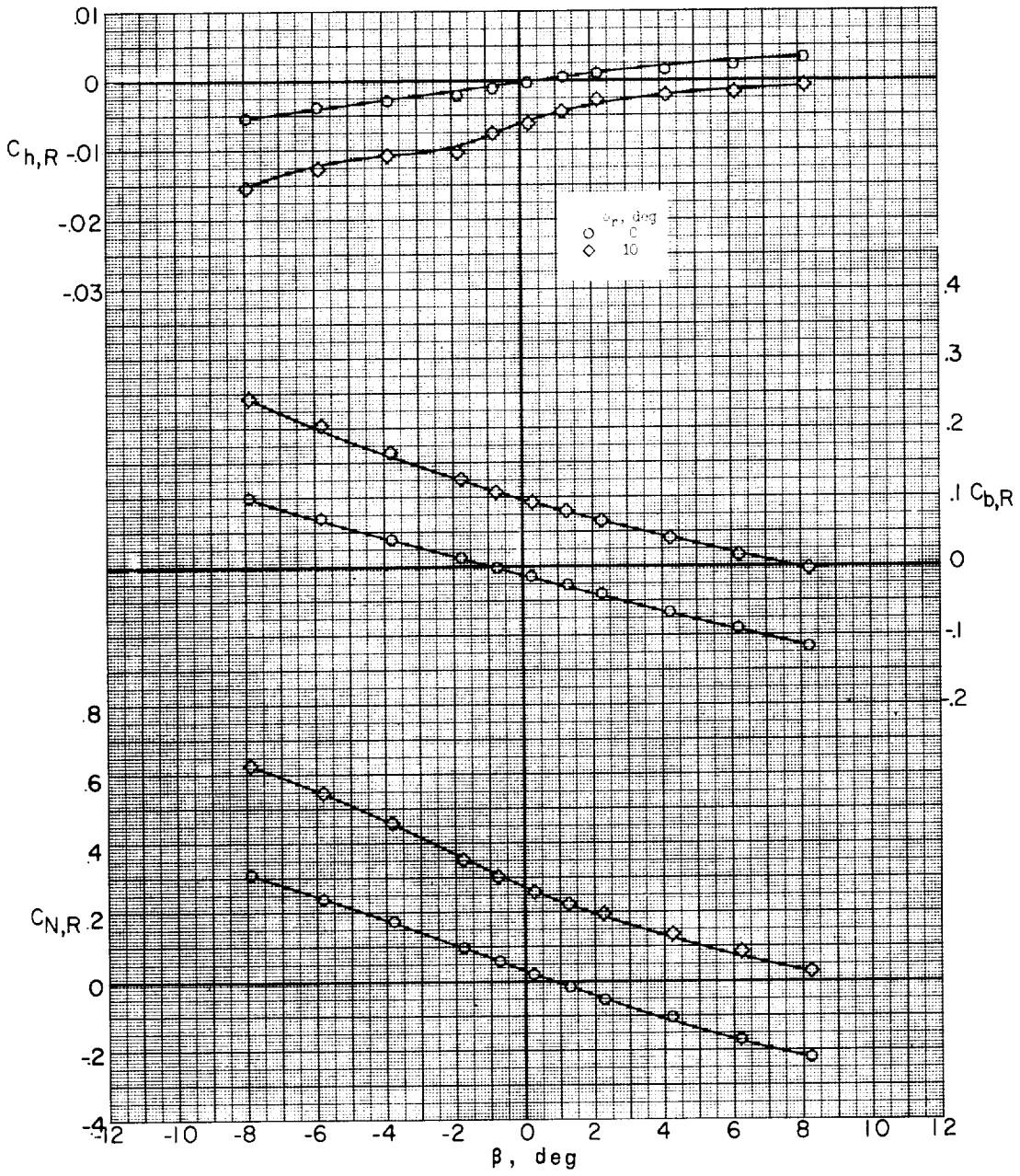
(b) M = 2.75; $\alpha = 0^{\circ}$.

Figure 23.- Continued.



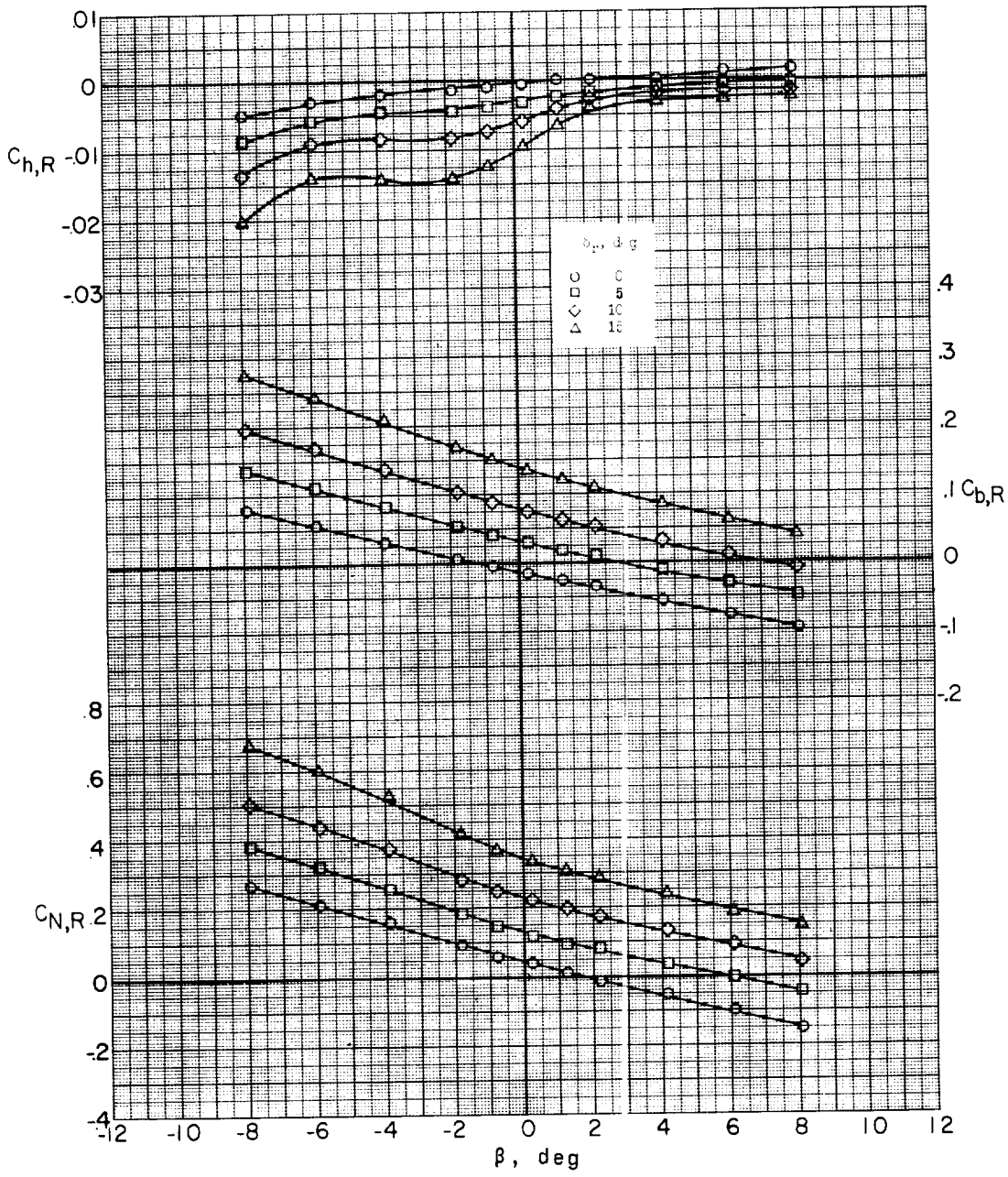
(c) M = 2.75; $\alpha = 5.0^{\circ}$.

Figure 23.- Continued.



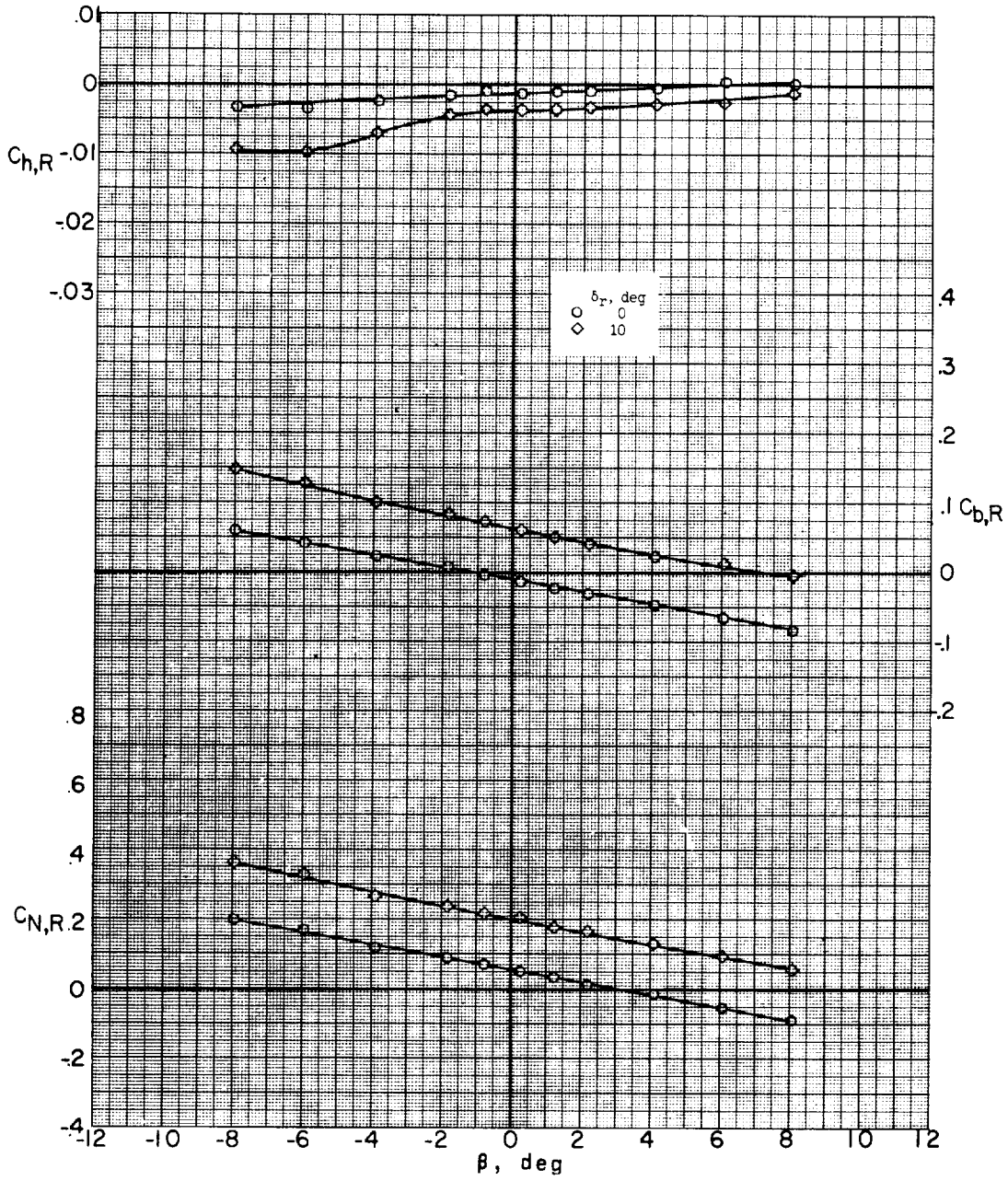
(d) M = 3.22; $\alpha = -5.0^{\circ}$.

Figure 23.- Continued.



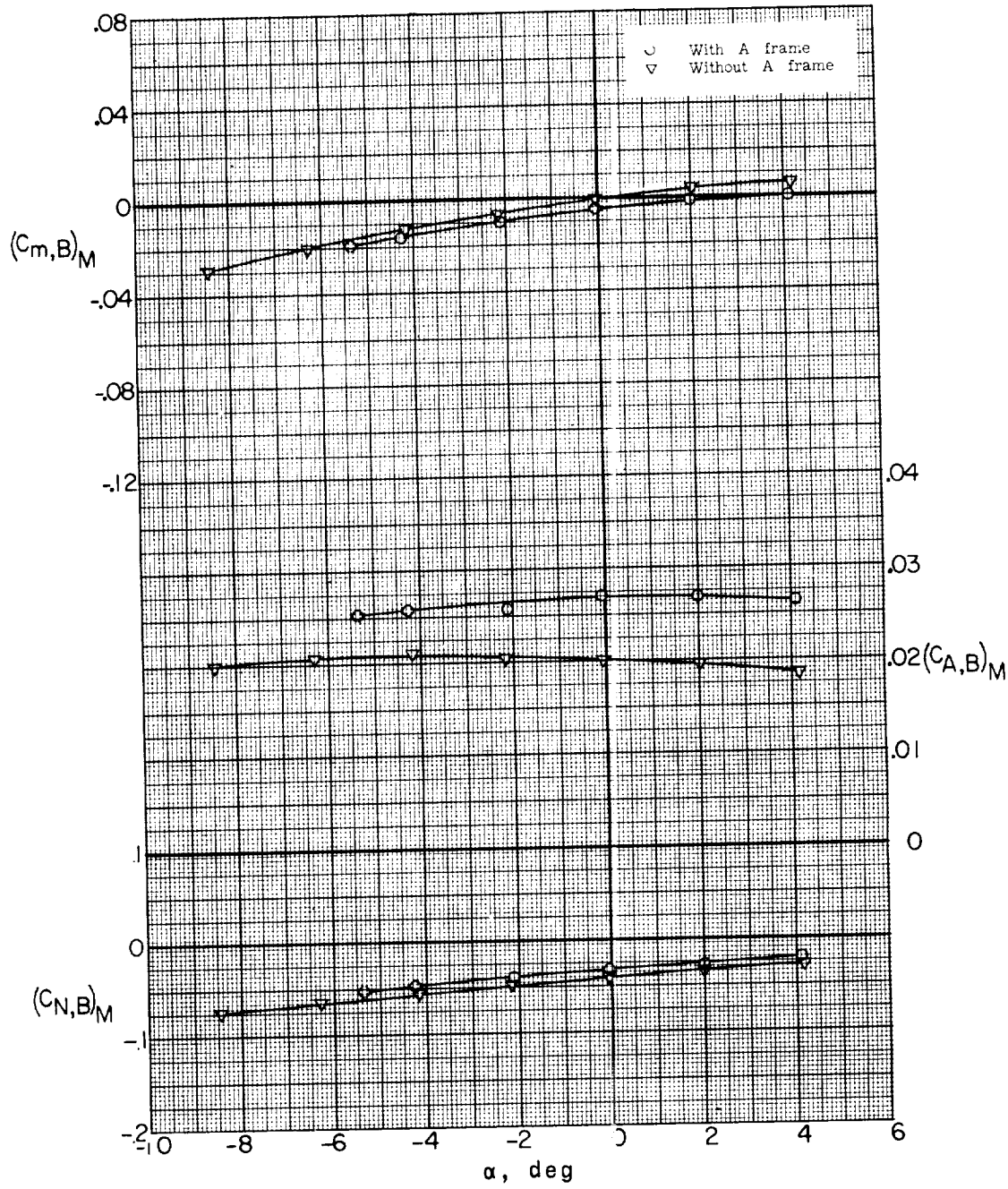
(e) M = 3.22; $\alpha = 0^{o}$.

Figure 23.- Continued.



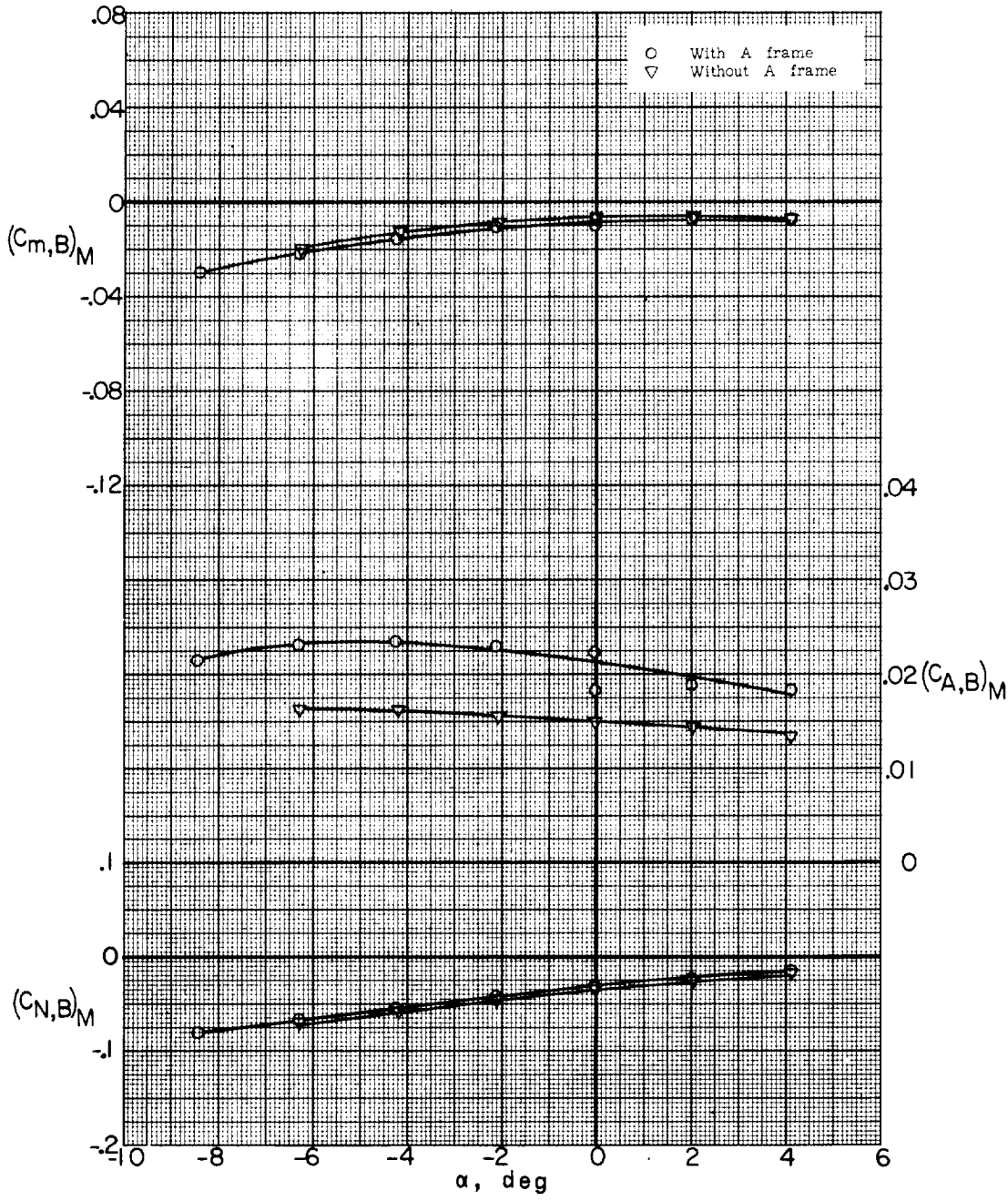
(f) M = 3.22; $\alpha = 5.0^{\circ}$.

Figure 23.- Concluded.



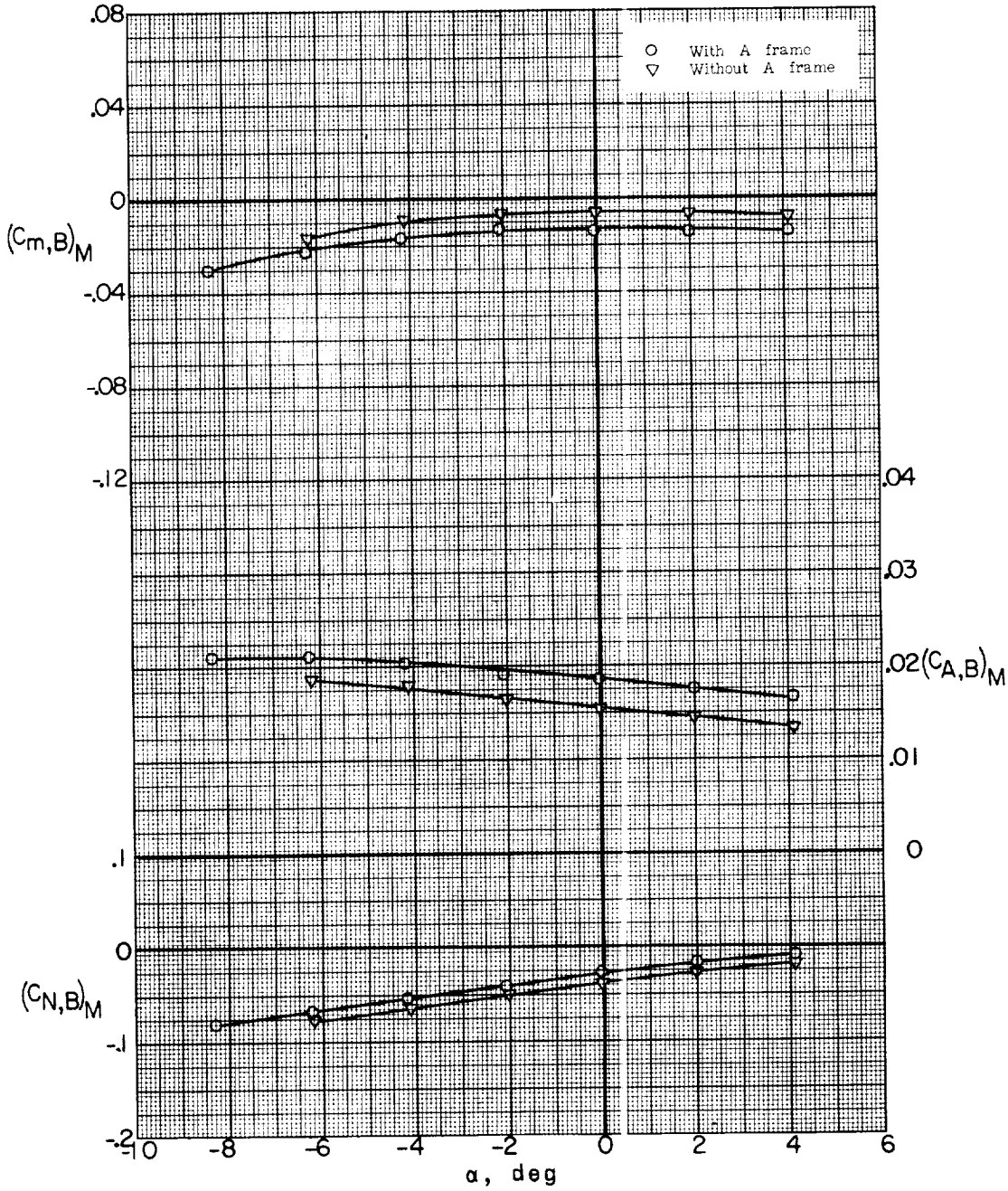
(a) M = 2.29.

Figure 24.- Effect of A-frame on pitch characteristics of booster. Missile-booster combination; $\delta_e = 0^o$; $\beta = 0.3^o$; sting A.



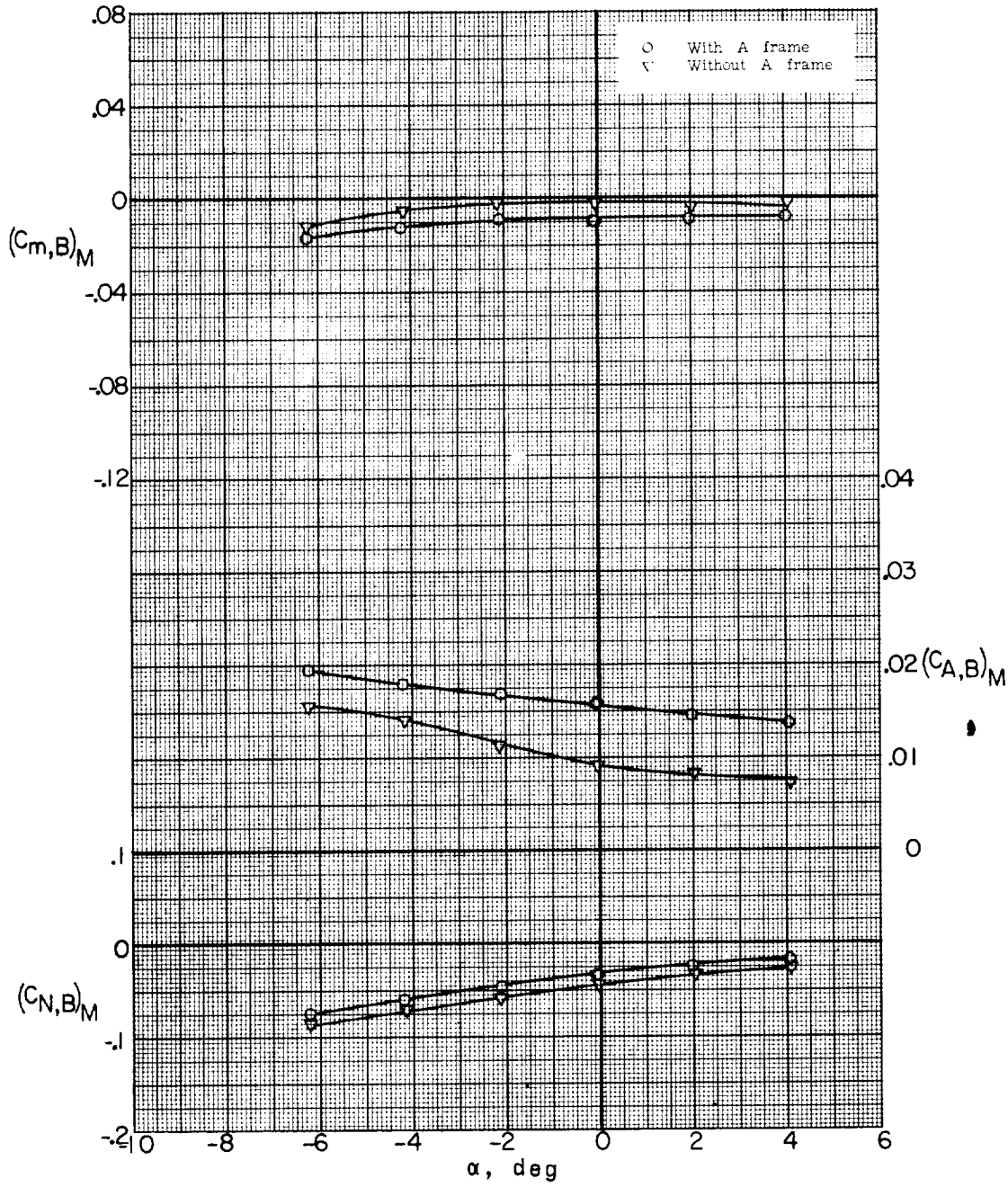
(b) M = 2.75.

Figure 24.- Continued.



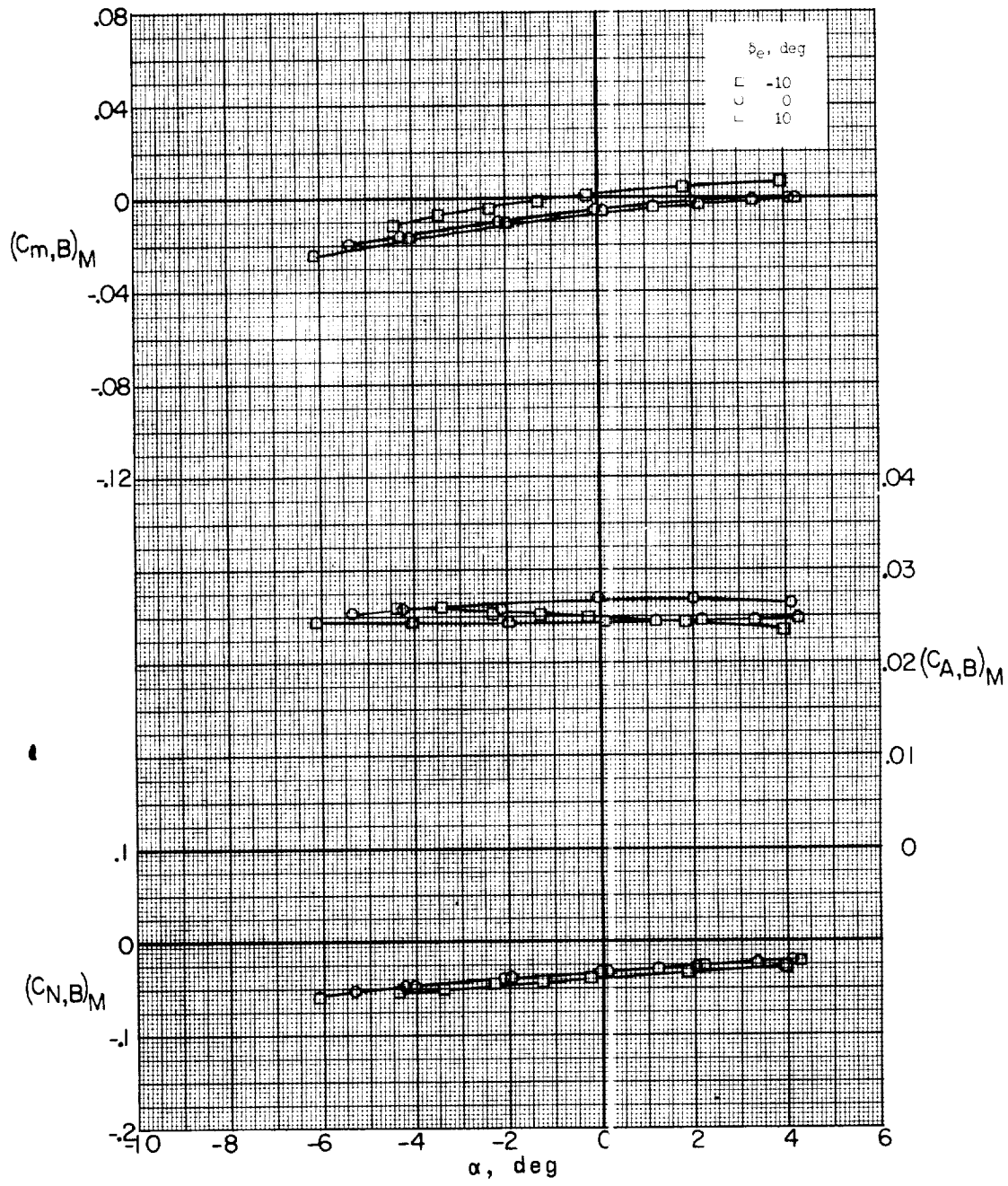
(c) M = 3.22.

Figure 24.- Continued.



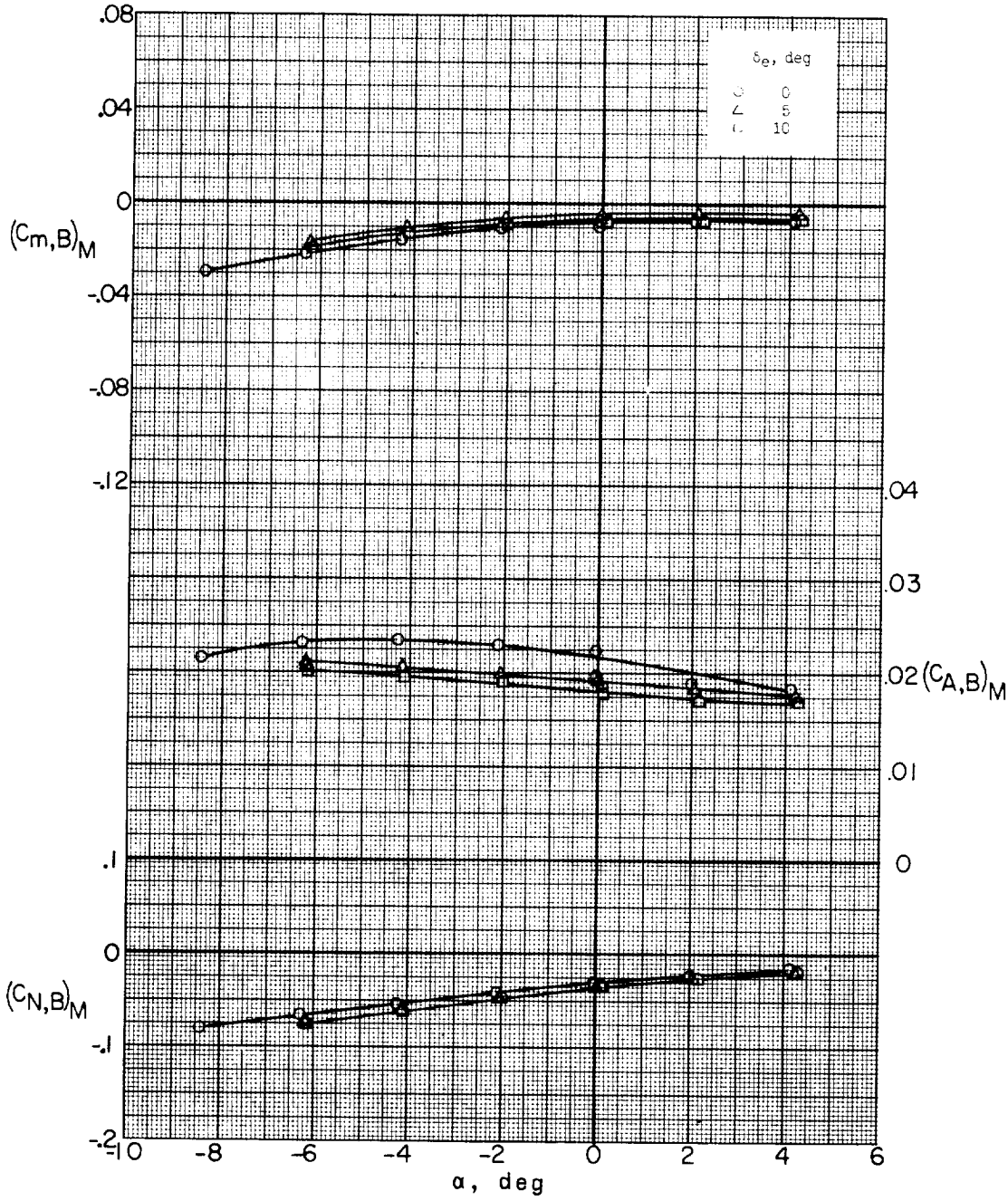
(d) M = 3.51.

Figure 24.- Concluded.



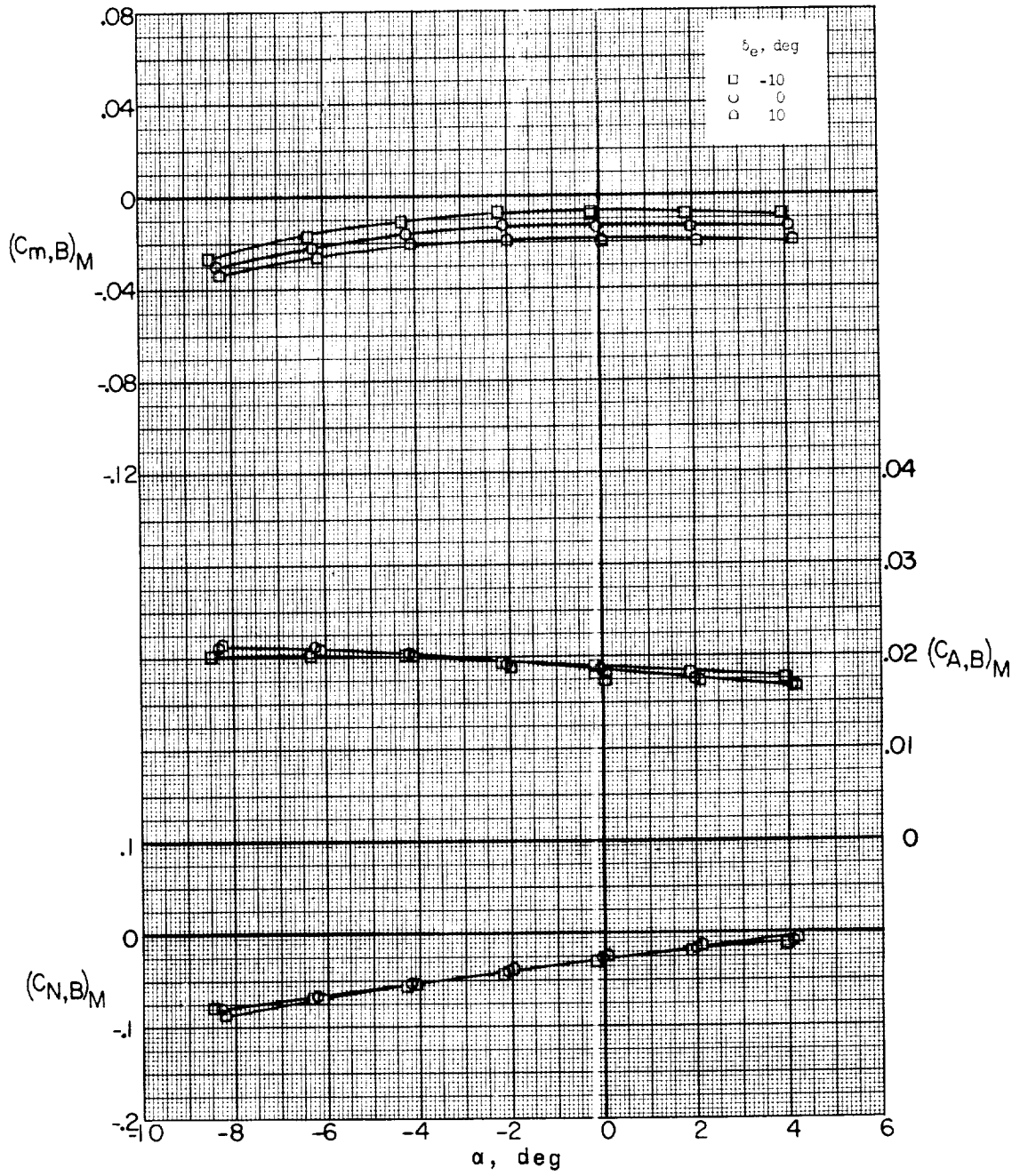
(a) M = 2.29.

Figure 25.- Effect of canard deflection on pitch characteristics of booster. Missile-booster combination with A-frame mounted; $\beta = 0.3^\circ$; sting A.



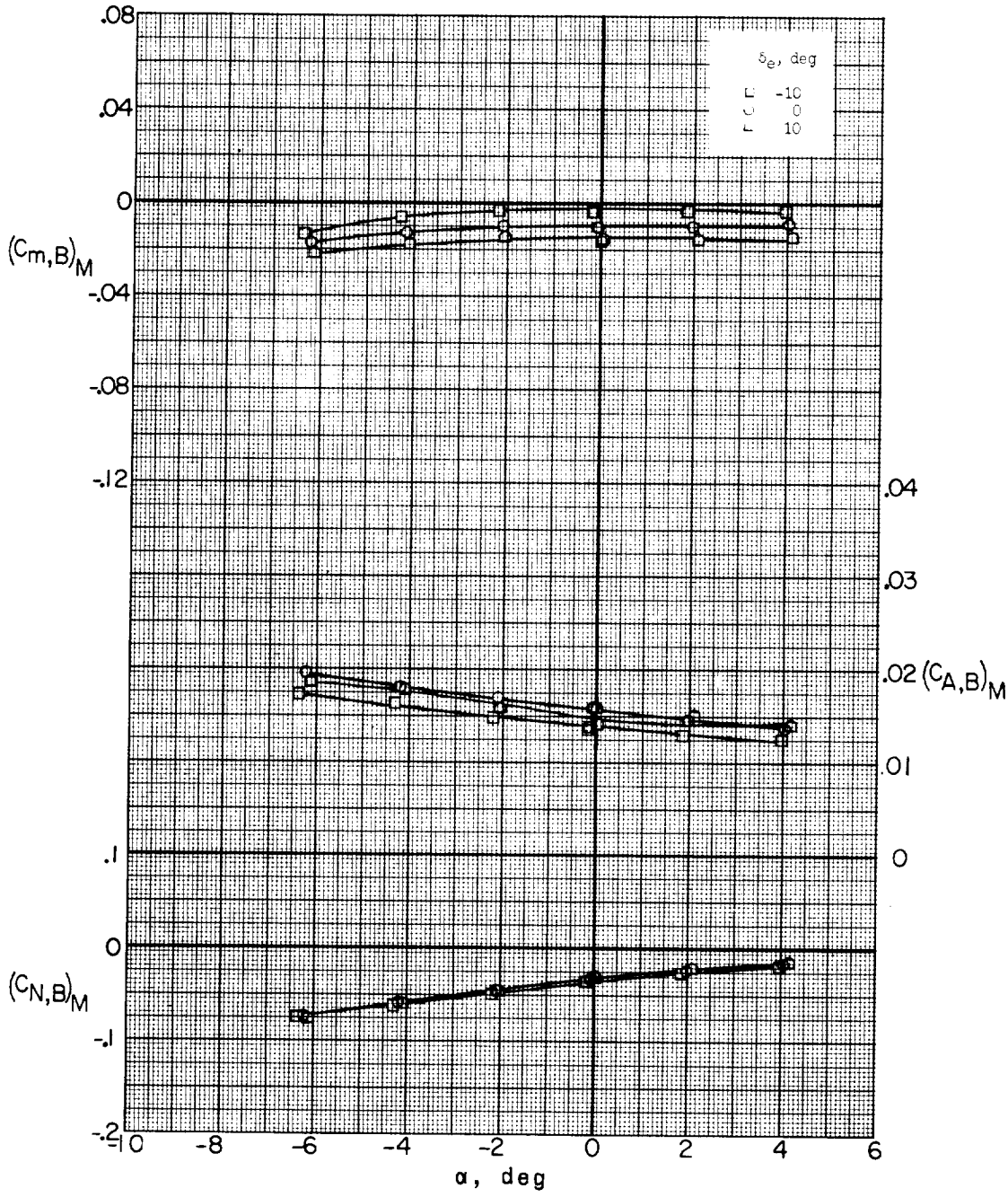
(b) M = 2.75.

Figure 25.- Continued.



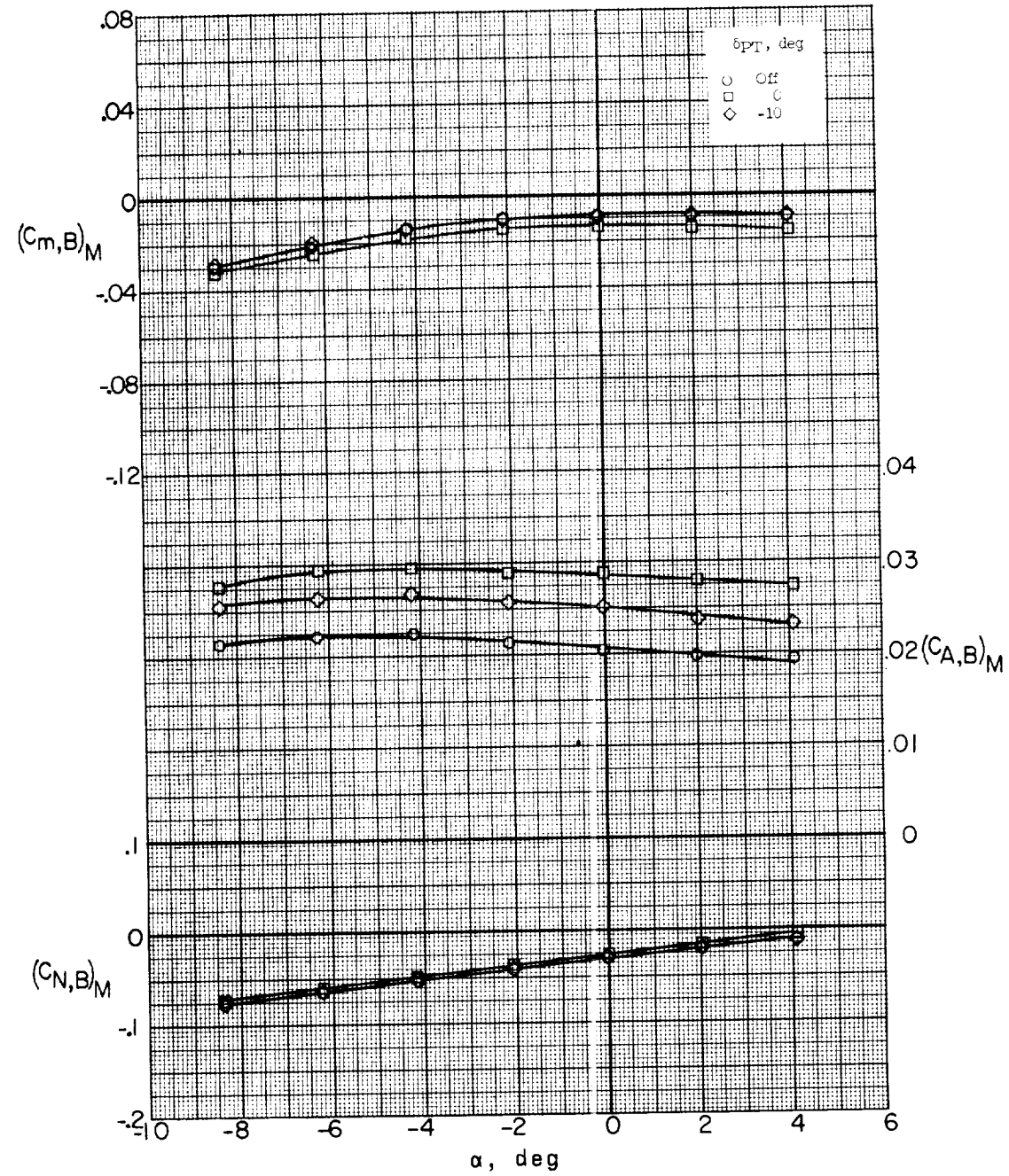
(c) M = 3.22.

Figure 25.- Continued.



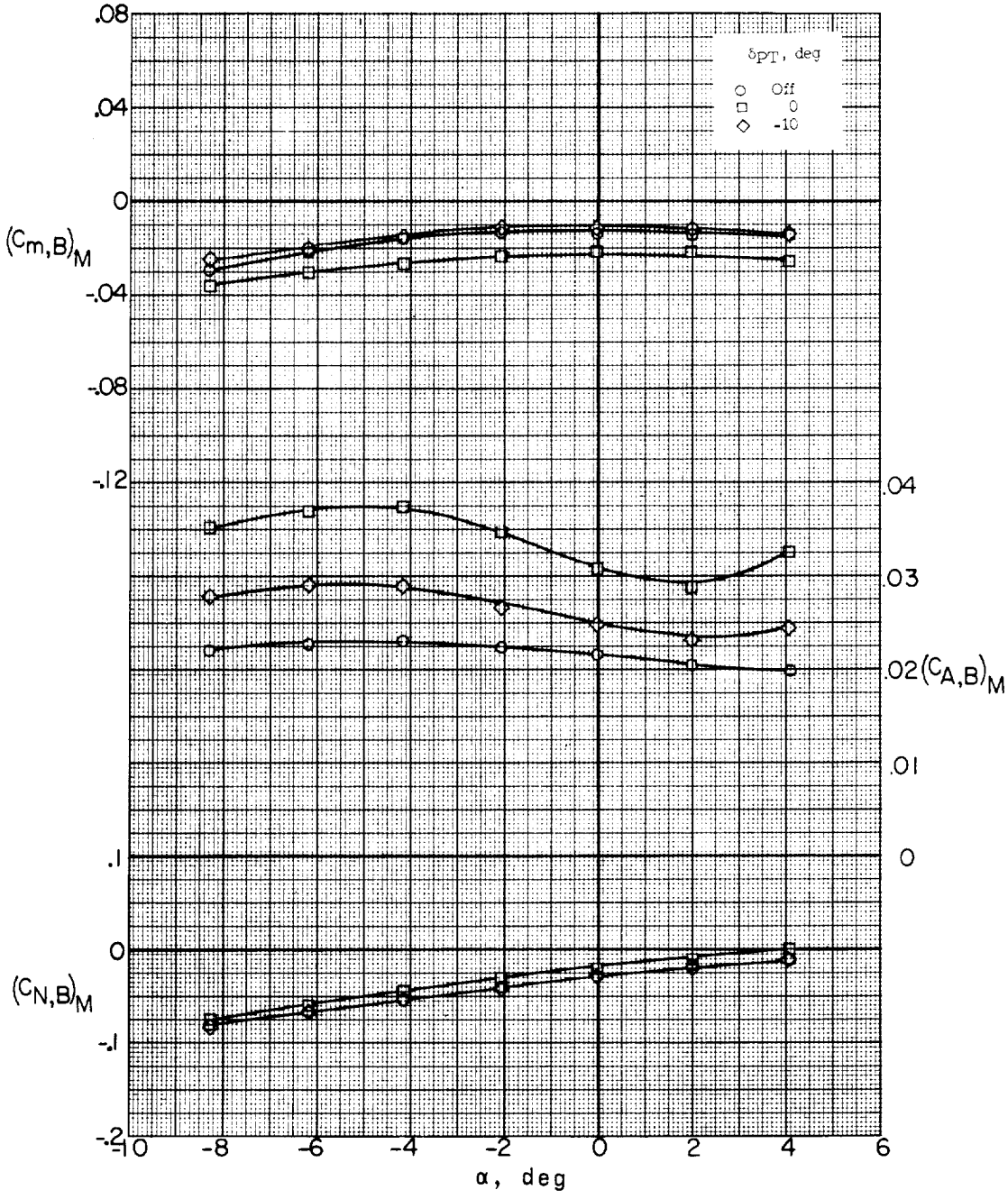
(d) M = 3.51.

Figure 25.- Concluded.



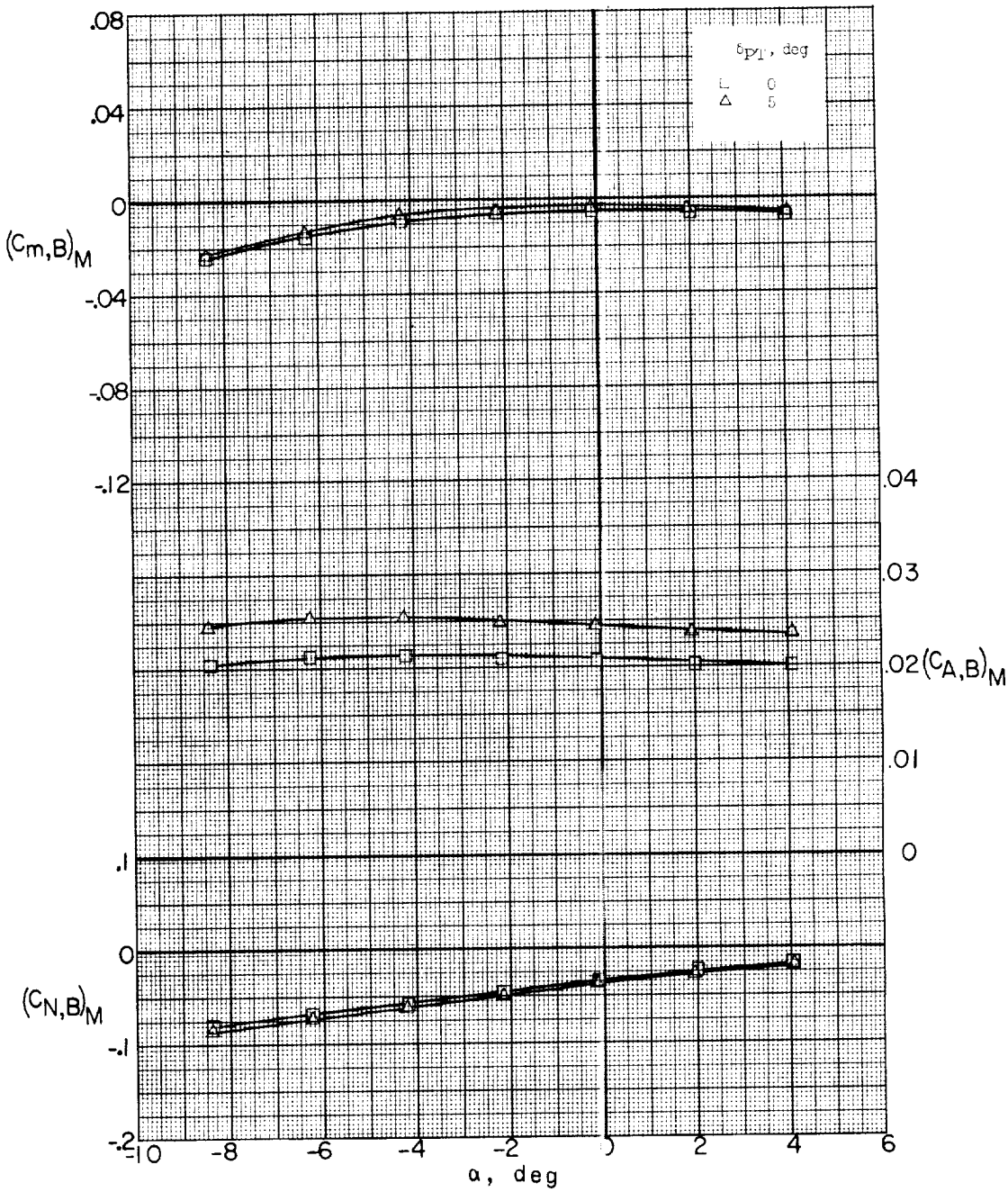
(a) M = 2.75; with bug-eye fairing.

Figure 26.- Effect of booster nozzle on pitch characteristics of booster. Missile-booster combination with A-frame mounted; $\delta_{YT} = 0^{\circ}$; $\beta = 0.2^{\circ}$; sting B.



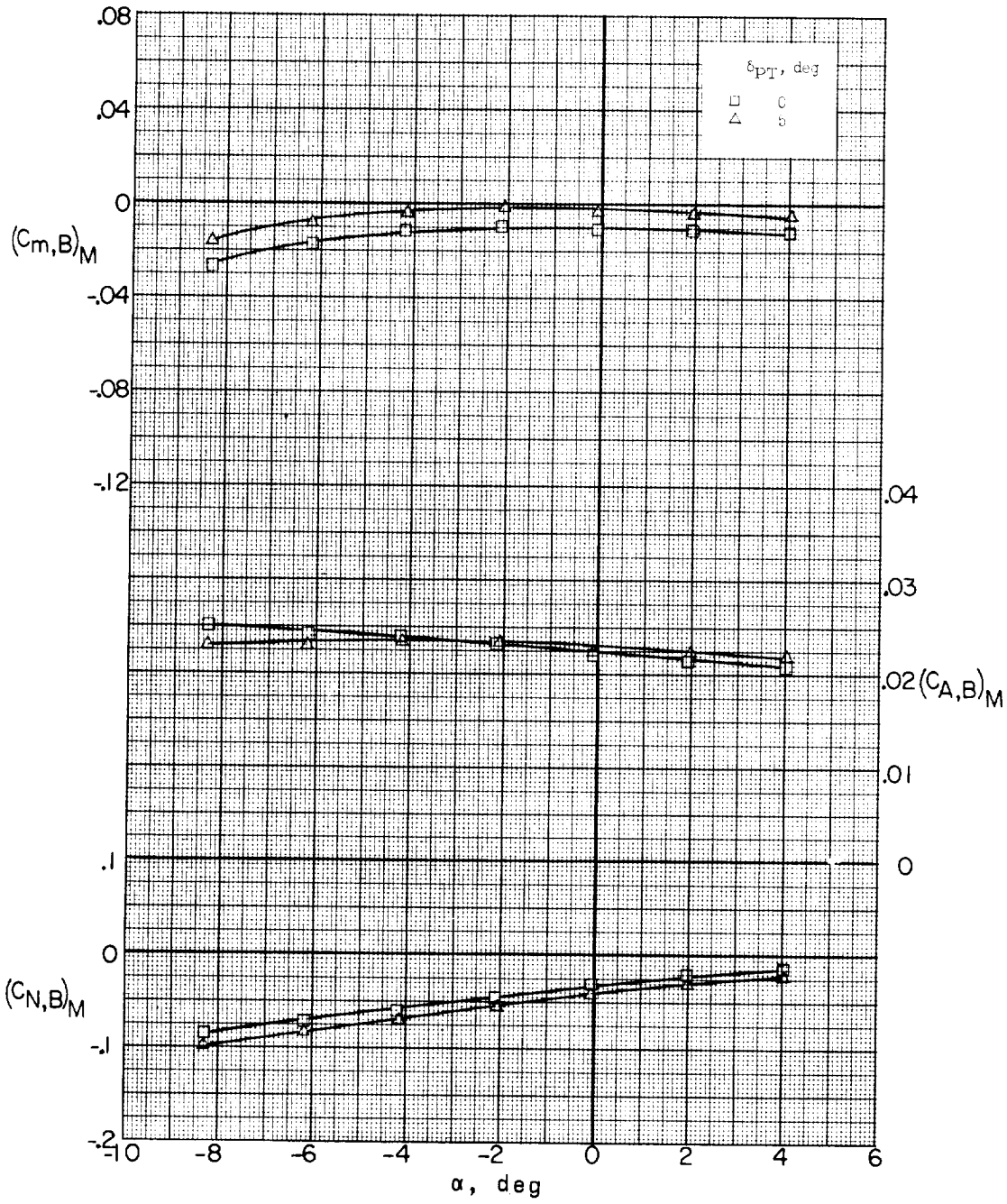
(b) M = 3.22; with bug-eye fairing.

Figure 26.- Continued.



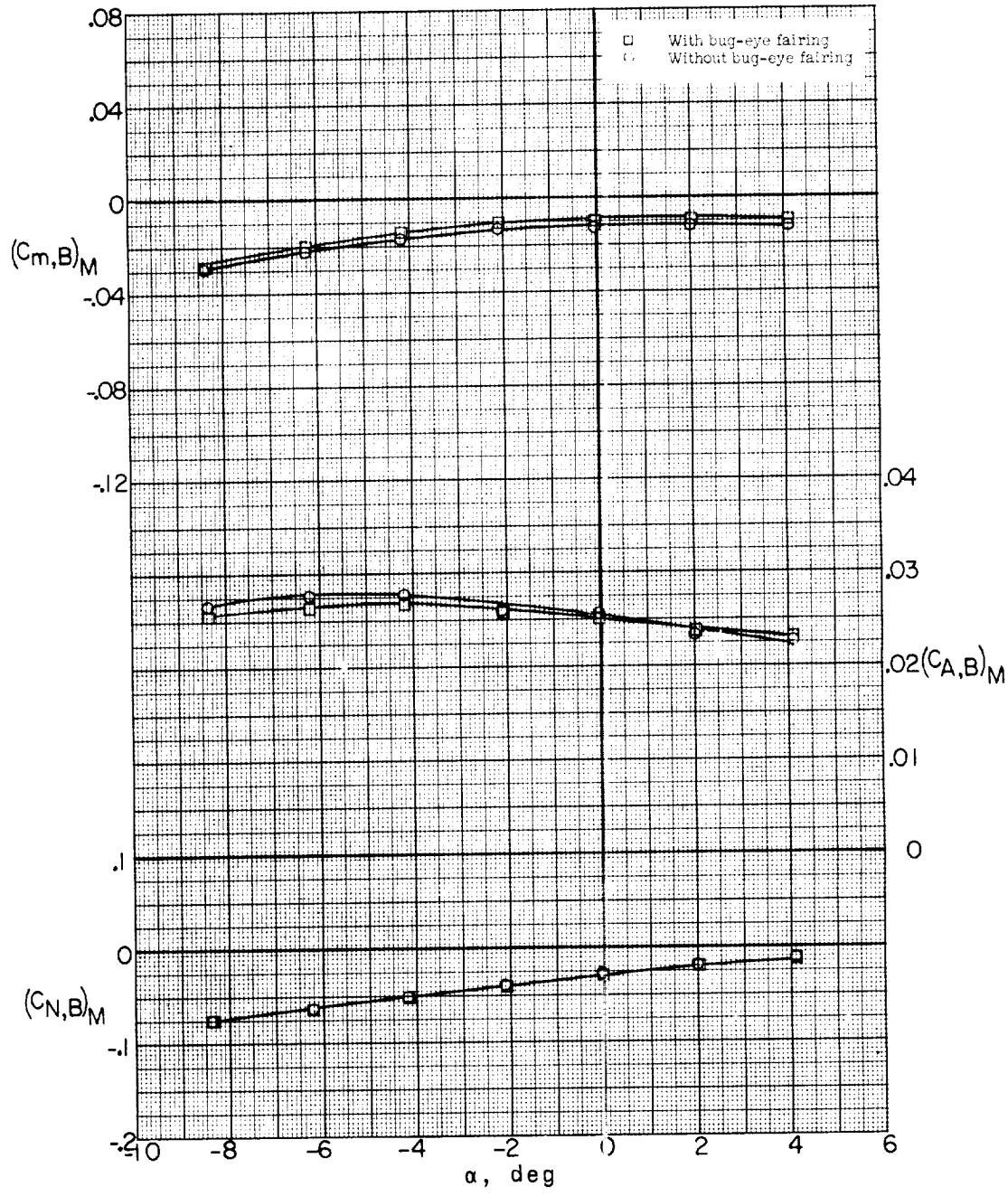
(c) M = 2.75; with bug-eye and nozzle-shroud fairings.

Figure 26.- Continued.



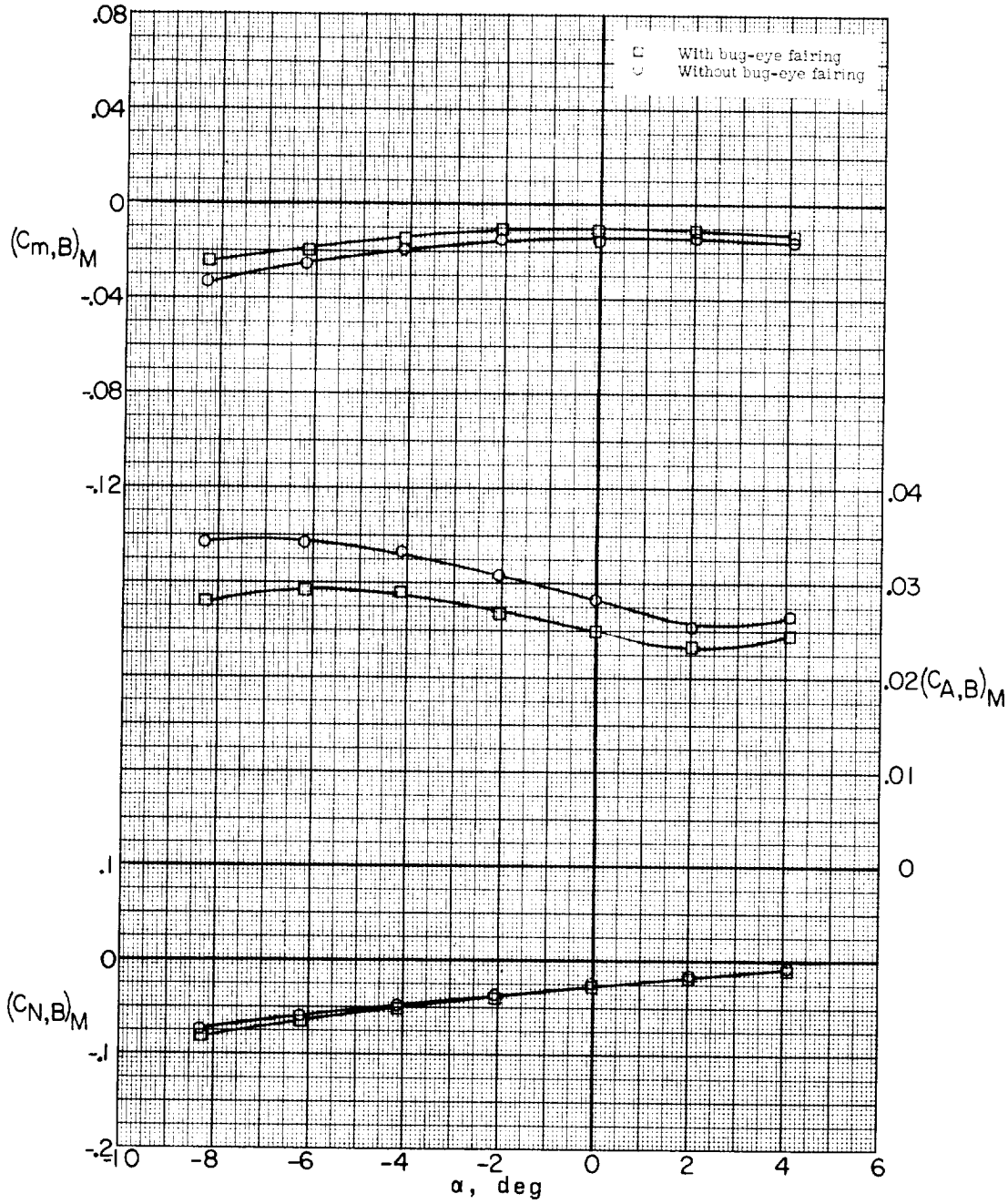
(d) M = 3.22; with bug-eye and nozzle-shroud fairings.

Figure 26.- Concluded.



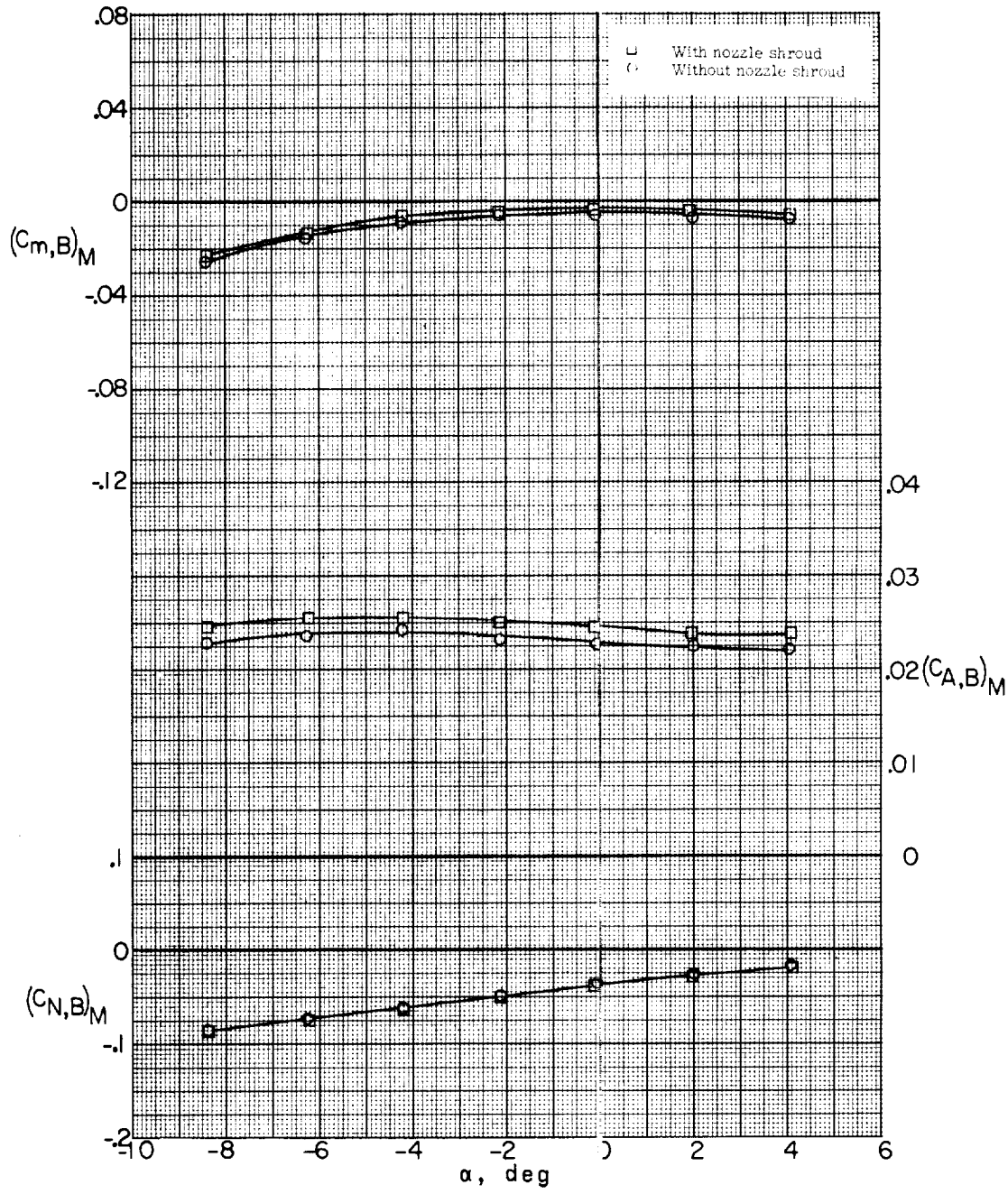
(a) M = 2.75.

Figure 27.- Effect of bug-eye fairing on pitch characteristics of booster. Missile-booster combination with A-frame mounted; $\delta_{PT} = -10^{\circ}$; $\delta_{YT} = 0^{\circ}$; $\beta = 0.2^{\circ}$; stirg B.



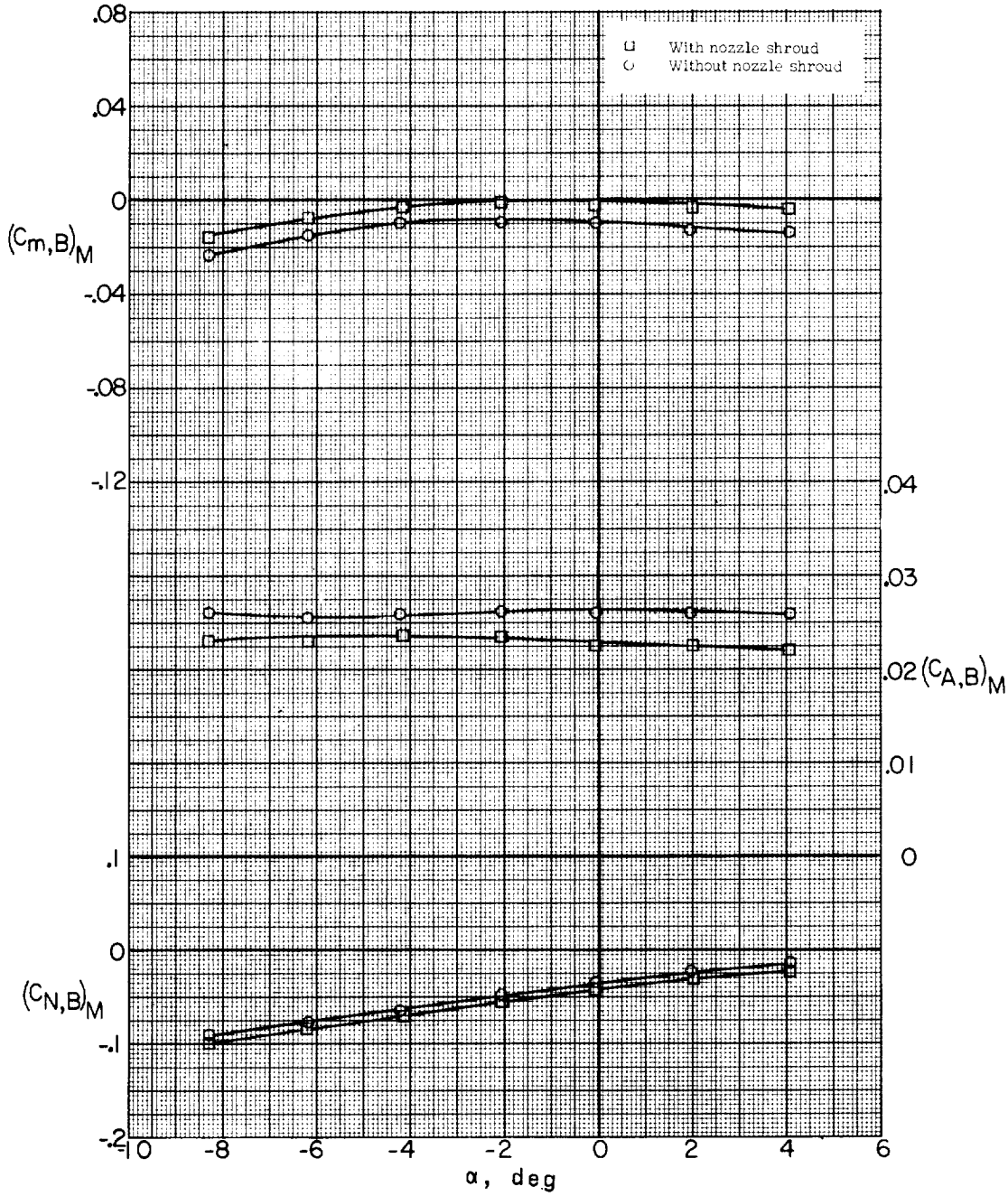
(b) M = 3.22.

Figure 27.- Concluded.



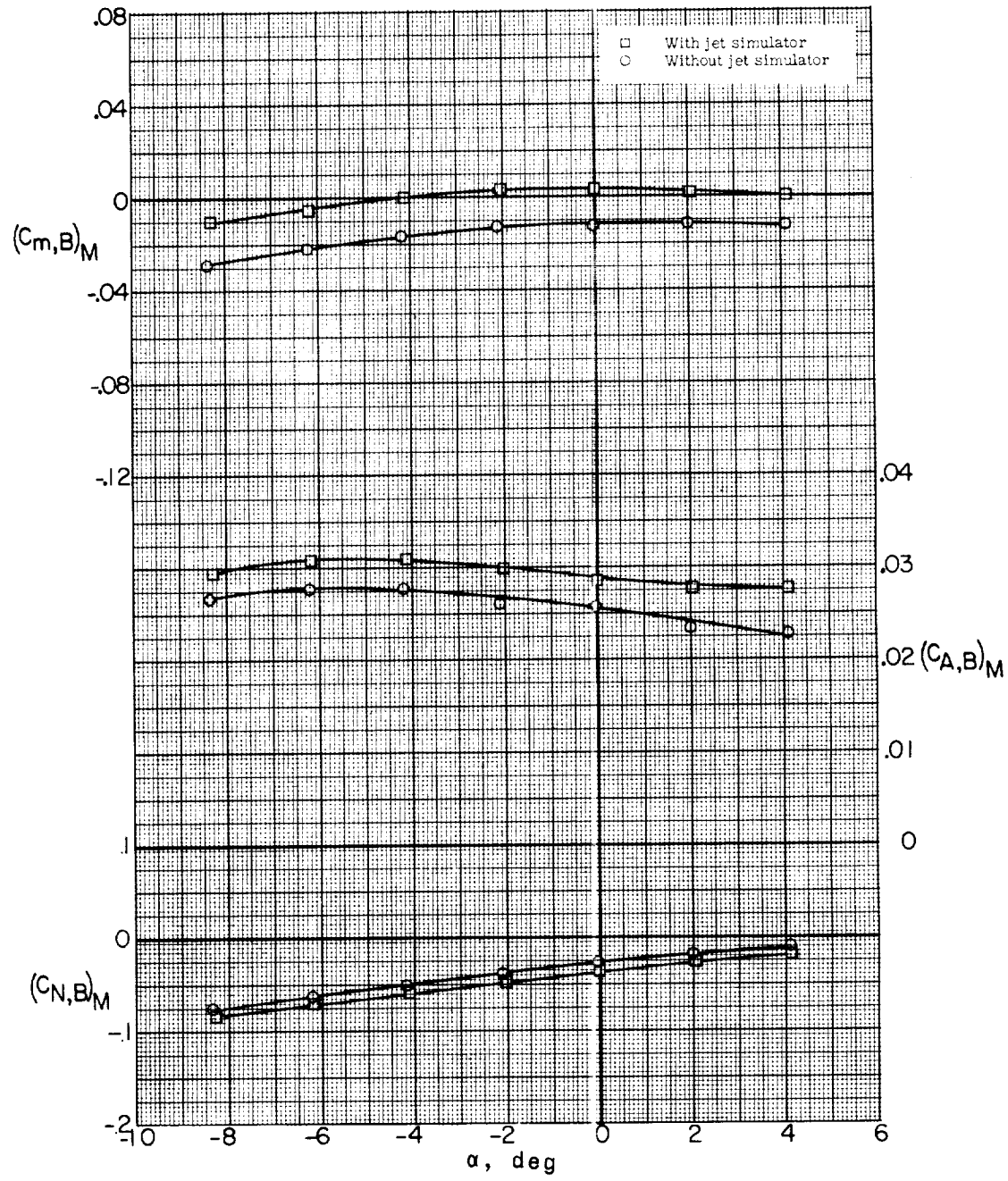
(a) M = 2.75.

Figure 28.- Effect of nozzle shrouds on pitch characteristics of booster. Missile-booster combination with bug-eye fairing and A-frame mounted; $\delta_{PT} = 5^\circ$; $\delta_{YT} = 0^\circ$; $\beta = 0.2^\circ$; sting B.



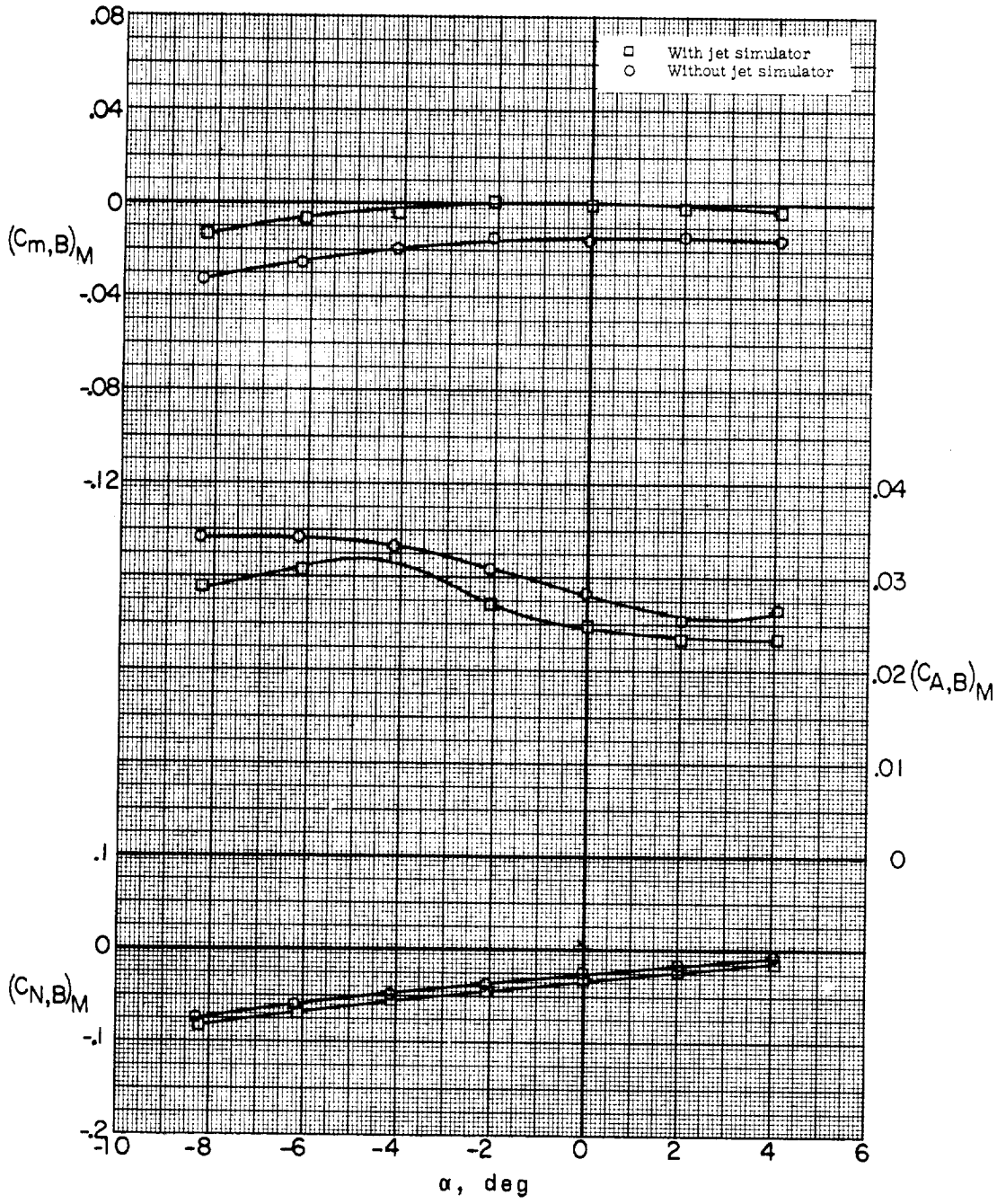
(b) M = 3.22.

Figure 28.- Concluded.



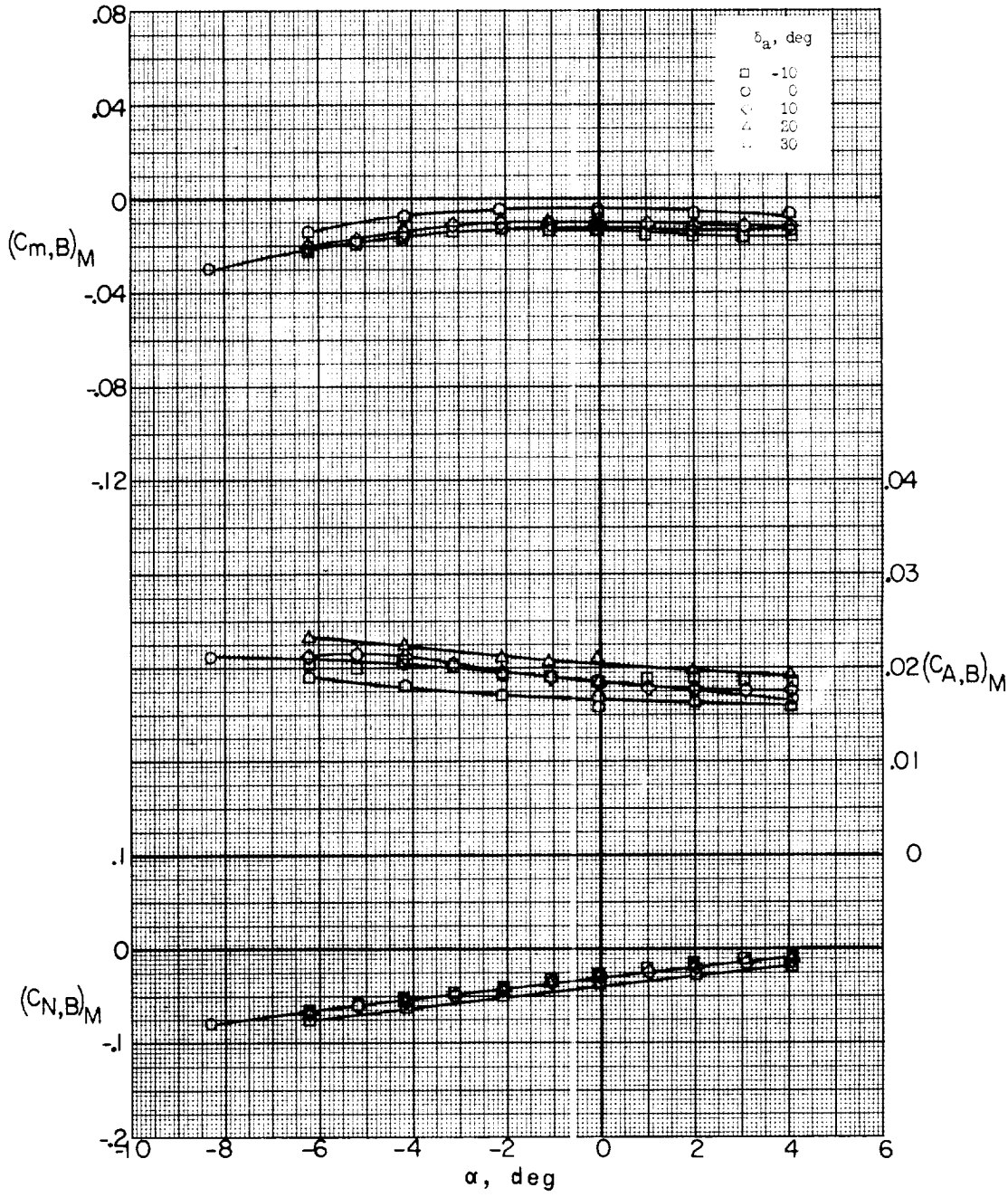
(a) M = 2.75.

Figure 29.- Effect of jet simulator mounted at rear of rocket nozzle on pitch characteristics of booster. Missile-booster combination with A-frame mounted; $\delta_{PT} = -10^{\circ}$; $\delta_{YT} = 0^{\circ}$; $\beta = 0.2^{\circ}$; sting B.



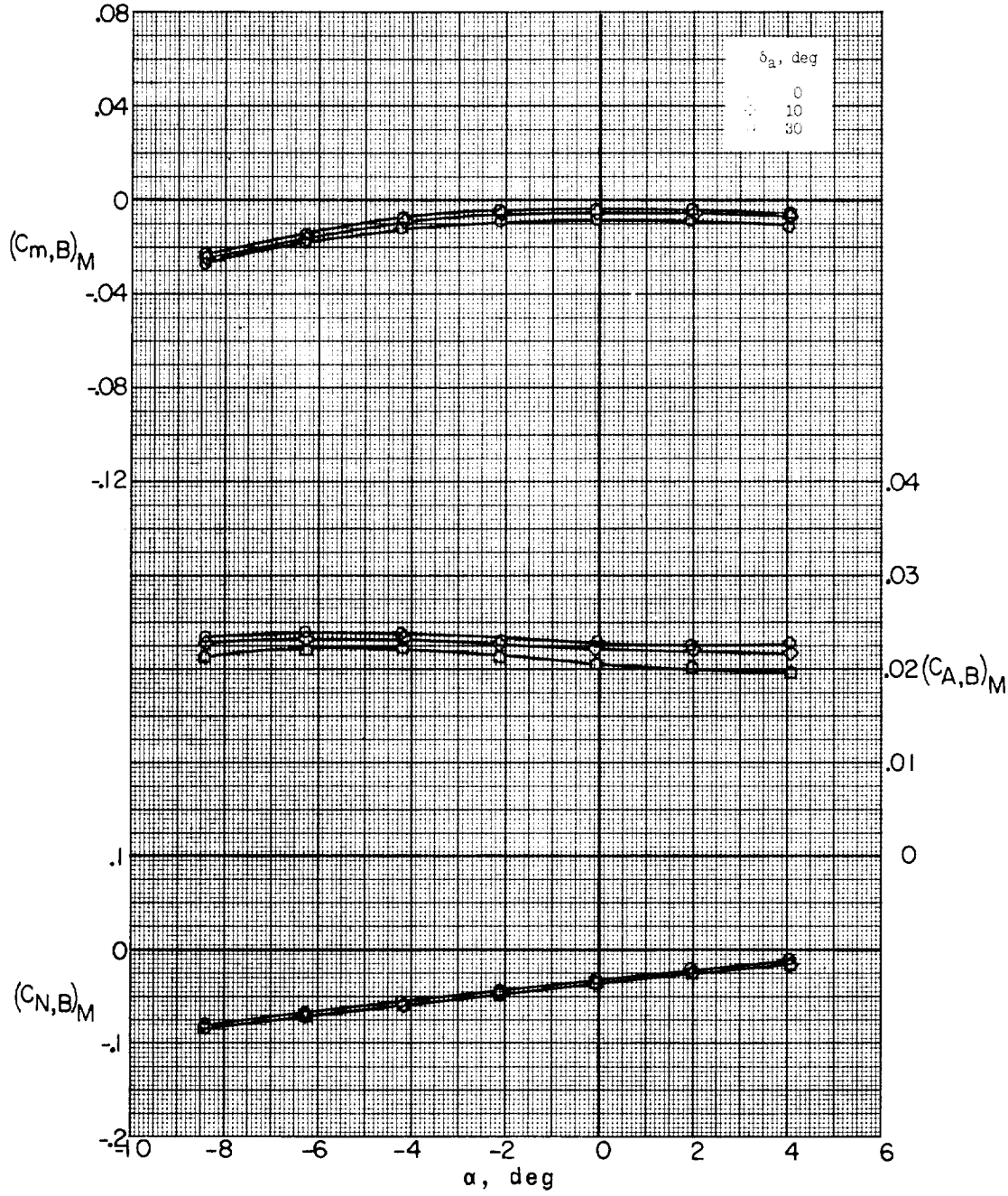
(b) M = 3.22.

Figure 29.- Concluded.



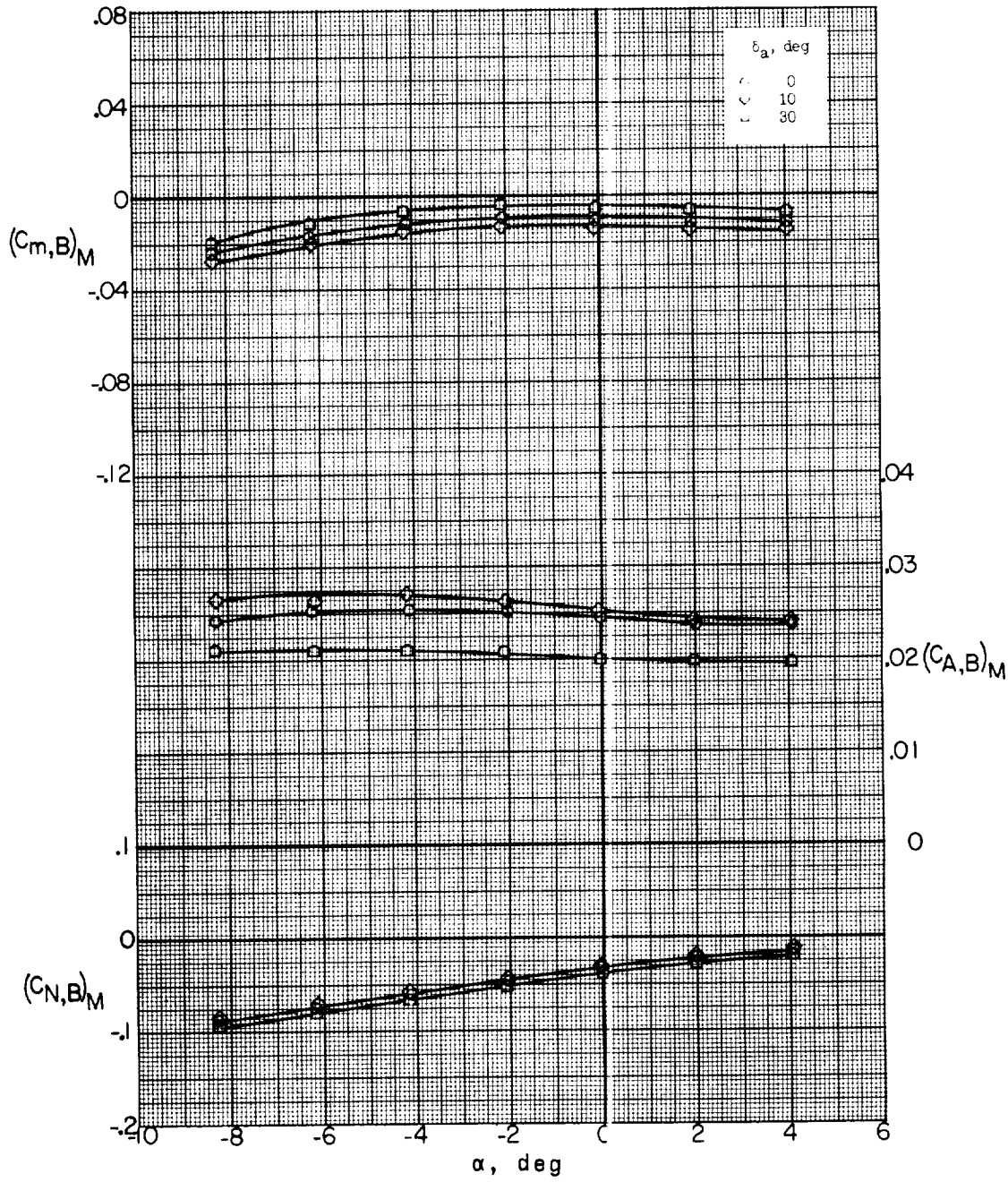
(a) M = 3.22; sting A.

Figure 30.- Effect of aileron deflection on pitch characteristics of booster. Missile-booster combination with A-frame mounted; $\delta_e = 0^\circ$; $\beta = 0.2^\circ$.



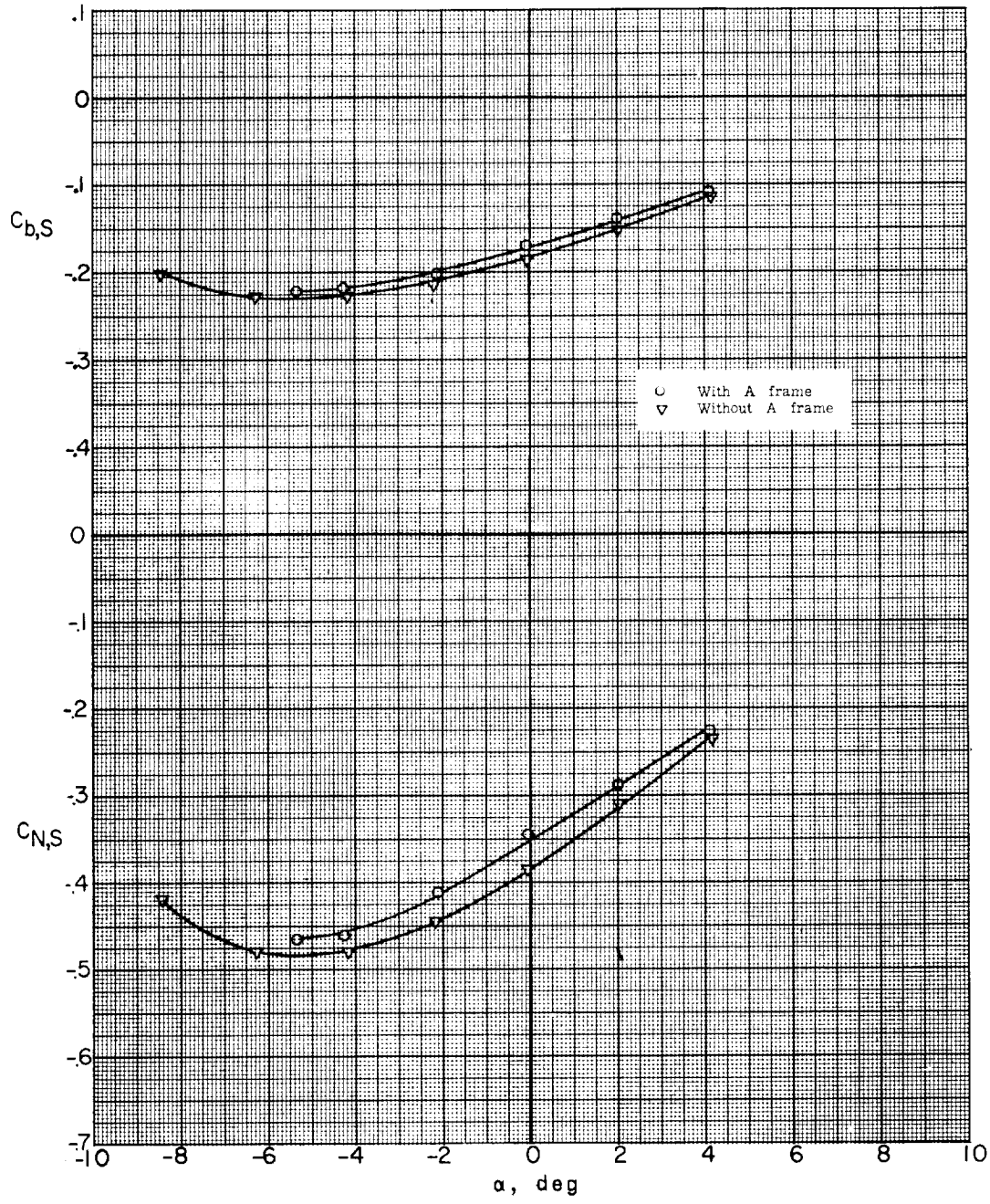
(b) M = 2.75; with missile aileron actuator housing; sting B.

Figure 30.- Continued.



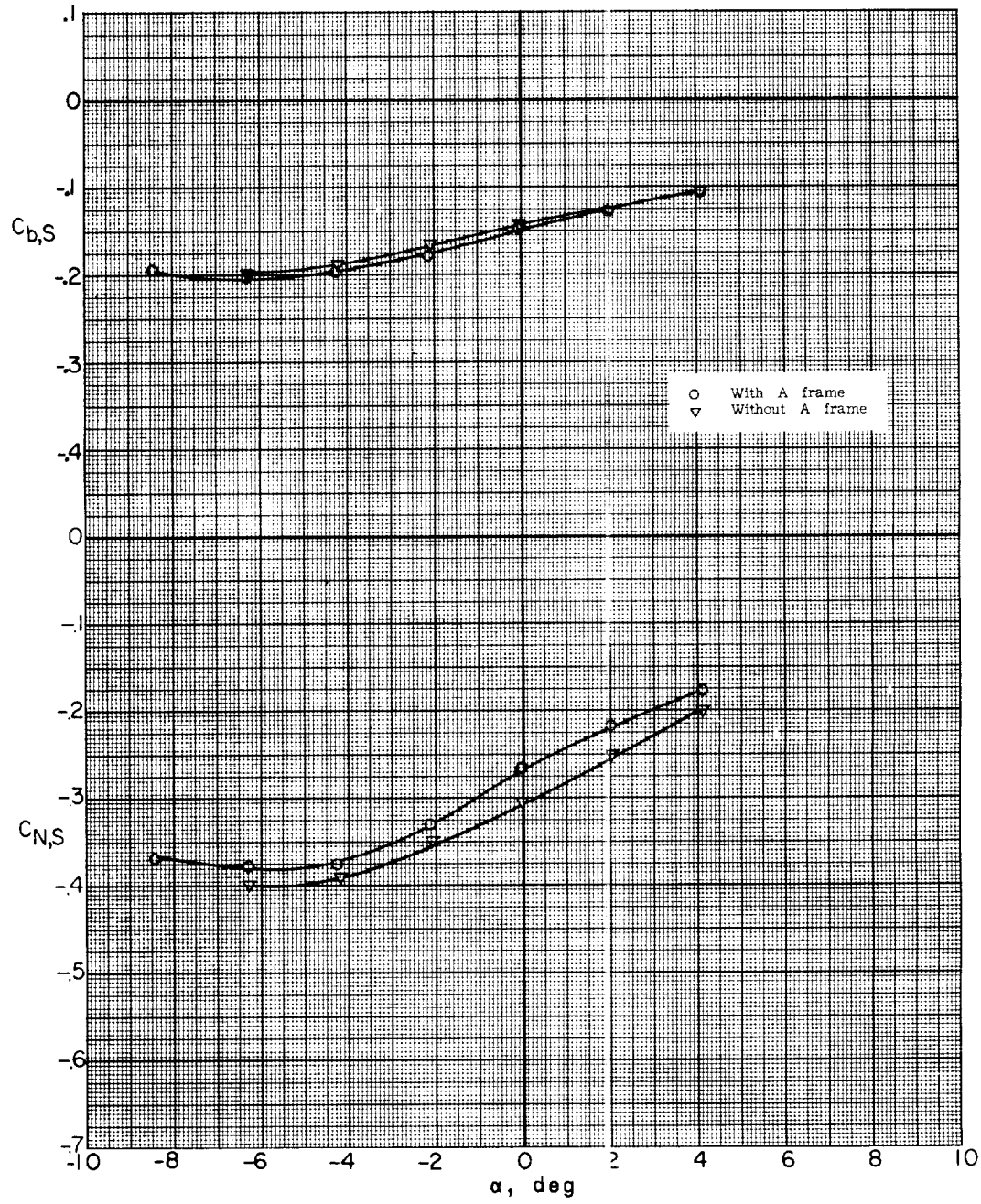
(c) M = 3.22; with missile aileron actuator housing; sting B.

Figure 30.- Concluded.



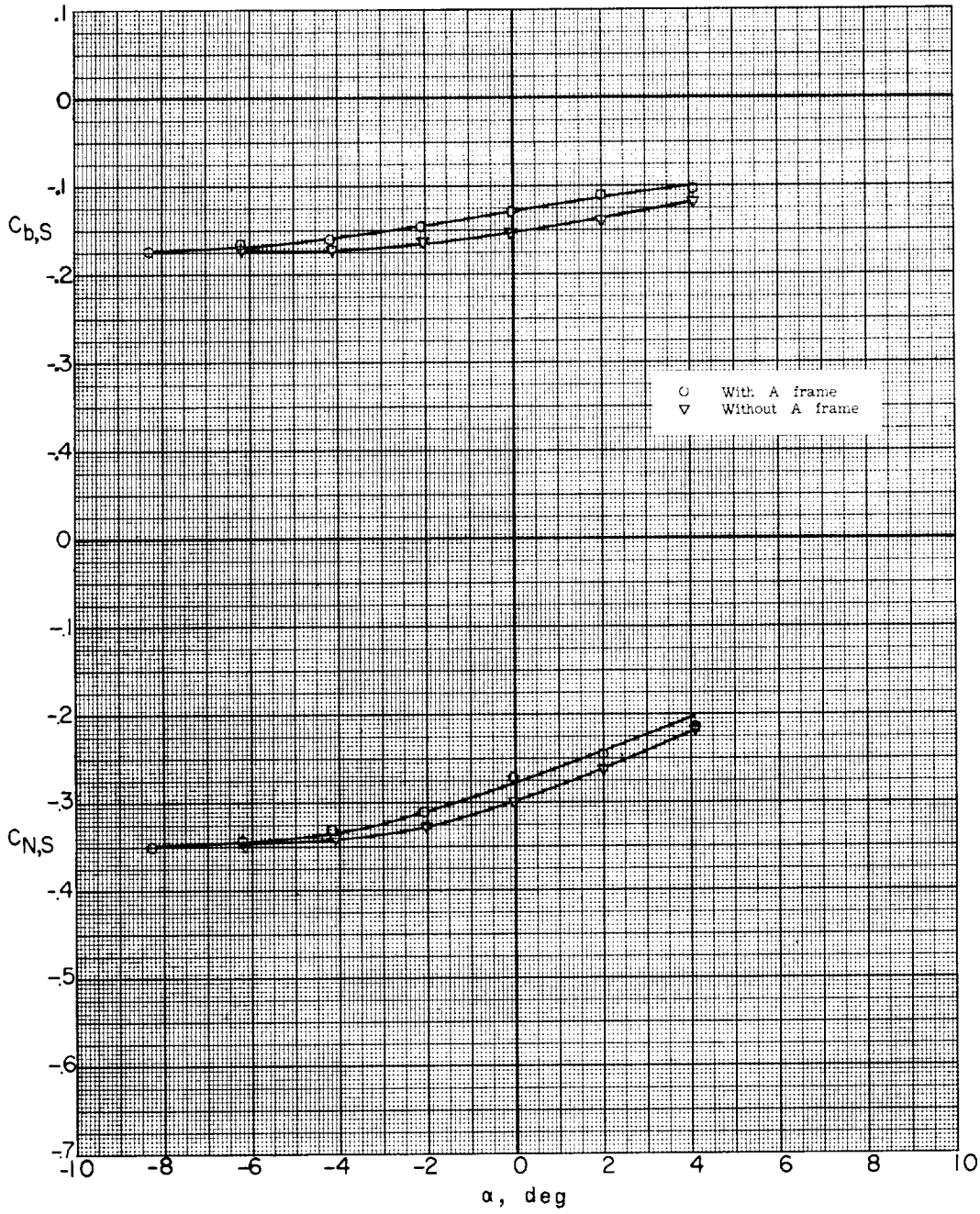
(a) M = 2.29.

Figure 31.- Effect of A-frame on pitch characteristics of booster separating surface. Missile-booster combination; $\delta_e = 0^\circ$; $\beta = 0.3^\circ$; sting A.



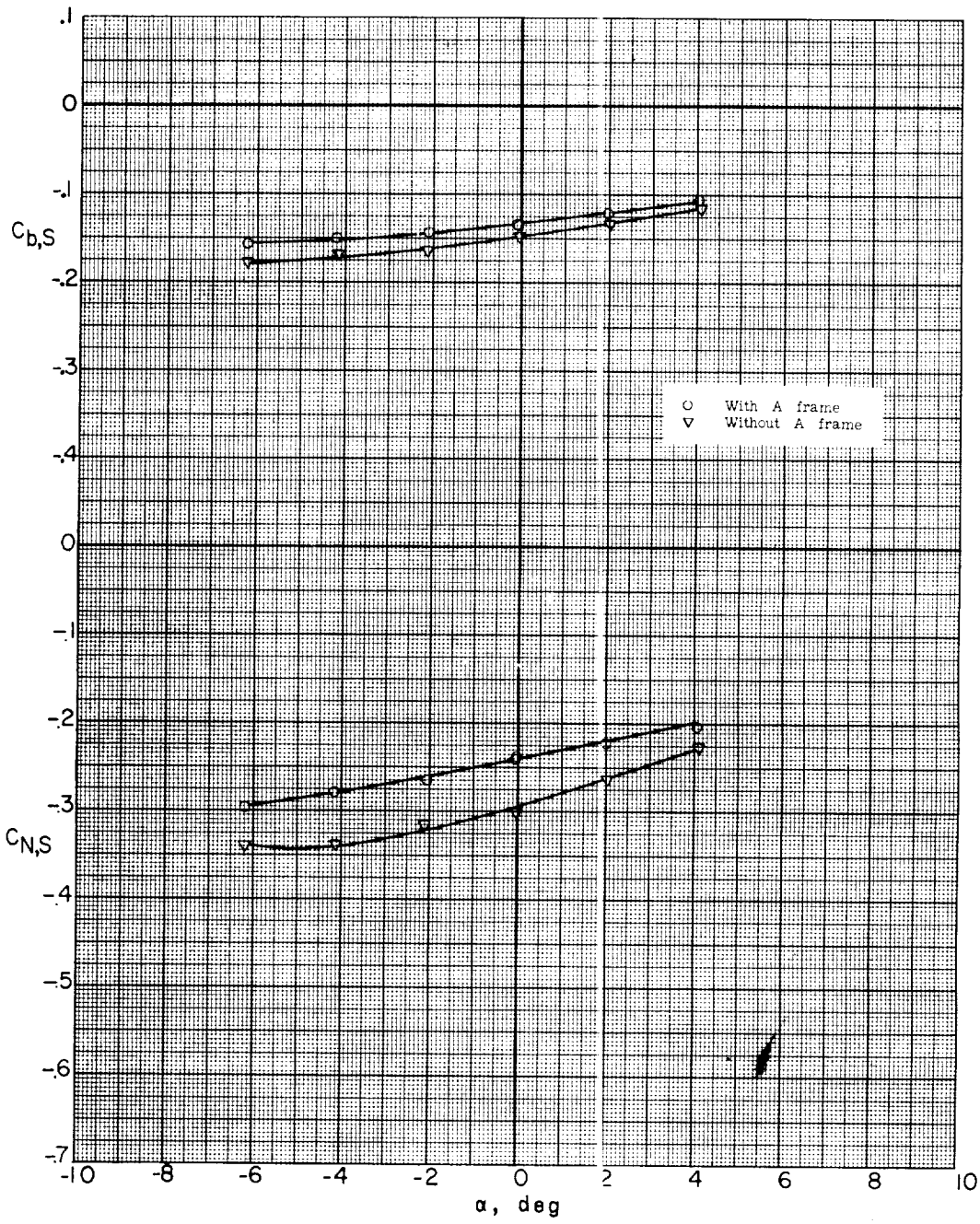
(b) M = 2.75.

Figure 31.- Continued.



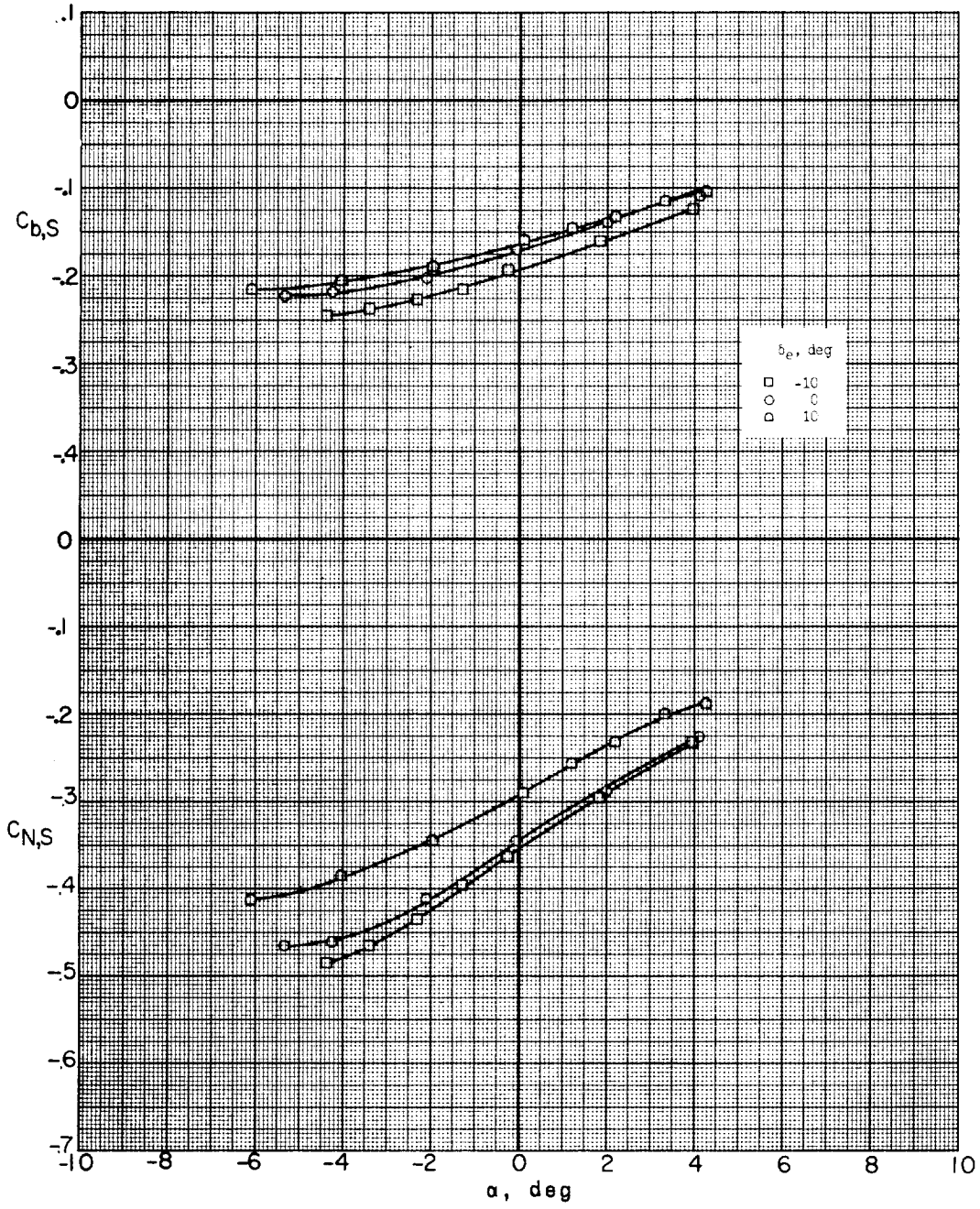
(c) M = 3.22.

Figure 31.- Continued.



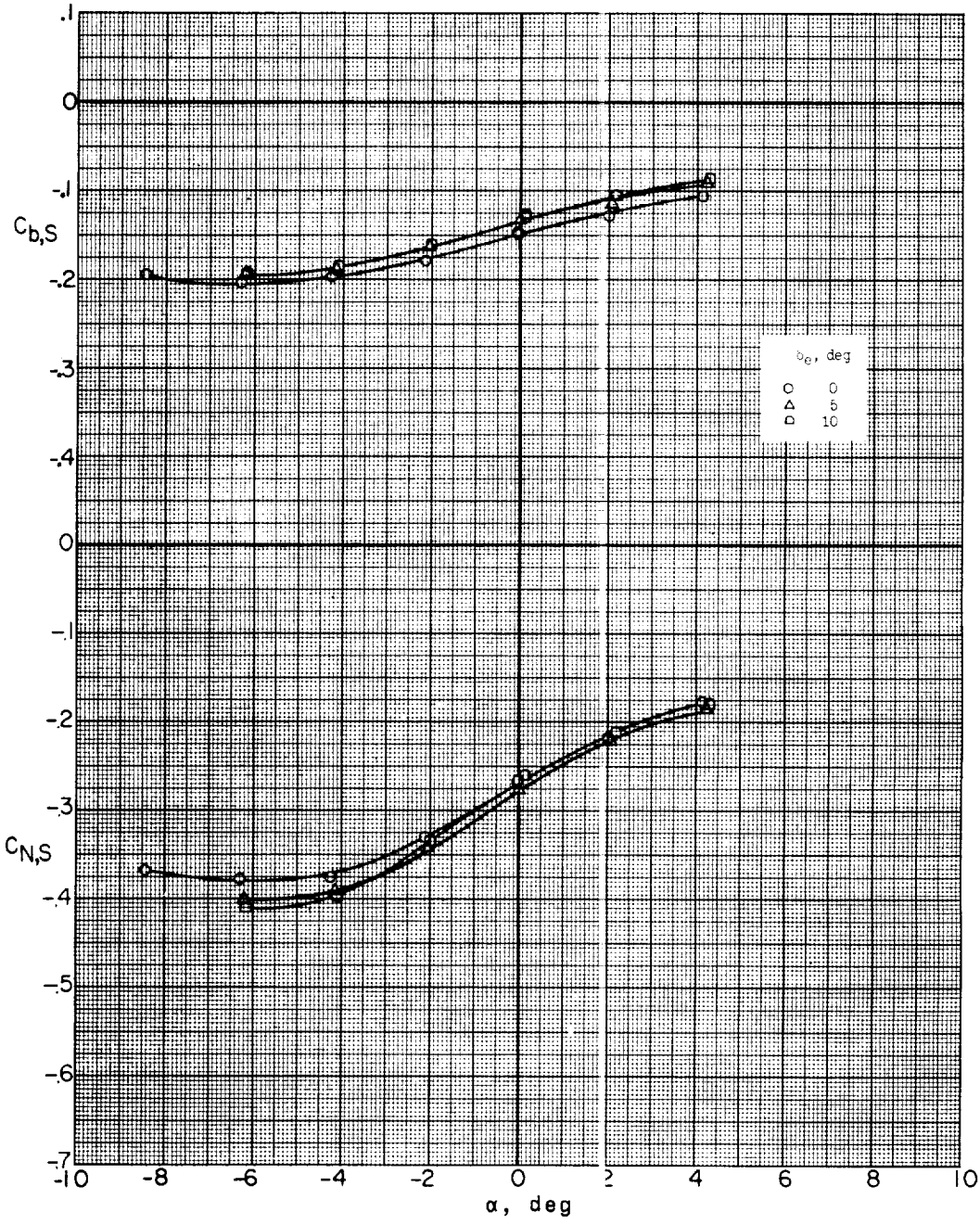
(d) M = 3.5.

Figure 31.- Concluded.



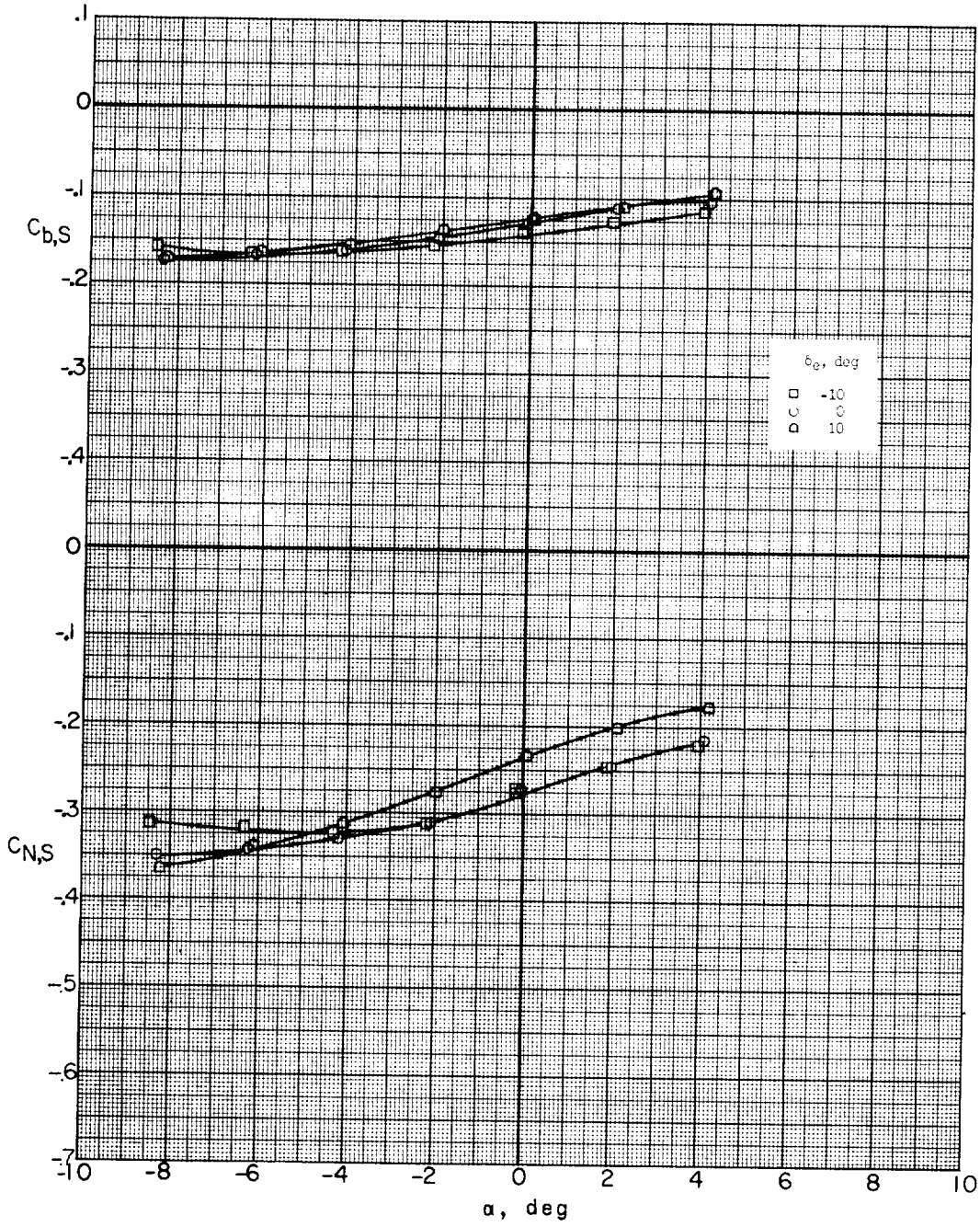
(a) M = 2.29.

Figure 32.- Effect of canard deflection on pitch characteristics of booster separating surface. Missile-booster combination with A-frame mounted; $\beta = 0.3^{\circ}$; sting A.



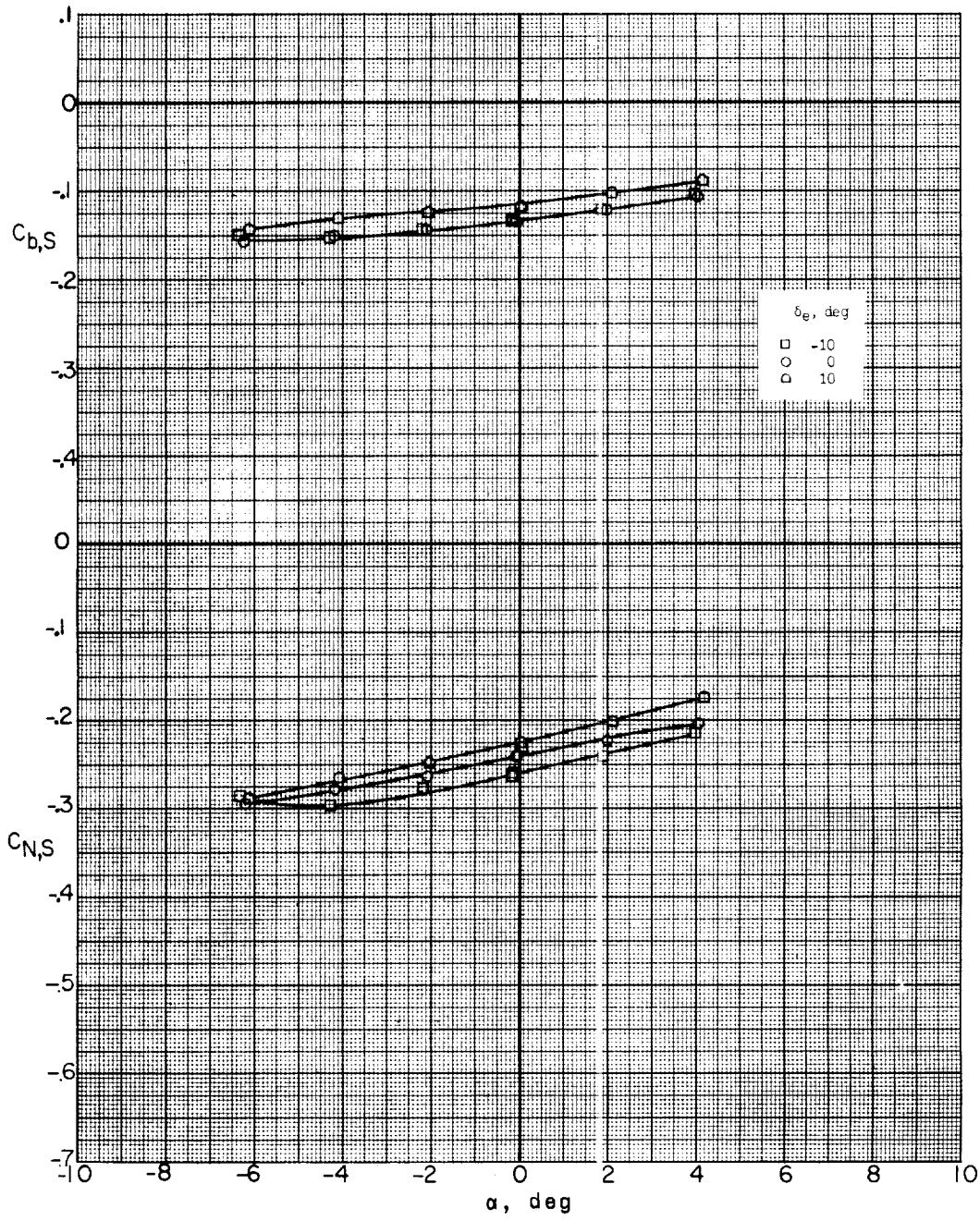
(b) M = 2.75.

Figure 32.- Continued.



(c) M = 3.22.

Figure 32.- Continued.



(d) M = 3.51.

Figure 32.- Concluded.

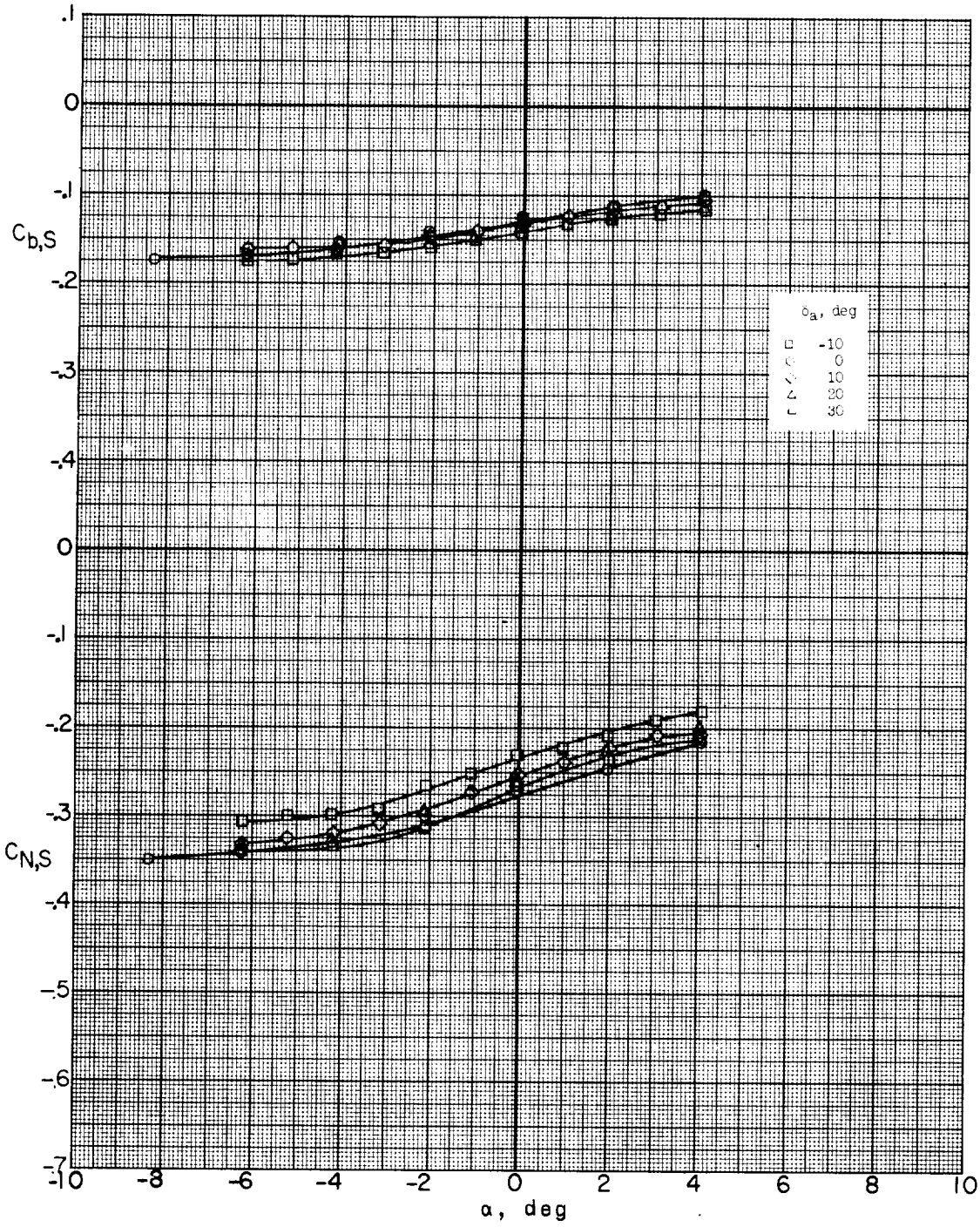
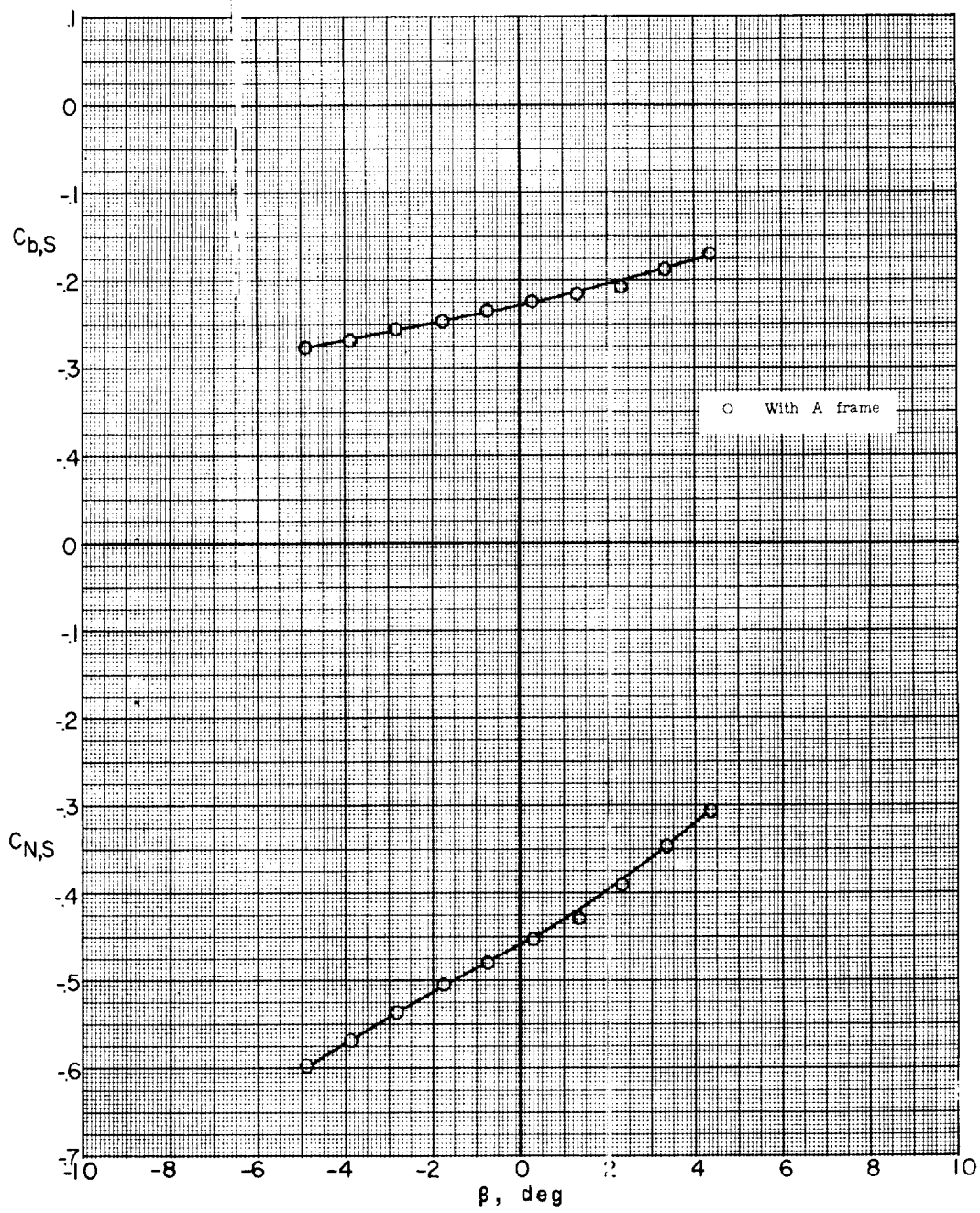
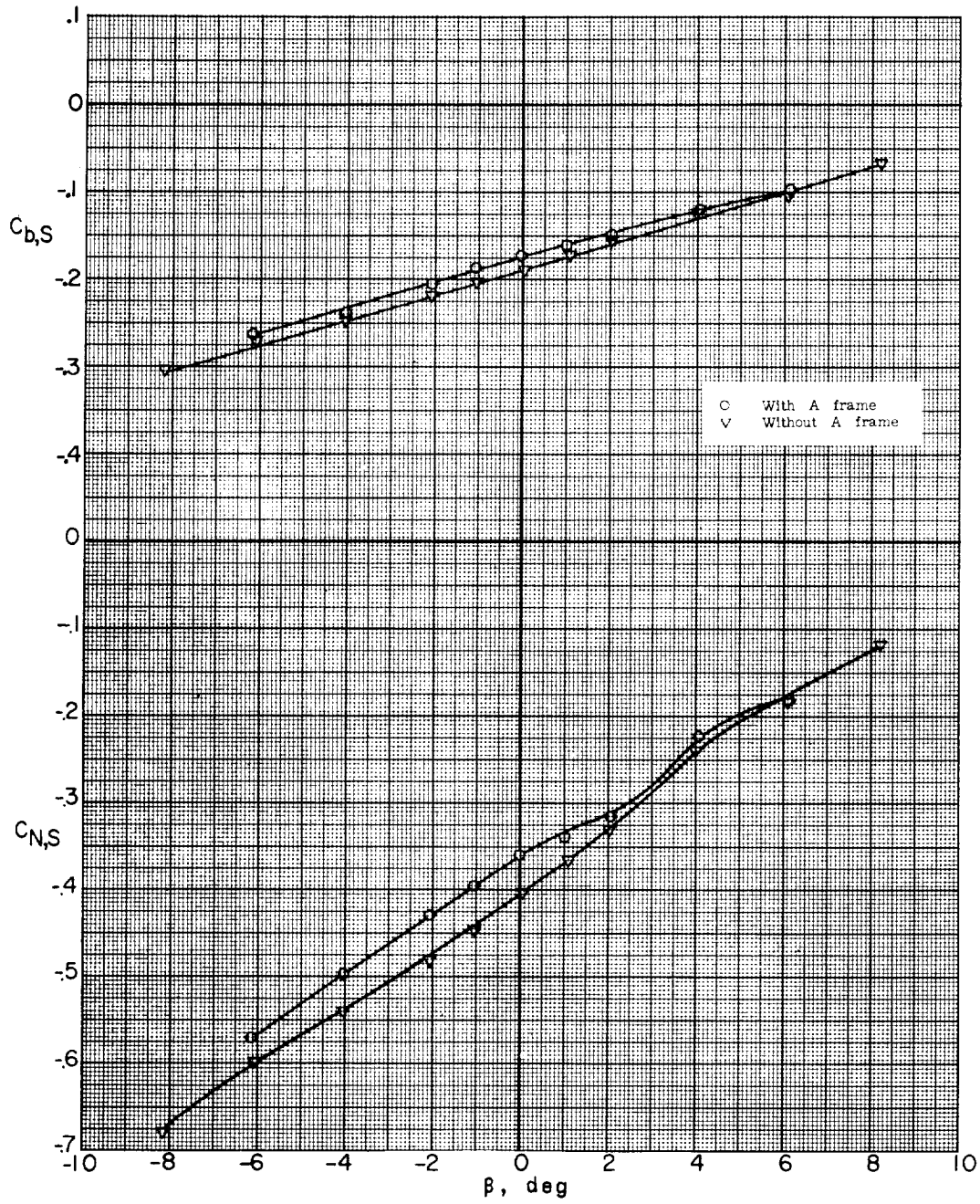


Figure 33.- Effect of aileron deflection on pitch characteristics of booster separating surface. Missile-booster combination with A-frame mounted; $\delta_e = 0^o$; $\beta = 0.2^o$; M = 3.22; sting A.



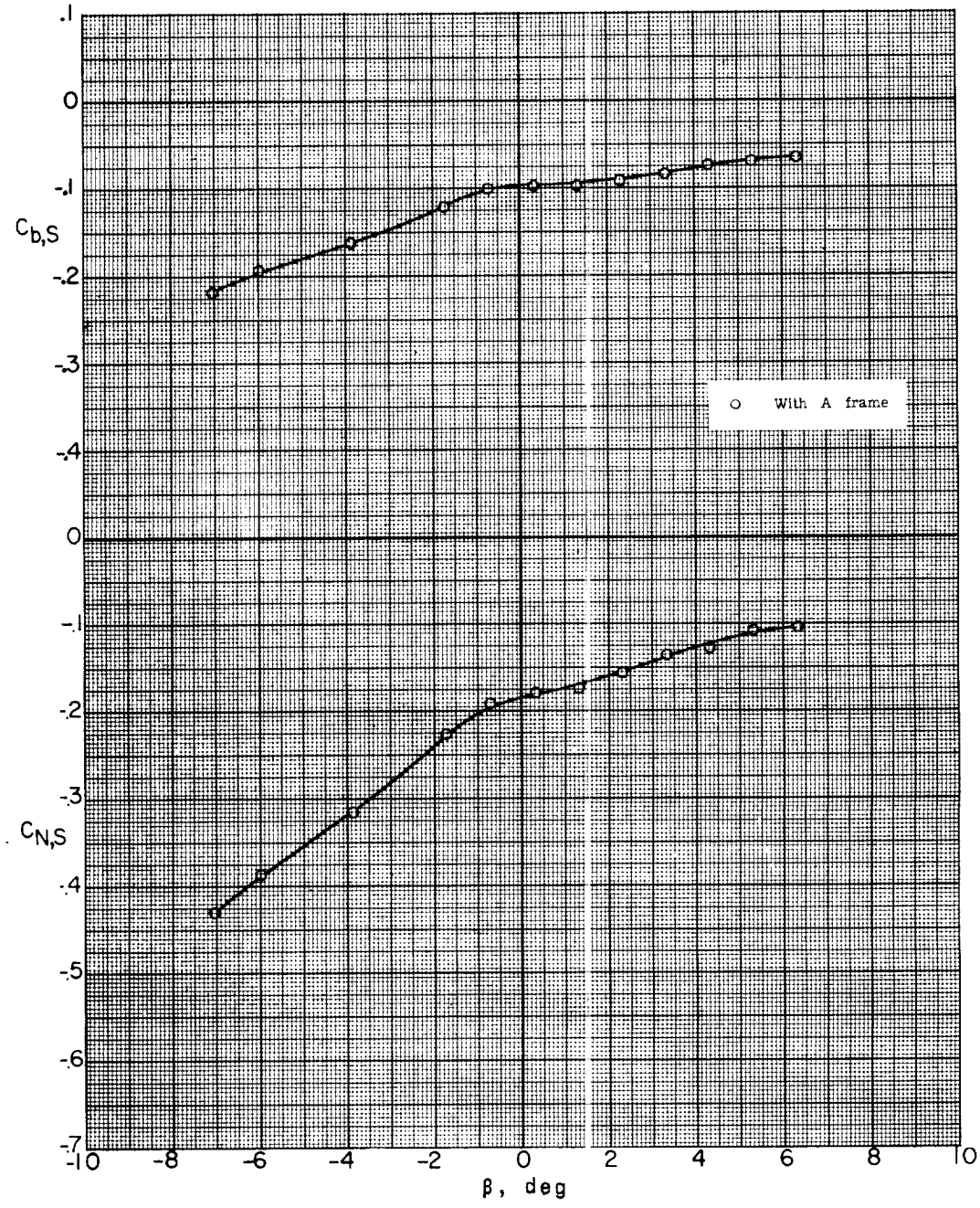
(a) M = 2.29; α = -5.3°.

Figure 34.- Effect of A-frame on lateral characteristics of booster separating surface. Missile-booster combination; δ_e = 0°; sting A.



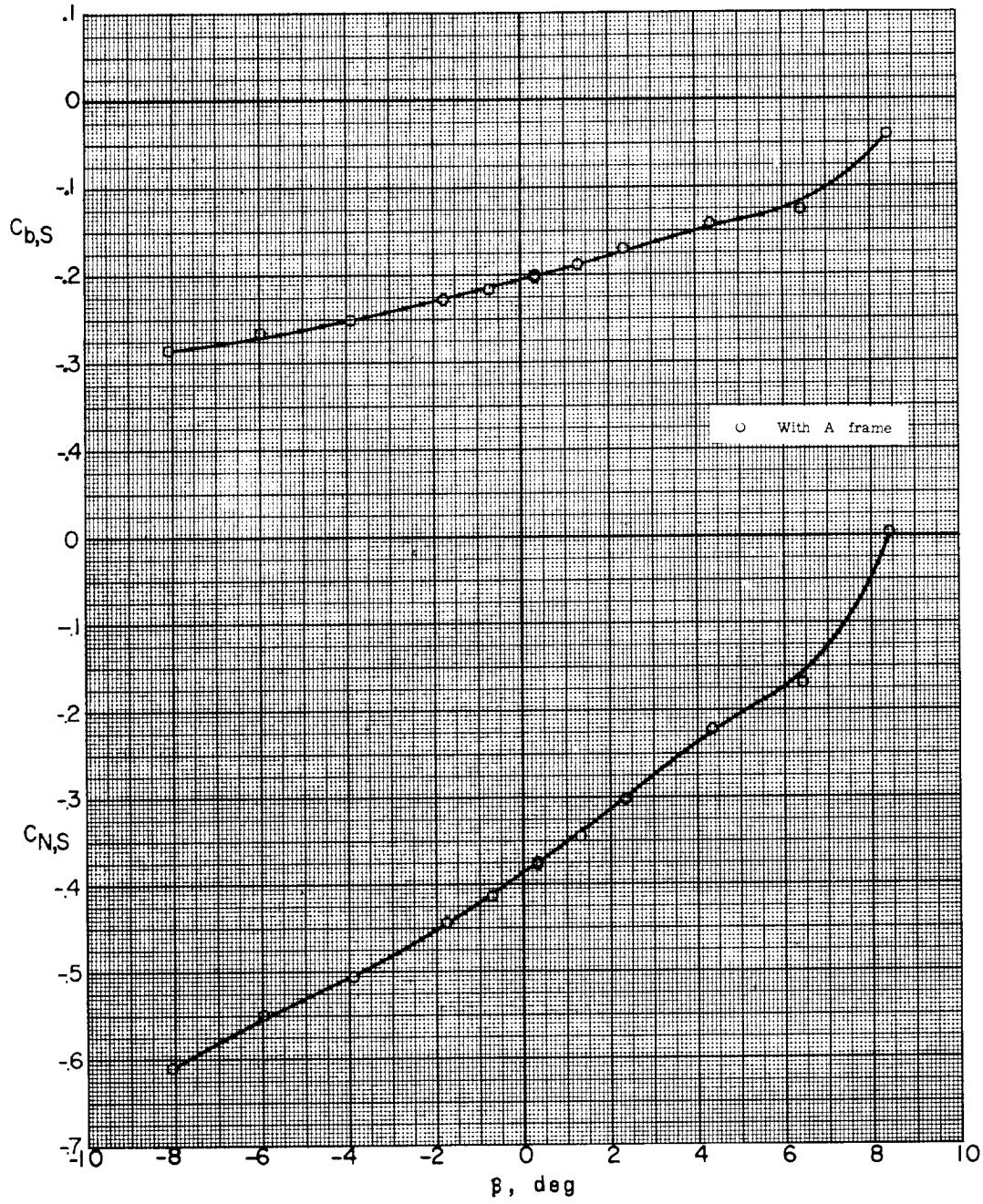
(b) M = 2.29; $\alpha = -0.3^{\circ}$.

Figure 34.- Continued.



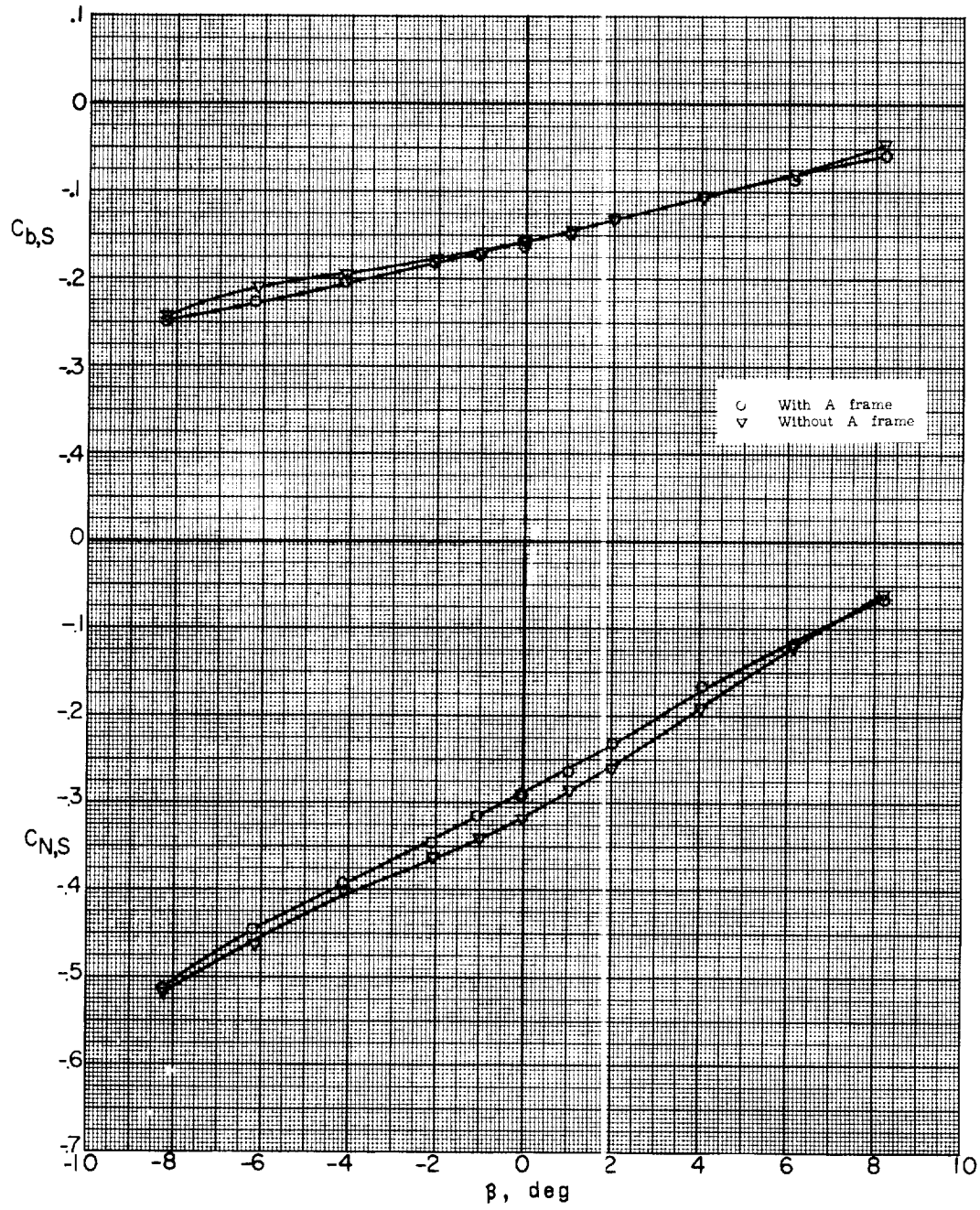
(c) M = 2.29; $\alpha = 5.1^{\circ}$.

Figure 34.- Continued.



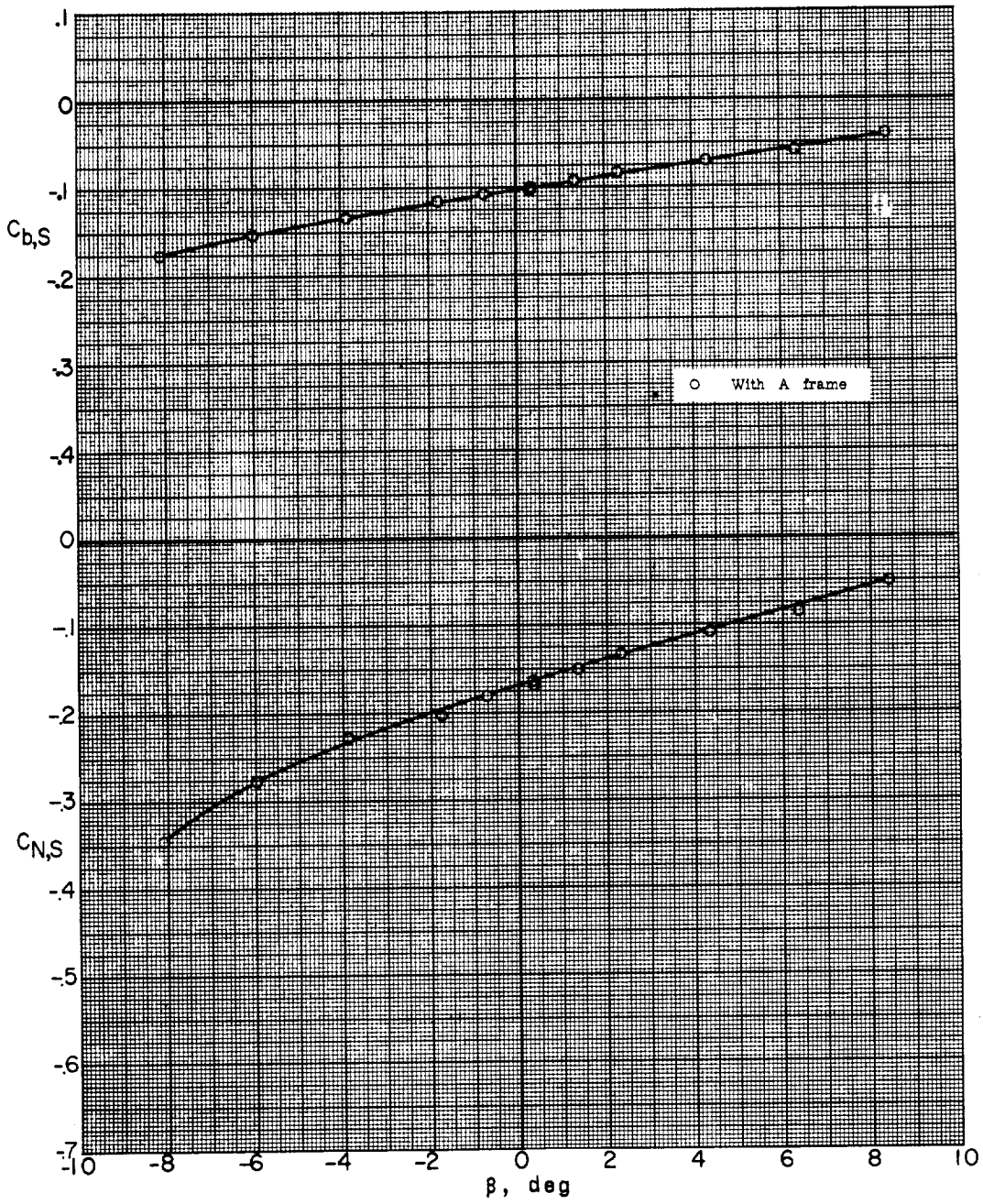
(d) $M = 2.75$; $\alpha = -5.3^{\circ}$.

Figure 34.- Continued.



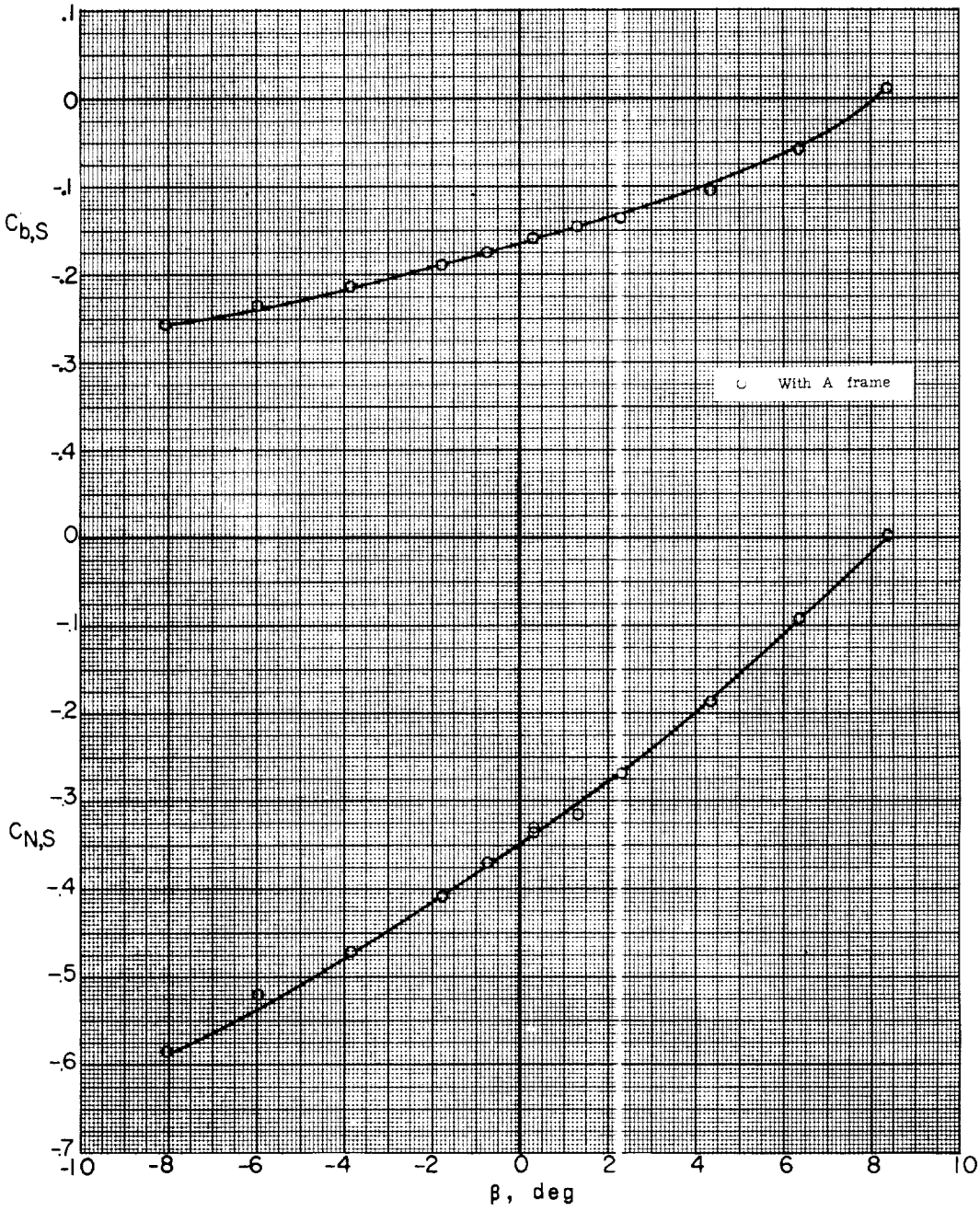
(e) M = 2.75; α = -0.3°.

Figure 34.- Continued.



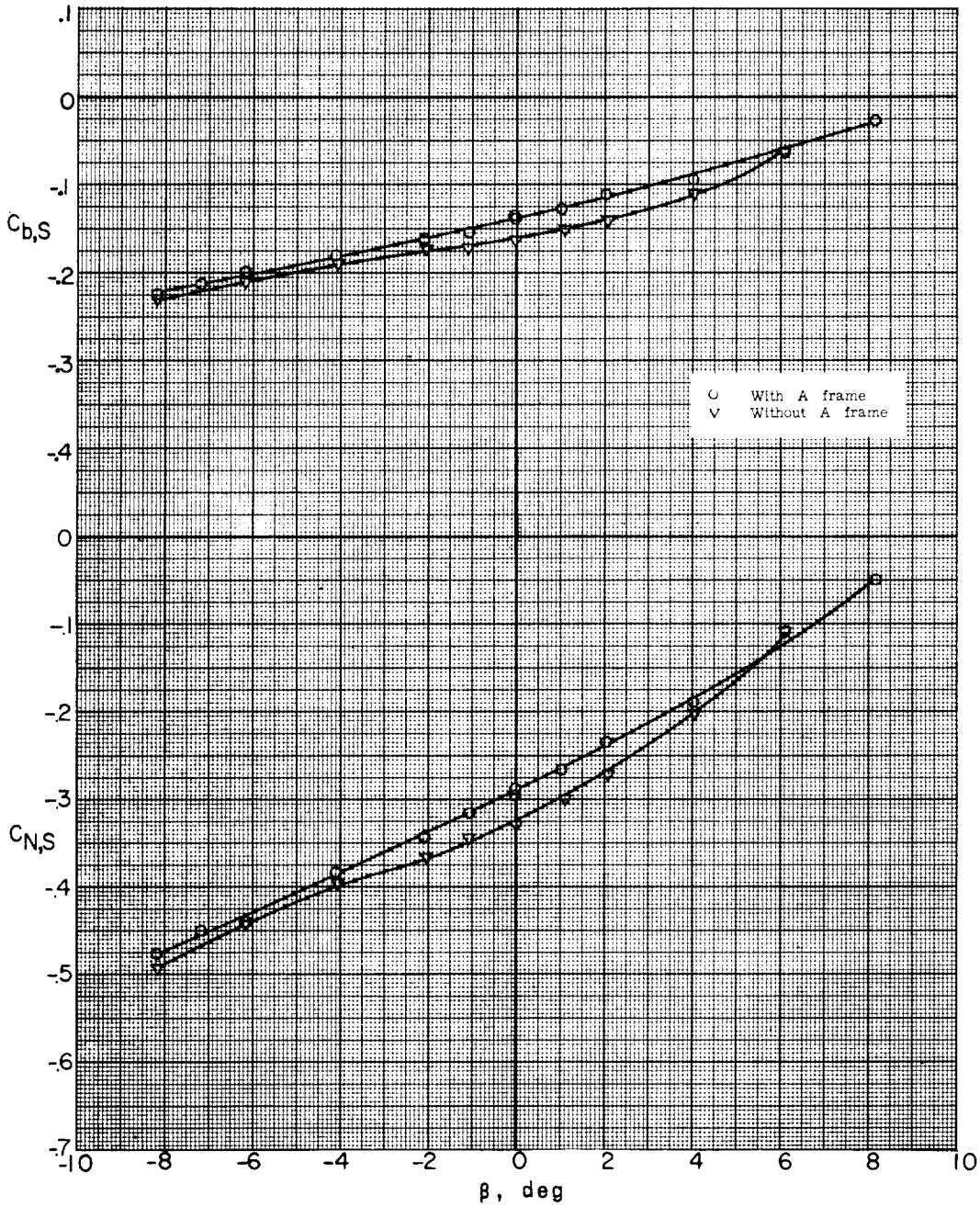
(f) M = 2.75; $\alpha = 5.2^{\circ}$.

Figure 34.- Continued.



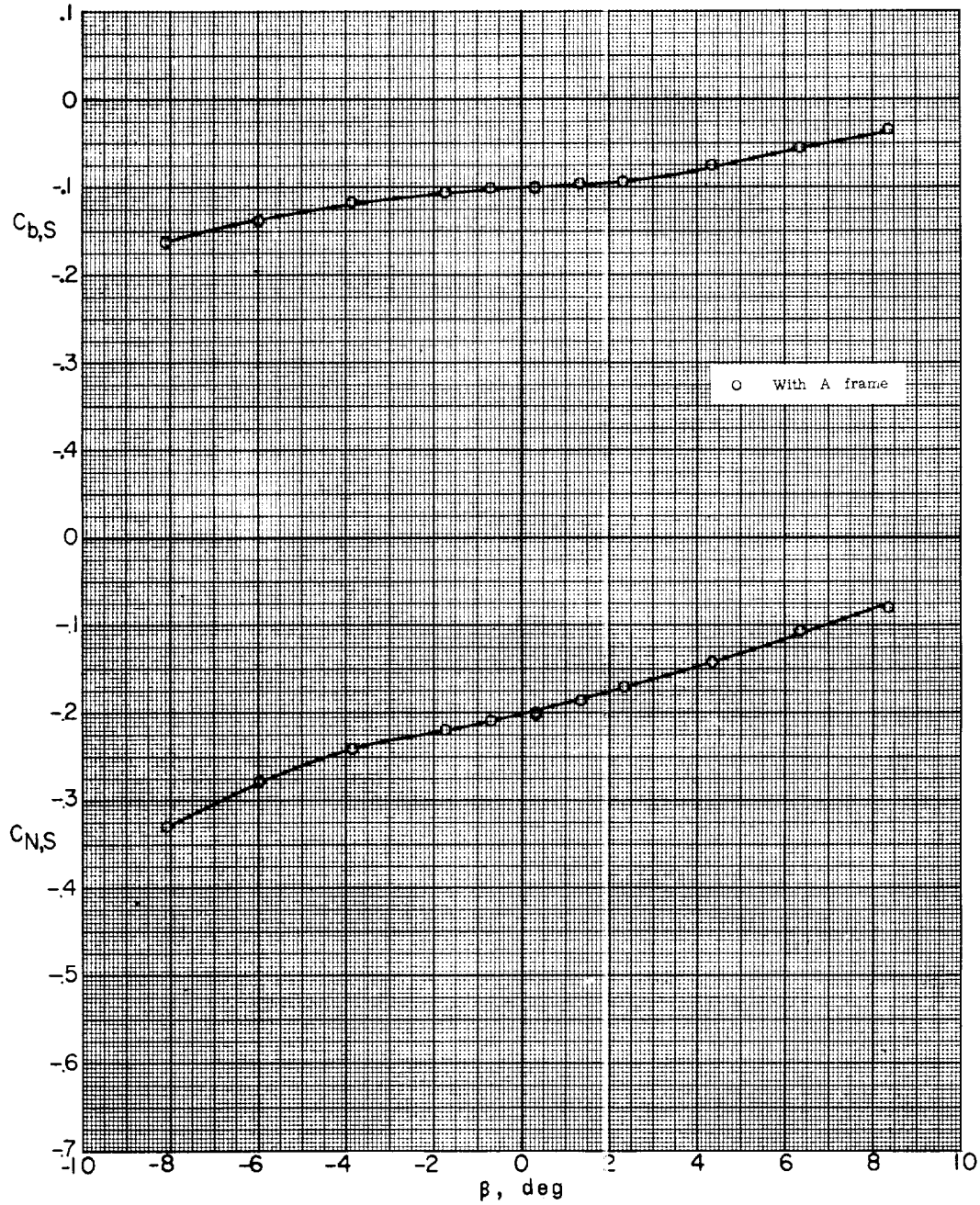
(g) M = 3.22; $\alpha = -5.2^{\circ}$.

Figure 34.- Continued.



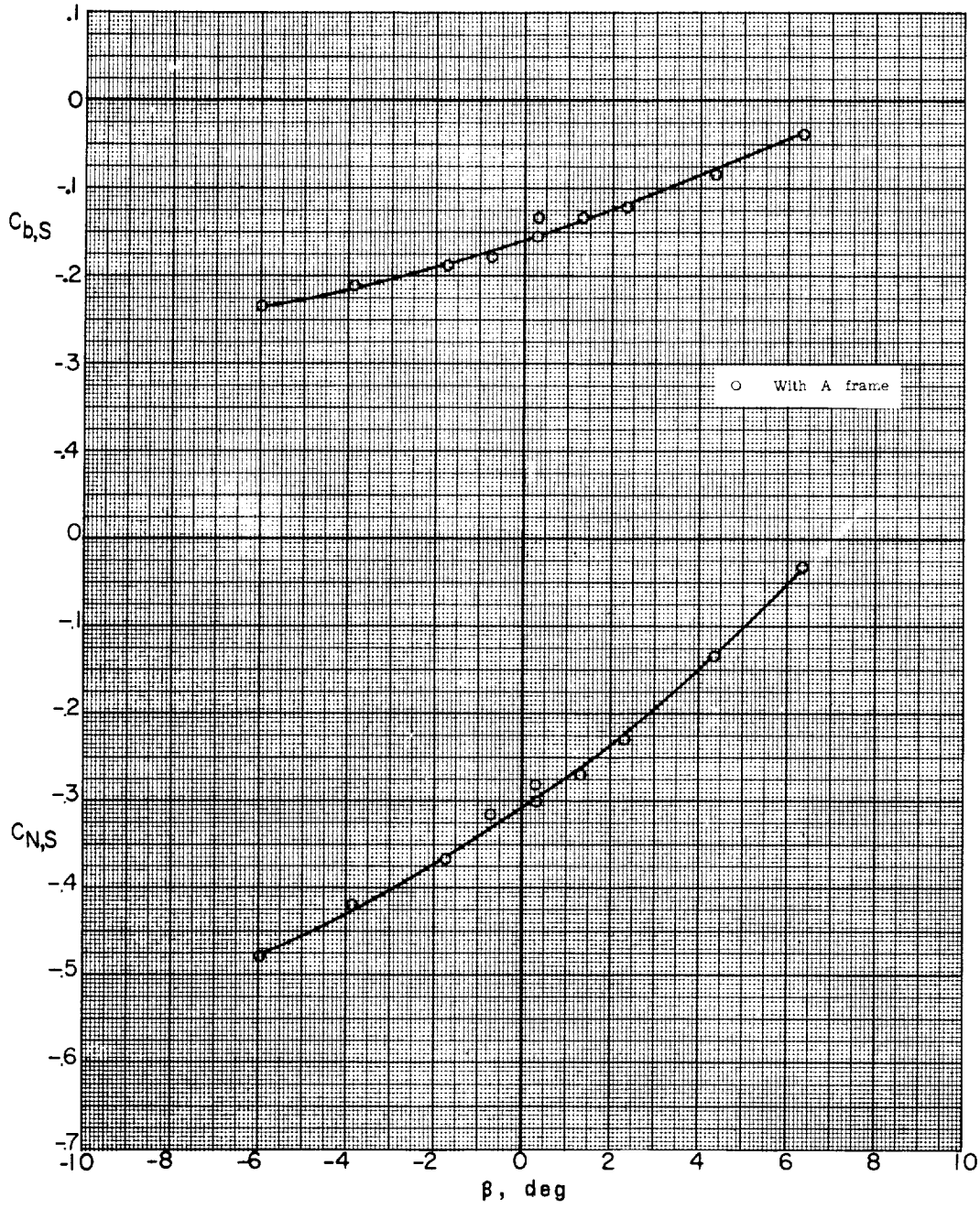
(h) M = 3.22; α = -0.3°.

Figure 34.- Continued.



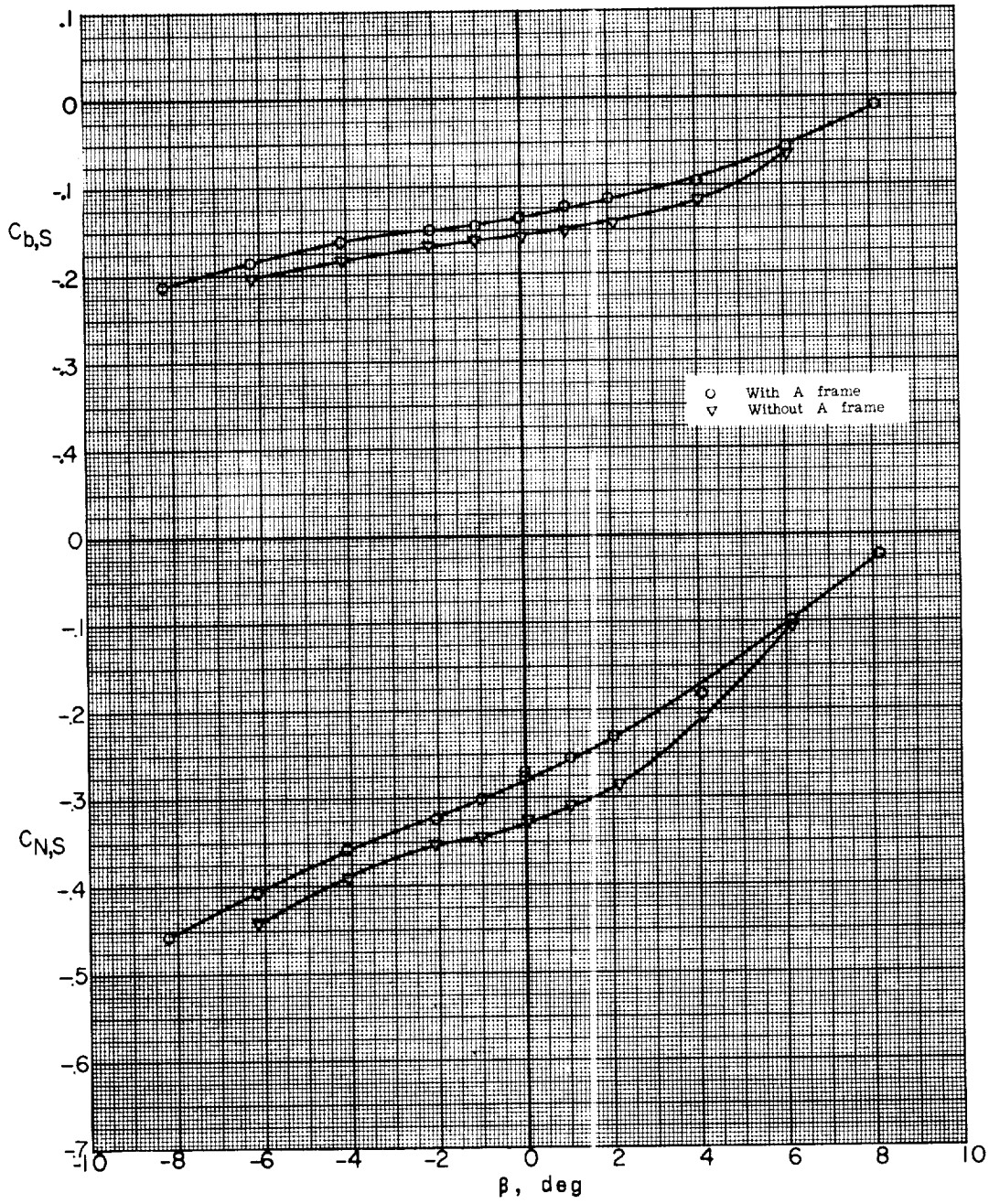
(i) M = 3.22; $\alpha = 5.1^{\circ}$.

Figure 34.- Continued.



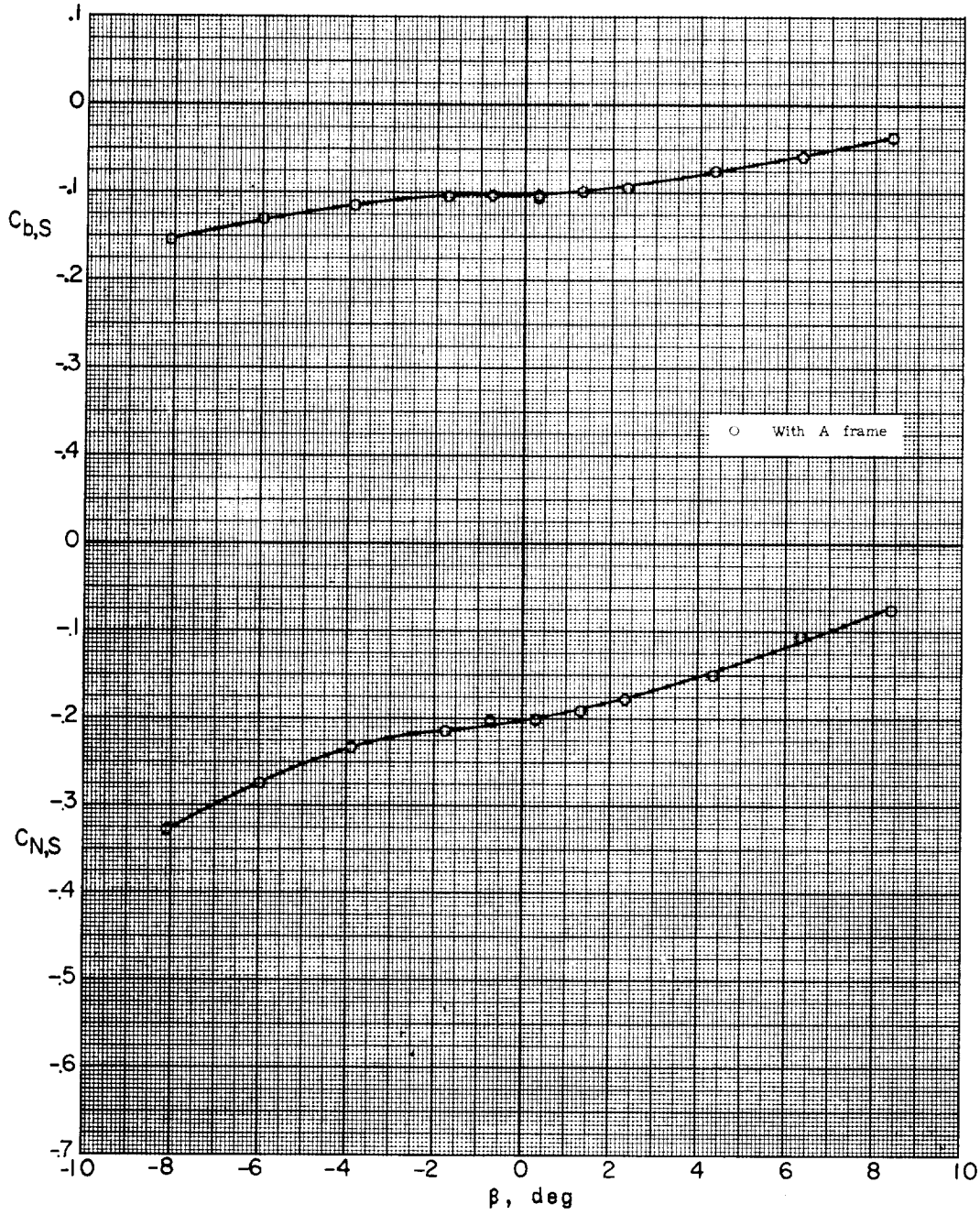
(j) M = 3.51; α = -5.2°.

Figure 34.- Continued.



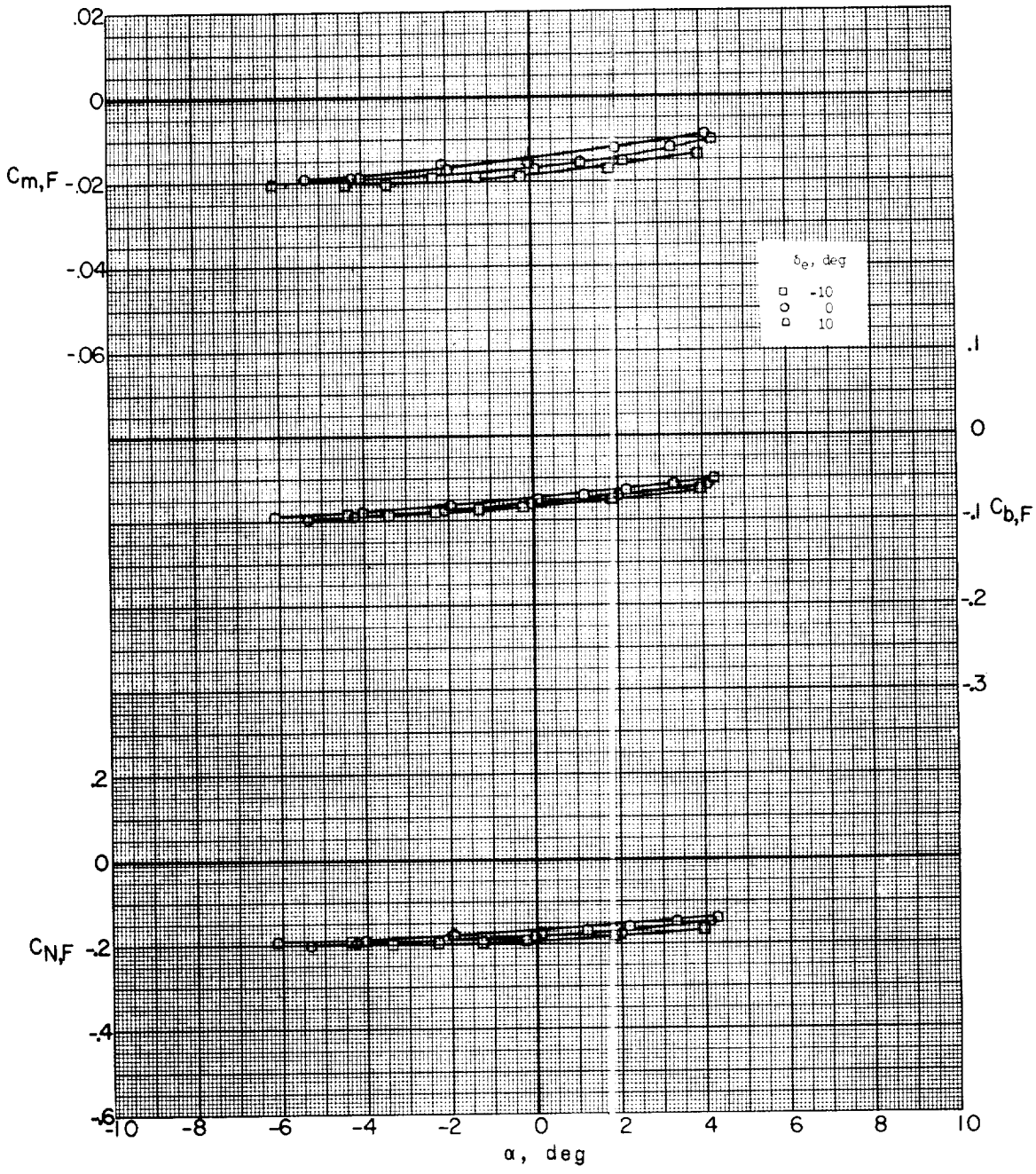
(k) M = 3.51; α = -0.3°.

Figure 34.- Continued.



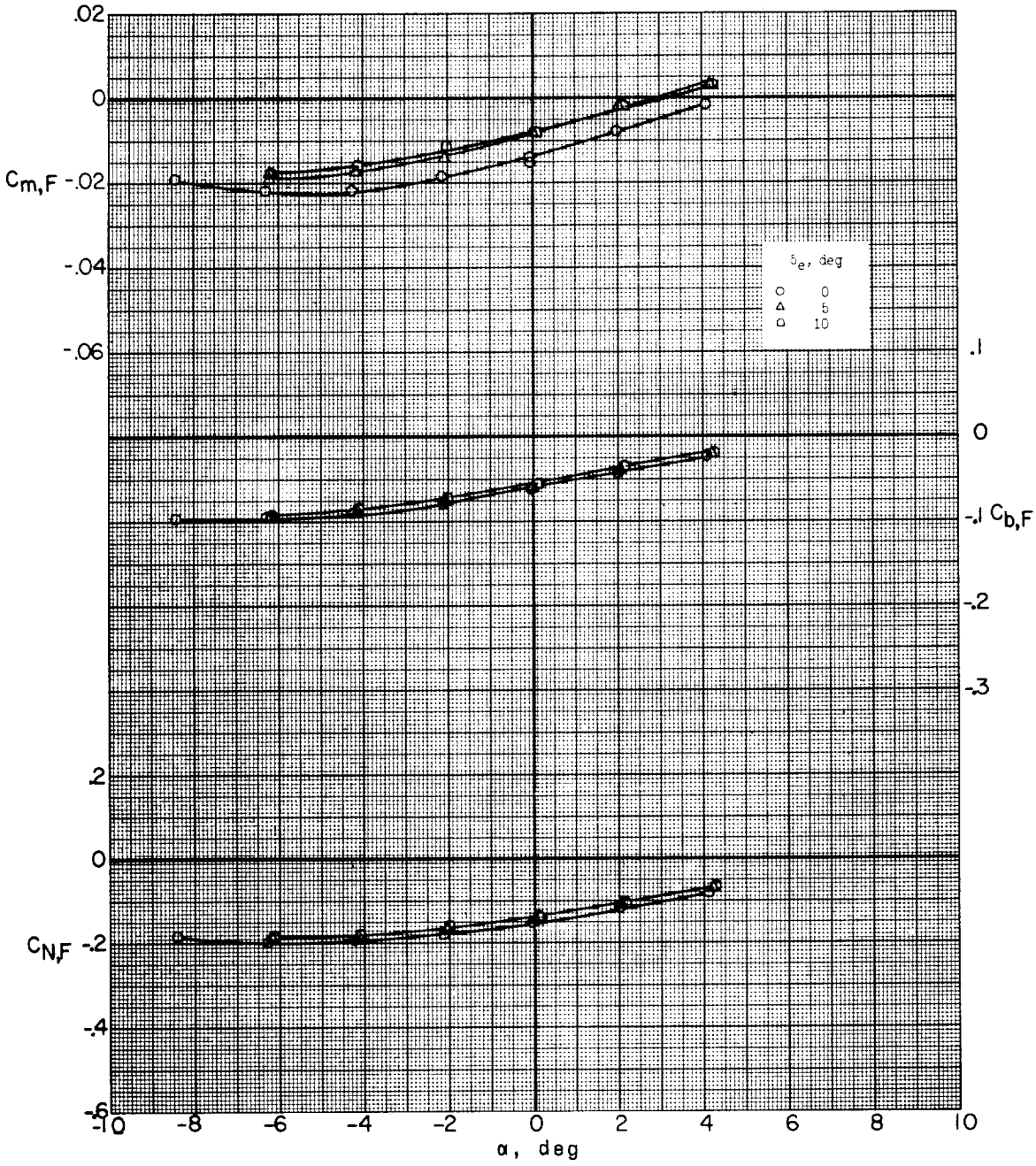
(l) M = 3.51; $\alpha = 5.1^{\circ}$.

Figure 34.- Concluded.



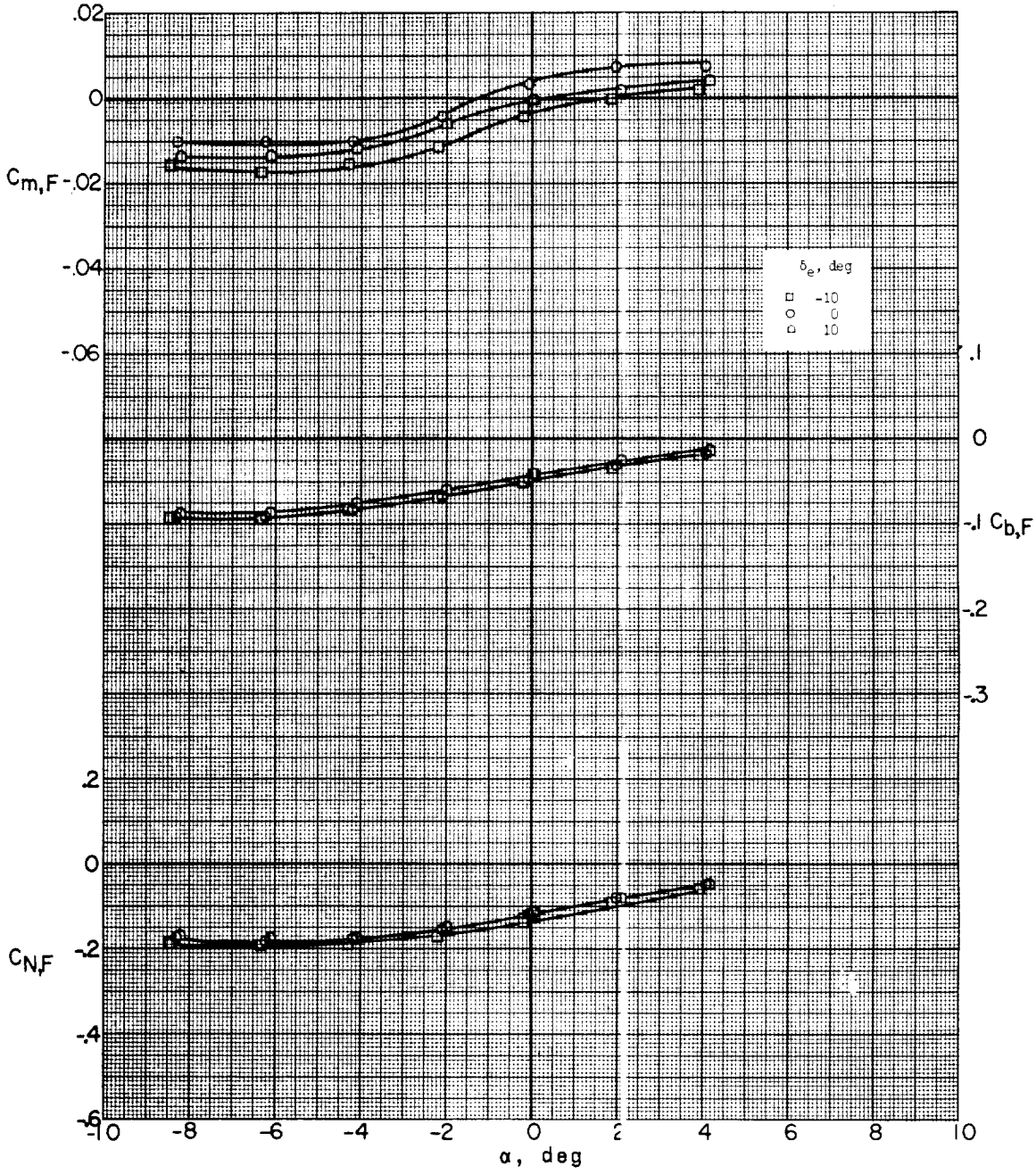
(a) M = 2.29

Figure 35.- Effect of canard deflection on pitch characteristics of booster fin. Missile-booster combination with A-frame mounted; $\beta = 0.3^{o}$; sting A.



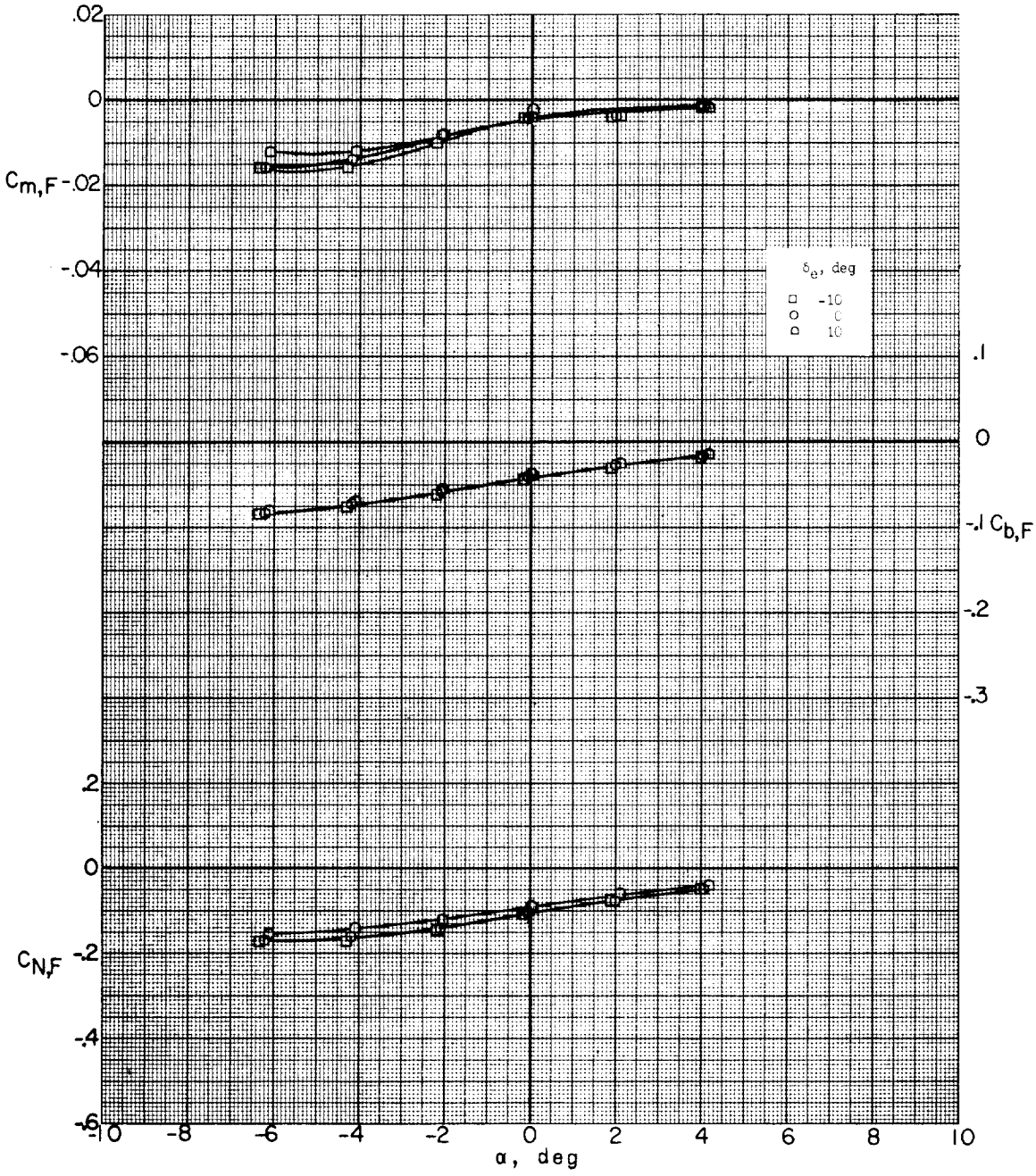
(b) M = 2.75.

Figure 35.- Continued.



(c) M = 3.22.

Figure 35.- Continued.



(d) M = 3.51.

Figure 35.- Concluded.

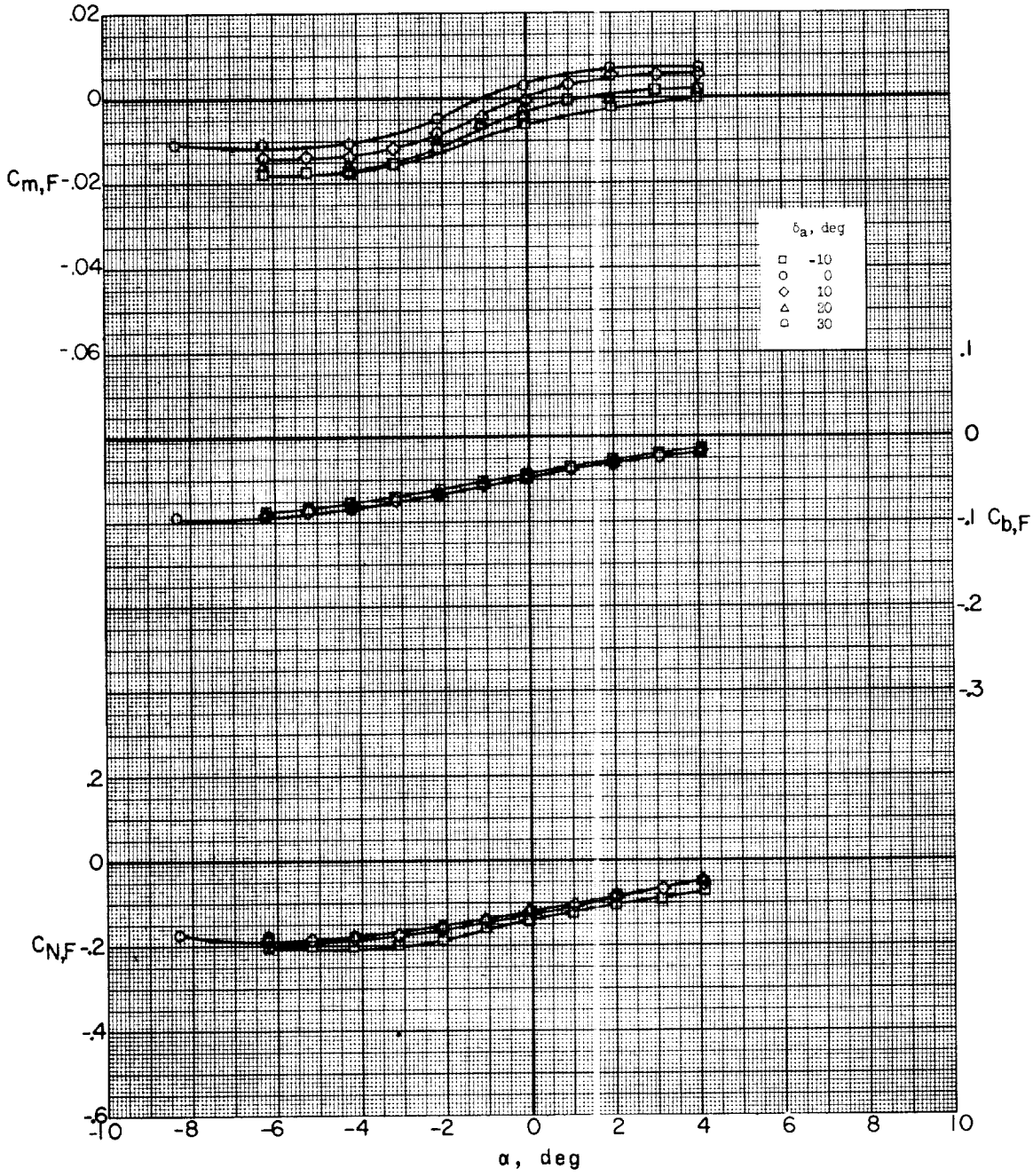
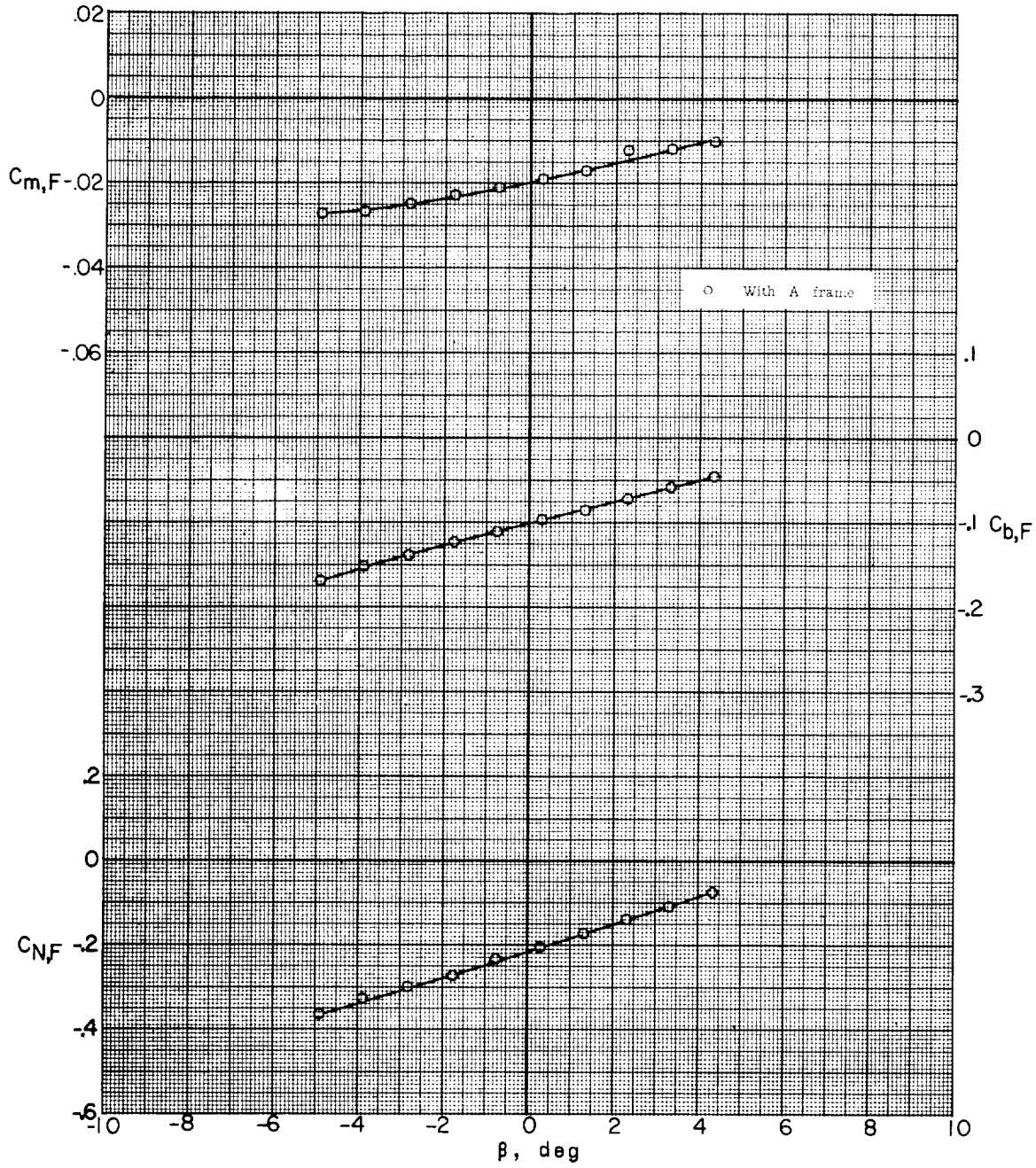
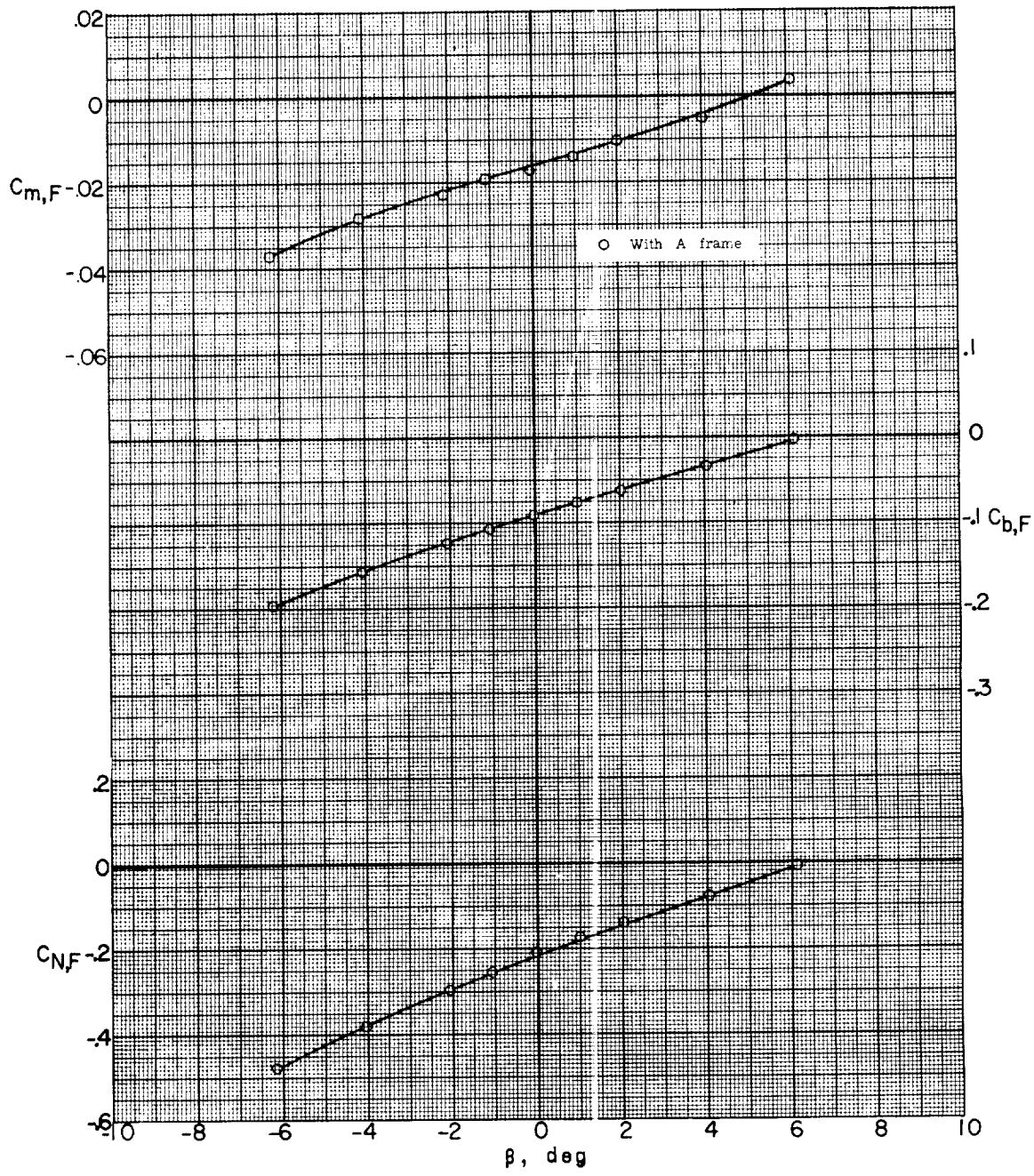


Figure 36.- Effect of aileron deflection on pitch characteristics of booster fin. Missile-booster combination with A-frame mounted; $\delta_e = 0^\circ$; $\beta = 0.2^\circ$; M = 3.22; sting A.



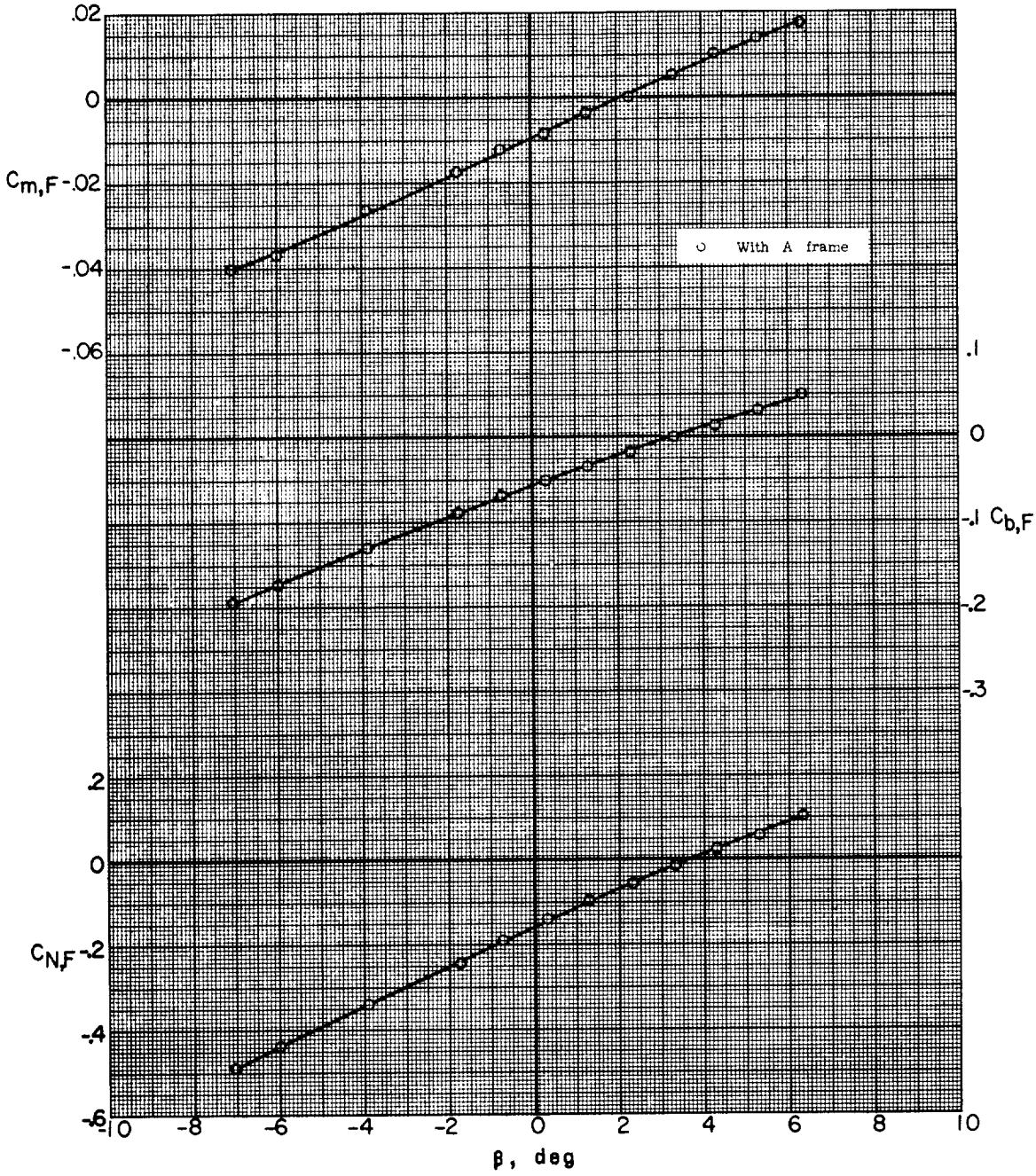
(a) $M = 2.29$; $\alpha = -5.3^{\circ}$.

Figure 37.- Lateral characteristics of booster fin. Missile-booster combination with A-frame mounted; $\delta_e = 0^{\circ}$; sting A.



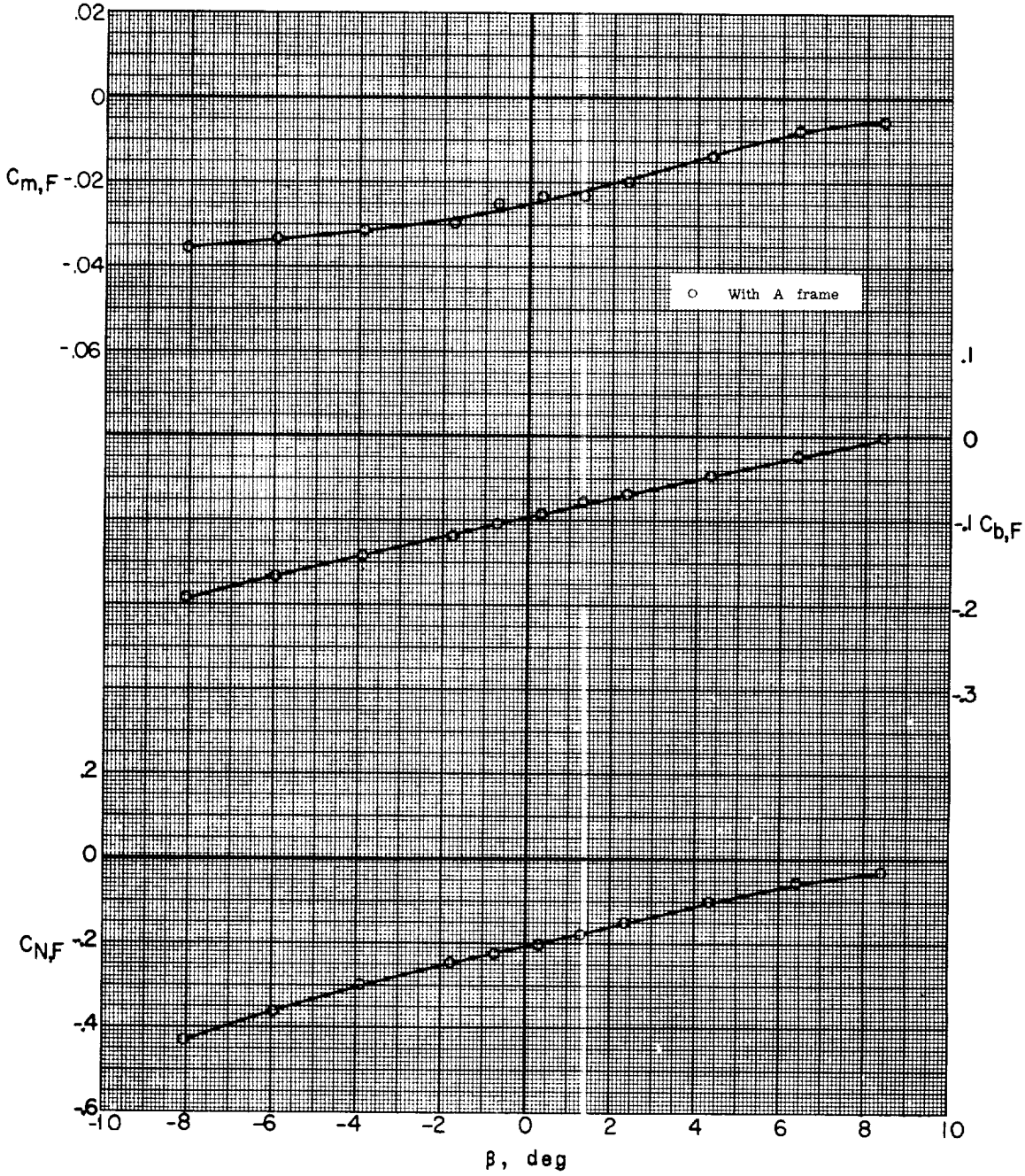
(b) M = 2.29; α = -0.3°.

Figure 37.- Continued.



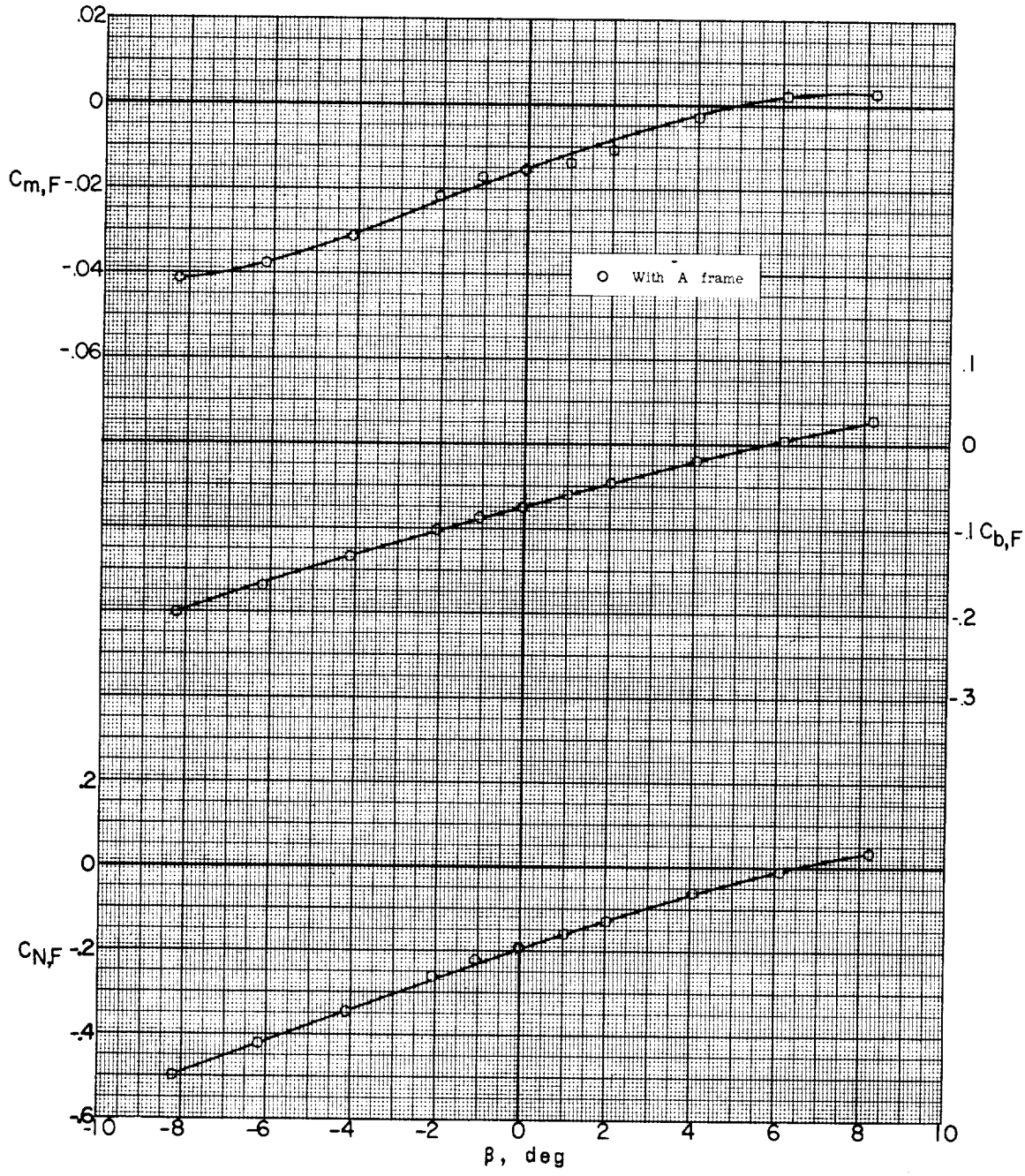
(c) M = 2.29; $\alpha = 5.1^{\circ}$.

Figure 37.- Continued.



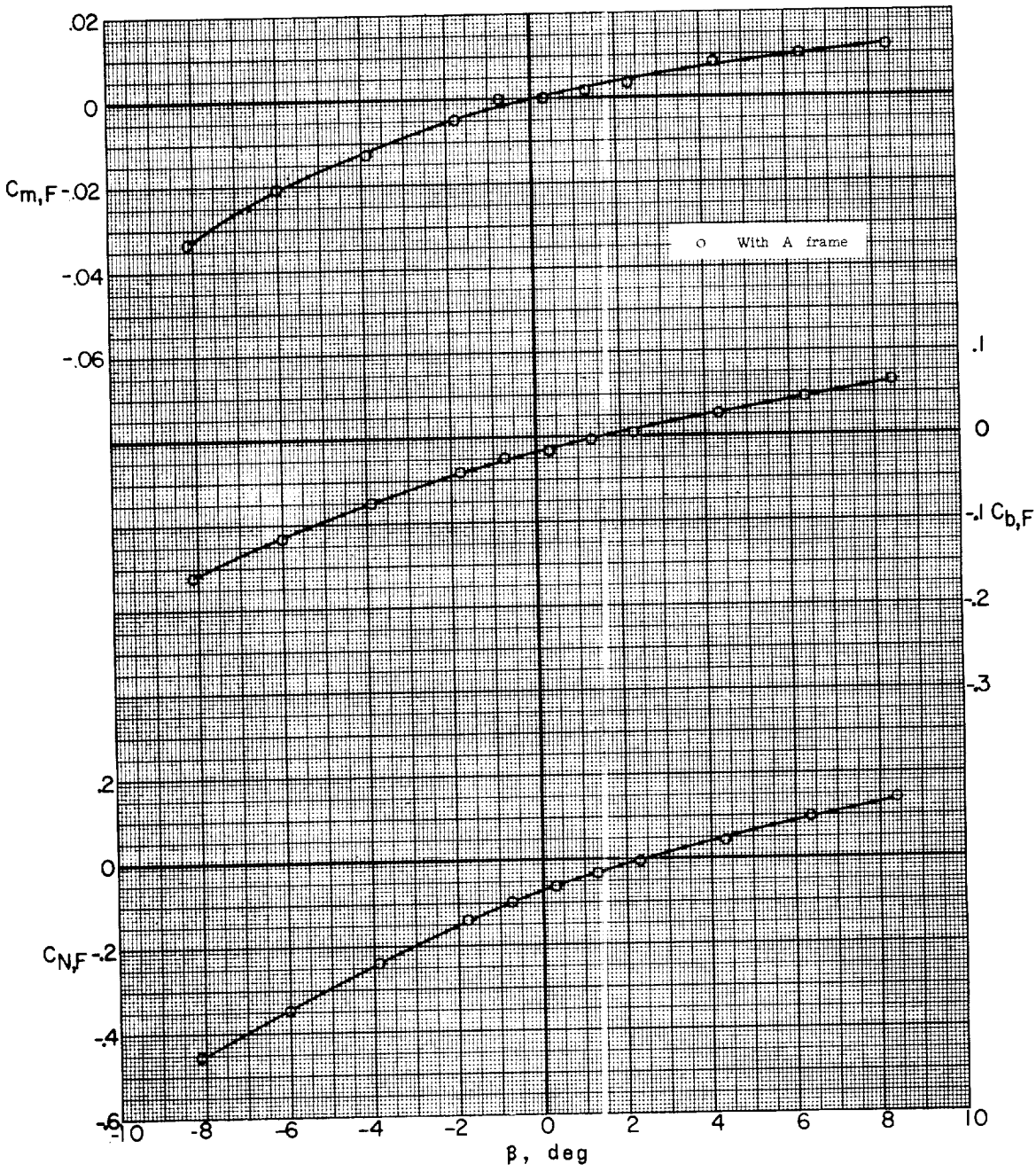
(d) M = 2.75; α = -5.3°.

Figure 37.- Continued.



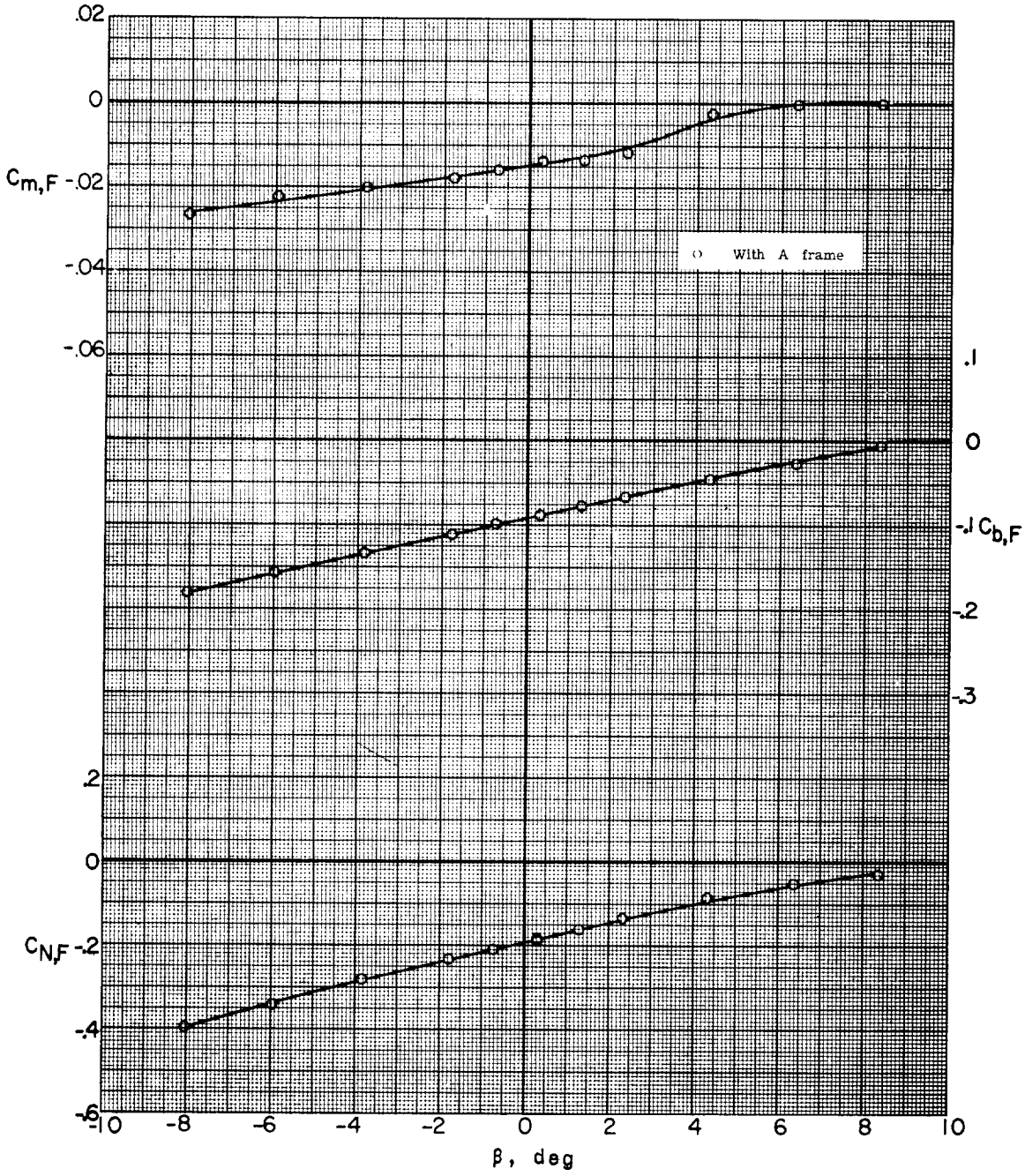
(e) M = 2.75; $\alpha = -0.3^{\circ}$.

Figure 37.- Continued.



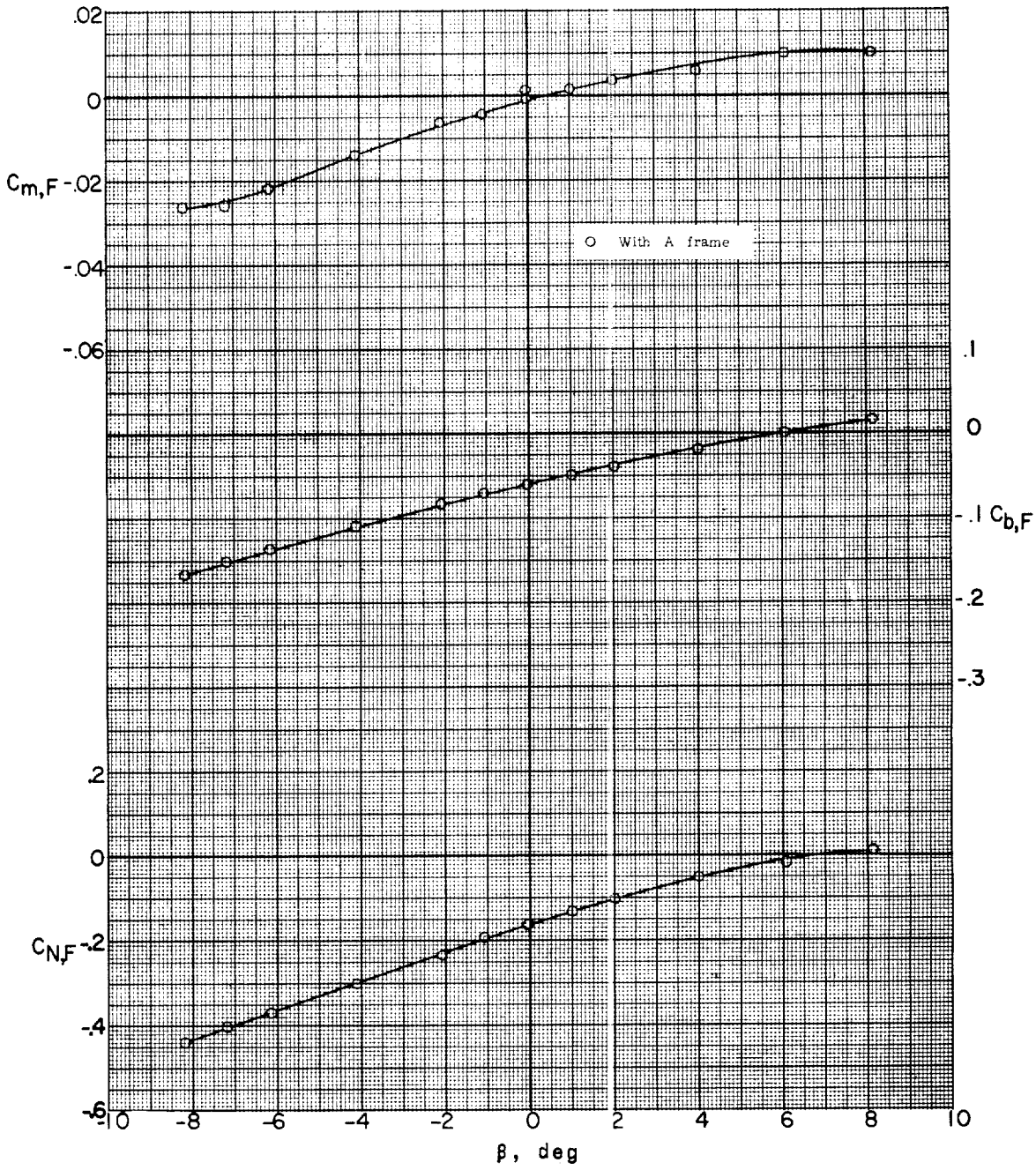
(f) M = 2.75; $\alpha = 5.2^{\circ}$.

Figure 37.- Continued.



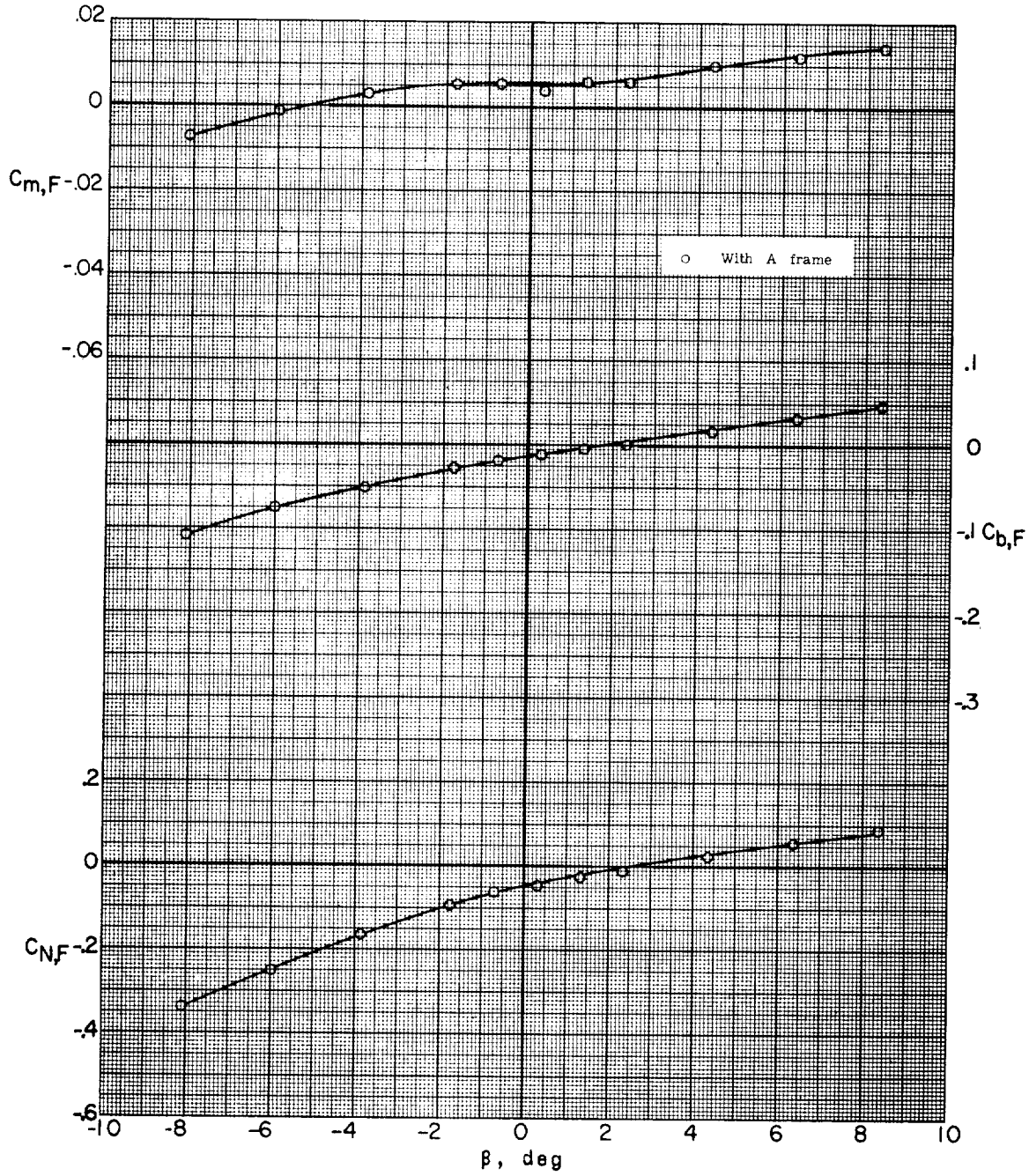
(g) M = 3.22; $\alpha = -5.2^{\circ}$.

Figure 37.- Continued.



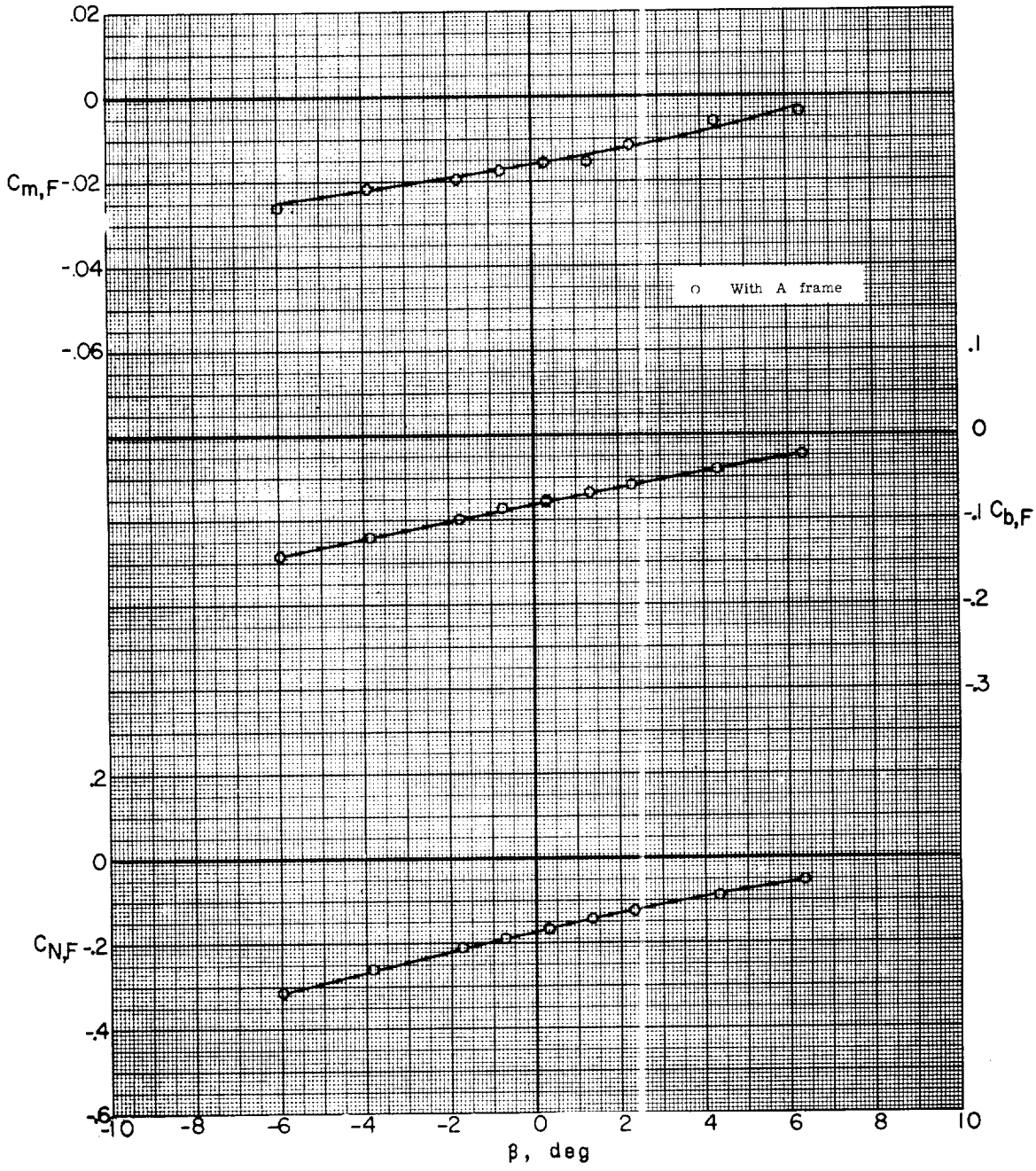
(h) M = 3.22; α = -0.3°.

Figure 37.- Continued.



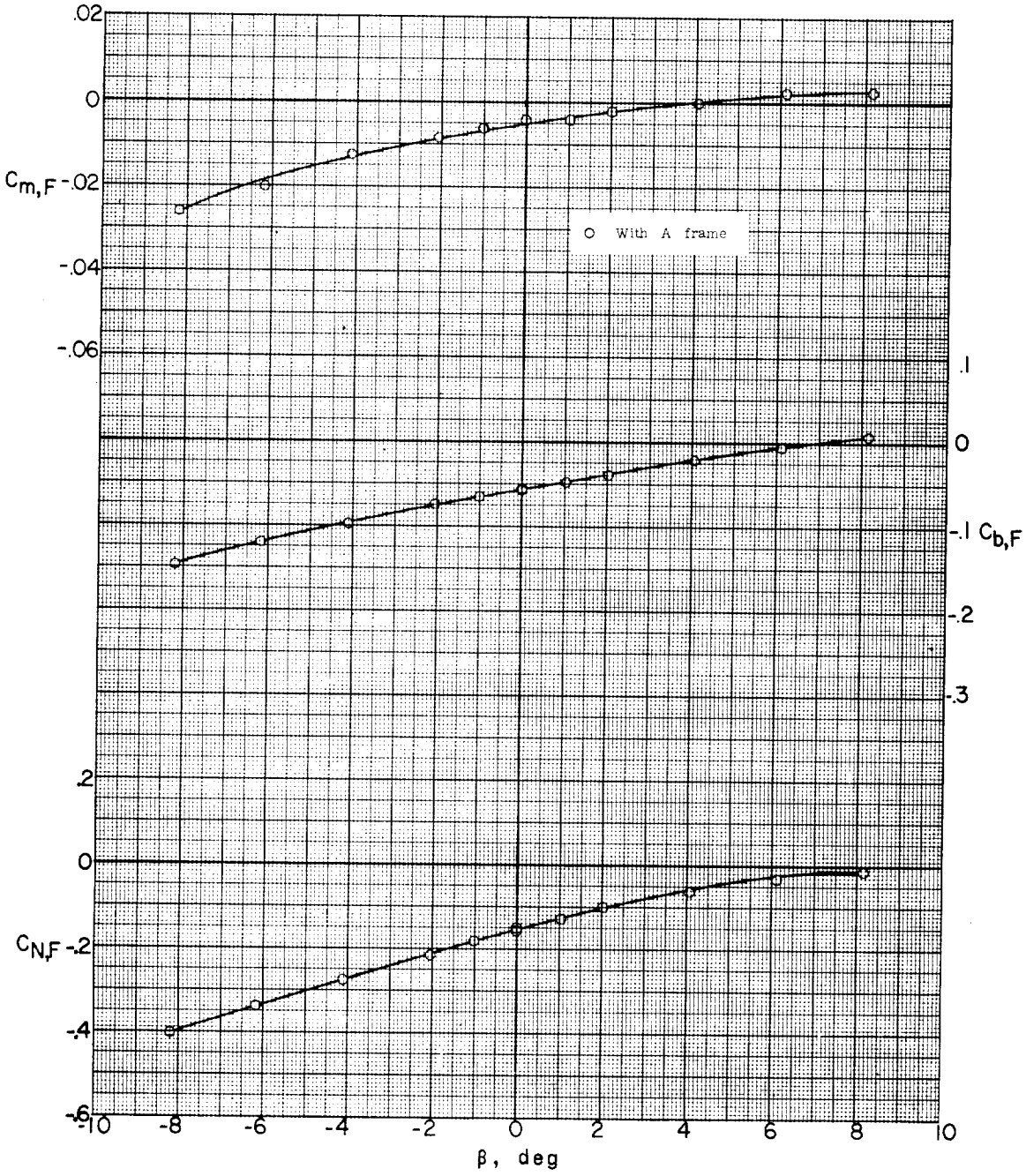
(i) M = 3.22; $\alpha = 5.1^{\circ}$.

Figure 37.- Continued.



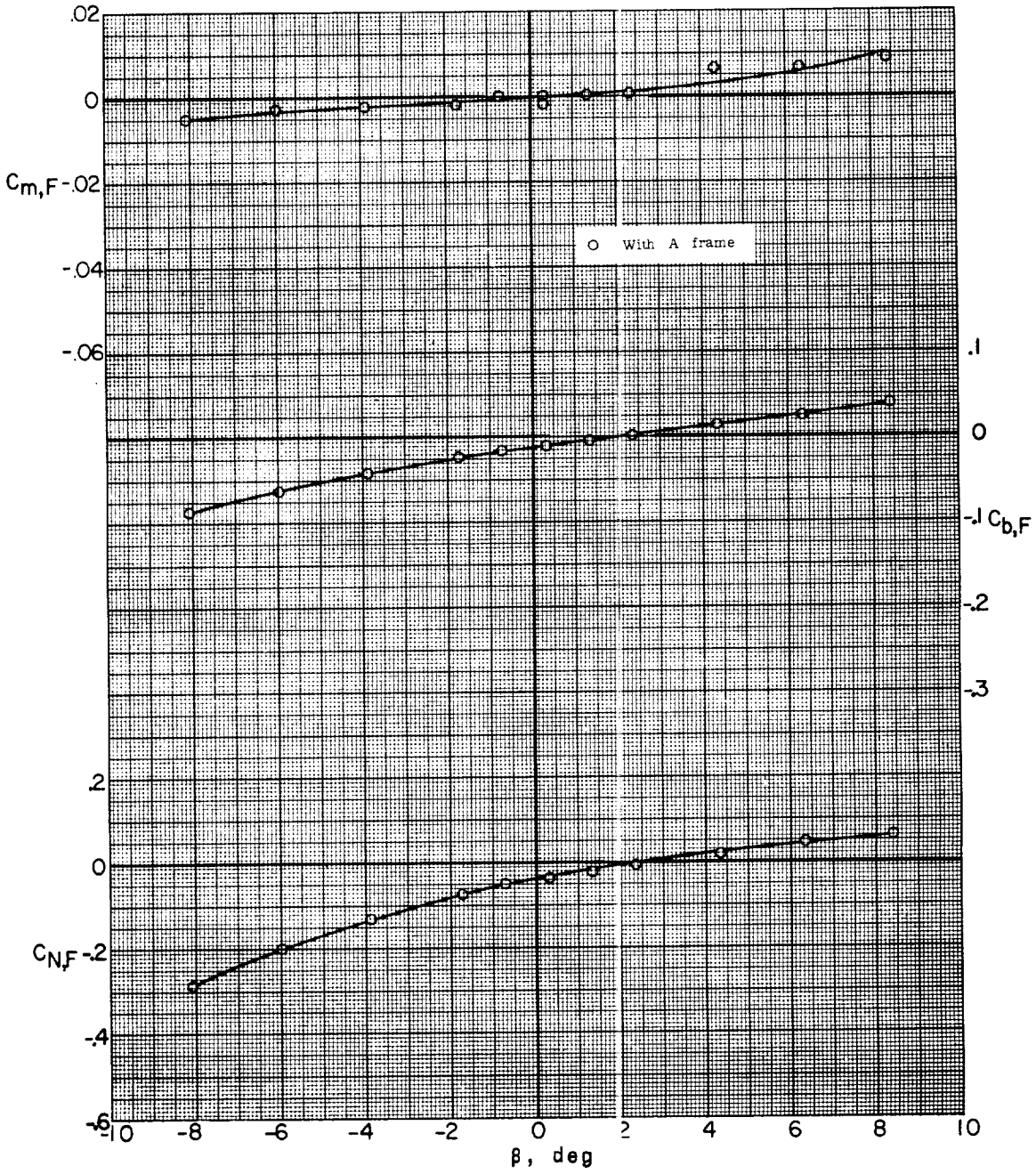
(j) M = 3.51; $\alpha = -5.2^{\circ}$.

Figure 37.- Continued.



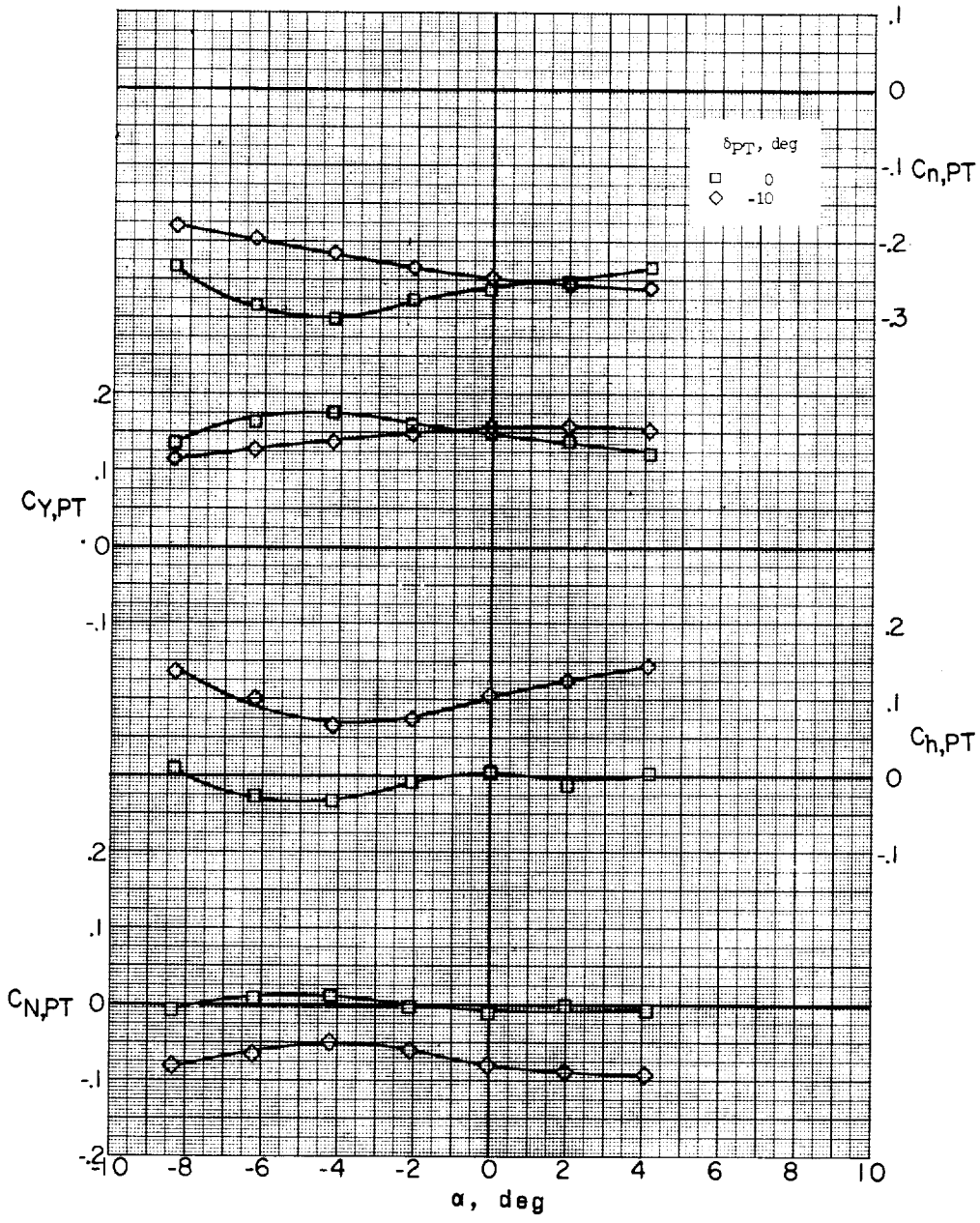
(k) M = 3.51; α = -0.3°.

Figure 37.- Continued.



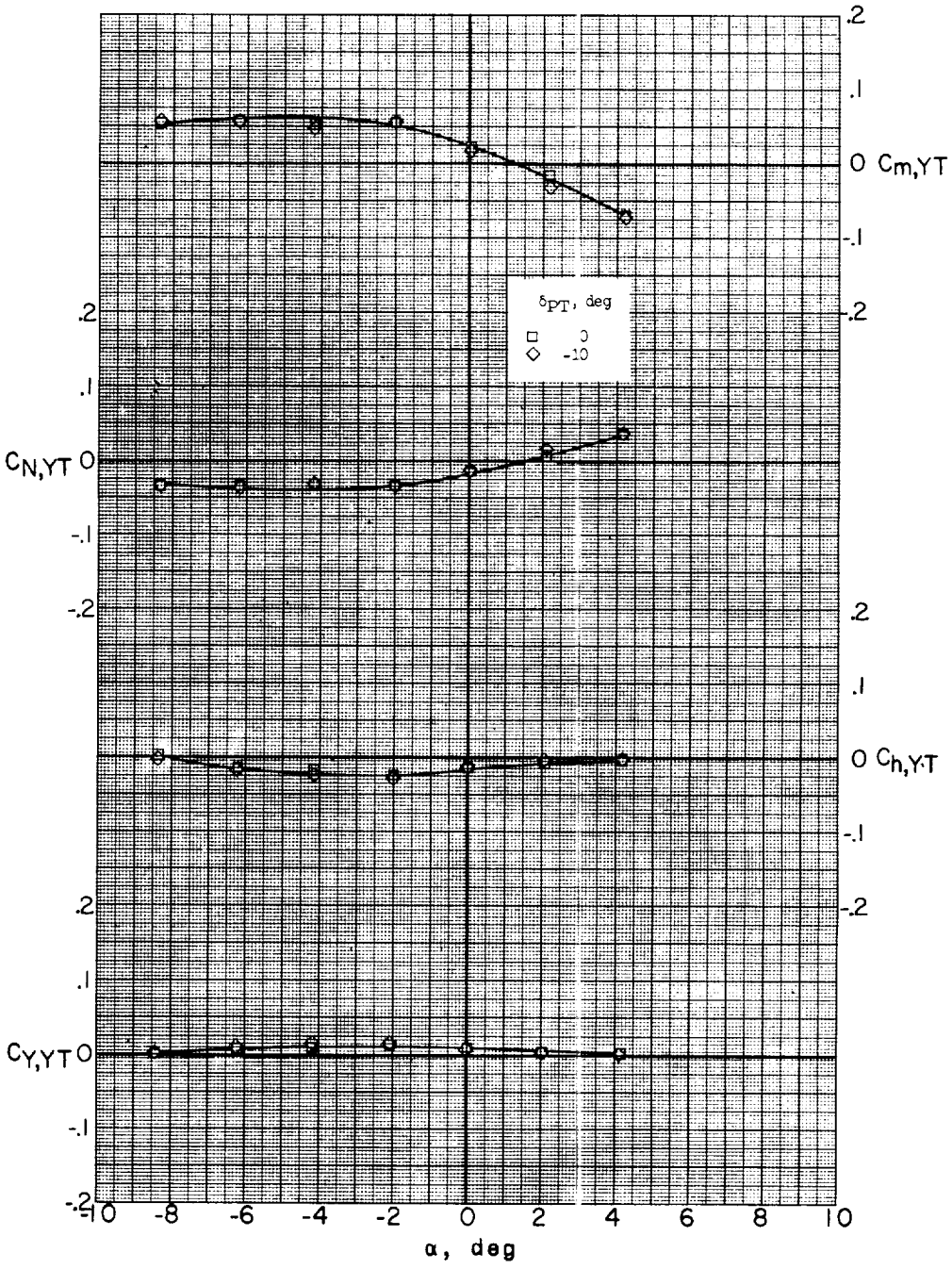
(l) M = 3.51; α = 5.1°.

Figure 37.- Concluded.



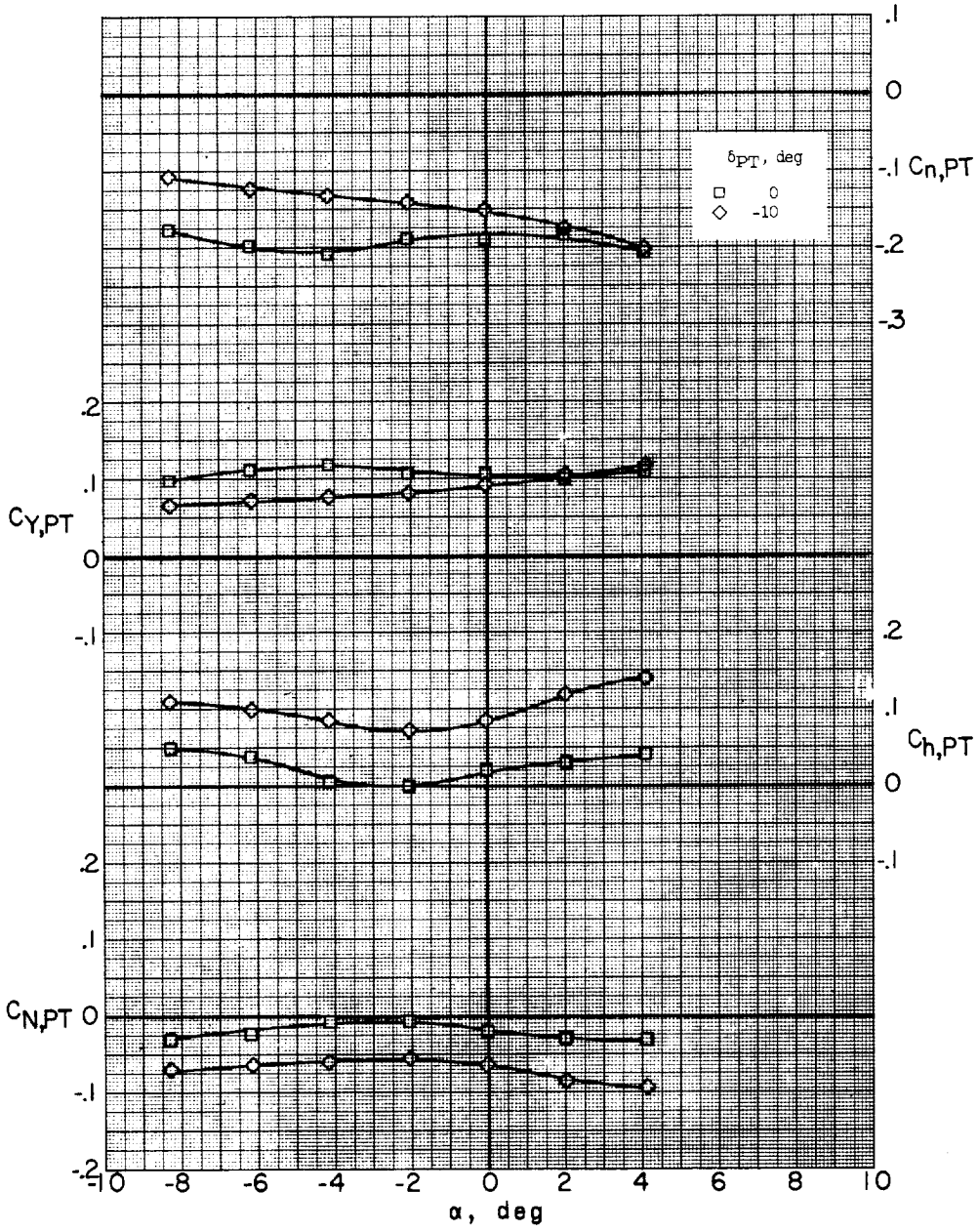
(a) M = 2.75; with bug-eye fairing.

Figure 38.- Effect of nozzle deflection on pitch characteristics of pitch and yaw thrust chambers. Missile-booster combination with A-frame mounted; $\delta_{YT} = 0^{o}$; $\beta = 0.2^{o}$; sting B.



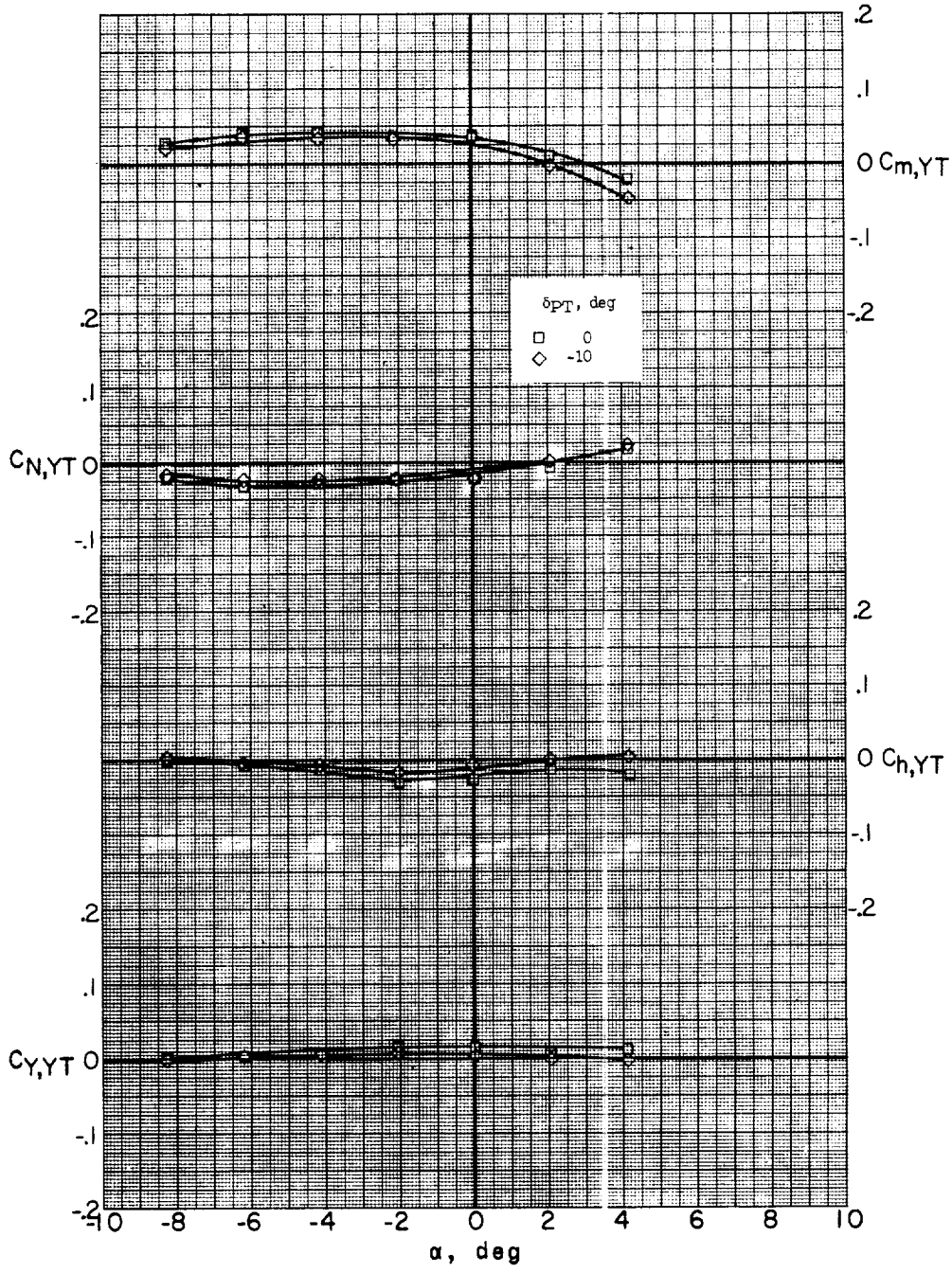
(a) Concluded.

Figure 38.- Continued.



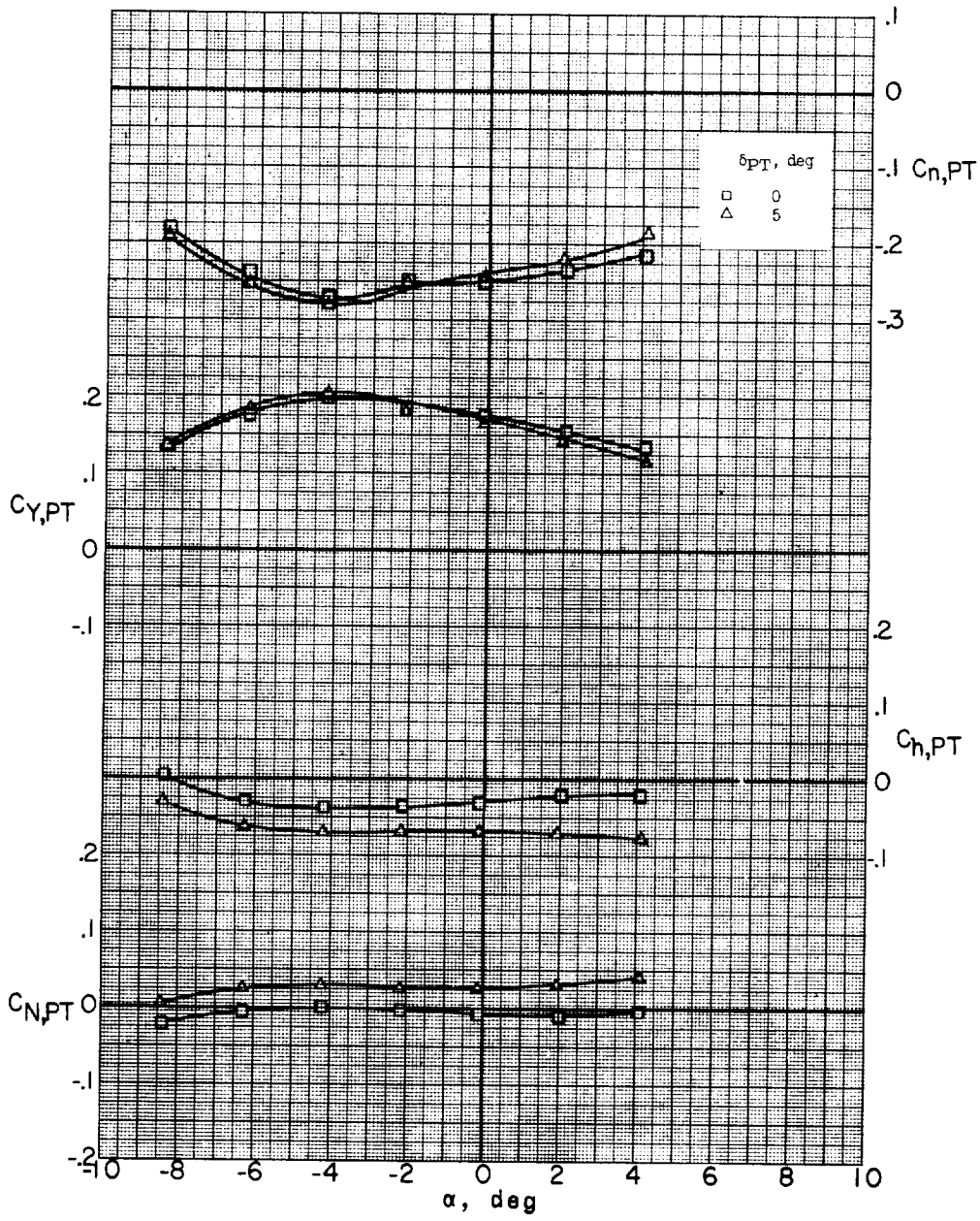
(b) M = 3.22; with bug-eye fairing.

Figure 38.- Continued.



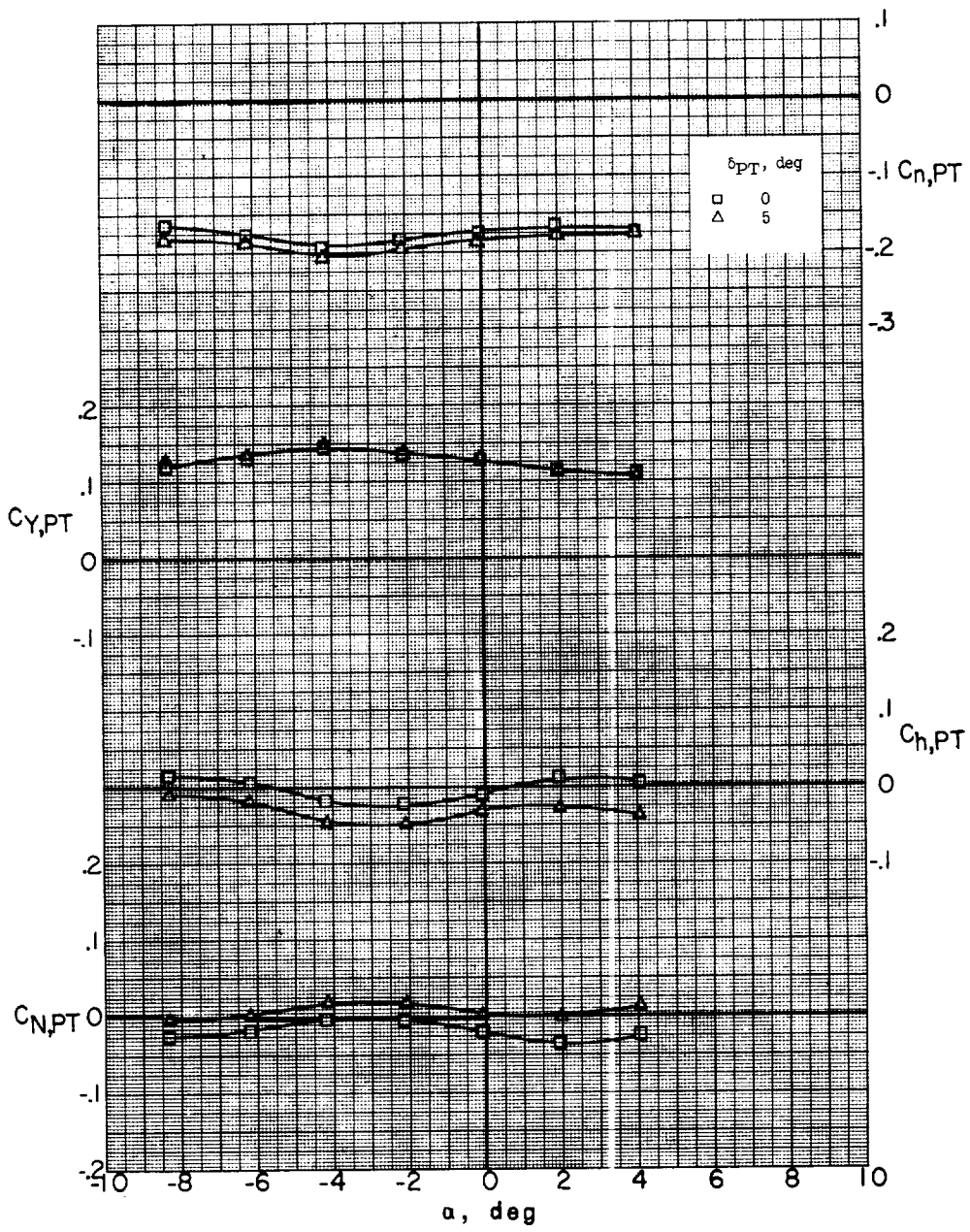
(b) Concluded.

Figure 38.- Continued.



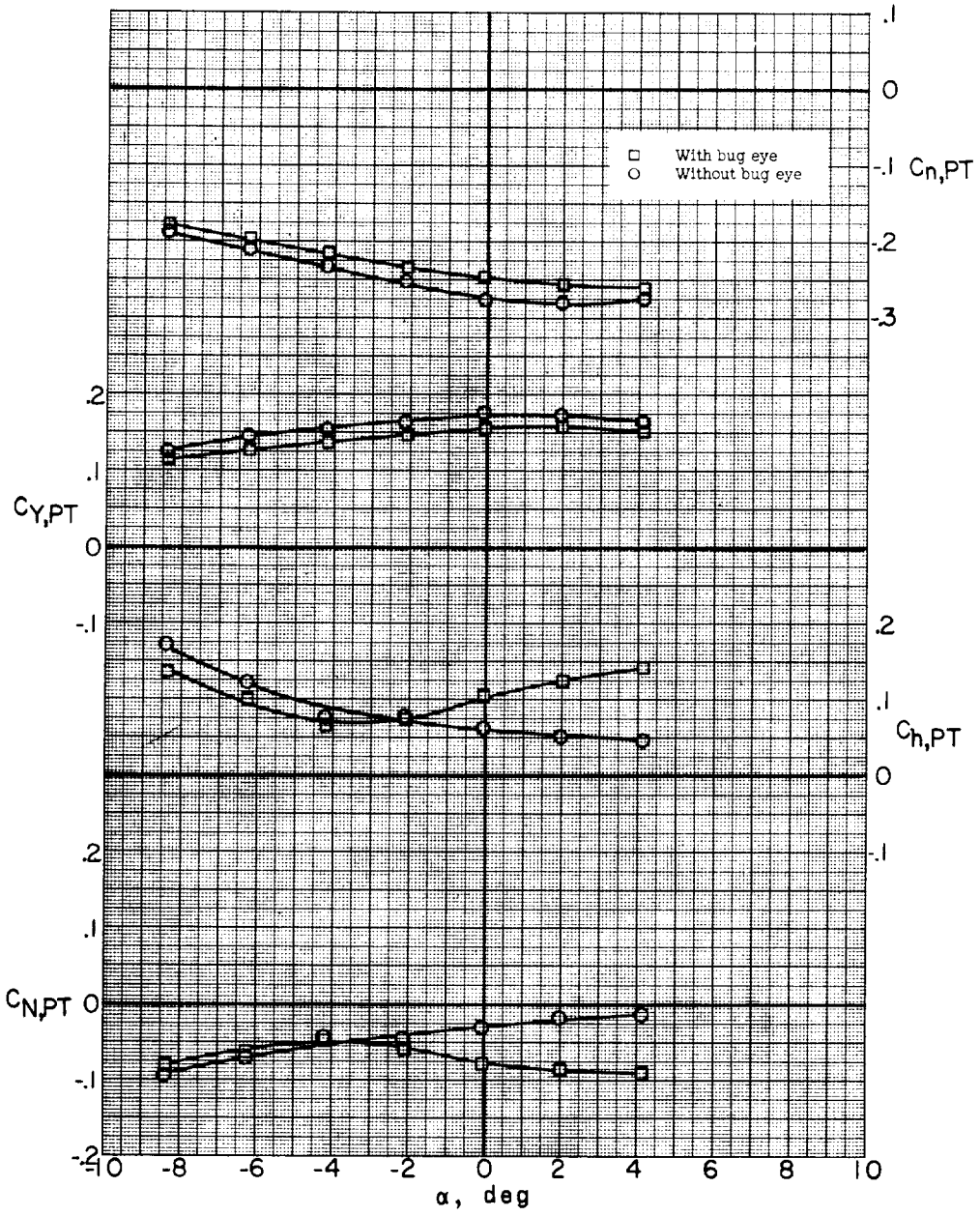
(c) M = 2.75; with bug-eye and nozzle-shroud fairings.

Figure 38.- Continued.



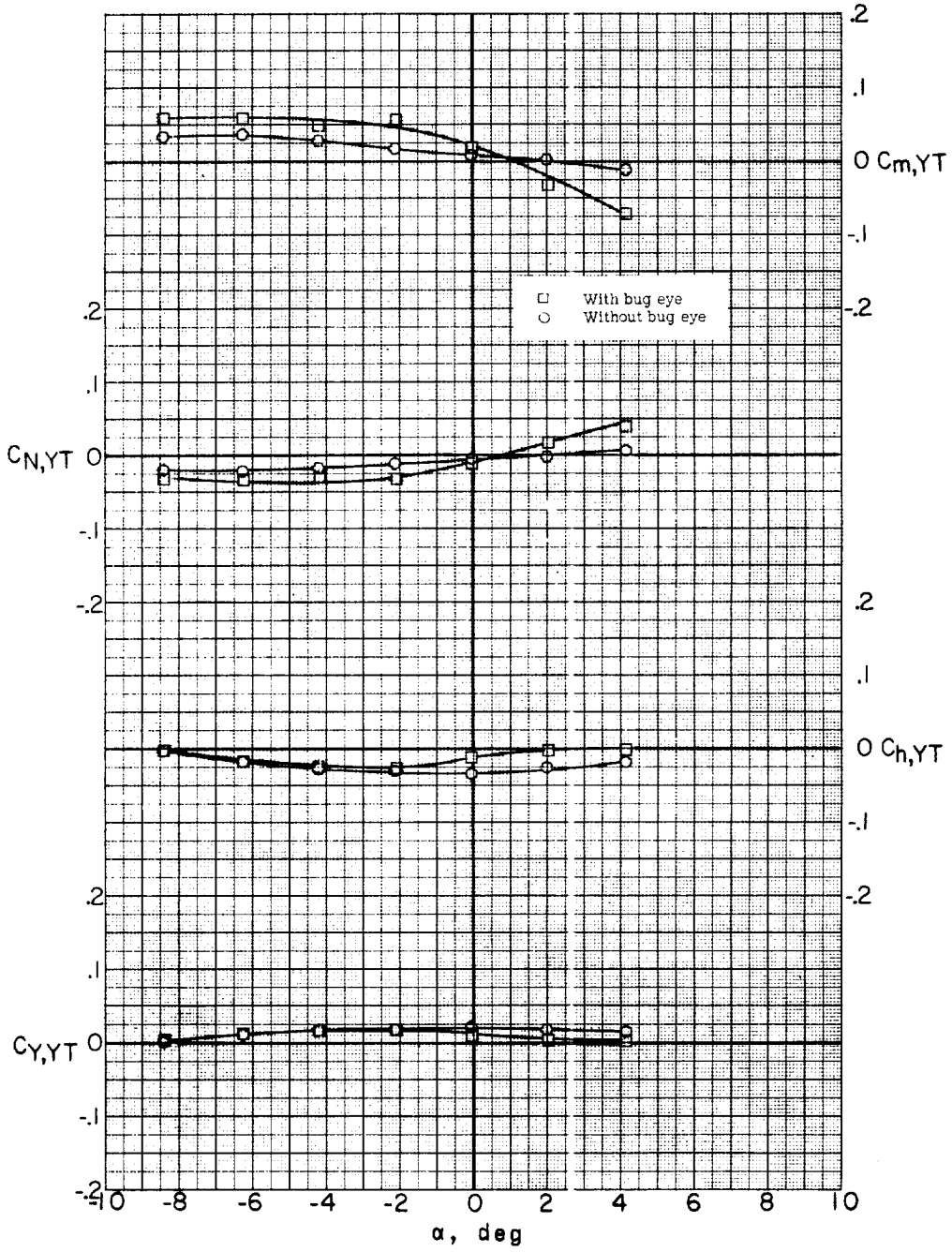
(d) M = 3.22; with bug-eye and nozzle-shroud fairings.

Figure 38.- Concluded.



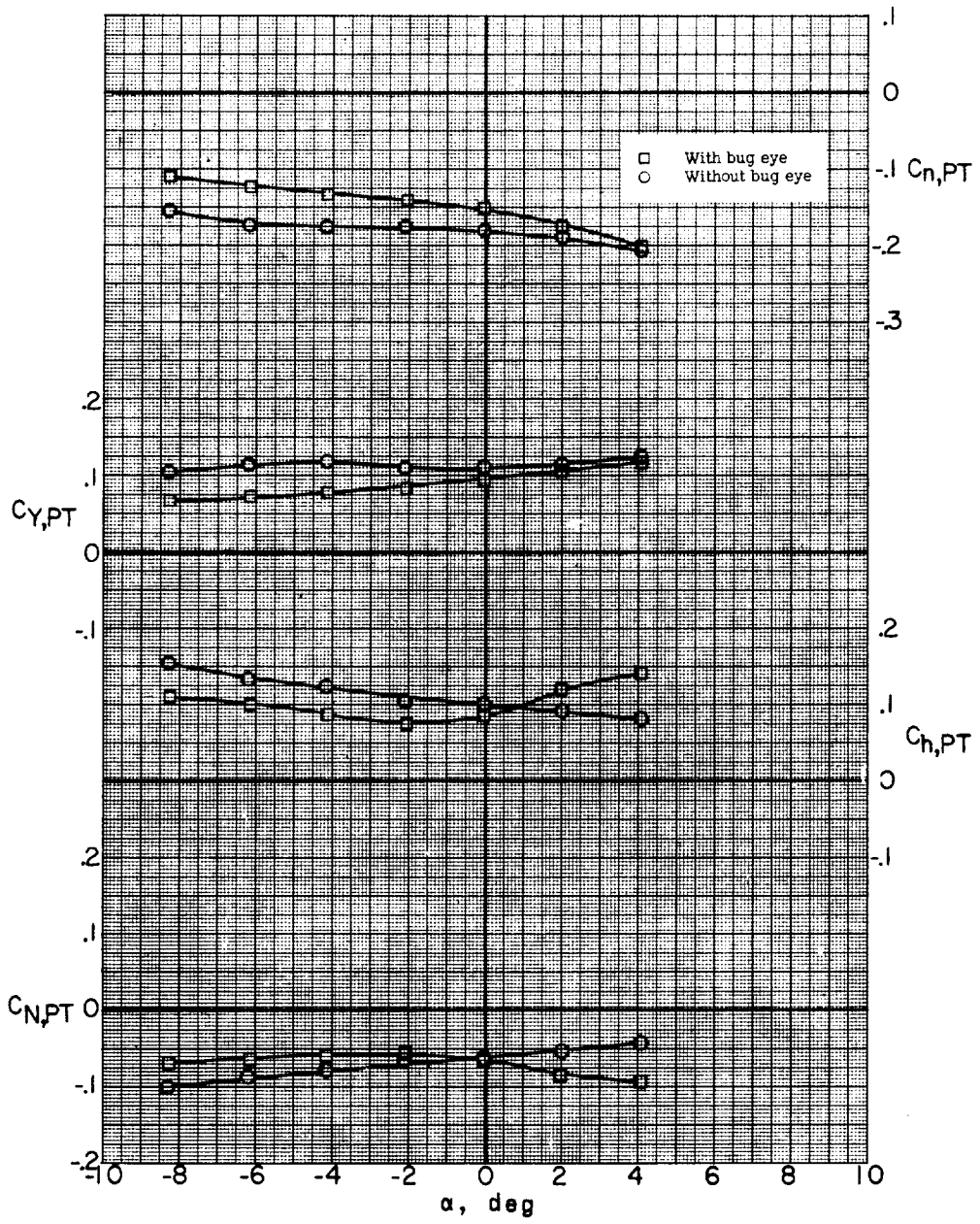
(a) M = 2.75.

Figure 39.- Effect of bug-eye fairing on pitch characteristics of pitch and yaw thrust chambers. Missile-booster combination with A-frame mounted; $\delta_{PT} = -10^{\circ}$; $\delta_{YT} = 0^{\circ}$; $\beta = 0.2^{\circ}$; sting B.



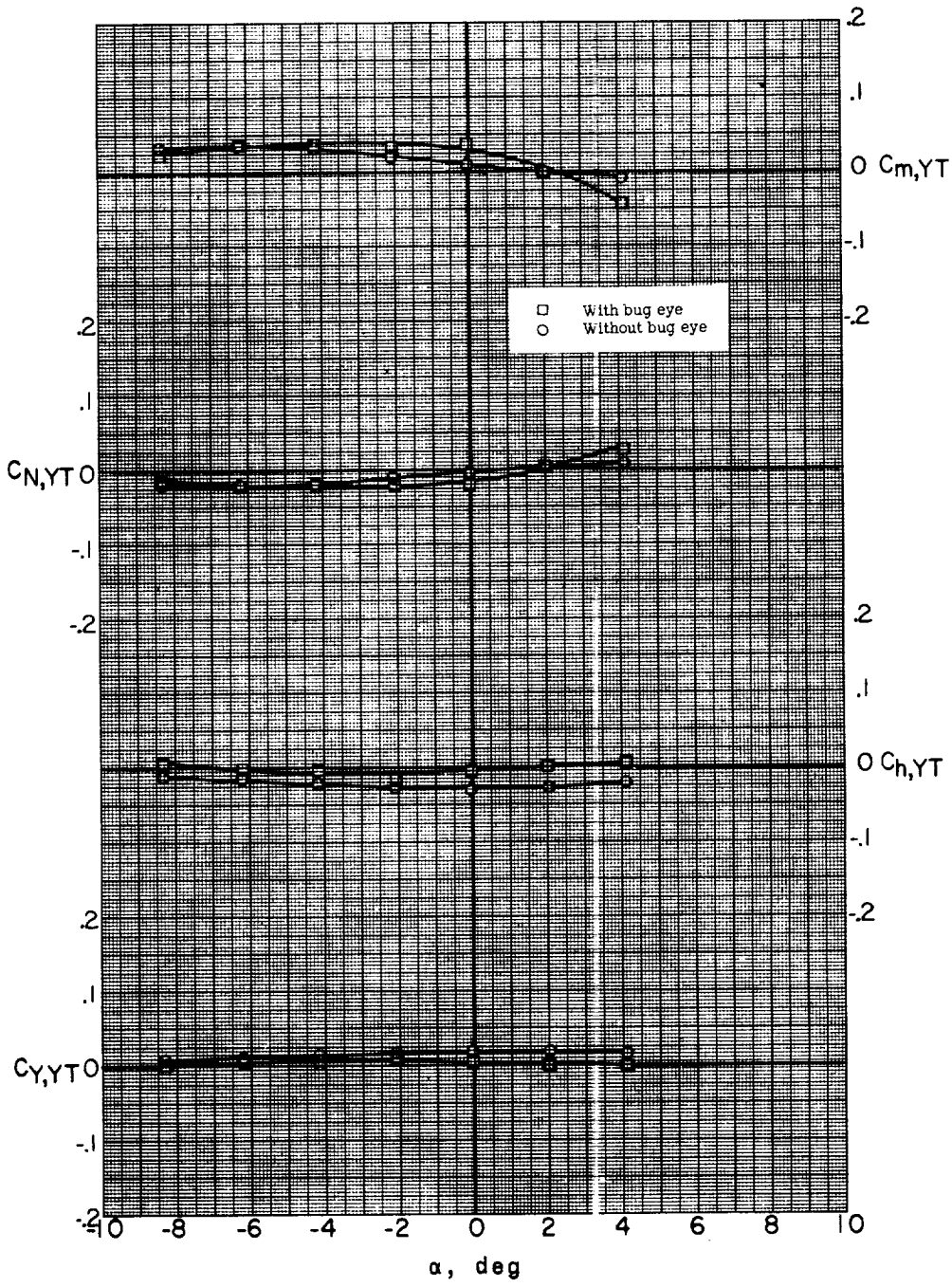
(a) Concluded.

Figure 39.- Continued.



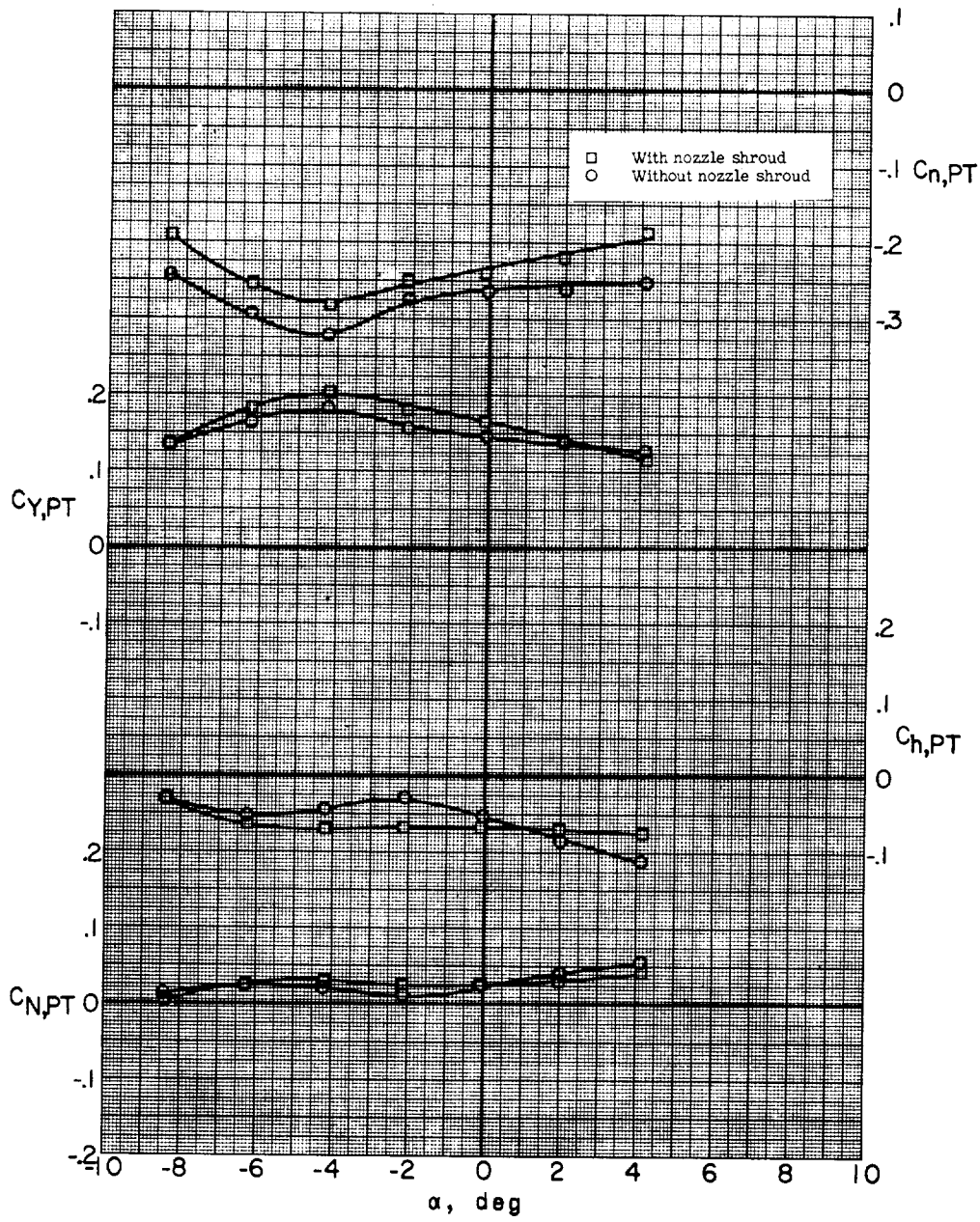
(b) M = 3.22.

Figure 39.- Continued.



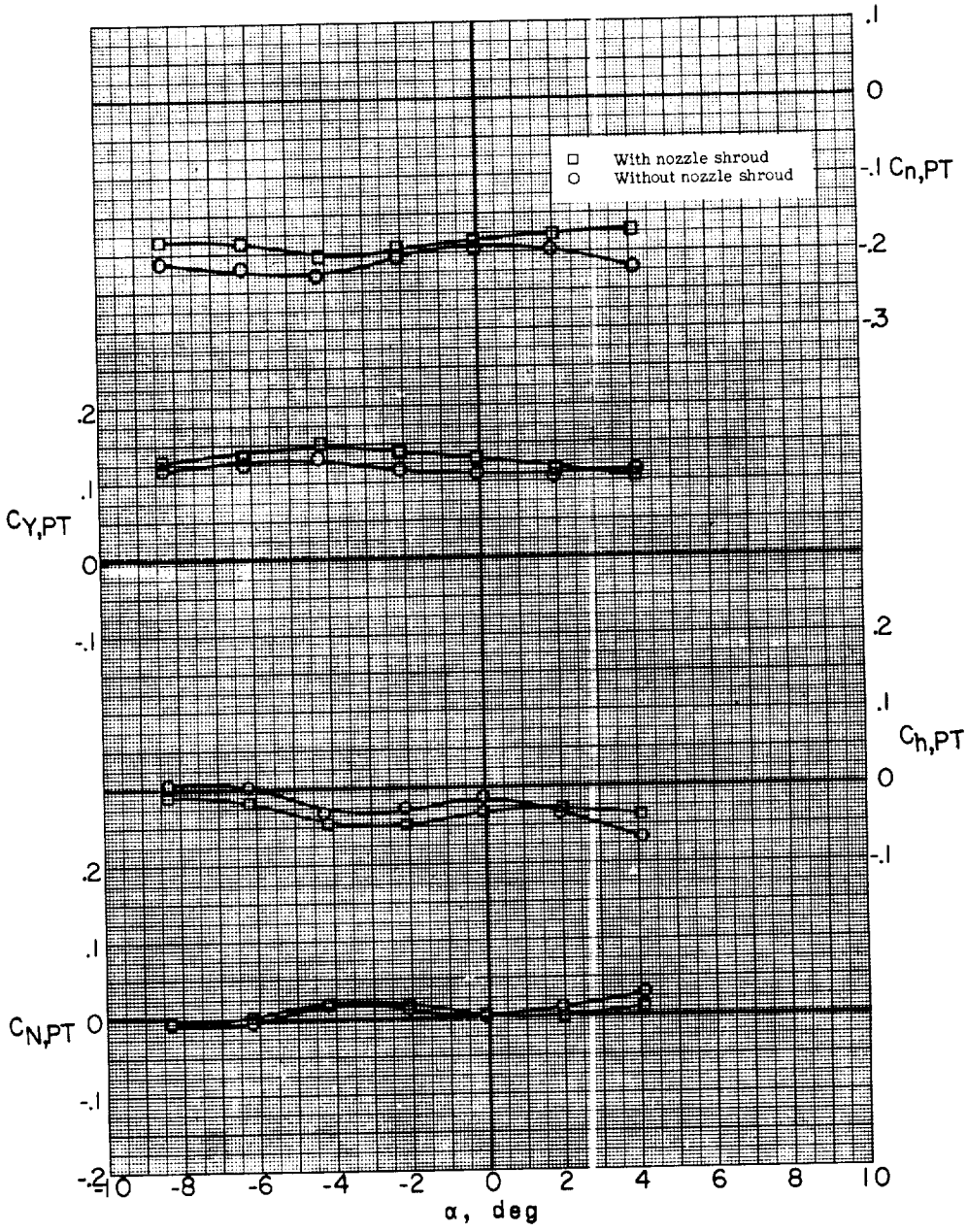
(b) Concluded.

Figure 39.- Concluded.



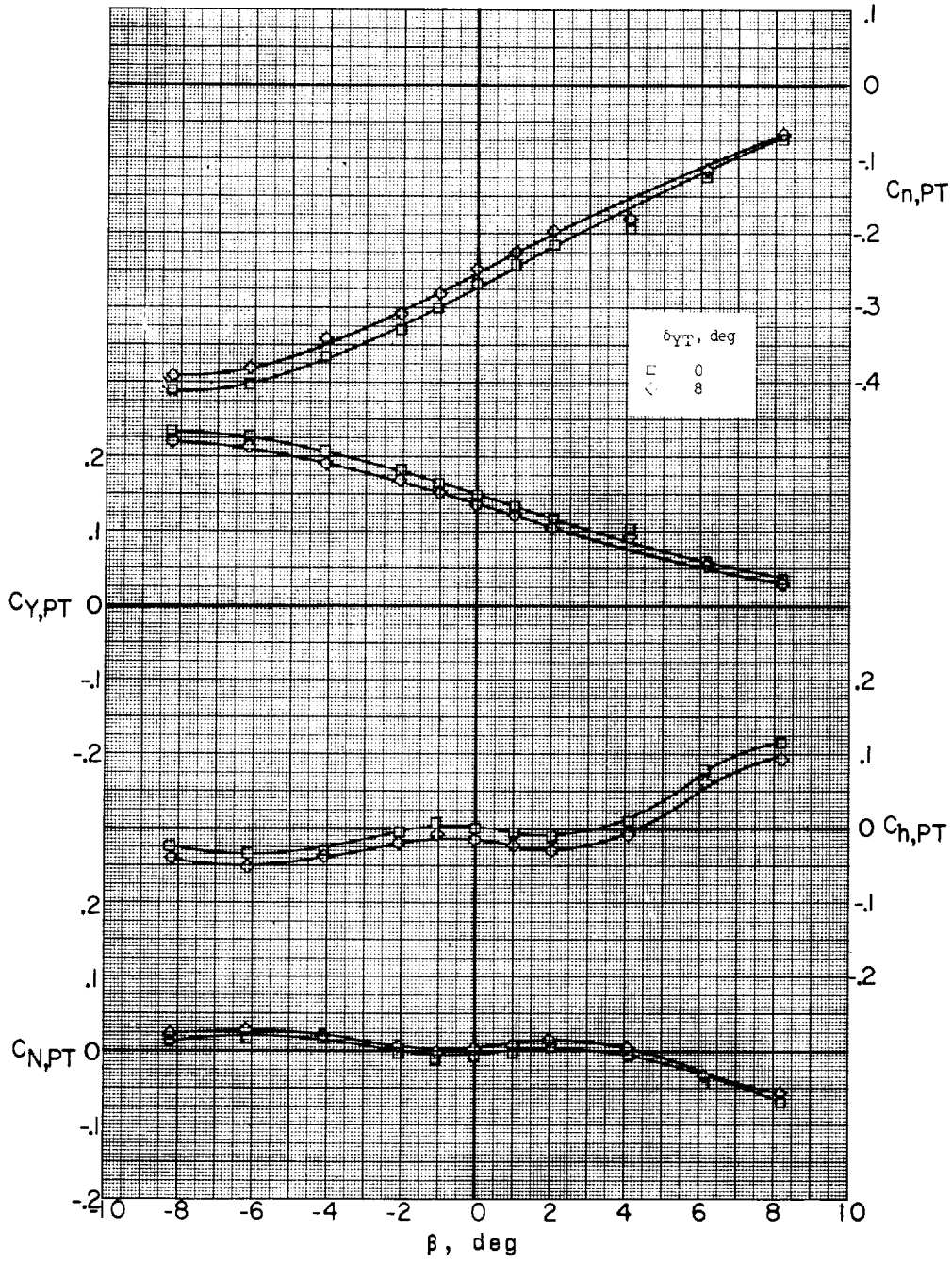
(a) M = 2.75.

Figure 40.- Effect of nozzle shrouds on pitch characteristics of pitch thrust chamber. Missile-booster combination with bug-eye fairing and A-frame mounted; $\delta_{PT} = 5^{\circ}$; $\delta_{YT} = 0^{\circ}$; $\beta = 0.2^{\circ}$; sting B.



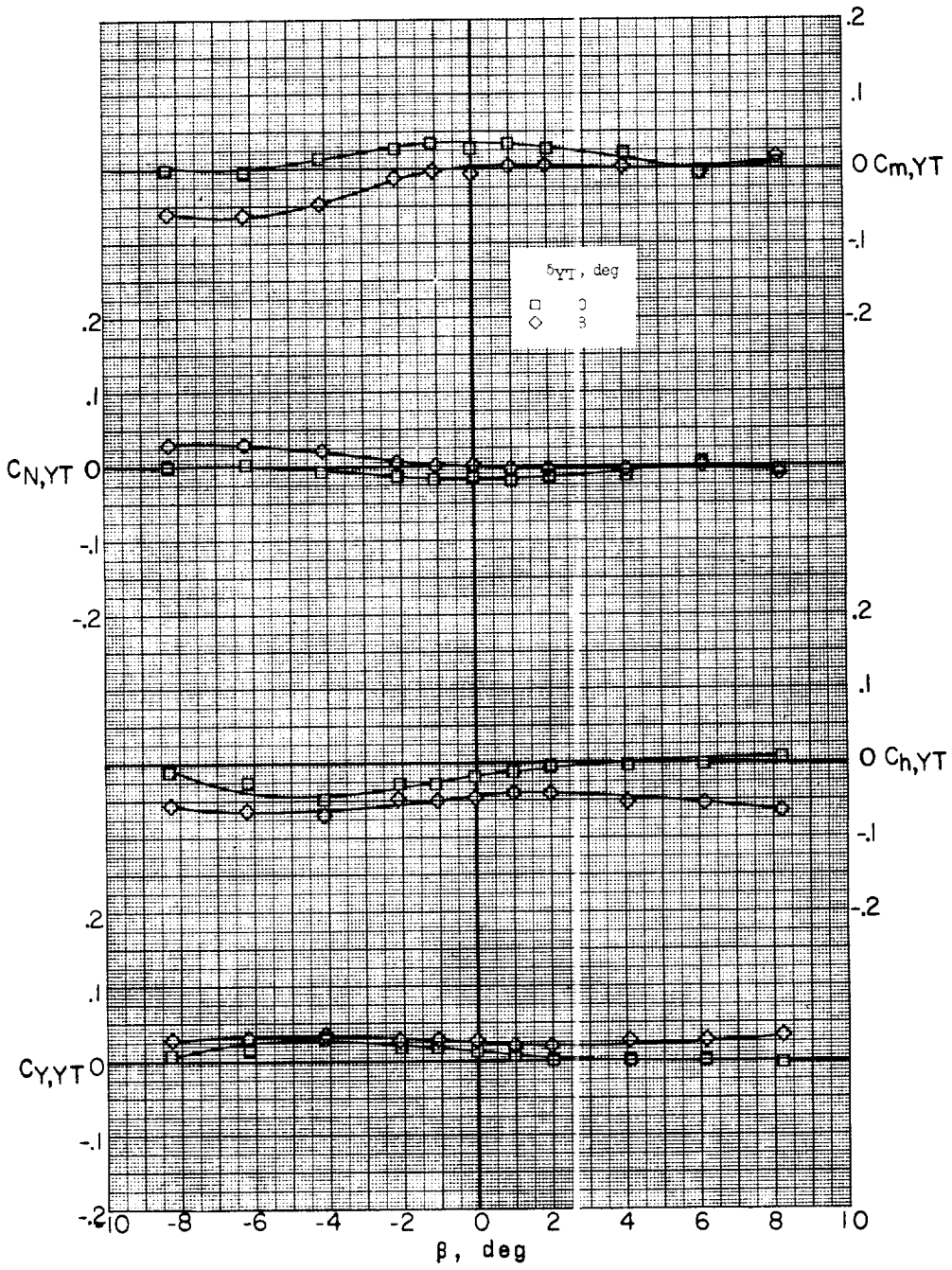
(b) M = 3.22.

Figure 40.- Concluded.



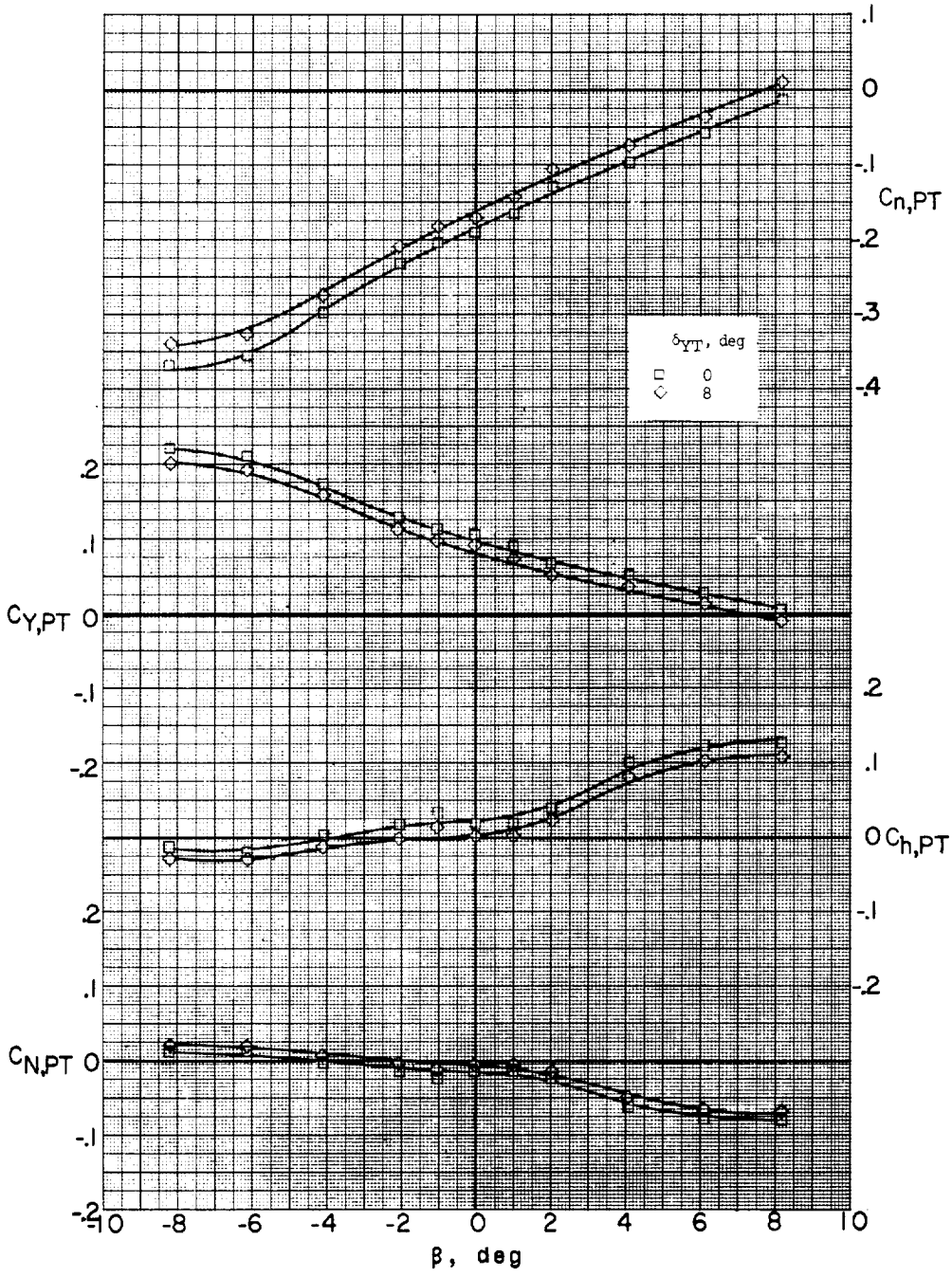
(a) M = 2.75.

Figure 41.- Effect of nozzle deflection on lateral characteristics of pitch and yaw thrust chamber. Missile-booster combination with bug-eye fairing and A-frame mounted; $\delta_{PT} = 0^{\circ}$; $\alpha = -0.3^{\circ}$; sting B.



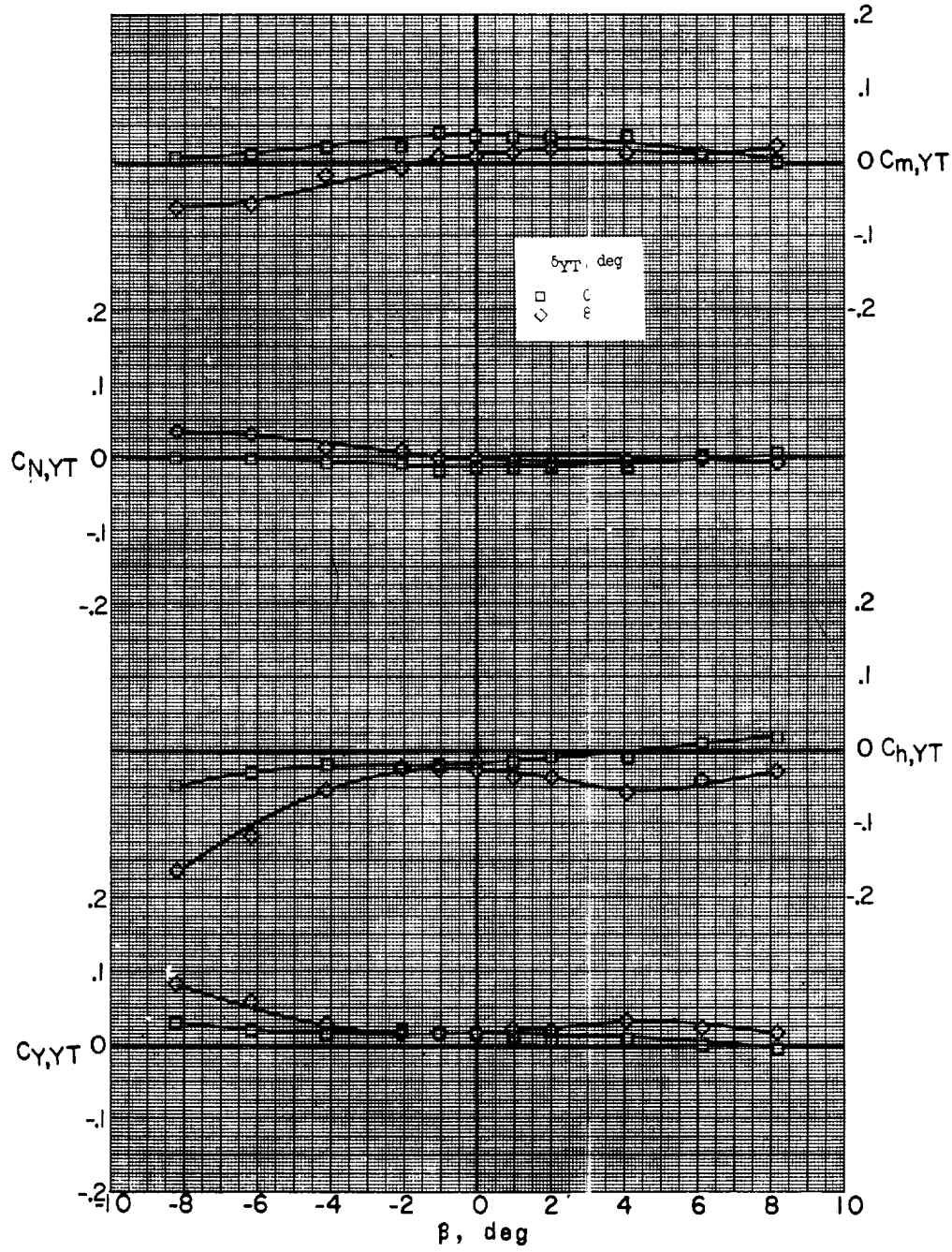
(a) Concluded.

Figure 41.- Continued.



(b) M = 3.22.

Figure 41.- Continued.



(b) Concluded.

Figure 41.- Concluded.

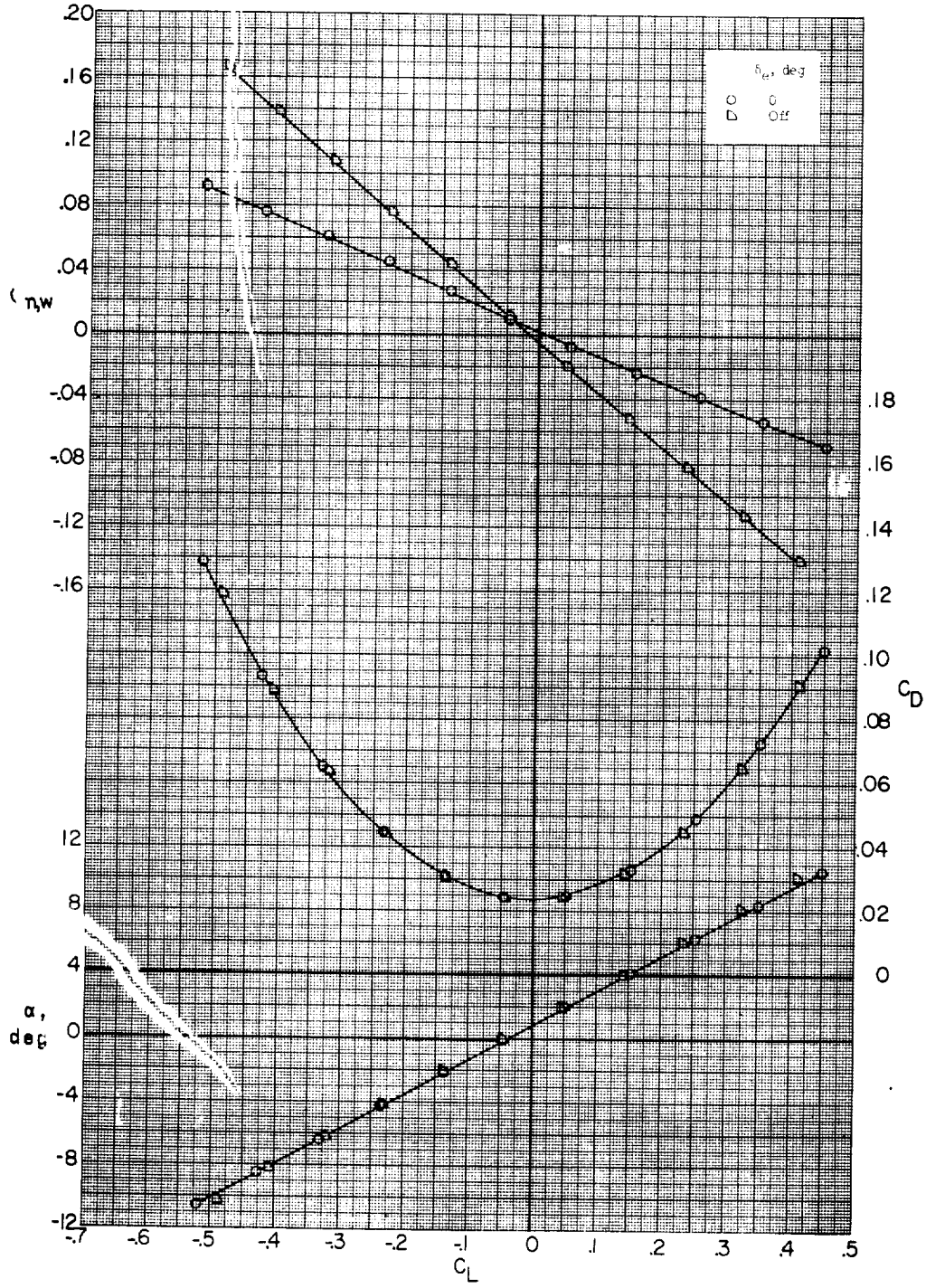
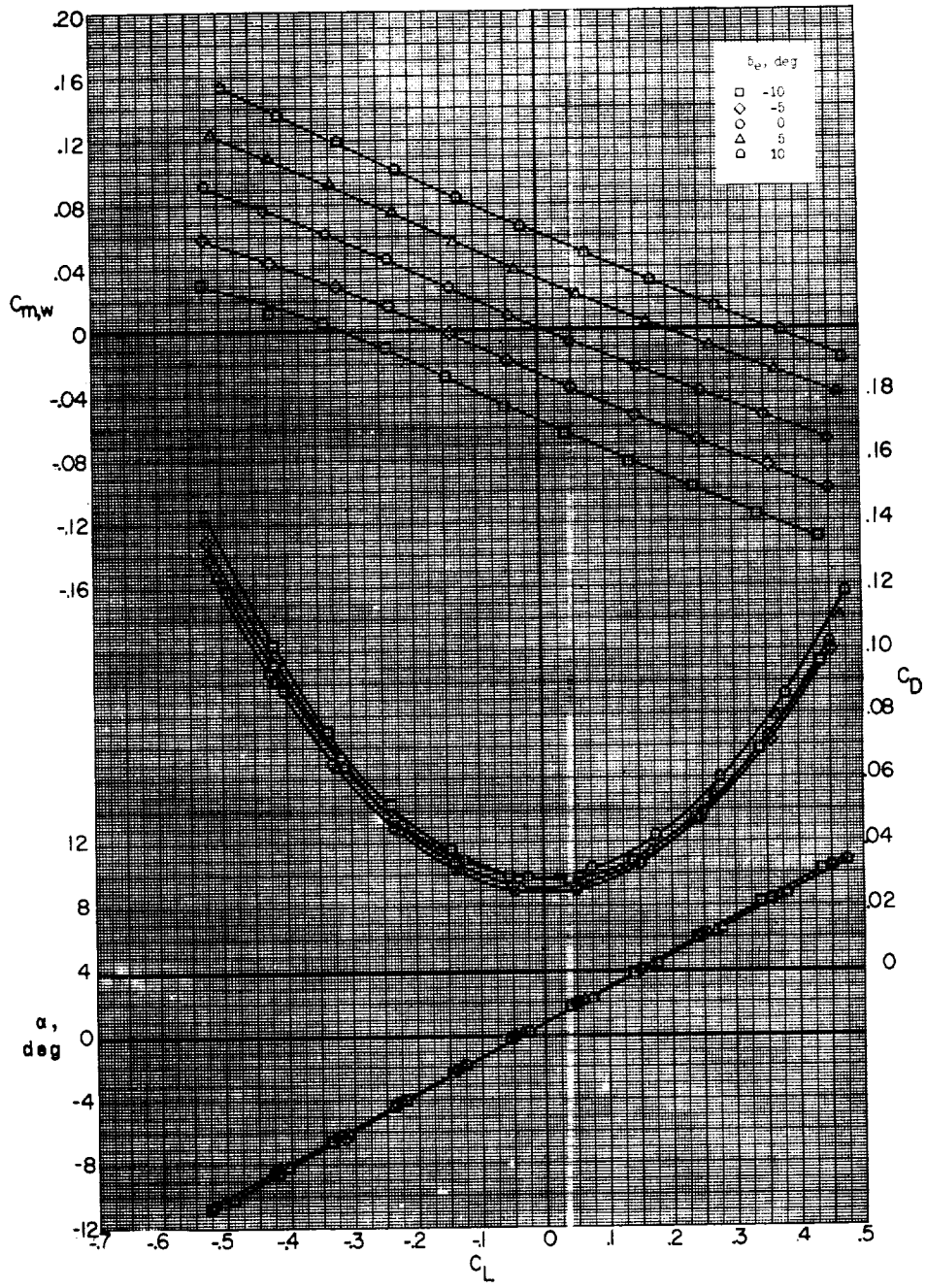
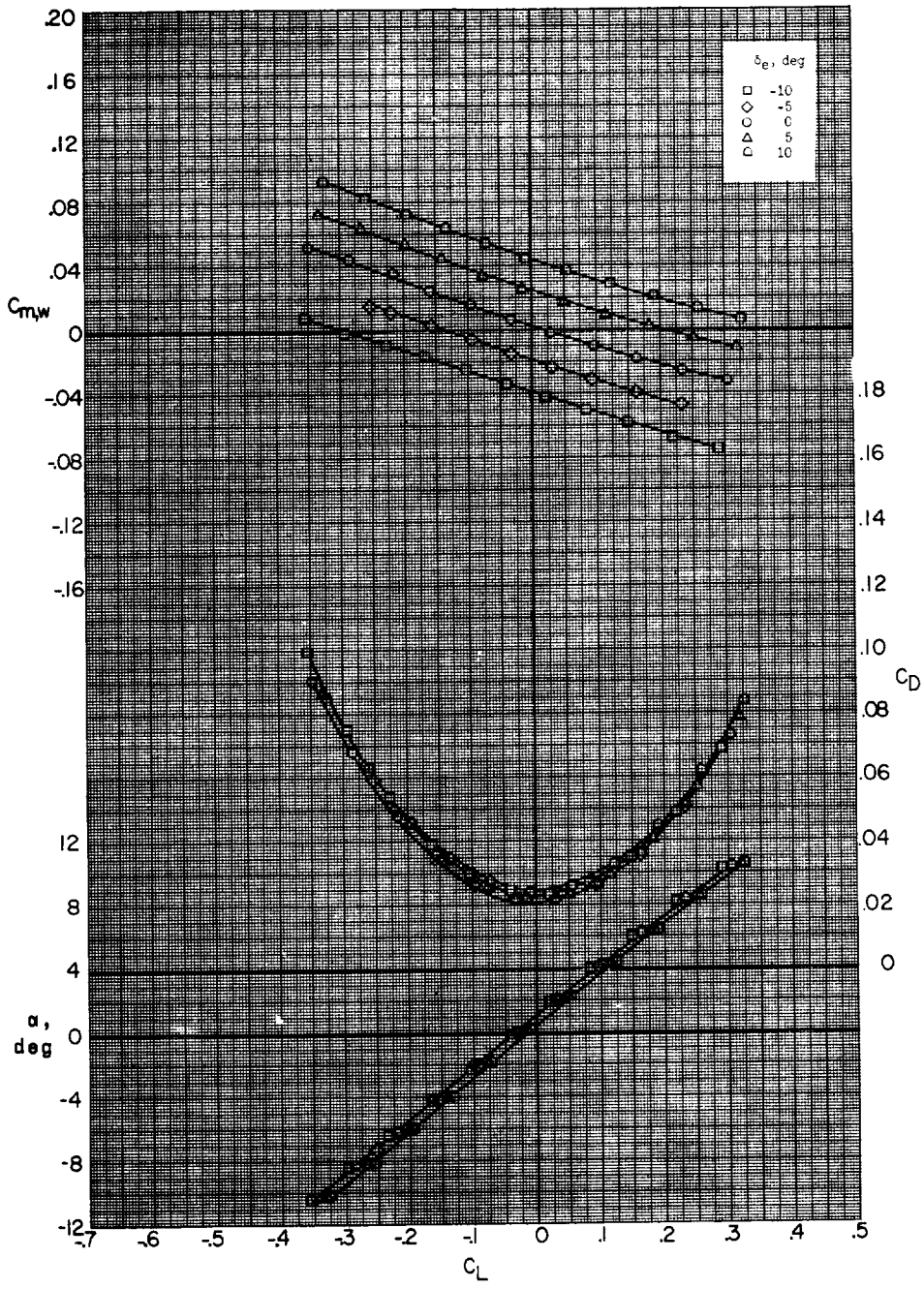


Figure 42.- Effect of canard surface on pitch characteristics of missile alone. $\beta = 0.2^{o}$; M = 1.77; sting A.



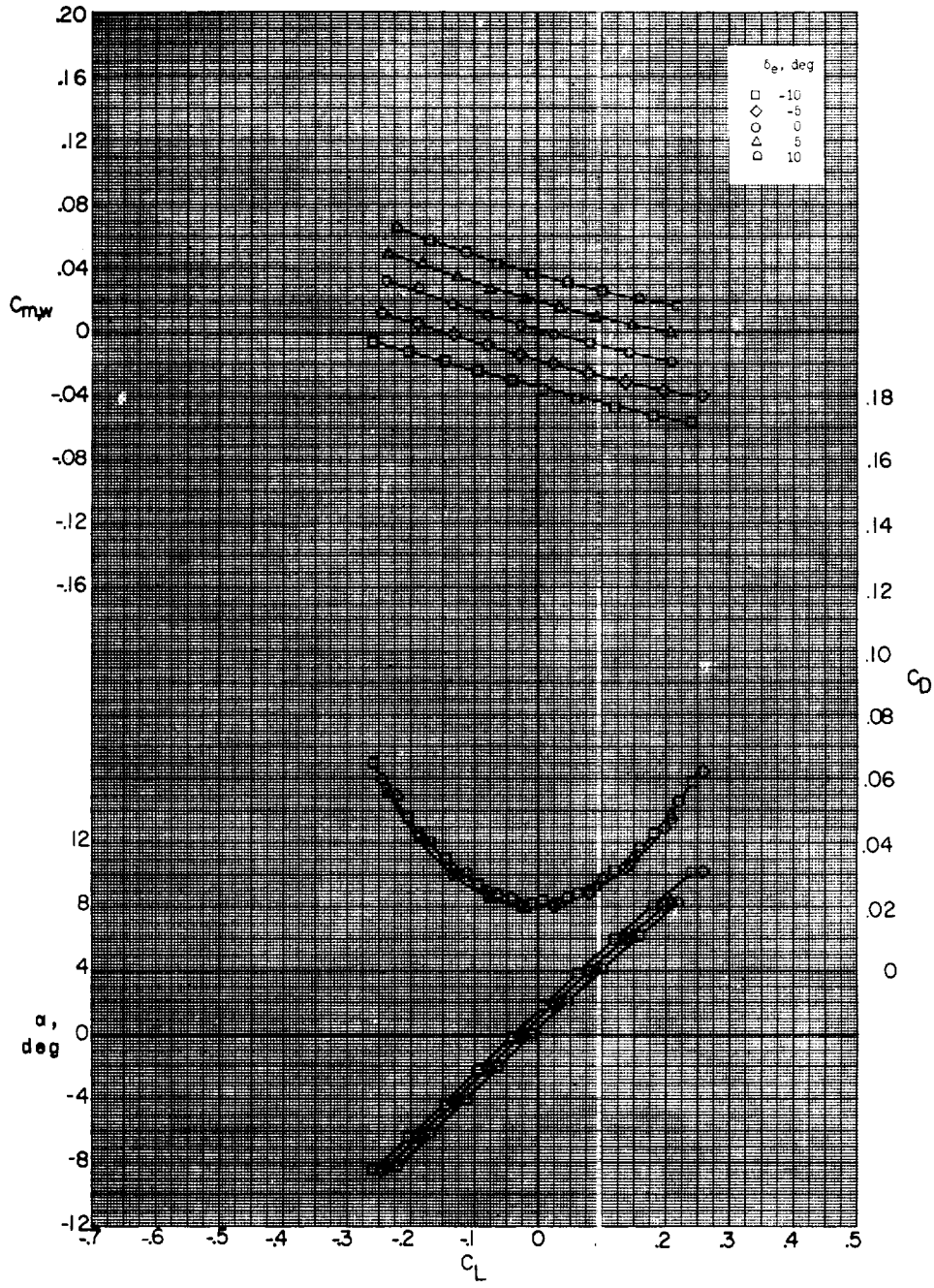
(a) M = 1.77.

Figure 43.- Effect of canard deflection on pitch characteristics of missile alone. $\beta = 0.2^{c}$; sting A.



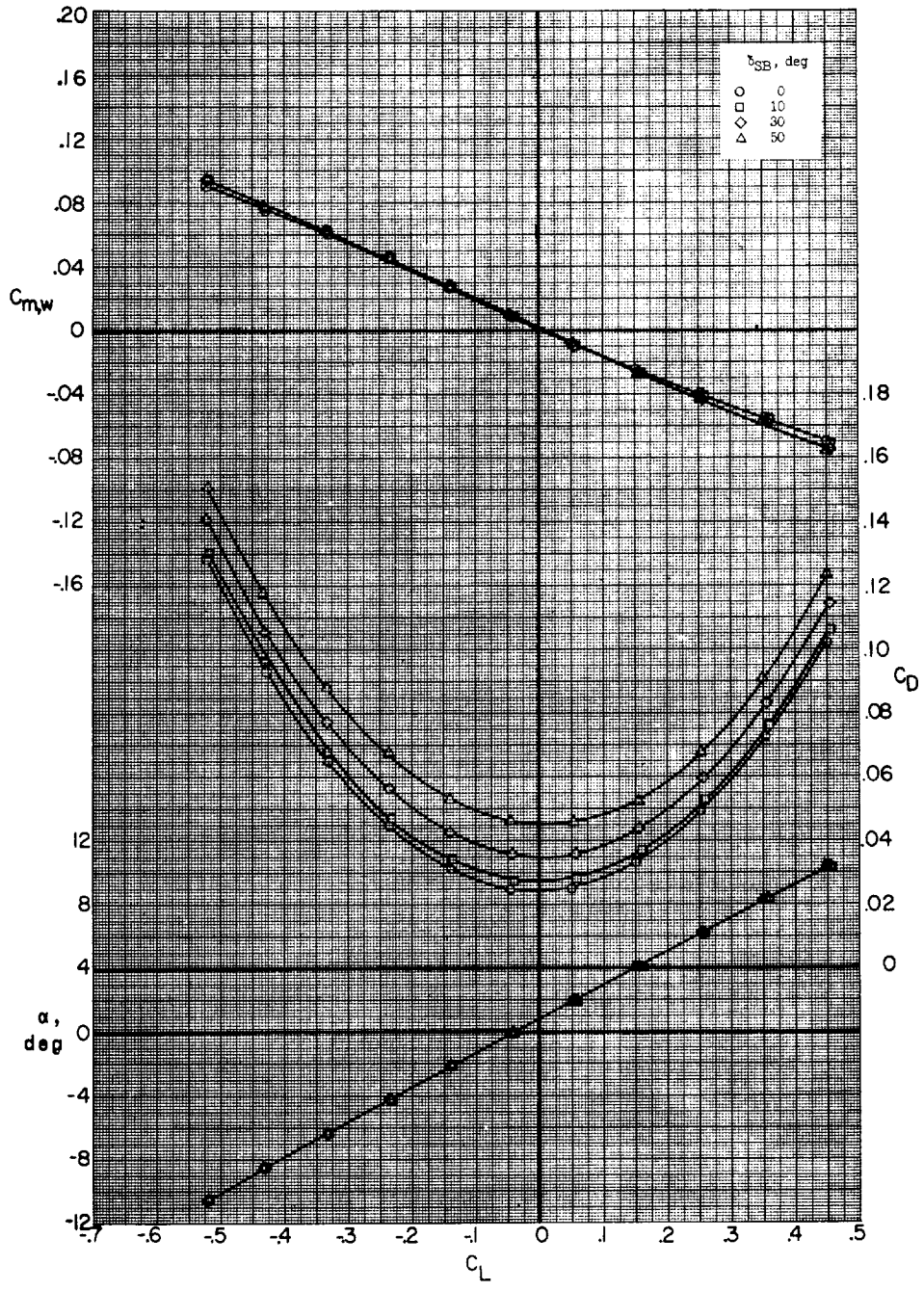
(b) M = 2.75.

Figure 43.- Continued.



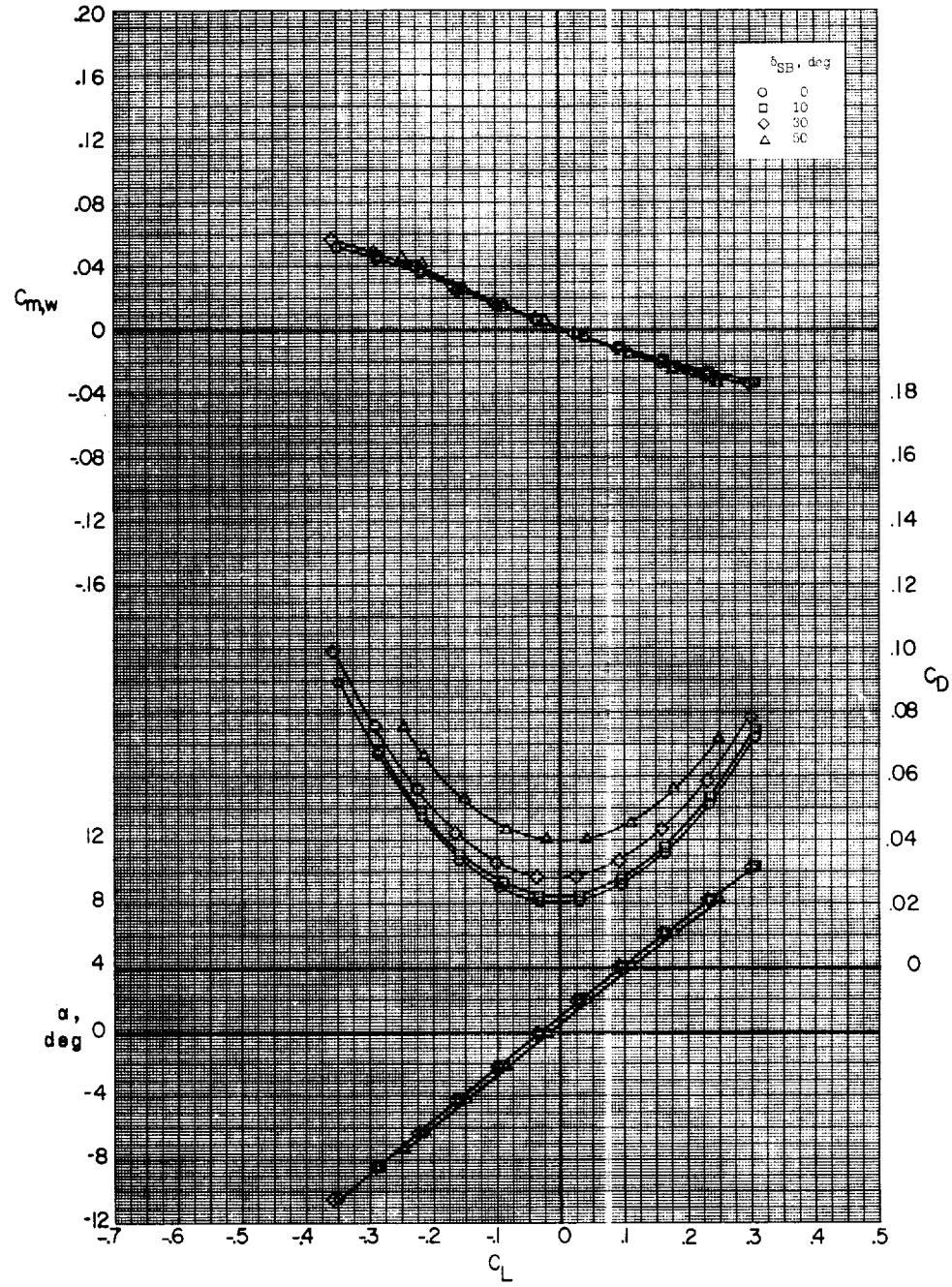
(c) M = 3.22.

Figure 43.- Concluded.



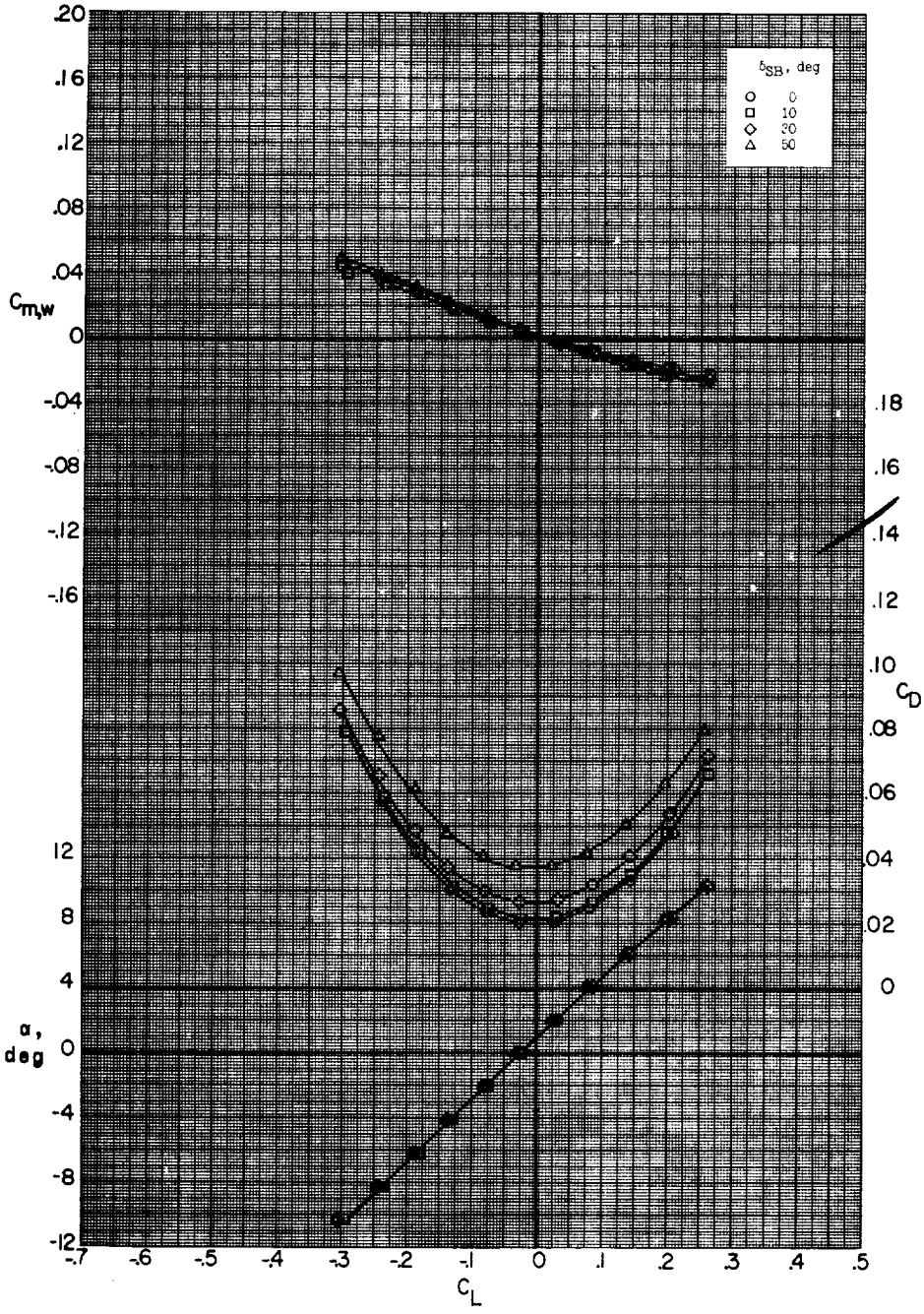
(a) M = 1.77.

Figure 44.- Effect of speed-brake deflection on pitch characteristics of missile alone. $\delta_e = 0^o$; $\beta = 0.2^o$; sting A.



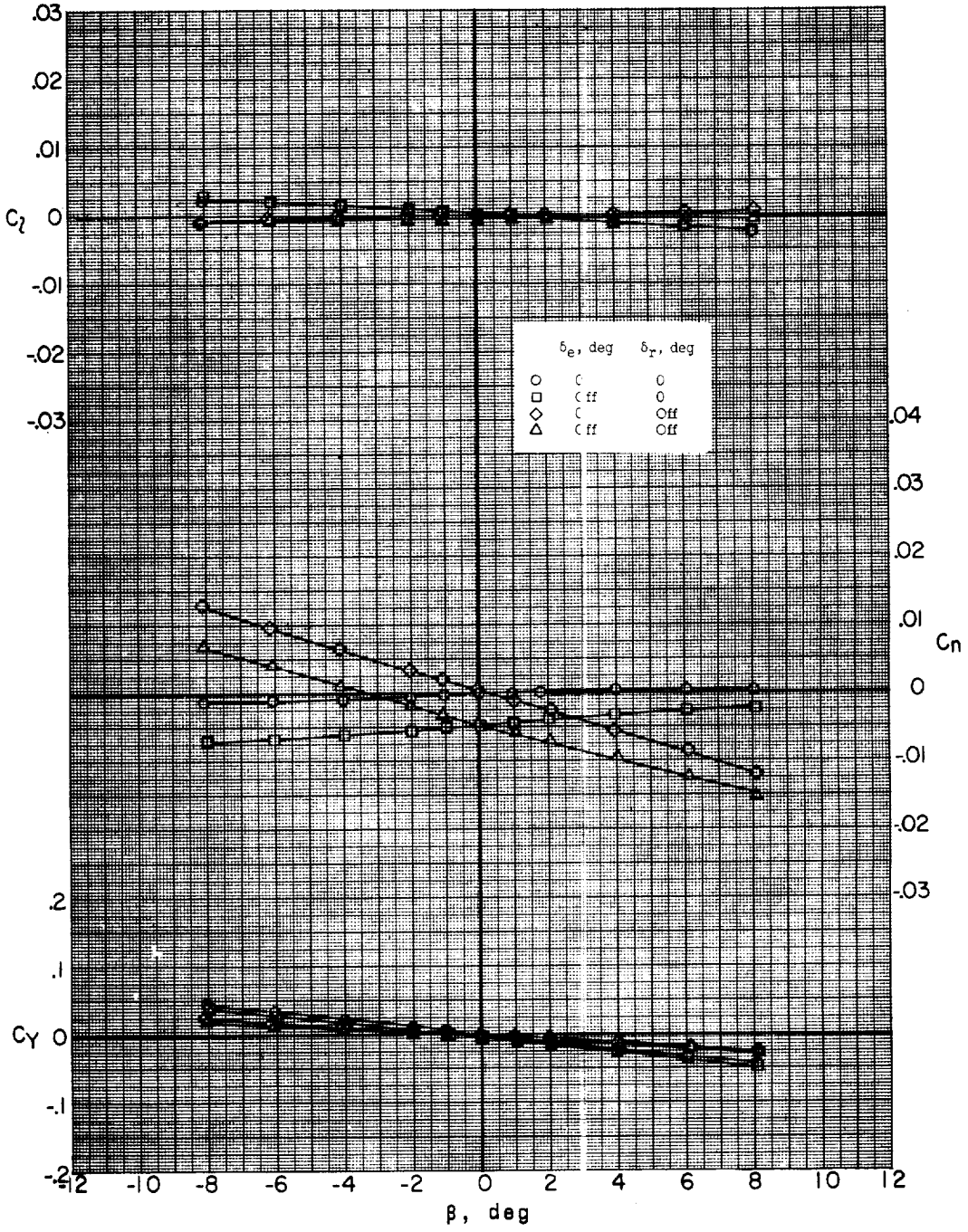
(b) M = 2.75.

Figure 44.- Continued.



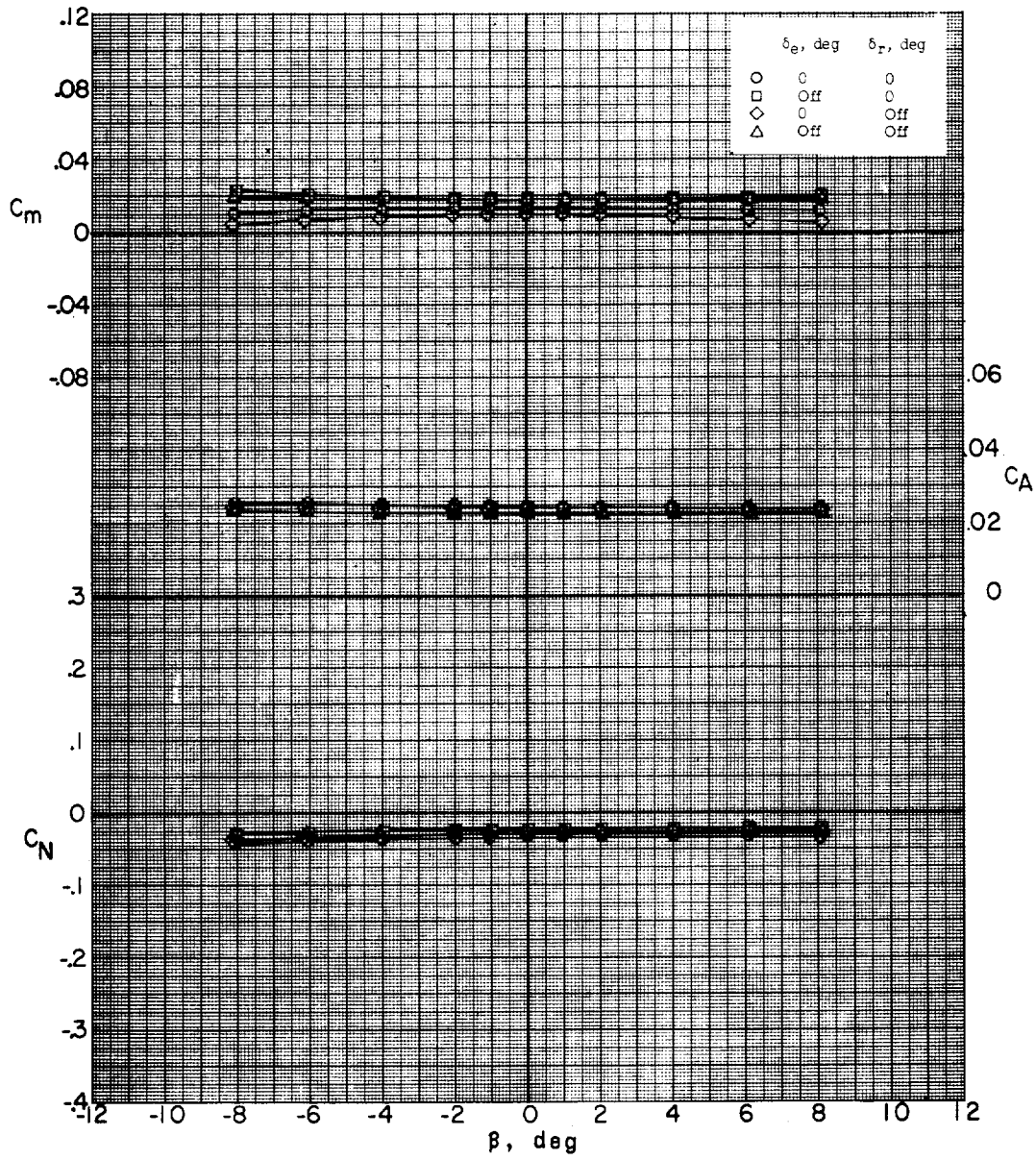
(c) M = 3.22.

Figure 44.- Concluded.



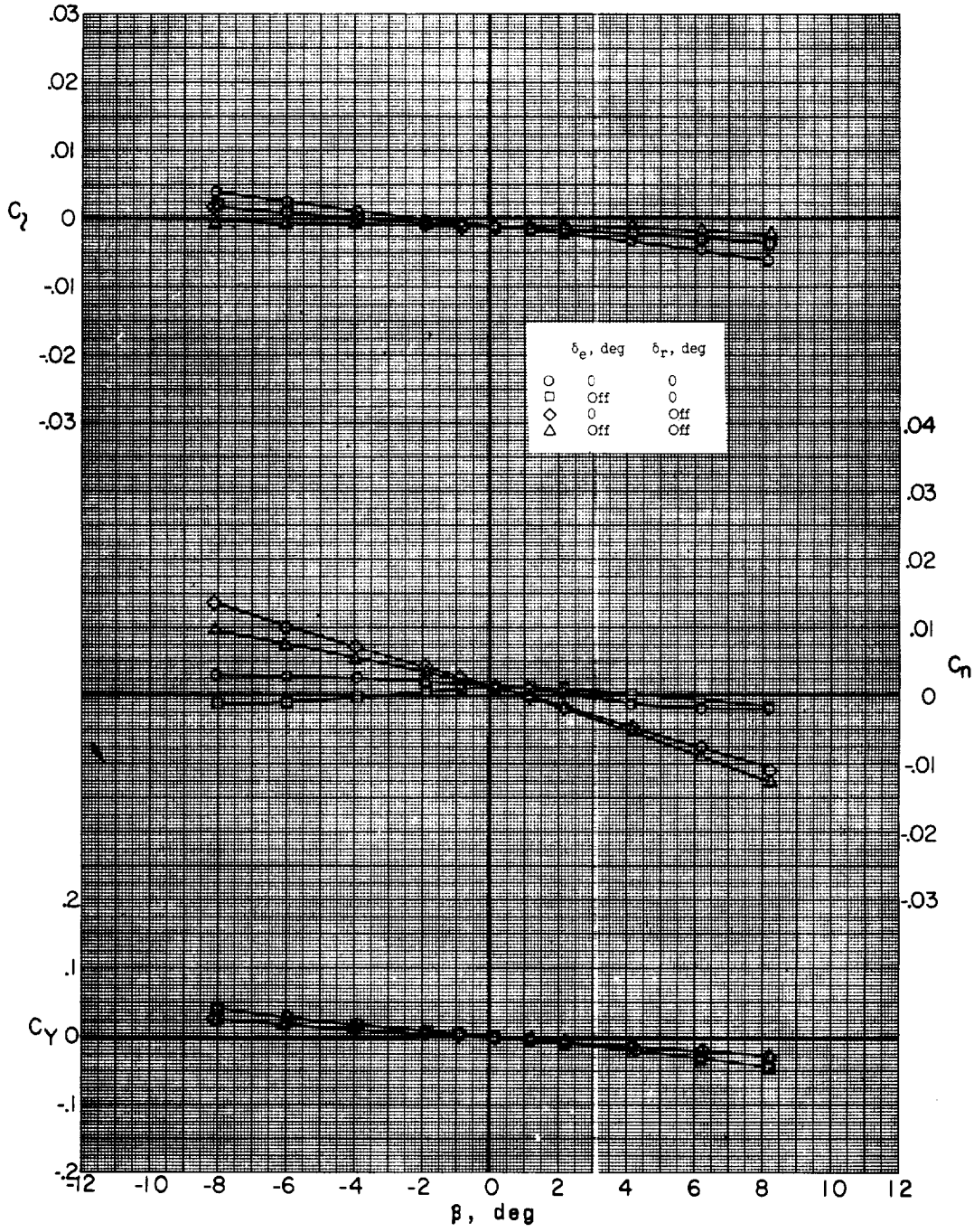
(a) $\alpha = -0.2^{\circ}$.

Figure 45.- Effect of canard and rudder surfaces on lateral characteristics of missile alone. M = 1.77; sting A.



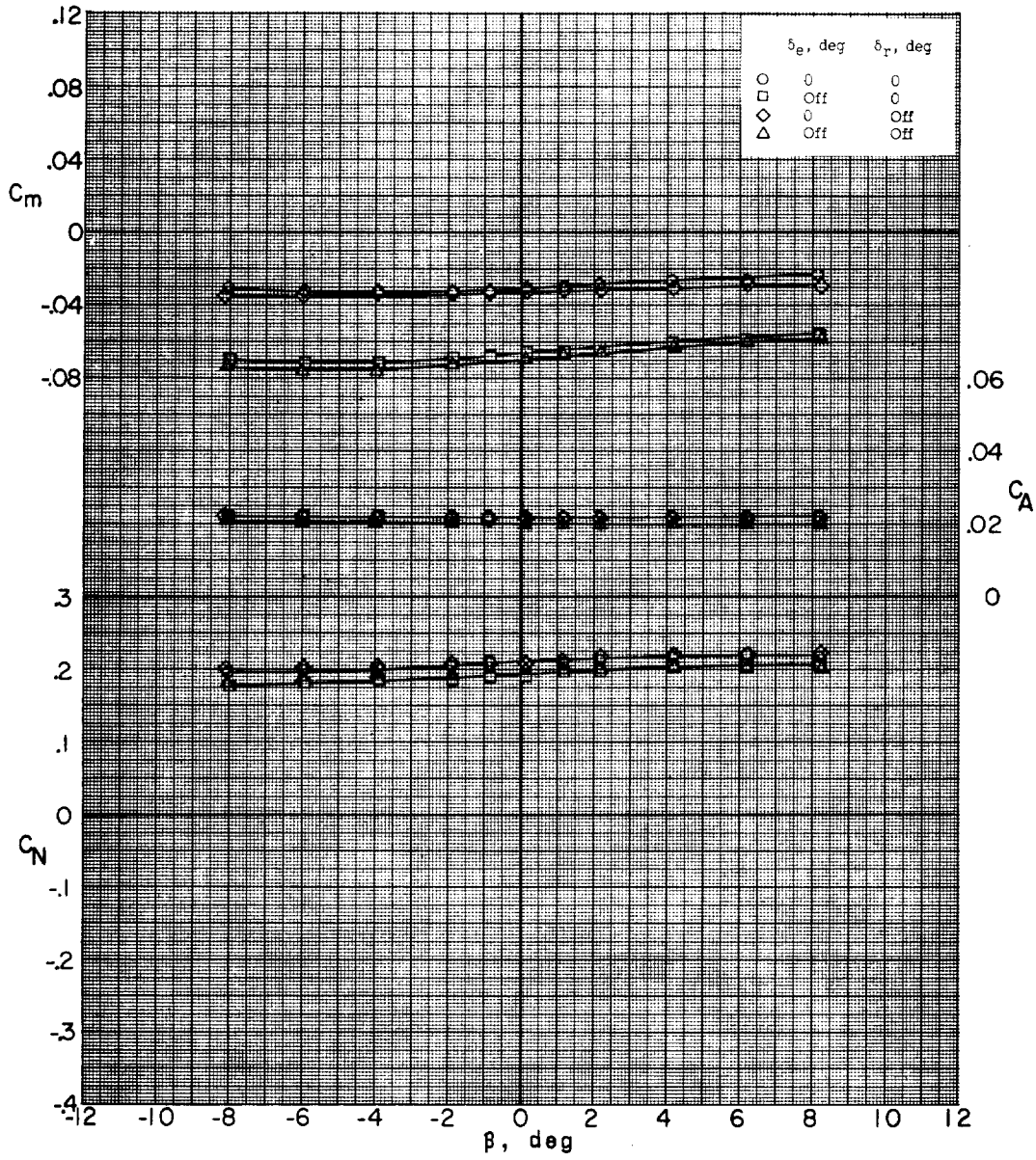
(a) Concluded.

Figure 45.- Continued.



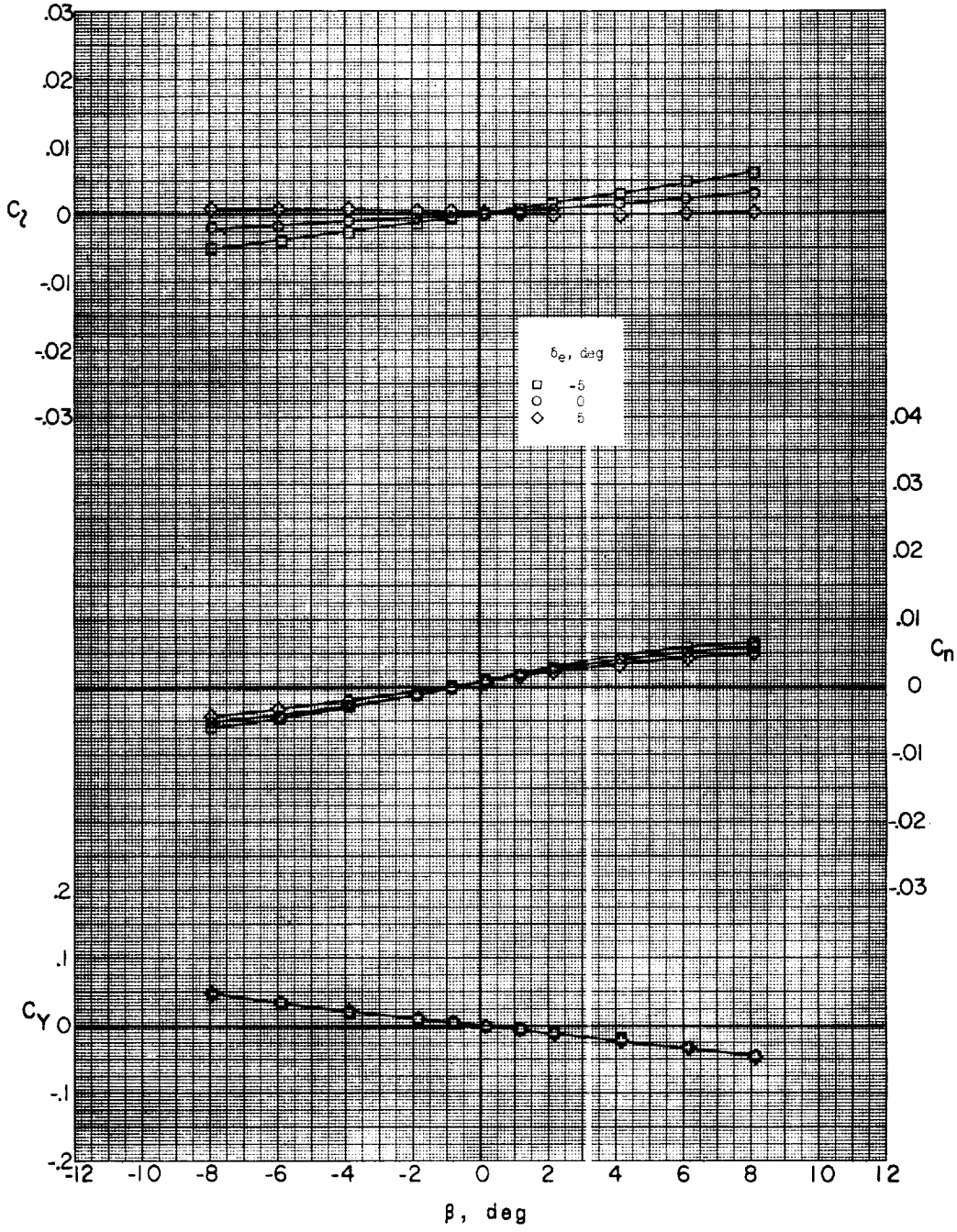
(b) $\alpha = 5.1^{\circ}$.

Figure 45.- Continued.



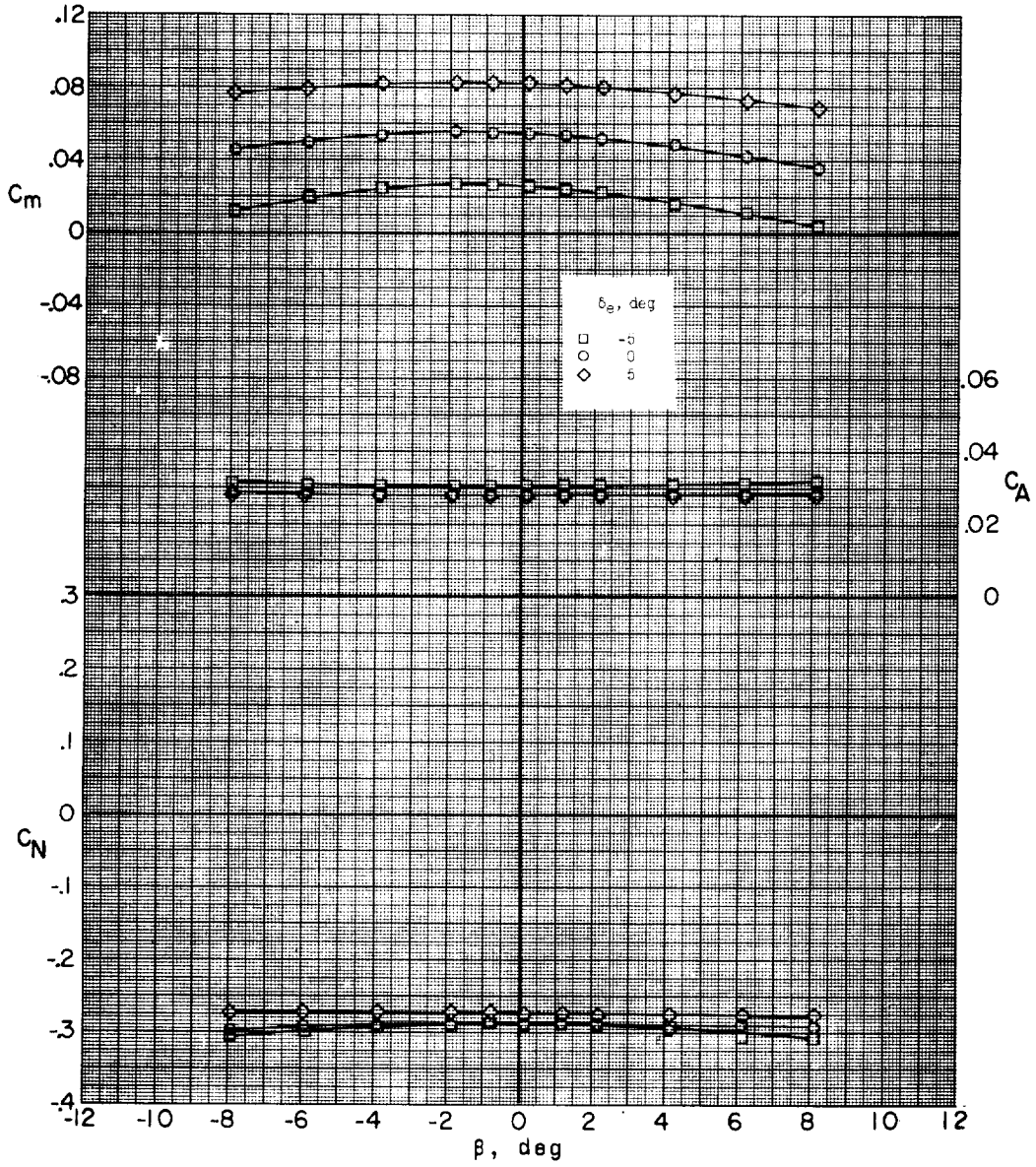
(b) Concluded.

Figure 45.- Concluded.



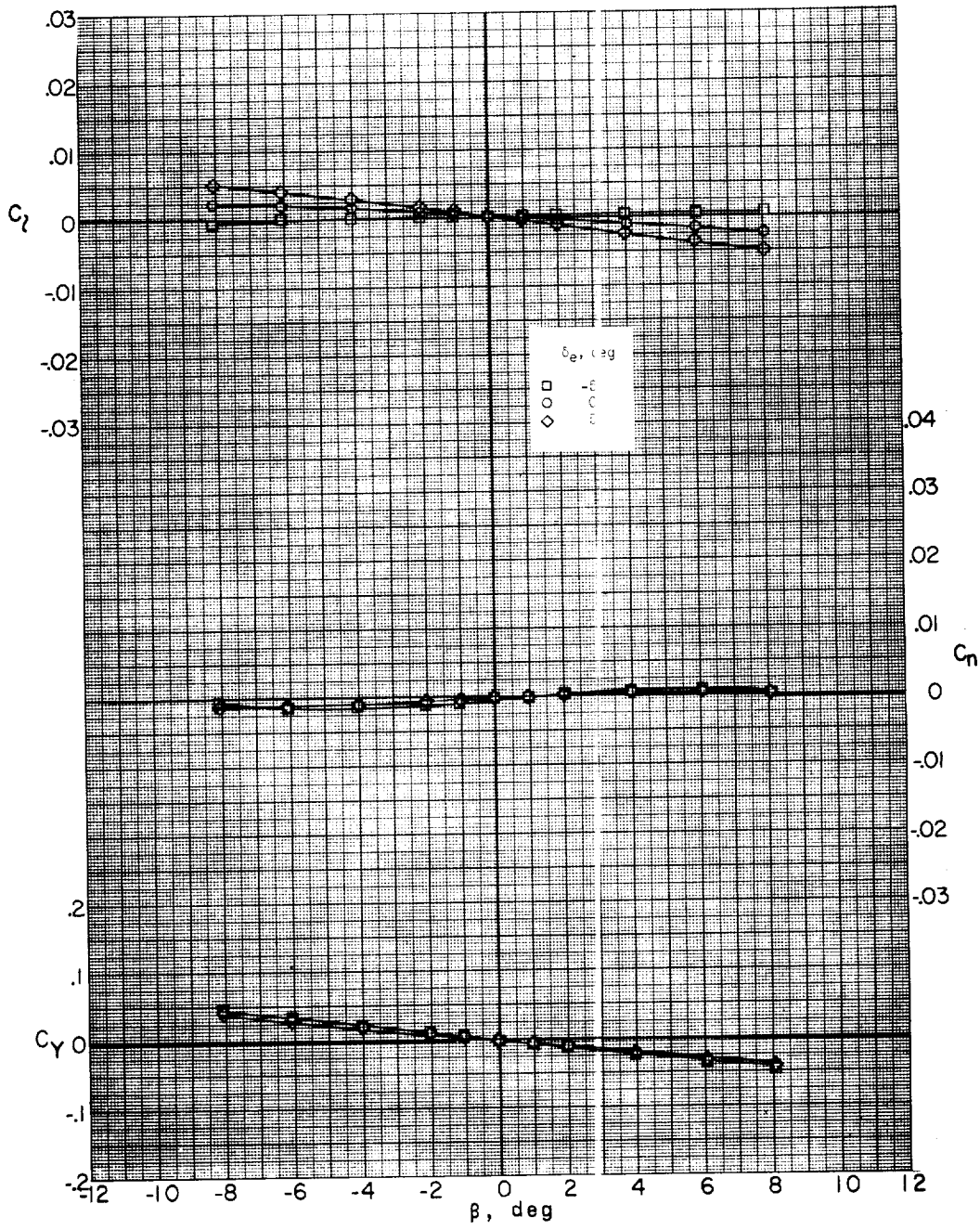
(a) M = 1.77; $\alpha = -5.3^{\circ}$.

Figure 46.- Effect of canard deflection on lateral characteristics of missile alone. Sting A.



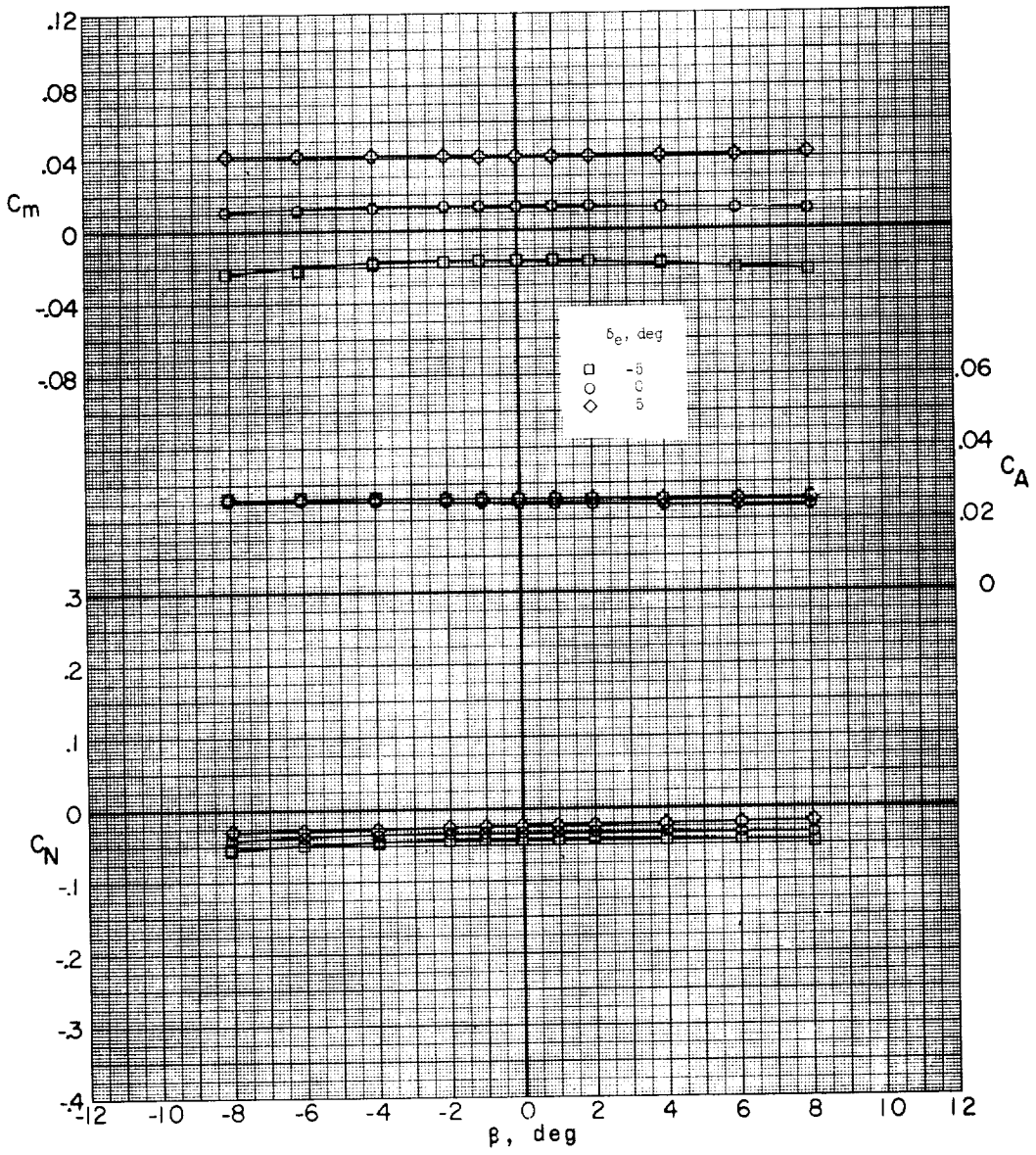
(a) Concluded.

Figure 46.- Continued.



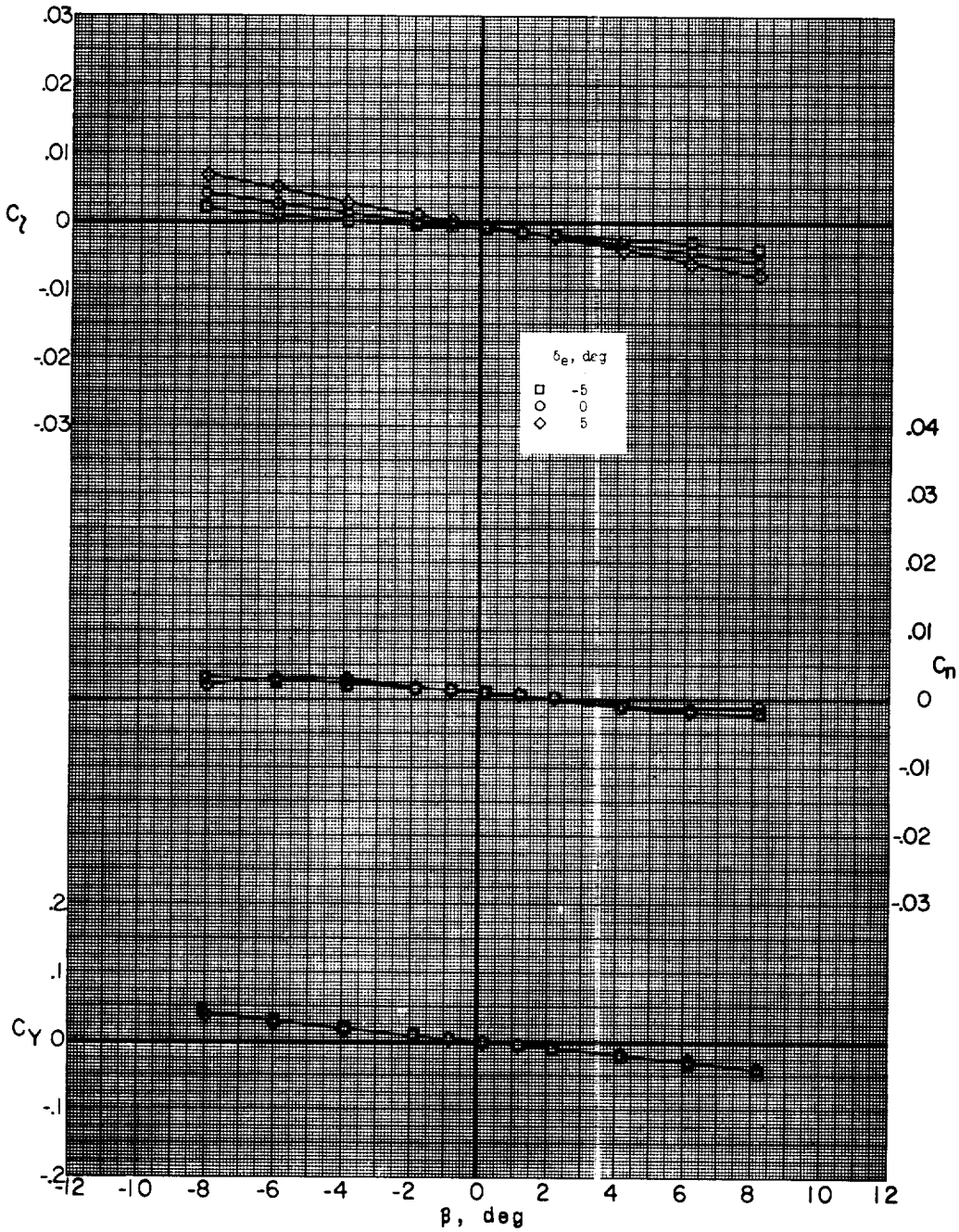
(b) M = 1.77; $\alpha = -0.2^{\circ}$.

Figure 46.- Continued.



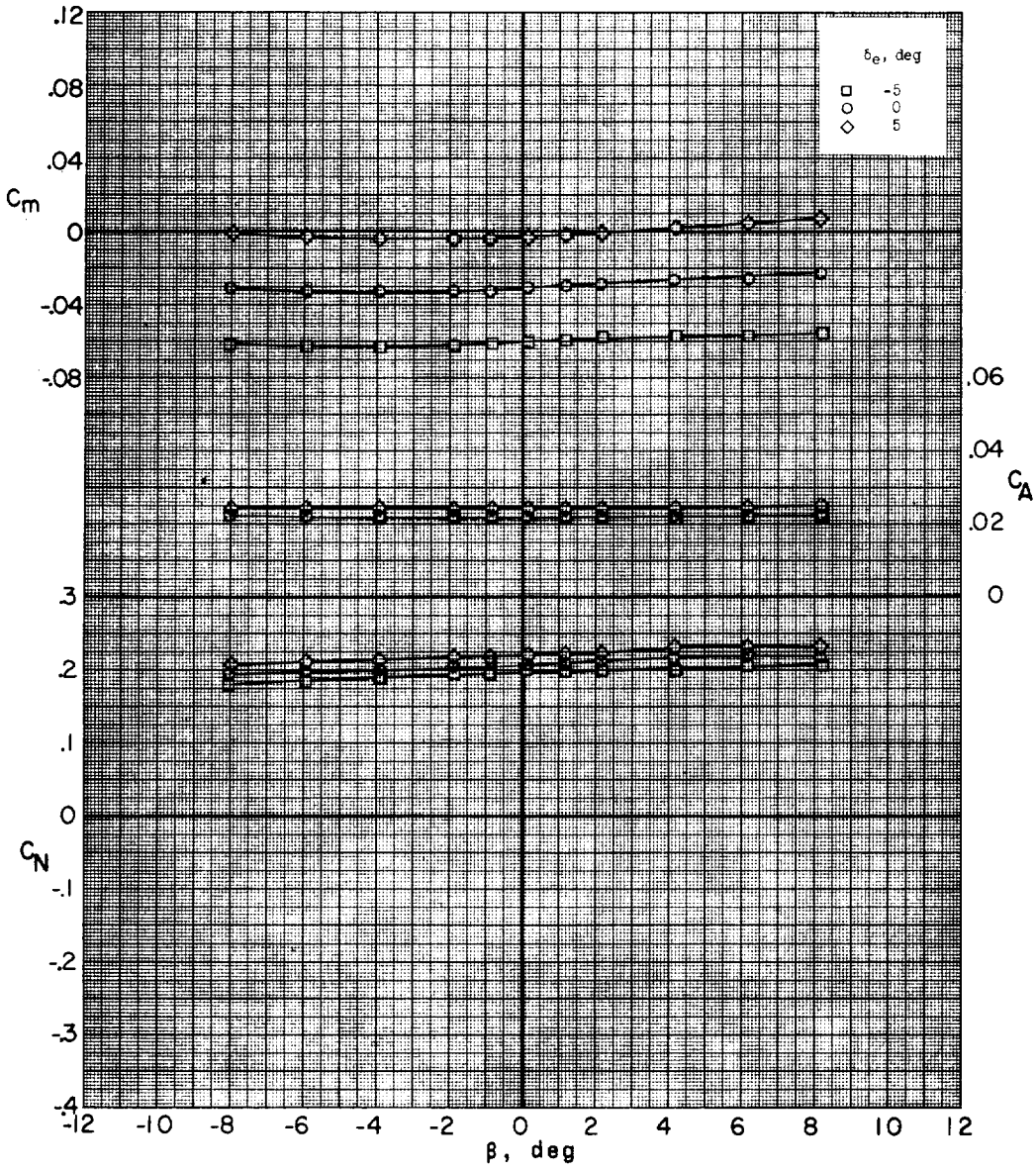
(b) Concluded.

Figure 46.- Continued.



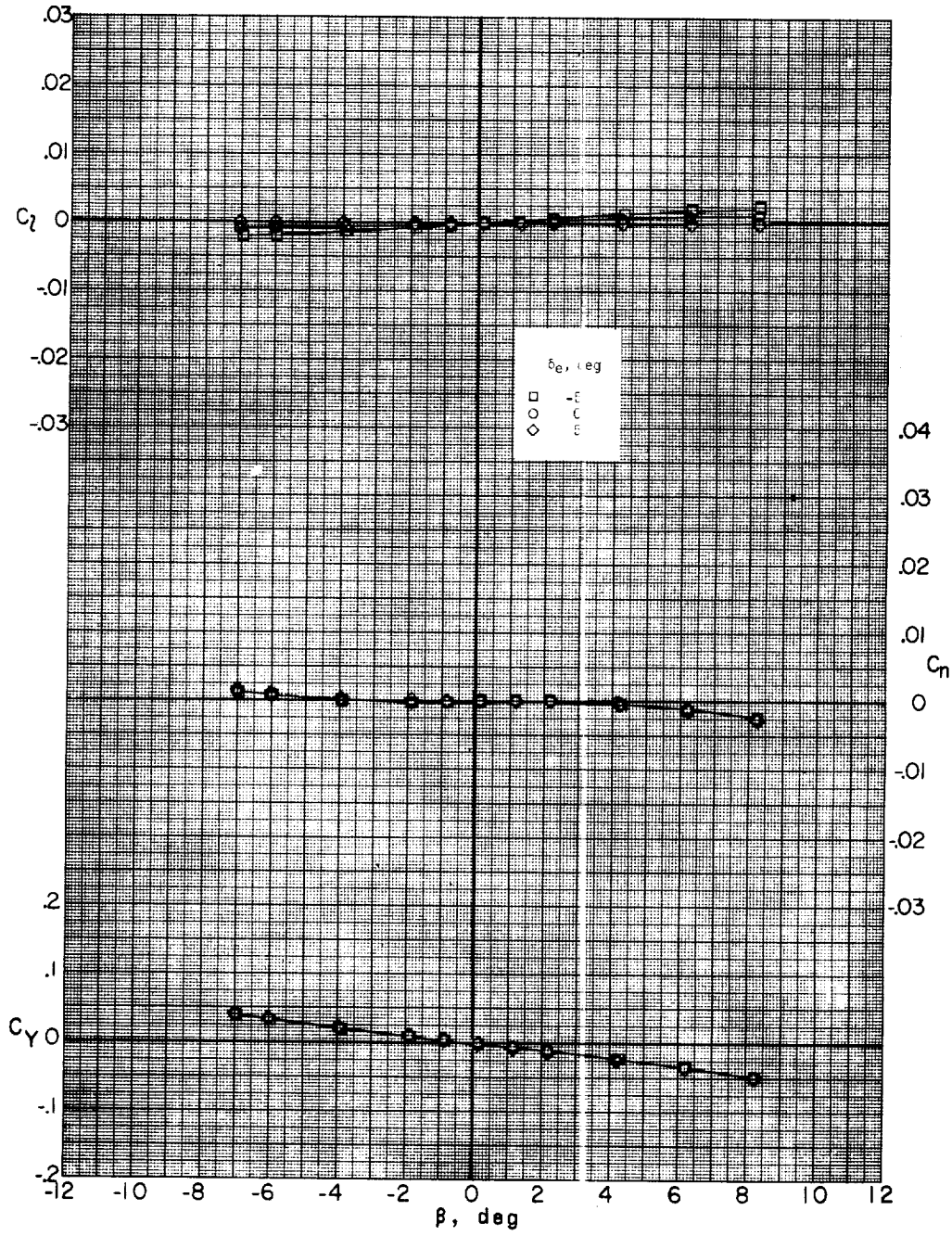
(c) M = 1.77; $\alpha = 5.2^{\circ}$.

Figure 46.- Continued.



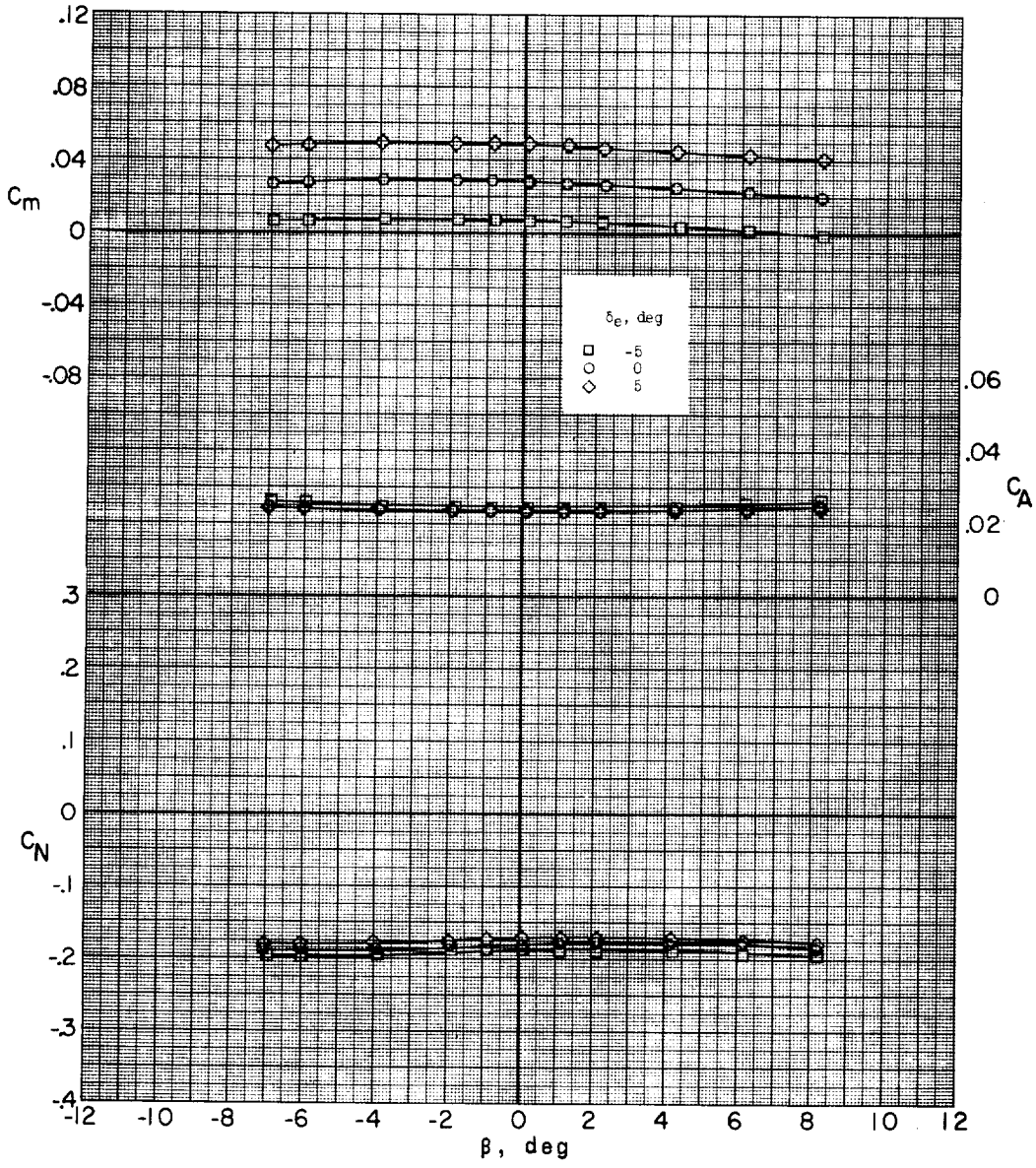
(c) Concluded.

Figure 46.- Continued.



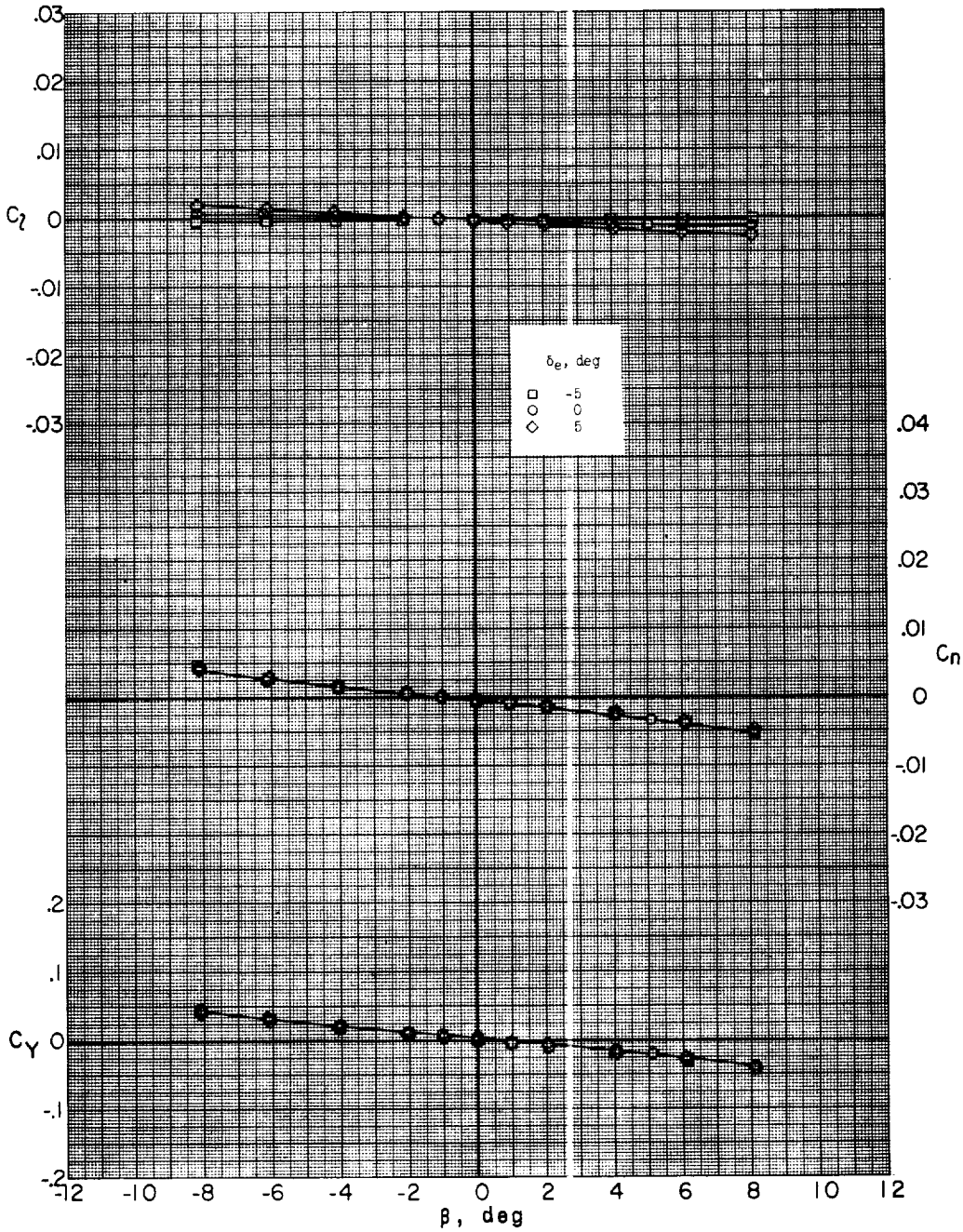
(d) M = 2.75; $\alpha = -5.2^{\circ}$.

Figure 46.- Continued.



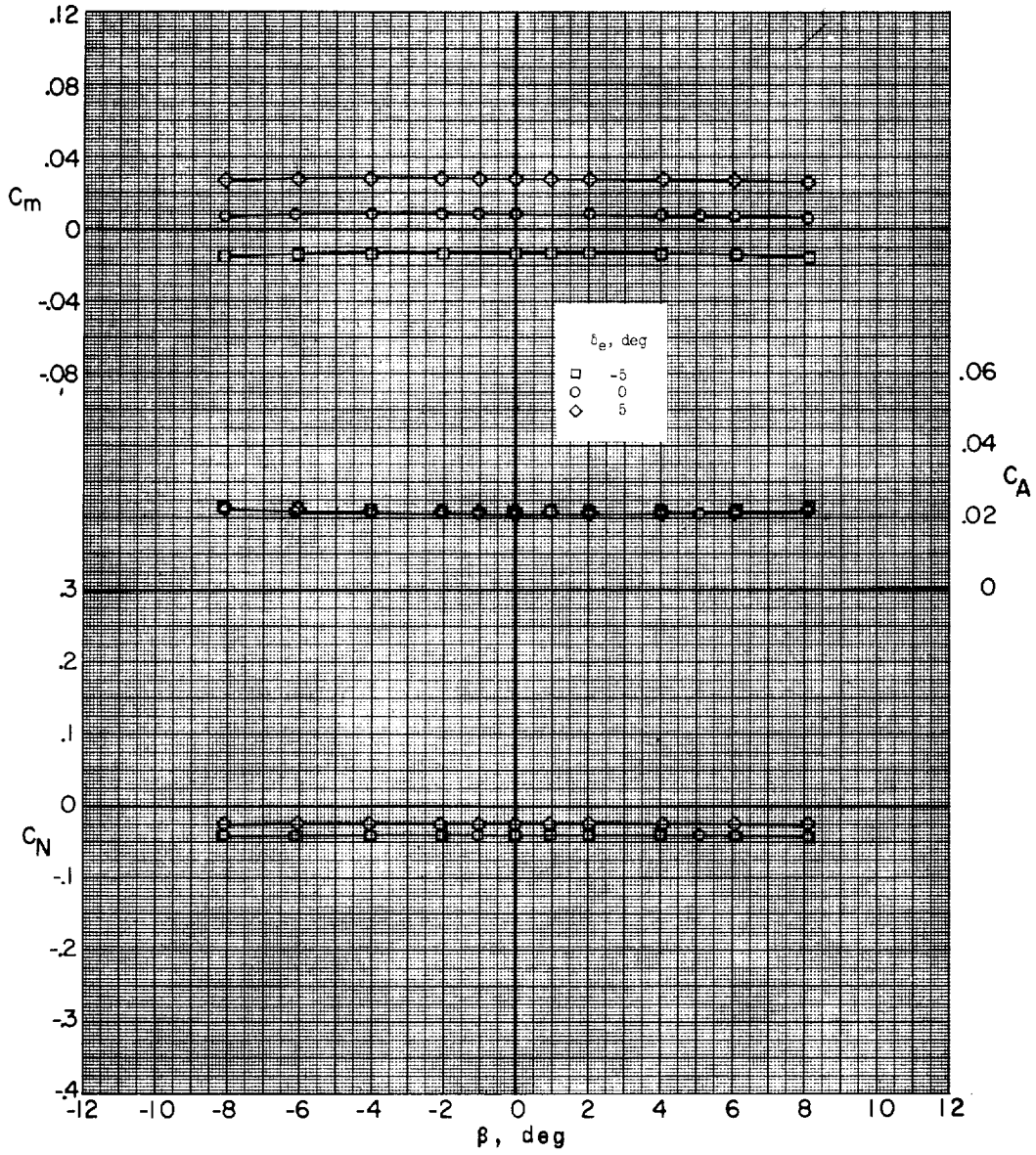
(d) Concluded.

Figure 46.- Continued.



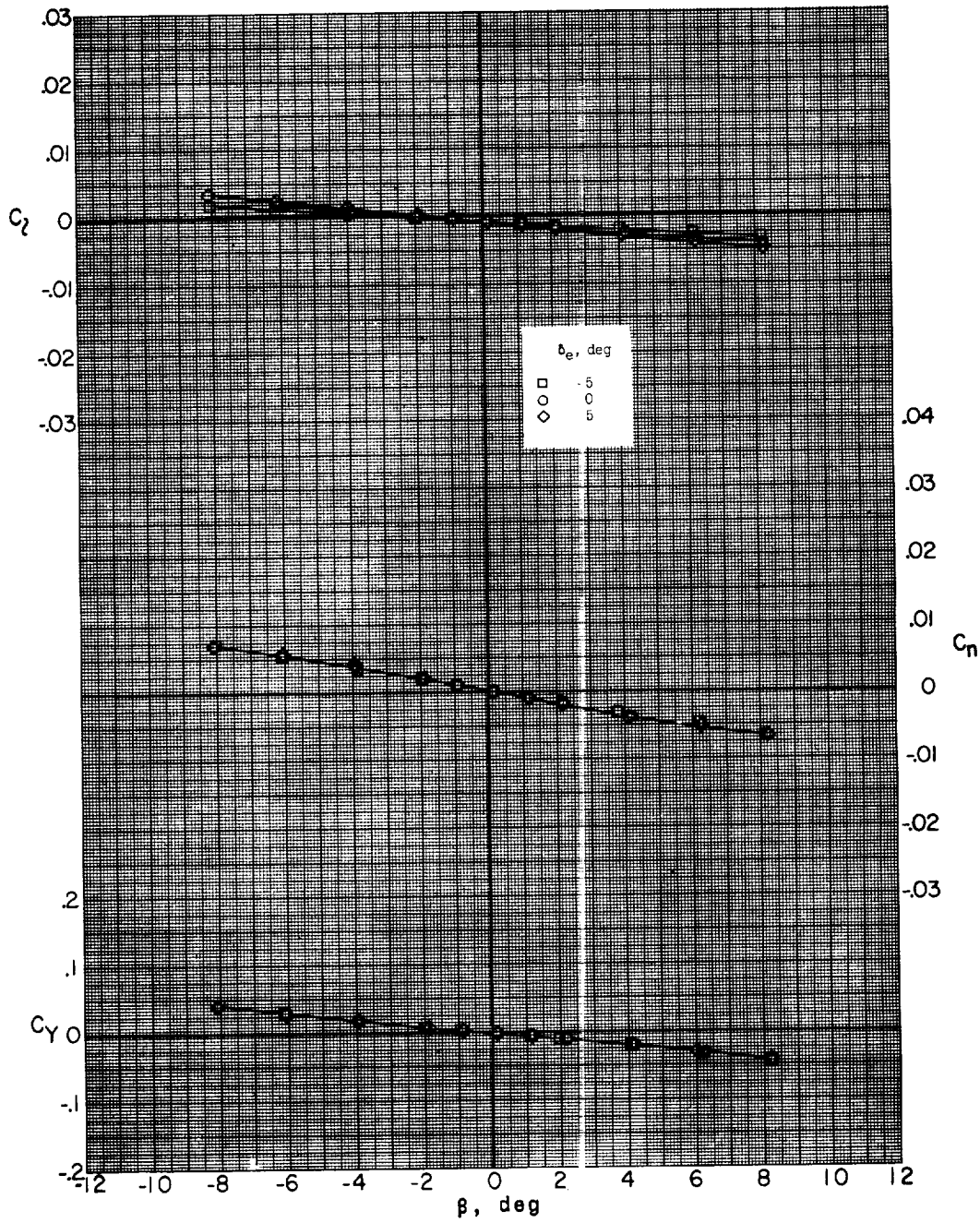
(e) M = 2.75; $\alpha = -0.2^{\circ}$.

Figure 46.- Continued.



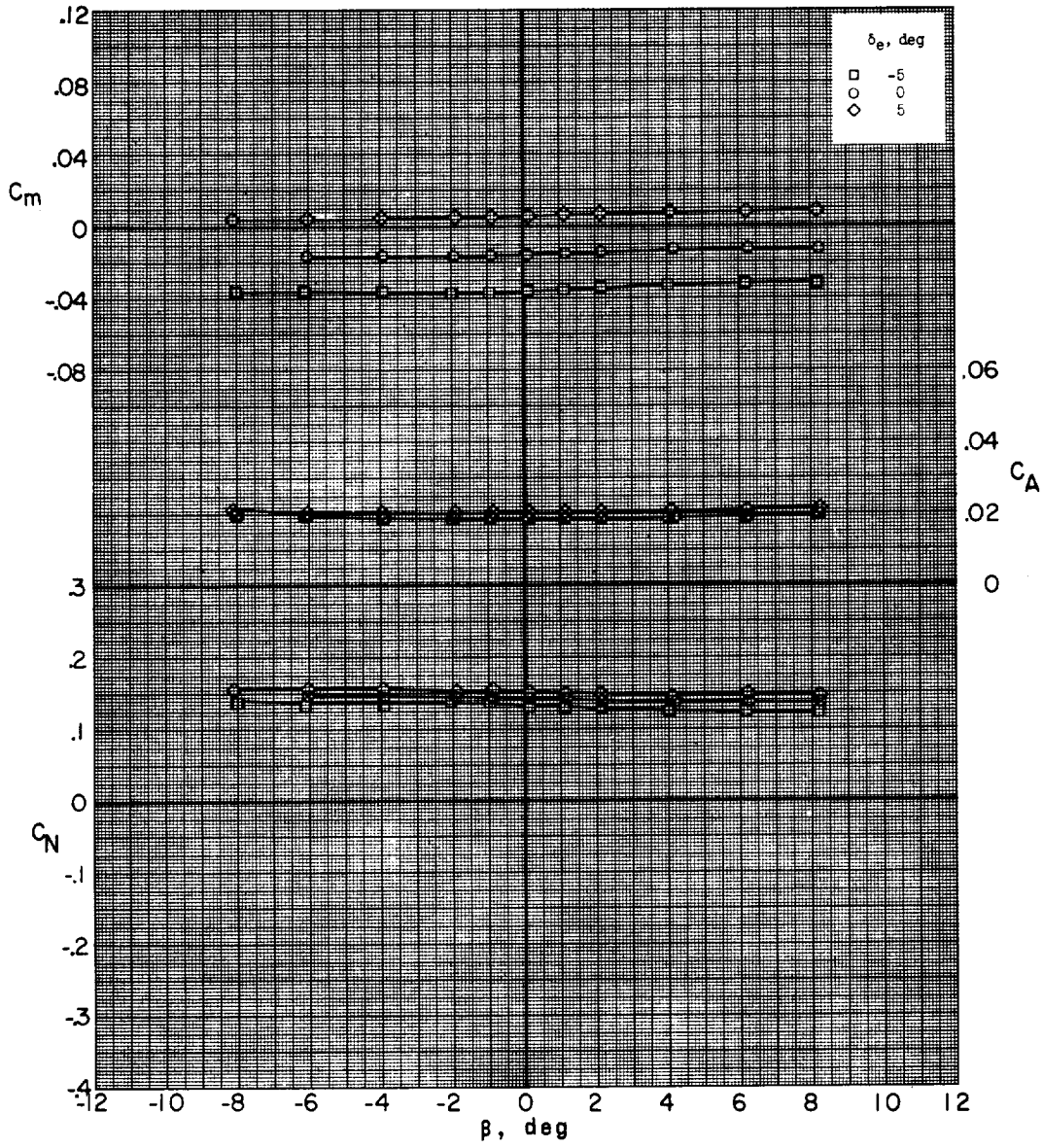
(e) Concluded.

Figure 46.- Continued.



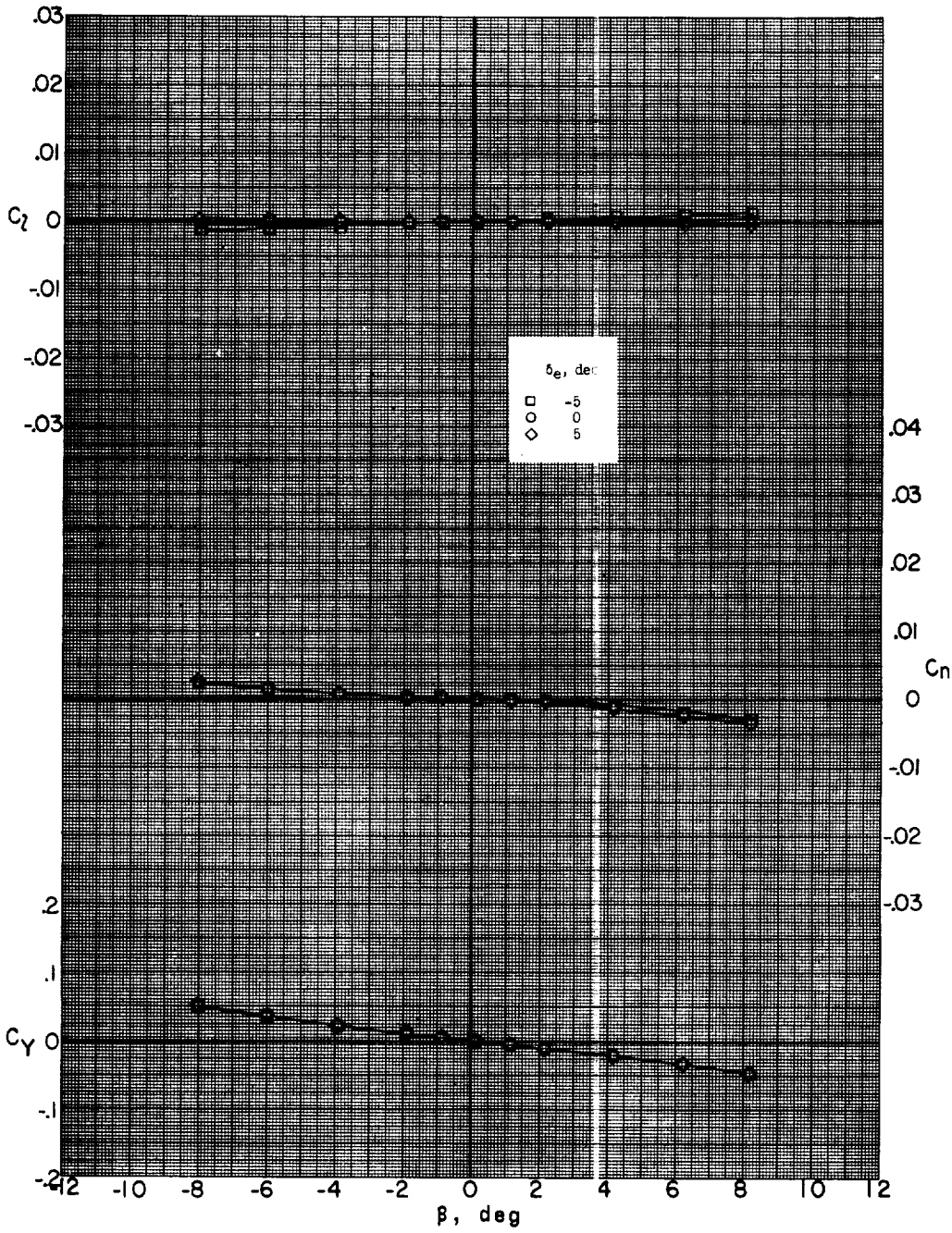
(f) M = 2.75; $\alpha = 5.2^{\circ}$.

Figure 46.- Continued.



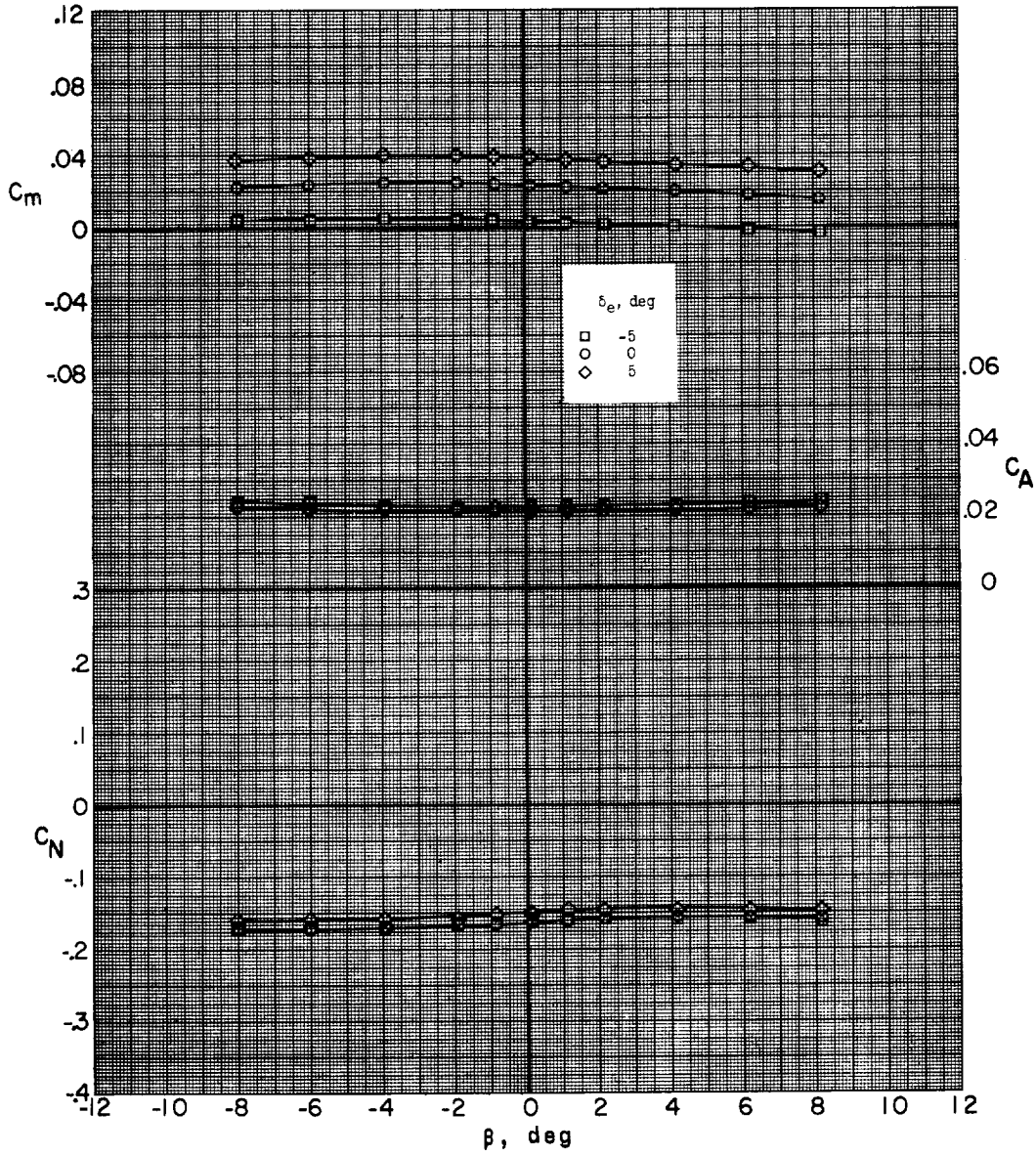
(f) Concluded.

Figure 46.- Continued.



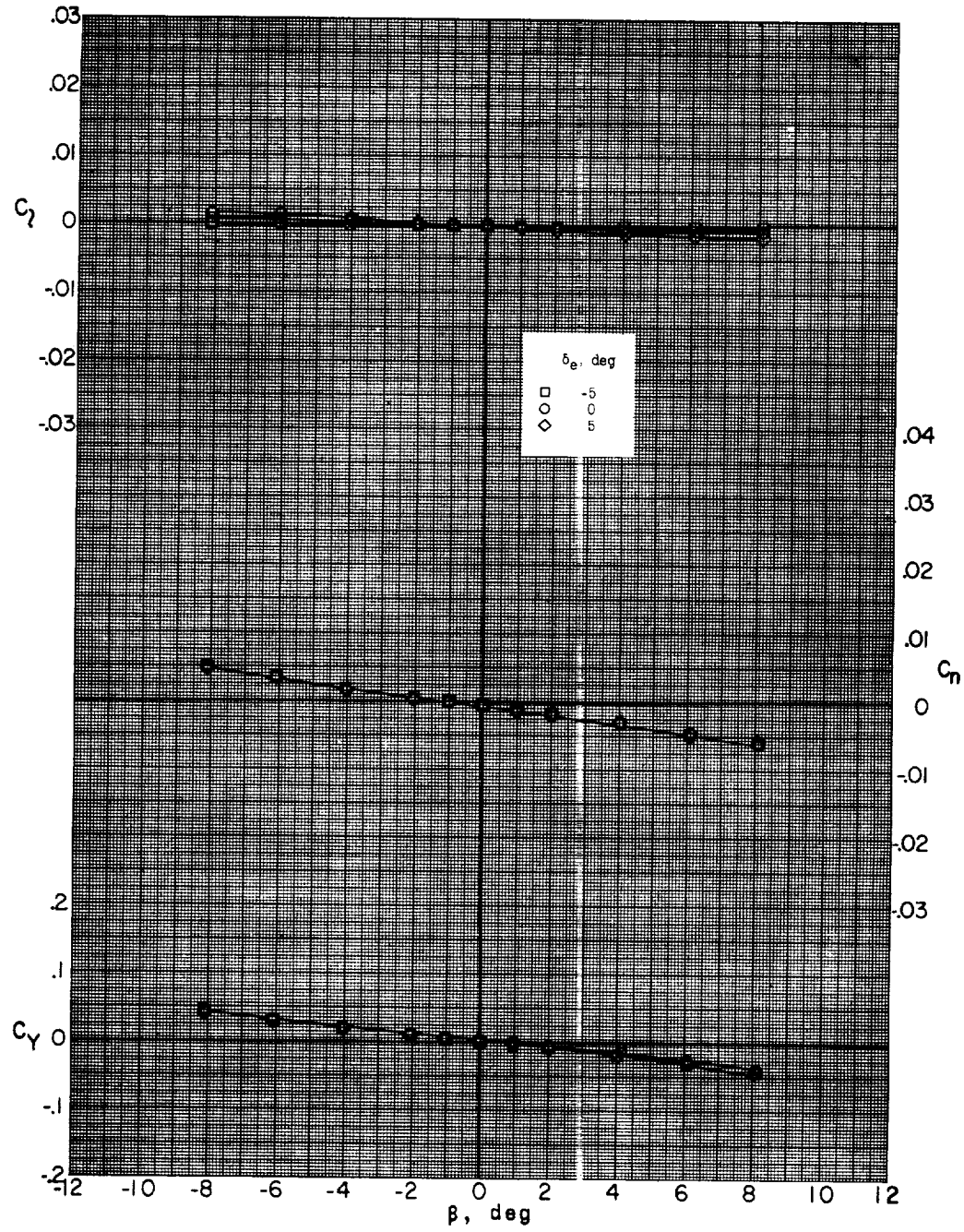
(g) M = 3.22; α = -5.1°.

Figure 46.- Continued.



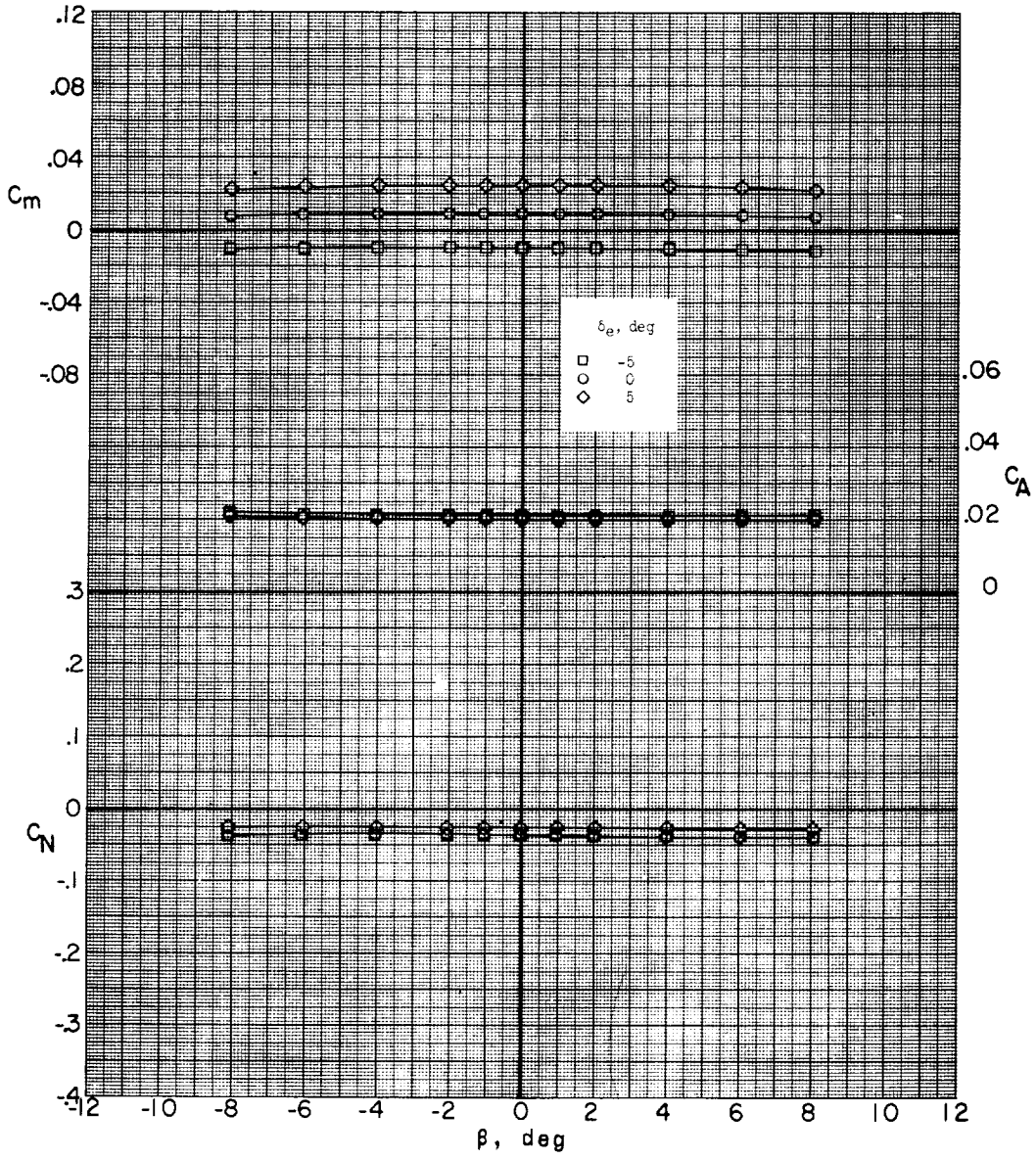
(g) Concluded.

Figure 46.- Continued.



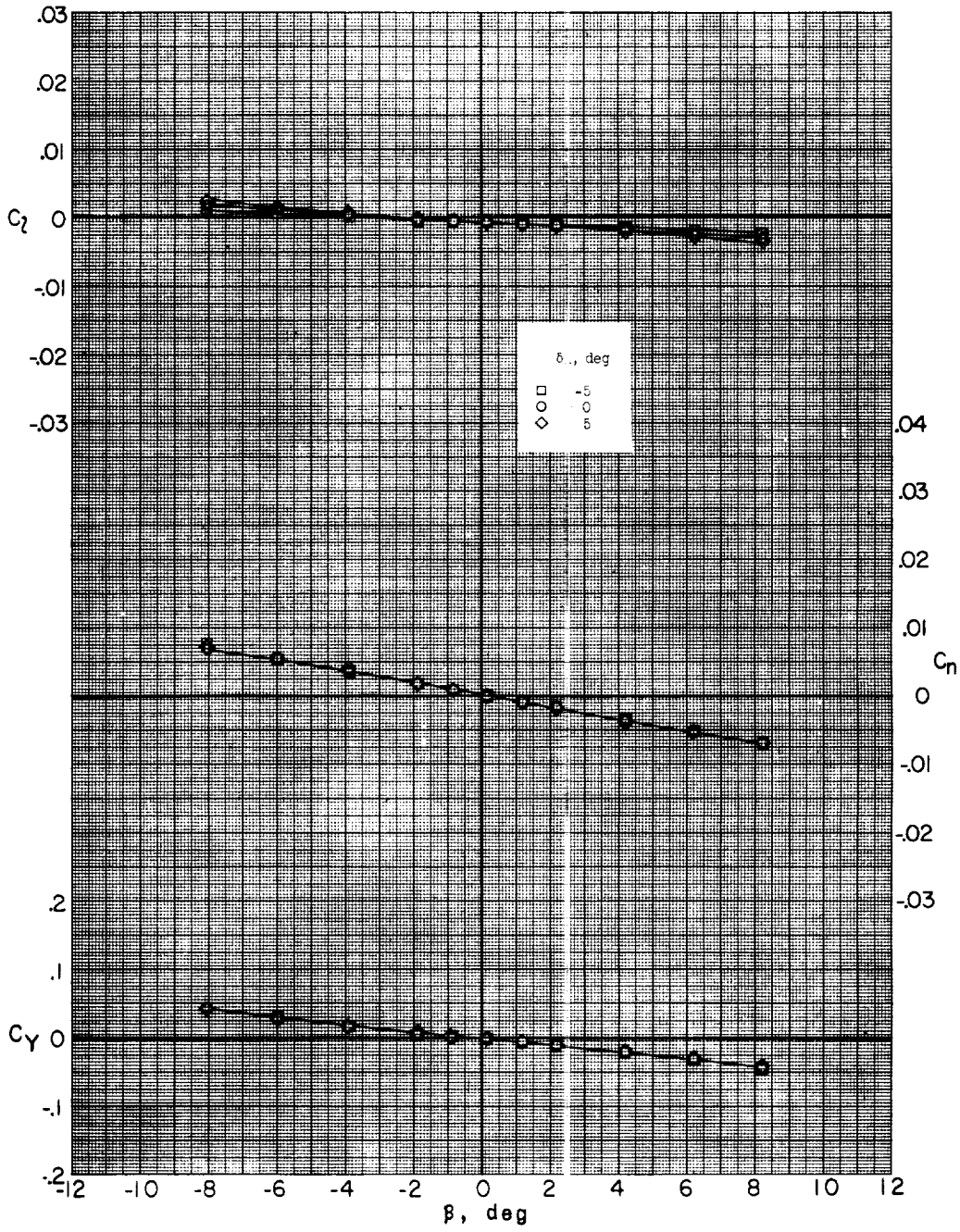
(h) M = 3.22; α = -0.2°.

Figure 46.- Continued.



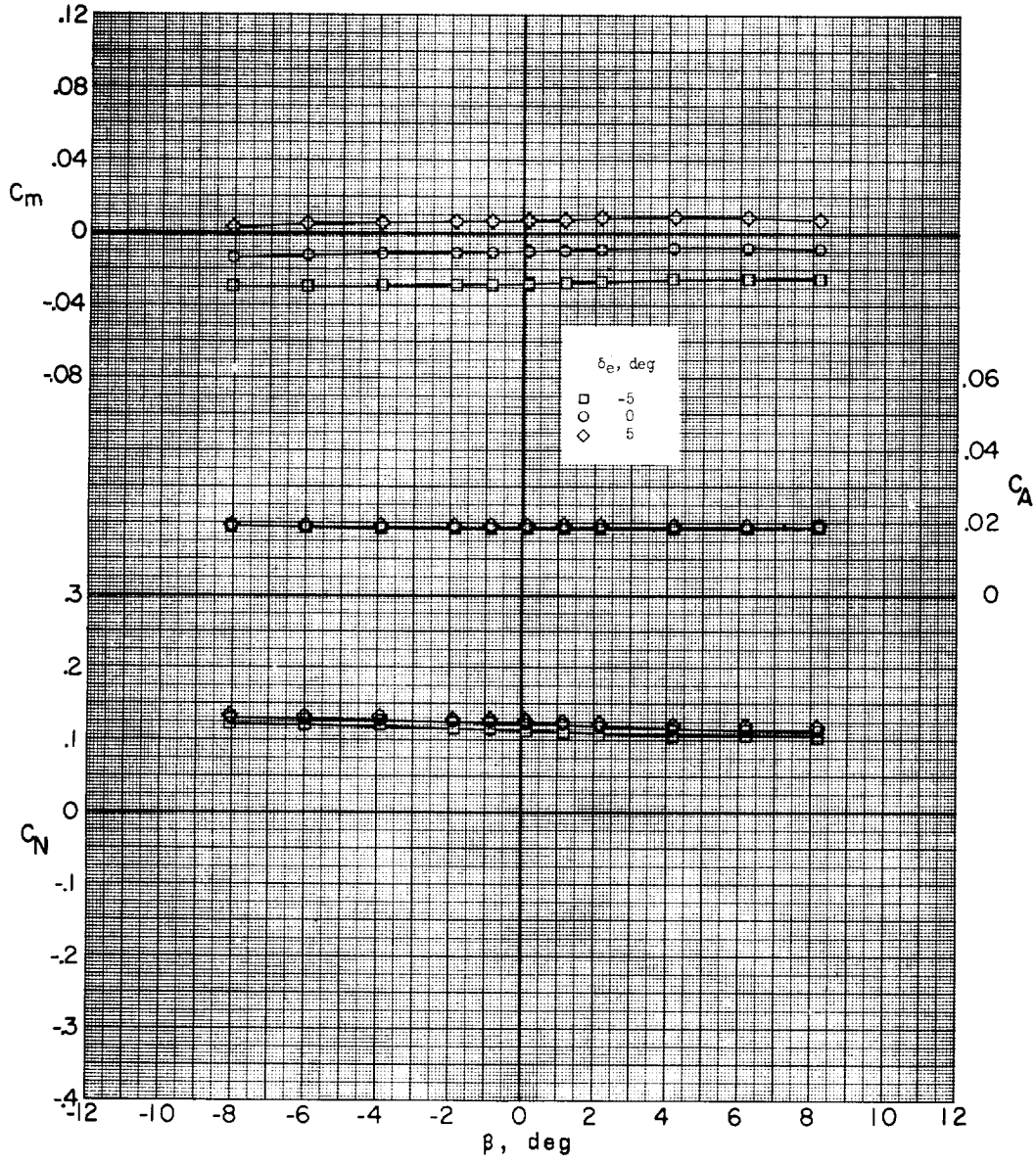
(h) Concluded.

Figure 46.- Continued.



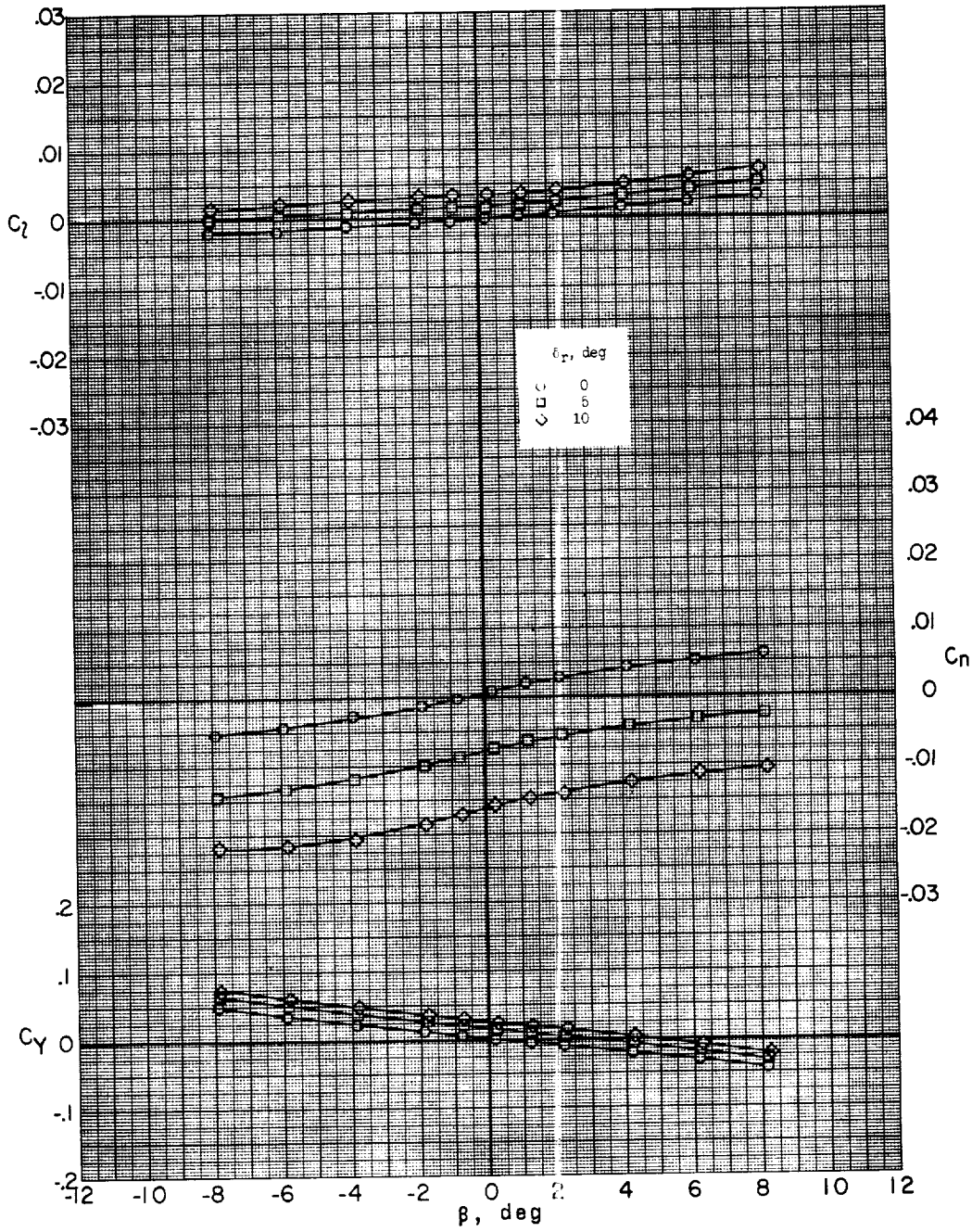
(i) M = 3.22; α = 5.1°.

Figure 46.- Continued.



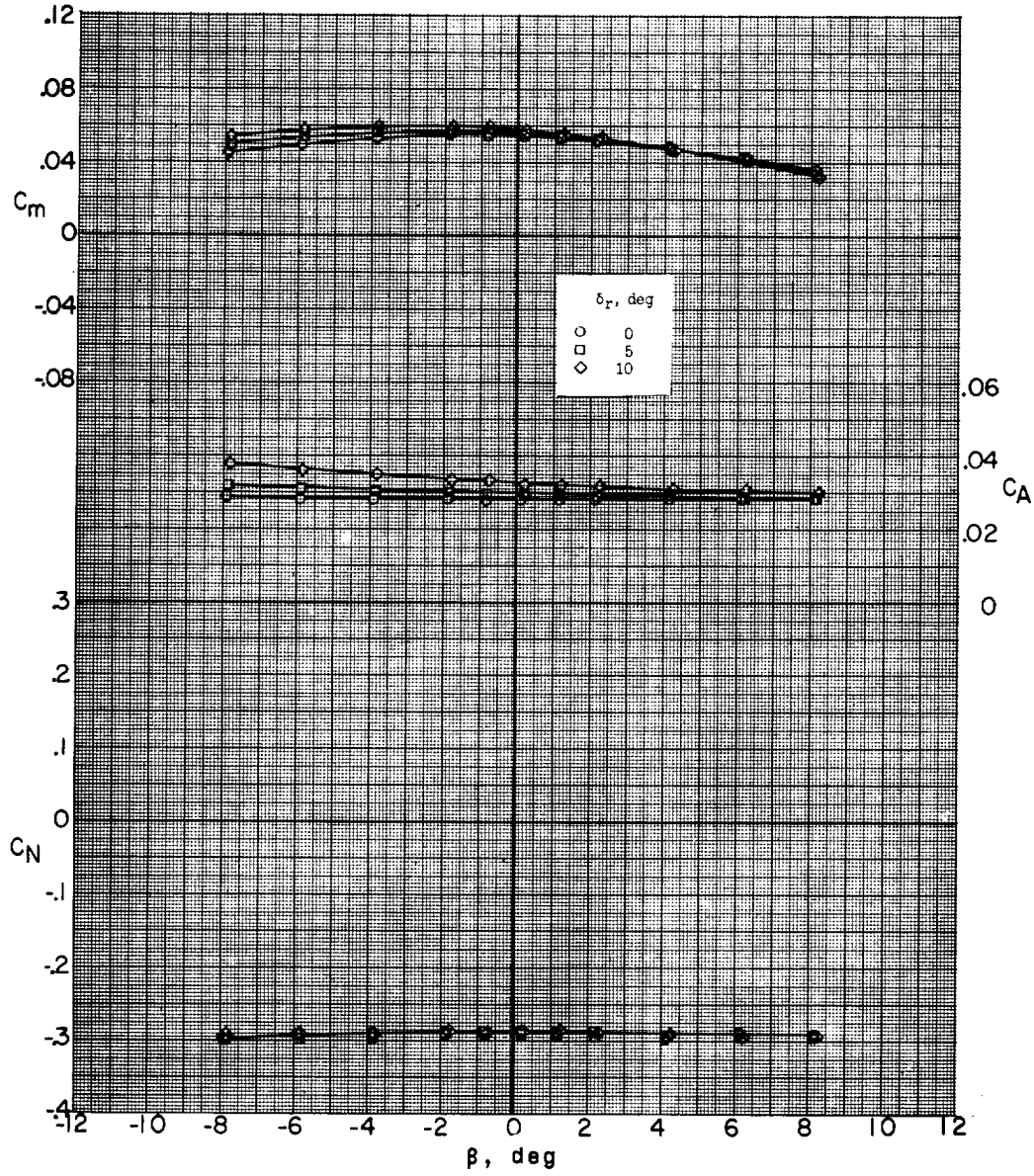
(i) Concluded.

Figure 46.- Concluded.



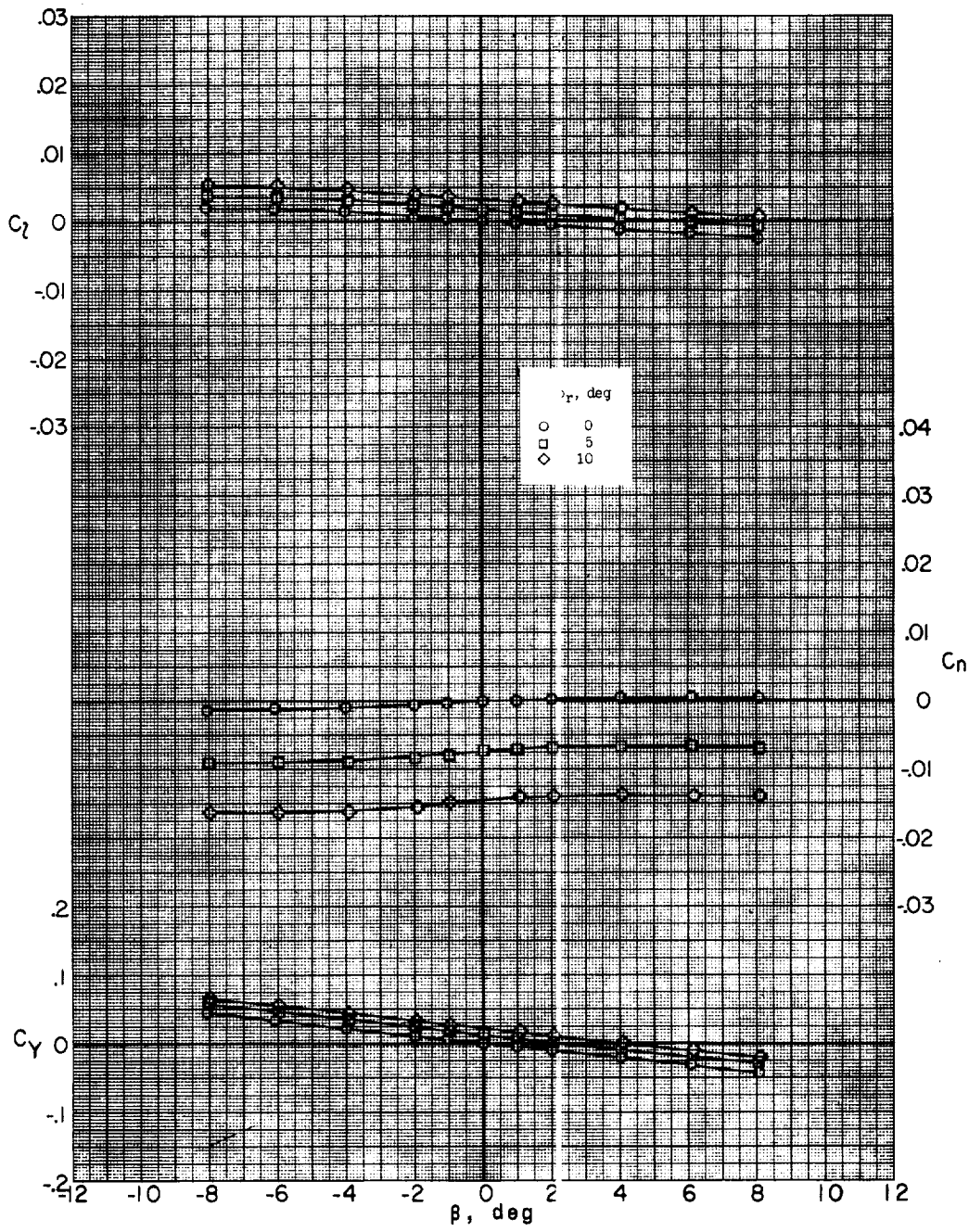
(a) M = 1.77; $\alpha = -5.3^{\circ}$.

Figure 47.- Effect of rudder deflection on lateral characteristics of missile alone. $\delta_e = 0^{\circ}$; sting A.



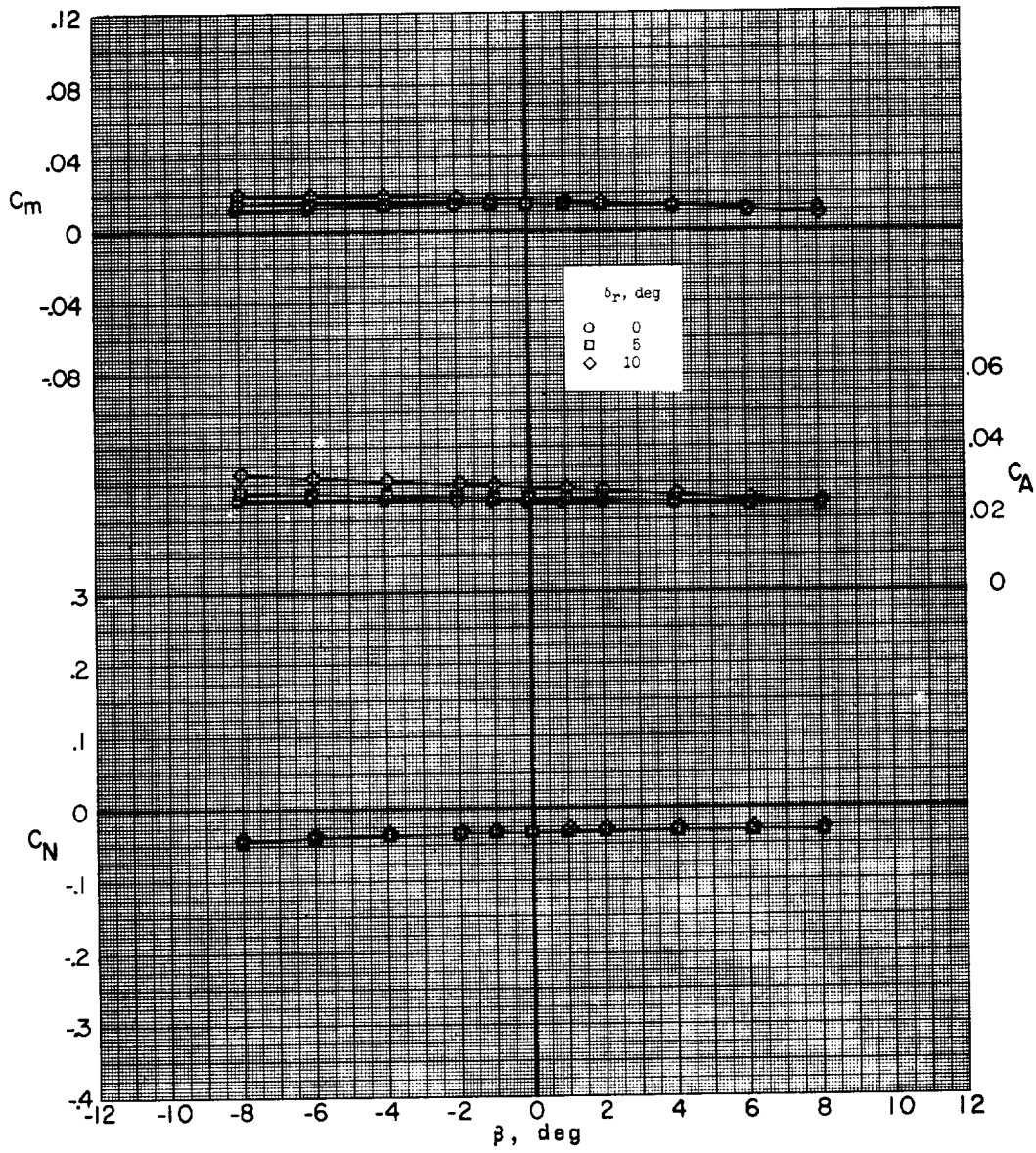
(a) Concluded.

Figure 47.- Continued.



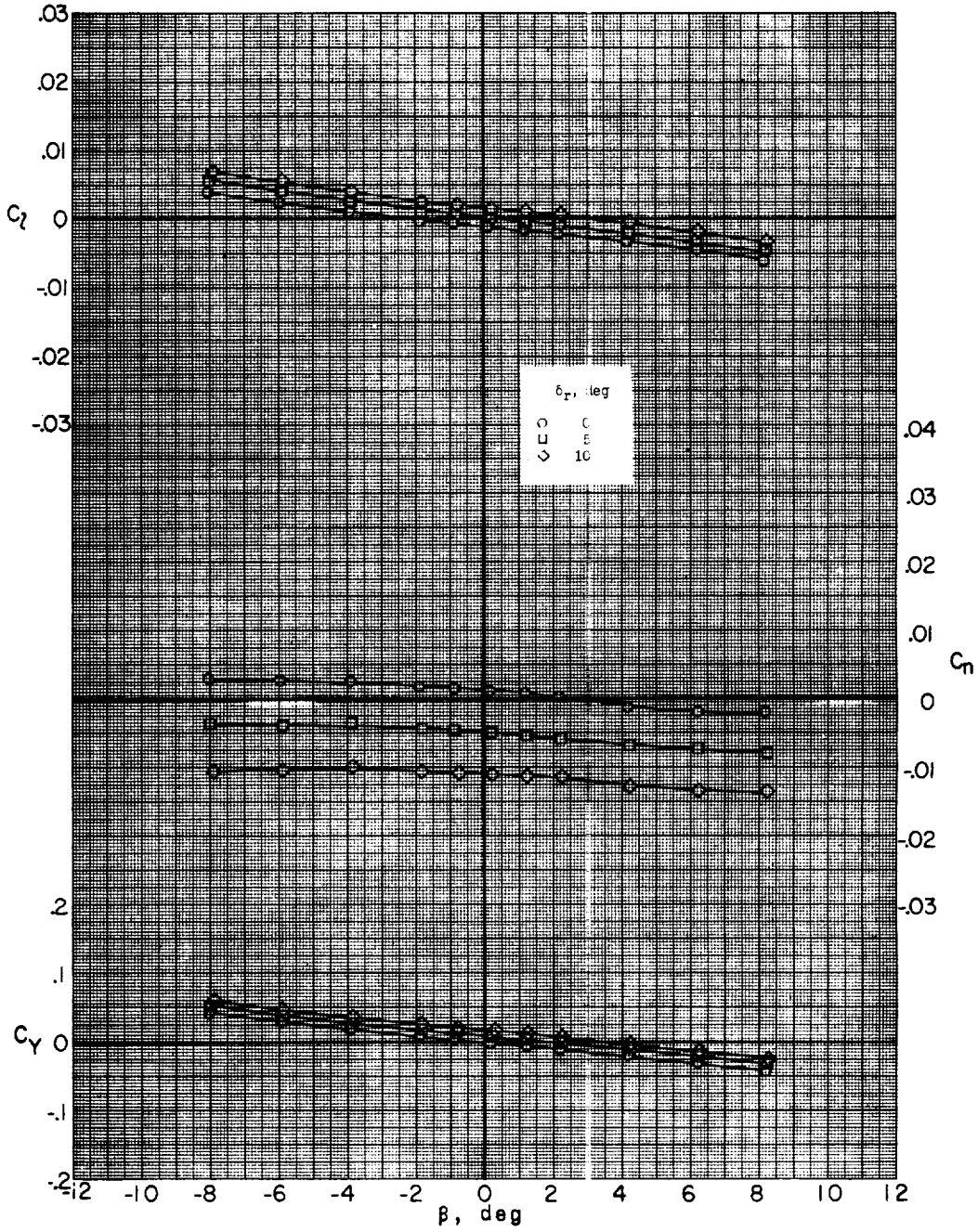
(b) M = 1.77; $\alpha = -0.2^{\circ}$.

Figure 47.- Continued.



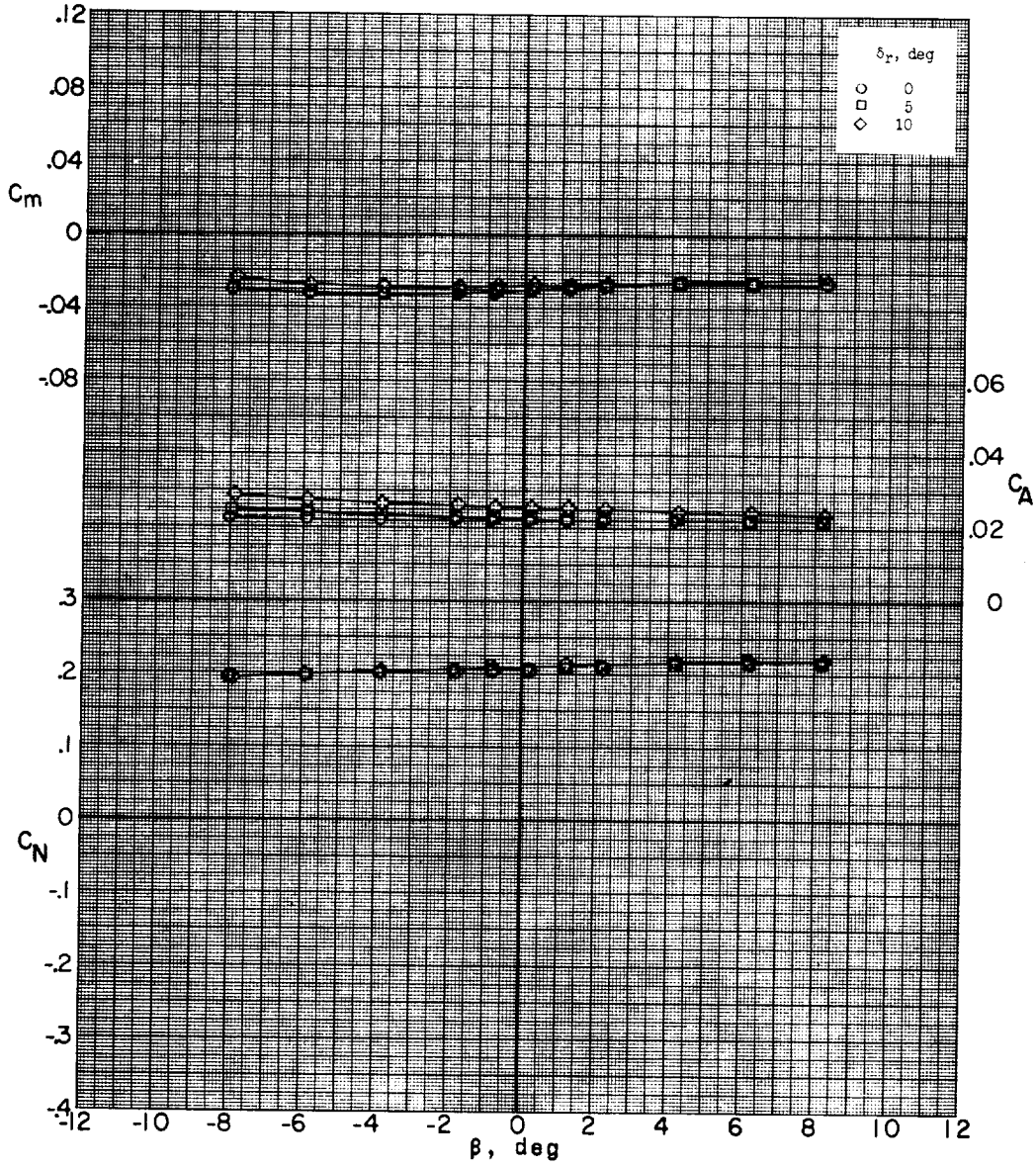
(b) Concluded.

Figure 47.- Continued.



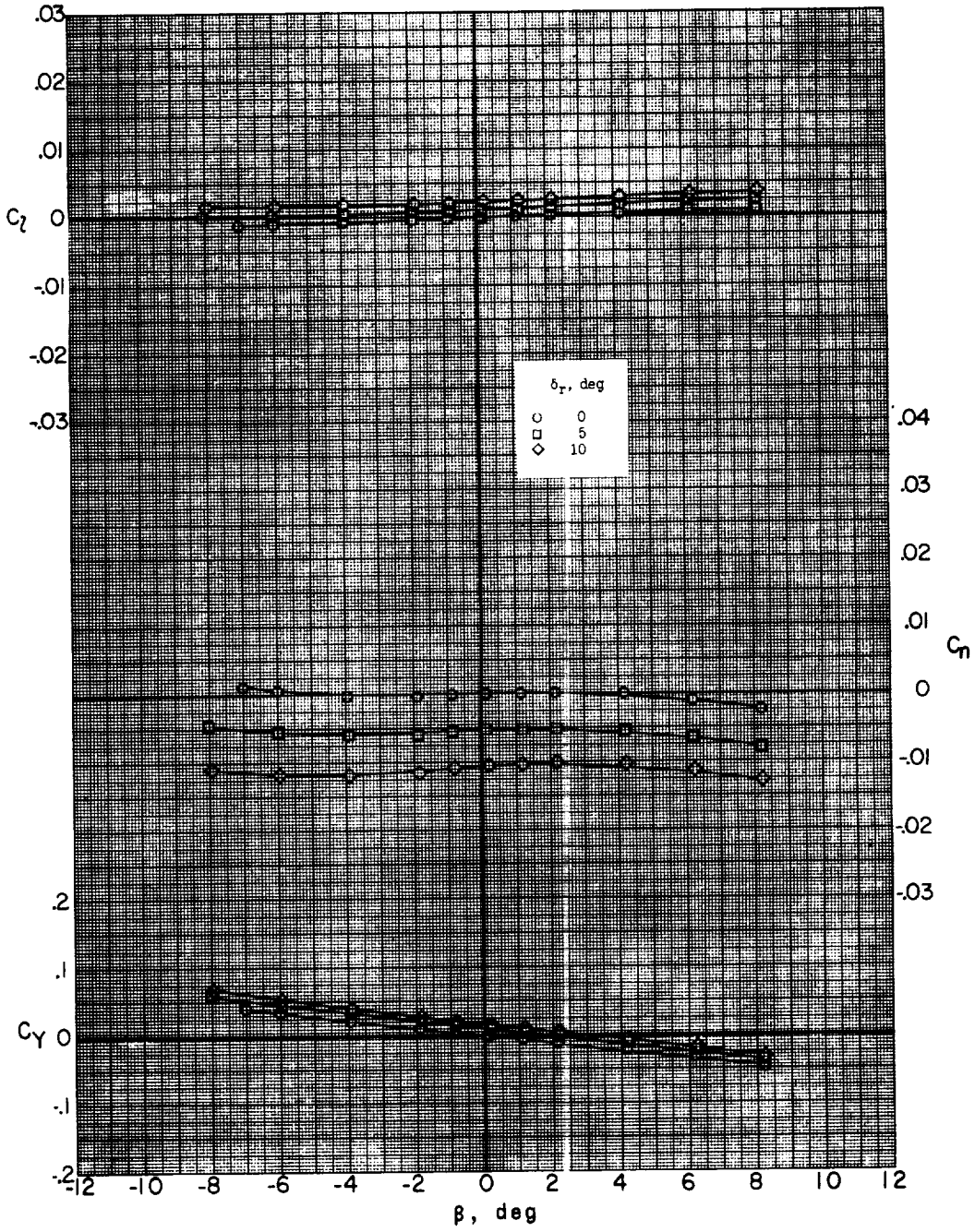
(c) M = 1.77; $\alpha = 5.2^{\circ}$.

Figure 47.- Continued.



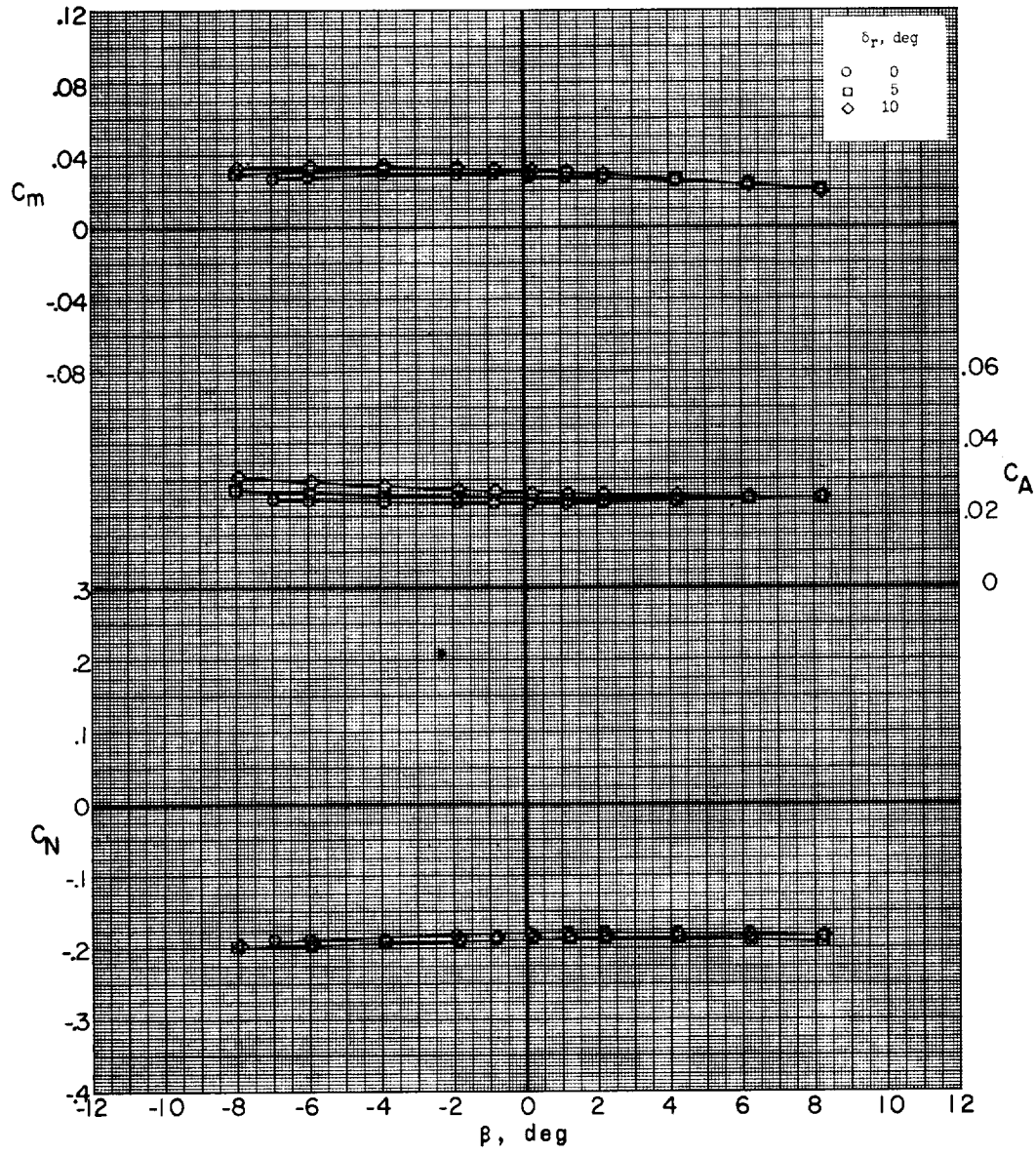
(c) Concluded.

Figure 47.- Continued.



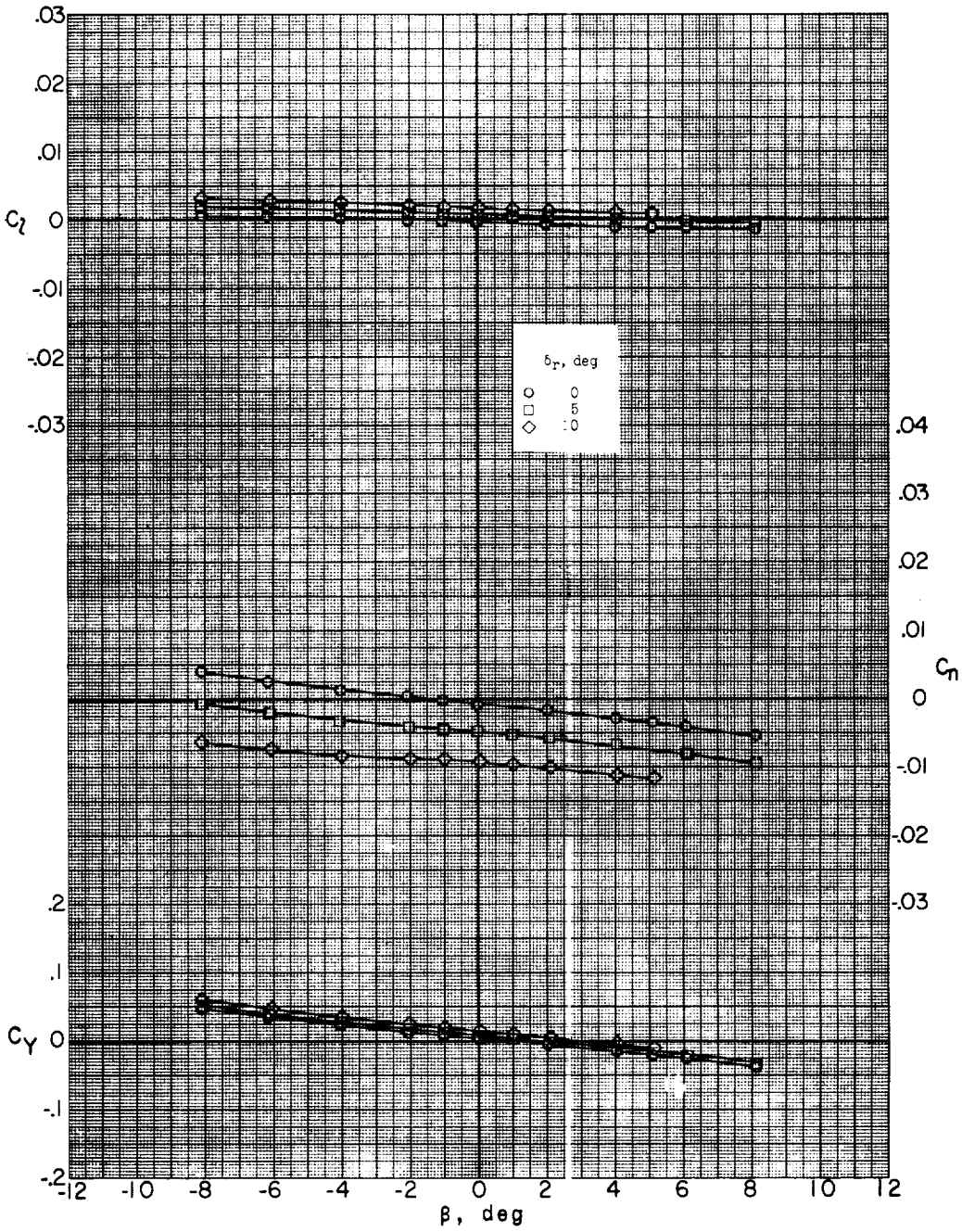
(d) M = 2.75; α = -5.2°.

Figure 47.- Continued.



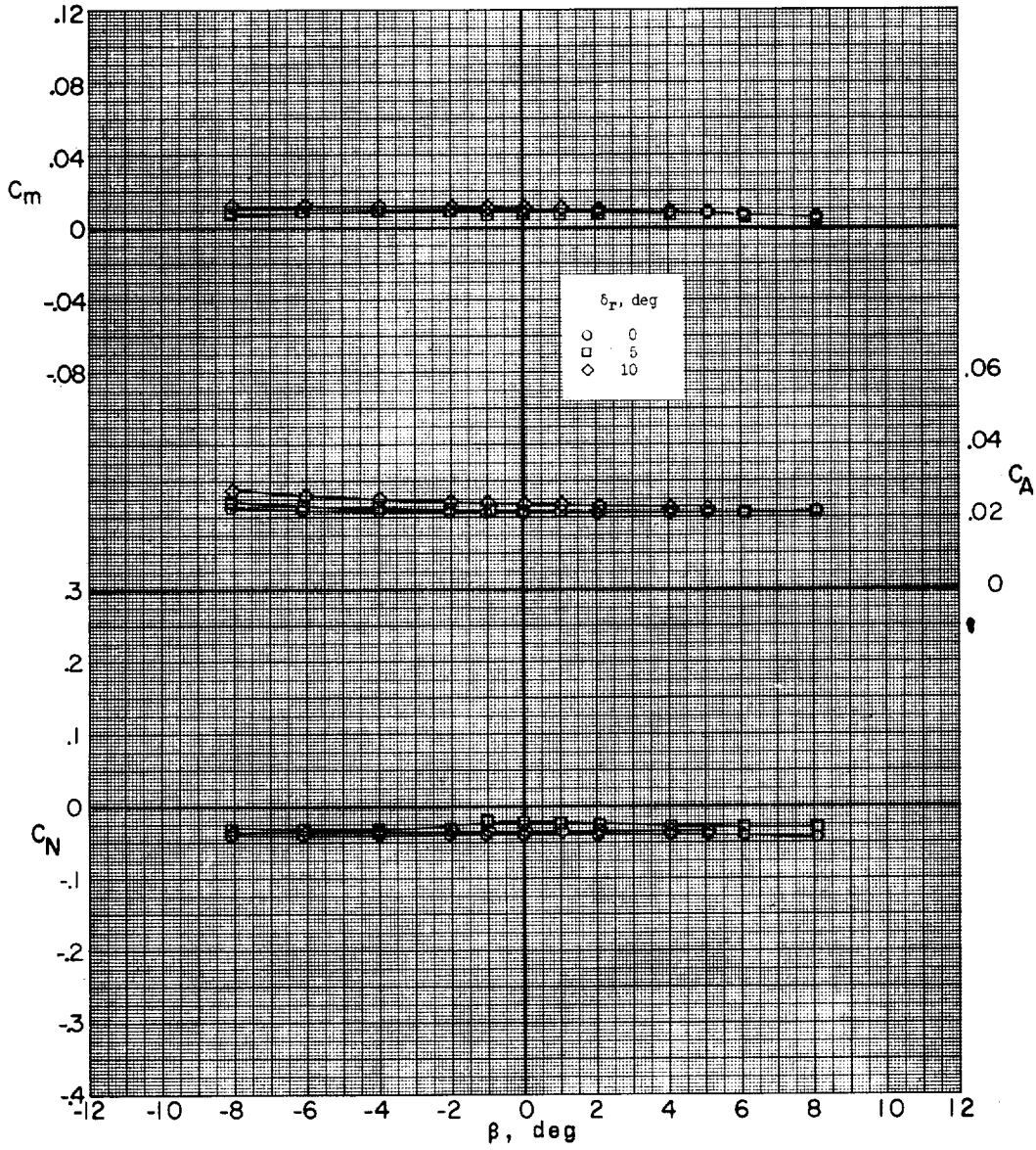
(d) Concluded.

Figure 47.- Continued.



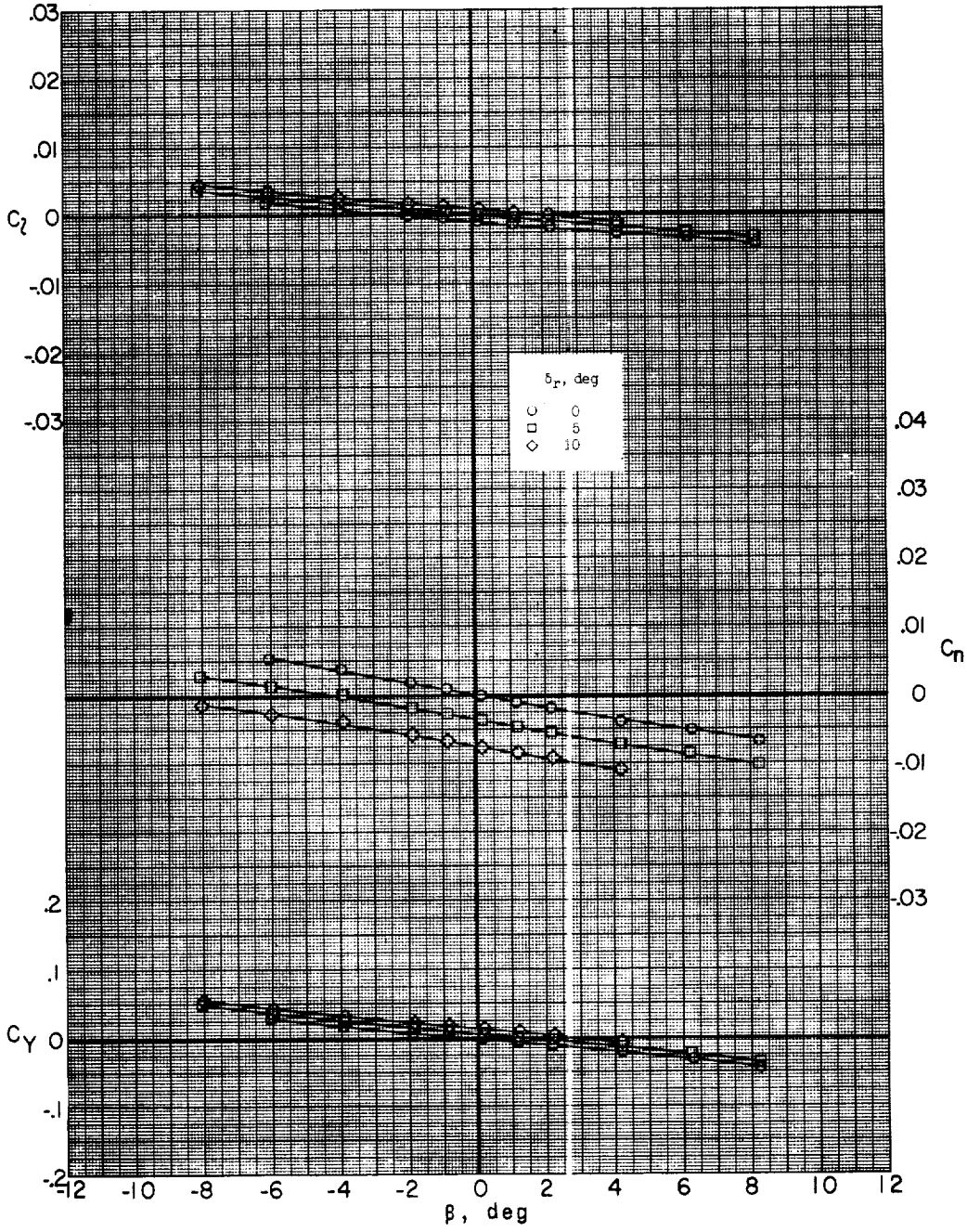
(e) M = 2.75; $\alpha = -0.2^\circ$.

Figure 47.- Continued.



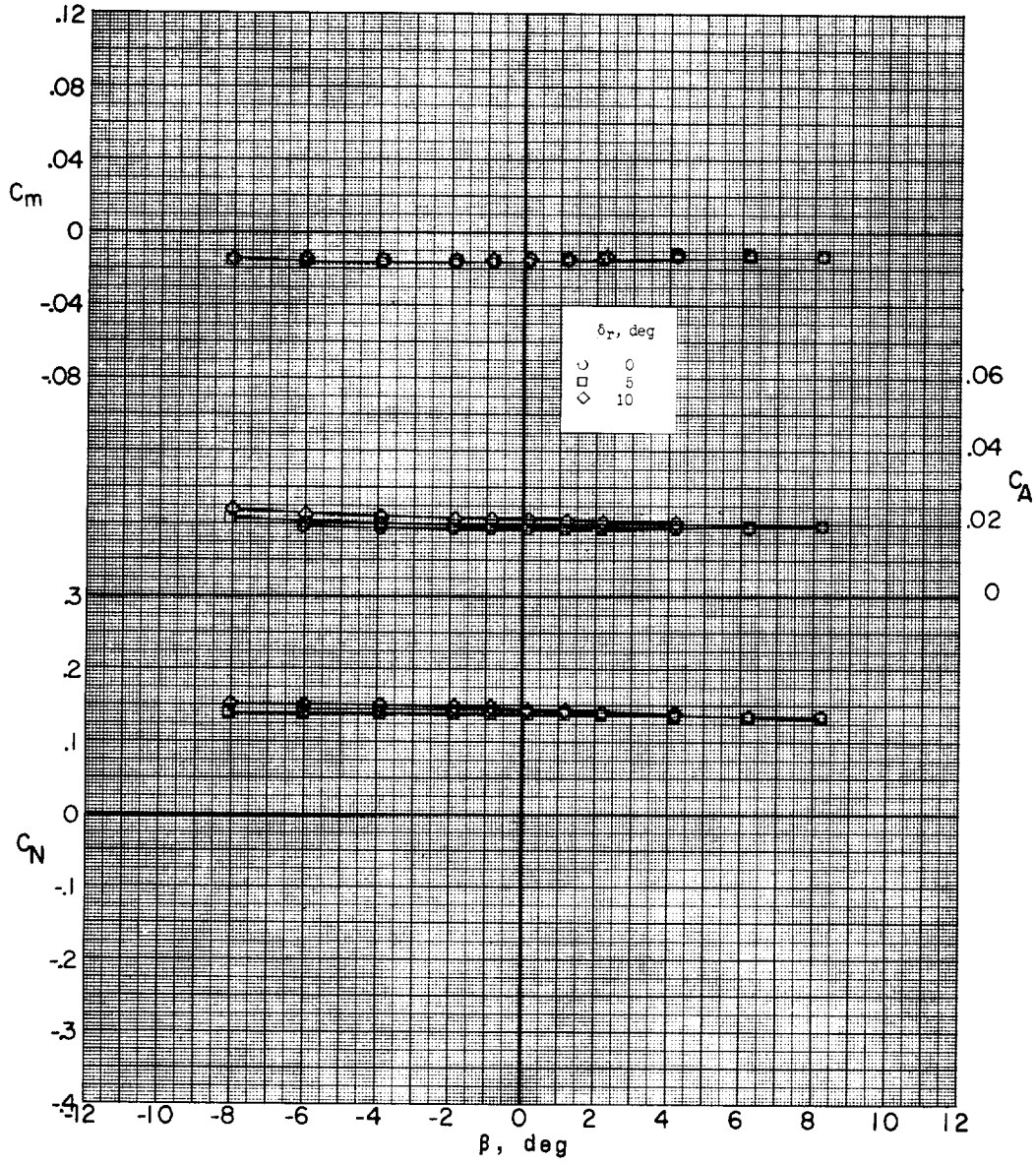
(e) Concluded.

Figure 47.- Continued.



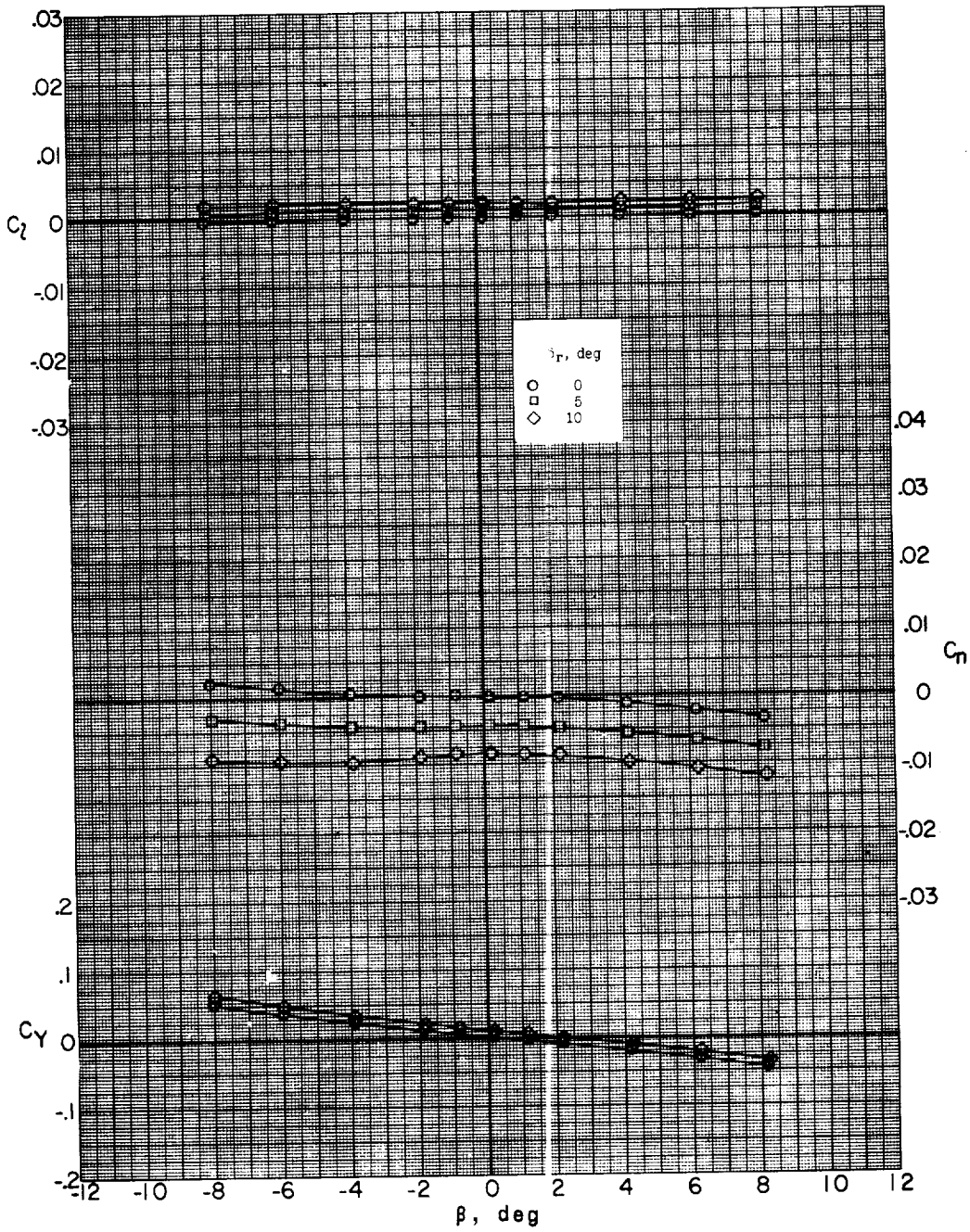
(f) M = 2.75; $\alpha = 5.2^{\circ}$.

Figure 47.- Continued.



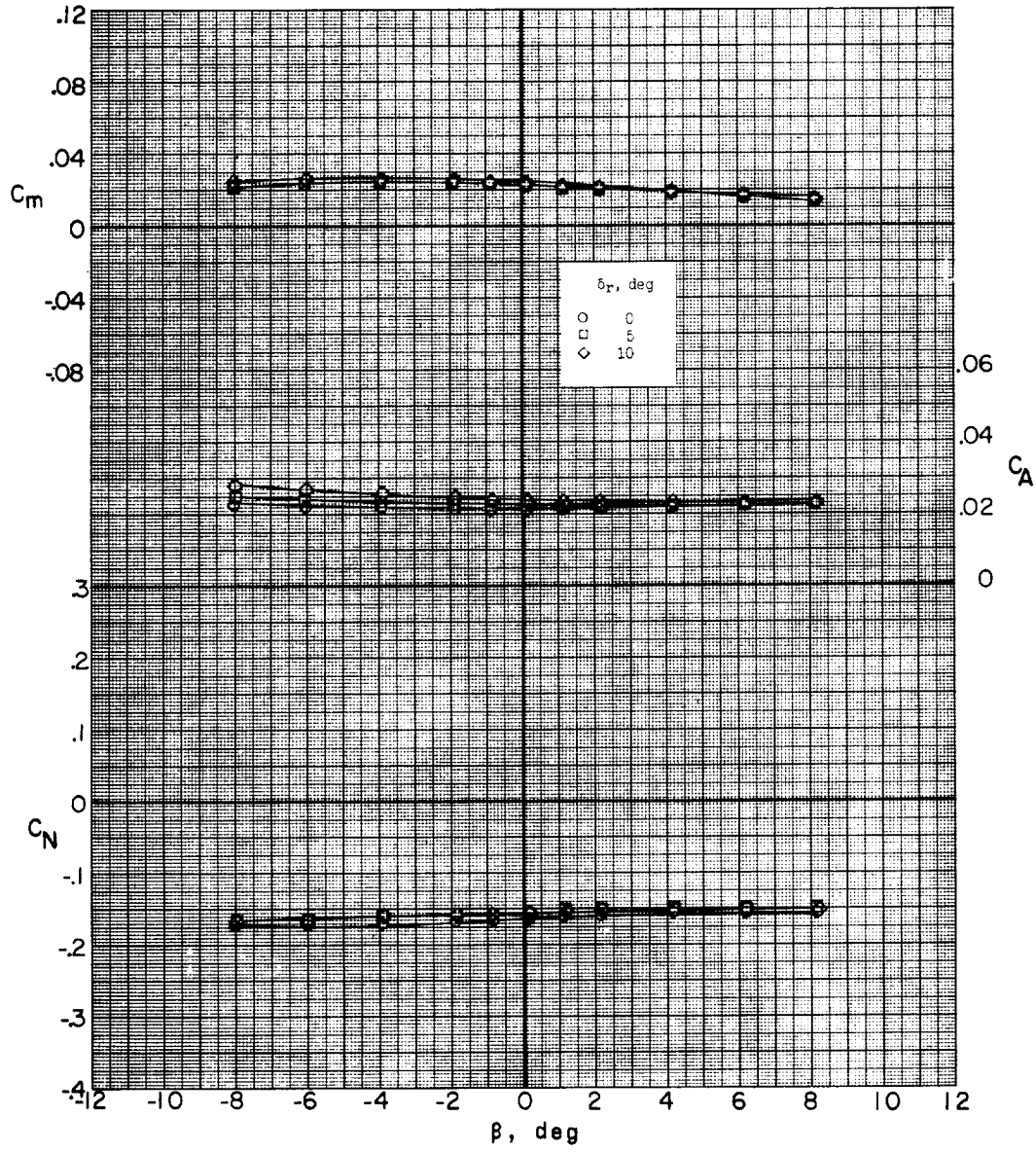
(f) Concluded.

Figure 47.- Continued.



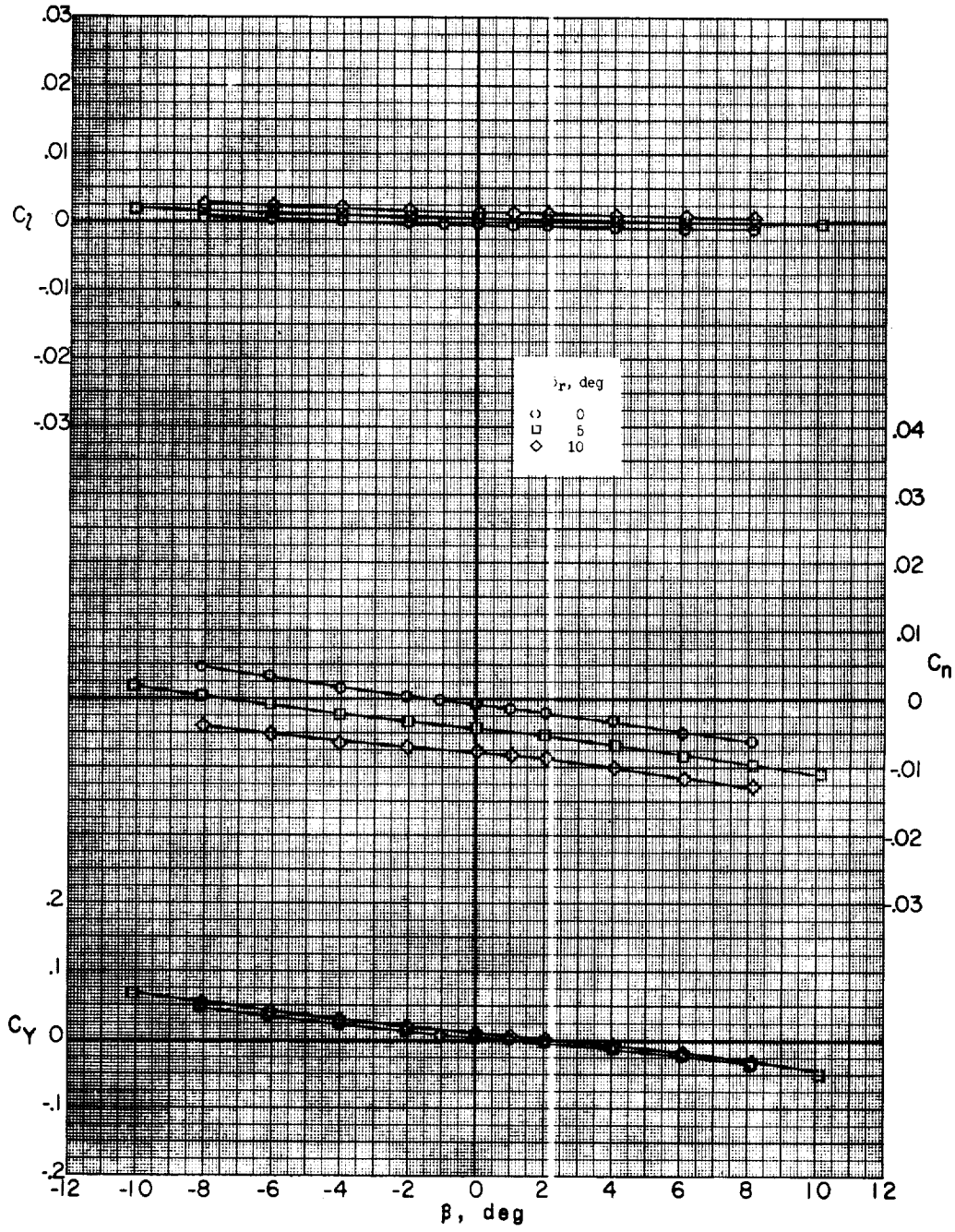
(g) M = 3.22; $\alpha = -5.1^{\circ}$.

Figure 47.- Continued.



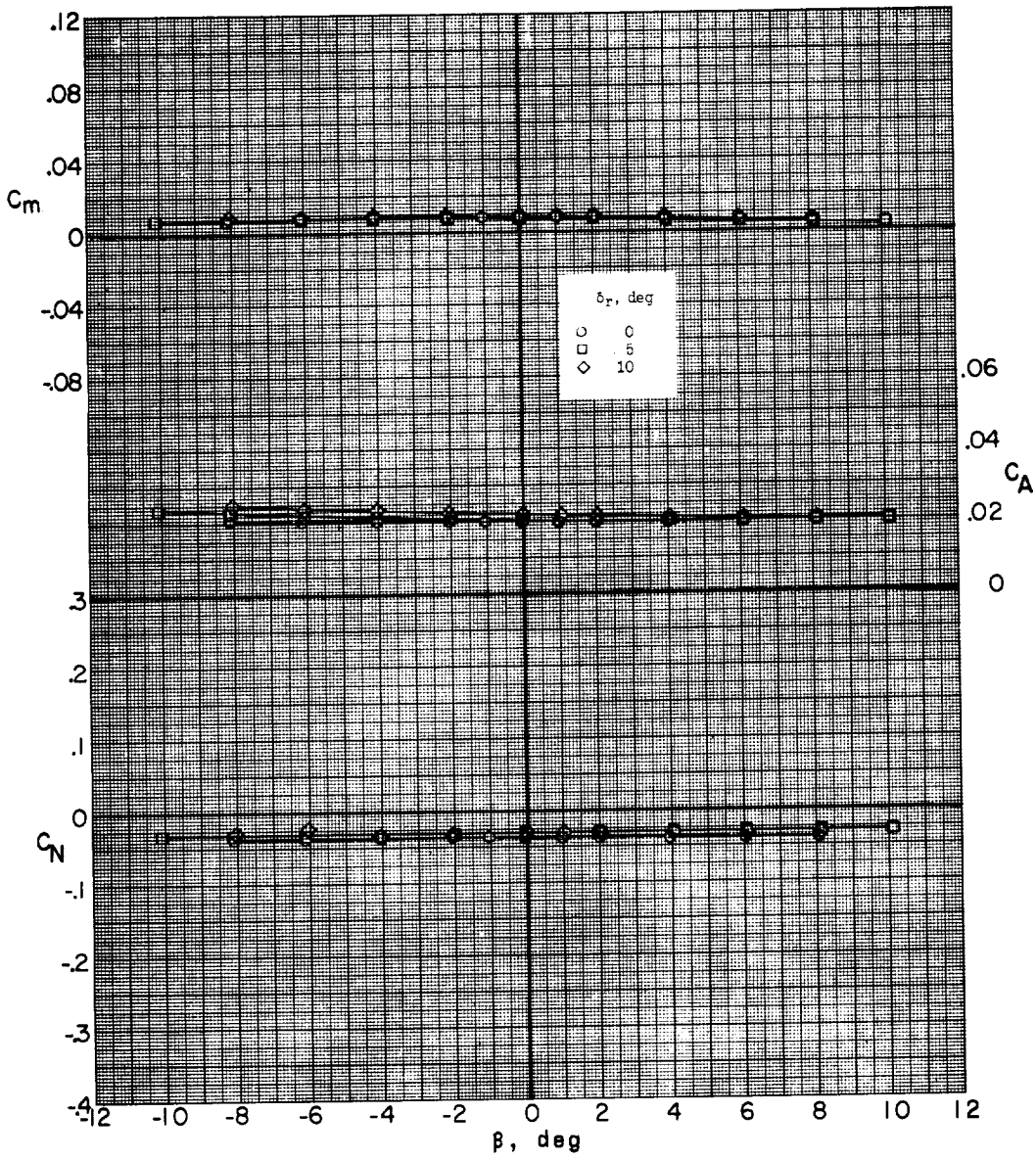
(g) Concluded.

Figure 47.- Continued.



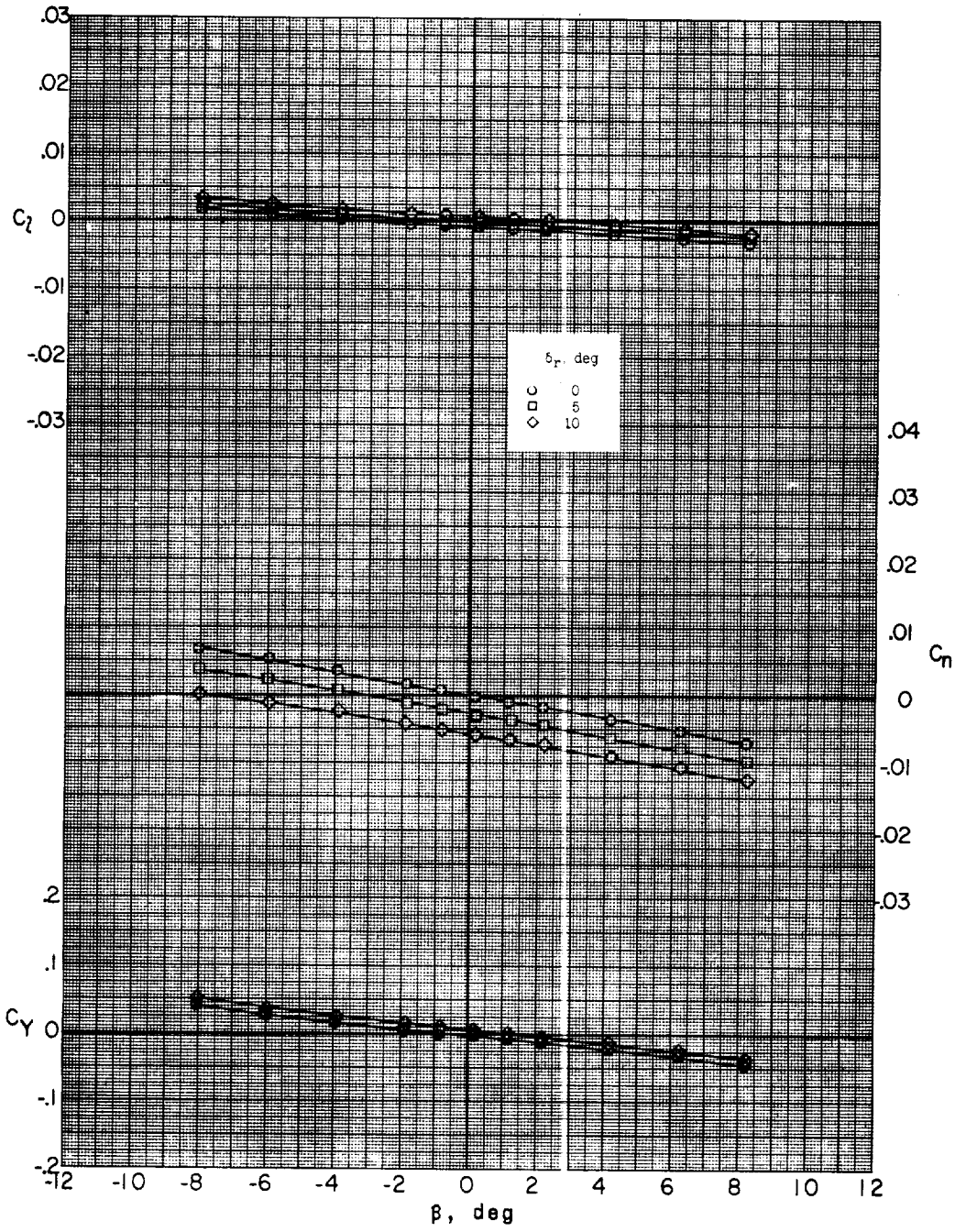
(h) M = 3.22; $\alpha = -0.2^{\circ}$.

Figure 47.- Continued.



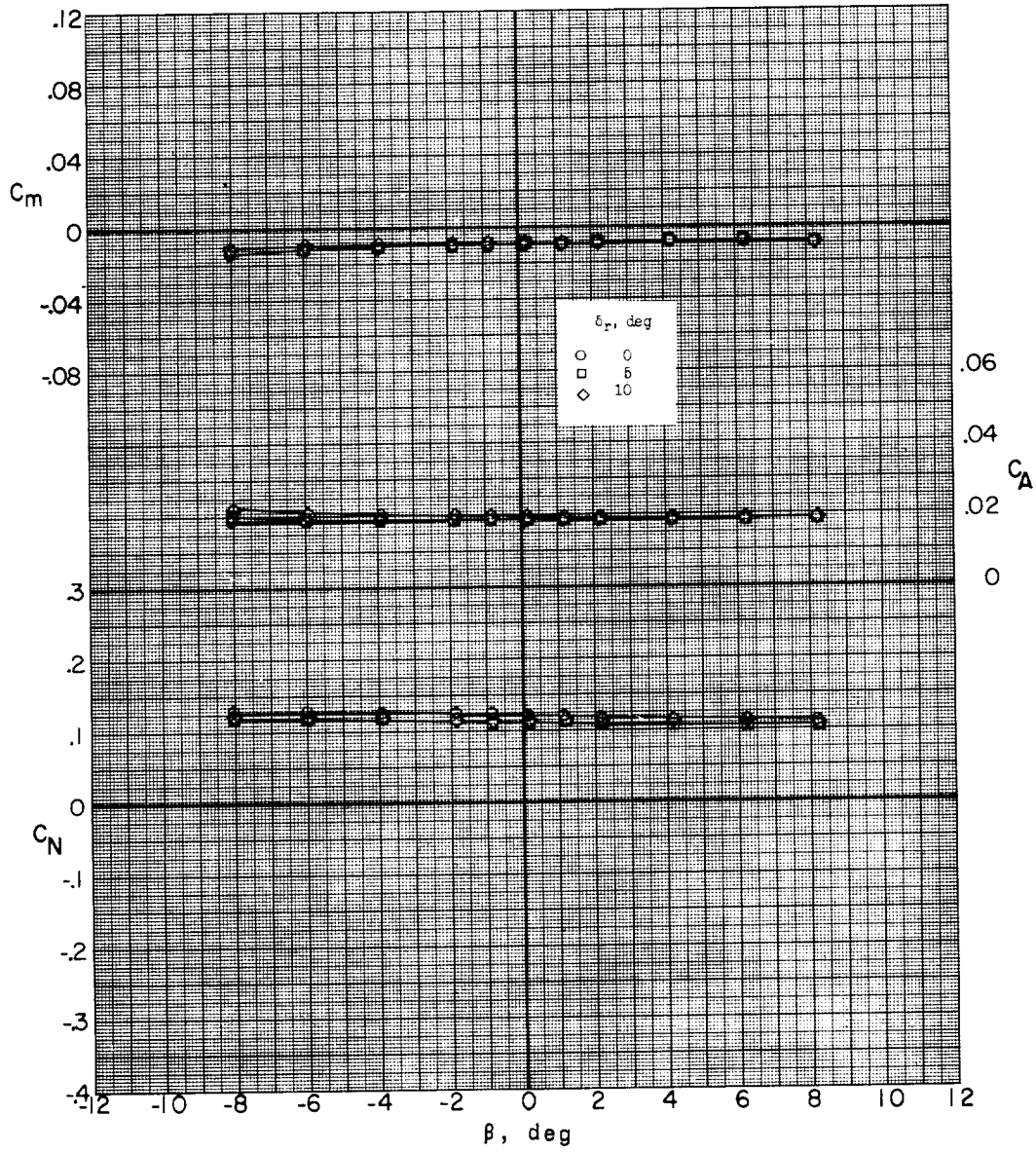
(h) Concluded.

Figure 47.- Continued.



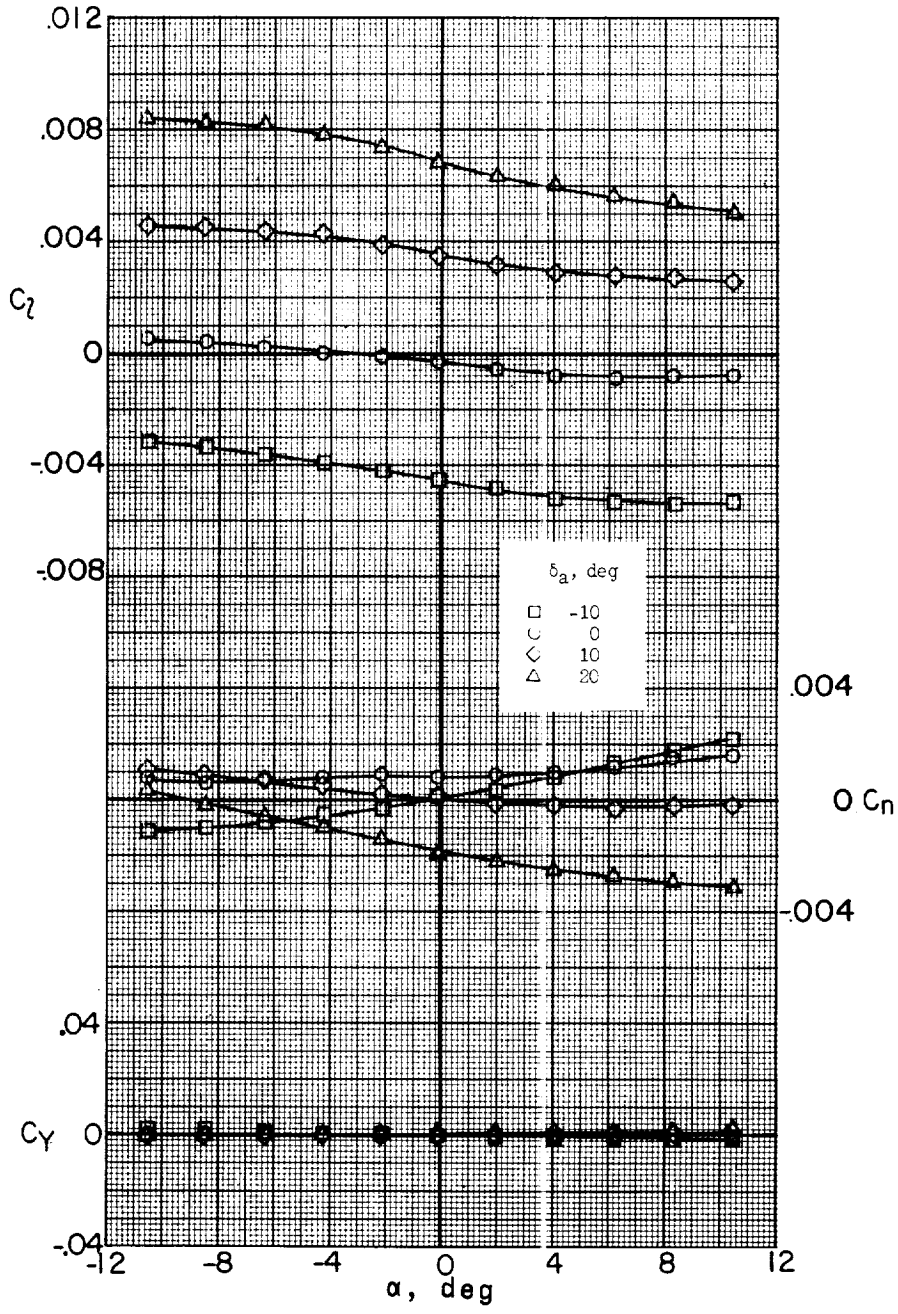
(i) $M = 3.22$; $\alpha = 5.1^{\circ}$.

Figure 47.- Continued.



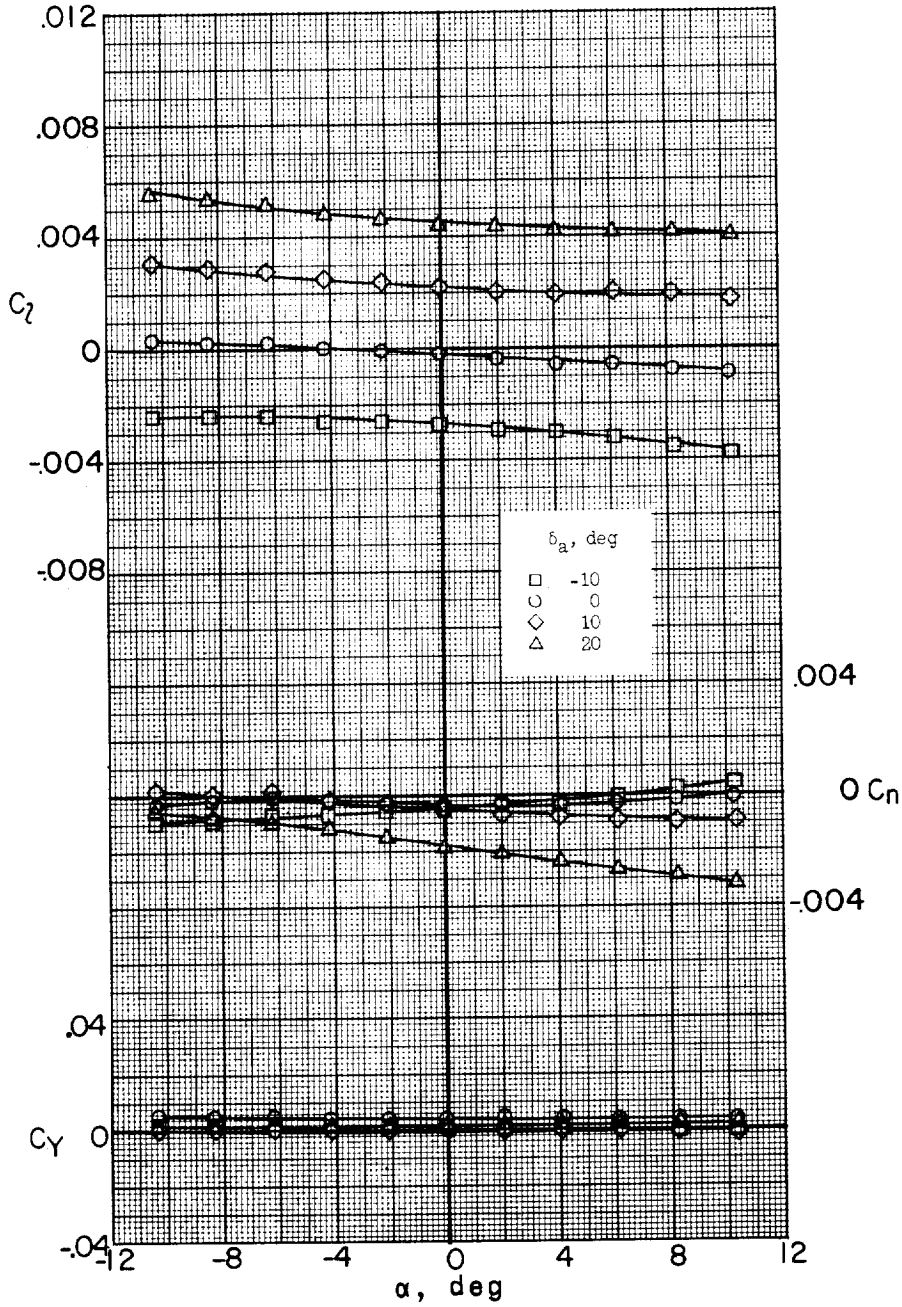
(i) Concluded.

Figure 47.- Concluded.



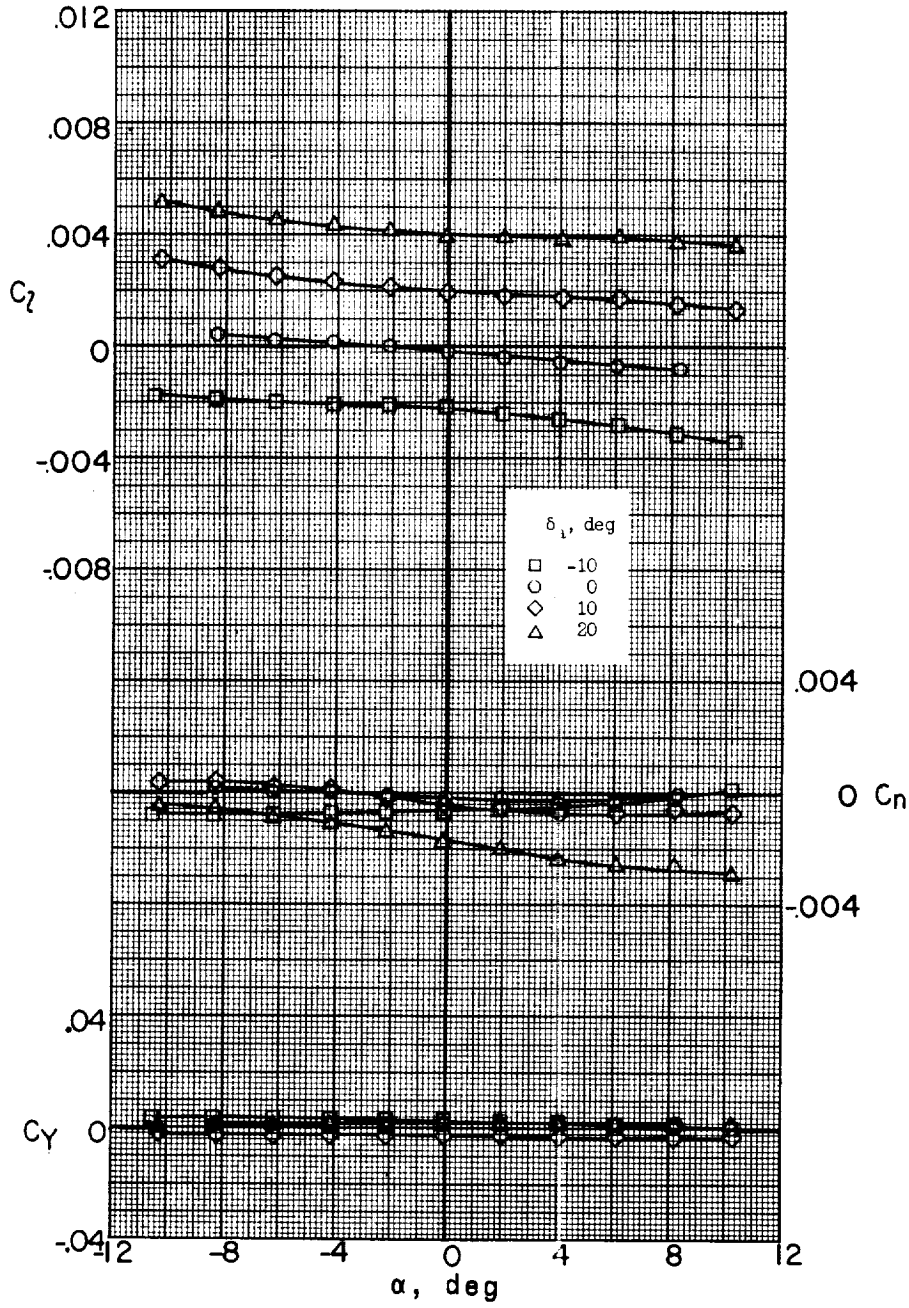
(a) M = 1.7''.

Figure 48.- Effect of aileron deflection on lateral characteristics of missile alone. $\delta_e = 0^\circ$; $\beta = 0.2^\circ$; sting A.



(b) M = 2.75.

Figure 48.- Continued.



(c) M = 3.22.

Figure 48.- Concluded.

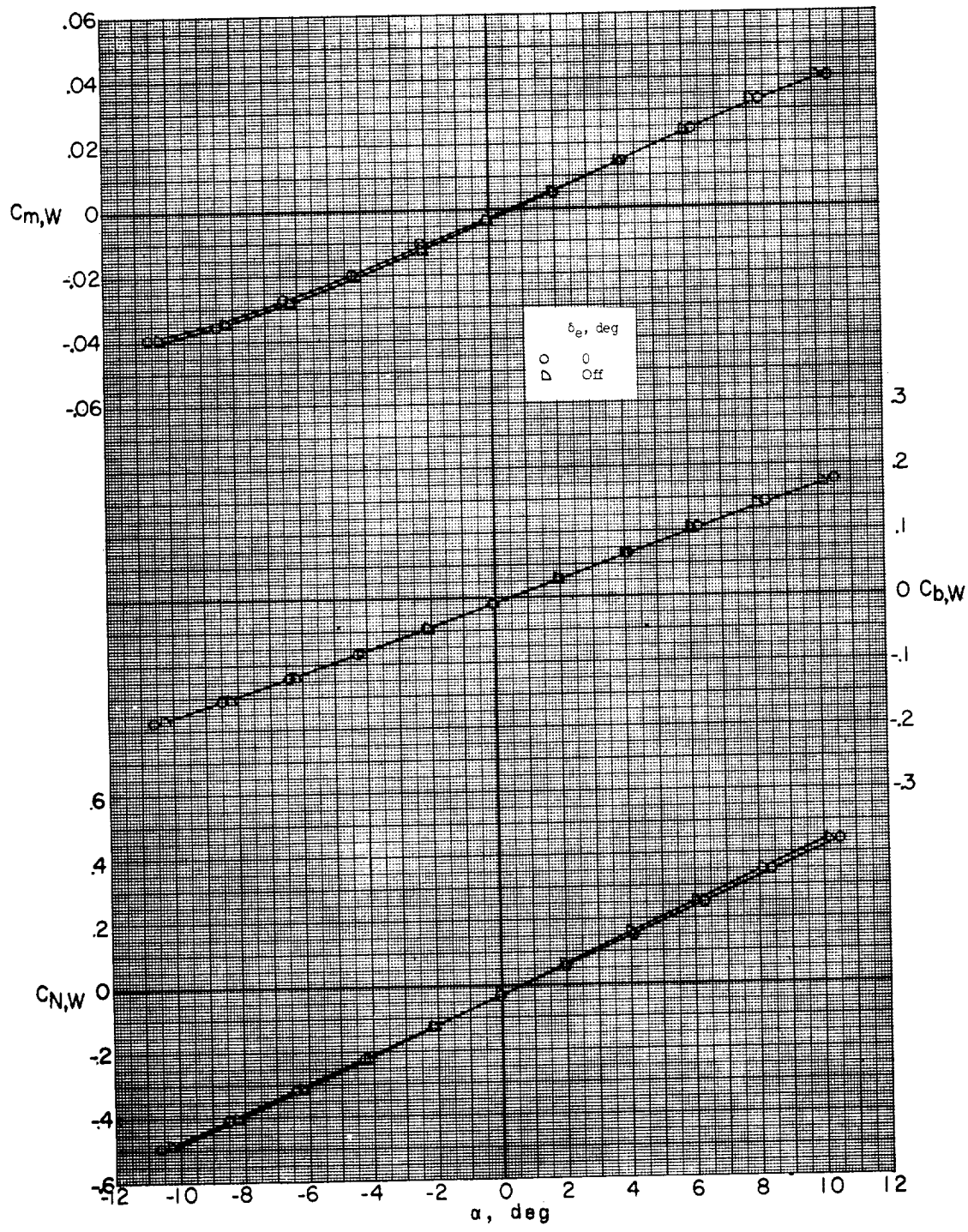
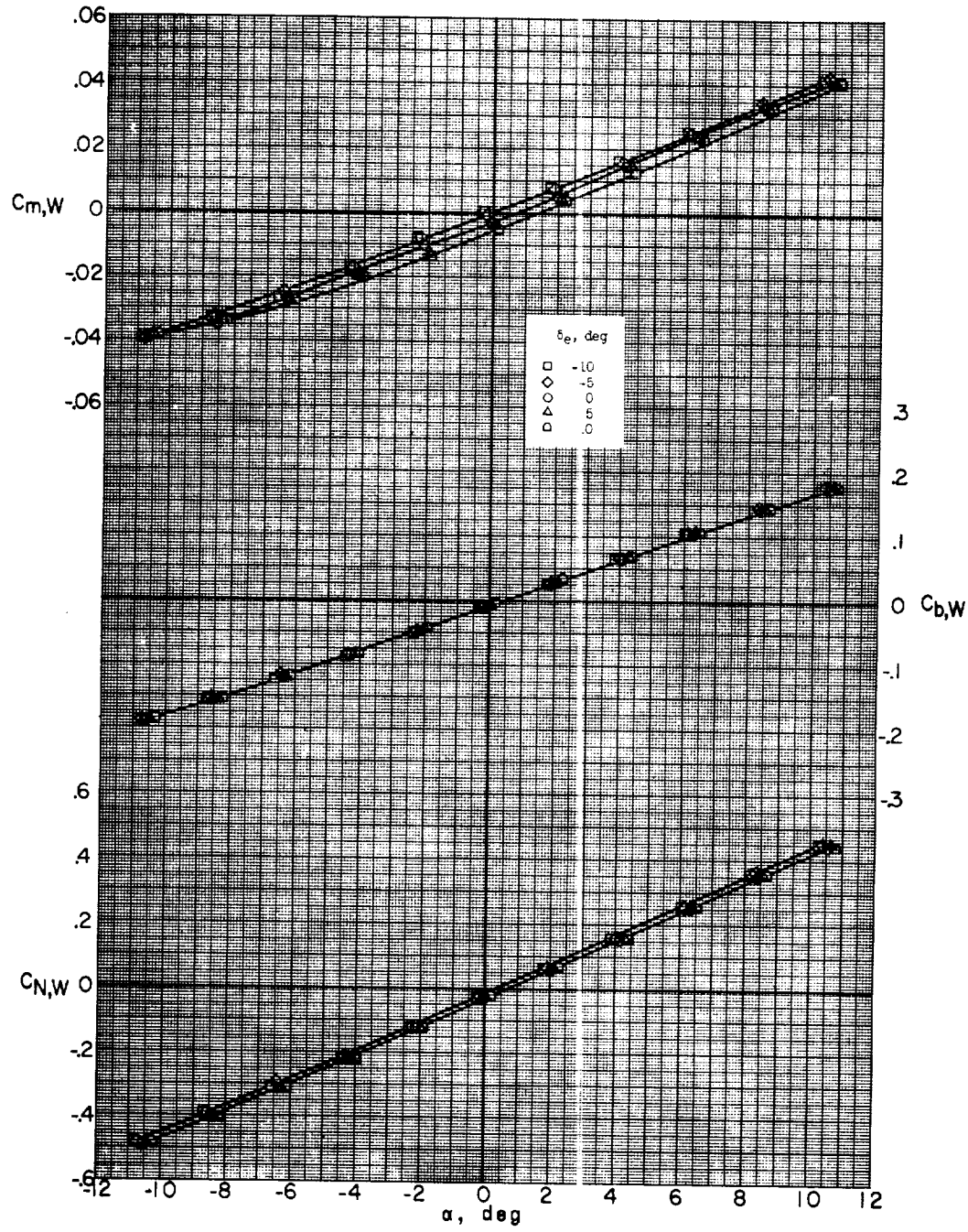
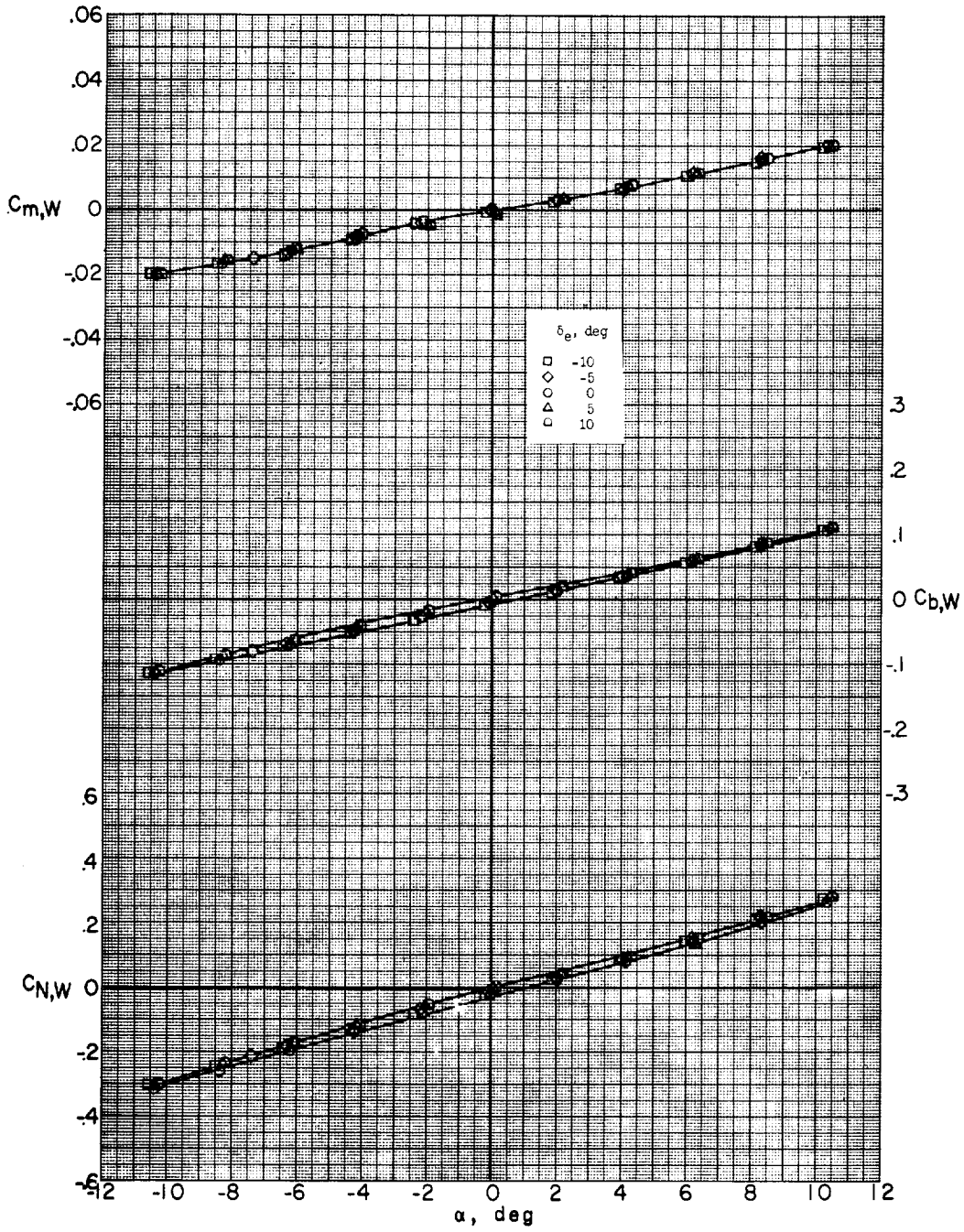


Figure 49.- Effect of canard surface on pitch characteristics of missile wing. Missile alone; $\beta = 0.2^{\circ}$; M = 1.77; sting A.



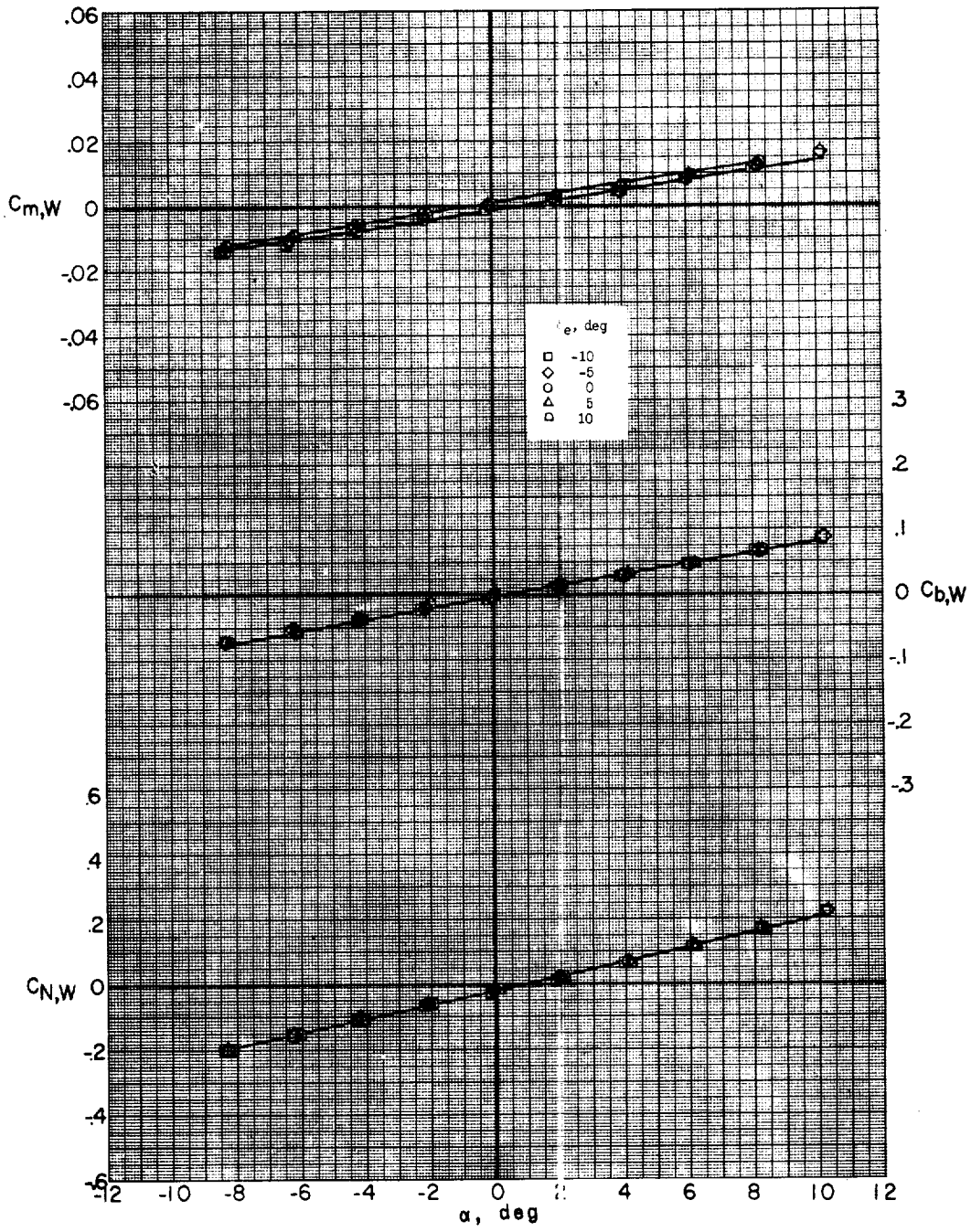
(a) M = 1.77.

Figure 50.- Effect of canard deflection on pitch characteristics of missile wing. Missile alone; $\beta = 0.2^{\circ}$; sting A.



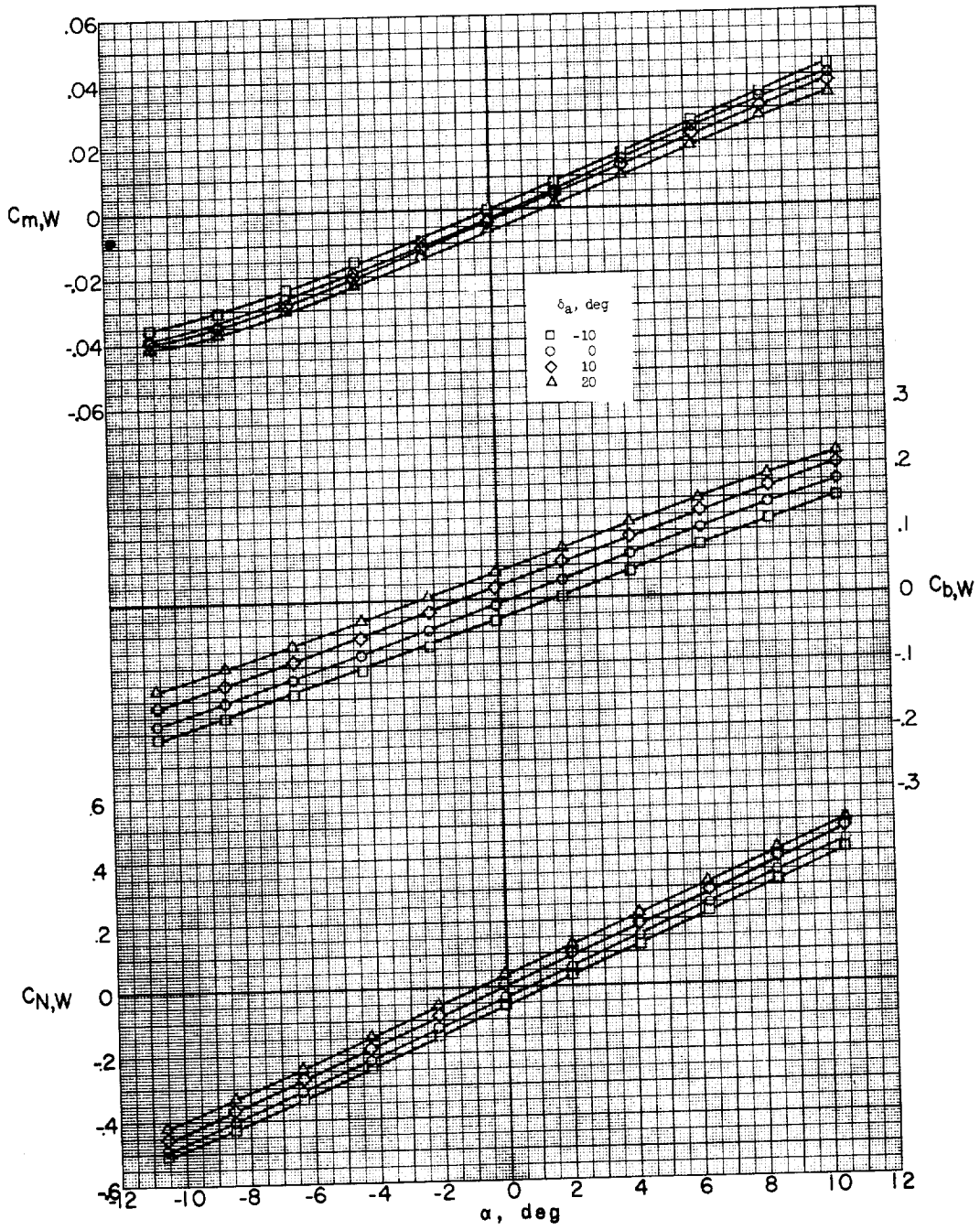
(b) M = 2.75.

Figure 50.- Continued.



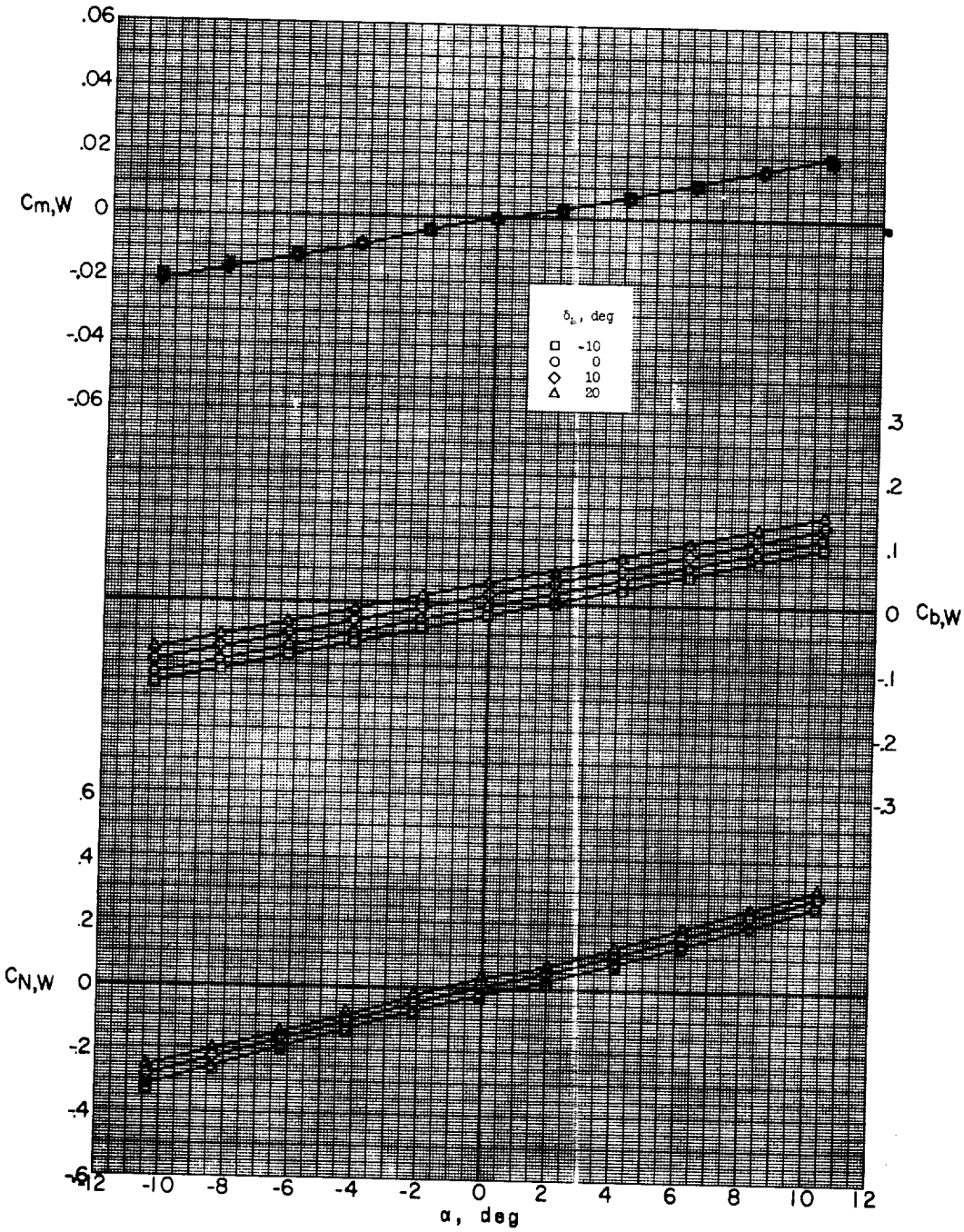
(c) M = .22.

Figure 50.- Concluded.



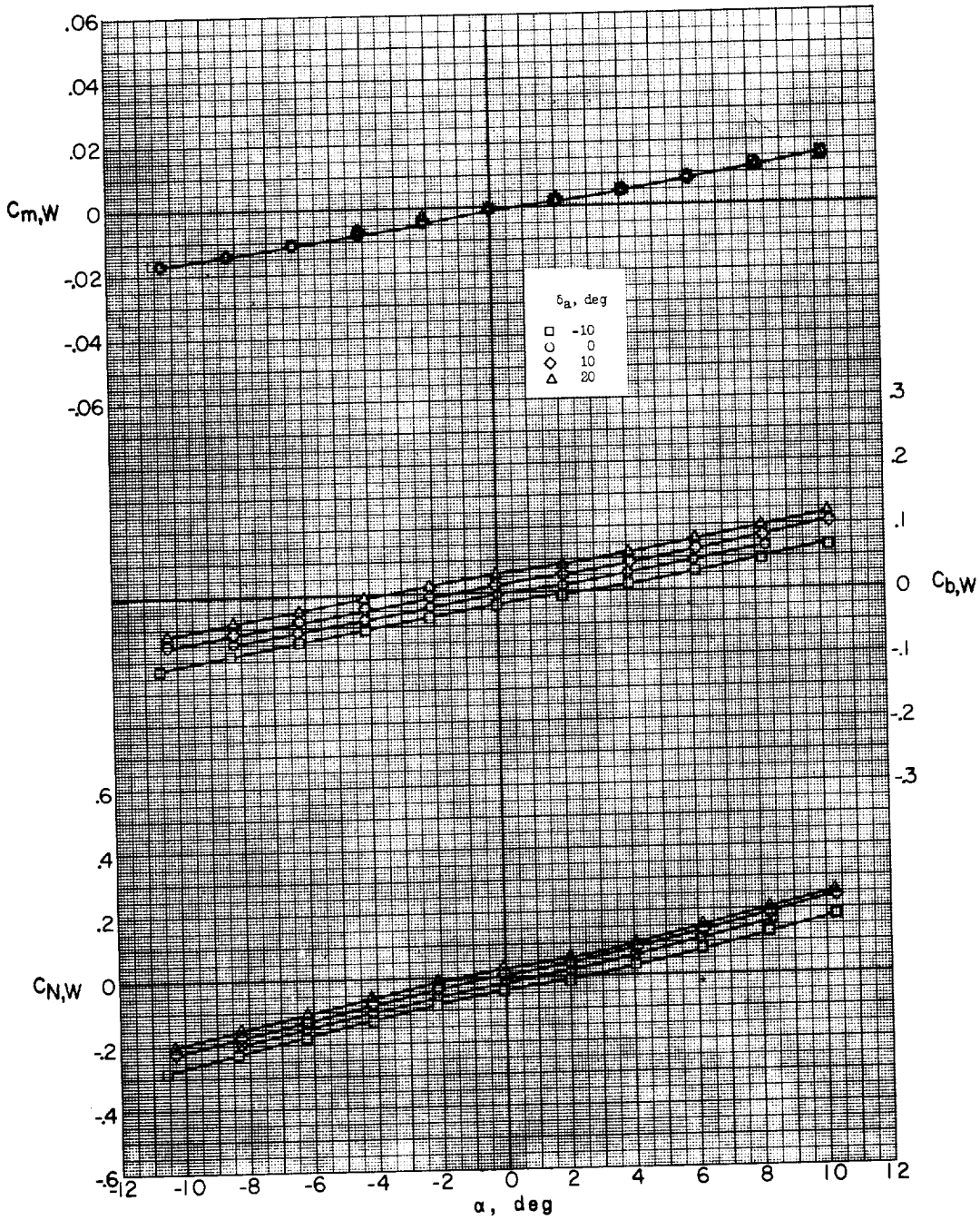
(a) M = 1.77.

Figure 51.- Effect of aileron deflection on pitch characteristics of missile wing. Missile alone; $\delta_e = 0^\circ$; $\beta = 0.2^\circ$; sting A.



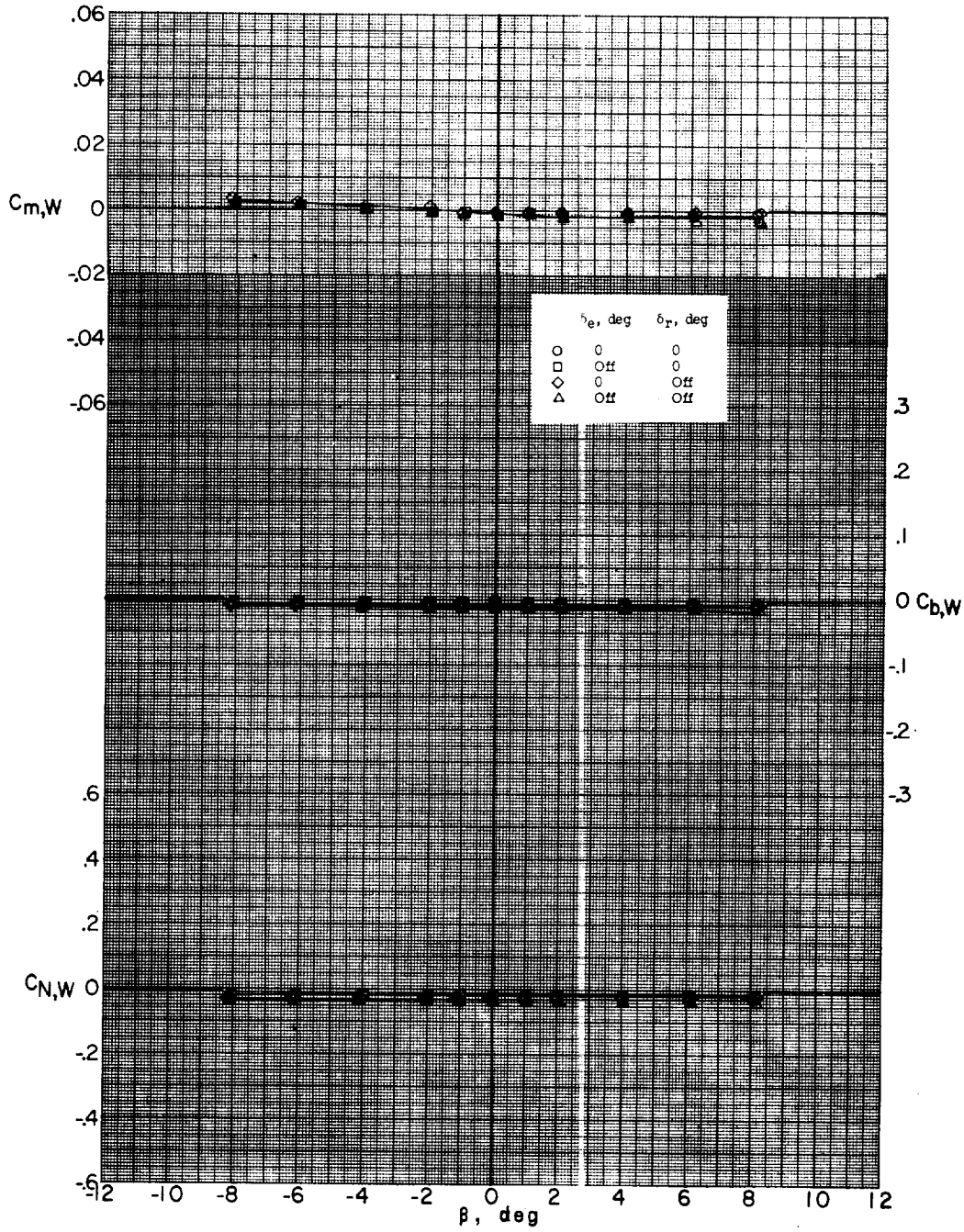
(b) M = 2.75.

Figure 51.- Continued.



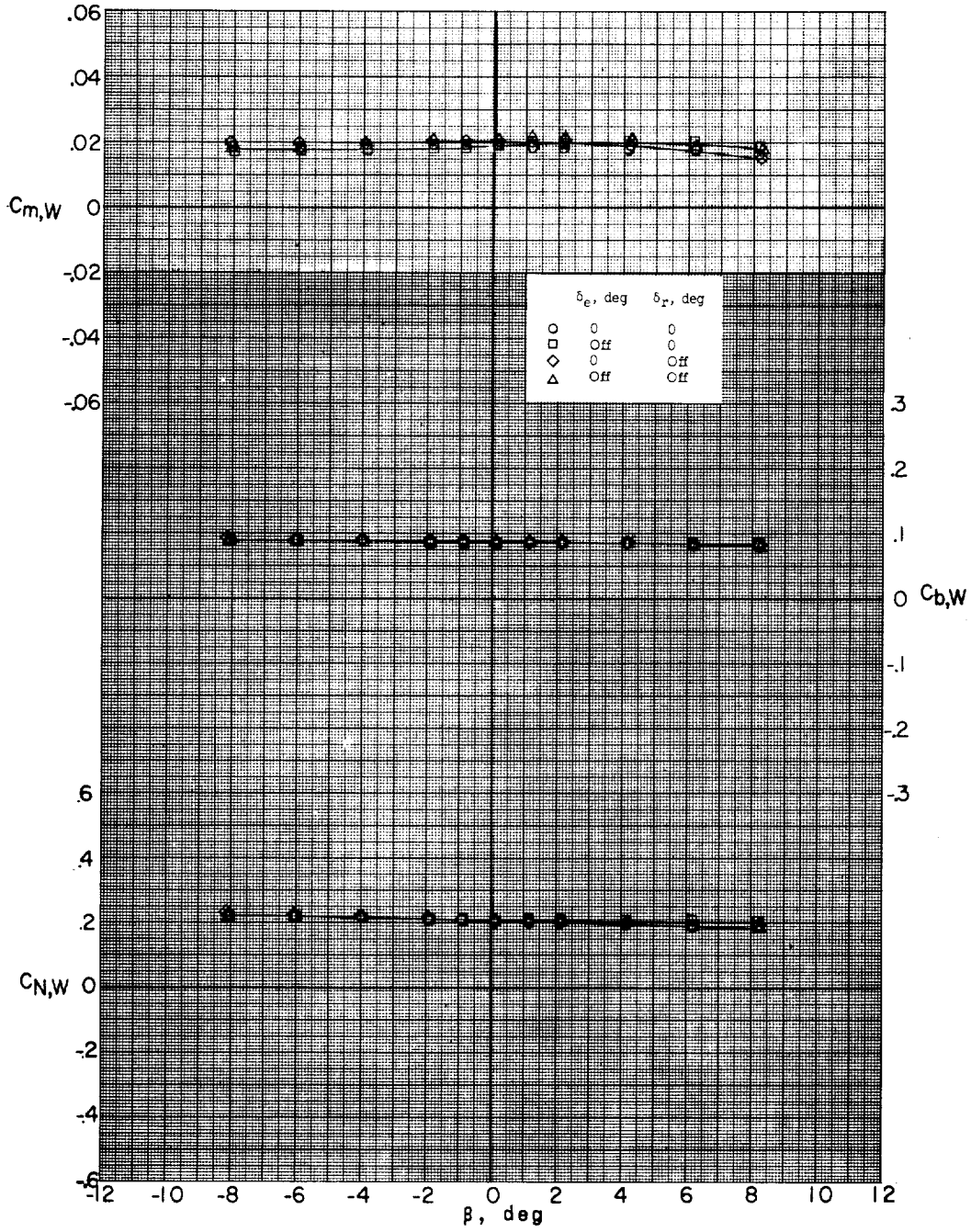
(c) M = 3.22.

Figure 51.- Concluded.



(a) $\alpha = -0.2^{\circ}$.

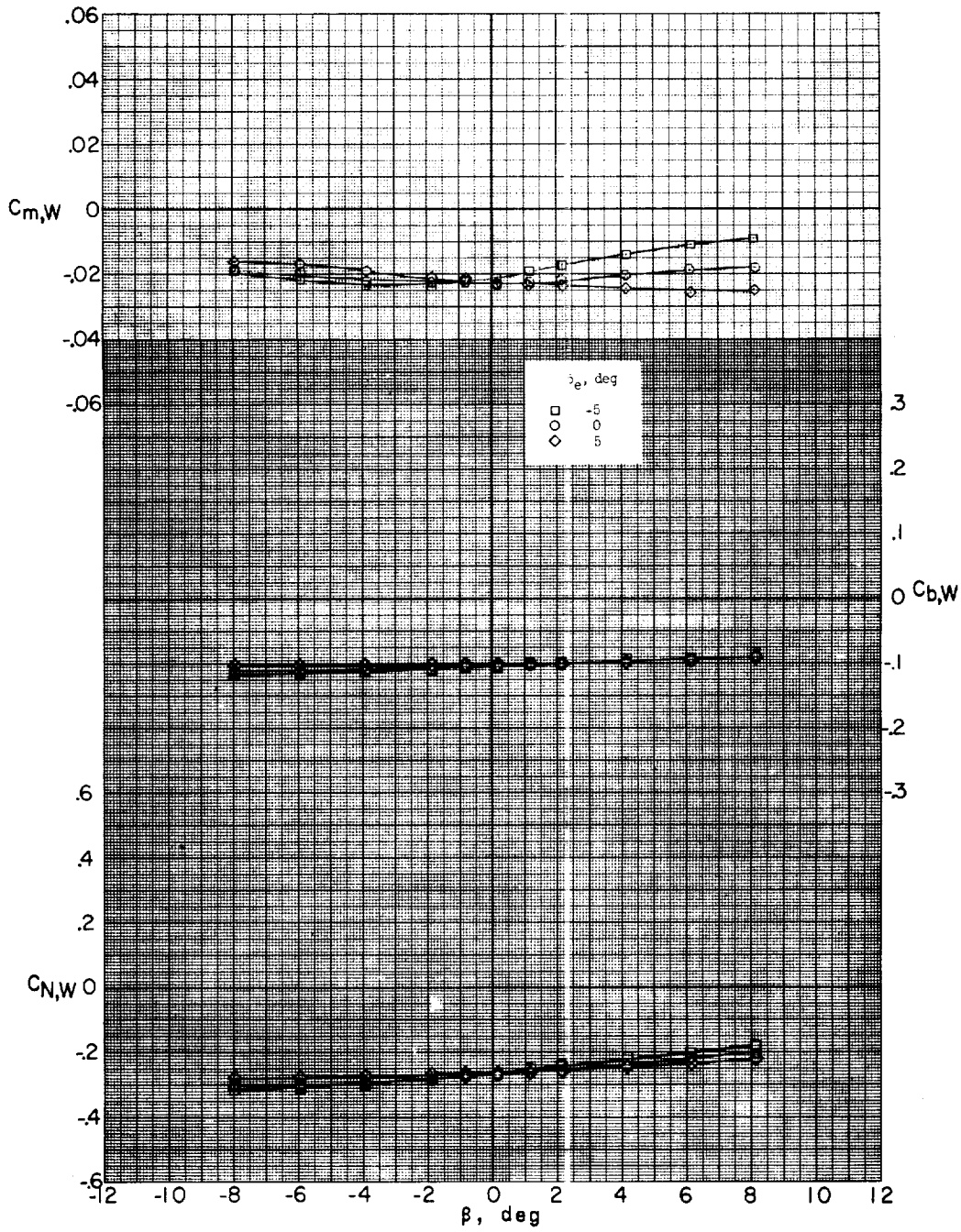
Figure 52.- Effect of canard and rudder surfaces on lateral characteristics of missile wing. Missile alone; M = 1.77; sting A.



(b) $\alpha = 5.1^{\circ}$.

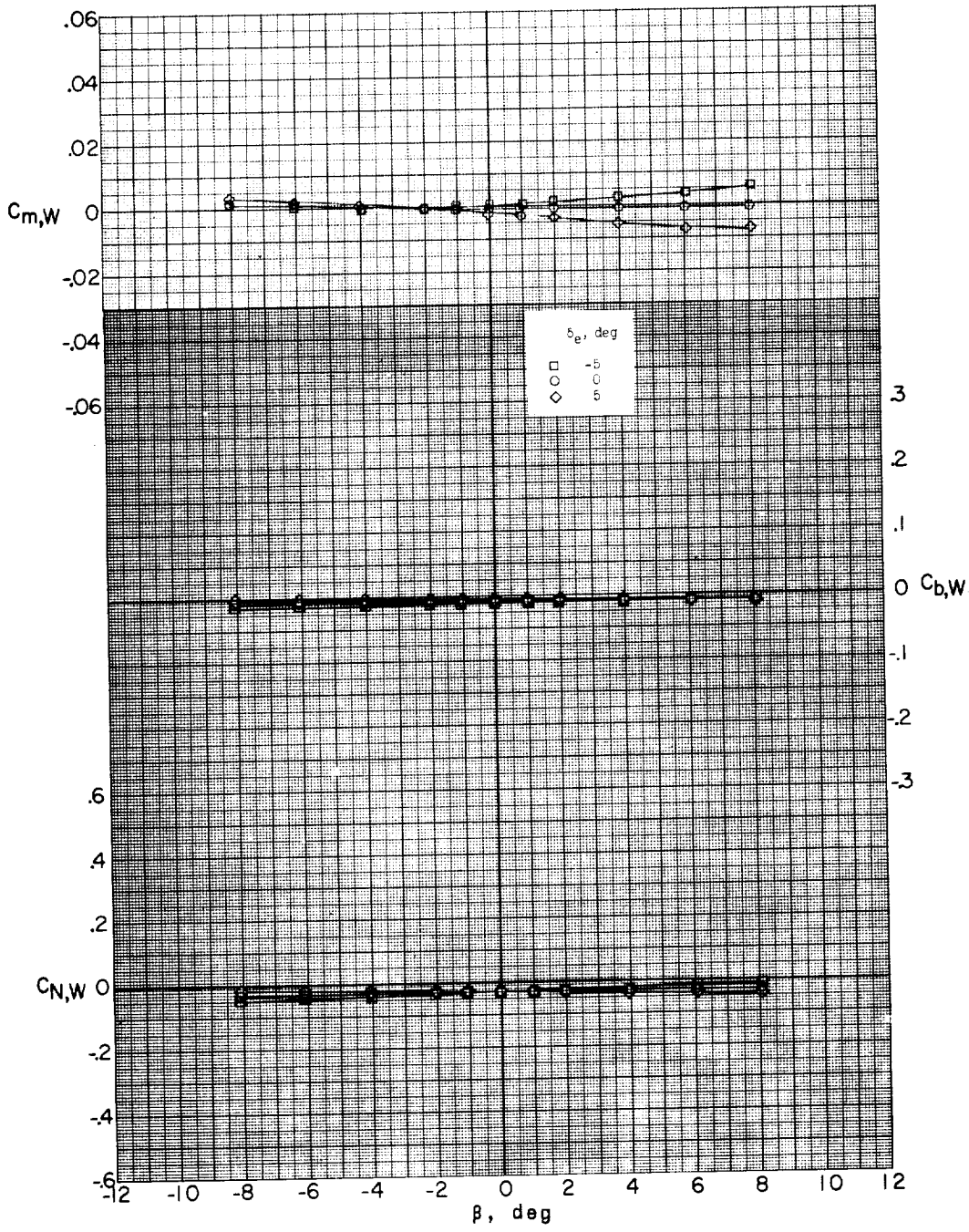
Figure 52.- Concluded.

[redacted]



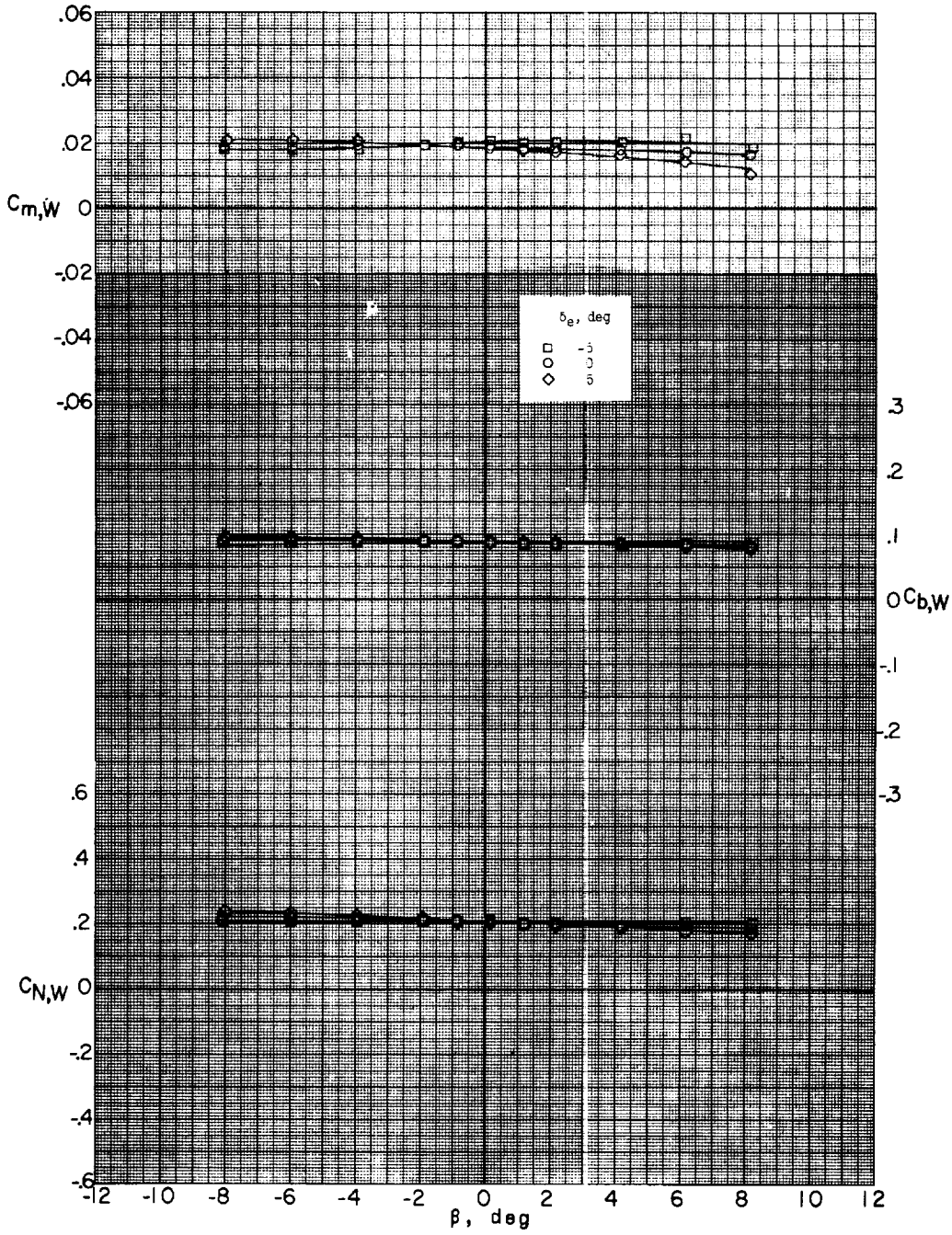
(a) M = 1.77; $\alpha = -5.3^{\circ}$.

Figure 53.- Effect of canard deflection on lateral characteristics of missile wing. Missile alone; sting A.



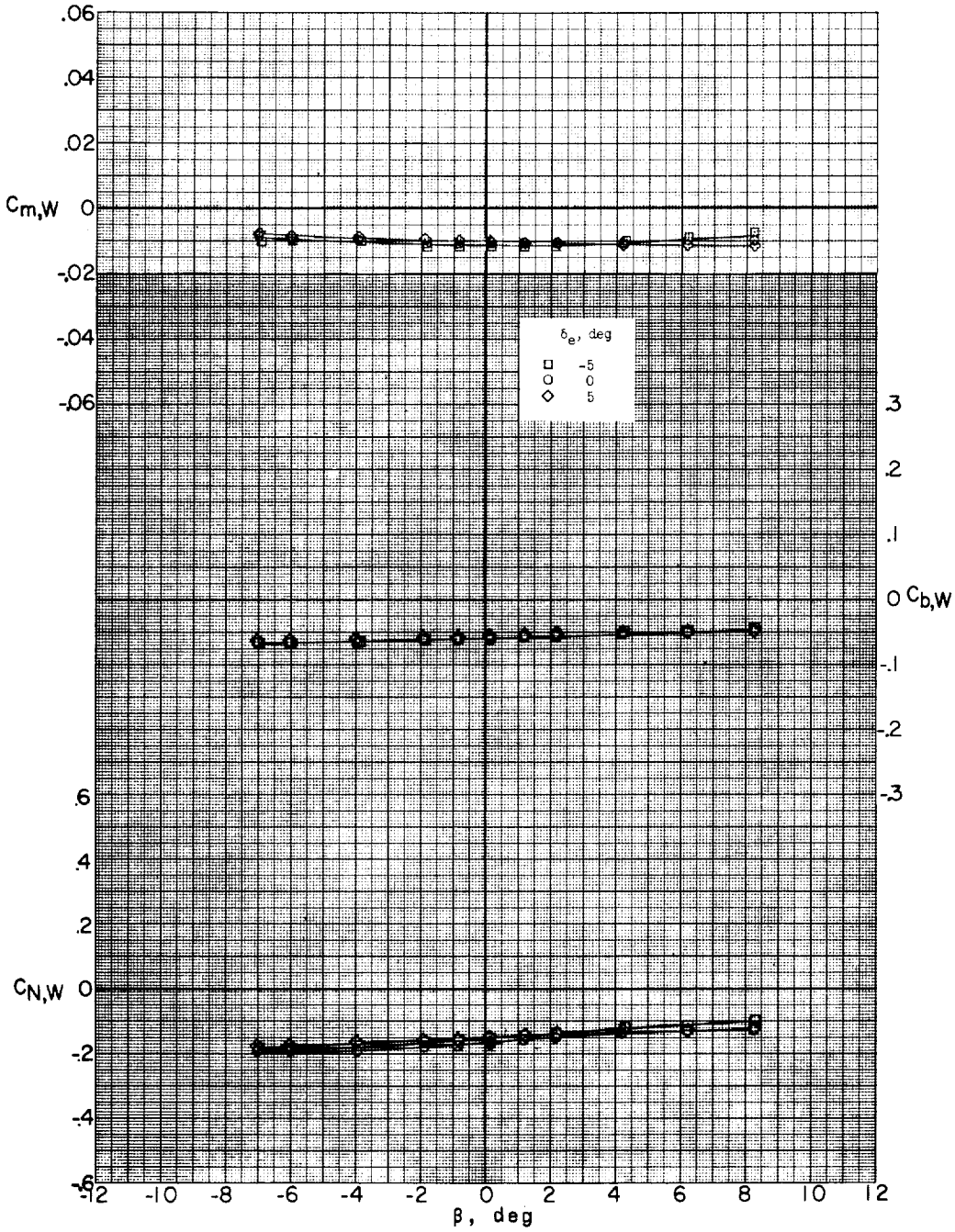
(b) M = 1.77; $\alpha = -0.2^{\circ}$.

Figure 53.- Continued.



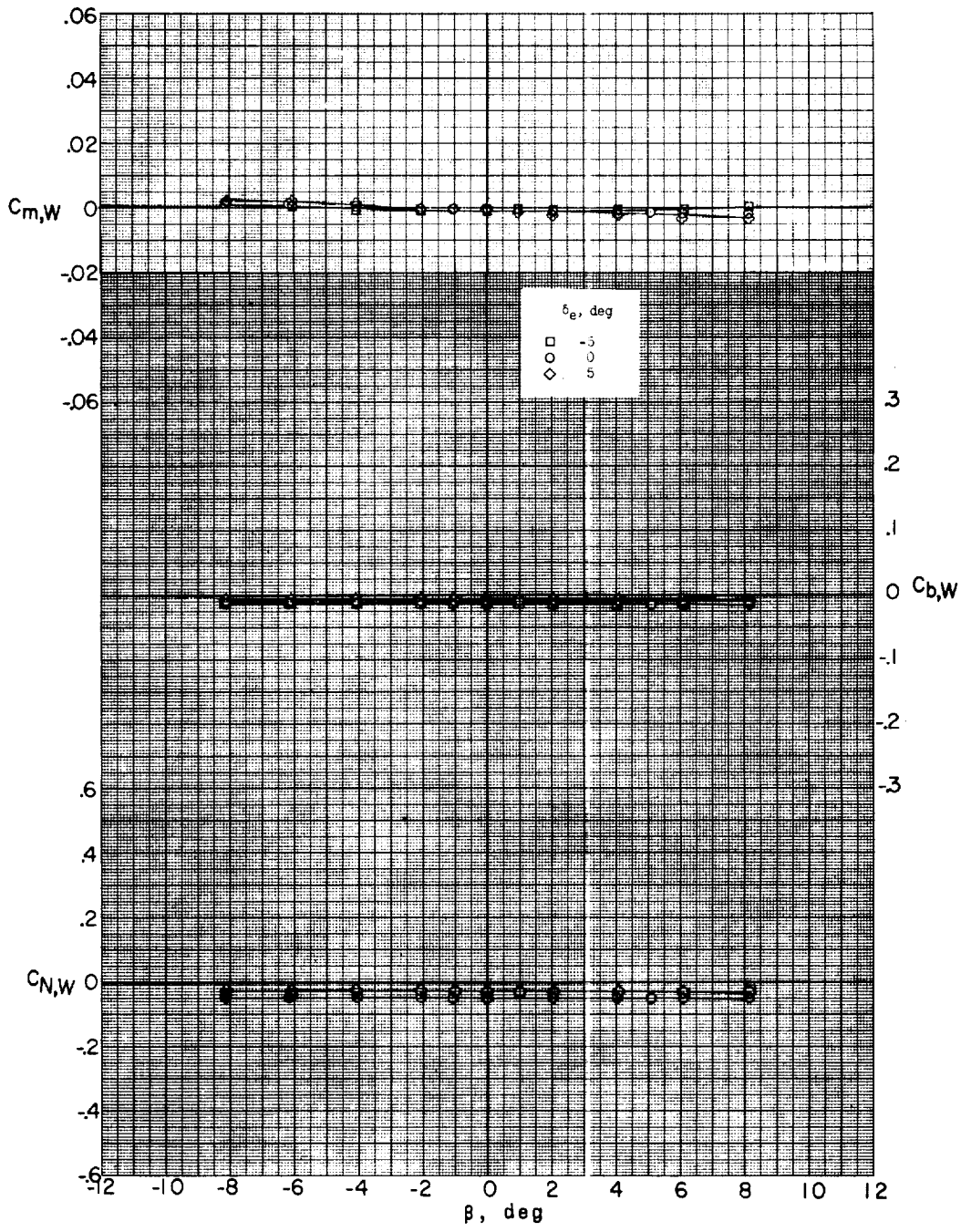
(c) M = 1.77; $\alpha = 5.2^{\circ}$.

Figure 53.- Continued.



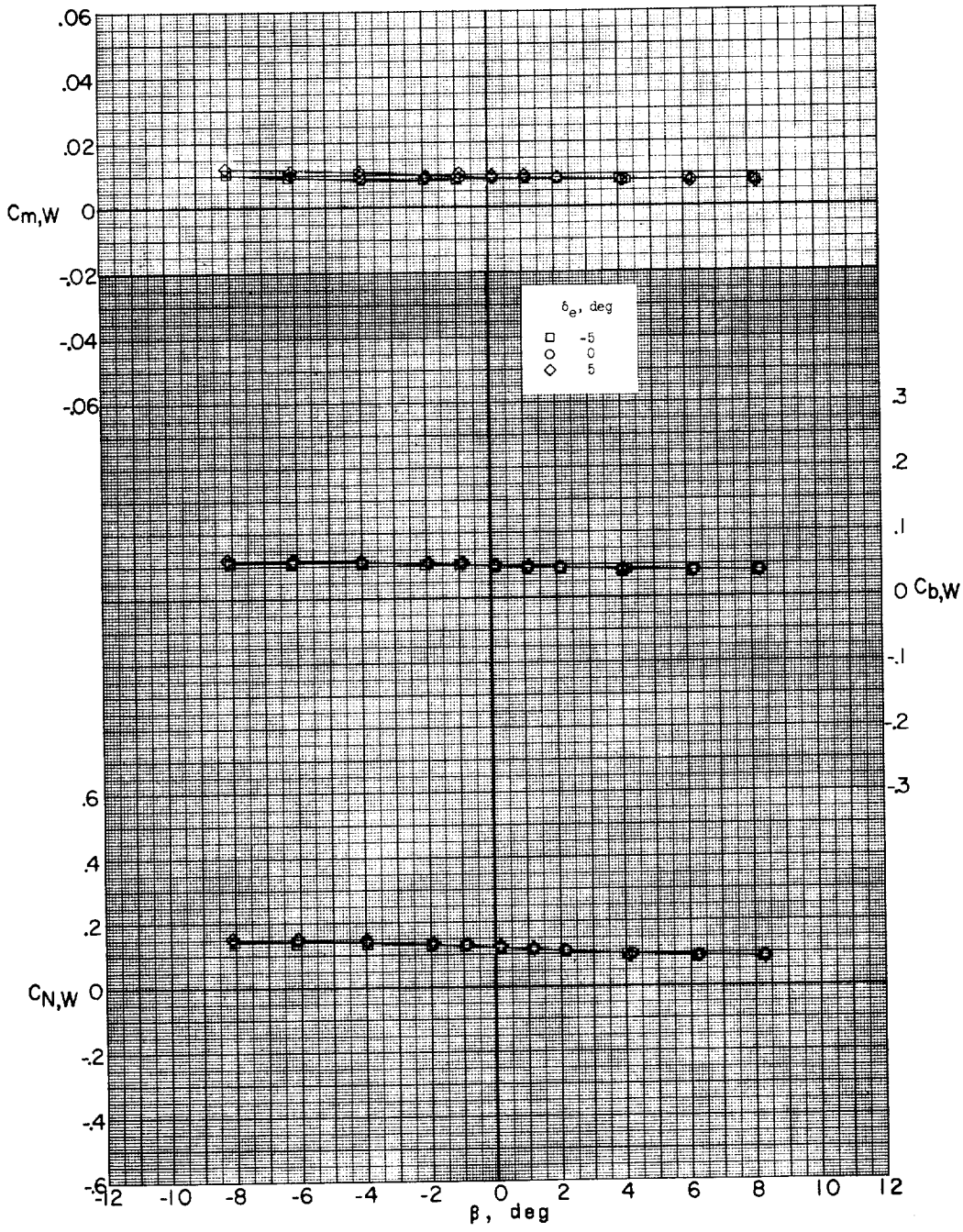
(d) M = 2.75; $\alpha = -5.2^{\circ}$.

Figure 53.- Continued.



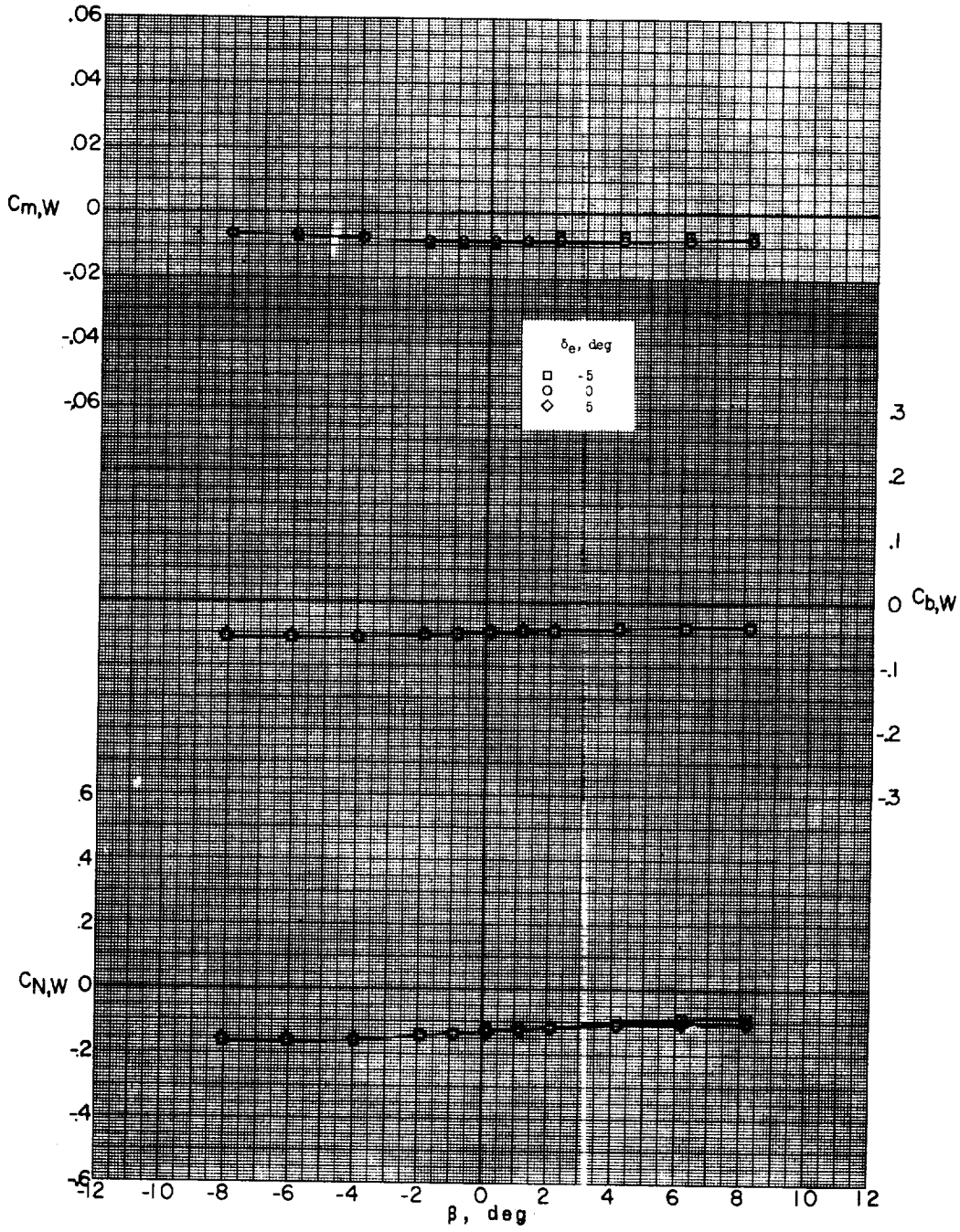
(e) M = 2.75; $\alpha = -0.2^{\circ}$.

Figure 53.- Continued.



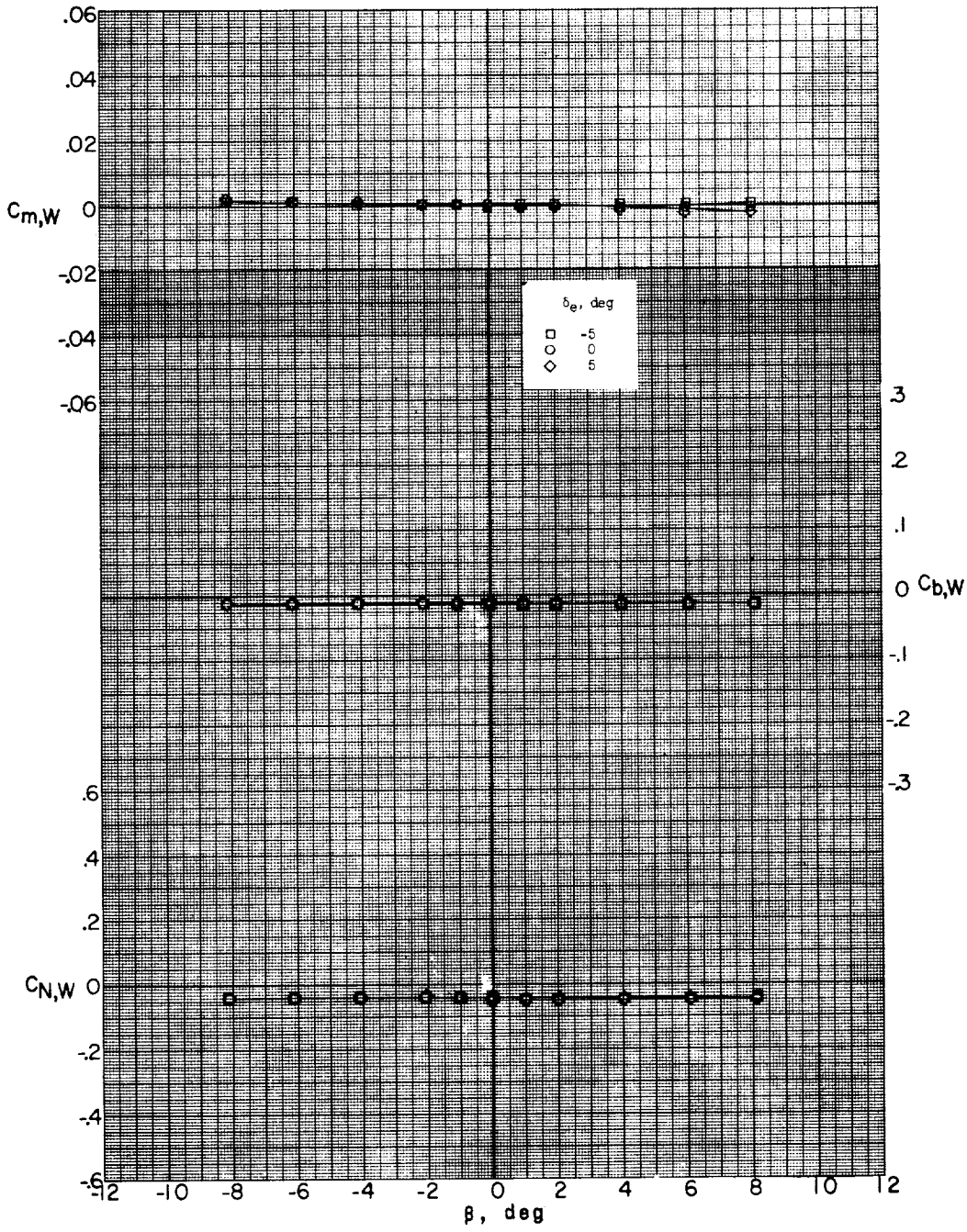
(f) M = 2.75; $\alpha = 5.2^{\circ}$.

Figure 53.- Continued.



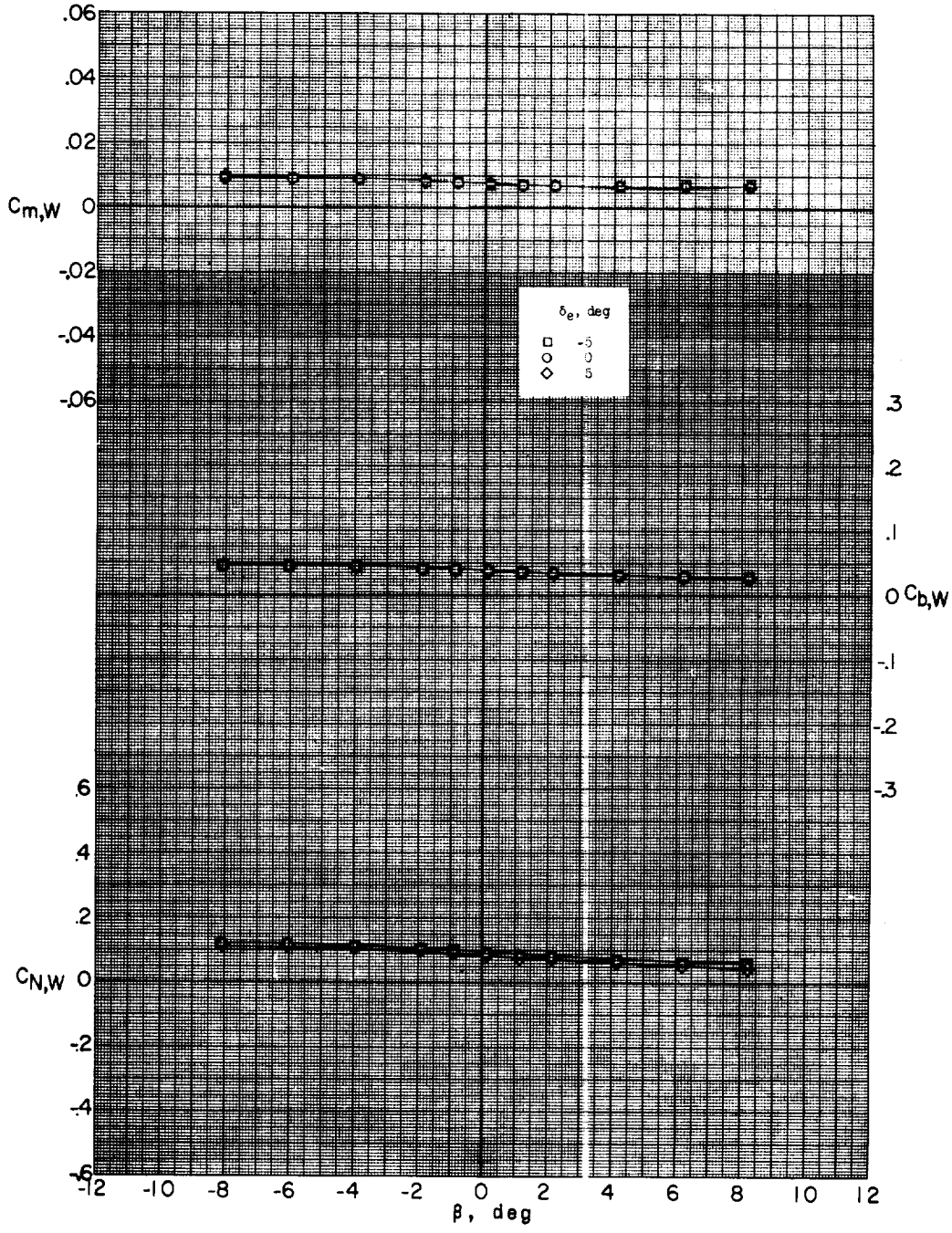
(g) M = 3.22; α = -5.1°.

Figure 53.- Continued.



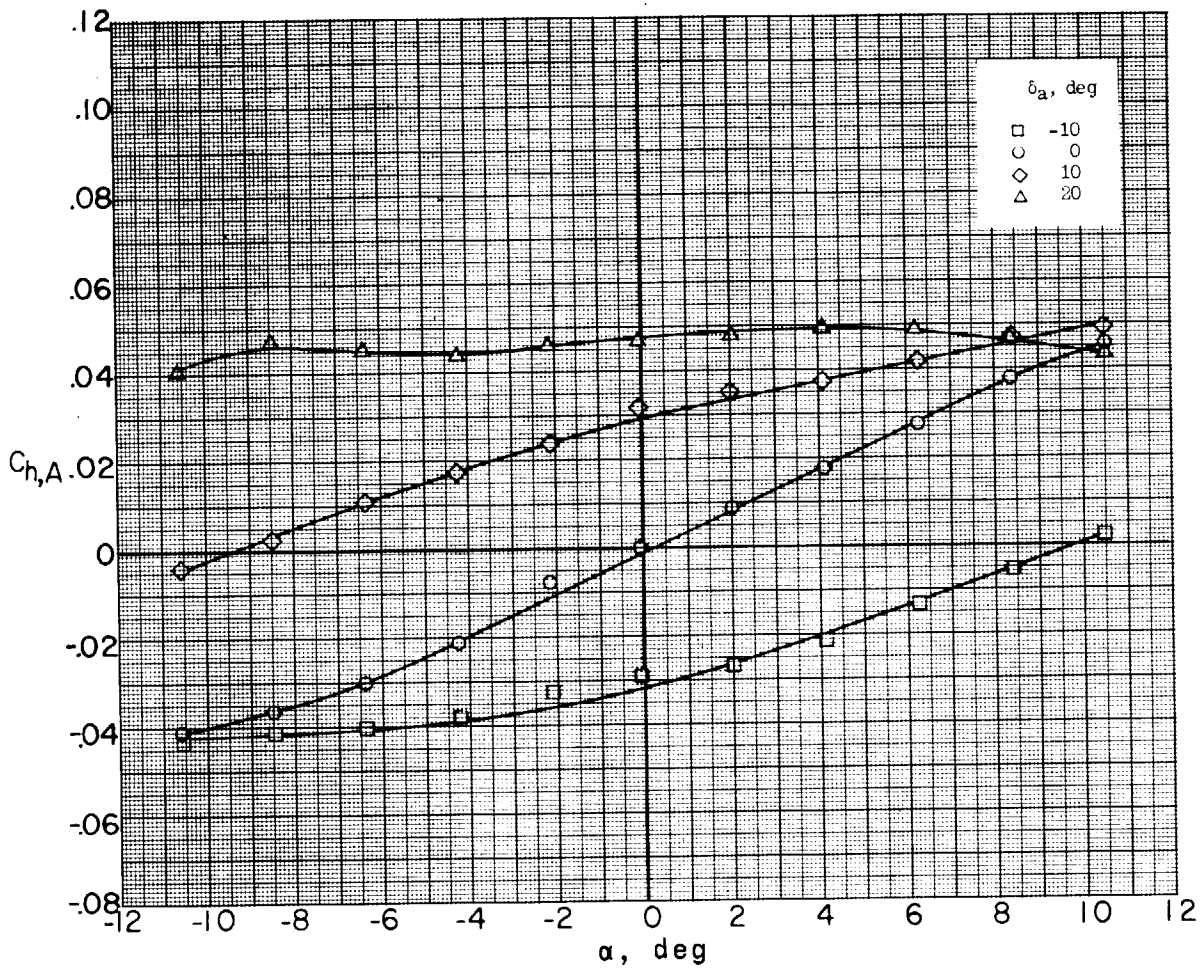
(h) M = 3.22; $\alpha = -0.2^{\circ}$.

Figure 53.- Continued.



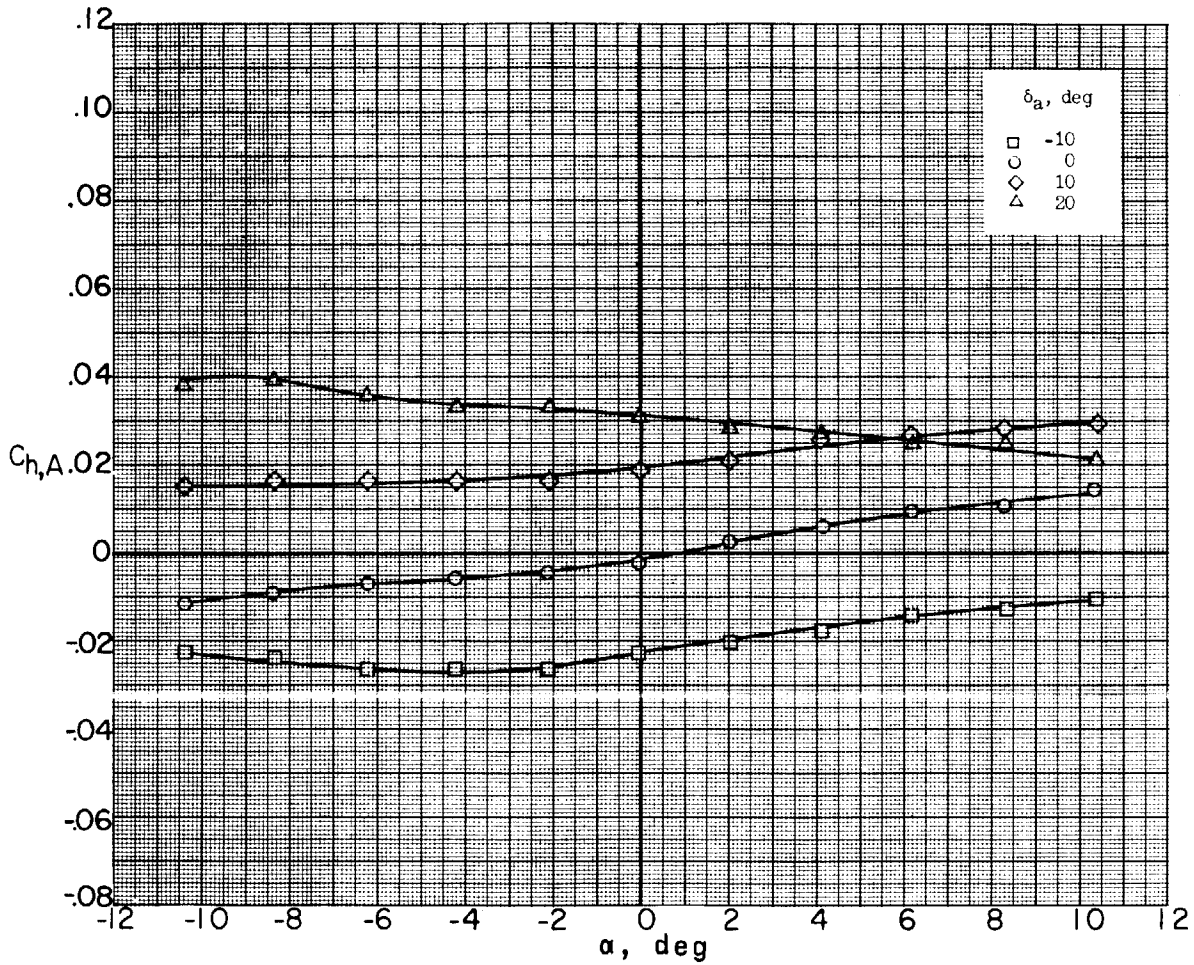
(i) $M = 3.22$; $\alpha = 5.1^{\circ}$.

Figure 53.- Concluded.



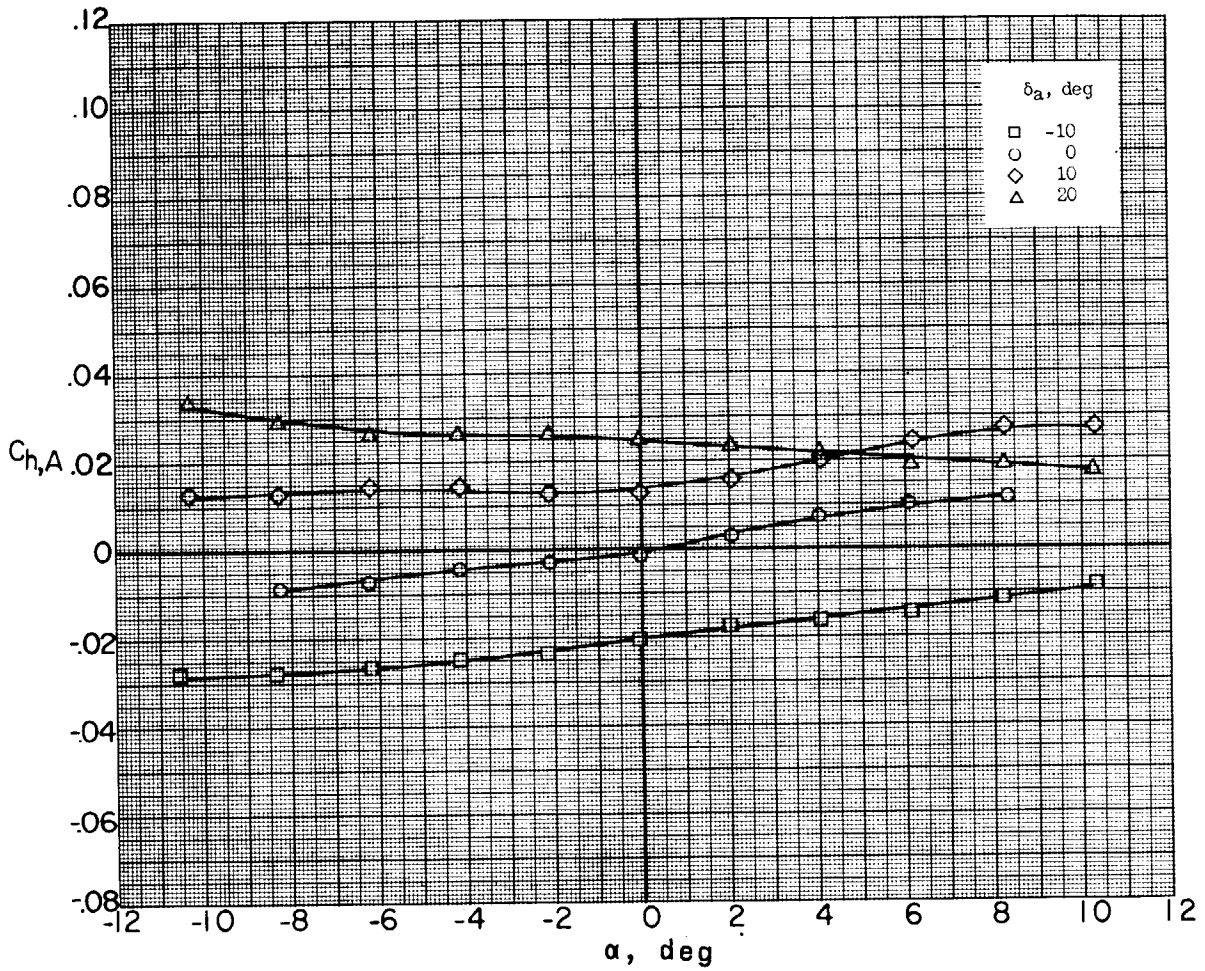
(a) M = 1.77.

Figure 54.- Effect of aileron deflection on aileron hinge-moment characteristics. Missile alone; $\delta_e = 0^o$; $\beta = 0.2^o$; sting A.



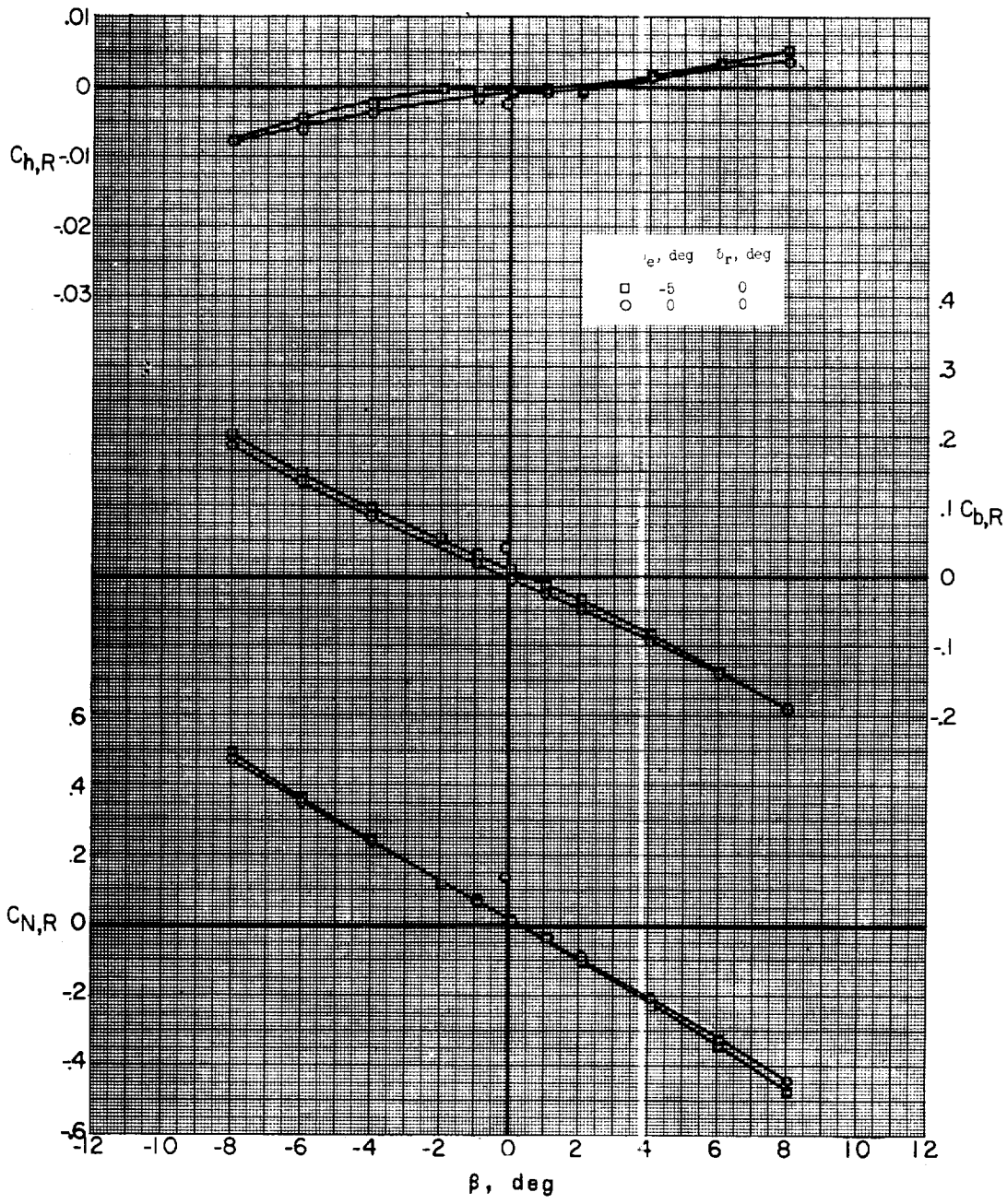
(b) M = 2.75.

Figure 54.- Continued.



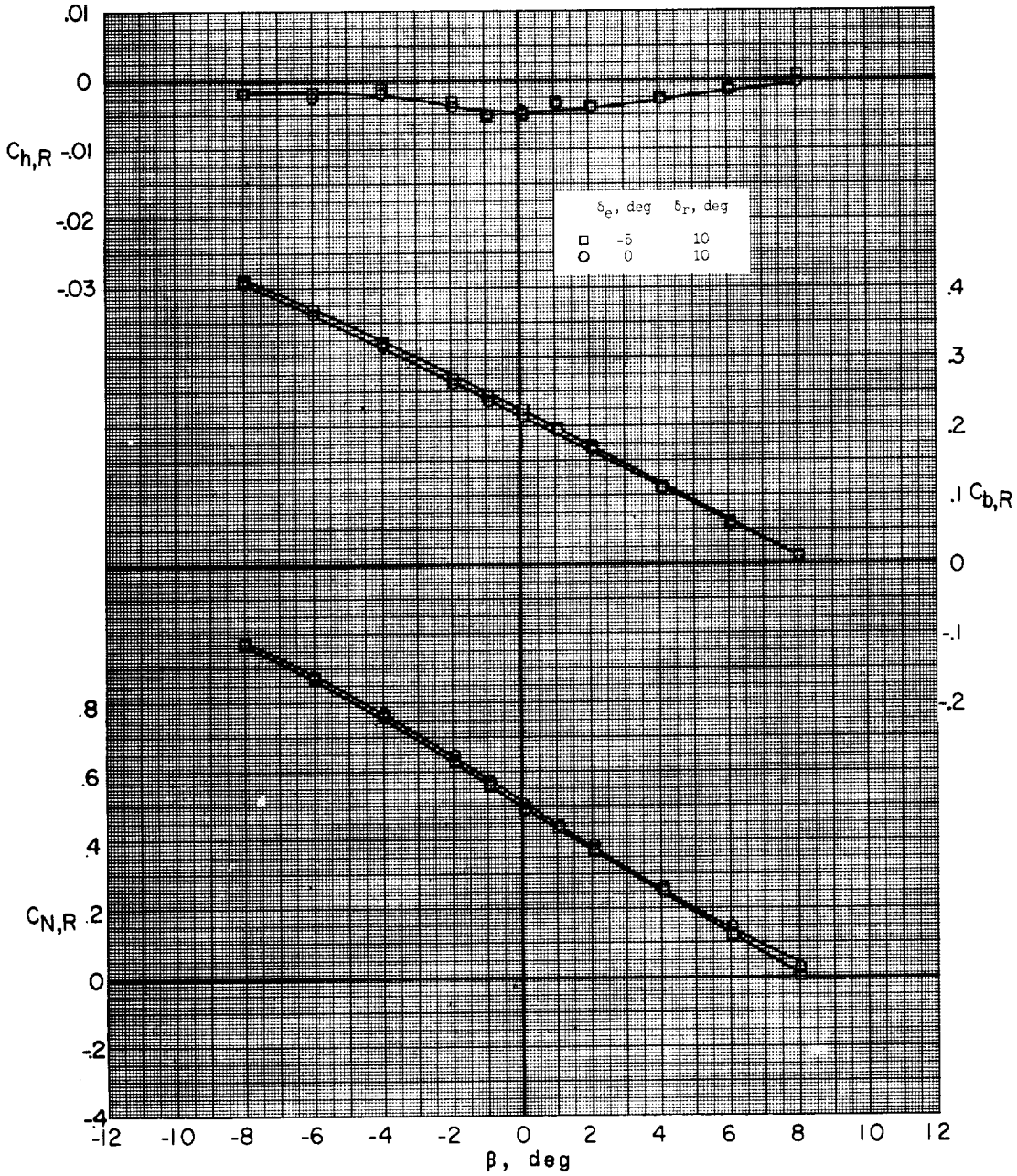
(c) M = 3.22.

Figure 54.- Concluded.



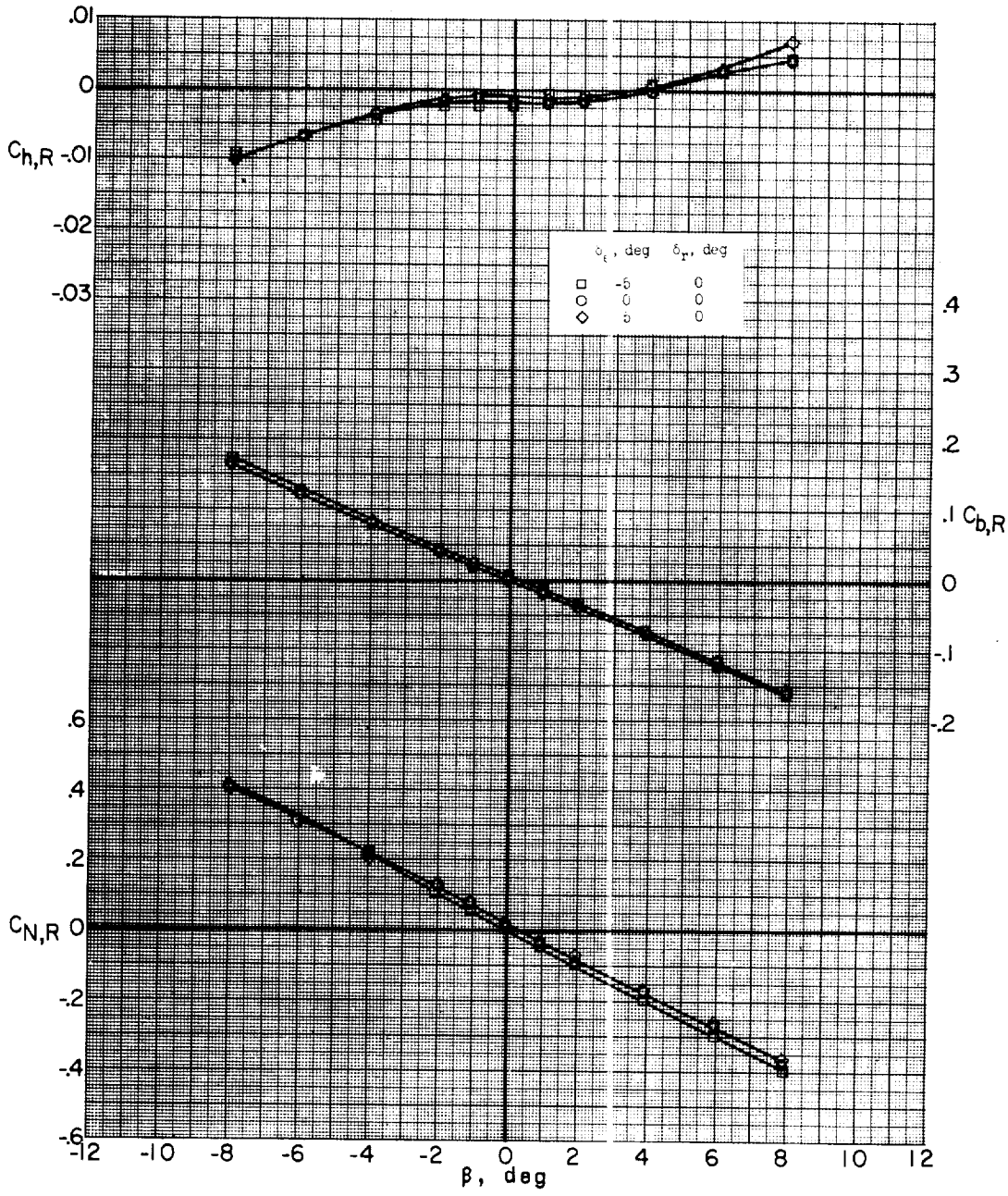
(a) M = 1.77; $\alpha = -5.0^{\circ}$.

Figure 55.- Effect of canard deflection on lateral characteristics of missile rudder at two rudder deflections. Missile alone; sting D.



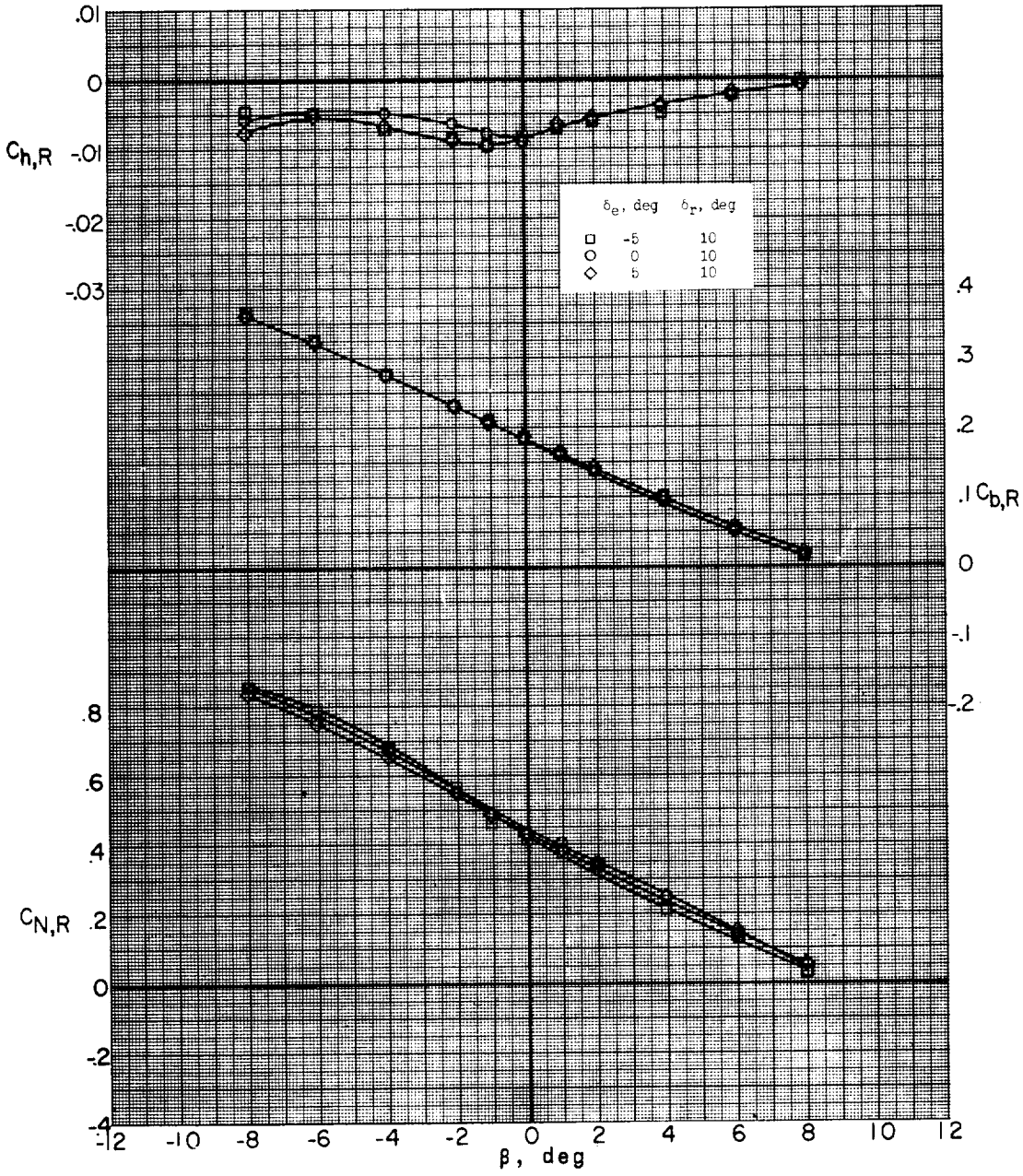
(a) Concluded.

Figure 55.- Continued.



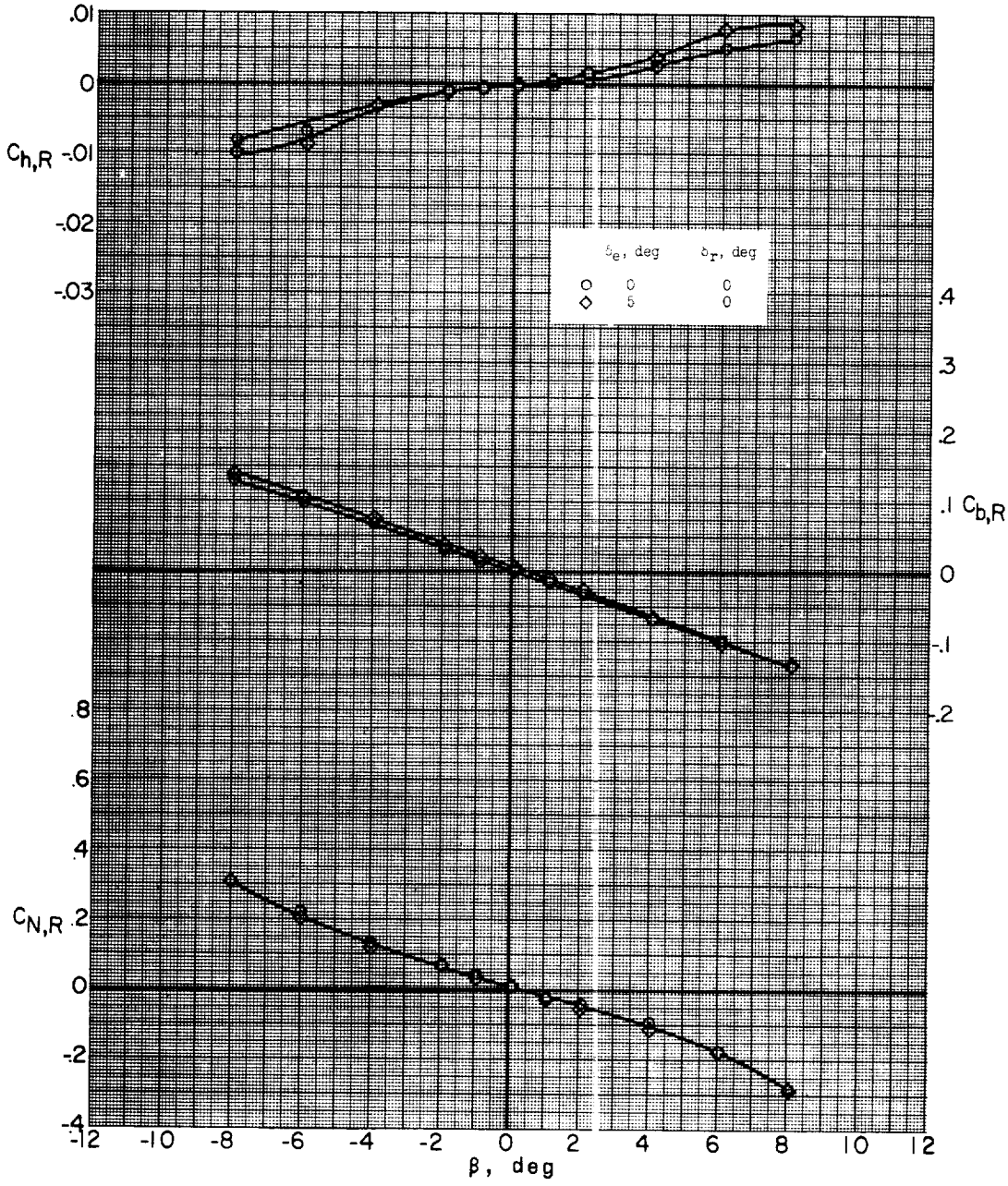
(b) M = 1.77; $\alpha = -0.1^\circ$.

Figure 55.- Continued.



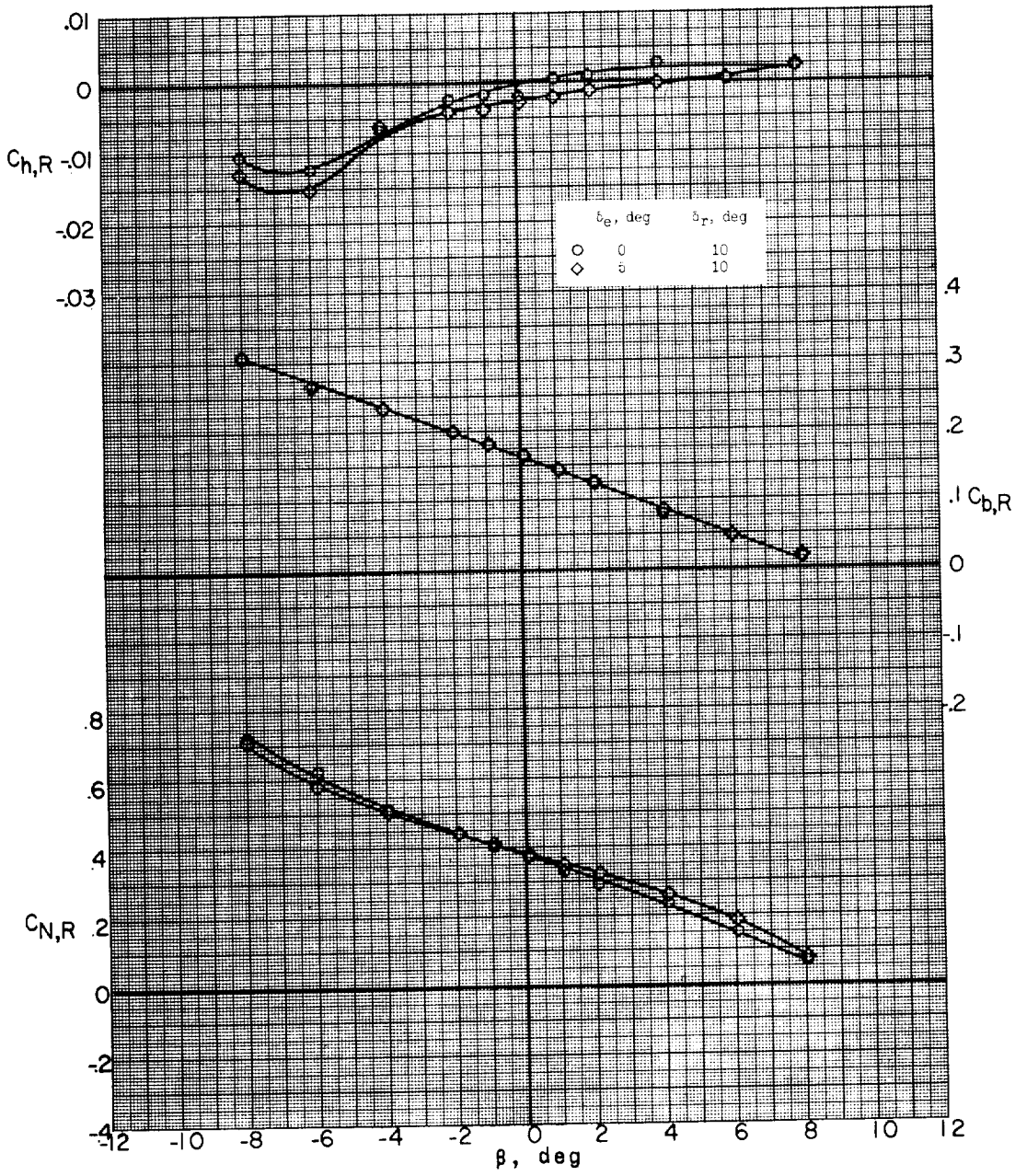
(b) Concluded.

Figure 55.- Continued.



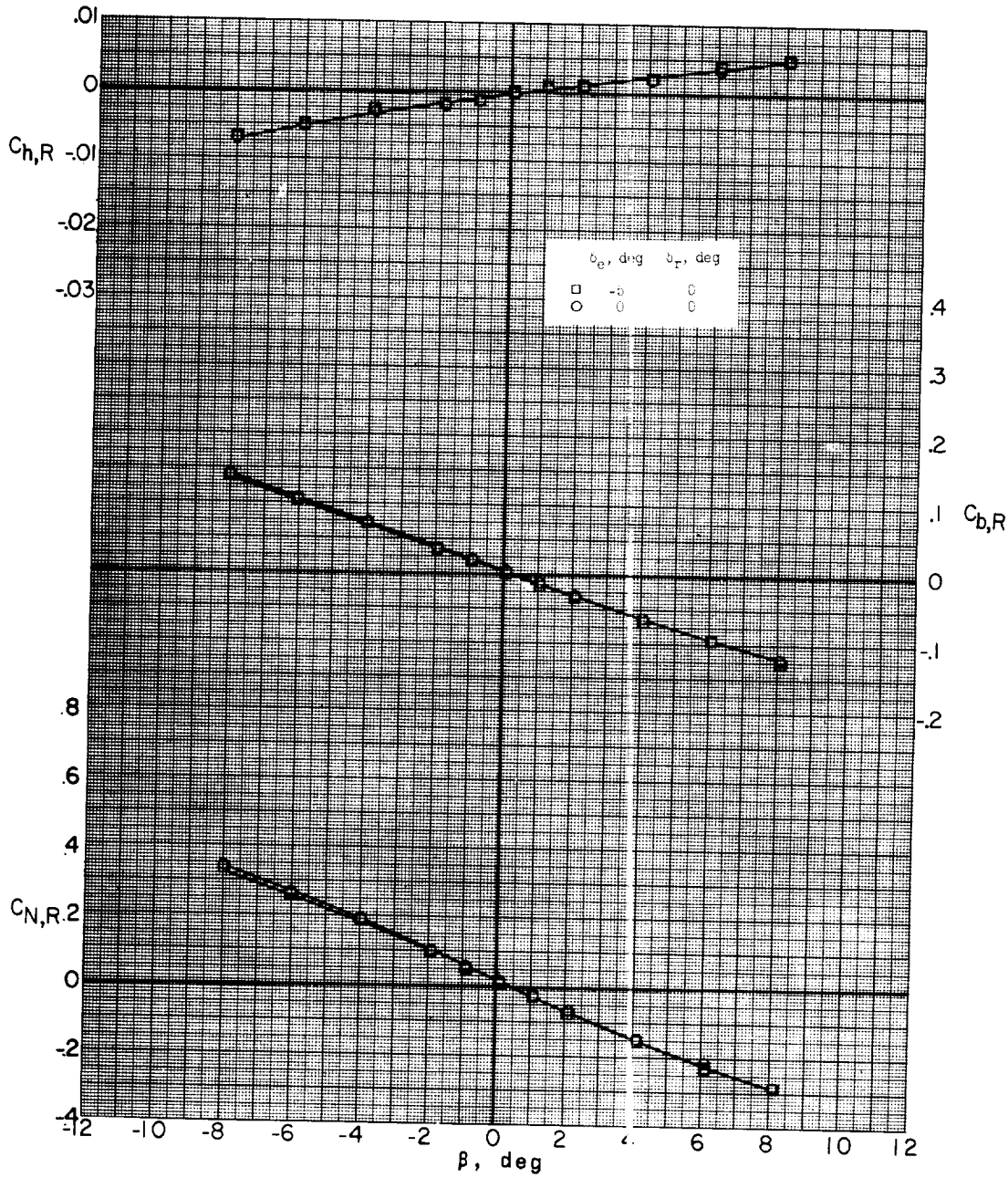
(c) M = 1.77; $\alpha = 5.0^\circ$.

Figure 55.- Continued.



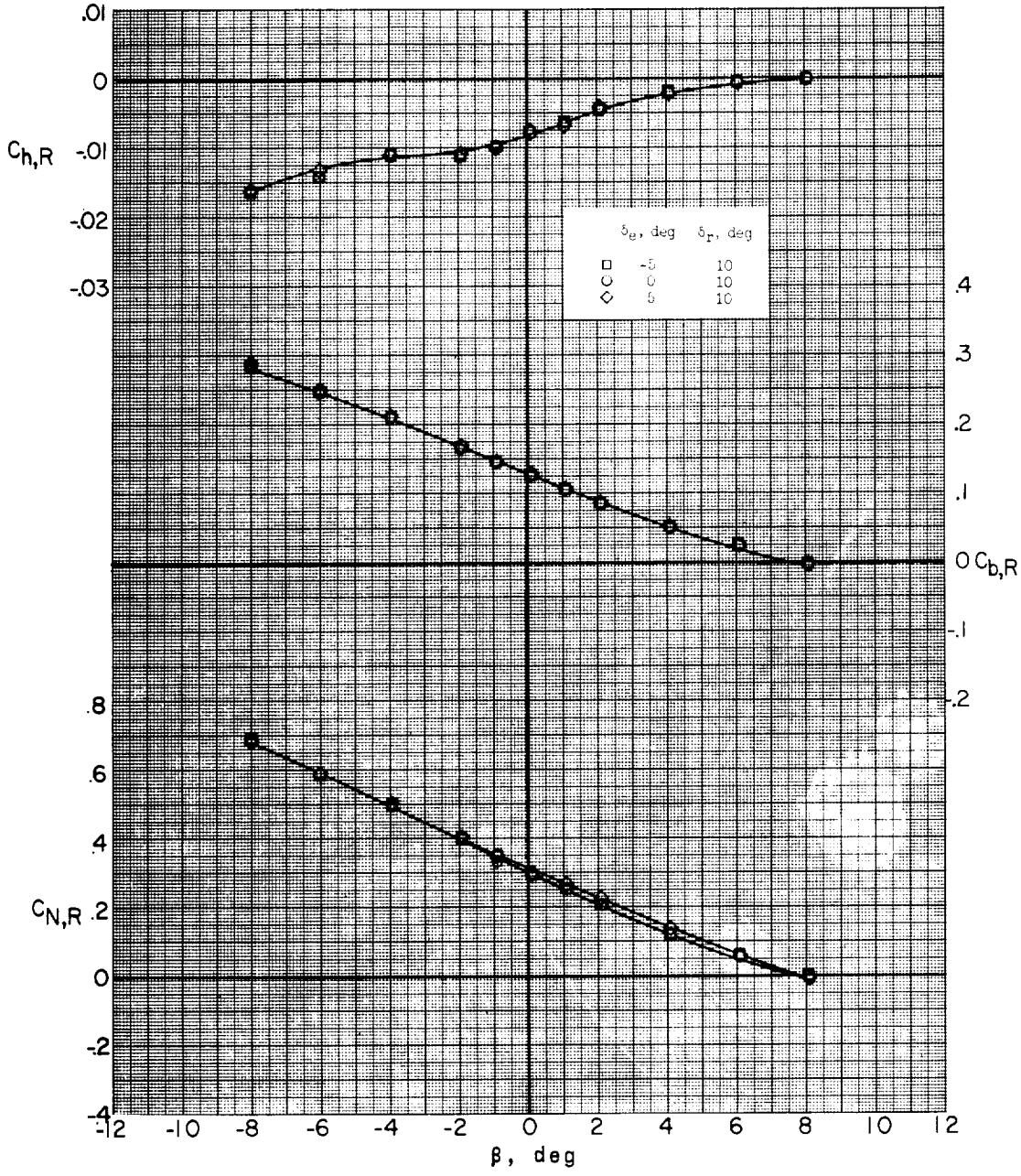
(c) Concluded.

Figure 55.- Continued.



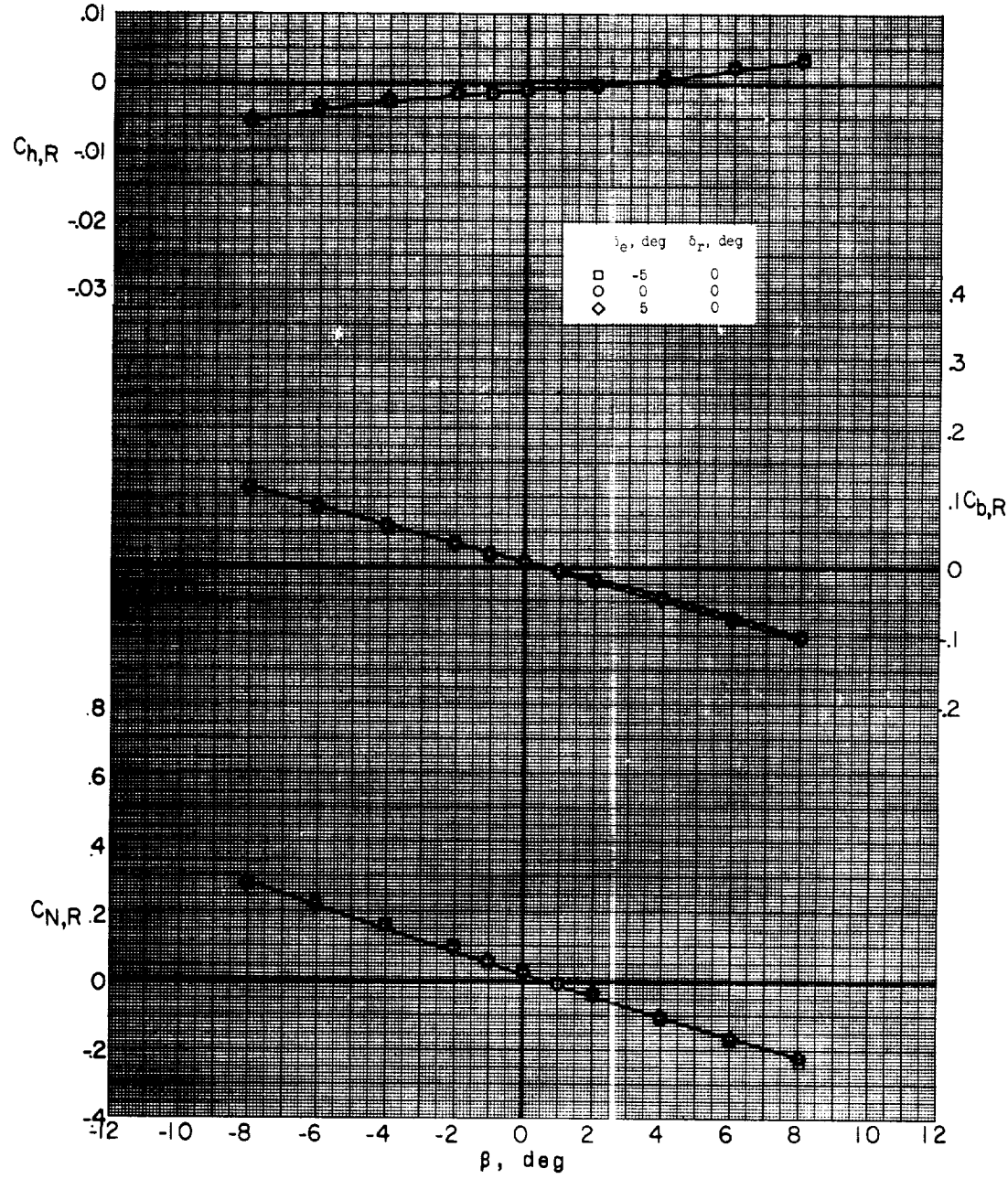
(d) M = 2.75; α = -5.0°.

Figure 55.- Continued.



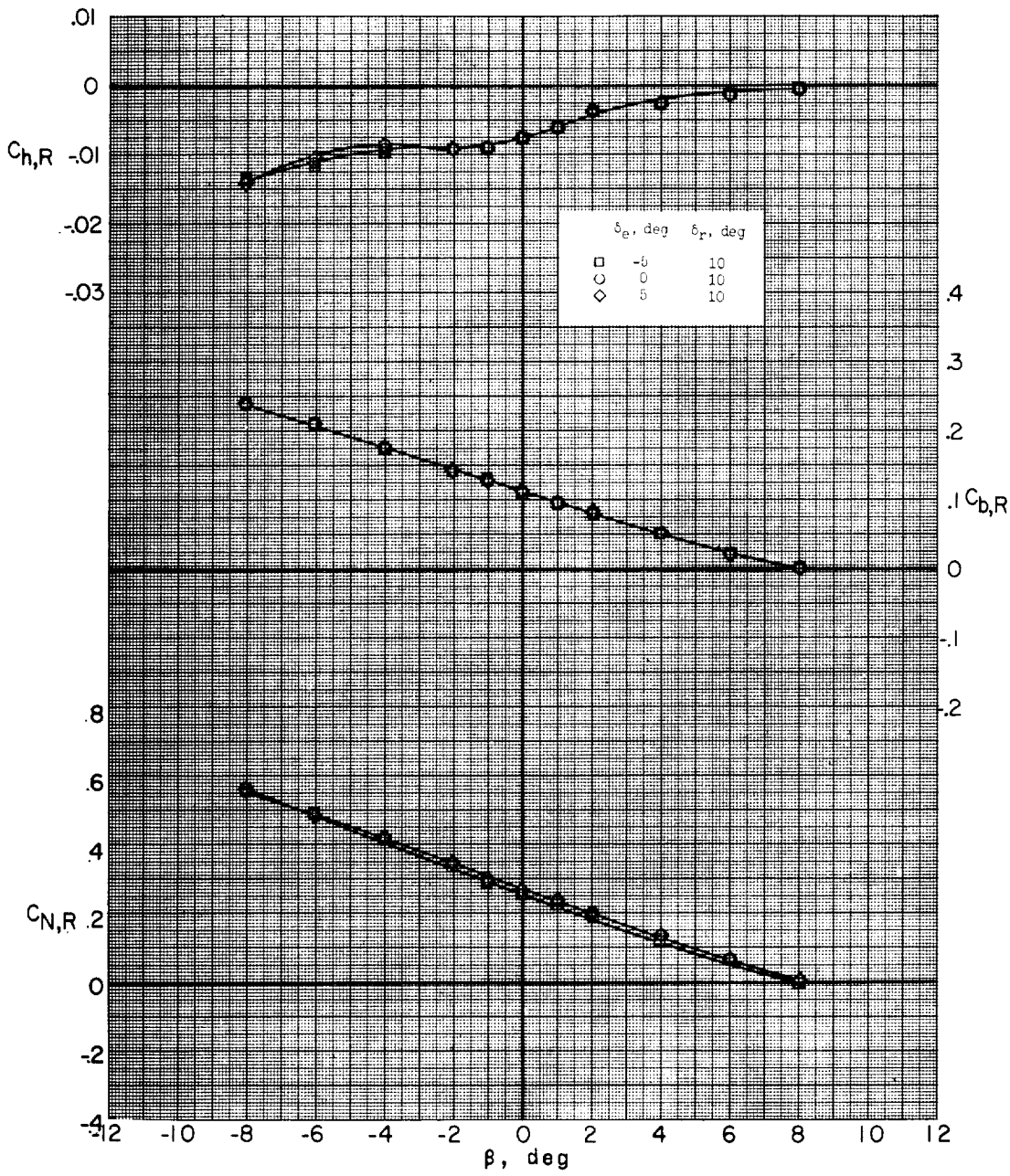
(d) Concluded.

Figure 55.- Continued.



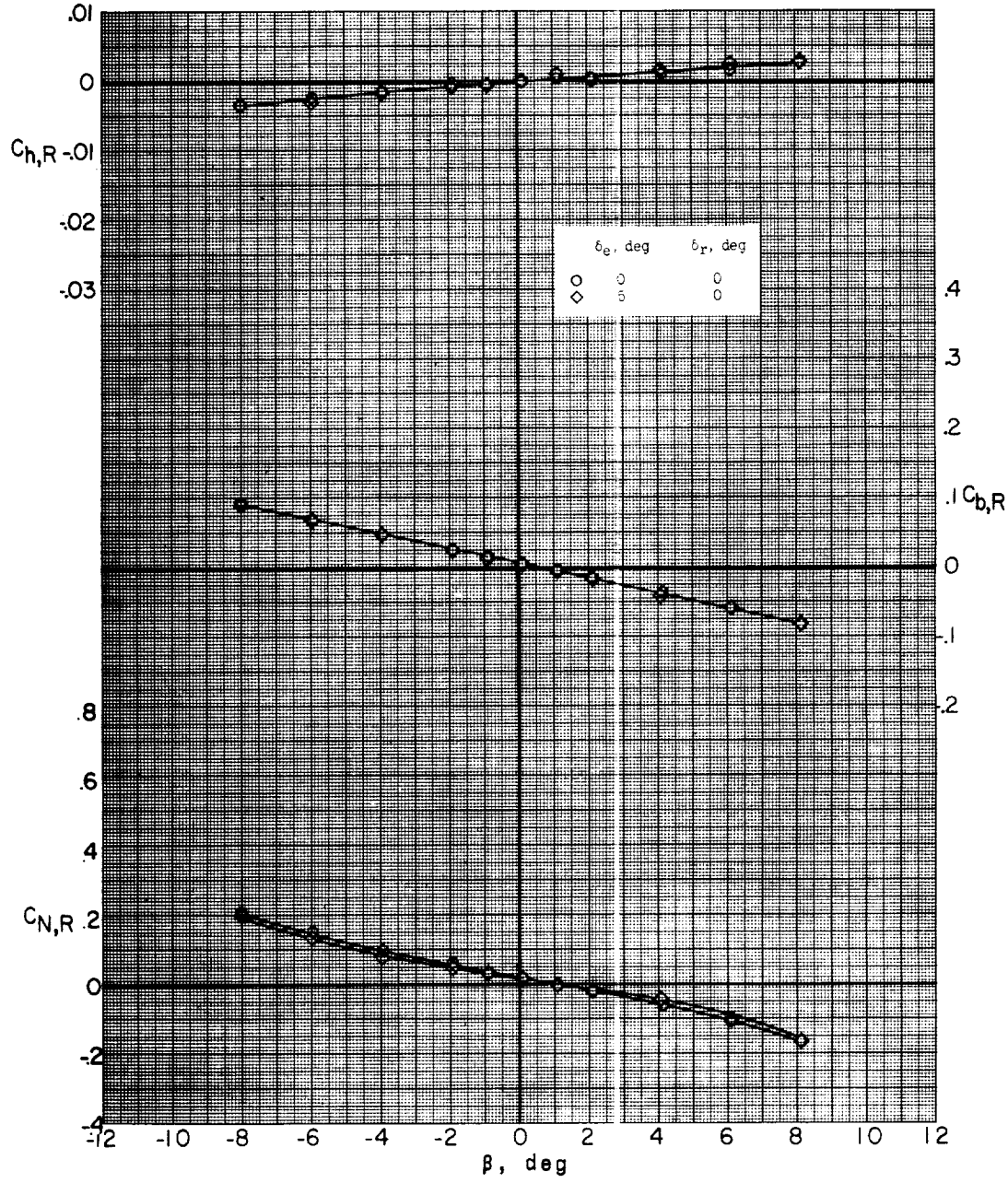
(e) M = 2.75; α = -0.1°.

Figure 55.- Continued.



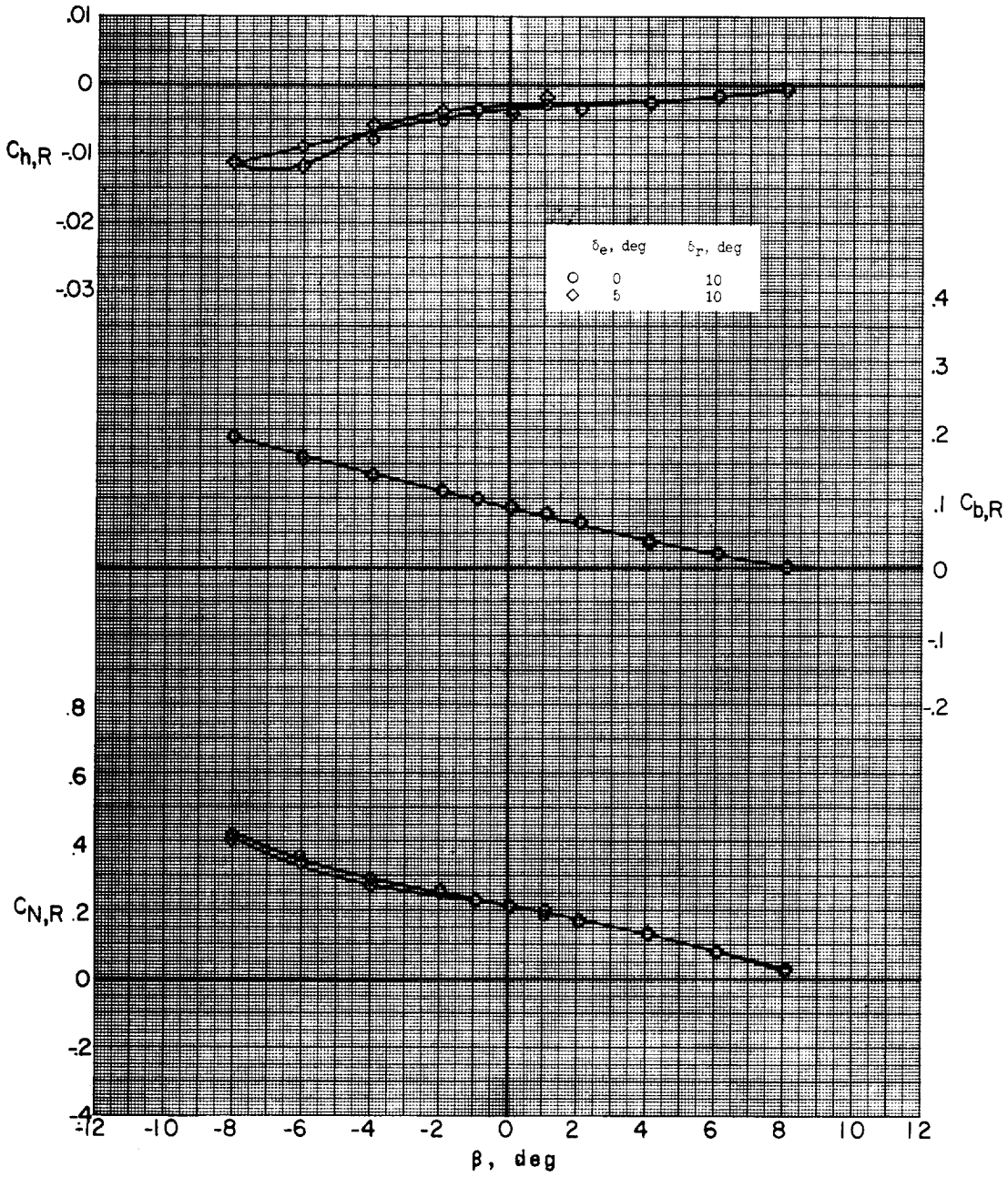
(e) Concluded.

Figure 55.- Continued.



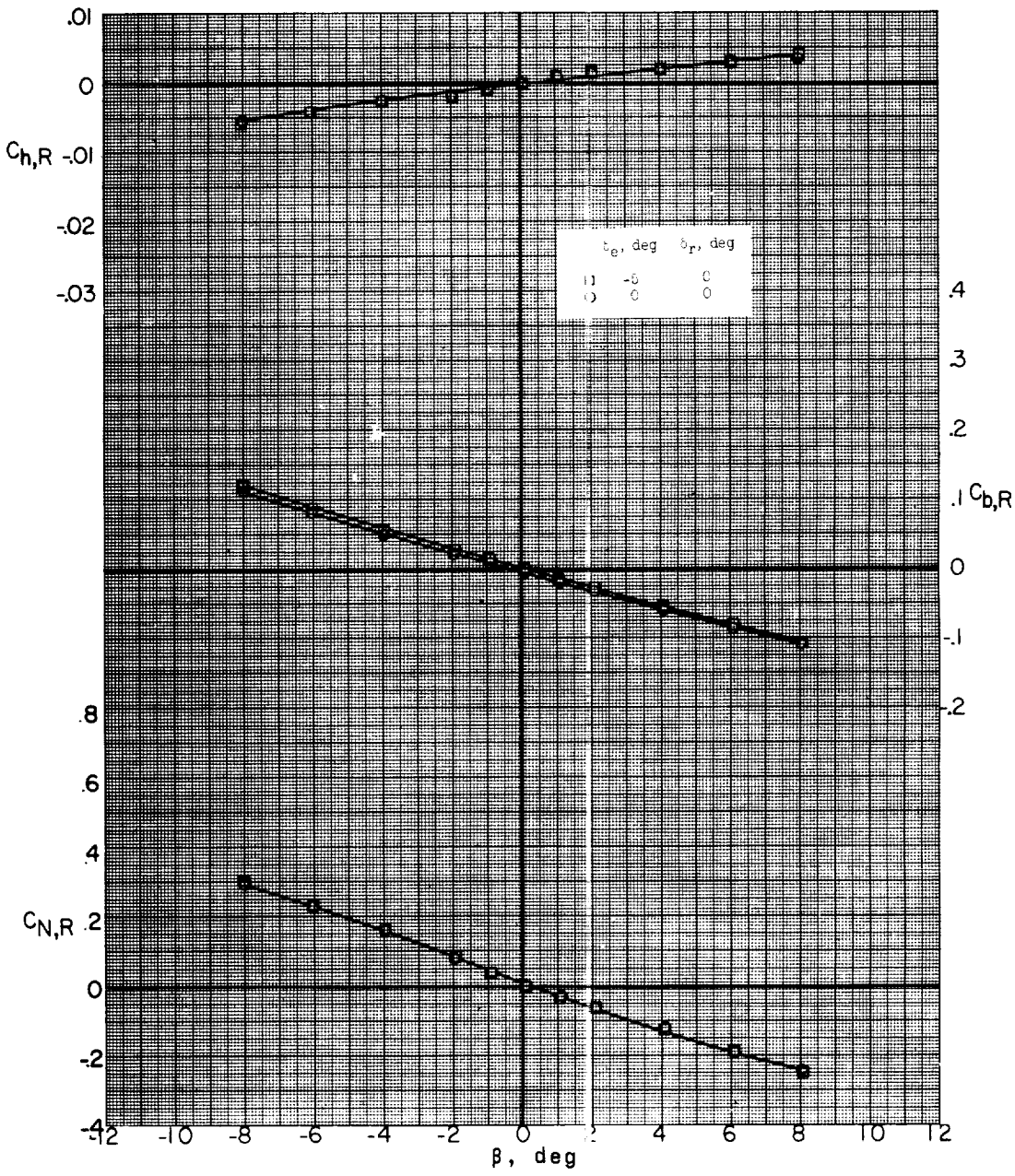
(f) M = 2.75; α = 5.0°.

Figure 55.- Continued.



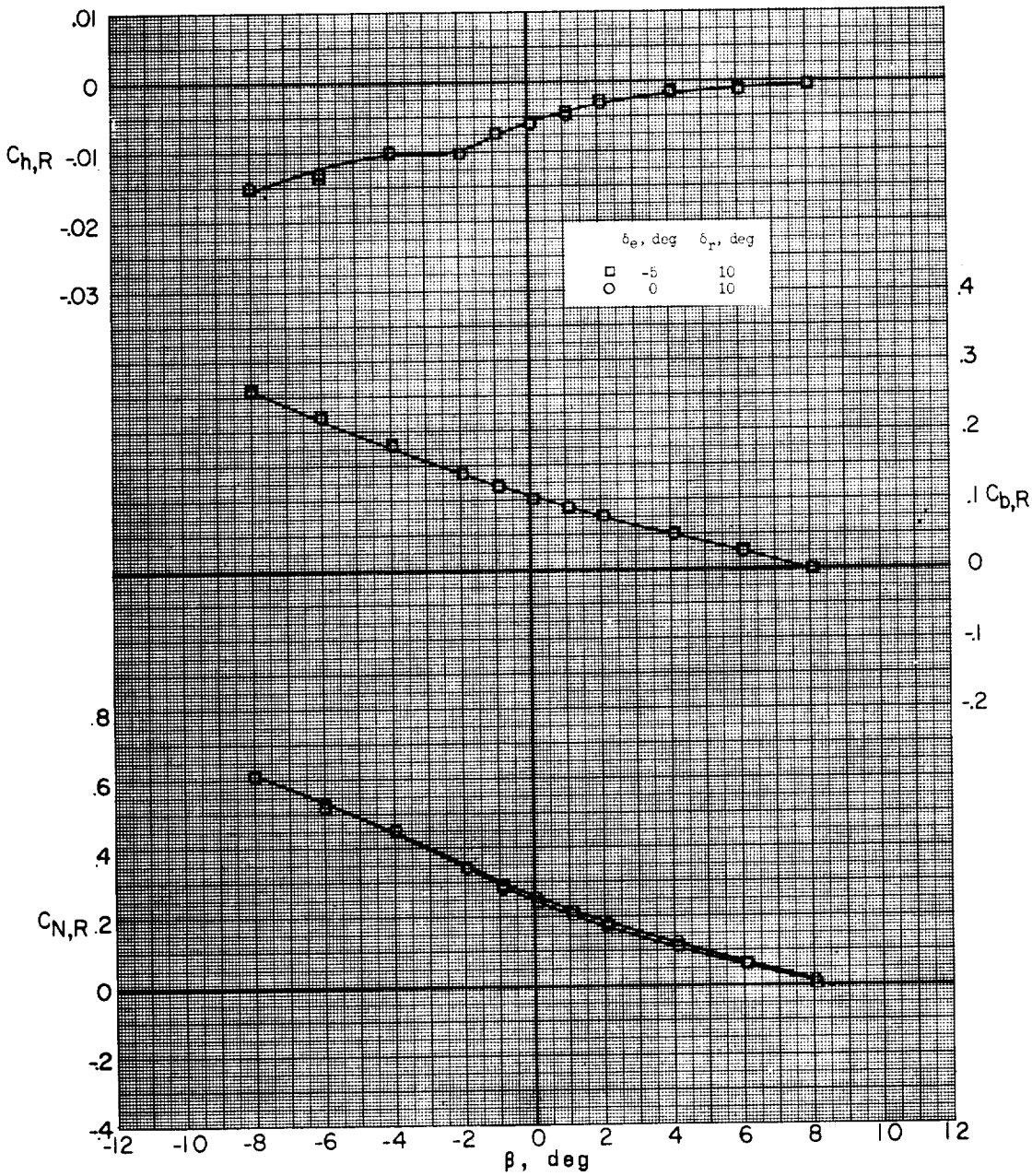
(f) Concluded.

Figure 55.- Continued.



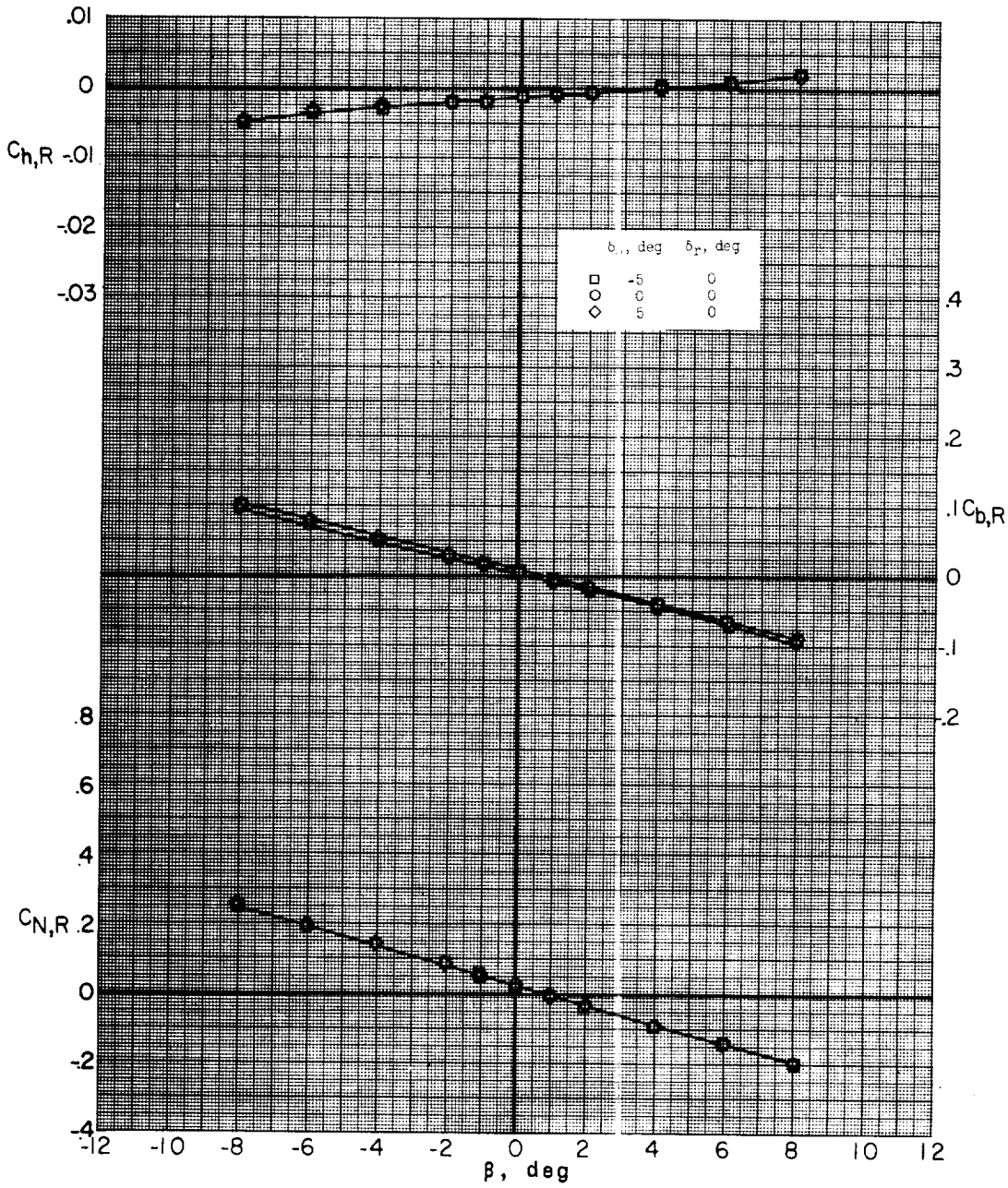
(g) M = 3.22; $\alpha = -5.0^{\circ}$.

Figure 55.- Continued.



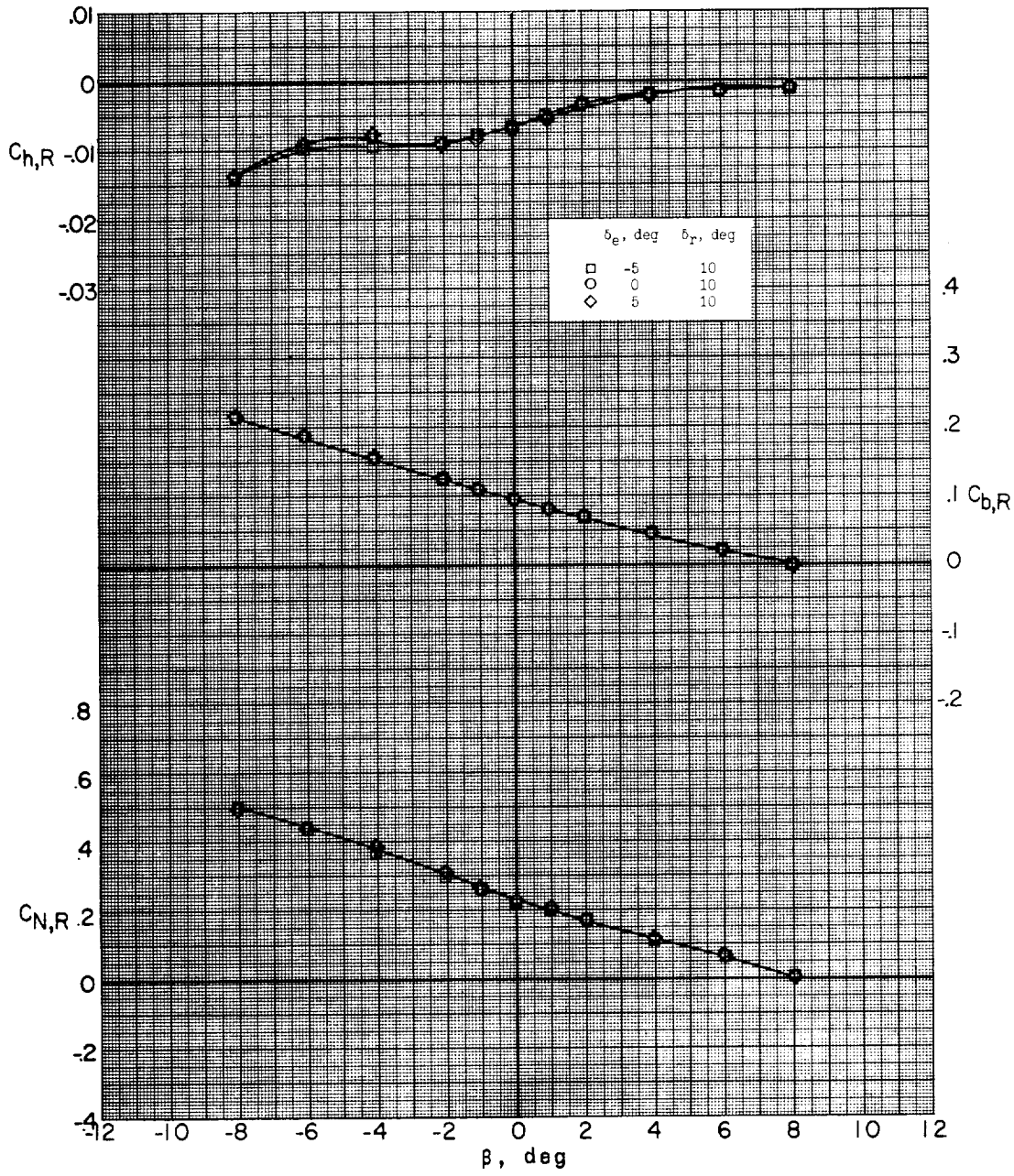
(g) Concluded.

Figure 55.- Continued.



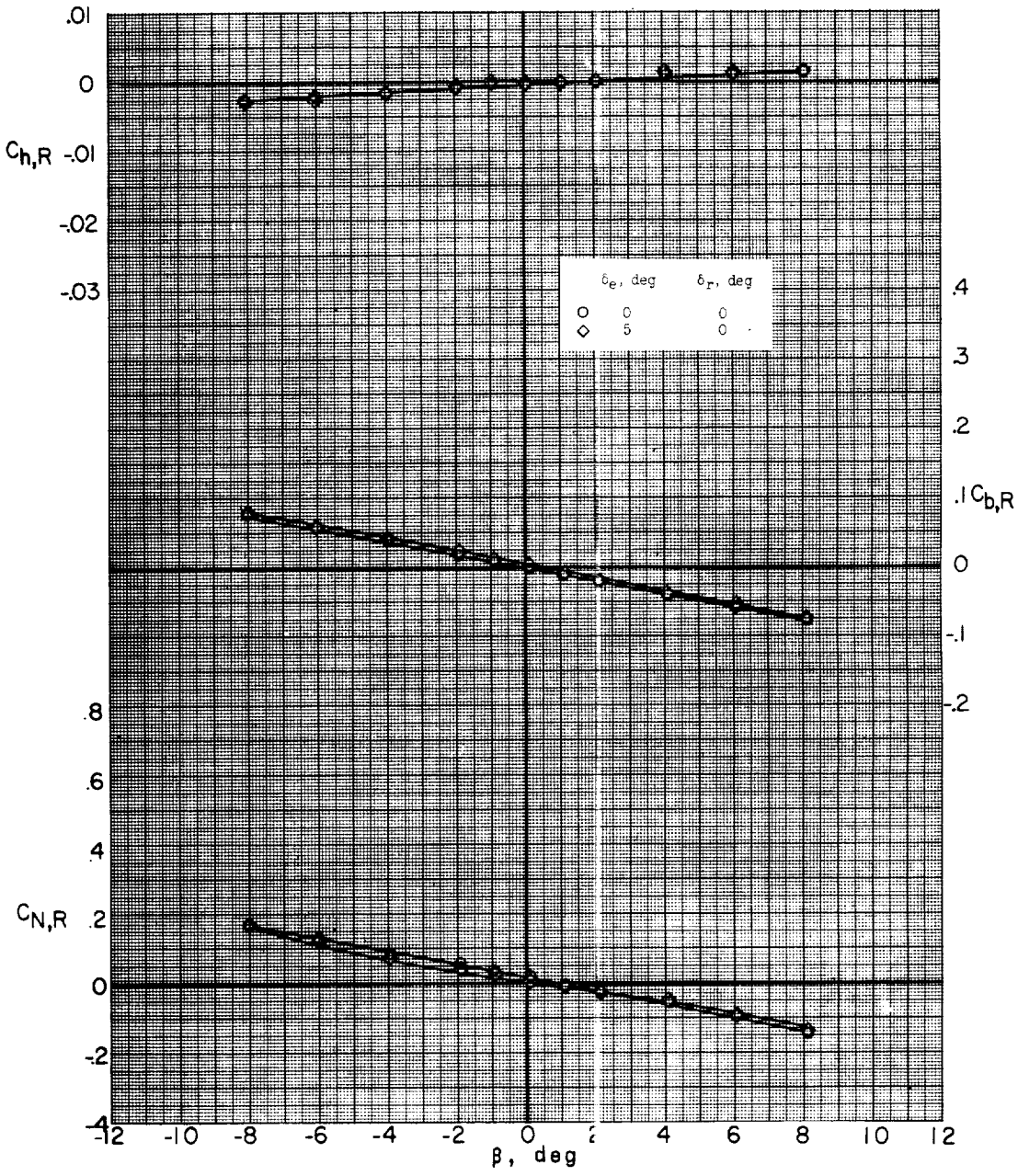
(h) M = 3.22; α = -0.1°.

Figure 55.- Continued.



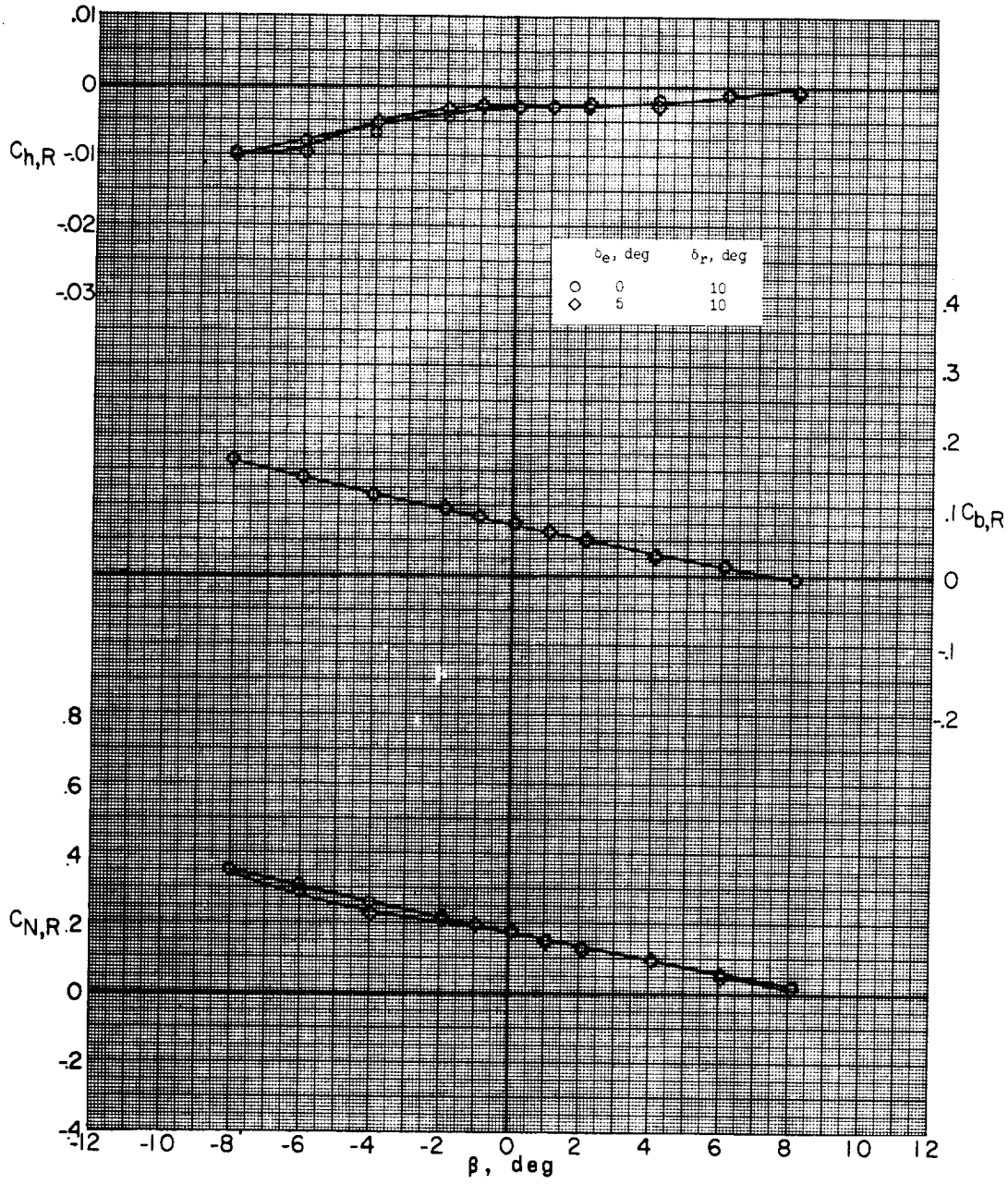
(h) Concluded.

Figure 55.- Continued.



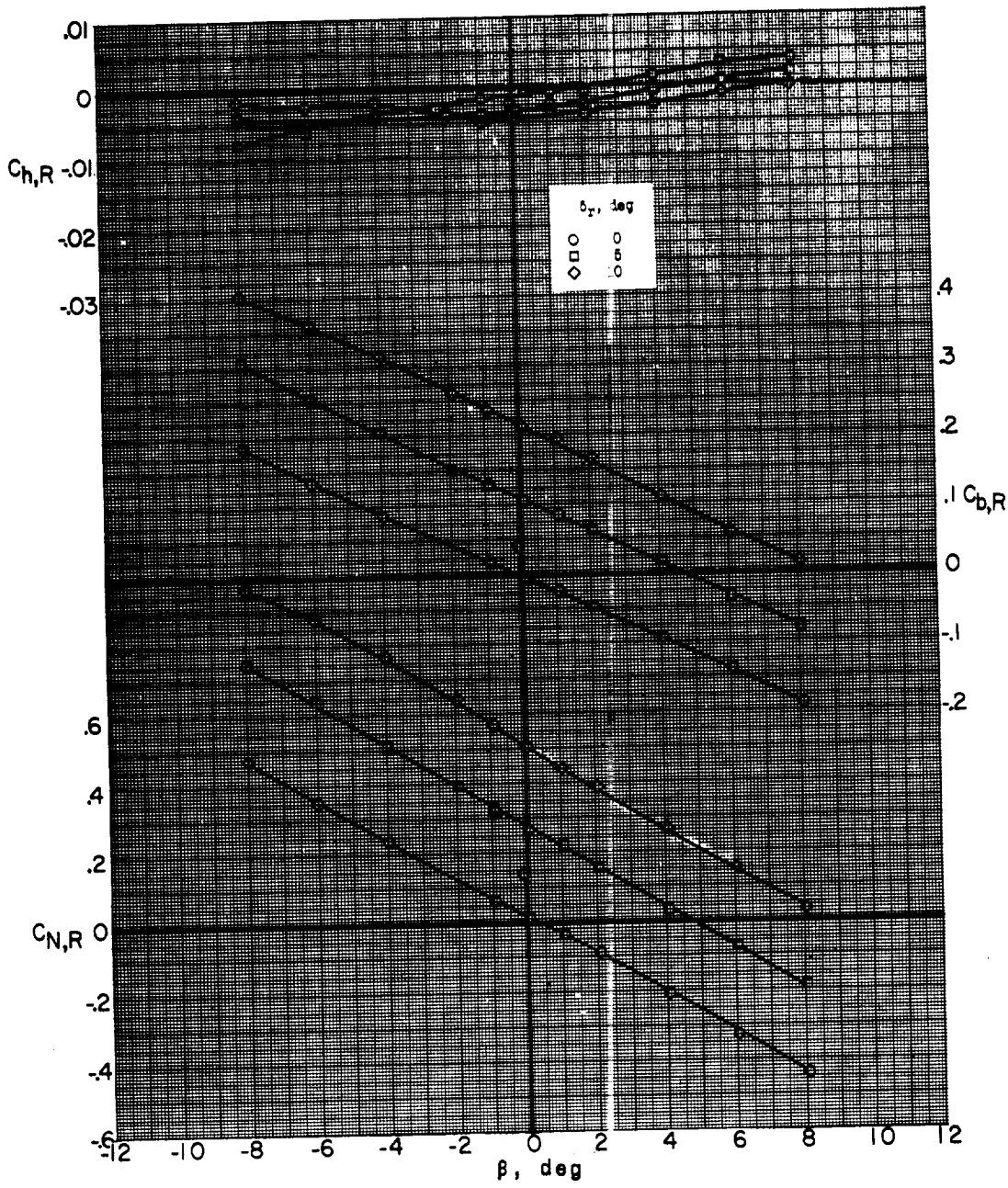
(i) M = 3.22; α = 5.0°.

Figure 55.- Continued.



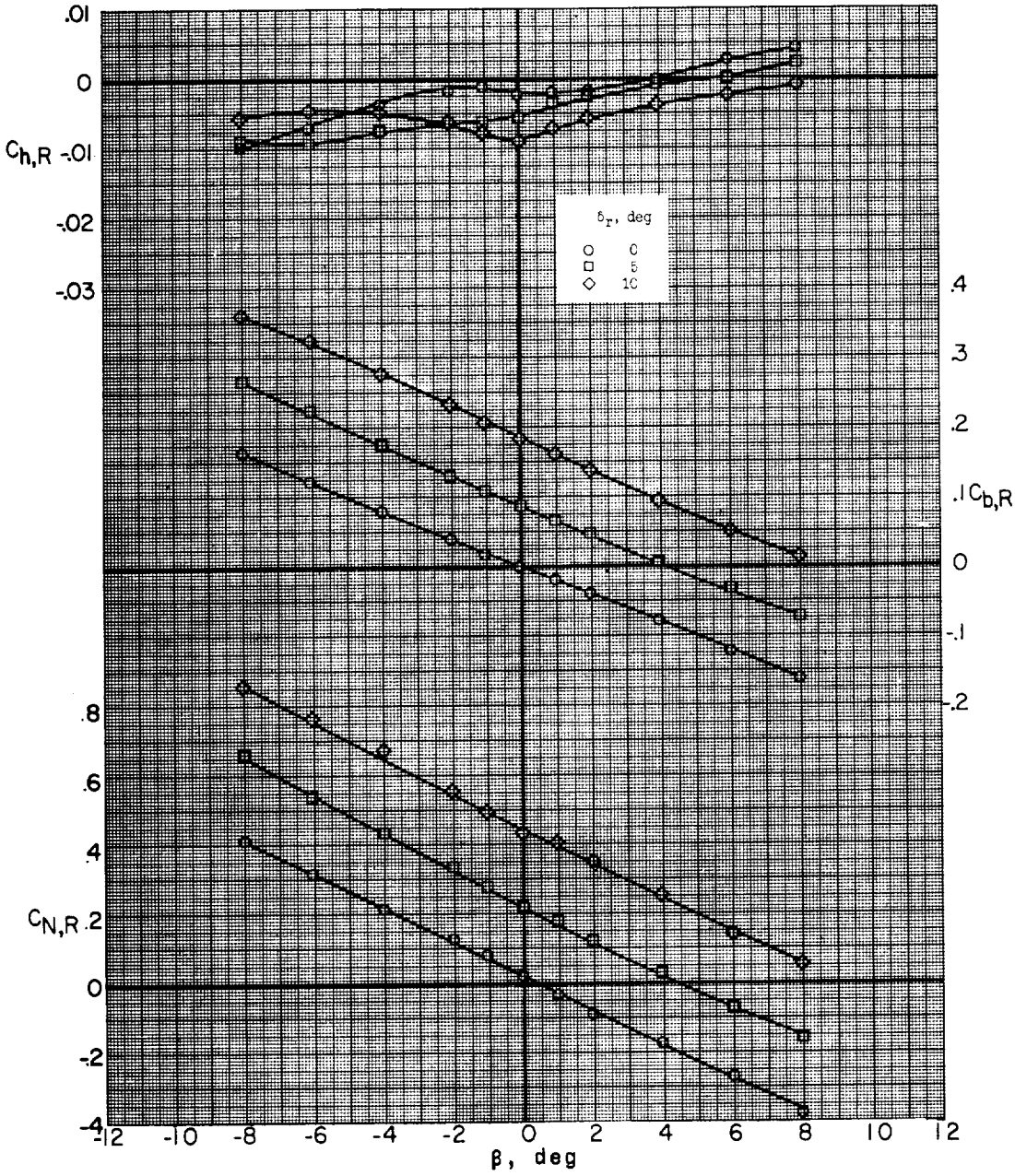
(i) Concluded.

Figure 55.- Concluded.



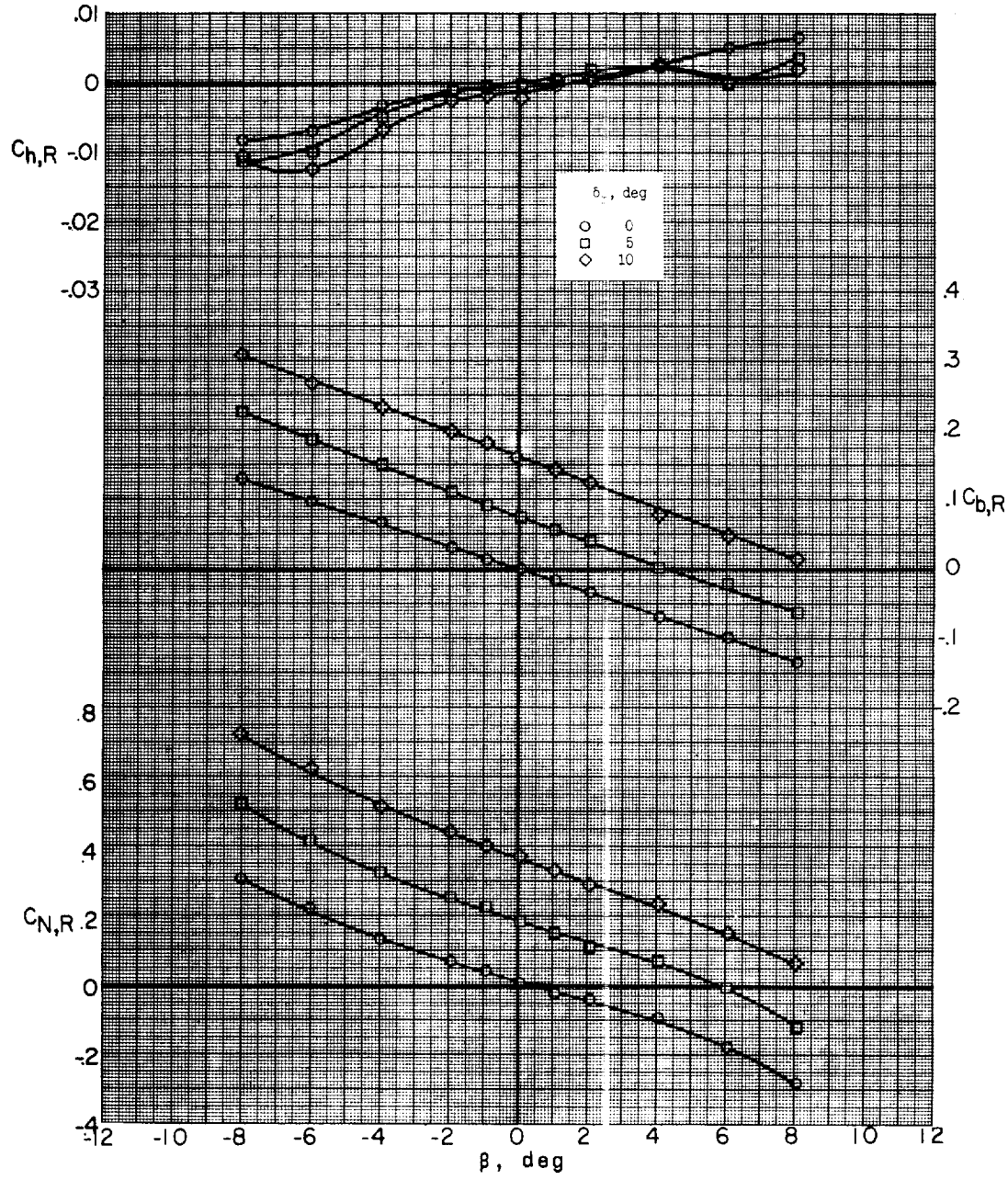
(a) M = 1.77; $\alpha = -5.0^{\circ}$.

Figure 56.- Effect of rudder deflection on lateral characteristics of missile rudder. Missile alone; sting D.



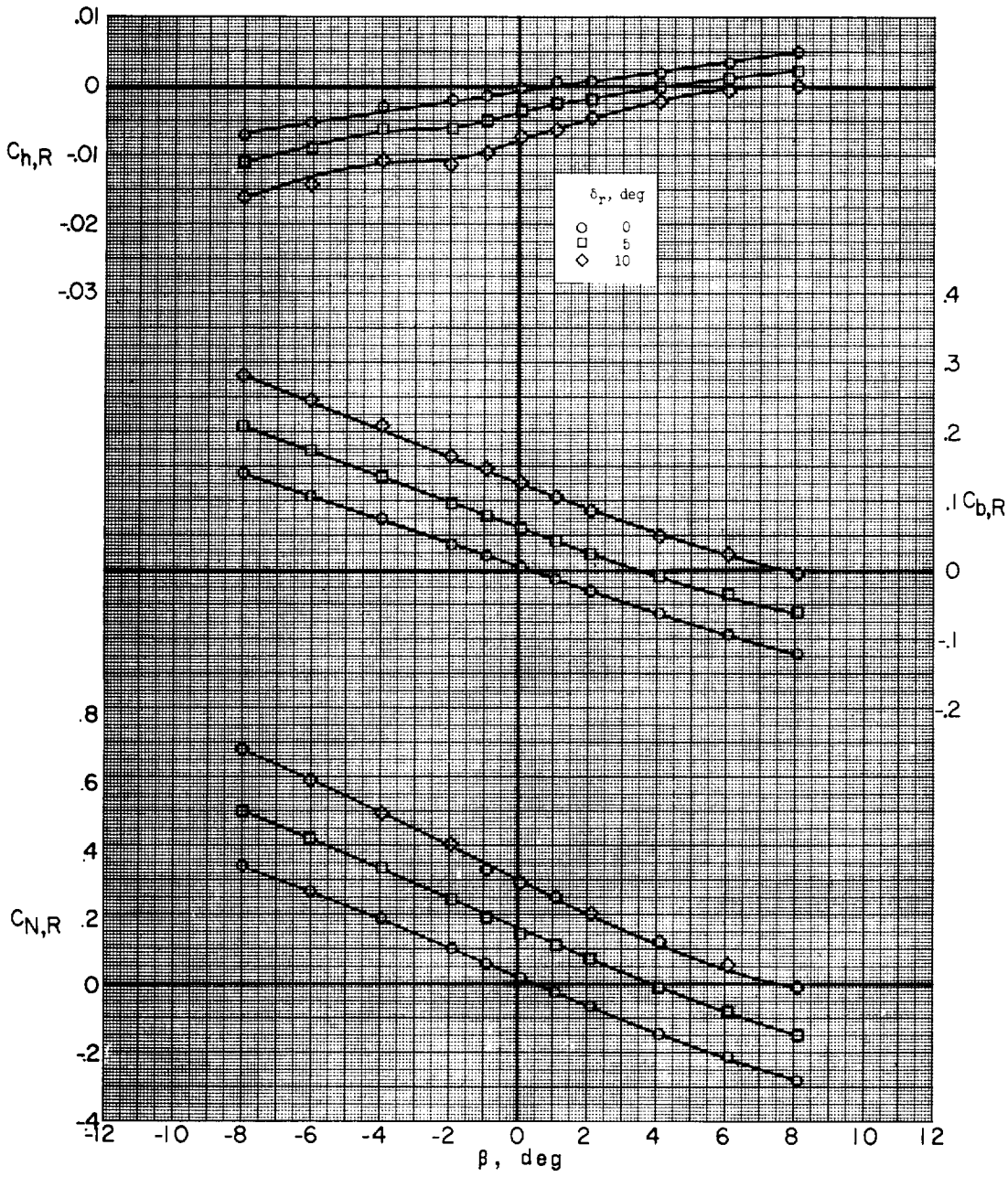
(b) M = 1.77; $\alpha = -0.2^{\circ}$.

Figure 56.- Continued.



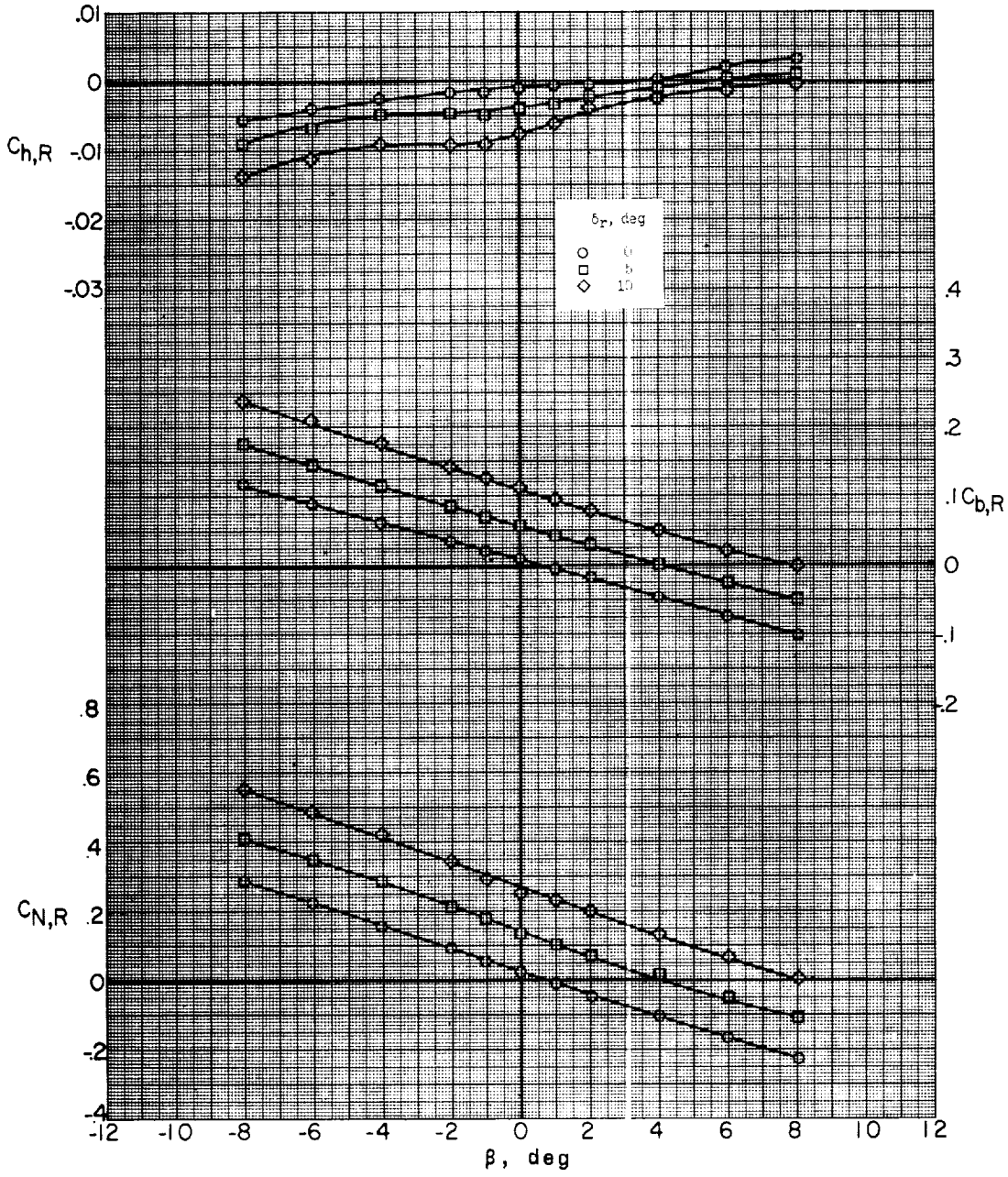
(c) M = 1.77; $\alpha = 5.0^{\circ}$.

Figure 56.- Continued.



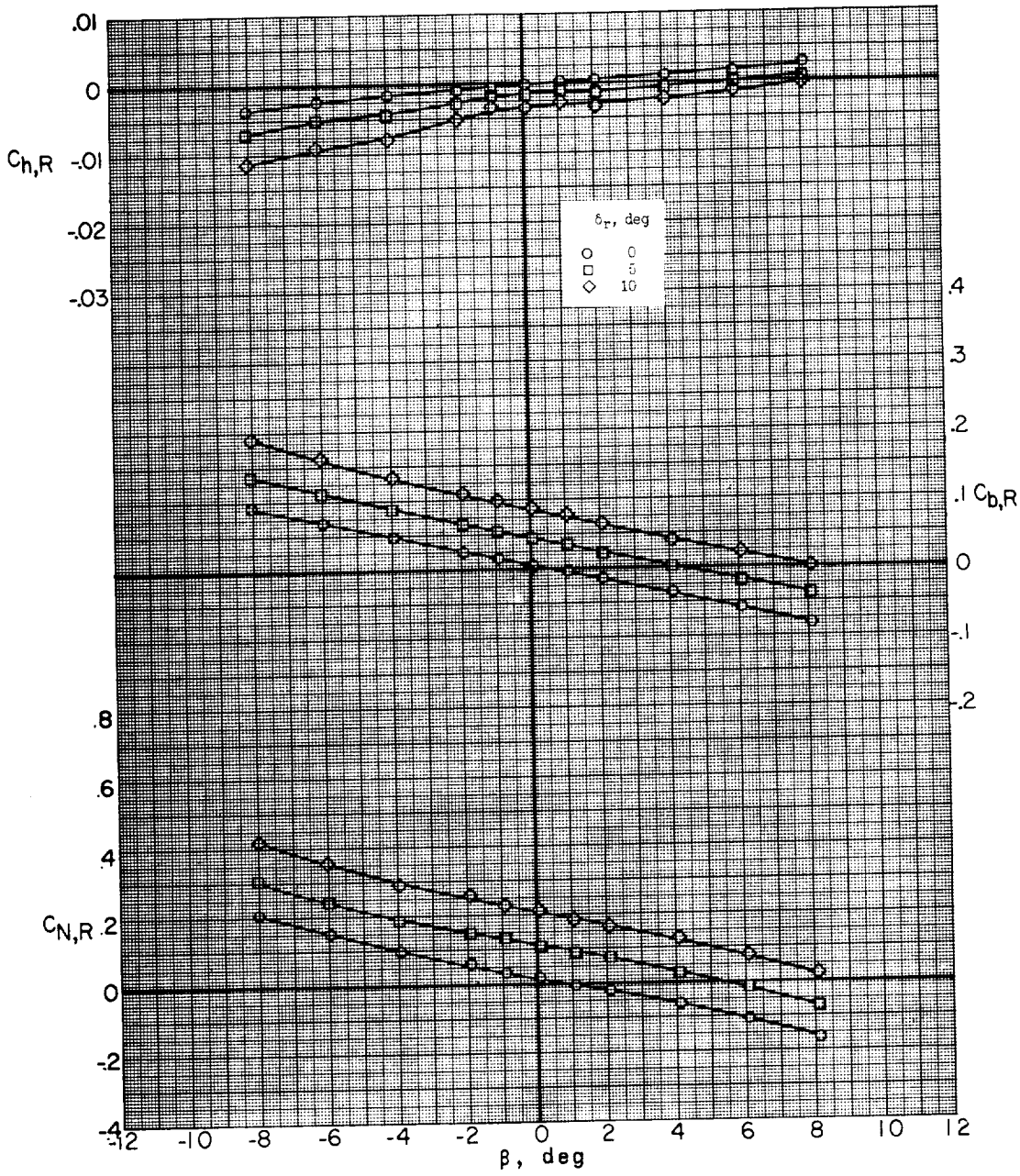
(d) M = 2.75; $\alpha = -5.0^{\circ}$.

Figure 56.- Continued.



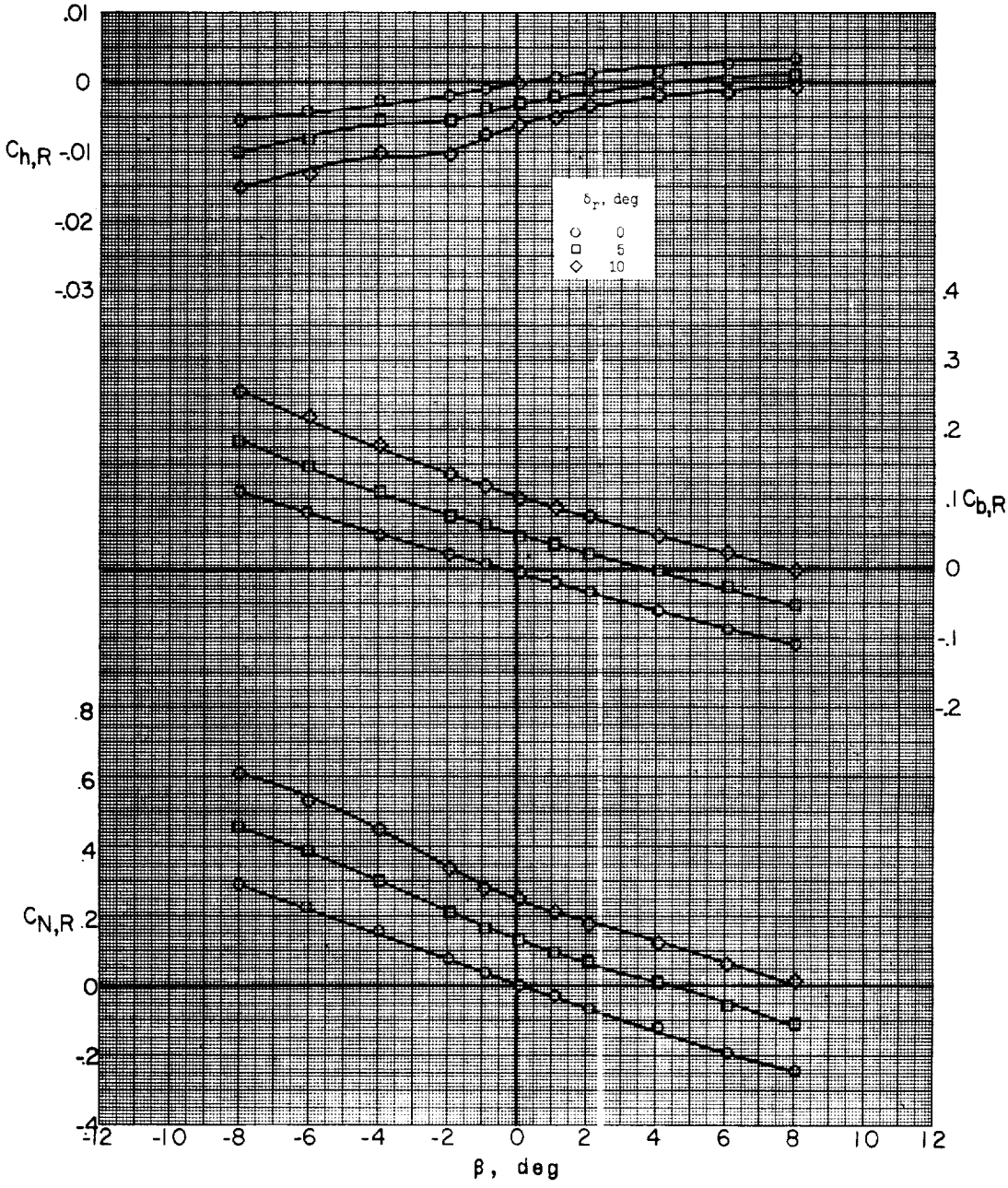
(e) M = 2.75; α = -0.1°.

Figure 56.- Continued.



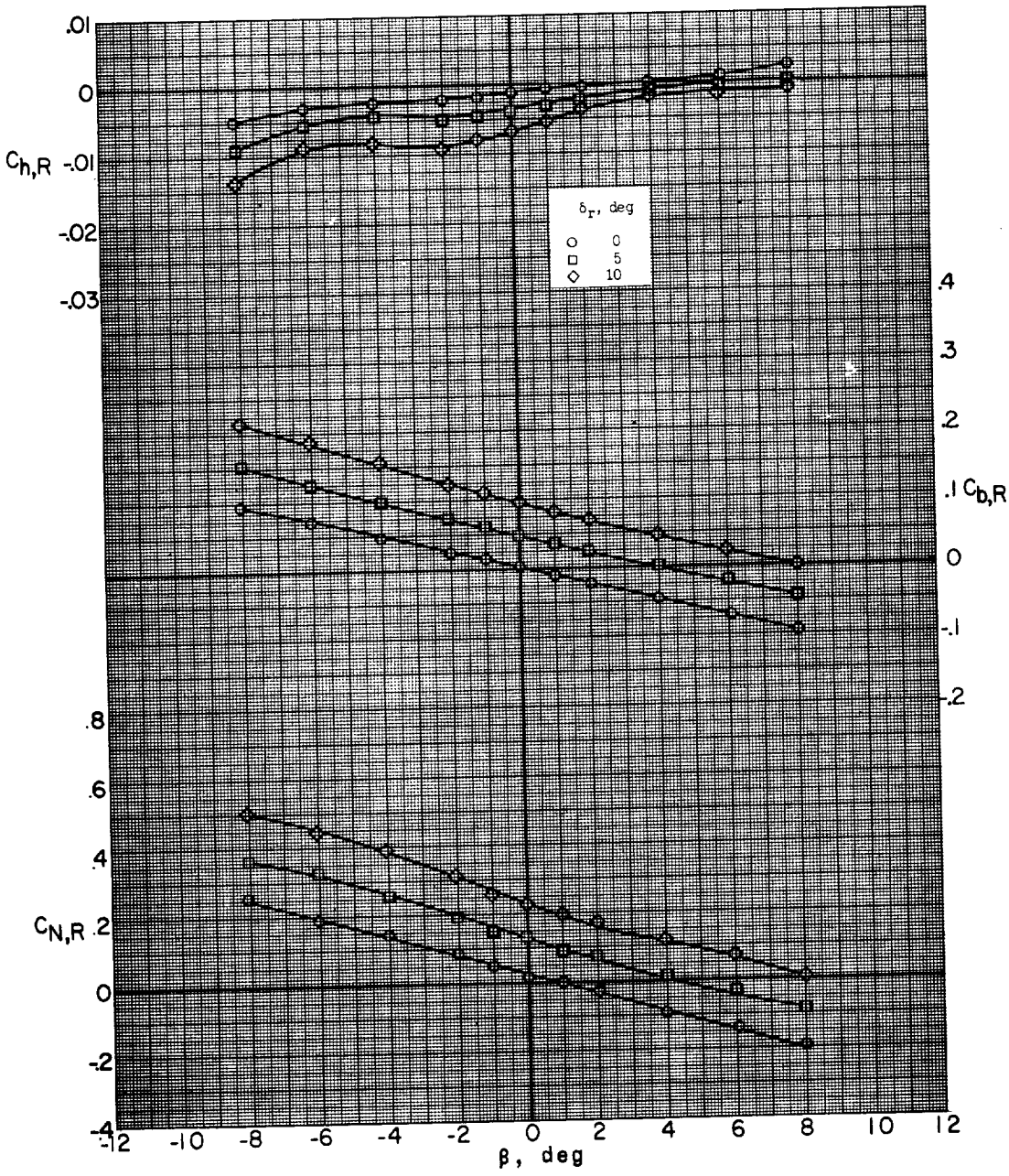
(f) M = 2.75; $\alpha = 5.0^{\circ}$.

Figure 56.- Continued.



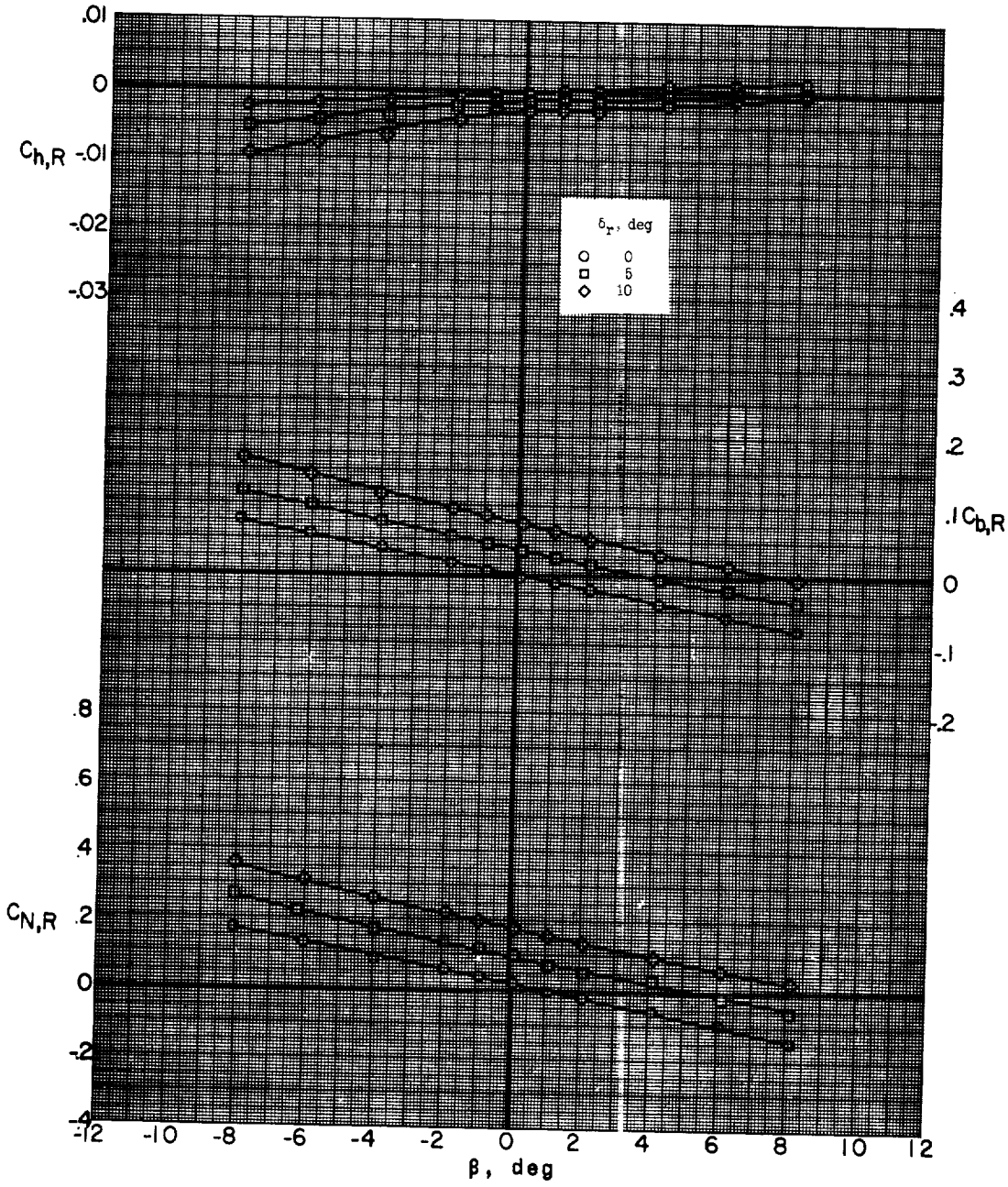
(g) M = 3.22; α = -5.0°.

Figure 56.- Continued.



(h) M = 3.22; $\alpha = -0.1^{\circ}$.

Figure 56.- Continued.



(i) M = 3.22; α = 5.0°.

Figure 56.- Concluded.